ISSN 0021-9673

VOL. 557 NOS. 1 + 2 SEPTEMBER 20, 1991

COMPLETE IN ONE ISSUE

Georges A. Guiochon Honour Volume
Part II

JOURNAL OF CHROMATOGRAPHY

INCLUDING ELECTROPHORESIS AND OTHER SEPARATION METHODS

SPECIAL VOLUME

ELSEVIER

Scope. The *Journal of Chromatography* publishes papers on all aspects of chromatography, electrophoresis and related methods. Contributions consist mainly of research papers dealing with chromatographic theory, instrumental development and their applications. The section *Biomedical Applications*, which is under separate editorship, deals with the following aspects: developments in and applications of chromatographic and electrophoretic techniques related to clinical diagnosis or alterations during medical treatment; screening and profiling of body fluids or tissues with special reference to metabolic disorders; results from basic medical research with direct consequences in clinical practice; drug level monitoring and pharmacokinetic studies; clinical toxicology; analytical studies in occupational medicine.

Submission of Papers. Manuscripts (in English; *four* copies are required) should be submitted to: Editorial Office of *Journal of Chromatography*, P.O. Box 681, 1000 AR Amsterdam, The Netherlands, Telefax (+31-20) 5862 304, or to: The Editor of *Journal of Chromatography, Biomedical Applications*, P.O. Box 681, 1000 AR Amsterdam, The Netherlands. Review articles are invited or proposed by letter to the Editors. An outline of the proposed review should first be forwarded to the Editors for preliminary discussion prior to preparation. Submission of an article is understood to imply that the article is original and unpublished and is not being considered for publication elsewhere. For copyright regulations, see below.

Publication. The *Journal of Chromatography* (incl. *Biomedical Applications*) has 38 volumes in 1991. The subscription prices for 1991 are:

J. Chromatogr. (incl. *Cum. Indexes, Vols. 501–550*) + *Biomed. Appl.* (Vols. 535–572):
Dfl. 7220.00 plus Dfl. 1140.00 (p.p.h.) (total *ca.* US$ 4400.00)

J. Chromatogr. (incl. *Cum. Indexes, Vols. 501–550*) only (Vols. 535–561):
Dfl. 5859.00 plus Dfl. 810.00 (p.p.h.) (total *ca.* US$ 3510.00)

Biomed. Appl. only (Vols. 562–572):
Dfl. 2387.00 plus Dfl. 330.00 (p.p.h.) (total *ca.* US$ 1430.00).

Subscription Orders. The Dutch guilder price is definitive. The US$ price is subject to exchange-rate fluctuations and is given as a guide. Subscriptions are accepted on a prepaid basis only, unless different terms have been previously agreed upon. Subscriptions orders can be entered only by calender year (Jan.–Dec.) and should be sent to Elsevier Science Publishers, Journal Department, P.O. Box 211, 1000 AE Amsterdam, The Netherlands, Tel. (+31-20) 5803 642, Telefax (+31-20) 5803 598, or to your usual subscription agent. Postage and handling charges include surface delivery except to the following countries where air delivery via SAL (Surface Air Lift) mail is ensured: Argentina, Australia, Brazil, Canada, Hong Kong, India, Israel, Japan*, Malaysia, Mexico, New Zealand, Pakistan, PR CHina, Singapore, South Africa, South Korea, Taiwan, Thailand, USA. * For Japan air delivery (SAL) requires 50% additional charge of the normal postage and handling charge. For all other countries airmail rates are available upon request. Claims for missing issues must be made within three months of our publication (mailing) date, otherwise such claims cannot be honoured free of charge. Back volumes of the *Journal of Chromatography* (Vols. 1–534) are available at Dfl. 208.00 (plus postage). Customers in the USA and Canada wishing information on this and other Elsevier journals, please contact Journal Information Center, Elsevier Science Publishing Co. Inc., 655 Avenue of the Americas, New York, NY 10010, USA, Tel. (+1-212) 633 3750, Telefax (+1-212) 633 3990.

Abstracts/Contents Lists published in Analytical Abstracts, Biochemical Abstracts, Biological Abstracts, Chemical Abstracts, Chemical Titles, Chromatography Abstracts, Clinical Chemistry Lookout, Current Contents/Life Sciences, Current Contents/Physical, Chemical & Earth Sciences, Deep-Sea Research/Part B: Oceanographic Literature Review, Excerpta Medica, Index Medicus, Mass Spectrometry Bulletin, PASCAL-CNRS, Pharmaceutical Abstracts, Referativnyi Zhurnal, Research Alert, Science Citation Index and Trends in Biotechnology.

See inside back cover for Publication Schedule, Information for Authors and information on Advertisements.

0021-9673/91/$03.50

This issue is printed on acid-free paper.

Printed in The Netherlands

For Contents, see p. VII

JOURNAL OF CHROMATOGRAPHY

VOL. 557 (1991)

JOURNAL of CHROMATOGRAPHY

INCLUDING ELECTROPHORESIS AND OTHER SEPARATION METHODS

SPECIAL VOLUME

ELSEVIER
AMSTERDAM — OXFORD — NEW YORK — TOKYO

J. Chromatogr., Vol. 557 (1991)

0021-9673/91/$03.50

Printed in The Netherlands

SPECIAL VOLUME

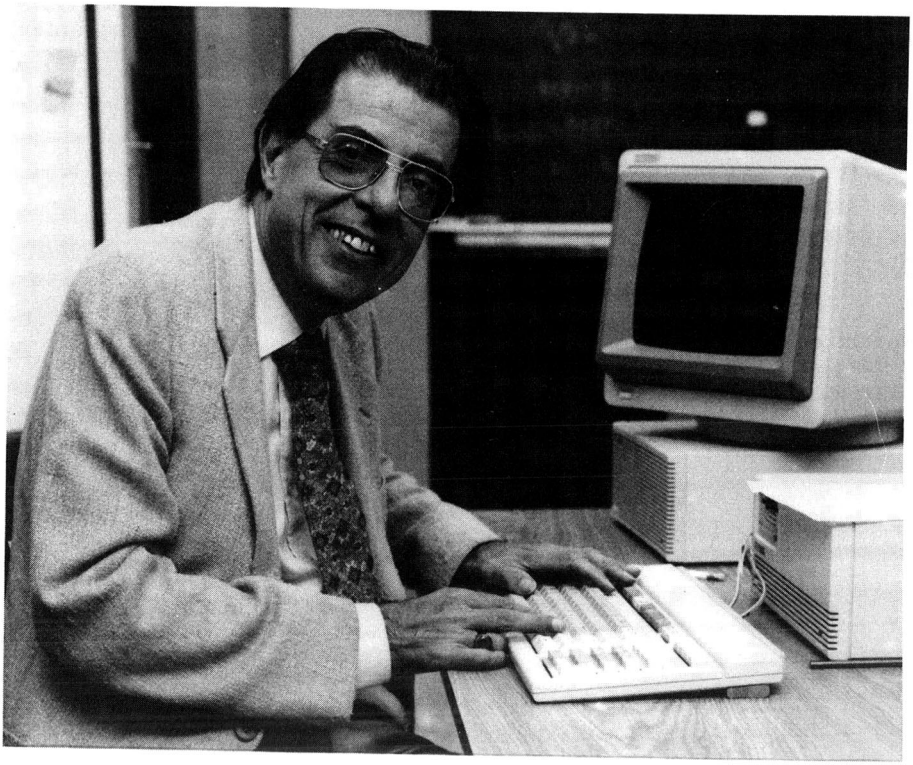

HONOUR VOLUMES

on the occasion of the 60th birthday of

GEORGES A. GUIOCHON

PART II

The papers submitted in honour of Professor **Georges A. Guiochon** on the occasion of his 60th birthday are published in two consecutive volumes of the *Journal of Chromatography*: Vols. 556 and 557 (1991). The Contents of both volumes are published in each of the volumes. A Preface by B. L. Karger appears in Vol. 556 and a Foreword by M. Martin in Vol. 557; a combined Author Index of both volumes is included in Vol. 557.

VOL. 557, NOS. 1+2 JOURNAL OF CHROMATOGRAPHY SEPTEMBER 20, 1991

CONTENTS

HONOUR VOLUMES ON THE OCCASION OF THE 60TH BIRTHDAY OF GEORGES A. GUIOCHON

PART II: VOLUME 557

PART I: VOLUME 556

In articles with more than one author, the name of the author to whom correspondence should be addressed is indicated in the article heading by a 6-pointed asterisk (*)

Journal of Chromatography, 557 (1991) XIII–XV
Elsevier Science Publishers B.V., Amsterdam

FOREWORD

Georges Guiochon was born in the French city of Nantes on September 6, 1931. He belongs to the small group of scientists who have made major and decisive contributions to the development of chromatography and to whom credit must deservedly be given for the fact that chromatography is, today, so widely and routinely used in nearly all branches of chemical and biochemical activities. It is therefore very appropriate and highly appreciated that two special volumes of the *Journal of Chromatography* are devoted to Georges in honour of his 60th birthday.

Entering a new decade in one's personal life is often the occasion of a particularly festive celebration. It is very fortunate that such a celebration could recently occur in the scientific community on the occasion of the *201st National Meeting of the American Chemical Society* in Atlanta, GA, last April during which Georges received an Award in Separation Science. Many of his friends and colleagues from several countries, as well as a group of his students and co-workers from the University of Tennessee were gathered around him. A family atmosphere emerged from this meeting, the more so as his oldest daughter, now a biologist, presented a lecture and Georges was proud and quite happy to introduce his grand-daughter to his friends. In addition, we were a small group of his former French students still active in chromatography and separation science who were very pleased to participate in this celebration. It was for us an occasion to remember the happy times we spent at École Polytechnique, first in Paris, then in Palaiseau where the École moved in 1975, when Georges was director of the Laboratoire de Chimie Analytique Physique.

I first met Georges in 1969 when I was looking for a thesis subject. High-performance liquid chromatography (HPLC), at that time called high-pressure liquid chromatography, was in its infancy and a German post-doctoral fellow from István Halász's laboratory in Frankfurt had just finished constructing a liquid chromatograph in the laboratory. I was asked to apply this new separation method to the analysis of steroids. But in fact, under the direction of Georges, the topic rapidly evolved and I never injected any steroid mixture into an HPLC column. I worked in tandem with a colleague and we first tried to evaluate the performance of the system. At that time, the finest particles available, something around 80 μm, were obtained by sieving commercial alumina or silica lots. But, after a short time, particles of around 30 μm became available which were either pellicular or totally porous; then, one day, Georges came to the laboratory with a batch of 7-μm silica particles with which we could pack a 7-cm long column with a high-pressure, high-capacity reciprocating pump initially intended to be used for preparative liquid chromatographic studies. Tremendous improvements in analysis time and separation resolution resulted from this substantial change in particle size. Steroids and my initial thesis subject were quickly forgotten. The subject matter of my thesis could not be anything other than the optimization of kinetic operating parameters in liquid chromatography, which made George very enthusiastic.

I remember how excited he was when we first pushed the pressure of the system to 80 atm and introduced a test compound with a syringe in a septum injector. He wanted to watch the experiment, a rather rare event, which gave us much confidence

in the relevance of the study which we were undertaking. Usually, Georges came from time to time into the laboratory to discuss the results. What was difficult for us to understand was then trivial to him and, after his visit, my colleague and I tried to remember his words with our poor, untrained student minds in order to unravel their meaning!

He is sometimes considered a theoretician. He certainly is willing to explore the depth of the phenomena involved in separation and is constantly striving to understand their fundamental aspects. He likes to model them. In fact, I have the feeling that Georges is really "the optimization man". He has the exceptional faculty of being able to envision the practical consequences that result from mastering equations and manipulating them in all possible directions. Because of this, Georges can be credited as having significantly influenced the evolution of column design and instrumentation in chromatography. For those of us who had the chance to be his students, this method of thinking has deeply influenced our way of approaching the chromatographic process.

He has been permanently on the lookout for new scientific fields in separation science and his intuition has been revealed to be particularly good in feeling which of them would become scientifically significant. He was one of the first scientists, and often the first in France, to become involved in many different fields, such as capillary gas chromatography, high-performance liquid chromatography, reversed-phase liquid chromatography, preparative gas chromatography, and preparative liquid chromatography.

Georges has also been concerned with the development of analytical chemistry and dissemination of scientific knowledge. He was quite active in GAMS, the Groupement pour l'Avancement des Méthodes Spectroscopiques et Physico-Chimiques d'Analyse (now Groupe pour l'Avancement des Sciences Analytiques), and served for some time as chairman of this organization, which is, in fact, the French society for analytical chemistry. In recognition of his very valuable services and his exceptional achievements in analytical chemistry, he was made an honourary member of GAMS. He is fascinated by the possibilities offered by the computer. He introduced the computer into the GAMS management, which greatly enhanced the efficiency of the society. The Laboratoire de Chimie Analytique Physique was the first at École Polytechnique to get a word processor. Today, this passion, combined with a deep understanding of the physico-chemical phenomena underlying the chromatographic process, culminates in the possibility offered by the computer to solve the differential mass balance equations involved in non-linear chromatography, work of very great significance which keeps Georges extremely active and productive and which greatly contributes in making liquid chromatography acceptable as an industrial production method.

Georges allowed his students a lot of freedom in which to conduct their studies. This was certainly not so easy to handle in the beginning when we, more or less tediously, were learning by experience the basics of chromatography, and some students may have wished to have had more guidance in the experiments. But, in fact, Georges was quite open and was generally available for those who wanted to discuss with him. Now we greatly appreciate this kind of relationship which allowed us to develop our own scientific personality. Moreover, because of Georges' international reputation, we benefited from frequent discussions with visitors from various West-

ern countries and we developed friendly relations with many scientists from Eastern Europe who spent months or years in the laboratory as a result of the strong involvement of Georges in the management of the Scientific Exchange Agreement Foundation.

Georges has been quite attentive to his students and co-workers. In fact, our relationship with him evolved from being one of hierarchical respect due to his position as a university professor (a rather highly regarded profession in France twenty or thirty years ago) and a person who we rapidly discovered had a prominent position in the international chromatographic community, to one of deep mutual personal respect for a person in whom we have progressively discovered great human qualities. Accordingly, when speaking to him, our address progressively shifted from "Monsieur Guiochon" to "Georges", a rather uncommon move in French traditional society.

Georges was concerned with the future of his students and he frequently helped them to find a job or a post-doctoral position in a foreign laboratory. When some of us obtained a permanent position in a French public research organisation, we chose to stay in the laboratory, in spite of the fact that a change in research topic and laboratory was recommended for career advancement, because of the propitious atmosphere for research in the laboratory under Georges' direction. We knew he put trust in us. He made time available for discussion in spite of the fact that he was busy with many different activities. Georges has a very high work capacity and, moreover, an exceptional ability to take decisions rapidly, which most often revealed themselves to be just and good decisions. This is undoubtedly one of the keys of his very succesful and prolific scientific career.

I am very glad to be able to take this opportunity to express my hearty thanks to him for the confidence and encouragement he always manifested to his students and co-workers, and for having given me the "research virus", which has exerted a definite influence on the orientation of my professional career, as well as for his significant help on many occasions and the numerous indications of his generosity. On behalf of his former students and co-workers, and his colleagues and friends, it is a great pleasure for me to wish Georges a very happy 60th birthday. I hope we will be able, for many more years, to read his significant scientific papers, listen to his provocative lectures at international symposia and enjoy the depth and pleasure of his friendship.

Paris (France) MICHEL MARTIN

Journal of Chromatography, 557 (1991) 1–12
Elsevier Science Publishers B.V., Amsterdam

CHROM. 23 323

Split injection into a capillary column at very low split ratios

STANISLAV WIČAR[a]
Laboratorní Přístroje, Prague (Czechoslovakia)

ABSTRACT

The solute zone in the inlet liner of a split injector at very low split ratios are split because of significant differences between the mean linear velocities in the capillary and in the liner. As the frontal part of the split zone of the solute moves through the liner with a velocity comparable with that in the capillary, radial diffusion is the limiting process. Given the diffusion coefficient of the solute, the radial mixing of the frontal part of the solute zone can be improved both by the inlet liner and the zone extension.

INTRODUCTION

The classical and still frequently used technique of introducing a sample into a capillary column is split injection. Compared with other techniques, such as on-column or splitless injection, the split technique reduces damage to the column caused by large amounts of liquid solvents and by non-volatile contaminants, and enables isothermal separation to be carried out. It is a typical sampling technique: only a part of the vaporized injected sample enters the column and is quantitatively evaluated; the principal open question is how representative is the analysed part with respect to the composition of the original liquid sample. A number of reviews have been published devoted to the split technique [1–4]. Unfortunately, there seems to be a lot of contradictory information, particularly concerning injection of larger sample volumes (*ca.* 2 μl of liquid) at very low split ratios (below 1:10). For example, Schomburg *et al.* [3] emphasize back-diffusion of high-boiling components with subsequent adsorption and condensation in the inlet lines at low split flow-rates, whereas Jennings [4] observed discrimination of more volatile hydrocarbon (C_{13}) compared with the less volatile one (C_{16}) if the split ratio was decreased below *ca.* 1:100. The latter observation seems to agree with that of Grob and Neukom [5]. Similar problems arise with the speed of evaporation of a sample in the liner. Bruderreck *et al.* [6] speak about seconds, but others use terms such as "flash" [1] or "explosion-like" [5] in this context. It was Wang *et al.* [7] who studied the effect of high temperature on solvent

[a] Present address: Barnett Institute, Northeastern University, 360 Huntington Avenue, 341 Mugar Building, Boston, MA 02115, USA.

0021-9673/91/$03.50

evaporation. Another question relates to the distribution of solutes in the solvent vapour in the liner. Ettre and Averill [8] contend that the linear function of a splitter is undermined by the absence of any "fractionation in the sample components during splitting because of difference in volatility". Because of this condition, vaporization tubes packed with glass wool plugs should help to "homogenize" the sample [3] or "thoroughly mix" the volatilized sample [1]. In spite of the contention of Ettre and Averill, German and Horning [9] recommend, instead of an inlet liner, a short piece of a packed column, where fractionation follows from the principle.

Practically no information exists about the dynamic behaviour of an inlet system consisting of an inlet valve (whether a part of an inlet pressure controller or a part of a flow controller), a splitter body, a capillary column and an outlet valve (whether an uncontrolled needle valve or a part of a back-pressure controller). Except for the report from Grob and Neukom [5] about the pressure wave that follows sample injection, only the steady-state properties of the basic control systems are discussed.

To study the processes that occur in an inlet liner after sample injection at high flow-rates is hardly possible; at low flow-rates the problem is less severe because we are dealing with a series of consecutive processes, which can be studied separately.

THEORY

Sample evaporation

Evaporation of a polycomponent liquid mixture on the glass wool in the inlet liner involves many factors, of which the following are the most important:

(1) Heat transfer to the boiling liquid, the injector temperature and the rate of evaporation.

(2) Composition of the vapour during evaporation.

(3) The volume changes accompanying evaporation.

(4) The possibility of sample decomposition on a solid hot surface.

The material balance of a binary solution during evaporation is expressed by the Rayleigh equation [10] of simple differential distillation:

$$\frac{dm}{m} = \frac{dx}{y - x} \tag{1}$$

where m is the mass of the liquid phase in moles, and x and y are the molar fractions of the volatile solvent in the liquid and the gas phase, respectively. Eqn. 1 is valid provided that the vapour is continuously removed from the boiling liquid.

To integrate eqn. 1 we need the equilibrium relation between x and y. For ideal solutions obeying the Raoult law

$$y = \frac{\alpha x}{1 + x(\alpha - 1)} \tag{2}$$

where $\alpha = P_s^0/P_i^0$ is the solvent relative volatility, and P_s^0 and P_i^0 are the saturated vapour pressures of solvent and solute, respectively, at the solvent boiling point. By integration of eqn. 1, using eqn. 2, we have

$$\ln \frac{m_0}{m} = \frac{1}{\alpha - 1}\left[\ln \frac{x_0}{x} + \alpha \ln \frac{1 - x}{1 - x_0}\right] \quad (3)$$

In eqn. 3, m_0 and x_0 are the initial mass of the liquid sample and the initial solvent molar fraction, respectively. For $\alpha \gg 1$ (a solute of low volatility in a volatile solvent) eqn. 3 can be simplified to

$$\frac{m}{m_0} = \frac{1 - x_0}{1 - x}$$

and evaporation of the major part of solvent results merely in concentration of the solute in the liquid phase; the gas phase during a substantial period of evaporation is formed practically by the pure solvent vapour. Consequently, the axial concentration distribution of the vapour plug in the liner is highly inhomogeneous. The front part of the vapour plug consists of pure solvent; somewhere towards the rear part there is a zone of the less volatile solute. The temperature of the boiling liquid remains at the boiling point of the solvent at the column inlet pressure (overheating cannot exceed 1°C), and rises at the end of evaporation to the boiling point of the less volatile solute or to the injector temperature.

If the injector temperature is below the boiling point of the particular solute, the solute saturated vapour pressure is complemented with the carrier to the total inlet liner pressure (distillation in a stream of inert gas), which inevitably leads to excessive dilution of the solute vapour with the carrier gas in the liner and, therefore, to additional broadening of the initial solute zone. Evaporation of larger volumes of a solvent (1–2 μl) on a glass wool plug is accompanied with a rapid local temperature fall. The limiting resistance to heat transfer is between the liner internal wall and the wool, because the wool is a good insulating material. At low split flow-rates the necessary heat excess cannot be transported by the overheated carrier gas and evaporation of less volatile solutes proceeds at a significantly lower temperature than that of the injector body.

The picture is substantially changed if the sample does not obey the Raoult law, and particularly if the solvent and the solute form an azeotropic mixture or if conditions for the extractive distillation prevail. In such cases the front part of the solvent vapour plug in the liner may contain solutes of interest, with consequences, as discussed later, for the pressure control and the liner void volume. This is probably the reason why discrepancies between the results obtained with test mixtures (hydrocarbons) and with solutes in real matrices are frequently reported.

Most chromatographers set the injector temperature somewhere close to the boiling point of the least volatile solute. With relatively volatile solvents, the temperature drop between the boiling liquid and any heated surface in the liner exceeds 100°C, and the solvent evaporation proceeds deep in the Leidenfrost region [11]; this means that every boiling droplet is surrounded by a continuous insulating layer of vapour, which reduces heat transfer to the boiling liquid. As the boiling liquid is in close contact with its vapour, a mutual mass transfer between both phases is possible, and fractionation may proceed behind that specified by eqn. 3. One can hardly speak about a "flash" evaporation in this context (evaporation of 2 μl of chloroform 200°C above its boiling point lasts from 2 to more then 6 s, depending on the I.D. of the liner).

As pointed out many times, the vaporization of an injected liquid sample is accompanied by a large increase in volume in the liner, which manifests itself by a pressure wave, propagated with the velocity of sound. The influence of this pressure wave on the liner function depends on the type of pressure control used.

Inlet pressure control

Pressure-control systems used in capillary GC fall into two basic categories. One type controls the supply of carrier gas into the injector by operating the inlet valve to guarantee constant pressure in the liner. The second type operates an outlet valve located in the vent line; an independent constant gas supply source in the inlet line (*e.g.*, a flow controller) is necessary for correct function of the pressure controller.

If the front part of a pressure wave produced by sample vaporization reaches the pressure sensor of a controller of the first type, the controller merely closes the inlet valve and simply waits until the pressure returns to its preset value. Such a controller is generally unable to eliminate the pressure wave. As the vapour propagation proceeds in all directions, some of the sample vapour may easily reach the septum part of the injector. Heavier components may be adsorbed on cooler surfaces and lighter ones may disappear through septum purge if the heated liner volumes on both sides of the evaporation point are not sufficient for the particular vapour volume. At lower split ratios the evaporation should thus proceed somewhere in the middle of the liner. This is probably the reason why Grob [2] emphasizes the importance of the distance between the needle exit and the column entrance.

The situation with the controllers of the second type is different. As soon as the front of the pressure wave reaches the controller sensor, the controller opens the outlet valve to compensate for the pressure increase by venting out part of the carrier present in the injector. If the pressure sensor is sufficiently sensitive, and if the valve operates rapidly to cope with the pressure changes, the pressure wave can be almost totally eliminated by converting it into a flow-rate wave. In this case the sample vapour is pushed down the heated liner at a speed determined by the sum of the preset injector flow-rate and the rate of evaporation. It is thus reasonable, in this particular case, to evaporate the sample in the upper part of the liner. Such an arrangement is advantageous, as it enables the use of syringes with short needles and reduces the danger of solvent evaporation from the heated syringe needle during injection.

To benefit from these advantages of the back-pressure controller, the dynamic properties of the control system and of the particular controllers (flow and pressure) used must be known. These are obtained by measuring both the transient characteristics of the control system with the open loop (between the sensor and the valve) and the reaction of the control system with the closed loop to pressure disturbances.

Convective diffusion of solute in the liner

As soon as the sample vapour is pushed down the liner, the flow lines that are established are governed by the continuity equation. At low split flow-rates, the mean linear velocity in the capillary is much greater than that in the liner and, consequently, a narrow cylindrical funnel moving significantly faster than the remaining annulus part is formed far above the column entrance. The resulting velocity profiles differ greatly from the parabolic profiles characteristic of open tubes and laminar flow. The convective process associated with the velocity funnel in the centre of the liner

transports the central part of the solute zone down the liner faster than the remaining part of the same solute, and is responsible for the formation of two close but separate zones at different liner depths. Radial solute diffusion transports some of the solute from the axial to the annular part of the liner, and another part of the solute from the annular to the axial part (Fig. 1). We have to deal with a typical axial solute zone splitting in the inlet liner. If there is enough liner length left above the capillary inlet, the split zones will merge by axial diffusion, otherwise we will observe peak splitting for peaks separated isothermally. The peak splitting disappears at temperature-programmed separations because the originally split solute zones are focused in the column. To suppress this unwanted effect of low split flow-rates, sufficient time must elapse for diffusion to occur before the solute zone reaches the column entrance. The stop-flow technique, proposed by Bayer and Liu [12], is unable to help here as convection in the central part of the pressurized liner proceeds even when the vent line is closed. The capacity of the inlet liner from the evaporation glass wool plug to the column entrance must thus be increased to exceed the sample vapour volume by at least a factor of three. The classical liner length (80–90 mm) is too short and should therefore be extended to at least 150 mm.

For ideal solutions following the Raoult law, the insufficient sample capacity of the liner may not be observed as the analyst is not interested in correct solvent splitting; the problems with the liner capacity may become evident for complex real solutions in which some components of analytical interest may be located in the front part of the solvent zone.

The process of sample vapour splitting

Let us consider conditions at the liner cross-section at the column inlet after sample injection and evaporation. For the mass of the i-th component of the mixture entering the column, $m_{c,i}$, in polar co-ordinates (r,Φ) it holds

$$m_{c,i} = \int_0^{\infty} \int_0^{2\pi} \int_0^{R} c_i(r,\Phi,t)\, u_c(r,\Phi,t)\, r\, \mathrm{d}r\, \mathrm{d}\Phi\, \mathrm{d}t \tag{4}$$

where R is the column internal radius, c_i and u_c are the i-th component concentration and linear flow velocity in the column, respectively, and t is time. A similar expression holds for the mass of the i-th component vented out of the liner, $m_{v,i}$:

$$m_{v,i} = \int_0^{\infty} \int_0^{2\pi} \int_{R_0}^{R_1} c_i(r,\Phi,t)\, u_v(r,\Phi,t)\, r\, \mathrm{d}r\, \mathrm{d}\Phi\, \mathrm{d}t \tag{5}$$

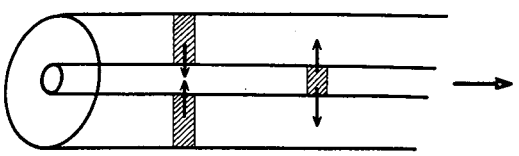

Fig. 1. Mechanism of the solute zone splitting in the inlet liner.

where R_0 and R_1 are the external radius of the column and the internal radius of the liner, respectively, and u_v is the linear flow velocity in the liner. In both expressions the diffusional mass transfer across the plane of interest has been omitted. The experimentally accessible steady-state volume flow-rate in the column, v_c, is

$$v_c = \int_0^{2\pi} \int_0^{R} u_c(r,\Phi)\, r\, dr\, d\Phi \tag{6}$$

and in the liner annulus, v_v:

$$v_v = \int_0^{2\pi} \int_{R_0}^{R_1} u_v(r,\Phi)\, r\, dr\, d\Phi \tag{7}$$

The ideal function of the liner is characterized by a series of equations

$$\frac{v_c}{v_v} = \frac{m_{c,i}}{m_{v,i}} = \text{const.} \tag{8}$$

for all sample components $i = 1, 2, 3, \ldots, n$, and for any split ratio v_c/v_v.

In order to approach to the liner ideal function, we have to satisfy two basic conditions:

(1) Perfect radial mixing of the solute in the liner.

(2) Steady flow conditions before the first sample component reaches the entrance of the column.

According to the first condition, c_i does not depend on r and Φ, and according to the second one, u_c and u_v do not depend on t; therefore

$$m_{c,i} = v_c \int_0^{\infty} c_i(t)\, dt \tag{4a}$$

$$m_{v,i} = v_v \int_0^{\infty} c_i(t)\, dt \tag{5a}$$

and eqn. 8 hold since the integrals in both eqns. 4a and 5a are identical, provided that condition 1 holds. It should be noted that the axial concentration profiles (*e.g.*, axial inhomogenities as split zones) expressed in the convection process as time functions $c_i(t)$, do not play any role here.

Unfortunately, any model based on perfect radial mixing is far from reality. This becomes clear if we include the velocity profiles in the liner above the column inlet in our considerations. The most critical zone with respect to radial diffusion is the frontal zone of each solute as it moves faster.

In practice, we are unable to guarantee steady flow immediately after the sample injection as required by eqns. 4a and 5a; steady flow conditions can be reached only after a certain time interval t_0. The magnitude of this interval is determined by the amount of the sample injected, by the heat transfer rate at the sample evaporation zone, and by the properties of the pressure control used.

It should be emphasized that all conclusions are valid only for totally evaporated samples. Splitting of two-phase systems, such as aerosols, is a matter of statistics and cannot be treated by tools developed for the physics of continuum. The conclusions made above are not valid either for injections into an empty liner, as sample droplets leaving the syringe needle hit the liner hot surface at various depths and the composition of the vapour and the corresponding diffusional paths are unpredictable.

EXPERIMENTAL

All experiments were carried out using the Chrom 61 gas chromatograph (Laboratorní Přístroje, Prague, Czechoslovakia). This apparatus is equipped with computer-controlled two-channel pneumatics for the carrier, hydrogen and air [13]. The original A-channel injector for packed columns was changed for a laboratory-made split injector (Fig. 2). The length of the quartz liner was 145 mm and the I.D. was 3.5 mm. The inlet part of the liner was packed with the glass wool (the plug length was 30 mm). The design of the top part of the liner enabled the 50-mm syringe needle to penetrate 15 mm deep into the liner (10 mm deep into the plug).

A glass capillary column (15 m × 0.25 mm I.D.) covered with immobilized SE-30 phase was used. The column ends were extended by standard fused-silica capillaries of 20 cm length. The column inlet was located 10 mm above the lower end of the liner.

Special attention was given to the design of the back-pressure controller. Grob and Neukom [5] explained discrimination by split-ratio changes during the various phases of a pressure wave accompanying the sample evaporation. To suppress the pressure wave, we need a very fast back-pressure controller that is able to cope with the rate of sample evaporation.

The control valve design is similar to that described earlier [13] in connection with the digital mass flow controller. The valve connected to the vent line of the injector consists of a short inlet tube (1.5 mm I.D.) followed by a seat (0.7 mm I.D.) and a closing element driven by a magnetically controlled lever. The valve mechanics is located inside the valve body of *ca.* 40 ml volume; the valve body is open to atmosphere. The valve operates with a constant period of 40 ms duration. At the beginning of each period the valve is opened for a calculated time interval; for the rest of the period the valve seat is closed. The opening intervals are set in 2 μs multiples.

A semiconductor tensometric pressure sensor is used to measure pressure in the injector. The normalized sensor signal, taken from the analogue Z-bus of Chrom 61, is converted by a dual-slope A/D converter, one digit of the converter reading corresponds to 100 Pa (0.001 atm). A modified PS controller program is used to control pressure by the 8080A type microcomputer SAPI 1 (Tesla Liberec, Czechoslovakia). The data from the converter are fed to the computer through a parallel input port, and every 40 ms the opening time interval is calculated on the basis of the actual sensor reading and sent to the valve through a programmable timer-counter interface.

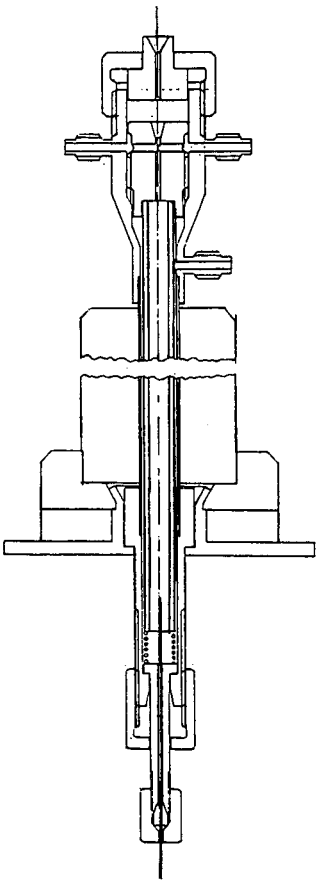

Fig. 2. Injector design.

The same data, along with the normalized pressure readings, are sent to respective D/A converters and plotted as time functions. The schematic diagram of the injector pneumatics is shown in Fig. 3, and the valve and inlet pressure response functions for 0.5, 1, and 2 μl of $CHCl_3$ at various injector temperatures are shown in Fig. 4. The valve responses demonstrate almost complete conversion of the pressure wave into the flow-rate changes in the liner.

As a test mixture, a solution of *n*-decane and *n*-octadecane in chloroform was used. The basic solution contained 0.24 μg of *n*-C_{10} and 0.384 μg of *n*-C_{18} in 1 μl of solution. This solution was further diluted 1:2 and 1:4, so that 0.5 μl of the basic solution contained the same amounts of solutes as 1 μl of the second or 2 μl of the third solution (0.12 and 0.192 μg, respectively). A Hamilton 701 N syringe was used to inject 1- and 2-μl samples, and a Hamilton 7001 N syringe with a needle spacer was used for 0.5-μl samples.

The necessary make-up gas for flame ionization detection (FID) was supplied by the B-channel carrier line. Nitrogen served both as the carrier gas and the make-up gas. The peak-area integration was performed with the CI-105 chromatographic integrator

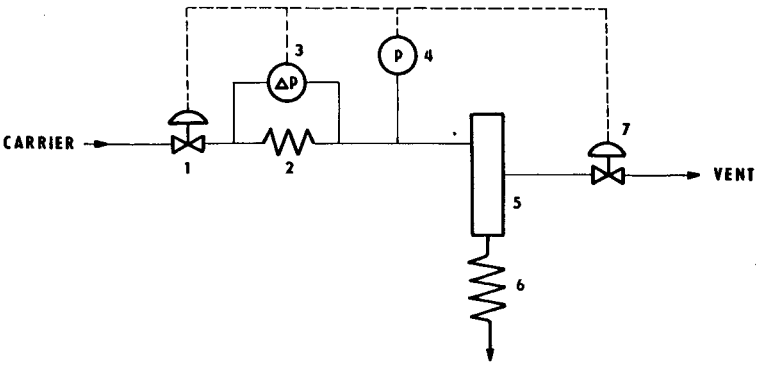

Fig. 3. Injector pneumatics: 1 = inlet valve; 2 = flow measuring capillary; 3 = differential pressure sensor; 4 = inlet pressure sensor; 5 = injector; 6 = column; 7 = outlet valve.

(Laboratorní Přístroje). The standard sampling interval (100 ms) was changed to 50 ms by making the necessary changes in the firmware ROMs.

The separation was carried out at programmed temperature. The programme started isothermally at 90°C, and after 3 min the temperature was raised at 40°C/min to 190°C where it remained for 6 min. The injector temperature was changed during the measurements.

To obtain FID responses to the original sample, 0.5 μl of the basic solution was analysed in a packed column (1.5 m, 3% SE-30 on Chromosorb^{R} W AW) at the same FID and electrometer conditions.

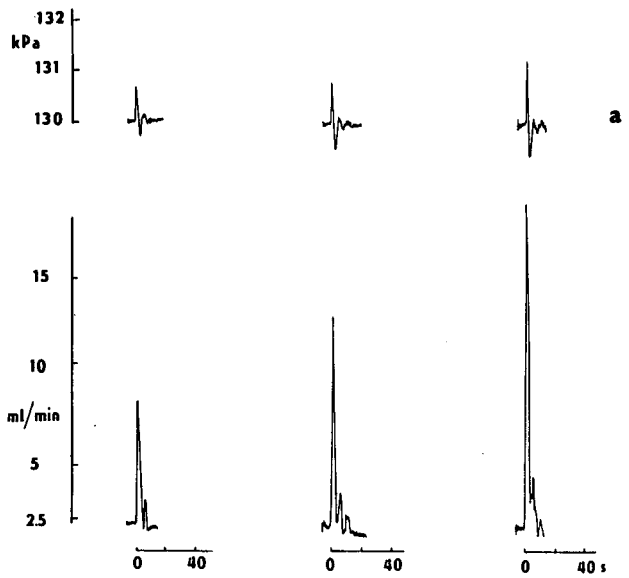

Fig. 4.

(Continued on p. 10)

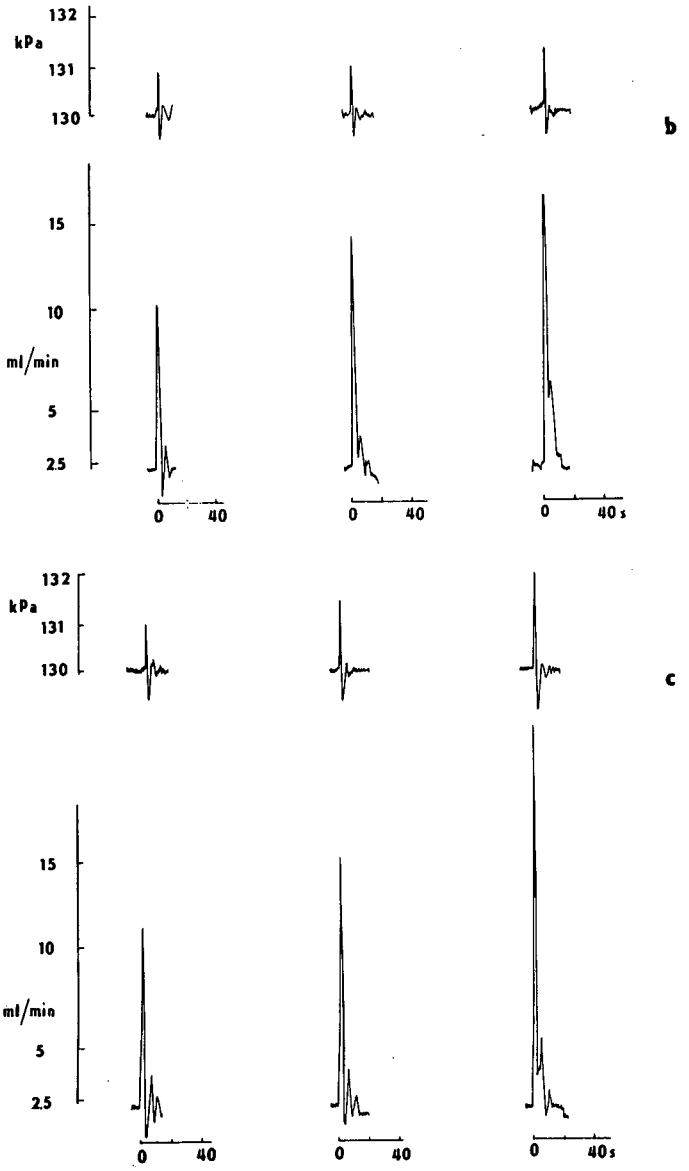

Fig. 4. Absolute pressure and outlet valve response functions to injection of (from the left to the right) 0.5, 1.0 and 2.0 μl of $CHCl_3$. Injector temperature: a = 200°C; b = 250°C; c = 300°C.

RESULTS AND DISCUSSION

The results for the capillary column are summarized in Table I. The data obtained with the 7001 (1 μl) syringe are *ca.* 10% lower than those obtained with the 701 (10 μl) syringe. By dividing the area counts for *n*-decane determined in the packed column (Table II) by 3.46 and 7.0, respectively, we obtain the theoretical responses for

TABLE I

CAPILLARY COLUMN DATA

Volume injected (μl)	Split ratio	Injection temperature (°C)	C_{10} area (μVs)	C_{18} area (μVs)	C_{18}/C_{10}
0.5	1:2.46	200	326 814 (2.5)[a]	497 428 (2.7)	1.52 (2.6)
		250	332 754 (2.0)	553 411 (2.5)	1.66 (3.0)
		300	337 959 (3.2)	725 110 (4.7)	2.15 (5.6)
1.0		200	369 771 (4.0)	556 800 (5.2)	1.51 (3.0)
		250	389 466 (1.7)	649 510 (4.0)	1.67 (2.8)
		300	396 583 (3.0)	808 056 (3.0)	2.04 (4.9)
2.0		200	370 048 (1.7)	561 398 (2.0)	1.52 (2.4)
		250	381 985 (1.9)	636 178 (1.7)	1.67 (1.6)
		300	363 677 (2.4)	820 859 (3.5)	2.26 (2.2)
0.5	1:6.0	200	151 282 (2.7)	236 375 (3.1)	1.56 (2.1)
		250	160 223 (2.0)	275 782 (3.7)	1.72 (4.1)
		300	163 868 (1.8)	340 884 (3.7)	2.08 (3.9)
1.0		200	177 050 (4.0)	265 011 (4.7)	1.50 (3.7)
		250	182 099 (5.0)	294 722 (3.6)	1.62 (4.5)
		300	172 236 (3.5)	374 897 (4.6)	2.18 (5.2)
2.0		200	171 587 (2.6)	261 363 (3.4)	1.52 (3.9)
		250	178 240 (1.2)	296 765 (5.3)	1.67 (5.3)
		300	183 359 (2.6)	368 109 (3.9)	2.01 (4.5)

[a] The data in brackets refer to the standard deviations expressed in % and valid for 10 measurements.

the preset split ratio 1:2.46 as 332 726 and for the preset split ratio 1:6.0 as 164 462. Both responses are in good agreement with the data obtained in the capillary. With 2-μl samples at injector temperatures 250°C and 300°C, *n*-decane peak splitting was frequently observed. In those cases both areas corresponding to *n*-decane were summed.

While the area counts for *n*-decane are independent of the injector temperature, a strong dependence of responses for *n*-octadecane on injector temperature is evident. Except for the injector temperature 200°C, the experimental responses exceed the theoretical ones (532 866 and 263 388, respectively). The corresponding C_{18}/C_{10} ratios increase with increasing injector temperature, and are practically independent of the preset split ratio. This fact can simply be explained if we realize that each solute

TABLE II

PACKED COLUMN DATA

Volume injected (μl)	C_{10} area (μVs)	C_{18} area (μVs)	C_{18}/C_{10}
0.5	1151 232 (1.7)	1843 716 (2.6)	1.60

enters into the capillary in the form of two discrete portions. As the velocity of the first portion is determined by the flow in the capillary (by the column inlet pressure), the radial mass transfer is insufficient for components with smaller diffusion coefficients, and more solute enters the column with the first portion as theoretically predicted. Given the velocity and diffusion path (inlet liner length reduced by the solvent vapour volume), the exposure of the first zone to diffusion can be extended by increasing the width of the particular zone. The principle is similar to that utilized by the slot shutter of a camera. The initial zone-broadening is here accomplished by decreasing the injector temperature far below the boiling point of the particular solute. This operation is of course dangerous, as condensation of less volatile components in relatively cold parts of the injector leading to discrimination cannot be excluded. This is probably the reason why the data for 200°C and *n*-octadecane are slightly below the theoretical values.

The correct solution to the problem lies in extending the inlet liner (the length of 250 mm is quite reasonable), in decreasing the liner internal diameter, and in changing nitrogen for hydrogen as the carrier gas. If the diffusional path is sufficient for the particular solute, the results should not depend on the injector temperature (as observed with *n*-decane).

REFERENCES

1 R. R. Freeman, *High Resolution Gas Chromatography*, Hewlett-Packard, 1979.
2 K. Grob, *Classical Split and Splitless Injection in Capillary GC*, Hüthig, Heidelberg, Basle, New York, 1988.
3 G. Schomburg, H. Behlau, R. Dielmann, F. Weeke and H. Husmann, *J. Chromatogr.*, 142 (1977) 87.
4 W. Jennings, *GC with Glass Capillary Columns*, Academic Press, New York, 2nd ed., 1980.
5 K. Grob, Jr. and H. P. Neukom, *J. High Resolut. Chromatogr. Chromatogr. Commun.*, 2 (1979) 563.
6 H. Bruderreck, W. Schneider and I. Halasz, *J. Gas Chromatogr.*, 5 (1967) 91.
7 F. S. Wang, H. Shanfield and A. Zlatkis, *J. High Resolut. Chromatogr. Chromatogr. Commun.*, 6 (1983) 471.
8 L. S. Ettre and W. Averill, *Anal. Chem.*, 33 (1961) 680.
9 A. L. German and E. C. Horning, *Anal. Lett.*, 5 (1972) 619.
10 Lord Rayleigh, *Phil. Mag.*, 4 (1902) 527.
11 T. B. Drew and A. C. Mueller, *Trans. Am. Inst. Chem. Eng.*, 33 (1937) 449.
12 E. Bayer and G. H. Liu, *J. Chromatogr.*, 256 (1983) 201.
13 S. Wičar, *J. Chromatogr.*, 295 (1984) 395.

Journal of Chromatography, 557 (1991) 13–21
Elsevier Science Publishers B.V., Amsterdam

CHROM. 23 322

On-line electrochemical reagent generation for liquid chromatography with luminol-based chemiluminescence detection

O. M. STEIJGER*
Department of Pharmaceutical Analysis, University of Utrecht, Sorbonnelaan 16, 3584 CA Utrecht (Netherlands)
G. J. DE JONG
Duphar B.V., C. J. van Houtenlaan 36, 1381 CP Weesp (Netherlands)
J. J. M. HOLTHUIS
EuroCetus BV, Paasheuvelweg 30, 1105 BJ Amsterdam (Netherlands)
and
U. A. Th. BRINKMAN
Department of Analytical Chemistry, Free University, De Boelelaan 1083, 1081 HV Amsterdam (Netherlands)

ABSTRACT

An on-line method for the generation of electrochemical reagent for liquid chromatography, with luminol-based chemiluminescence detection, has been developed. An ESA Coulochem guard cell, equipped with a porous graphite working electrode, operated at −600 mV and inserted after the column, produces an oxidative reagent for the luminol-based reaction. This method has been compared with the conventional method with post-column addition of hydrogen peroxide as the oxidative reagent. With this novel method a detection limit of 0.15 pmol of ibuprofen (labelled with an isoluminol derivative) can be obtained, and a good alternative for post-column addition of hydrogen peroxide is presented.

INTRODUCTION

High sensitivity is often required for the trace-level determination of drugs in biological samples. In liquid chromatography (LC), chemiluminescence (CL) detection offers good possibilities to improve detection limits over those of more conventional detection methods, *e.g.* fluorescence detection. Various CL reactions can be applied for detection in LC, but the most frequently used detection system is based on the peroxyoxalate CL reaction. A disadvantage of the CL system is the poor solubility and stability of the oxalates in common reversed-phase LC solvents.

The CL reaction of luminol (5-amino-2,3-dihydro-1,4-phthalazinedione) with hydrogen peroxide in the presence of a catalyst in alkaline solution is another well-known CL reaction (Fig. 1). Despite the fact that CL of luminol has been under

0021-9673/91/$03.50

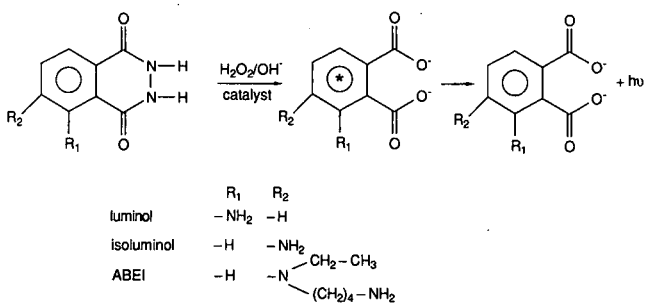

Fig. 1. CL reaction of luminol and analogues.

investigation since 1928 [1], the mechanism of this reaction is still not exactly known. A variety of oxidants, such as hydrogen peroxide, oxygen, persulphate, bromine and hypochlorite can be used [2–5], but hydrogen peroxide is the most effective. With hydrogen peroxide as the oxidant, a catalyst is required. Typical catalysts are peroxidases, hemin, transition-metal ions and hexacyanoferrate(III) [2,3]. The luminol CL reaction can be used as the detection system in LC for the determination of hydrogen peroxide (also hydrogen peroxide generated by (enzyme) reactions) [6,7], hydroperoxides [8–11], certain metal ions [12,13] or complexes containing metal ions [14], chelate-forming agents [15–17] and analytes labelled with specially modified luminol [18–20]. In the case of analytes containing a carboxylic group, the label used is N-(4-aminobutyl)-N-ethylisoluminol (ABEI) [18,19].

Normally in LC, hydrogen peroxide and the catalyst are added post-column as two separate solutions [18,19], because hydrogen peroxide reacts with the catalyst. The inconvenience of handling three flowing solutions (eluent, hydrogen peroxide and catalyst) can be circumvented by using electrochemical generation of hydrogen peroxide. This reagent is electrochemically generated on-line from oxygen present in the mobile phase. An electrochemical flow-cell containing a porous graphite electrode is placed at the column outlet. At this electrode, oxygen present in the mobile phase is reduced to hydrogen peroxide.

In this paper, on-line electrochemical generation of hydrogen peroxide is compared with addition of hydrogen peroxide by a pump, using the determination of ABEI-labelled ibuprofen as a model system. Microperoxidase, added to the eluate just before detection, is used as catalyst.

EXPERIMENTAL

Chromatographic conditions

The conventional LC–CL system, with separate post-column addition of hydrogen peroxide and the catalyst, is simplified by on-line electrochemical generation of hydrogen peroxide (Fig. 2). The electrochemical flow-cell used was an ESA Coulochem guard cell (Model 5020, Bedford, MA, USA) containing a porous graphite working electrode and connected to a laboratory-made potentiostat operated at −600 mV. (The reference electrode was constructed of a proprietary material and was typically placed within a millimetre of the working electrode).

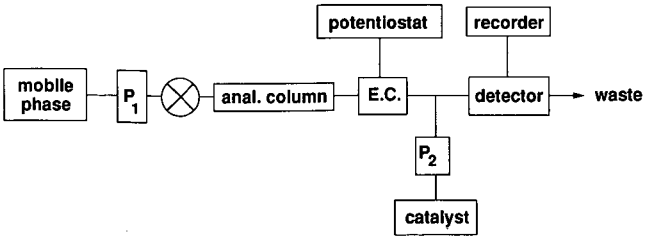

Fig. 2. Block diagram of the LC–CL system with on-line electrochemical reagent generation. E.C. = electrochemical flow-cell, operating at −600 mV; P_1 = acetonitrile–10 m*M* carbonate buffer of pH 10.5 (27:73, v/v); P_2 = 1 μM microperoxidase in 10 m*M* carbonate buffer (pH 10.5). In the LC–CL system with reagent addition, the E.C. is replaced by a third pump, P_3, for the addition of hydrogen peroxide in water. When an FIA system was used, the column was removed and 5 μl of 0.1 μM ABEI in carrier solution was injected.

The mobile phase, acetonitrile–aqueous 10 m*M* carbonate buffer (pH 10.5) (27:83, v/v) was delivered by a Kratos Spectroflow 400 pump (Applied Biosystems, Ramsey, NJ, USA) at a flow-rate of 0.8 ml/min. The catalyst microperoxidase (1.0 μM in 10 m*M* carbonate buffer of pH 10.5) (Sigma, St. Louis, MO, USA) was added post-column by an LKB pump (Model 2150; Pharmacia LKB Biotechnology, Uppsala, Sweden) at a flow-rate of 0.4 ml/min and, in the case of the addition of hydrogen peroxide (30% v/v, Baker, Deventer, The Netherlands), a solution in water was delivered by a Kratos Spectroflow 400 pump (Applied Biosystems) at a flow-rate of 0.05 ml/min.

A solution containing ibuprofen and the internal standard naproxen (both from Sigma) derivatized with ABEI, or a 0.1 μM solution of ABEI (Sigma) in the mobile phase was injected by a Waters U6K injector (Waters Assoc., Milford, MA, USA) or a laboratory-made injector with a 18-μl sample loop. A polymer PLRP-S column (150 × 4.6 mm I.D., particle size 5 μm; Polymer Labs., Church Stretton, UK) was used, and the detector was a Kratos Spectroflow 980 fluorescence detector (Applied Biosystems) with the lamp disconnected and equipped with a 25-μl flow-cell and a cut-off filter of 389 nm.

Determination of hydrogen peroxide

For the determination of hydrogen peroxide generated in the ESA electrochemical flow-cell, which was incorporated in the LC system described, a flow-injection (FIA) system with electrochemical detection (ED) was used. The carrier, a solution of 10 m*M* carbonate buffer (pH 10.5), was delivered by a Kratos Spectroflow 400 pump (Applied Biosystems) at a flow-rate of 0.8 ml/min. The electrochemical detector consisted of a confined wall-jet system (PB-2) equipped with a platinum working electrode (diameter 6 mm, Beckman Instruments, Mijdrecht, Netherlands) operated at a potential of +600 mV *vs.* SCE, and an auxiliary electrode of glassy carbon (diameter 6 mm) at a distance of 50 μm from the platinum working electrode. The generating current was set at 2 μA.

Calibration samples of hydrogen peroxide (0.2, 0.5, 1.0, 2.0, 5.0 and 10.0 · 10^{-4}%) were prepared in carrier solution, and 10 μl were injected into the FIA system. From a flow system consisting of a Kratos Spectroflow 400 pump (Applied

Biosystems) delivering the same carrier solution at a flow-rate of 0.8 ml/min, and the ESA cell, a sample was taken every 30 s for the determination of the concentration of the generated hydrogen peroxide.

Derivatization procedure

A 50-μl volume of a standard solution of ibuprofen (0.05 mg/ml) and naproxen (0.15 mg/ml) in methanol was evaporated under nitrogen in a 1.5-ml reaction vial (Model 3810; Eppendorf, Hamburg, Germany) at ambient temperature. Next, 50 μl of 1-hydroxybenzotriazole (HOBT) (Janssen Chimica, Beerse, Belgium) in chloroform (0.25 mg/ml), 100 μl of a solution of N-ethyl-N'-3-dimethylaminopropylcarbodiimide (DAC) (Fluka, Buchs, Switzerland) in chloroform (1.875 mg/ml) and 20 μl of ABEI in a 0.04 *M* methanolic potassium hydroxide solution (5.0 mg/ml) were added to the reaction vial. After 30 s of vortexing, the carboxylic acids were derivatized at 50°C in a water-bath during 10 min. Extraction of excess ABEI was carried out with 170 μl of an aqueous hydrochloric acid solution (pH 0.5). A 100-μl volume of the chloroform layer was evaporated to dryness at ambient temperature, and the residue was dissolved in 100 μl of methanol. This solution was diluted in the mobile phase to the desired concentration and injected in the LC–CL system.

RESULTS AND DISCUSSION

Optimization of parameters

In this study a comparison has been made between on-line electrochemical generation of hydrogen peroxide and hydrogen peroxide addition by a pump, using the determination of ABEI-labelled ibuprofen as a model system. Before the comparison could be made, several experiments had to be carried out in order to optimize the electrochemical reagent generation at the porous graphite working electrode in the ESA cell. For these experiments, the analytical column was removed from the system shown in Fig. 2.

In the first place, the optimum potential of the electrode was determined by injecting an ABEI solution into the system. The CL intensity proved to be optimal at a potential of -600 mV (Fig. 3). In this case acetonitrile–carbonate buffer (27:83, v/v)

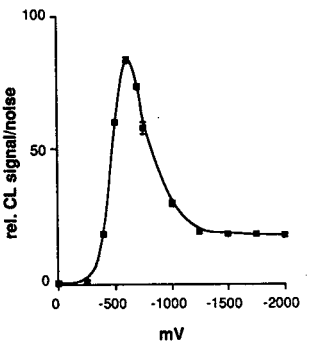

Fig. 3. CL signal-to-noise ratio as a function of electrode potential. For conditions of the FIA system, see Fig. 2. Indicated are the S.D. values, which resulted in a maximum R.S.D. of 4% (n = 2).

was used as the carrier stream, but the same optimum was found for a carrier of pure buffer. Studies of the reduction of oxygen at a porous graphite electrode have never been published, but Taylor and Humffray [21] described oxygen reduction at a glassy carbon electrode, which is similar to a porous graphite electrode. At pH > 10, they found that the most likely reactions at a potential less negative than *ca.* −1.2 V (with maximum current at *ca.* −500 mV) to be:

$$O_2 + H_2O + 2e^- \rightarrow HO_2^- + OH^- \quad (1)$$

and

$$O_2 + 2H_2O + 4e^- \rightarrow 4OH^- \quad (2)$$

The first reaction is the sum of the following reactions:

$$O_2 + e^- \rightarrow O_2^- \quad (1a)$$

and

$$O_2^- + H_2O + e^- \rightarrow HO_2^- + OH^- \quad (1b)$$

Reaction 2 constitutes only a small proportion of the overall process. At potentials more negative than *ca.* −1.2 V, reduction of the peroxide ion according to

$$HO_2^- + H_2O + 2e^- \rightarrow 3OH^- \quad (3)$$

or the formation of hydrogen according to

$$2H_2O + 2e^- \rightarrow 2OH^- + H_2 \quad (4)$$

is the most likely reaction; possibly, these processes occur simultaneously.

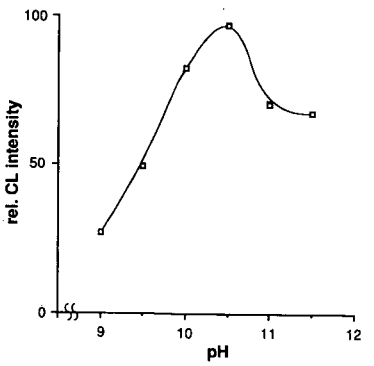

Fig. 4. Effect of pH on CL intensity. Conditions of the FIA system as in Fig. 2 except P_1 = 10 m*M* carbonate buffer (pH 10.5). Indicated are the S.D. values, which resulted in a maximum R.S.D. of 1.5% (n=3).

The optimum potentials found by Taylor and Humffray [21] are comparable with our results: we have found an optimum at −600 mV, and above *ca.* −1250 mV no change in the CL intensity was found.

Secondly, the effect of the pH on the CL intensity obtained with electrogenerated hydrogen peroxide was studied; the results are shown in Fig. 4. The maximum CL intensity was reached at pH 10.5, which is in agreement with the optimum for electrochemiluminescence of luminol [22].

Before we can compare the CL intensity obtained with the ESA cell with the CL intensity observed following addition of hydrogen peroxide, the optimum concentration of hydrogen peroxide has to be determined. Fig. 5 shows the CL intensity as a function of the percentage of hydrogen peroxide; 0.5% hydrogen peroxide (160 m*M*) gives the highest CL intensity, both for a carrier of pure buffer and for acetonitrile–buffer (27:73, v/v). The addition of acetonitrile results in a decrease in the CL intensity; in the case of 27% acetonitrile a five-fold decrease was observed in the CL intensity, as was a two-fold decrease in the CL signal-to-noise (S/N) ratio (see also Fig. 6).

Fig. 5 also shows the CL intensity obtained with the ESA cell; in this case, instead of a hydrogen peroxide solution, the third pump delivered water. The CL signal obtained with the ESA cell is *ca.* 10 times lower than the CL signal obtained with 0.5% hydrogen peroxide but, with the former method, the noise is also lower than in the latter case (S/N = 300 for the former and 850 for the latter system). In other words, the sensitivity is about three-fold higher for the CL system with hydrogen peroxide addition.

From the open-square curve in Fig. 5, one can estimate the concentration of hydrogen peroxide generated at the electrode in the ESA set-up with a carrier consisting of the carbonate buffer (A); the value turns out to be $1.75 \cdot 10^{-3}$%, or 570 μM.

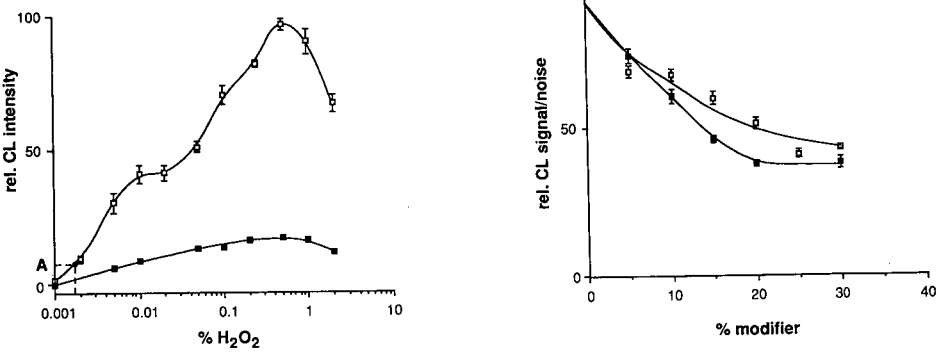

Fig. 5. CL intensity as a function of hydrogen peroxide percentage: (□) P_1 = 10 m*M* carbonate buffer (pH 10.5); (A) CL intensity obtained with electrochemical reagent generation; (■) P_1 = acetonitrile–10 m*M* carbonate buffer (pH 10.5) (27:73, v/v). For P_2 and P_3 see Fig. 2. Indicated are the S.D. values, which resulted in a maximum R.S.D. of 11.5% (□) and 6% (■) (n=4).

Fig. 6. Effect of modifiers on CL intensity. P_1 = modifier, 10 m*M* carbonate buffer (pH 10.5). For other conditions of the FIA system, see Fig. 2. Modifier: (□) acetonitrile; (■) methanol. Indicated are the S.D. values, which resulted in a maximum R.S.D. value of 5% for methanol and 4.5% for acetonitrile (n=4).

For the determination of the exact percentage of hydrogen peroxide generated at the porous graphite electrode, an FIA system with ED as described above was used. The calibration graph was linear over at least the range of $(0.02–1)\cdot10^{-3}\%$ (6.5–325 μm) of hydrogen peroxide, with a correlation coefficient of 0.9994 and an intercept of 2.2492 ($n = 4$). The sample taken from the system with the ESA cell contained $0.067 \cdot 10^{-3}\%$ (22 μM) hydrogen peroxide. This is *ca.* 25-fold lower than expected from the results given in Fig. 5.

The fact that the concentration of hydrogen peroxide generated at the electrode is much lower than the concentration deduced from the $[H_2O_2]$ *vs.* CL intensity curve, seems to imply that the CL intensity obtained with the ESA cell is not caused by the presence of hydrogen peroxide only. Probably, as well as the hydrogen peroxide anion (reactions 1a and 1b), the superoxide anion O_2^- is responsible for the CL reaction. Earlier studies also reported data that suggest that O_2^- can participate in the luminol CL reaction [23–25].

Further, the effect of the addition of a modifier on the CL intensity was investigated. Fig. 6 shows the effect of methanol and acetonitrile on the S/N ratio. Both modifiers cause a decrease in the CL S/N ratio, but at percentages above *ca.* 25% the S/N ratio becomes essentially constant. The S/N ratio obtained with acetonitrile is slightly better than that obtained with methanol. The decrease in the CL intensity is not caused by a decrease in the generation of hydrogen peroxide in the presence of a modifier: a decrease in the CL S/N ratio was also observed during the hydrogen peroxide addition method. Systematic investigation on the effect of organic solvents are scarce [26]; however, it is known that modifiers generally decrease the CL intensity, although the effect is very solvent- and catalyst-dependent.

The effect of the flow-rate of the carrier that is led through the ESA cell was also investigated, because it may be expected that a lower flow-rate of the carrier will generate more hydrogen peroxide. However, not only will the electrochemical reduction of oxygen to hydrogen peroxide be influenced by the flow-rate, but the total amount of light measured in the flow-cell of the detector will also change; on lowering the flow-rate of the carrier, the residence time between the ESA cell and the detector will be longer. Apart from these two effects, there will also be a change of solvent composition in the detector cell, which can effect the CL intensity. In practice, a two-fold reduction of the flow-rate (0.4 ml/min) caused an increase in the CL intensity by a factor of 1.6; however, the S/N ratio remained essentially constant between 0.4 and 0.8 ml/min.

Determination of ABEI-labelled ibuprofen

The determination of ABEI-labelled ibuprofen obtained with electrochemical reagent generation was compared with that obtained on addition of a hydrogen peroxide solution in water (0.5%) via a third pump (Fig. 7). As well as ibuprofen, naproxen, another arylpropionic acid, was also determined, because in further studies this drug will be used an an internal standard. The peaks of ibuprofen and naproxen observed in the chromatogram when using the electrochemical reagent generation method (Fig. 7b) are smaller those obtained with the hydrogen peroxide addition method (Fig. 7c). However, comparison of the S/N ratios for both substances gives a slightly better result (*ca.* 30%) for the CL detection method than for the electrochemical reagent generation; obviously, the addition of a solution (in this case hydrogen

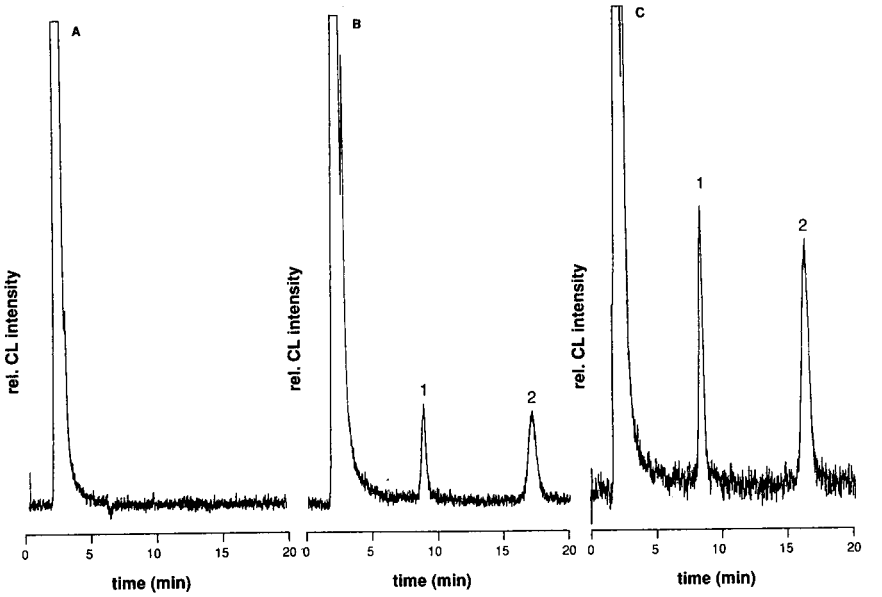

Fig. 7. Determination of ABEI-labelled ibuprofen. The injection volume was 18 μl of a 1000-fold diluted solution of derivatized drugs in mobile phase; for other conditions, see Fig. 2. (A) Blank (without ibuprofen and naproxen); detection with ESA cell. (B) ABEI-derivatized ibuprofen (1.3 pmol injection) (2) and ABEI-derivatized naproxen (3.4 pmol injection) (1); detection with ESA cell. (C) Same solution of ibuprofen and naproxen as in (B), detection with hydrogen peroxide addition, P_3 = 0.5% hydrogen peroxide in water.

peroxide) by an extra pump introduces additional noise. However, when the electrochemical reagent generation method was performed with addition of water by the third pump, the S/N ratio of the peroxide addition method was three times greater. Fig. 7a shows a chromatogram of a reaction mixture without ibuprofen and naproxen using the electrochemical reagent generation method.

The detection response of the LC–CL system with on-line electrochemical reagent generation was investigated by diluting the solution of the ABEI-labelled ibuprofen and naproxen 10, 100 and 1000 times. The responses was linear in the range 1.3–130 pmol of ABEI-labelled ibuprofen (r = 0.9995) and the detection limit was 0.15 pmol. (For ABEI-labelled naproxen a detection limit of 0.45 pmol was reached.)

When oxygen was bubbled through the mobile phase or an ultrasonic bath was used for degassing for 30 min, no change in the peak heights of the analytes was observed. Determination of the oxygen concentration showed a 10% decrease for the degassed mobile phase and a two-to-three-fold increase after oxygen bubbling, compared with the original mobile phase. Apparently, only a part of the oxygen dissolved in the mobile phase is used to generate the oxidative reagent(s). The efficiency of the electrochemical reaction of oxygen could probably be increased by increasing the surface area of the electrode.

CONCLUSIONS

On-line electrochemical reagent generation has a wide potential for LC with luminol-based CL detection, and is a good alternative to post-column addition of hydrogen peroxide. The present LC–CL system is much easier to handle than the conventional luminol-based LC–CL system, because instead of a third pump for hydrogen peroxide addition, an on-line electrochemical flow-cell is used, which can be easily inserted. It should be emphasized that with every new ESA Coulochem guard cell a single injection of a concentrated ABEI solution is required for it to show constant and reliable performance.

With the present LC–CL method, a detection limit of 0.15 pmol of ABEI-derivatized ibuprofen (and 0.45 pmol of ABEI-derivatized naproxen) can be obtained, which allows the use of the system for drug analysis at trace levels.

The use of a polymer-based analytical column offers the opportunity to use a mobile phase of high pH. This eliminates the need for the post-column introduction of a solution of high pH.

A further paper will deal with the optimization of the derivatization of ibuprofen with ABEI for the determination of this analyte and other drugs containing a carboxylic acid group in biological fluids.

REFERENCES

1 H.O. Albrecht, *Z. Phys. Chem.*, 136 (1928) 321.
2 W. R. Seitz, *CRC Crit. Rev. Anal. Chem.*, 13 (1981) 1.
3 H. R. Schroeder and F. M. Yeager, *Anal. Chem.*, 50 (1978) 1114.
4 W. R. Seitz and D. M. Hercules, *Anal. Chem.*, 44 (1972) 2143.
5 I. M. A. Shakir and A. T. Faizullah, *Analyst*, 114 (1989) 951.
6 M. S. Gandelman and J. W. Birks, *J. Chromatogr.*, 242 (1982) 21.
7 P. J. Koerner and T. A. Nieman, *J. Chromatogr.*, 449 (1988) 217.
8 Y. Yamamoto, M. H. Brodsky, J. C. Baker and B. N. Ames, *Anal. Biochem.*, 160 (1987) 7.
9 Y. Yamamoto and B. N. Ames, *Free Rad. Biol. Med.*, 3 (1987) 359.
10 B. Frei, Y. Yamamoto, D. Niclas and B. N. Ames, *Anal. Biochem.*, 175 (1988) 120.
11 T. Miyazawa, K. Yasuda, K. Fujimoto and T. Kaneda, *Anal. Lett.*, 21 (1988) 1033.
12 M. P. Neary, R. Seitz and D. M. Hercules, *Anal. Lett.*, 7 (1974) 583.
13 P. Jones, T. Williams and L. Ebdon, *Anal. Chim. Acta*, 217 (1989) 157.
14 V. G. Maltsev, T. M. Zimina, A. B. Khvatov and B. G. Belenkii, *J. Chromatogr.*, 416 (1987) 45.
15 T. Hara, M. Toriyama and T. Ebuchi, *Bull. Chem. Soc. Jpn.*, 58 (1985) 109.
16 T. Hara, M. Toriyama, T. Ebuchi and M. Imaki, *Bull. Chem. Soc. Jpn.*, 59 (1986) 2368.
17 A. MacDonald and T. A. Nieman, *Anal. Chem.*, 57 (1985) 936.
18 T. Kawasaki, M. Maeda and A. Tsuji, *J. Chromatogr.*, 328 (1985) 121.
19 H. Yuki, Y. Azuma, N. Maeda and H. Kawasaki, *Chem. Pharm. Bull.*, 36 (1988) 1905.
20 S. R. Spurlin and M. M. Cooper, *Anal. Lett.*, 19 (1986) 2277.
21 R. J. Taylor and A. A. Humffray, *J. Electroanal. Chem.*, 64 (1975) 63.
22 K. E. Haapakka and J. J. Kankare, *Anal. Chim. Acta*, 138 (1982) 263.
23 E. K. Hodgson and I. Fridovich, *Photochem. Photobiol.*, 18 (1973) 451.
24 H. P. Misra and P. M. Squatrito, *Arch. Biochem. Biophys.*, 215 (1982) 59.
25 G. Merényi, J. Lind and T. E. Eriksen, *Photochem. Photobiol.*, 41 (1985) 203.
26 T. A. Nieman, in J. W. Birks (Editor), *Chemiluminescence and Photochemical Reaction Detection in Chromatography*, VCH Publishers, New York, 1989, p. 99.

Journal of Chromatography, 557 (1991) 23–37
Elsevier Science Publishers B.V., Amsterdam

CHROM. 23 296

Quantitative determination limit in chromatography: computer-based simulations

M. ZOUBAÏR EL FALLAH[a] and MICHEL MARTIN*

Ecole Supérieure de Physique et Chimie Industrielles, Laboratoire de Physique et Mécanique des Milieux Hétérogènes (URA CNRS 857), 10 Rue Vauquelin, 75231 Paris Cedex 05 (France)

ABSTRACT

Following the previously developed statistical approach of the peak overlapping phenomenon in the chromatography of complex mixtures, computer-simulated chromatograms were generated to investigate the influence of this phenomenon on the accuracy of quantitative determinations. The probabilities of performing the quantitative determination, with an error smaller than or equal to a given value, of the most abundant component in a peak observed in the chromatogram, and of a given sample component were computed as a function of the relative height or area of the observed peak and of the relative area of the component, respectively, for different values of the accepted error. In addition, these probabilities were shown to depend significantly on the chromatographic saturation factor, which reflects the degree of occupancy of the space available for the separation by the sample. Surprisingly, it appears that small peaks observed in the chromatogram are more likely than large peaks to be pure. However, the probability of the correct quantitative determination of a sample component increases with its concentration in the sample. The determination limit, defined as the minimum relative amount of a component in the sample required to have a given probability of performing its quantitative determination with an error smaller than or equal to a given value, when taking into account the peak overlap phenomenon, was derived.

INTRODUCTION

Recent developments in chromatographic techniques, such as an increase in column efficiency through the use of columns with very small inner diameters in gas chromatography and of very fine particles in liquid chromatography, the preparation of stationary phases with improved stability and reproducibility, the use of highly sensitive detectors and the achievement of high reproducibility in injection and mobile phase delivery systems, have allowed chromatographers to analyse more and more complex matrices. The quantitative determination of particular compounds remains the major goal of such analyses. In a complex matrix, the main source of errors, when performing quantitative determinations, is essentially due to the peak interference phenomenon, which is obviously greater for mixtures containing a large

[a] Present address: Department of Chemistry, University of Tennessee, Knoxville, TN 37996-1600, USA.

0021-9673/91/$03.50

number of solutes. The seriousness of the peak overlap phenomenon and its effect on the analytical information losses have been already pointed out [1–5].

It has been shown that in a crowded chromatogram, the probability of obtaining a single uncontaminated peak, with a reasonable fixed degree of purity, is extremely low. It depends on what can be called the chromatographic saturation, *i.e.*, on the extent to which the space available for the separation, which can be expressed in terms of the peak capacity of the system [6], is to be occupied by all the sample components. Then, one can regard the accuracy of the quantitative determinations in chromatography from a probabilistic point of view. Hence, in a crowded chromatogram, we have only a limited probability of performing the quantitative determination, with an error smaller than or equal to a fixed value, of any solute belonging to the mixture. This probability depends on the degree of saturation of the chromatogram, but also on the relative analytical response of the solute. This relative response may be expressed as the ratio of the area of the so-called parent peak (*i.e.*, the peak which would be obtained if an amount of the solute under consideration equal to that present in the sample was chromatographed alone, under experimental conditions identical with those selected for the analysis of the mixture) to the sum of the areas of all parent peaks, which is also the area of the whole chromatogram. In fact, when the response of the solute parent peak represents an important fraction of the whole chromatogram response, the probability of performing its quantitative determination, with an error smaller than or equal to a fixed value, is relatively high, because the height and area of the largest chromatographic parent peaks are most likely to remain almost unmodified by the interference with the other parent peaks of the mixture. However, when the parent peak relative response is weak, the latter probability will become relatively low because the small parent peaks, when interfering with the others, exhibit a greater probability of being hidden by the largest ones. Accordingly, a small parent peak will most likely belong to a cluster which has a height and an area greatly different from those of the parent peak considered. In the following, the peaks of the envelope of the chromatogram will be called observed peaks. Each observed peak contains one or several parent peaks.

Nagels and co-workers [7,8] were the first to use this probabilistic point of view in their computer simulation studies of the effect of peak interference on the correctness of quantitative chromatographic determinations, when analysing plant extracts by reversed-phase high-performance gradient elution liquid chromatography. In order to simulate a typical plant extract chromatogram, a parent peak area distribution function was required. They used a distribution which was estimated from the observed peak area distribution function, itself obtained by chromatographing 62 plant extracts. They computed the probability that the most abundant component (in terms of detector response) belonging to an observed peak represents more than 50, 90 or 95% of the total relative area of this observed peak. Then, the error associated with the quantitative determination of the most abundant component was smaller than 50, 10 or 5%, respectively. In addition, they computed the probability of performing a quantitative determination, with an error smaller than or equal to a fixed value, of a parent peak with a given relative response. They showed that these two probabilities depend on the peak capacity of the system and on the relative response of the peak. In order to characterize the ability of the chromatographic system to perform quantitative determinations, they introduced a parameter termed the quantitative determina-

tion limit, DL_e^p, which corresponds to the minimum relative response that a parent peak solute must have in the chromatogram in order to have a given probability, p, of performing its quantitative determination with an error smaller than or equal to a fixed value, e. At a fixed probability level of performing the quantitative determination with a fixed relative error, it is clear that the parameter DL_e^p varies with the peak capacity of the system. The higher is the resolving power of the chromatographic system, the lower will be DL_e^p, and hence the lower are the amounts of solutes that can be determined with a fixed probability and a certain error.

It should be pointed out that the conversion of DL_e^p, expressed in terms of solute relative response, to its value in terms of solute amount (weight fraction of solute in the analysed mixture), leads, when response factors are known, to a specific quantitative determination limit parameter SDL_e^p, which characterizes the ability of the system to determine a specific compound. Accordingly, the optimization of quantitative determinations for a complex matrix corresponds to a search of experimental conditions in order to reach a global minimum for all the SDL_e^p corresponding to the components of interest, *i.e.*, a simplex optimization performed on a space dimension equal to the number of components of interest plus the number of the experimental parameters to be optimized.

The parameter SDL_e^p is to be distinguished from the classical "limit of determination" [9,10], which is conventionally defined as the minimum amount of a component producing an analytical signal above which it is considered that the solute can be quantified consistently, within a level of confidence. Of course, in the estimation of the classical limit of determination, apart from the instrumental intrinsic sources of error, none of the other sources of signal perturbations are to be taken into account such as those induced by the presence of the other solutes in the sample. In this study, assuming that the sources of errors in quantitative determinations from complex chromatograms are principally due to peak overlap phenomena, the concept of the quantitative determination limit, DL_e^p, allows one to take into account, in probabilistic terms, the matrix effects as a function of the resolving power of the chromatographic system.

The probability of performing a quantitative determination of a parent peak, with an error smaller than or equal to a fixed value, and thus DL_e^p, depends on the chromatographic saturation factor, *i.e.*, the ratio of the real number of detectable components, m, in the sample to the dimensionless length of the separation space, T. In elution chromatography, T represents the ratio of the distance over which the chromatogram is spread (expressed in time units) to some appropriate reference time. When the standard deviation is the same for all the parent peaks, which is generally acceptable assumption in liquid chromatography with linear solvent strength gradient elution and in gas chromatography with linear temperature programming [11,12], T is linearly proportional to the peak capacity, n_c, of the system. Under these chromatographic conditions, one may express, for convenience, T in standard deviation units. Thus, for a given sample with m detectable components, the above probability and DL_e^p depend on the system peak capacity, n_c. However, Nagels and coworkers [7,8] did not state precisely the number of parent peaks, m, used in their computer simulations in order to estimate the different probabilities of quantitative determinations. Unfortunately, the different curves they presented cannot be used for practical estimations of the quantitative determination limits in real chromatograms,

because the saturation factors to which the resulting curves correspond are not known. In addition, although the quasi-exponential peak-height distribution function used by these authors is similar, for a large number of components, to the theoretical one [13], it is a specific one corresponding only to phenolic plant extracts. Further, the procedure they used to estimate the distribution function of the parent peak areas seems to be very sensitive to the degree of chromatographic saturation, and thus this estimation is not an unequivocal operation.

The objective of this study was to generalize the different probabilities curves of quantitative determinations by utilizing a theoretical parent peak-height distribution function and also by expressing those probabilities and DL_e^p as a function of the chromatographic saturation factor, m/T. The use of m/T is preferred to that of m/n_c as the former, in contrast to the latter, does not imply the selection, on an arbitrary basis, of a value for the critical resolution needed to compute n_c. Indeed, it has been shown that this critical resolution depends on the peak-height distribution of the parent peaks [14]. One can note that the saturation factor, m/T, defined above is one quarter of the saturation parameter, m/n_c, used by Davis and Giddings [1] on the basis of a four standard deviation (4σ) separation between consecutive peaks. In the following, the method selected for quantitative measurements (peak height or peak area) is first discussed, together with its effect on the quantitative determination probabilities. Two different quantitative determination probabilities will be calculated by means of computer simulations: for an observed peak, having a given relative response, we estimated the probability of performing the quantitative determination, with an error smaller than or equal to a fixed value, of the major parent peak belonging to this observed peak. This probability depends on the relative response of the observed peak and on the chromatographic saturation factor. Then, the probability of performing the quantitative determination, with an error smaller than or equal to a fixed value, of a parent peak of a given relative abundance in the chromatogram is estimated. This probability depends on the relative abundance of the parent peak and on the saturation factor. Finally, the estimation of DL_e^p is performed for different values of p and e, using the latter probability curves.

MODEL AND COMPUTER SIMULATION PROCEDURE

In order to simplify the computational procedure of synthetic chromatograms, one assumes that the parent peaks are Gaussian with a constant standard deviation along the retention axis. Under these conditions, the parent peak-height distribution is identical with the distribution of the products of the concentration (in the sample) by the detection response factor of the sample components. One assumes that this distribution is the same as the distribution of the concentrations of the sample components, *i.e.*, that the convolution of the concentration distribution by the component distribution does not affect or affects only slightly the concentration distribution. It was found that there is some support for this hypothesis in liquid chromatography [15]. Thus, under these conditions, the parent peak-height distribution is identical with the component concentration distribution, which is determined from a statistical theory of concentration distribution in complex samples [13].

A program written in Pascal and run on an SPS-7 computer (Bull, Louveciennes, France) allows the simulation of the synthetic chromatograms. To obtain a

chromatogram with a fixed saturation factor, m/T, first two components are selected and the difference between their retention times is set to T standard deviations, then the $m-2$ other components are randomly distributed within this time interval. The random function was available from the Pascal Library and has a period equal to $2^{32}-1$; its sequence can be modified by changing the function argument. This function was used to obtain both the retention times of the randomly positioned parent peaks and their heights from a random selection through a file where all the peaks heights are listed. The arguments of the random functions for the retention time and peak-height selection are different. Different simulated chromatograms are obtained simply by changing the random function arguments. As discussed above, the assumptions of randomness of the distribution of retention times of the sample components and of constant deviation have been shown to be realistic in the case of some analyses using linear solvent strength gradient elution in liquid chromatography or linear temperature programming in gas chromatography, for solutes with no well defined correlation in the molecular structure [11,12,15].

For each simulated chromatogram, a procedure permits the determination of the area and the height of each observed peak, in addition to the retention time of each valley appearing in the chromatogram. An observed peak corresponds to the feature of the chromatogram appearing either between two consecutive valleys or before the first valley or after the last one. Accordingly, there are as many observed peaks as there are maxima in the chromatogram. It is then necessary to identify each observed peak. For this, the following procedure is adopted: any parent peak which has its retention time between the retention times of two consecutive valleys is considered to belong to the observed peak defined by those valleys. Parent peaks whose retention times are either before the retention time of the first valley or after the retention time of the last valley are considered to belong to the first and to the last observed peaks, respectively.

In the following, each parent peak is characterized by its relative height, Hr_p, and its relative area, Ar_p. As the parent peaks are assumed to be Gaussian and to have the same standard deviation, these two quantities are identical. For each simulation, the relative area, Ar_o, and the relative height, Hr_o, of each observed peak are computed. Ar_o is the ratio of the area of the observed peak, as defined above, to the total area of the chromatogram. Hr_o is the ratio of the height of the observed peak to the sum of the heights of all observed peaks. With each observed peak is associated a most abundant parent peak, which corresponds to the parent peak, belonging to this observed peak, which exhibits a relative area larger than that of any other parent peak belonging to the same observed peak. This parent is assumed to be the most abundant one even though a fraction of its area may be outside either limits of the observed peak. Of course, owing to parent peak interference phenomena, the correlation between Ar_o and Hr_o is not obvious, and it depends on the degree of chromatographic saturation.

In all simulations discussed in the following, the number of parent peaks, m, was set to 50. Some simulations, not reported here, were also performed with 25 or 100 parent peaks. The distribution of peak heights, resulting from the adaptation of a theoretical model derived for a very large number of components to finite numbers of components [13], are not exactly the same for the different values of m. Therefore, the differences which appear in the absolute values of the probability curves, to be

described below, for different m can most likely be attributed to this artifact. However, it is remarkable that the curves obtained at different m values but for a given saturation factor, m/T, are all parallel and very close to each other while curves corresponding to a given m value but to different saturation factors are fairly distant from each other and have a different shape. This confirms that the saturation is the key parameter affecting chromatographic performances.

RESULTS AND DISCUSSION

Probability of performing a quantitative determination, with an error smaller than or equal to a given value, of the most abundant parent peak in a given observed peak

Usually, the chromatographer does not have a precise and complete idea about all the components of the mixture under investigation; what he or she has is a chromatogram containing several observed peaks, and he or she may be interested in determining quantitatively one or several particular components for which the retention times are known, under given chromatographic conditions. Generally, the observed peak in the chromatogram which has a retention time (time corresponding to the peak maximum) relatively close to that of the component of interest is attributed to that component. Sometimes, further investigations (such as NMR and spectral analyses of some collected fractions or on-line coupling with mass spectrometry or Fourier transform infrared spectrometry, for instance) are needed to confirm the purity of all the peaks of interest. Nevertheless, in spite of the very high resolving power of some of these combined systems, such as gas chromatography–mass spectrometry, the complete identification of a mixture has been demonstrated, in one case, to be impossible both experimentally and from a statistical point of view [16]. Thus, there is only a limited probability that the most abundant parent peak in an observed peak will correspond to the one the analyst wants to quantify. Therefore, one of the most important questions is to know the probability of performing such quantitative determinations, with an error smaller than or equal to e_0. This probability is denoted $P_{o,h}(e \leqslant e_0)$ or $P_{o,a}(e \leqslant e_0)$ depending on whether the quantitative determination is performed by measuring the height or the area of the observed peak, respectively. Obviously, these probabilities depend on Hr_o and Ar_o, respectively, but also on the saturation factor, m/T.

Here the error, e_0, is computed with respect to the difference between the value of the height or area of the observed peak and that of most abundant peak. Accordingly, when measuring heights, the error is always positive owing to the increase in the peak height when interferences occur, whereas the error associated with area measurements may be either positive or negative. Therefore, in the following, the absolute value of e_0 is used for the area determinations.

For a fixed saturation factor, 10 000 simulations were done ($N_s = 10\,000$). For a given parent peak, exhibiting a given Hr_p (or Ar_p) value, the computation procedure consists in the evaluation of the number of times, $N_{maj,h}(Hr_p, e \leqslant e_0)$, where this particular parent peak was found to be the most abundant one in the observed peak to which it belongs and where the error associated with its height determination is smaller than a given value, e_0. Similarly is evaluated the number of times, $N_{maj,a}$ $(Ar_p, e \leqslant e_0)$, where the given parent peak was found to be the most abundant one in the observed peak to which it belongs and where an error smaller than e_0 is made in

its area determination. One is interested in the variation of the probabilities $P_{o,h}$ and $P_{o,a}$ with Hr_o and Ar_o, respectively. However, the height and area of the observed peak where the given parent peak is found to be the most abundant and where the determination is made with an error $e \leqslant e_0$ are different from one simulation to another. Therefore, the variation of the probabilities $P_{o,h}$ and $P_{o,a}$ with Hr_o and Ar_o can be obtained only indirectly. Each time that the parent peak with a given Hr_p (or Ar_p) is found to be the most abundant in an observed peak with $e \leqslant e_0$, the height, or area, of the observed peak is tabulated and, at the end, the averages, $Hr_{o,av}$ and $Ar_{o,av}$, of all tabulated values are calculated. The values of the probabilities are then given by

$$P_{o,h}(Hr_{o,av}, e \leqslant e_0) = N_{maj,h}(Hr_p, e \leqslant e_0) / N_s \quad (1)$$

$$P_{0.a}(Ar_{o.av}, e \leqslant e_0) = N_{maj,a}(Ar_p, e \leqslant e_0) / N_s \quad (2)$$

Comparison between area and height measurement performances on the basis of the probability computations

It is interesting to compare the two probability values (based on area and height measurements) obtained for a similar mean value of Hr_o and Ar_o. This comparison was made with 10 000 simulations and for both a relatively low-density chromatogram having a saturation factor $m/T = 0.05$ and a relatively dense chromatogram five times more crowded ($m/T = 0.25$). The admitted relative error, e_0, was set to 10%. Fig. 1 shows the variation of $P_{o,h}(e \leqslant 0.1)$ and $P_{o,a}(e \leqslant 0.1)$ as a function of Hr_o and Ar_o, respectively, for these two values of the saturation factor.

Both probabilities decrease with increasing relative area and height of the observed peaks, which leads to the conclusion that the larger is the observed peak, the higher is its probability of being contaminated. The probabilities are lower at high

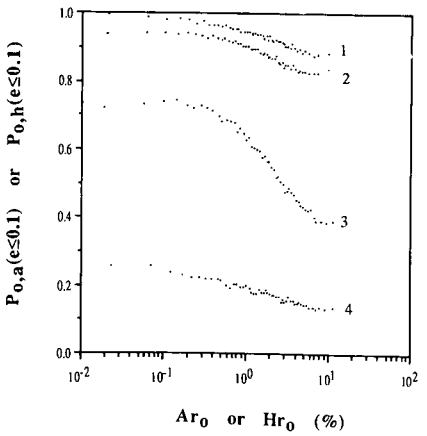

Fig. 1. Variation of the probability of performing a quantitative determination of the height of the major parent peak in an observed peak, with an error smaller than or equal to 0.1, $P_{o,h}(e \leqslant 0.1)$, as a function of the relative height of the observed peak, Hr_o, for a saturation factor $m/T = 0.05$ (curve 1) and 0.25 (curve 4), respectively. Variation of the probability of performing a quantitative determination of the area of the major parent peak in an observed peak, with an error smaller than or equal to 0.1 $P_{o,a}(e \leqslant 0.1)$, as a function of the relative area of the observed peak, Ar_o, for a saturation factor $m/T = 0.05$ (curve 2) and 0.25 (curve 3), respectively.

saturation than at low saturation, which reflects the fact that peaks are more likely to be contamined when the chromatographic saturation is high. At low saturation factors, the decrease in both probabilities is less pronounced than that at high saturation factors. Moreover, the simulations show that at high saturation, the probability of a correct quantitative determination is higher when the peak area rather than the peak height is used for the measurements. Nevertheless, this observation is no longer valid at low saturation factors, for which the probability of correct determination using height measurements was found to be higher than that of area measurements. However, in this instance the difference between the two probabilities is smaller than at high saturation and is expected to decrease as the saturation decreases. Indeed, at very low saturation, *i.e.*, when m/T tends toward 0, both measurements will be equivalent and will lead to determination probabilities which tend toward 1. Therefore, it seems that, for relatively high chromatographic saturations, peak heights will be more seriously affected by interferences than will peak areas. As the problem of quantitative determination is more serious when the saturation is relatively high and as most commercial integrators express quantitative results by mean of area measurements, we shall only consider the area measurements in the following to express the determination probabilities.

Variation of $P_{o,a}(e \leqslant e_0)$ with the relative area of the observed peaks

For a given chromatographic saturation, the probability of performing a quantitative determination of the most abundant peak in an observed peak, with an error smaller than or equal to e_0, depends on the relative area of this observed peak. The general shape for the variation of this probability as a function of Ar_0, for different values of the accepted error, e_0, and for a saturation factor $m/T=0.25$, is shown in Fig. 2. As expected, for a fixed value of Ar_0, the higher is the tolerated error the higher is the probability of correct determination. However, it may seem surprising that, for a relatively large domain of low Ar_0 values, *i.e.*, $Ar_0 \leqslant 0.3\%$, the probability remains almost constant, then decreases rapidly as Ar_0 increases (however, there is one excep-

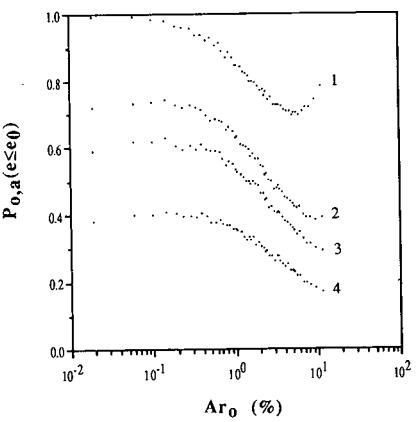

Fig. 2. Variation of the probability $P_{o,a}(e \leqslant e_0)$ as a function of the relative area of the observed peak, Ar_0, for different values of the accepted error, e_0, and for a saturation factor $m/T=0.25$. e_0: (1) 0.5; (2) 0.1; (3) 0.05; (4) 0.01.

tion to this behaviour for the curve corresponding to $e \leqslant 0.5$, which exhibits a minimum at about $Ar_o = 5\%$). The conclusion drawn from these curves is that if a small observed peak were to be found in a chromatogram, the probability of performing correctly the determination of its most abundant component is relatively high. In other words, a small peak has little chance of being observed in the chromatogram, but once it is observed, it is likely to be relatively pure. The probability $P_{o,a}$ decreases when the observed peak becomes larger. Therefore, larger parent peaks have more chance of representing the most abundant peaks in the observed peak, but they are most likely to be contaminated by the interferences with other parent peaks.

The exception found when $e \leqslant 0.5$ can be explained by the fact that it is rare that the error in the measurement of the area of a large parent peak exceeds 50%. A similar result was obtained by Nagels *et al.* [7], but with a minimum at $Ar_o = 3\%$. This corresponding Ar_o value is most likely to vary with the saturation factor. The present simulation allows the estimation of the probability of correct determination for observed peaks with relative areas as low as 0.01%, which is ten times lower than the results obtained by Nagels *et al.*, probably because they used a relatively small number of parent peaks in their simulations. In fact, owing to the sampling from the parent peak-area distribution, the achievement of lower values of Ar_p relies on the simulation of a larger number of parent peaks, m, in the chromatogram, whereas the achievement of lower Ar_o values depends also on the saturation of the chromatogram.

Fig. 3. shows the variation of $P_{o,a}(e \leqslant 0.1)$ as a function of Ar_o for different values of the saturation factor, m/T. These curves can be used to estimate the probability of performing the quantitative determination of the most abundant peak in an observed peak, for different values of the saturation factor. As expected, at a fixed value of Ar_o, this probability of correct determination increases as the chromatographic saturation decreases. In addition, at a fixed value of Ar_o, the rate of increase of the probability with decreasing saturation factors is larger for larger values of the saturation factor. Thus, for $Ar_o = 1\%$, when the saturation factor decreases from 0.5 to 0.25 the probability $P_{o,a}(e \leqslant 0.1)$ increases by 44.5%, whereas starting with a saturation factor equal to 0.25 and decreasing it by half to 0.125 leads to an increase in the probability of only 23%.

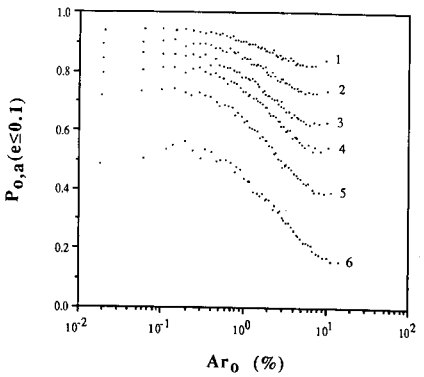

Fig. 3. Variation of the probability $P_{o,a}(e \leqslant 0.1)$ as a function of the relative area of the observed peak, Ar_o, for different values of the saturation factor m/T. m/T: (1) 1/20; (2) 1/12; (3) 1/8; (4) 1/6; (5) 1/4; (6) 1/2.

From these computations we can also represent the variation of $P_{o,a}(e \leqslant 0.1)$ as a function of the saturation factor, at different values of Ar_o. The variation of this probability, for different values of Ar_o, is reported on Figure 4, as a function of the reciprocal of the saturation factor, which is a more convenient representation as we know that the probability of correct determination tends towards zero for an infinite saturation factor. At a fixed Ar_o, as the saturation decreases, *i.e.*, as T increases for m fixed, $P_{o,a}(e \leqslant 0.1)$ increases rapidly at first, then tends more slowly toward 1. As discussed above, one sees that, for a fixed saturation factor, $P_{o,a}(e \leqslant 0.1)$ increases with decreasing Ar_o.

Probability of performing a quantitative determination, with an error smaller than or equal to a given value, of a given parent peak

In addition to the probability of performing the quantitative analysis of the most abundant peak in an observed peak, the chromatographer is also interested in knowing the probability associated with the quantitative determination, with an fixed error, of a given parent peak. Actually we are looking for the quantitative determination of a particular parent peak, in contrast to the previous probability where we were investigating each observed peak in the chromatogram, and computing the probability of determining the most abundant peak. Again, the probability of quantitative determination of a parent peak, with a fixed error, depends also on the degree of saturation in the chromatogram and on the relative area of the parent peak, Ar_p. This probability is referred to as $P_{p,a}(e \leqslant e_0)$. The error, e, is calculated on the basis of the comparison between the observed peak containing the parent peak and the parent peak itself. This probability is computed by accounting the number of times, N_a $(e \leqslant e_0)$, where the parent peak can be determined with an error smaller than or equal to e_0, when N_s simulations are performed. Hence the probability is calculated as

$$P_{p,a}(e \leqslant e_0) = N_a(e \leqslant e_0) \,/\, N_s \tag{3}$$

Variation of $P_{p,a}(e \leqslant e_0)$ with the relative area of a parent peak

For a fixed saturation factor, more than 10 000 simulations are performed in

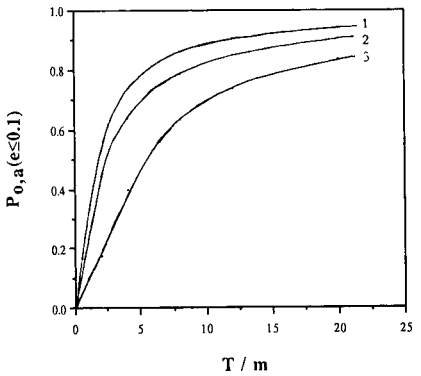

Fig. 4. Variation of the probability $P_{o,a}(e \leqslant 0.1)$ as a function of T/m, the reciprocal of the saturation factor, for different values of the relative area of the observed peak, Ar_o. Ar_o: (1) 0.1%; (2) 1%; (3) 10%.

order to estimate $P_{p,a}$ for different values of the accepted error. Fig. 5 shows the variation of $P_{p,a}(e \leqslant e_0)$ for a saturation factor equal to 0.25 and for different values of e_0. Obviously, for a fixed Ar_p and a given saturation factor, the probability of a correct quantitative determination increases as the accepted error increases. At a fixed saturation factor, it seems that the general shape of the curve of variation of $P_{p,a}$ $(e \leqslant e_0)$ with Ar_p depends on the value of the accepted error. Nevertheless, the global behaviour observed is an increase in the probability with increasing Ar_p, which differs strongly from the behaviour observed in Fig. 2 for $P_{o,a}(e \leqslant e_0)$ *versus* Ar_o. It is expected that the probability of performing a correct quantitative determination of a parent peak increases with its area, as larger parent peaks are relatively less affected by the overlap with smaller parent peaks. Nevertheless, it seems that this observation is not valid when the accepted error is relatively low, as the curves for $e \leqslant 0.01$ and, to a lesser extent, for $e \leqslant 0.05$ appear to become approximately constant when Ar_p exceeds 3% or even to exhibit a maximum at about $Ar_p = 3\%$. No simple explanation can be envisioned to account for this unexpected observation, which is associated with a relatively high saturation factor. This phenomenon is reported here for the first time. The calculations performed by Nagels *et al.* [7] did not show a similar observation, probably because the saturation factor corresponding to their computations was not high enough.

Fig. 6a and b show the variation of $P_{p,a}$ as a function of Ar_p for different values of the saturation factor, m/T, at two different accepted errors, $e_0 = 0.1$ and 0.5, respectively. Again, for a given saturation factor, the probability of correct quantitative determination is seen to increase as the area of the parent peak increases. This increase is almost linear for the curves in Fig. 6a corresponding to $e_0 = 0.1$, which means that the probability of correct determination varies exponentially with the relative area of the parent peak, whereas the rate of increase of the probability with Ar_p for $e_0 = 0.5$ (Fig. 6b) is much more pronounced, especially at relatively high saturation factors. For a fixed parent peak, the probability of its correct quantitative determination increases as the saturation factor decreases, because interferences between par-

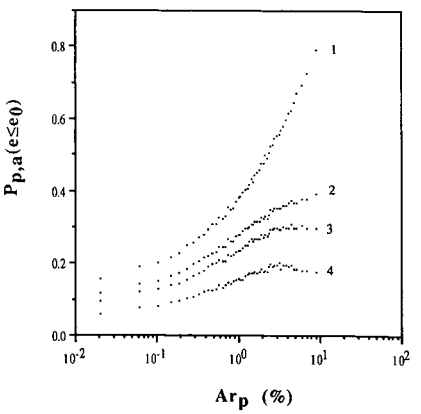

Fig. 5. Variation of the probability, $P_{p,a}(e \leqslant e_0)$, of performing a quantitative determination of the area of a parent peak, with an error smaller than or equal to e_0, as a function of the relative area of the parent peak, Ar_p, for a saturation factor $m/T = 0.25$, and for different values of the accepted error, e_0. e_0: (1) 0.5; (2) 0.1; (3) 0.05; (4) 0.01.

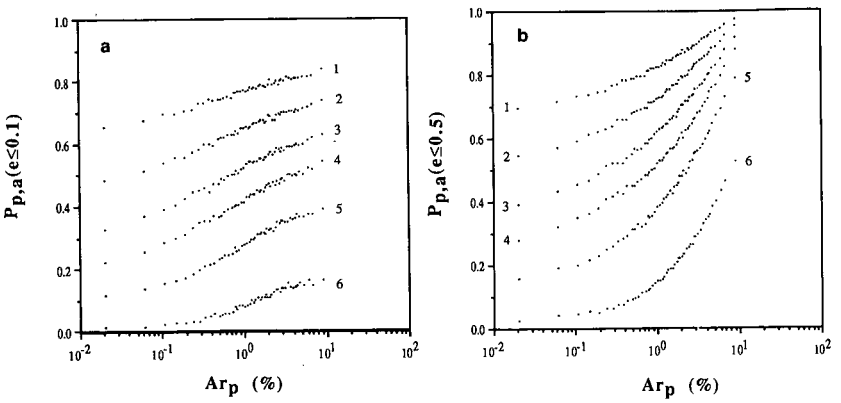

Fig. 6. (a) Variation of $P_{p,a}(e \leqslant 0.1)$ as a function of the relative area of the parent peak, Ar_p, for different values of the saturation factor. m/T: (1) 1/20; (2) 1/12; (3) 1/8; (4) 1/6; (5) 1/4; (6) 1/2. (b) Variation of $P_{p,a}(e \leqslant 0.5)$ as a function of the relative area of the parent peak, AR_p, for different values of the saturation factor. m/T: (1) 1/20; (2) 1/12; (3) 1/8; (4) 1/6; (5) 1/4; (6) 1/2.

ents peaks diminish when the degree of chromatographic saturation decreases.

These curves can be used in order to estimate the probability of correct determination for a given parent peak. In addition, they provide a means of estimating the upper limit of the saturation factor, *i.e.*, the minimum resolving power, required to achieve a given probability of performing correctly a quantitative determination within some tolerated error.

Computation of the quantitative determination limit

The quantitative determination limit, DL_e^p, corresponds to the minimum relative abundance of a parent peak, expressed as a percentage of the whole chromatographic response, which leads to a probability, p, of performing its quantitative determination with an error smaller than or equal to some fixed value e. Since the variation of the probability, $P_{p,a}(e \leqslant e_0)$, of quantitative determination, with an error smaller than or equal to e_0, of a parent peak of given relative area, Ar_p, has already been studied, it is then possible to estimate DL_e^p, for a given saturation factor, by using one of the curves in either Fig. 6a or b, depending on the chosen value of the accepted error. Hence, DL, for a given accepted error, corresponds to the value of Ar_p, estimated from the curve corresponding to the appropriate saturation factor, which leads to the desired probability of correct quantitative determination. Reversing the coordinates in Fig. 6a and b shows that, for a fixed accepted error and for a given saturation factor, DL_e^p increases very steeply with the required probability, p. In addition, for a given required probability, p, the smaller is the accepted error, the greater is the value of the determination limit.

The domain of the saturation factor, m/T, investigated in this study lies between 0.05 and 0.5. In other words, this corresponds to a degree of occupancy of the chromatographic space between 10% and 100% of the peak capacity, if the peak capacity is calculated on the basis of a 2σ separation. The corresponding interval becomes 14.2–142% of n_c, if n_c is calculated on the basis of a 2.84σ separation, as it should be in order to see as many maxima as there are peaks in the chromatogram when taking

into account the distribution of peak heights [14]. Within this domain of saturation investigated, it appears from Fig. 6a that it is impossible to achieve a probability of determination of the parent peak equal to 0.9 for an accepted error smaller than or equal to 10%. This means that in order to achieve a probability of determination as high as 0.9 with an error smaller than or equal to 0.1, the chromatographic saturation factor must be well below 0.05, even for the largest parent peaks in the mixture. However, if one chooses a probability of determination equal to 0.5, with an associated error smaller than or equal to 0.1, the quantitative determination limit, $DL_{0.1}^{0.5}$, is then equal to 8% and 1%, for $m/T = 0.167$ and 0.125, respectively. Fig. 6b shows that, with an accepted error of 0.5, it is possible to achieve probabilities of quantitative determinations as high as 0.9, especially at low saturation factors.

Fig. 7 shows the variation of two quantitative determination limit parameters, $DL_{0.1}^{0.5}$ and $DL_{0.5}^{0.9}$, as a function of the saturation factor. Both DL are seen to increase as the saturation increases, but this increase is more pronounced for $DL_{0.1}^{0.5}$, which is certainly due to the fact that the probability of correct determination is more sensitive to the increase in the saturation factor for low rather than for high values of the accepted error. Ultimately, whatever e and p, all DL curves will tend toward 100% at very large saturation factors.

In practice, for a given complex chromatogram, the saturation factor can be calculated by means of one of the recently developed procedures for estimating the number of sample components [1–5]. Then the values of various DL_e^p parameters can be estimated from curves such as those in Fig. 7. Alternatively, they can be used to evaluate the reduction of the DL values resulting in the improvement of the separation power of a chromatographic system or from switching to another more efficient separation system.

CONCLUSION

The problem of quantitative analysis from chromatograms of complex mixtures appears to be very serious. From a statistical point of view, even for the largest

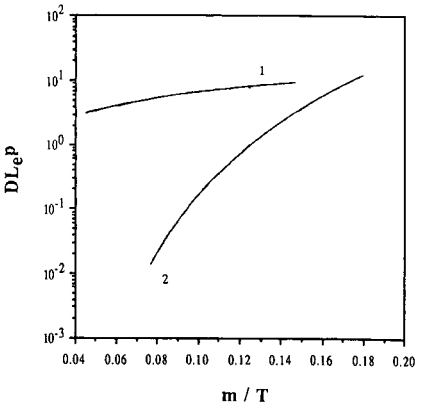

Fig. 7. Variation of the quantitative determination limit, DL_e^p, corresponding to a probability p of performing a quantitative determination of a parent peak with an error smaller than of equal to e as a function of the saturation factor m/T. (1) $p=0.9$ and $e=0.5$; (2) $p=0.5$ and $e=0.1$

parent peaks the probability associated with their quantitative determination, with an error smaller than or equal to given value, can be very low, especially if the chromatographic saturation factor is relatively high. In order to achieve a reasonable probability of correctly performing a quantitative determination, the chromatographic system must exhibit a very high resolving power, *i.e.*, it must have a peak capacity greatly exceeding the number of components in the sample. In addition, it was found that small observed peak are most likely to be pure but on the other hand, the probability of finding them in a typical complex chromatogram is relatively low. One must be more careful when quantifying large observed peaks, as they are most likely to be the result of two or more parent peaks lumped together.

The use of the quantitative determination limit, DL_e^p, permits the quantification, in probabilistic terms, of the effect of peak overlap phenomena on quantitative determinations. This parameter is expressed in terms of a fraction of the whole chromatographic response. Thus, for a component of interest, it is easy, when its response factor is known, to convert DL into a specific parameter, SDL_e^p expressed as the weight fraction of solute in the analysed mixture, which allows one to quantify the ability of the chromatographic system to analyse this particular solute, in the studied matrix. Indeed, the parameter SDL_e^p, which is associated with the "horizontal" sources of error (the interferences between parent peaks), can be compared with the classical limit of determination, which reflects the effect of the "vertical" source of error (the influence of noise in the signal). As they most likely are independent, the largest of these two parameters will impose the overall limit of determination. In addition, the curves of the variation of DL_e^p (or SDL_e^p) as a function of the saturation factor allow one to estimate the efficiency of the chromatographic system required to obtained a reasonable probability of performing the quantitative determination of a given parent peak within some tolerated error.

Of major importance here is the fact that the larger is the response factor of a solute with a particular detector, with respect to the whole chromatographic response, the lower is the amount of this component which can be determined with a reasonable probability and an accepted error, that is, the more likely is the chance that this solute produces a chromatographic signal which is above the *DL* level. In addition to seeking an increase in the resolving power of the chromatographic system when analysing complex mixtures, it seems that one of the major tasks for the analyst interested in the quantitative determination of one or a few components is certainly the optimization of the detection, in order to make it more selective for the components of interest. This step in any development of an analytical procedure can be decisive for its success. In this respect, the present statistical study allows one to express quantitatively the improvement brought into the validity of the quantitative determination of a component by any increase in its relative response factor.

This study has been presented within the context of chromatography, but it is clear that its results can be extended to any kind of zonal separation method provided that the hypotheses underlying the simulation model (randomly distributed Gaussian zones with constant standard deviation) can correspond to realistic attributes of the method.

ACKNOWLEDGEMENTS

The authors are very grateful to P. Cousot of the Computer Centre of the Ecole Polytechnique (Palaiseau, France) for allowing them free access to the facilities of the Centre. They are also grateful to Rhône-Poulenc Recherches (Courbevoie, France) for partially supporting this research. M.Z.E. thanks the Ecole Polytechnique for financial support during his Thesis work. This work was presented in part at the *13th International Symposium on Column Liquid Chromatography, Stockholm, June 25–30, 1989.*

REFERENCES

1 J. M. Davis and J. C. Giddings, *Anal. Chem.*, 55 (1983) 418.
2 M. Martin, D. P. Herman and G. Guiochon, *Anal. Chem.*, 58 (1986) 2200.
3 M. Z. El Fallah and M. Martin, paper presented at the *17th International Symposium on Chromatography, Vienna, September 25–30, 1988.*
4 J. M. Davis, *J. Chromatogr.*, 449 (1988) 41.
5 A. Felinger, L. Pasti and F. Dondi, *Anal. Chem.*, 62 (1990) 1846.
6 J. C. Giddings, *Anal. Chem.*, 39 (1967) 1072.
7 L. J. Nagels, W. L. Creten and P. M. Vanpeperstræte, *Anal. Chem.*, 55 (1983) 216.
8 L. J. Nagels and W. L. Creten, *Anal. Chem.*, 59 (1987) 822.
9 L. A. Currie, *Anal. Chem.*, 40 (1968) 586.
10 P. W. J. M. Boumans, *Spectrochim. Acta Part B*, 33 (1978) 625.
11 L. R. Snyder, *High performance Chromatography, Advances and Perspectives*, Vol. 1, Academic Press, New York, 1980, p. 207.
12 H. W. Habgood and W. E. Harris, *Anal. Chem.*, 32 (1960) 450.
13 M. Martin, to be published.
14 M. Z. El Fallah and M. Martin, *Chromatographia*, 27 (1987) 115.
15 M. Martin and G. Guiochon, *Anal. Chem.*, 57 (1985) 289.
16 D. Rosenthal, *Anal. Chem.*, 52 (1982) 63.

Journal of Chromatography, 557 (1991) 39–46
Elsevier Science Publishers B.V., Amsterdam

CHROM. 22 971

Laser-excited fluorescence detection of gas-phase chromatography eluates

SCOTT J. HEIN[a] and EDWARD H. PIEPMEIER
Department of Chemistry, Oregon State University, Corvallis, OR 97031 (USA)
and
LAWRENCE C. THOMAS*
Department of Chemistry, Seattle University, Seattle, WA 98122 (USA)

ABSTRACT

A high-spectral-resolution laser-excited molecular fluorescence gas chromatographic (GC) detection system is evaluated. It utilizes a pulsed supersonic jet expansion to yield very-narrow-bandwidth (*e.g.* $\leq$ 0.1 nm) fluorescence excitation spectra that may be rapidly scanned via a tunable dye laser. A microcomputer synchronizes the entire system, collects data, performs calculations, and creates visual displays of results. The laser-excited fluorescence detection system was interfaced to a gas chromatograph to exploit both the selectivity of the chromatography and the excellent spectral selectivity of the detector. Fluorescence excitation chromatograms were acquired by monitoring fluorescence emission from selected transition wavelengths characteristic of the GC eluates. The excitation wavelengths were also programmed to change at appropriate retention times to provide greatest selectivities for individual analytes as they eluted, and to allow multiple analytes to be determined in a single elution. Response factors for the system varied appreciably from run to run, which precluded the use of external standard quantitation procedures. However, excellent stabilites for within-run relative response factors were sufficient to allow for good quantitative measurements using internal standard techniques.

INTRODUCTION

Aromatic compounds such as polynuclear aromatic compounds (PNAs) typically have strong molecular absorbance bands between 180 and 350 nm. Multi-ring PNAs also tend to exhibit high fluorescence quantum efficiencies, resulting in part from their rigid molecular structures that exhibit few vibrational degrees of freedom, and thus limit non-radiative internal conversion. At room temperatures PNAs tend to exhibit broad-bandwidth fluorescence excitation spectra due to transitions from many overlapping electronic, vibrational, and rotational energy states. Correspondingly, at higher temperatures characteristic of gas chromatographic (GC) eluates, *e.g.*, $>250°C$, absorbance and fluorescence excitation spectra of PNAs lack detail, typically exhibiting three broad bands arising from electronic $\pi \rightarrow \pi^*$ transitions in the UV region [1,2].

[a] Present address: Dow Chemical, Western Research and Development, Analytical Research Labs., P.O. Box 1398, Pittsburg, CA 94565, USA.

0021-9673/91/$03.50

Most gas-phase UV fluorescence detectors have monitored emission from a fixed excitation waveband to produce chromatograms [3–10]. However, other systems allow fluorescence spectra to be acquired [11,12]. Limits of detection have been below nanogram levels, but vary considerably [3,4,8,11]. The fluorescence detectors show great selectivities, allowing PNA eluates to be measured in the presence of other non-fluorescencing, coeluting compounds. Judicious choice of the excitation band further enhances selectivities and sensitivities. The temporal resolution of the GC system supplements the powerful spectral selectivities of those detectors. Some of the detectors have allowed concurrent measurements of high-temperature GC eluates by both absorbance and fluorescence [3,4,11]. One of the systems [11] provides rapid-scanning capabilities and variable-wavelength illumination that may be changed easily as the chromatography separation develops. Several of the gas-phase fluorescence detectors are compact, of simple design, show excellent sensitivities, and exhibit low limits of detection.

Supersonic jet expansions (SJEs) are extremely useful for high-spectral-resolution fluorescence measurements [13], allowing for fluorescence spectra to be observed which are characteristic of very low temperatures, *e.g.*, <10–100 K, and thereby show little of the vibrational and rotational sequence congestion observed in high-temperature spectra. The high spectral resolution has been exploited for GC eluates using constant-wavelength laser excitation [10,14–17]. Mass *versus* response relations were shown, and low nanogram limits of detection were achieved [15], however, no evaluation of potential quantitative GC analysis utility was done, and difficulties that plague GC calibrations and determinations were not addressed.

In this work, we evaluate a specially constructed GC detection system that exploits the unique spectral qualities of laser-induced fluorescence (LIF) and pulsed-flow SJEs of GC eluates. Herein we show superior selectivities offered by the system and evaluate quantitative GC applications for which it is suited.

EXPERIMENTAL

Reagents

Fluorene ($>98\%$ pure) and 1-methylfluorene ($>99\%$ pure) were purchased from Aldrich. Dichloromethane solvent was pesticide-grade quality, and all other chemicals used were reagent grade. Solutions were maintained in a darkened refrigerator at 0°C in PTFE-capped gas-tight vials between use. Gases used were $>99.999\%$ pure.

Apparatus

A block diagram of the entire system is illustrated in Fig. 1. Samples were introduced to the measurement cell via one of two methods. In one case, a small amount of one of the test compounds was placed in a Pyrex glass thimble inserted into a heated Swagelok Tee. Helium was then allowed to flow through the Tee, carrying the vaporized test compound continuously into the measurement cell. The second method utilized a Hewlett-Packard Model 5710A gas chromatograph for GC separations through a 1 m $\times$ 4 mm I.D. glass column filled with 100–120 mesh Supelcoport solid support coated at 3% with SP-2250 liquid phase. The oven temperature was programmed from 100 to 250°C at 16°C min^{-1} and held at 250°C for 10–30 min.

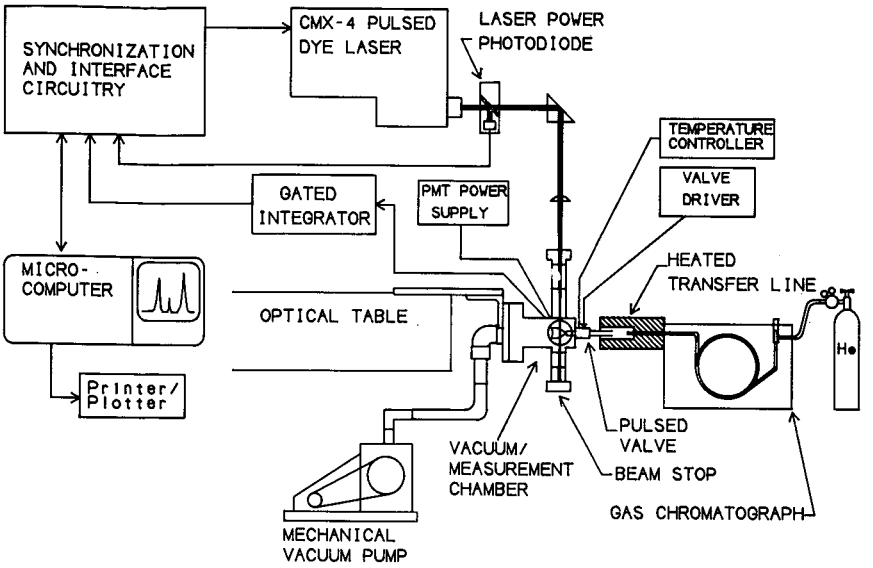

Fig. 1. Block diagram of the gas chromatography–laser-excited fluorescence–supersonic jet expansion experimental system.

Helium carrier gas was used at 30 ml min^{-1} with 40 p.s.i. inlet pressure. Injected volumes ranged from 0.1 to 2 μl into the 300°C injection port. Eluates from the GC system were transported to the SJE–LIF detector via the heated interface of the 5710A gas chromatograph, which had formerly been used with a Hewlett-Packard 5892 gas chromatographic–mass spectrometric (GC–MS) system. An 18-kg lead ingot was placed on top of the GC system and a 5-kg lead block on the transfer line to dampen mechanical vibrations. However, the GC fan remained a principal source of mechanical vibrations and thus fluorescence signal noise in the detector.

The SJE–LIF measurement cell (Fig. 2) was constructed from aluminum and was anodized black to reduce scattering of the laser excitation radiation. All vacuum seals were made with Viton O-rings. The entrance window was a 1-in. diameter, 0.25-in. thick fused-silica disc. Three entrance baffles with 0.196-in. diameter apertures were spaced along the 6-in. entrance arm of the cell to reduce stray and scattered light. The laser beam exited into a 4-in. deep beam stop through two additional baffles. The overall body of the cell was heated by a 2.5-in. I.D., 1.5-in. wide mica band heater, while the flange containing the pulsed valve was maintained at 145°C by an additional temperature-controlled cartridge heater. The measurement cell was evacuated to a pessure of 10^{-3} Torr via an Edwards ED200 200-LPM two-stage mechanical vacuum pump (Edwards High Vacuum, Sussex, UK).

The pulsed-nozzle device was a modified BMW automobile fuel injector with a 0.33-mm diameter axis-symmetric nozzle, controlled by special timing circuitry. The pulsed valve was maintained at 145°C to prevent condensation of the GC eluates, which were pulsed into the cell in 1- or 2-ms bursts at a frequency of 5 or 10 Hz. The Chromatix CMX-4 flashlamp-pumped tunable dye laser (Chromatix, Sunnyvale, CA, USA) was synchronized to fire 0.5–1.5 ms after the beginning of the SJE pulse and was

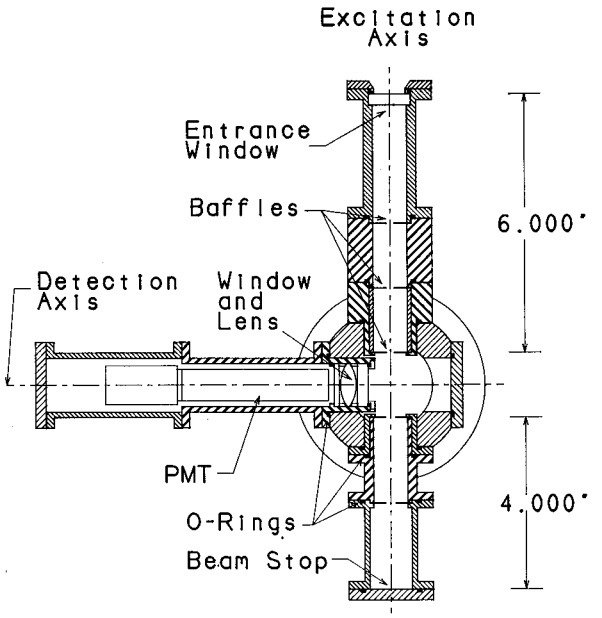

Fig. 2. Front view (looking down the expansion axis) of the supersonic jet expansion measurement cell. The supersonic nozzle and front flange are not shown.

aligned to intersect the central expansion axis 1 mm downstream from the nozzle tip. Total fluorescence emission was collected at right angles to both the expansion and excitation axes through a f/1 fused-silica bi-convex lens, which focused the fluorescence emission onto the photocathode of a Hamamatsu R1464 head-on photomultiplier tube (Hamamatsu, Middlesex, NJ, USA) maintained at −725 V. The PMT photoanodic current arising from the pulse of fluorescence emission was collected by an Evans gated integrator (Model 4120, Evans Assoc., Berkeley, CA, USA) and was digitized by a Metrabyte Dash-8, 12-bit-resolution analog-to-digital converter (ADC) (Metrabyte, Taunton, MA, USA). The ADC system was controlled by a Corona microcomputer (Cordata, Thousand Oaks, CA, USA). The computer served as the central control device for all synchronized parts of the system, and for the data collection, computations, and graphical displays.

The dye laser was wavelength-calibrated over the Rhodamine-590 laser dye tuning range using an optogalvanic technique [18]. In addition, the laser was modified to rapidly scan ultraviolet wavelength between 290 and 300 nm via automated computer control. Wavelength scanning via the birefringent filter tuning element and corrections for pulse-to-pulse variations of laser power were accomplished as has been done by other researchers [18]. The automation of the system allowed the laser to rapidly change from one wavelength to another during the course of a chromatographic run, allowing measurements of multiple analytes.

RESULTS AND DISCUSSION

Initial experiments involved characterization of the system with continuously introduced fluorene and 1-methylfluorene. High-resolution fluorescence excitation spectra were acquired using either argon or helium as a diluent gas. Spectra were acquired by stepwise adjustments of the laser's birefringent filter to achieve 0.01-nm increments. The fluorescence excitation spectra of fluorene and 1-methylfluorene in a helium supersonic expansion using the SJE–LIF system are shown in Fig. 3. The peak widths (full width at half maximum) were approximately 0.1 nm, as compared with bandwidths of 20–30 nm found in the solution and gas-phase spectra. Excitation wavelengths of 296.0 nm for fluorene and 294.7 nm for 1-methylfluorene were used in chromatographic experiments discussed below.

Fixed-wavelength fluorescence excitation chromatograms of a mixture of 100 ng fluorene and 100 ng of 1-methylfluorene taken at 296.0 and 294.7 nm are shown in Fig. 4. Chromatographic peak widths of 10–15 s were typically obtained, with slight tailing of the peaks due to cold trapping of the analyte on the pulsed valve, which could be heated no hotter than 145°C to protect internal plastic parts. The programmed

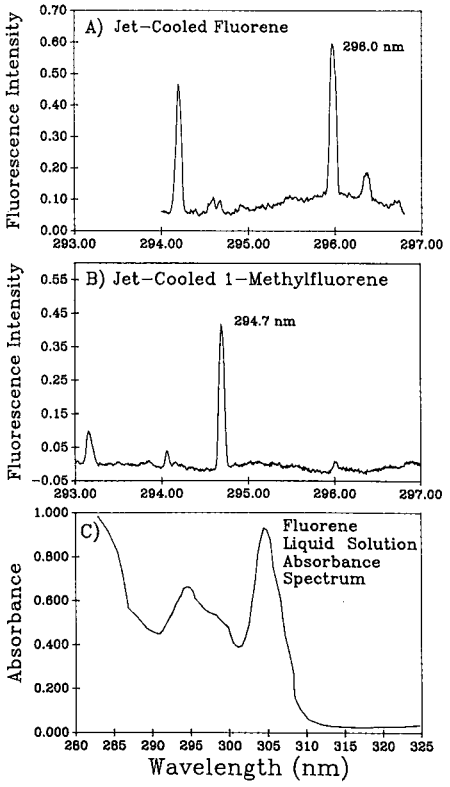

Fig. 3. Fluorescence excitation spectrum of (A) fluorene and (B) 1-methylfluorene acquired using the experimental system described herein, compared with (C) the conventional liquid solution absorbance spectrum of 5 μg/ml fluorene in cyclohexane.

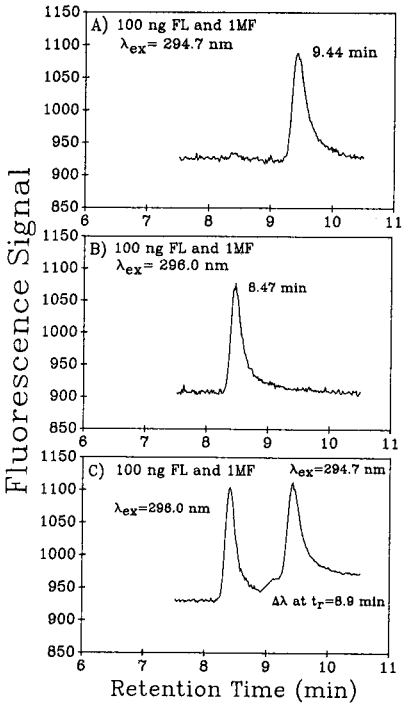

Fig. 4. Fluorescence excitation chromatograms of a mixture of 100 ng each of fluorene (FL) and 1-methylfluorene (1MF) acquired at fixed wavelengths of (A) 294.7 nm and (B) 296.0 nm, and (C) the chromatogram of the same mixture produced by a programmed excitation wavelength scan.

excitation wavelength fluorescence excitation chromatogram of the same mixture is also shown in Fig. 4. In this case, the system was programmed to change from 296.0 to 294.7 nm just after elution of the fluorene.

Good sensitivities were routinely achieved with the system, *e.g.*, 24.4 $\pm$ 0.7 area units ng^{-1} at 95% confidence. Consequent limits of detection approximated 5 ng, even with considerable background noise caused by mechanical vibrations from the GC fan and the vacuum pump. Selectivities were outstanding with little interference between the closely related test compounds, except for a slight response for 1-methylfluorene with 296.0-nm excitation due to minor spectral overlap. Excellent selectivities were also exhibited during the analyses of a very complex mixture. Fig. 5 shows fluorescence excitation chromatograms acquired using selective excitation wavelengths for fluorene and 1-methylfluorene for a hydrothermal oil sample taken from a deep-ocean hydrothermal vent located in the Guaymas Basin of the Gulf of California. This sample was also analyzed by GC–MS and contained a wide variety of PNAs including fluorene and four methylfluorene isomers. The only significant responses observed in these chromatograms were due to fluorene and 1-methylfluorene despite the fact that many other PNAs and the three other methylfluorene isomers were present at similar or greater concentrations.

Because of the complexity of the instrumentation, however, sensitivity of the

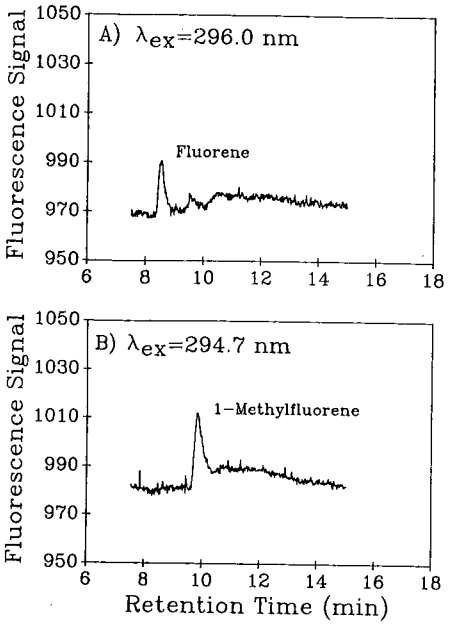

Fig. 5. Fluorescence excitation chromatograms resulting from 2-μl injections of a hydrothermal oil sample taken from the Guaymas Basin seabed in the Gulf of California.

detector system varied appreciably from day to day, and often from run to run, and therefore required repeated optimization to ensure good performance. Because of this variability, precise quantitation would be difficult if the external standard method were used, *e.g.*, for most fixed-excitation-wavelength analyses. However, with the programmed excitation wavelength system developed in this work, multiple analytes can be measured from a single elution, providing the potential for internal standard quantitation to be used. Response factors evaluated for eight replicate measurements of a fluorene and 1-methylfluorene mixture over the course of one day showed a relative standard deviation (R.S.D.) of 18 and 19%, respectively, while the R.S.D. for the relative response factor of 1-methylfluorene to fluorene was 3.5% for the same eight measurements. Thus, the detection system can provide good precisions for determinations via the internal standard technique, but may be unsuitable for the external standard method.

The GC–SJE–LIF system described herein provides programmed excitation wavelength selection and rapid wavelength scanning, thereby allowing multiple analytes to be determined for each chromatographic separation, with great selectivities for each measured analyte. However, irreproducibilities in sensitivities varied greatly from run to run, precluding reliable external standard measurements. Fortunately, relative sensitivities were very reproducible and thus reliable internal standard measurements are feasible with this detector system. Future instrumental improvements should diminish mechanical vibration-induced signal noise to considerably enhance limits of detection. In addition, alternative internal standards, such as deuterated isomers of desired analytes, are being investigated and may help to improve the utility of the technique.

ACKNOWLEDGEMENTS

The authors thank the National Institutes of Health and the Oregon State University Research Council for financial support. In addition, we thank Orest Kawka of the Department of Oceanography at OSU for access to the Guaymas basin hydrothermal oil sample.

REFERENCES

1 H. H. Jaffe and M. Orchin, *Theory of Ultraviolet Spectroscopy*, Wiley, New York, 1962.
2 J. B. Birks, *Photophysics of Aromatic Molecules*, Wiley-Interscience, London, 1970.
3 A. K. Adams, D. L. Van Engelen and L. C. Thomas, *J. Chromatogr.*, 303 (1984) 341.
4 D. L. Van Engelen, A. K. Adams and L. C. Thomas, *J. Chromatogr.*, 331 (1985) 77.
5 H. P. Burchfield, E. E. Green, R. J. Wheeler and S. M. Belledeau, *J. Chromatogr.*, 99 (1974) 697.
6 R. P. Cooney and J. D. Winefordner, *Anal. Chim. Acta*, 89 (1977) 9.
7 J. W. Robinson and J. P. Goodbread, *Anal. Chim. Acta*, 66 (1973) 239.
8 L. C. Thomas and A. K. Adams, *Anal. Chem.*, 54 (1982) 2597.
9 R. P. Cooney and J. D. Winefordner, *Anal. Chem.*, 49 (1977) 1057.
10 J. M. Hayes and G. J. Small, *Anal. Chem.*, 54 (1982) 1202.
11 D. L. Van Engelen, L. C. Thomas and E. H. Piepmeier, *J. Chromatogr.*, 405 (1987) 191.
12 D. J. Freed and L. R. Faulkner, *Anal. Chem.*, 44 (1972) 1194.
13 D. H. Levy, *Ann. Rev. Phys. Chem.*, 31 (1980) 197.
14 J. A. Warren, J. M. Hayes and G. J. Small, *Anal. Chem.*, 54 (1982) 138.
15 B. V. Pepich, J. B. Callis, D. H. Burns, M. Gouterman and D. A. Kalman, *Anal. Chem.*, 58 (1986) 2825.
16 S. W. Stiller and M. V. Johnston, *Anal. Chem.*, 59 (1987) 567.
17 S. W. Stiller and M. V. Johnston, *Appl. Spectrosc.*, 41 (1987) 1357.
18 G. J. Beenen, J. W. Hosch and E. H. Piepmeier, *Anal. Chem.*, 51 (1981) 239.

Journal of Chromatography, 557 (1991) 47–58
Elsevier Science Publishers B.V., Amsterdam

CHROM. 23 241

Separation of *trans/cis*- α- and β-carotenes by supercritical fluid chromatography

I. Effects of temperature, pressure and organic modifiers on the retention of carotenes

M.-C. AUBERT, C. R. LEE and A. M. KRSTULOVIĆ*
Synthélabo Recherche (L.E.R.S.), Recherche Analytique et Contrôle Pharmaceutique, 23/25 Avenue Morane Saulnier, 92360 Meudon la Forêt (France)
and
E. LESELLIER, M.-R. PÉCHARD and A. TCHAPLA
LETIAM, Institut Universitaire de Technologie d'Orsay, BP 127, 91403 Orsay Cedex (France)

ABSTRACT

A partial separation of the isomers of α- and β-carotenes has previously been achieved by non-aqueous reversed-phase chromatography on octadecyl silica columns eluted with mixtures of hexane and polar modifiers. We show that improved results are obtained by the use of mobile phases based on liquid or supercritical carbon dioxide. Polar modifiers have similar effects on chromatographic selectivity in the non-aqueous reversed-phase and supercritical fluid chromatography systems, suggesting that the retention mechanism is the same in both cases (predominantly partition). With the carbon dioxide-based mobile phases, it was possible to optimize chromatographic efficiency by varying the temperature and pressure. The use of both binary and ternary mixtures was investigated.

INTRODUCTION

The carotenoids are natural pigments that are responsible for the orange–yellow colour of numerous plant tissues. Carotenes are carotenoid hydrocarbons of which several types are known. The most abundant of these, designated α- and β-carotenes, are the principal forms of provitamin A in the diet of humans. Certain carotenes (notably β-carotene) are anticarcinogenic [1,2].

In fresh plant tissue, all of the double bonds have the *trans* configuration (all-*trans*), which is the most stable thermodynamically [3–5]. Isomerization to *cis* configurations results in a loss of nutritional value [3–5]; the determination of these isomers is necessary for the quality control of fresh foodstuffs and for the evaluation of the effects of food-processing on freshness.

The analysis of carotene isomers is usually carried out by high-performance

0021-9673/91/$03.50

liquid chromatography (HPLC) with either normal-phase [6,7] or reversed-phase [8–10] systems. The simultaneous analysis of the *cis* and *trans* isomers of the α- and β-carotenes has also been achieved with an isocratic non-aqueous reversed-phase NARP) system [10]. In these studies, conventional octadecyl-substituted silica columns were eluted with hexane, to which was added various polar modifiers. Nevertheless, analysis times were long (45 min) and all compounds of interest could not be separated under these conditions.

Supercritical fluids have lower viscosities than liquids and thus solute diffusion coefficients are higher than in conventional solvents; reports of the supercritical fluid extraction [11] and chromatography [12,13] of carotenes have already appeared. Since the solvent polarity of supercritical carbon dioxide is similar to that of hexane, it was a logical step to investigate the use of carbon dioxide for NARP chromatography. The elution power of supercritical (or nearly supercritical) fluids can be varied, not only by the use of solvent modifiers but also by means of changes in temperature and pressure. In this report, we describe the influence of these experimental variables on the separation of carotenes by NARP with high-pressure carbon dioxide as the main constituent of the eluent.

EXPERIMENTAL

Chemicals

The solvents of HPLC grade were purchased either from Prolabo (Paris, France) or Carlo Erba (Milan, Italy). Carbon dioxide (N45 grade, containing $\leqslant 7$ ppm water) was purchased from Alphagaz (Bois d'Arcy, France).

Preparation of samples

Pigments were extracted from carrots (Nantaise variety) with a mixture of hexane, diethyl ether and acetone (50:20:30, v/v/v), as previously described [4]. Dried extracts were stored at -25°C. Before being analysed, the extracts were dissolved in a mixture of methanol and dichloromethane (80:20, v/v) and exposed to ambient light for a few hours. Authentic samples of all-*trans* α- and β-carotenes were purchased from Sigma (St. Louis, MO, USA).

Apparatus

Chromatography was performed using equipment manufactured by Jasco (Tokyo, Japan; supplied by Prolabo). The two pumps (Model 880-PU) were connected for gradient elution by means of a Model 801-SC controller and a Model MX-50 dynamic high-pressure mixing unit. The head of the pump used for carbon dioxide was cooled to -2°C. The mixing unit was connected to a standard injector (Rheodyne, Cotati, CA, USA; Model 7125) fitted with a 20-μl loop, via a pressure-relief valve (Rheodyne; Model 7037). The column was mounted in a thermostatically controlled oven. The UV detector (Model 875-UV) was fitted with the standard high-pressure cell (4 μl; 5 mm path length). Chromatograms were recorded at 340 or 450 nm. The eluent was discharged via an automatic back-pressure regulator (Model 880-81). Chromatograms were recorded using an electronic integrator (Shimadzu, Kyoto, Japan, Model C-R3A; supplied by Roucaire, Vélizy-Villacoublay, France).

The chromatographic columns tested in the course of this study were the fol-

lowing: 5 μm Spheri-5 ODS-5A (250 × 4.6 mm I.D.), Brownlee Labs., Santa Clara, CA, USA; 5 μm Ultrabase UB225 (250 × 4.6 mm I.D.), S.F.C.C., Gagny, France; 5 μm Nucleosil C_{18} (250 × 4.6 mm I.D.) Macherey-Nagel, Düren, Germany; 5 μm Superspher 100 RP-18 (250 × 4.0 mm I.D.), Merck, Darmstadt, Germany; 5 μm LiChrospher 100 RP-18 (200 × 4.0 mm I.D.), Merck; 5 μm LiChrospher 100 RP-18E (200 × 4.0 mm I.D.), Merck; 5 μm ChromTech CT-Sil C_{18} (150 × 4.6 mm I.D.), ChromTech, Norborg, Sweden; and 3-μm Spherisorb ODS-2 (100 × 4.6 mm I.D.), Phase Separations, Deeside, UK.

RESULTS AND DISCUSSION

Effects of variations in pressure and temperature

This part of the study was carried out with a Spheri-5 ODS-5A column that had successfully been used for NARP liquid chromatography [10]. With supercritical fluid chromatography (SFC), the order of elution of the carotenes was the same as with NARP: all-*trans* α-carotene, *cis* isomers of α-carotene, all-*trans* β-carotene, *cis* isomers of β-carotene.

Effect of temperature. When the mobile phase in SFC is carbon dioxide without modifiers, the capacity factor (k') increases in proportion to the temperature (at constant pressure), whether the stationary phase is bare or octadecyl-grafted silica. This effect can most likely be explained by the temperature-dependent decrease in density of the mobile phase [15]. On the other hand, when the carotenes are eluted with carbon dioxide containing 12% methanol, k' decreases with increasing temperatures between 22°C and 55°C (Fig. 1), an effect that is typical of liquid chromatographic separations. It seems that the temperature-dependent increase in solute–solvent interactions more than compensates for the decrease in density.

The resolution between the all-*trans* α- and β-carotenes decreases as the temperature is increased (Fig. 2). Since the selectivity remains constant, the improvement observed on lowering the temperature must be due to the increase in k' or to increased

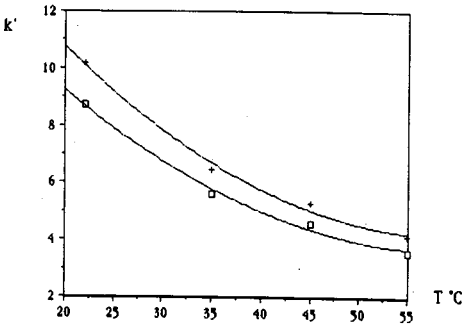

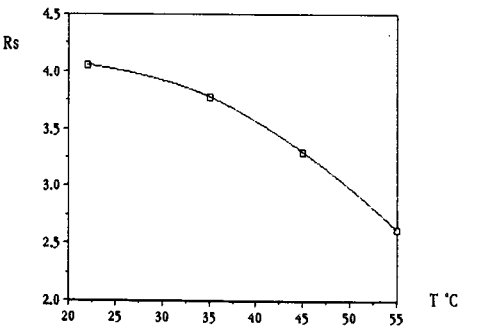

Fig. 1. Dependence of k' values of carotenes on temperature at constant pressure (250 bar, 25 MPa). Column Spheri-5 ODS-5A; mobile phase carbon dioxide–methanol (80:20, v/v); flow-rate 3.0 ml/min; detection 450 nm. Key: □ = all-*trans* α-carotene; + = all-*trans* β-carotene.

Fig. 2. Resolution R_s of all-*trans* α- and β-carotenes as a function of temperature. The chromatographic conditions are indicated in the legend to Fig. 1.

efficiency (theoretical plate number, N). The efficiency is related to the reduced plate height (h) by the equation:

$$N = L/hd_p \tag{1}$$

where L is the column length and d_p the particle size.

The two principal factors determining the reduced plate height are k' and the solute diffusion coefficient (D_m), which appear in terms B and C of eqn. 2:

$$h = A + B/v + Cv \tag{2}$$

where v is the reduced mobile phase velocity.

Term B, which describes the longitudinal diffusion, is generally considered constant and close to 2. Mourier [15] has shown that term C, which describes mass transfer, depends on k' according to eqn. 3:

$$C = k'/30(1 + k') \cdot D_m/D_s \tag{3}$$

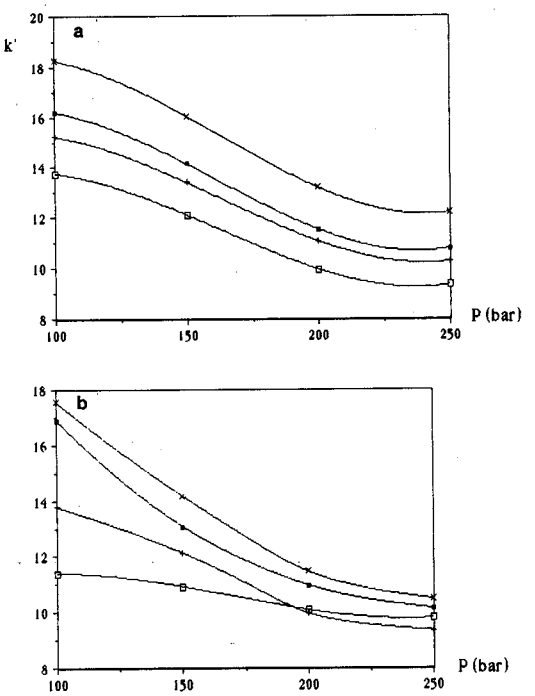

Fig. 3. (a) Dependence of k' values of carotenes on pressure (p) at constant temperature (22°C). The chromatographic conditions were otherwise as indicated in the legend to Fig. 1. Key: □ = all-*trans* α-carotene; + = *cis* α-carotenes; ■ = all-*trans* β-carotene; × = *cis* β-carotenes. (b) Dependence of k' values of carotenes on pressure, with different percentages of organic modifier (methanol). The temperature was 25°C and the other chromatographic conditions were as indicated in the legend to Fig. 1. Key: □ = all-*trans* α-carotene eluted with carbon dioxide–methanol (80:20, v/v); + = *cis* α-carotenes eluted with carbon dioxide–methanol (85:15, v/v); ■ = all-*trans* β-carotene eluted with carbon dioxide–methanol (88:12, v/v); × = *cis* β-carotenes eluted with carbon dioxide–methanol (88:12, v/v).

TABLE I

EFFECT OF PRESSURE ON RESOLUTION (R_s) OF CAROTENES

Pressure (MPa)	Resolution of β/α all-*trans*			Resolution of β *trans*/α *cis*		
	Methanol 20%	Methanol 15%	Methanol 12%	Methanol 20%	Methanol 15%	Methanol 12%
10	4.61	5.17	4.79	1.40	1.91	1.91
15	4.19	4.73	4.73	1.28	1.64	1.75
20	4.31	4.56	4.34	1.31	1.58	1.57
25	3.85	4.29	4.20	1.11	1.47	1.59

Hence C decreases as k' increases, and therefore an increase in k' is associated with increased efficiency. In fact, the increase in retention time should favour increased solute diffusion D_s at the surface of the stationary phase [15], an effect that would lead to a further reduction in the mass transfer term. At carbon dioxide densities greater than 0.6 g/cm^3, D_m can be evaluated from the equation of Wilke and Chang, adapted to SFC [15]:

$$D_m = 7.4 \cdot 10^{-15} \cdot (\psi \cdot M_s)^{0.5}/(\eta V_s)^{0.6} \quad (4)$$

The optimum temperature appears to be between 22 and 25°C; clearly, the mobile phase is subcritical. This is of no consequence, since there is no discontinuity in the physical properties of the fluid at the critical point. In some applications, particularly chiral separations, the best selectivities between isomers are obtained under subcritical conditions [16]. Also, the optimal temperature for NARP separations is between 20 and 25°C [10]; fortunately, this is low enough for the study of thermolabile carotenoids.

Effect of pressure. We studied the effects of varying the mobile phase pressure between 100 and 250 bar (10 and 25 MPa), at 22°C. Increasing the pressure led to decreased capacity factors (Fig. 3), an effect that can be explained by enhanced solubility of the solutes with increasing density of the mobile phase. The capacity factors appear to decrease less rapidly at pressures above 200 bar (20 MPa), probably because of the non-linearity of the P–T curve of carbon dioxide which, at 22°C, becomes progressively less compressible (Fig. 3a). The capacity factor also becomes less pres-

TABLE II

EFFECT OF PRESSURE ON EFFICIENCY (N) CALCULATED FOR ALL-*trans* β-CAROTENE

Methanol (%)	Efficiency (N)			
	10 MPa	15 MPa	20 MPa	25 MPa
15	16550	15900	15400	14300
12	17700	17000	14900	14500
10	17500	15950	15600	15400

sure-dependent as the concentration of methanol is increased (Fig. 3b), indicating that the modifier diminishes the compressibility of the fluid, which becomes almost incompressible at 20% methanol.

The selectivity between the all-*trans* α- and β-carotenes, as well as that between the *cis* and *trans* isomers, is independent of both pressure and temperature (and therefore of the fluid density). The resolution between the different isomers decreases with increasing pressure (Table I), and the separation between the *cis* α-carotenes and all-*trans* β-carotene is adequate only at the lowest pressures that were used. Since the selectivity is constant, the pressure-dependent changes in resolution must be due to changes in efficiency (Table II). Increasing the pressure increases the mobile phase viscosity, thus decreasing the mass transfer term C (eqn. 3) and the diffusion coefficient (eqn. 4). In the present case, when the retention time is increased by decreasing the pressure, the unfavourable effects of the increased diffusion coefficient (term D_m) are more than compensated by a reduction in the peak broadening that is due to the finite rate of solute diffusion at the surface of the stationary phase (term D_s).

In practice, it is preferable to avoid working at pressures at which the fluid is very compressible, as the pressure drop along the column is associated with a density gradient and reduced efficiency. Hence a pressure of 15 MPa was preferred to 10 MPa.

A chromatogram of a carrot extract on a Spheri-5 ODS-5A column, obtained under optimized conditions of pressure and temperature, is shown in Fig. 4. Total analysis time was 16 min, whereas the analysis required 45 min when the same column was used in NARP HPLC [10]. In addition, the SFC analysis revealed a peak (retention time 15.5 min, labelled 4b in Fig. 4) that was not detected by HPLC [10], probably because of its long retention time. This peak absorbs strongly at 340 nm; it is probably due to 9- or 13-*cis* β-carotene.

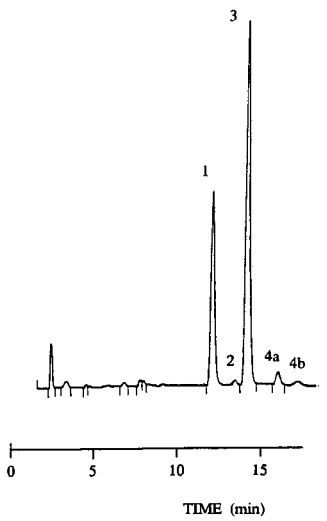

Fig. 4. Separation of the components of a carrot extract on a Spheri-5 ODS-5A column. Peaks: 1 = all-*trans* α-carotene; 2 = *cis* isomers of α-carotene; 3 = all-*trans* β-carotene; 4a = *cis* isomers of β-carotene; 4b = unknown, probably 9- or 13-*cis* β-carotene.

Effects of mobile phase modifiers

Published studies of the effects of modifiers in SFC have generally concerned the chromatography of polar compounds such as phenols [15,17]. Whether the stationary phase is bare or octadecyl silica, the addition of modifiers to supercritical carbon dioxide leads to reduced capacity factors. When the modifier is a polar compound, such as methanol, this reduction is probably due to deactivation of silanol groups and to specific interactions between the solutes and the modifier. However, some reports in the literature [18] do show a direct correlation between solute retention and elution strength of the mobile phase. With carbon dioxide based mobile phases, the effects of apolar modifiers such as hexane are most easily explained by an increase in density of the mobile phase, an effect that is also likely to occur with polar modifiers.

We have studied the effects of a range of solvent modifiers in NARP-SFC of carotenes: methanol, acetonitrile, tetrahydrofuran (THF), dichloromethane and trichlorotrifluoroethane (TTE). Binary or ternary mixtures with carbon dioxide contained 3–20% (v/v) of the modifiers.

Binary mixtures

Each modifier produced a concentration-dependent decrease in the capacity factors of the carotenes (Fig. 5). The effectiveness of the modifiers was not directly correlated with their densities (Table III), which increase in the order: acetonitrile < methanol < THF–methanol < dichloromethane < TTE. The solvent power of these modifiers, at equal concentrations, increases in the order: methanol < acetonitrile < THF–methanol < TTE < dichloromethane. This order correlates neither with the densities nor with the polarities of the modifiers. It appears, therefore, that specific interactions between the solutes and the modifiers are important, particularly in the case of the polar solvent acetonitrile.

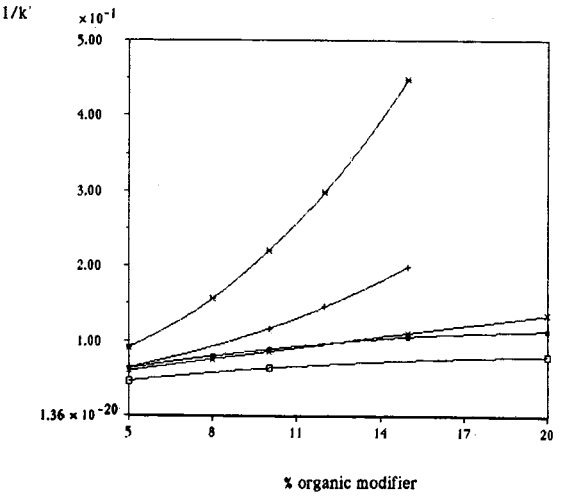

Fig. 5. Variation of $1/k'$ of all-*trans* α-carotene as a function of the concentrations of different modifiers. Chromatographic conditions as in Fig. 1, except that the column was Ultrabase UB225. Key: □ = methanol; ∗ = dichloromethane; ■ = acetonitrile; × THF–methanol; + = trichlorotrifluoroethane.

TABLE III

DENSITIES AND POLARITIES (ACCORDING TO ROHRSCHNEIDER [20]) OF DIFFERENT SOLVENTS USED AS MODIFIERS

	Solvents				
	Acetonitrile	Methanol	THF	Dichloromethane	TTE
Density (g/l)	0.781	0.79	0.88	1.33	1.57
Polarity	5.8	5.1	4.1	3.1	< 1

Minimal retention was obtained with the strongest modifier, dichloromethane, which is the one that is closest to the dipole–dipole interaction pole of Snyder's triangle [19]. THF–methanol was the only modifier that gave a linear plot of $1/k'$ against concentration. With modifiers more polar than this, the line curved slightly downwards, as would be expected where an increase in solvent polarity favours solute–solvent interactions. Conversely, an exponential (upwards) curvature was found for the non-polar modifiers, suggesting that the solubility of the carotenes is enhanced by an amount that is independent of the concentration of modifier. Essentially the opposite effects have been observed for the chromatography of phenols [15].

The retention of the carotenes appears to be uninfluenced by the presence of residual silanol groups, as the addition of 2% water to a methanol–carbon dioxide

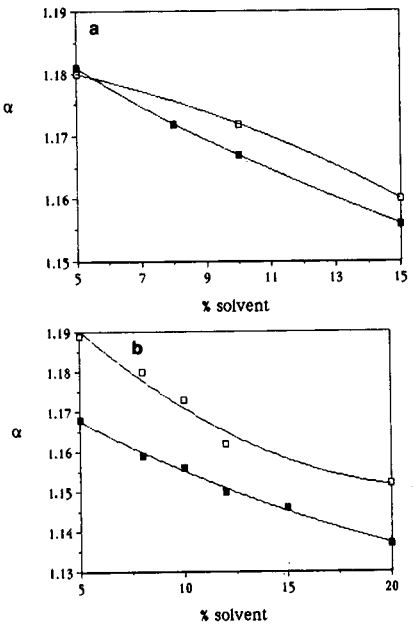

Fig. 6. Variation of the selectivity between the all-*trans* α- and β-carotenes as a function of percentages of the organic modifiers methanol (a) and acetonitrile (b). Key: ■ = Nucleosil C_{18} column; □ = Ultrabase UB225 column. The other chromatographic conditions were as in Fig. 1.

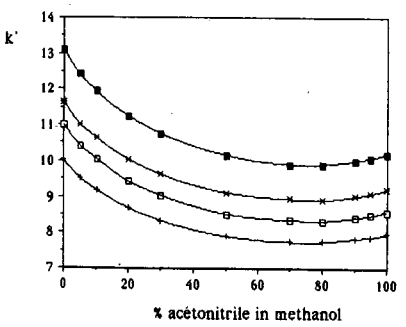

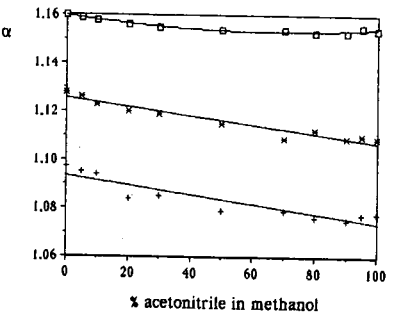

Fig. 7. Variation of k' values of carotenes as a function of the concentration of acetonitrile in methanol, the total concentration of modifier being 15%. Column Ultrabase UB225; pressure 150 bar (15 MPa); temperature 30°C; flow-rate 3.0 ml/min; detection 450 nm. Key: + = all-*trans* α-carotene; □ = *cis* α-carotenes; * = all-*trans* β-carotene; ■ = *cis* β-carotenes.

Fig. 8. Variation of the selectivity between different carotenes as a function of the concentration of acetonitrile in methanol, the total concentration of modifier being 15%. Chromatographic conditions as in Fig. 7. Key: □ = all-*trans* β-carotene/all-*trans* α-carotene; + = *cis* α-carotenes/all-*trans* α-carotene; * = *cis* β-carotenes/all-*trans* β-carotene.

mixture (15:85, v/v) resulted in increased rather than decreased capacity factors. The retention mechanism is by partition, with no adsorptive contribution.

Selectivity between the all-*trans* α- and β-carotenes is affected in a similar manner by methanol (Fig. 6a) and acetonitrile (Fig. 6b). The Ultrabase C_{18} column provided better selectivity than the Nucleosil C_{18} column. In contrast, the selectivity between *trans* and *cis* isomers is unaffected by the modifiers. With increasing percentage of modifier, the selectivity between the α- and β-all-*trans* compounds is diminished (Fig. 6), although it does not fall below 1.15 for 15% modifier.

Ternary mixtures

Analyses were carried out at 22, 25 and 30°C, with the total modifier concentration being maintained constant at 15%. In the first study, the concentration of acetonitrile in methanol was varied between 0 and 100%. The trends in selectivity and retention time were similar at all three temperatures. Although both modifiers have similar densities, they are not equivalent as far as capacity factors are concerned (Fig. 7). Retention diminishes as the methanol–acetonitrile ratio is increased up to about 70%, above which it slightly rises.

This effect, which has already been seen with NARP-HPLC [10], can be ascribed on the one hand to π–π bonding between acetonitrile and the π bonds of the carotenes, and on the other hand to increased solvent polarity (calculated by Rohrschneider's method [20]). It should be noted that acetonitrile is a stronger eluent than methanol in SFC (where the total modifier concentration is 15%), whereas the inverse is true when these solvents are used at 100% concentration in NARP-HPLC [10]. These results described here were reproduced using the following columns: Nucleosil C_{18}, LiChrospher 100 RP-18, LiChrospher 100 RP-18E, Spherisorb ODS-2, ChromTech CT-Sil C_{18}, Superspher 100 RP-18.

The selectivity between the α and β all-*trans* carotenes is independent of the

TABLE IV

SELECTIVITY BETWEEN THE UNIDENTIFIED PEAK AND ALL-*trans* α-CAROTENE AS A FUNCTION OF PERCENTAGE ACETONITRILE

Acetonitrile (%)	Selectivity
20	1.00
30	1.049
50	1.068
70	1.079
90	1.091

methanol–acetonitrile ratio (Fig. 8). However, the selectivity between *trans* and *cis* isomers falls as the proportion of acetonitrile is increased, for both the α- and β-carotenes. This specific effect on the geometric but not on the positional isomers is the reverse of that noted above for binary solvent mixtures. This may be due to differences in topology of the stationary phase between the two cases.

The reduction in selectivity between the *trans* and *cis* isomers produced by acetonitrile was used to advantage in optimizing the separation shown in Fig. 4. Since, with methanol–carbon dioxide, the peaks the least well resolved were those of

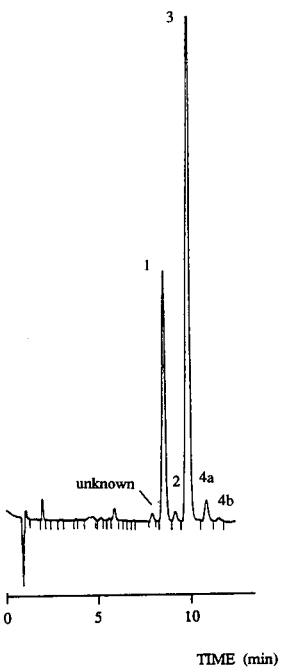

Fig. 9. Separation of the components of a carrot extract on an Ultrabase UB225 column. Mobile phase carbon dioxide–acetonitrile–methanol (85:14.25:0.75, v/v/v); temperature 22°C; pressure 150 bar (15 MPa); flow-rate 3.0 ml/min; detection 450 nm. The peaks are numbered as in Fig. 4. The peak labelled "unknown" is possibly γ- or ζ-carotene (see text).

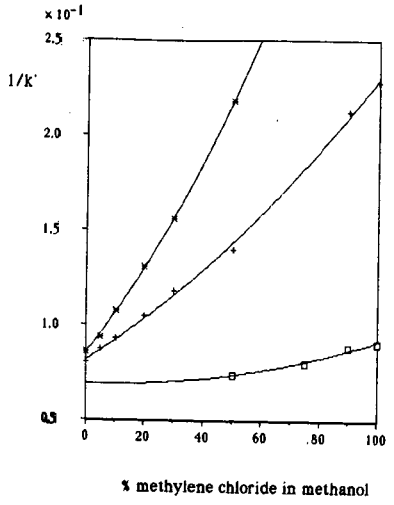

Fig. 10. Variation of $1/k'$ as a function of the percentage of dichloromethane in methanol. Column Ultrabase UB225; pressure 150 bar (15 MPa). The other chromatographic conditions were as indicated in the legend to Fig. 1. Key: □ = total modifier concentration 5%, temperature 22°C; + = total modifier concentration 10%, temperature 30°C; × = total modifier concentration 15%, temperature 22°C.

the *cis* isomers of α-carotene and all-*trans* β-carotene, the separation could be improved by replacing part of the methanol with acetonitrile. This does not cause the *trans* and *cis* isomers to overlap, as there is a good margin between them. Addition of acetonitrile revealed an additional component in the extract of carrots (Table IV), which elutes before all-*trans* α-carotene, and is completely resolved at acetonitrile–methanol ratios greater than 7:3 (Fig. 9). Since the absorbance of this compound at 340 nm is very weak, it is unlikely to be a *cis* isomer. It could be γ- or ζ-carotene, as these two compounds have structures very similar to that of α-carotene.

Some studies were carried out with ternary mixtures of carbon dioxide, methanol and dichloromethane. Total modifier concentrations were 5 and 15% at 22°C, and 10% at 30°C. Increasing the ratio of dichloromethane to methanol led to decreased capacity factors, particularly at high total modifier concentrations (Fig. 10). Plots of $1/k'$ against modifier concentration were exponential, as with the binary mixtures. Unlike acetonitrile, dichloromethane produced a general decrease in selectivities; the α- and β-carotenes were less well separated, as were the *cis* and *trans* isomers. This is probably due to reduced interactions between the solutes and the stationary phase, as all the carotenes have high affinities for this solvent.

CONCLUSIONS

The separation of *cis* and *trans* α- and β-carotenes is improved by the use of SFC techniques in place of HPLC: the analysis time is considerably shortened, and an additional *cis* isomer of β-carotene is resolved.

Pressure- and temperature-induced changes in the density of carbon dioxide affect the chromatographic efficiency, but not the selectivity. Conversely, the selectivity can be varied by the use of eluent modifiers, which do not appear to influence

the efficiency. This effect varies as a function of the type of organic modifier used in both binary and ternary mixtures.

The effects of eluent modifiers on the capacity factors and solubilities of the pigments are similar whether SFC or HPLC is used. This strongly suggests that the retention mechanism(s) are similar in both techniques. The dominant mechanism is partition, with adsorption having little or no rôle.

Ternary mixtures of acetonitrile, methanol and carbon dioxide revealed a presently unidentified compound whose peak otherwise overlapped that of all-*trans* α-carotene. However, the results obtained with this eluent depend on the C_{18} stationary phase that is employed, and they will be discussed in the following paper [21].

ACKNOWLEDGEMENT

The authors wish to acknowledge Jean-Pierre Porziemsky for his technical assistance.

REFERENCES

1 R. C. Moon and L. M. Itri, in M. B. Sporn, A. B. Roberts and D. S. Goodman (Editors), *The Retinoids*, Academic Press, New York, 1984, p. 2.
2 D. E. Ong and F. Chytil, in G. D. Aurbach (Editor), *Vitamins and Hormones*, Academic Press, New York, 1983, p. 103.
3 A. T. Ogunlesi and C. Y. Lee, *Food Chem.*, 4 (1979) 311.
4 J. P. Sweeny and A. C. March, *J. Am. Diet. Assoc.*, 59 (1971) 238.
5 L. A. Chandler and S. J. Schwartz, *J. Agric. Food Chem.*, 36 (1988) 129.
6 K. Tsukida, K. Saiki, T. Takii and Y. Koyana, *J. Chromatogr.*, 245 (1982) 359.
7 M. Vecchi, G. Englert, R. Maurer and U. Meduna, *Helv. Chim. Eng.*, 1 (1981) 264.
8 R. J. Buchway, *J. Liq. Chromatogr.*, 8 (1985) 1527.
9 F. W. Quackenbush, *J. Liq. Chromatogr.*, 10 (1987) 643.
10 E. Lesellier, C. Marty, C. Berset and A. Tchapla, *J. High Chromatogr. Chromatogr. Commun.*, 12 (1989) 447.
11 F. Favati, J. W. King, J. P. Friedrich and K. Eskins, *J. Food Sci.*, 53 (1988) 1532.
12 H. H. Schmitz, W. E. Artz, C. L. Poor, J. M. Dietz and J. W. Erdman, *J. Chromatogr.*, 479 (1989) 261.
13 D. R. Gere, *Hewlett Packard Application Note 800-5*, Hewlett Packard, Avondale, 1983.
14 E. Lesellier, *Thesis*, Paris 7 University, Paris, 1990.
15 P. Mourier, *Thesis*, Paris University, 1986.
16 C. R. Lee, J.-P. Porziemsky, M.-C. Aubert and A. M. Krstulović, *J. Chromatogr.*, 539 (1991) 55.
17 J. G. M. Jansen, P. J. Schoenmakers and C. A. Cramers, *J. High Resolut. Chromatogr. Chromatogr. Commun.*, 12 (1989) 645.
18 T. A. Berger and J. F. Deye, *Anal. Chem.*, 62 (1990) 1181.
19 L. R. Snyder, *J. Chromatogr.*, 92 (1974) 223.
20 L. Rohrschneider, *Anal. Chem.*, 45 (1973) 1241.
21 E. Lesellier, M.-R. Péchard, A. Tchapla, M.-C. Aubert, C. R. Lee and A. M. Krstulović, *J. Chromatogr.*, 557 (1991) 59.

Journal of Chromatography, 557 (1991) 59–67
Elsevier Science Publishers B.V., Amsterdam

CHROM. 23 242

Separation of *trans/cis* α- and β-carotenes by supercritical fluid chromatography

II. Effect of the type of octadecyl-bonded stationary phase on retention and selectivity of carotenes

E. LESELLIER and A. TCHAPLA
LETIAM, Institut Universitaire de Technologie d'Orsay, BP 127, 91403 Orsay Cedex (France)
and
M.-R. PÉCHARD, C. R. LEE and A. M. KRSTULOVIĆ*
Synthélabo Recherche (L.E.R.S.), Recherche Analytique et Contrôle Pharmaceutique, 23/25 Avenue Morane Saulnier, 92360 Meudon la Forêt (France)

ABSTRACT

Described in this paper are the effects of the type of bonding (monomeric *versus* arborescent-polymeric) of 22 octadecyl-bonded phases and of carbon loading on the separation of *cis* and *trans* isomers of α- and β-carotenes. Only arborescent-polymeric phases afforded the separation of *cis* and *trans* isomers, regardless of the degree of carbon loading. Incomplete separation of the α- and β-carotenes is obtained if the capacity factor for α-carotene is below 6. Also described is a method for estimating the void volume in supercritical fluid chromatography, derived from the two-solvent weight-difference method used in high-performance liquid chromatography. The porosity values are in good agreement with those reported in the literature.

INTRODUCTION

Commercial stationary phases of octadecyl-bonded silica have widely differing properties, and it is sometimes difficult to transpose a separation from one make of column to another. Among the factors that determine the performance of a column, such as the shape and size of the particles, the pore size, the specific surface area and the percentage surface coverage, the kind of function that is bonded to the support is particularly important.

Where the stationary phase is prepared with a monofunctional alkylsilane, there is one-to-one bonding between the reagent and the silanol groups, giving a "brush-type" structure [1]. Di- and trifunctional silanes can bond to more than one silanol group on the silica support to give essentially the same type of "brush-type"

0021-9673/91/$03.50

stationary phases as monofunctional silanes. However, they can also polymerize in the presence of traces of water [2]; under suitable conditions, a stationary phase can be prepared in which each alkylsilane that is bonded to the surface of the silica gives rise to an arborescent-polymeric structure that is not brush-like. Such stationary phases are frequently (and correctly) described in the literature as "polymeric", but as this can lead to confusion with column packings in which the support itself is polymeric we shall use the term "arborescent-polymeric" in this paper. Arborescent-polymeric stationary phases appear to be particularly suitable for separating closely related compounds that differ in the degree of planarity of their structures [3,4]. Although no systematic studies have been carried out, the best published reversed-phase separations of *cis*- and *trans*-carotenes have been obtained on this type of stationary phase, particularly with Vydac [5,6] and Spheri-5 [7] columns.

Several techniques have been applied to the study of the structure of bonded phases, but in most cases the results do not reflect the state of a phase in the presence of the mobile phase. More empirical studies have established the behaviour of different stationary phases in terms of capacity factors (k') and selectivities (α) [1,8–10]. As part of a study of the simultaneous separation of α and β *cis* and *trans* carotenes extracted from carrots [11], we have compared the results obtained on columns containing monofunctional and arborescent-polymeric C_{18} bonded phases, including some whose nature was not revealed by the manufacturer.

EXPERIMENTAL

Details of sample preparation and of the chromatographic system have been given in the preceding paper [11]. The octadecyl-bonded silica columns that were used are listed in Table I.

The void volume of a column was determined by first flushing it with pure carbon dioxide at 3 ml/min for 10 min. The column was then depressurized and left open to the atmosphere for another 10 min, by which time the mass was stable. It was weighed with the stoppers in place, then filled and equilibrated with methanol by pumping the solvent for 30 min, and finally stoppered and reweighed.

The extra-column void volume (0.206 μl) was estimated from the retention times for repeated injections of solvents (acetonitrile of methanol), the column being replaced by a union of negligible volume. The appropriate time was taken as the retention time of a positive peak that appeared shortly after the injections. Ten determinations of this time gave a relative standard deviation of 1.5%.

RESULTS AND DISCUSSION

The *cis* and *trans* α- and β-carotenes were separated by non-aqueous reversed-phase (NARP) high-performance liquid chromatography (HPLC), on a Spheri-5 ODS-5A column, which had an arborescent-polymeric bonded octadecyl stationary phase [7]. A column having a monomeric stationary phase (Spheri-5 ODS-5A) was not satisfactory. In the preceding paper [11], we showed that an improved separation can be obtained with the arborescent stationary phase by using mobile phases based on high-pressure carbon dioxide, the retention mechanism being the same. This technique is generally referred to as supercritical fluid chromatography (SFC), despite the

fact that in many cases, including the present one, the mobile phase is in the liquid state. However, since the chromatographically relevant physical properties (including compressibility) do not change abruptly at the critical temperature, it is usual to retain the term "SFC", even when the temperature is somewhat below the critical point. We have evaluated the performance of the other columns, using the SFC conditions (22°C, 150 bar, 15% methanol) that were found to be optimal for the Brownlee arborescent-polymeric column. Particular attention is paid to the estimation of k' for the analytes, because this parameter characterizes the stationary phase independently of factors such as the size and porosity of the column.

Determination of dead volumes in SFC

For an incompressible mobile phase, the capacity factor is given by the equation:

$$k' = (V_r - V_{0(\text{total})})/V_{0(\text{column})} \quad (1)$$

where V_r is the retention volume of an analyte and the V_0 terms represent the void volumes; the void volumes of the column and of the equipment must be known individually. Various methods have been proposed for estimating the column void volume: by injection of non-retained solvents, by extrapolation of retention volumes of solutes forming homologous series, and by weighing the column equilibrated with solvents of different densities [12]. The first two methods are the most sound from the theoretical point of view, because V_0 is determined under the conditions that will be used for chromatography. However, in the case of SFC, the density gradient along the column leads to complications that render precise definitions of V_0 and k' difficult to achieve in practice when (as in the present work) the mobile phase is used at temperatures and pressures not far removed from the critical values. Furthermore, since the temperature of the mobile phase is lower at the chilled pump head than at the top of the column, the average flow-rate (in ml/min) through the column is greater than that supplied by the pump.

Since our objective was to compare columns of fairly similar dimensions and particle size, and not to establish thermodynamic constants, we chose to neglect the errors due to compressibility. The void volume was taken as the volume of methanol (calculated from the mass) required to fill the columns that had previously been

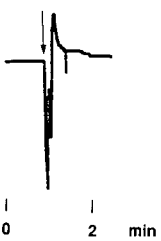

Fig. 1. Blank injection for determination of the void volume. Column: Nucleosil C_{18} (250 × 4.6 mm I.D.), 5 μm. Mobile phase: carbon dioxide–methanol (85:15, v/v). Temperature 22°C, pressure 15 MPa, flow-rate 3 ml/min, λ = 450 nm.

TABLE I

POROSITIES OF OCTADECYL-BONDED COLUMNS USED FOR SUPERCRITICAL FLUID CHROMATOGRAPHY, RETENTION PARAMETERS OF ALL-*trans* α-CAROTENE AND SELECTIVITIES AND RESOLUTIONS OF THE SEPARATION OF *cis* AND *trans* α- AND β-CAROTENES ON DIFFERENT C_{18} COLUMNS

M = monofunctional C_{18} groups; D = difunctional C_{18} groups; P = arborescent-polymeric C_{18} groups; – = exact nature unknown.

Column	L (mm)	V_0	Porosity ε (%)	Type of bonding	t_r α-carotene (min)	k' α-carotene	Separation of α- and β-carotenes	Selectivity of *trans/cis* β-carotene isomers	Resolution of *trans/cis* β-carotene isomers	Separation of α- and β-carotenes *trans/cis* isomers
Ultrabase UB 225	250	2.463	59	M	11.22	12.58	Yes	> 1	> 1.5	Yes
Spheri-5 ODS-5A	250	2.456	59	P (A)	11.40	12.85	Yes	> 1	> 1.5	Yes
LiChrospher 100 RP 18	250	2.150	68	D	8.35	10.57	Yes	> 1	> 1.5	Yes
LiChrospher 100 PR 18e	250	2.187	70	D	9.60	12.05	Yes	> 1	> 1.5	Yes
Nucleosil C_{18}	250	2.866	69	P (A)	7.38	6.66	Yes	> 1	> 1.5	Yes
ChromTech CT-Sil C_{18}	150	1.545	62	–	4.89	8.36	Yes	> 1	> 1.5	Yes
Superspher 100 RP_{18}	250	2.106	67	D	8.16	8.02	Yes	> 1	> 1.5	Yes
Spherisorb ODS-2	100	1.029	62	P (A)	3.75	9.73	Yes	> 1	> 1.5	Yes
Supelcosil LC-PAH	150	1.768	71	P (A)	2.05	2.37	Yes	> 1	< 1.5	No
Erbasil C18	150	1.656	66	P (A)	3.60	5.4	Yes	> 1	< 1.5	No
Suplex pKb-100	150	1.623	65	–	2.38	3.27	Yes	> 1	> 1.5	No
Ultracarb 5-ODS 20	150	1.789	72	–	10.32	16.2	Yes	> 1	> 1.5	No
Zorbax ODS	250	2.678	64	M	4.98	4.5	Yes	= 1	< 1.5	No
Ultrasphere ODS	250	2.520	61	M	2.48	1.86	No	= 1	–	No
Vydac 201 HS	150	1.760	70	M	5.43	8.13	No	= 1	–	No
Partisil 5 ODS-3	250	2.803	67	M	7.70	7.17	No	= 1	–	No
μBondapak C_{18}	300	2.908	70		6.29	5.42	No	= 1	–	No
Vydac 210 TP	150	1.680	67	P (A)	1.6	1.73	Yes	> 1	< 1.5	No
Perkin-Elmer HC-ODS/PAH	250	1.327	88	P (A)	1.25	2.05	Yes	> 1	< 1.5	No
Vydac 218 Tp	250	2.898	70	P (A)	3.28	2.32	Yes	> 1	> 1.5	No
Hypersil $15C_{18}$	150	2.635	63	M	7.01	6.9	No	= 1	–	No
Synchropak SCD-100	150	1.874	75	M	1.68	1.59	Yes	> 1	< 1.5	No

flushed with supercritical carbon dioxide and equilibrated with air. Methanol was used because it is not absorbed to a significant extent by the stationary phase [13].

The value of V_0 for each of the columns is given in Table I, together with the porosity, calculated from V_0 and the total column volume. A representative HPLC trace is given in Fig. 1. As expected for C_{18} bonded-phase columns, the porosity ranged from 60 to 70%, except for the Perkin-Elmer analytical HC-ODS/PAH column, for which the value was anomalously high.

Influence of the type of stationary phase on the separation of carotenes

The effect of the stationary phase can be evaluated from overall variations in capacity factors or from variations in the extent of separation of different pairs or groups of compounds, such as:

(a) α- and β-carotenes (the isomers not being separated),
(b) *cis* and *trans* isomers of β-carotene, or
(c) *cis*/*trans* α- and β-carotenes.

Separation of α- from β-carotenes. All but five of the columns in Table I separated two classes of carotene (resultion, $R_s > 1.5$), under the conditions that had been optimized for the Spheri-5 ODS-5A column. Two of these five stationary phases are of the monofunctional type (Ultrasphere and Hypersil), one (μBondapak) is of an undetermined nature and the other two are arborescent-polymeric (Vydac 201TP and Synchropak SCD-100). The failure of the last two columns to provide a separation can be accounted for by the exceptionally low capacity factors (Table I), which are due to low percentages of carbon loading and, in the case of the Vydac 201 TP column, to a pore size of 30 nm. It is interesting that the end-capped version of this column, Vydac 218 TP, give higher capacity factors (for example 2.32 compared with 1.73 for α-carotene), together with an improved separation.

Four of the five columns that were unsatisfactory under the standard conditions gave adequate separations when the percentage of modifier in the mobile phase was reduced, confirming the suggestion that, as far as this particular separation is concerned, the major difference between the columns is in the degree of carbon loading. The only exception was the μBondapak column, which was already been reported to give anomalous results in a study of homologous series [9].

Separation of the cis and trans isomers of β-carotene. During a previous liquid chromatographic study, it was found that the separation of the *cis*- and *trans*-carotene isomers at ordinary temperatures (> 15°C) required a stationary phase of the arborescent-polymeric type. The same generalization applies to separations by SFC, since all the columns that failed to give this separation were of the monofunctional type: Hypersil $15C_{18}$, Vydac 201 HS, Zorbax ODS, Ultrasphere ODS, μBondapak C_{18} and Partisil 5 ODS-3.

All of the columns with arborescent-polymeric stationary phases (including those that did not separate the α- and β-carotenes) gave selectivity factors (α) greater than 1 for the separation of the *cis* and *trans* isomers (Table I). However, the resolution (R_s) was not always satisfactory, especially when the capacity factor (measured for α-carotene) was less than 6. To summarize, this separation requires a arborescent-polymeric stationary phase and the percentage carbon loading must be sufficient to

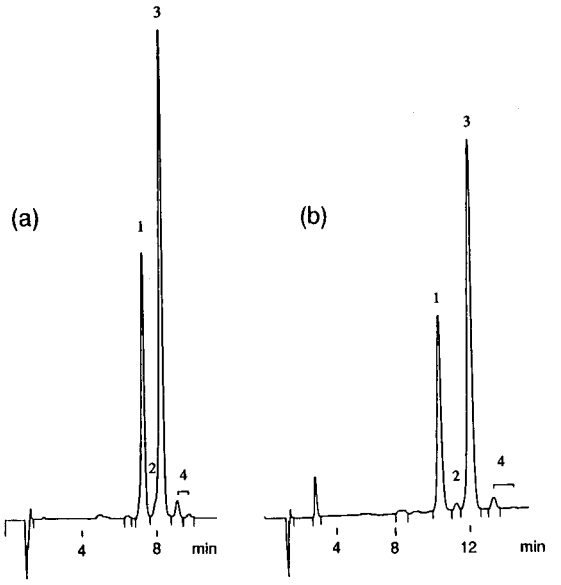

Fig. 2. Comparison of two chromatograms of a carrot extract, analysed on a Nucleosil C_{18} column (250 × 4.6 mm I.D.). Mobile phase: (a) carbon dioxide–methanol (85:15, v/v) at 15 MPa; (b) carbon dioxide–methanol (95:5, v/v) at 20 MPa. Temperature 22°C, flow-rate 3 ml/min, λ = 450 nm. Identification of peaks: 1, all-*trans* α-carotene, 2, *cis* isomers of α-carotene, 3, all-*trans* β-carotene, 4, *cis* isomers of β-carotene.

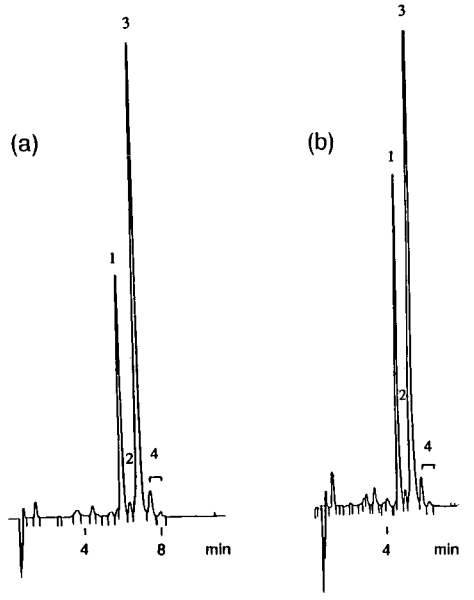

Fig. 3. Chromatograms of a carrot extract on (a) ChromTech CT-Sil C_{18} (150 × 4.6 mm I.D.), (b) Spherisorb ODS-2 (100 × 4.6 mm I.D.). Mobile phase: carbon dioxide–methanol (90:10, v/v). Temperature 22°C, pressure 15 MPa, flow-rate 3 ml/min, λ = 450 nm. Identification of peaks: see legend to Fig. 2.

TABLE II

EFFECT OF ADDITION OF ACETONITRILE TO THE MOBILE PHASE ON THE CAPACITY FACTOR (k') OF ALL-*trans* α-CAROTENE AND ON THE SEPARATION OF *cis* AND *trans* β-CAROTENES ON DIFFERENT C_{18} BONDED COLUMNS

Columns	k' of α-carotene with 15% organic modifier		Separation of β-carotene *trans*/*cis* isomers with 15% organic modifier [methanol–acetonitrile (1:1, v/v)]
	Methanol	Methanol–acetonitrile (1:1, v/v)	
Ultrabase UB 225	12.58	10.91	Yes
Spheri-5 ODS-5A	12.85	10.69	No
LiChrospher 100 RP 18	10.57	9.95	No
LiChrospher 100 RP 18e	12.05	9.4	No
Nucleosil C_{18}	6.66	6.15	Yes
ChromTech CT-Sil C_{18}	8.36	7.1	Yes
Superspher 100 RP-18	8.02	7.08	Yes
Spherisorb ODS-2	9.73	8.48	No

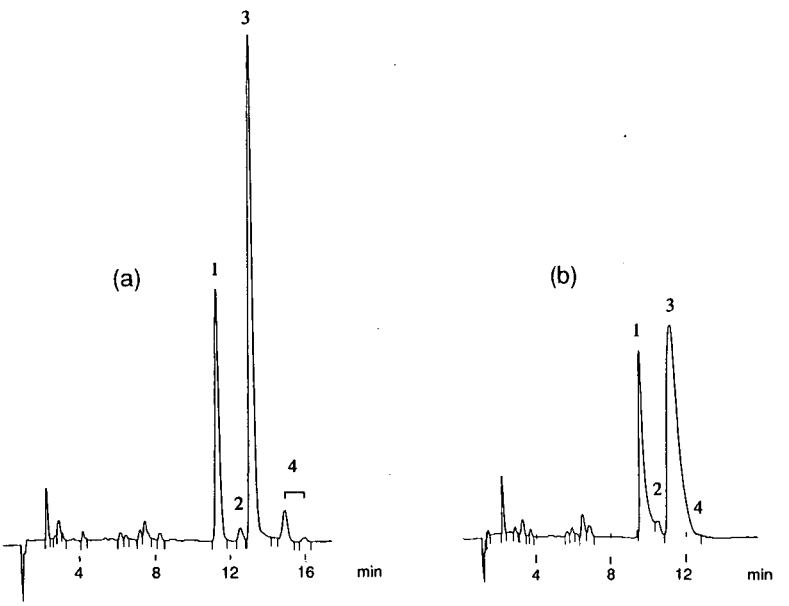

Fig. 4. Influence of the organic modifier on the chromatographic profile of a carrot extract analysed on an arborescent-polymeric column (Spheri-5 ODS-5A; 250 × 4.6 mm I.D.). Mobile phase: (a) carbon dioxide–methanol (85:15, v/v), (b) carbondioxide–methanol–acetonitrile (85:7.5:7.5, v/v). Temperature 22°C, pressure 15 MPa, flow-rate 3 ml/min, λ = 450 nm. Identification of peaks: see legend to Fig. 2. The early-eluting peaks are probably oxygen-containing degradation products.

give a capacity factor of at least 6 under the described conditions. The only column that deviated from this rule was Suplex pKb-100, which gave an adequate separation with a capacity factor of less than 6. However, the packing material of this column has been specially treated, in a manner that has not been divulged, to render it suitable for the chromatography of basic compounds.

Separation of the cis and trans isomers of α- and β-carotenes. The simultaneous separation of the *cis* and *trans* α- and β-carotenes was achieved on 8 of the 22 columns that were tested. Of these, six columns were of the arborescent-polymeric type: Spheri-5 ODS-5A, LiChrospher 100 RP 18, LiChrospher 100 RP 18e, Superspher 100 RP18 and Nucleosil C_{18}. In the four cases where capacity factors were less than 10 under the conditions that were optimal for Spheri 5 ODS-5A (ChromTech CT-Sil C_{18}, Superspher, Spherisorb ODS-2 and Nucleosil C_{18}), it was necessary to reduce the concentration of mobile phase modifier to 5 or 10% in order to obtain a clean separation of the *cis* isomers of α-carotene (Fig. 2). The consequent increase in retention times could be reduced by raising the pressure to 200 bar. The shortest analysis times (less than 8 min for a complete separation) were provided by ChromTech CT-Sil C_{18} and Spherisorb ODS-2 columns, which are the shortest of those tested (Fig. 3).

The quality of the separation obtained on the Ultrabase column is surprising for a monofunctional stationary phase (See Fig. 9 of preceding paper [11]). As with the Suplex pKb-100 column mentioned in the previous section, this column is specially deactivated for the analysis of basic compounds. Clearly, the proprietary treatment modifies the chromatographic properties for non-basic compounds.

Effects of the mobile phase modifier as a function of the stationary phase. The kinetics of mass transfer between the phases is influenced by the nature of the mobile phase modifier [14]. In the chromatography of phenolic compounds on unmodified silica, the addition of acetonitrile to the mobile phase leads to severe peak broadening, and in certain cases a loss of selectivity. We tested the effects of replacing half of the methanol in the mobile phase with acetonitrile (carbon dioxide–methanol–acetonitrile, 85:7.5:7.5, v/v/v), for the chromatography of carrot carotenes on the eight columns that gave a complete separation (Table II). In all cases, the capacity factors were reduced. With four of the columns, neither efficiency nor selectivity was

TABLE III

PERCENTAGE OF ACETONITRILE THAT PRODUCES A SIGNIFICANT LOSS IN EFFICIENCY ON DIFFERENT OCTADECYL-BONDED COLUMNS, IN RELATION TO THE CAPACITY FACTOR OF ALL-*trans* α-CAROTENE

Columns	k' of α-carotene with with 15% organic modifier [methanol–acetonitrile (1:1, v/v)]	Acetonitrile (%)
Spheri-5 ODS 5A	10.69	5
LiChrospher 100 RP 18	9.95	50
LiChrospher 100 RP 18e	9.4	70
Spherisorb ODS-2	8.48	95

reduced, and, as noted previously [11], a previously undetected peak was resolved when acetonitrile was used.

However, with the remaining four columns (Spheri-5 ODS-5A, LiChrospher 100 RP 18, LiChrospher 100 RP 18e and Spherisorb ODS-2) the peaks were broadened, so that the resolution between the *cis* and *trans* isomers was reduced (Fig. 4). These four columns, which are arborescent-polymeric, have the greatest carbon loadings of the columns of this type that were tested. It appears from the data in Table III that the deleterious effect of acetonitrile is directly correlated with the carbon loading (as estimated from the capacity factors). The peak broadening did not occur with the monofunctional Ultrabase column, despite its high carbon loading ($k' = 12.6$).

CONCLUSION

Both the type and the percentage carbon loading of the stationary phase influence the separation of the carotenes by SFC. Except for Ultrabase UB225, the stationary phases of the monofunctional type do not separate the *cis* and *trans* isomers. On arborescent-polymeric columns, the separation of α- and β-carotenes is incomplete if the capacity factor for α-carotene is below 6. Where the capacity factor is above 9.5 under the described conditions (high percentage carbon loading), the efficiency of the column decreases if part of the methanol in the mobile phase is replaced by acetonitrile; with less heavily loaded supports, the nature of the mobile phase modifier is relatively unimportant.

REFERENCES

1 K. Karch, T. Sebastian and I. Halász, *J. Chromatogr.*, 122 (1976) 3.
2 J. J. Kirkland and J. J. DeStefano, *J. Chromatogr. Sci.*, 8 (1970) 309.
3 S. A. Wise and L. C. Sander, *J. High Resolut. Chromatogr. Chromatogr. Commun.*, 8 (1985) 248.
4 L. C. Sander and S. A. Wise, *J. High Resolut. Chromatogr. Chromatogr. Commun.*, 11 (1988) 383.
5 R. J. Buschway, *J. Agric. Food Chem.*, 34 (1986) 409.
6 F. W. Quackenbush and R. L. Smallidge, *J. Assoc. Off. Anal. Chem.*, 69 (1986) 767.
7 E. Lesellier, C. Marty, C. Berset and A. Tchapla, *J. High Resolut. Chromatogr. Chromatogr. Commun.*, 12 (1989) 447.
8 R. Rosset, *Analusis*, 15 (1987) 1.
9 A. Tchapla, H. Colin and G. Guiochon, *Anal. Chem.*, 56 (1984) 621.
10 S. Heron and A. Tchapla, *J. Chromatogr.*, 556 (1991) 219.
11 M.-C. Aubert, C. R. Lee, A. M. Krstulović, E. Lesellier, M.-R. Péchard and A. Tchapla, *J. Chromatogr.*, 557 (1991) 47.
12 A. M. Krstulovic, H. Colin and G. Guiochon, *Anal. Chem.*, 54 (1982) 2438.
13 F. Riedo and E. Kováts, *J. Chromatogr.*, 239 (1982) 1.
14 P. Mourier, *Thesis*, Paris VI University, Paris, 1986.

Journal of Chromatography, 557 (1991) 69–83
Elsevier Science Publishers B.V., Amsterdam

CHROM. 23 391

Magnitude of the diffusion coefficient anomaly in the critical region and its effect on supercritical fluid chromatogrpahy

K. D. BARTLE, D. L. BAULCH, A. A. CLIFFORD* and S. E. COLEBY
School of Chemistry, University of Leeds, Leeds LS2 9JT (UK)

ABSTRACT

Literature measurements of diffusion in a supercritical fluid, especially those of naphthalene in supercritical fluid carbon dioxide, are discussed. These show that at very high dilution there is no measurable anomaly, but that large reductions in the apparent diffusion coefficient are observed at higher, though still low, concentrations. Three effects contributing to the anomaly are described: those of chemical potential, augmented density and fluid motion. Measurements were made of the effect of on-column naphthalene solute concentration on column efficiency in supercritical fluid chromatography using carbon dioxide as the mobile phase. The experiments were performed at 35°C (308 K) at a variety of mobile phase densities and a constant linear flow-rate. The results are interpreted in terms of the above-mentioned phenomena and their implications for the Van Deemter and Golay equations. Calculations of quantities related to chemical potential, augmented density and fluid motion were performed for the same system (naphthalene in carbon dioxide) in order to estimate their importance. The significance of the diffusion coefficient anomaly for analytical and preparative supercritical fluid chromatography is discussed.

INTRODUCTION

Since supercritical fluid chromatography (SFC) is usually carried out at flow-rates above the optimum for the minimum theoretical plate height, h_{min}, as a compromise between satisfactory resolution and workable analysis time, the C_m term in the Van Deemter equation for h in terms of the mean mobile phase velocity u,

$$h = A + B/u + C_m u + C_s u \quad (1)$$

makes an important contribution. C_m is inversely proportional to the diffusion coefficient of the solute in the mobile phase, D_m, as it arises from the variation of velocity in the mobile phase and is reduced by the effect of diffusion across the velocity profile. The principal advantage of SFC over liquid chromatography is that D_m is higher in supercritical fluids, allowing greater efficiency of separation or shorter analysis times.

Transport properties, such as diffusion, in supercritical fluids can exhibit so-called anomalous behaviour in the critical region [1], meaning that their values undergo a variation, which is sometimes dramatic, at temperatures just above the critical temperature and around the critical density. The diffusion coefficient tends to zero at

0021-9673/91/$03.50

the critical point and along an isotherm above the critical temperature exhibits a drop, which is a maximum close to the critical density. In the limit of infinite dilution, this "anomaly" becomes vanishingly small.

Thus, chromatographic peak widths in SFC should be greater in the region around the critical point than away from it, and some of its advantage over liquid chromatography may be lost. There are two reasons why this is often inconsequential. First, chromatography is usually carried out at low concentrations which are close enough to the infinite-dilution limit for the diffusion coefficient anomaly to be negligible. However, measurements of diffusion coefficients using the chromatographic peak-broadening effect have sometimes been found to be affected by the amount of solute injected [2]. (It should be noted that preparative-scale SFC uses moderate solute concentrations, so the diffusion coefficient anomaly may then be important.) Second, the maximum in the anomaly is associated with the critical density. SFC is carried out at pressures above the critical pressure: increasing the temperature above the critical temperature will shift the maximum to higher pressures. The purpose of this study was to investigate the extent of the anomaly in the diffusion coefficient for a solute in high dilution, both experimentally and by thermodynamic argument, using the system of naphthalene in carbon dioxide, and to discuss its significance for SFC.

LITERATURE MEASUREMENTS OF DIFFUSION COEFFICIENTS IN SUPERCRITICAL FLUIDS

The large number of experimental measurements of diffusion coefficients in supercritical fluids fall into two classes. First, there are those made by chromatographic peak broadening (also known as Taylor dispersion), under conditions which approximate infinite dilution and mostly show no measurable anomaly in the critical region. The latter include measurements made by a variety of measurements at higher concentrations, which can show large anomalies.

The results of measurements of the former type for naphthalene in carbon dioxide at 313 K, made by a number of workers [3–5], are shown in Fig. 1 as a graph of ρD_m *vs.* density, ρ. Also shown is a value of ρD_m close to zero density calculated from the value measured in air [6] using rigorous kinetic theory [7]. The continous line in Fig. 1 gives the predictions of Thorne–Enskog theory [7], which is expected to be valid, at least qualitatively, at lower densities. Hence, the quantity ρD_m does not change dramatically over the whole density range and its general form is given by the dashed line. The curve falls initially with density, in accordance with Thorne–Enskog theory, and then rises to a fairly level region. We suggest that the rising portion of the curve is due to the fall in the rate of rotational diffusion with density, whereas edgewise motion of the naphthalene molecules persists longer.

Measurements of the diffusion coefficient of naphthalene in carbon dioxide at higher concentrations have been made by Tsekhanskaya [8] at 308 K. These show a dramatic drop from a value of $4.8 \cdot 10^{-9}$ m^2 s^{-1} at a density of 250 kg m^{-3} to $0.006 \cdot 10^{-9}$ m^2 s^{-1} near the critical density and then a rise to a value of $6.9 \cdot 10^{-9}$ m^2 s^{-1} at a density of 592 kg m^{-3}. As is explained in the next section, this fall is not all due to a decrease in the diffusion coefficient itself.

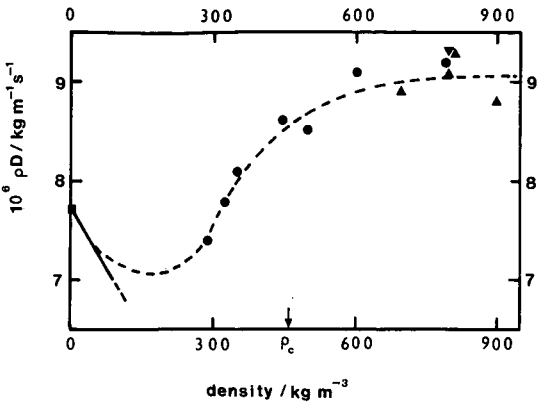

Fig. 1. Plot of the product of the diffusion coefficient, D_m, and density ρ, for naphthalene in dilute solution in carbon dioxide at 313 K: ■ = calculated from D_m in air [6]; ● = Feist and Schneider [3]; ▲ = Lauer *et al.* [4]; ▼ = Funazukuri *et al.* [5]. The arrow shows the critical density.

EXPERIMENTAL

The effects on peak width of solute concentration and mobile phase density in the critical region were studied using a Lee Scientific 501 supercritical fluid chromatograph (Dionex). Solutions of naphthalene (Gold Label, scintallation grade, 99 + %; Aldrich) in dichloromethane (DCM) (high-performance liquid chromatographic grade, 99.8 + %, May and Baker) were injected onto a phenyl-substituted polysiloxane capillary column, 15 m × 100 μm I.D. (Lee Scientific). The column dimensions were selected to maximize the residence time and facilitate the measurement of any anomalous effects.

The temperature of the system was maintained at 35.0°C by immersing the complete column in a water-bath. The temperature was monitored by a chromel thermocouple connected to a digital voltmeter (Keithly) with an accuracy of ±0.001 mV. Measurements were made within a temperature range expressed as (35.000 ±0.085)°C. The flow-rate of carbon dioxide (SFC grade; Air Products) was regulated by means of different lengths of linear restrictor tubing (12 μm I.D.) (Polymicro Technologies), butt-connected to the main capillary column. The lengths of linear restrictors were in the range 58.5–75.0 cm. The apparatus is shown schematically in Fig. 2. The pressure was programmed to give a retention time of the unretained peak (the injection solvent) of 19.67 min at each linear restrictor length, so that mean linear flow-rate, u, of the Golay equation was constant throughout the experiments. Densities corresponding to the experimental temperature and pressure were calculated using a principle of corresponding states method.

The pneumatic injection valve (A90; Valco) was fitted with a 60-nl sample loop. The long injection time of 6 s ensured that the entire contents of this loop were delivered onto the column. At the residence times used, this was assumed not to distort the peak shape appreciably from Gaussian.

Flame ionization at 400°C detection was applied. The flow-rate of hydrogen was 30 cm^3 min^{-1} and of air 300 cm^3 min^{-1}. The make-up gas was helium at 28 cm^3

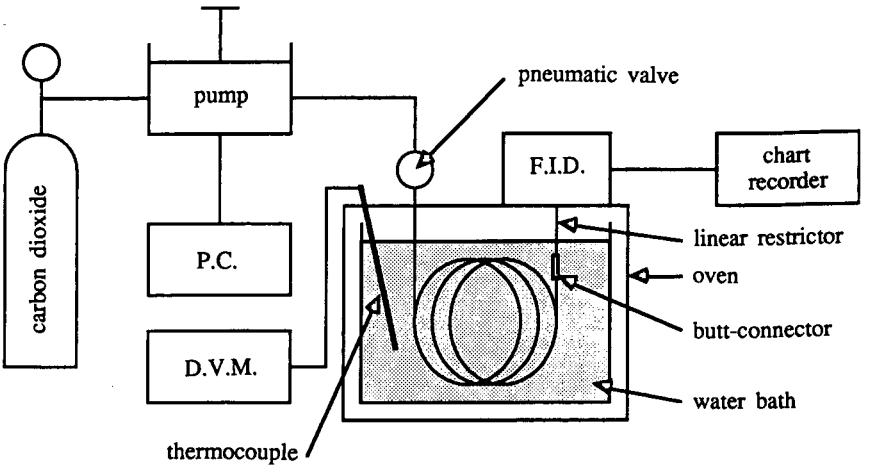

Fig. 2. Schematic diagram of the apparatus in which the experiments were performed. P.C. = personal computer; D.V.M. = digital voltmeter; F.I.D. = flame ionization detector.

min^{-1}. Output was relayed to a potentiometric chart recorder (Smiths) operating at speed of 120 mm min^{-1}. The baseline width of the solute peak was measured from the recorder trace. This, with a knowledge of the column dimensions and mean mobile phase flow-rate, permitted the calculation of the peak volume at elution.

The peak volume at detection was assumed to be representative of the solute peak volume travelling down the column, especially as peak broadening is a function of the square root of residence time, *i.e.*, half the broadening occurs after one quarter of the passage along the column. At a known density, and given a desired mole fraction of naphthalene in carbon dioxide on the column, the appropriate concentration of naphthalene in DCM to be injected can be determined.

At each density studied, at least five replicate runs were made for solutions of naphthalene in DCM equivalent to on-column mole fraction concentrations of $1 \cdot 10^{-4}$, $2 \cdot 10^{-4}$, $3 \cdot 10^{-4}$ and $4 \cdot 10^{-4}$. The differences in the retention times of the unretained injection solvent, DCM, and the solute, denoted $t_r - t_m$, and the width at half-height, $w_{d_{0.5}}$, were measured from the chart recorder traces to an accuracy of ± 0.05 cm, and used to determine the efficiency of the column as a function of solute concentration at a variety of densities.

RESULTS AND DISCUSSION

The expanded Golay equation for capillary columns is

$$h = \frac{2D_m}{u} + \frac{d_c^2(1 + 6k + 11k^2)u}{96(1 + k^2)D_m} + \frac{2kd_f^2u}{(1 + k)^2D_s} \qquad (2)$$

where u is the average mobile phase velocity along the column d_c is the column inside diameter, k is the capacity ratio, d_f is the stationary phase film thickness and D_m and

TABLE I

EXPERIMENTAL DATA, AT 35.0°C, FOR DIFFERENCES OF RETENTION OF THE SOLUTE PEAK AND UNRETAINED SOLVENT PEAK AT $t_r - t_m$ AND THE WIDTH AT HALF-HEIGHT, $w_{d0.5}$, OF THE NAPHTHALENE SOLUTE PEAK

35.0°C		Concentration (mole fraction of naphthalene)							
p (bar)	ρ (kg m^{-3})	$1 \cdot 10^{-4}$		$2 \cdot 10^{-4}$		$3 \cdot 10^{-4}$		$4 \cdot 10^{-4}$	
		$t_r - t_m$ (cm)	$w_{d0.5}$ (cm)	$t_r - t_m$ (cm)	$w_{d0.5}$ (cm)	$t_r - t_m$ (cm)	$w_{d0.5}$ (cm)	$t_r - t_m$ (cm)	$w_{d0.5}$ (cm)
78.0	407.1	17.02	3.45	17.12	3.55	17.05	3.65	16.89	3.73
79.8	458.5	16.17	3.54	16.15	3.69	16.18	3.87	16.16	4.08
80.4	474.6	16.13	3.55	16.12	3.71	16.19	3.98	16.22	4.16
81.7	507.3	16.11	3.47	16.15	3.56	16.22	3.73	16.22	3.85
83.0	547.6	15.70	3.29	15.63	3.37	15.71	3.52	15.76	3.72
85.5	602.9	15.53	3.21	15.60	3.27	15.64	3.34	15.72	3.37
90.0	671.0	14.74	2.91	14.86	2.98	14.91	2.93	14.99	3.02

D_s are the diffusion coefficients in the mobile and stationary phase, respectively. Under SFC conditions, which normally operate at flow-rates above the optimum for maximum efficiency (typically by a factor of ten), the term in C_m of the Van Deemter equation (eqn. 1) increases the significance of its contribution relative to the term in B.

In order to obtain results which could be compared in terms of diffusional effects on the Golay equation for column efficiency, it was essential to perform chromatographic separations at the same mean linear flow-rate of the mobile phase and with the same on-column concentration of naphthalene. The manner in which this was done is outlined under Experimental. The flow-rate used in this study was 1.277 cm s^{-1}.

Table I gives the retention differences of the solute peak and the unretained solvent peak (DCM) as $t_r - t_m$ and the width at half-height of the naphthalene solute peak. The former value was found to be in the region of 16 min. However, at densities above 474.6 kg m^{-3} the peaks of solute at high concentration were generally retained longer than those at low concentrations, whereas below this density the reverse applied. The effect was not marked under the conditions used. At all densities, the width at half-height, $w_{d0.5}$, was found to increase with increasing concentration. This phenomenon increased in magnitude with increasing density to a density close to 474.6 kg m^{-3} (note that the critical density, *i.e.*, the density at the critical temperature and pressure, of carbon dioxide is 470.1 kg m^{-3}). Any further increase in density to the limit of the study (671.0 kg m^{-3}) was observed to reduce the magnitude of the effect. At densities higher than 671.0 kg m^{-3}, any effects were of the same order of magnitude as the experimental uncertainties.

Fig. 3 shows a plot of h, derived from the experimental values, *versus* the density of the mobile phase, ρ. The number of plates in the column, and the corresponding plate heights, determined from the experimental data are given in Table II. The heights evaluated under these experimental conditions are slightly larger than those generally used in SFC (typically of the order of 0.2 mm at ten times the optimum

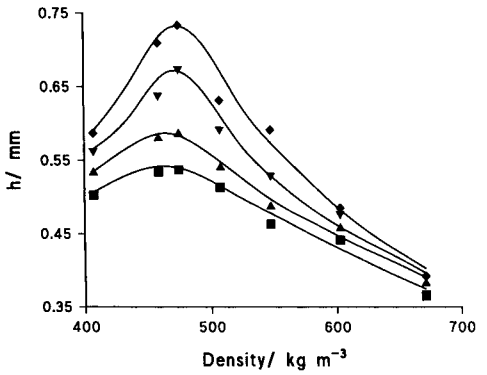

Fig. 3. Plot of the experimentally derived h *versus* density, ρ. Lines join data of the same on-column concentrations of naphthalene, x_2: ■, $x_2 = 1 \cdot 10^{-4}$ mole fraction; ▲, $x_2 = 2 \cdot 10^{-4}$ mole fraction; ▼, $x_2 = 3 \cdot 10^{-4}$ mole fraction; ◆, $x_2 = 4 \cdot 10^{-4}$ mole fraction.

mean linear flow-rate, $10u_{opt}$, on the preferred 50 μm I.D. column and 0.4 mm at $10u_{opt}$ on a 100 μm I.D. column). The effect of concentration on h is depicted in Fig. 4 over the range of densities studied.

Peak broadening arises from a reduction in the diffusive transport, behaviour typified by a heavier solute in a supercritical fluid in the critical region. Three factors contribute to this effect. The first is a reduction in the diffusion coefficient itself. According to non-equilibrium themodynamics [9,10], the diffusive flux is driven by the gradient of chemical potential rather than concentration, although it is defined in terms of the latter. The theoretical expression for D_m therefore contains the important factor

$$\zeta = (1/RT)(\delta\mu_2/\delta \ln x_2)_{p,T} \tag{3}$$

TABLE II

NUMBER OF PLATES IN THE COLUMN, n, DERIVED FROM THE EXPERIMENTAL DATA, AT 35.0°C, AND THE CORRESPONDING PLATE HEIGHTS, h

35.0°C		Concentration (mole fraction of naphthalene)							
p (bar)	ρ (kg m^{-3})	$1 \cdot 10^{-4}$		$2 \cdot 10^{-4}$		$3 \cdot 10^{-4}$		$4 \cdot 10^{-4}$	
		n	h (mm)	n	h (mm)	n	h (mm)	n	h (mm)
78.0	407.1	29 798	0.503	28 165	0.533	26 629	0.563	25 534	0.587
79.8	458.5	28 112	0.534	25 869	0.580	22 243	0.638	21 161	0.709
80.4	474.6	27 945	0.537	25 584	0.586	22 243	0.674	20 463	0.733
81.7	507.3	29 244	0.513	27 793	0.540	25 331	0.592	23 776	0.631
83.3	547.6	32 425	0.463	30 887	0.487	28 329	0.529	25 374	0.591
85.5	602.9	34 016	0.441	32 797	0.457	31 447	0.477	30 909	0.485
90.0	671.0	41 134	0.365	39 259	0.382	40 627	0.369	38 266	0.392

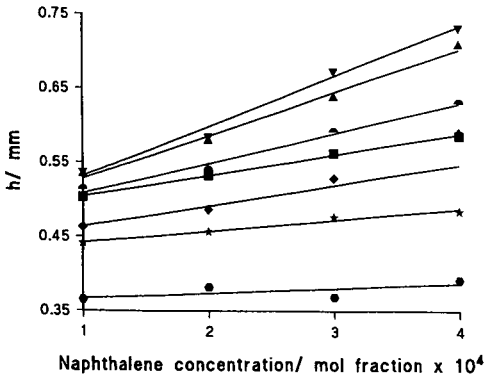

Fig. 4. Plot of the experimentally determined h as a function of on-column mole fraction concentration, x_2, of naphthalene. The data are shown for a variety of densities: ■, 407.1; ▲, 458.5; ▼, 474.5; ◓, 507.3; ◆, 547.6; ★, 602.9; ●, 671.0 kg m^{-3}.

where μ_2 is the chemical potential of the solute and x_2 its mole fraction. At the critical point ζ tends to zero, except at the limit of infinite dilution. The physical explanation of this is that, towards the critical point, a situation is approached in which the fluid will split into two phases in which the solute will have the same chemical potential but different concentrations (except in the limit of zero concentration where both concentration are tending to zero).

The second factor is a smaller one, but it does reinforce the above effect. Arising because of the attraction of the heavier solute molecule for the solvent molecules, it results in a solvent density in the region of the solute peak which is higher than that in the column as a whole. This augmentation of local solvent density is largest in the critical region. As shown in Fig. 5, the quantity ρD_m usually does not change greatly with density, and the diffusion coefficient will be lower in the region of the solute peak by a factor of around ρ_0/ρ, where ρ is the density in the presence of solute and ρ_0 is the density of the pure solvent.

Finally, a more serious effect, which is difficult to quantify, concerns fluid motion during the diffusion process. The diffusion coefficient and the fluxes of solute to which it relates are defined barycentrically, *i.e.*, with respect to the mass of the fluid at any point, and therefore the frame of reference will be in motion. In chromatography, there will be the motion of the fluid along the column, with velocity increasing towards the centre of an open capillary or passage through a packed column, which is taken into account in the theory of chromatography. There will be additionally, however, a motion of the fluid towards any region in which the concentration is increased by the diffusion process, in order to achieve the higher density corresponding to the higher concentration. This motion will mean that the flux of solute with respect to space-fixed coordinates is different to that with respect to the barycentre. In accurate liquid diffusion studies in static cells, this effect is taken into account: a one-dimensional solution to the problem is sufficient [11]. In SFC in the critical region this is potentially a more serious effect, and a three-dimensional solution is required. It can be shown [12] that the fluid velocity, $\mathbf{v}$ arising from this effect is related to the flux of the solute, $\mathbf{J}_2$, by

$$\mathrm{div}\mathbf{v} = -\rho(V_2/M_2 - V_1/M_1)\mathrm{div}\mathbf{J}_2 \qquad (4)$$

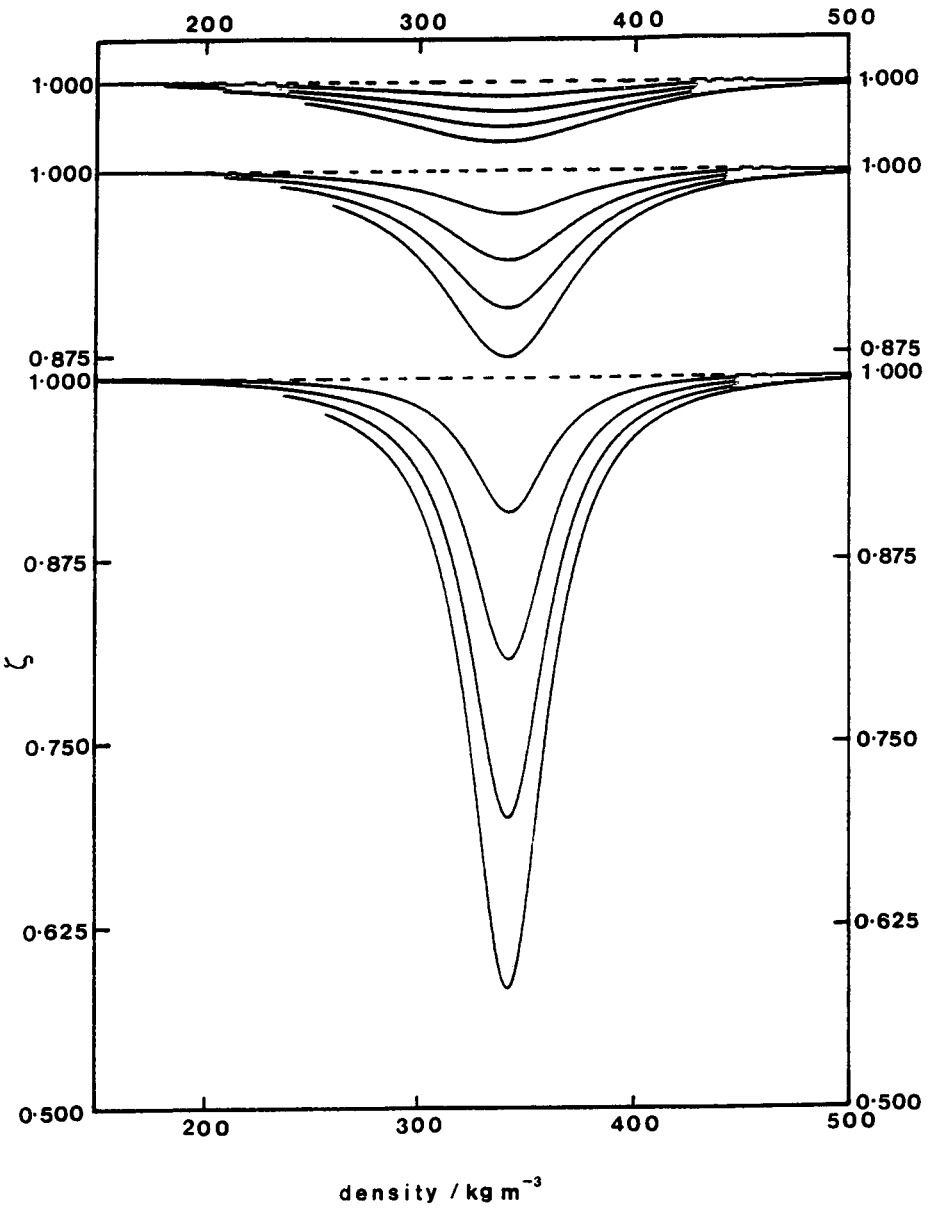

Fig. 5. Plots of ζ *versus* density, ρ, for solutions of naphthalene in carbon dioxide at temperature 1, 3 and 9 K above the critical temperature of the pure solvent, calculated from the Van der Waals equation. Mole fractions of naphthalene are $1 \cdot 10^{-4}$, $2 \cdot 10^{-4}$, $3 \cdot 10^{-4}$, and $4 \cdot 10^{-4}$, with deviations of ζ from unity increasing with increasing concentration. The scale factor on the ζ axis is the same at all three temperatures. Note that the critical density according to the Van der Waals equation, with the parameters used, is 343 kg m^{-3}.

where V_1 and V_2 are partial molar volumes and M_1 and M_2 are the molar masses of the solvent and solute, respectively. In the critical region, the partial molar volumes of

typical solutes are large and negative, as will be discussed in more detail in the next section. The effect is therefore potentially a large one, but is also proportional to the rate of change of solute flux with distance, and thus will also become negligible in the limit of infinite dilution.

Two examples of this third effect are now discussed. First, when a solid is being dissolved into a supercritical fluid, the flux of solute falls off with increasing distance from the solid surface and so, according to eqn. 4, there is fluid motion towards this surface, reducing the solute transport away from the solid with respect to space-fixed coordinates. This contributes to the reduction in the diffusive flux observed in the Tsekhanskaya diffusion experiment [8], for example. As a second example, in the case of a one-dimensional Gaussian distribution of solute concentration, application of eqn. 4 shows that the fluid moves away from the centre of the distribution, with the velocity rising from zero at the centre to a maximum and then falling towards zero at the edges. These, therefore, are two contrasting examples. In the first, new solute is being introduced, which attracts solvent towards it, reducing the diffusive flux. In the second, the solute already in solution transports its associated solvent molecules with it as it moves, increasing the diffusive flux with respect to space-fixed coordinates.

The incorporation of this effect into the theory of chromatography is a daunting prospect, as the dependence of D_m, ρ and $\mathbf{v}$ on concentration make the diffusion equation, solved for example in the Golay treatment [13], non-linear. The situation is further complicated by the fact that, because of the fluid motion associated with diffusion, a full hydrodynamic analysis may be necessary, which takes into account viscous and inertial effects in addition to solving the diffusion equation. In the absence of a proper analysis, the following qualitative argument and conclusion seem likely to be valid. The solute peak, averaged over the cross-section of the tube, travels along an open chromatographic column in an approximately Gaussian form with respect to the longitudinal coordinate. As it travels it is spread by various effects corresponding to the terms in eqn. 1 and when this happens it is further spread by fluid motion away from the centre of the peak, as in the Gaussian example above. Thus, fluid motion will cause increased spreading in SFC, especially in the critical region. This effect is difficult to quantify, but will be less important for very dilute solutions.

Thermodynamic arguments for a diffusion coefficient anomaly

In this section estimates are made of the quantities illustrating the importance of the genuine reduction in mutual diffusion coefficient itself (via chemical potential), augmented density and fluid motion. The Van der Waals equation of state is used, and although this is less successful than later equations in predicting thermodynamic quantities which agree with experiment; it is adequate for the purpose of estimating the importance of the effects. The simpler form of the Van der Waals equation,

$$p = RT/(V-b) - a/V^2 \tag{5}$$

is used, where p is the pressure, V the molar volume and the constants a and b are given by

$$a = [(a_{11})^{1/2}x_1 + (a_{22})^{1/2}x_2]^2$$

$$a_{12} = (a_{11}a_{22})^{1/2}$$

$$b = b_1x_1 + b_2x_2 \tag{6}$$

The Van der Waals parameters used for carbon dioxide were $a_{11} = 0.364675$ J m^3 mol^{-1} and $b_1 = 42.7514 \cdot 10^{-6}$ m^3 mol^{-1}, calculated from a critical temperature of 304 K and a critical pressure of 7.39 MPa [14] (the large number of significant figures used ensures that the predicted critical temperature of the pure solvent is close to 304 K). The corresponding values for naphthalene used were $a_{22} = 3.97$ J m^3 mol^{-1} and $b_2 = 189 \cdot 10^{-6}$ m^3 mol^{-1} obtained from a critical temperature of 758 K and a critical pressure of 4.11 MPa [14].

Quantities related to these three effects are now made. For the first of these, the diffusion coefficient itself, the relevant parameter is ζ, defined by eqn. 3. This can be shown, by using standard thermodynamic procedures and the Van der Waals equation, to be given by

$$\zeta = 1 - [2x_1x_2/RTV^2(V-b)^2\varphi]\{(a_{11}+a_{22}-2a_{12})V + a(b_1-b_2)/V - 2[(a_{11}-a_{12})x_1 - (a_{22}-a_{12})x_2](b_1-b_2)\} \tag{7}$$

where

$$\varphi = 1(V-b)^2 - 2a/RTV^3 \tag{8}$$

Sample calculations were made and are shown in Figs. 5 and 6. Fig. 5 shows ζ falling below unity around the critical density to an extent increasing with concentration and proximity to the critical temperature. The curves are only shown for condition where correlations of experimental solubilities [15] using the Peng–Robinson equation of state [16] indicate that saturation has not occured. Fig. 5 shows that a decrease in ζ by about half can occur 1 K above the critical temperature of the pure solvent, but that the decrease is only a few percent 9 K above the critical temperature. These plots compare with Fig. 3, the variation of h with density at the same four concentrations, almost as inversions. Note, however, that results of calculations are not shown for the precise experimental temperature. Fig. 6 shows the values for the highest concentration plotted as a function of pressure. Here the effect is sharper and moves to higher temperature, both these features reflecting the p–V–T behaviour of the fluid.

For the second effect, that of increased density, calculations of ρ_0/ρ were made and are shown in Fig. 7 as a function of pressure. This is seen to be a smaller effect, which does, however, reinforce the first.

The third effect, arising from fluid motion, is a function of the differences in the partial molar volumes of the solute and solvent. Calculations of this quantity for the solvent, V_1, show that it is not markedly different from the molar volume of pure carbon dioxide at the same temperature and pressure. V_2, for the solute, is given by

$$V_2 = [1/(V-b) + b_2/(V-b)^2 - 2(a_{12}x_1+a_{22}x_2)/RTV^2]/\varphi \tag{9}$$

according to the Van der Waals equation.

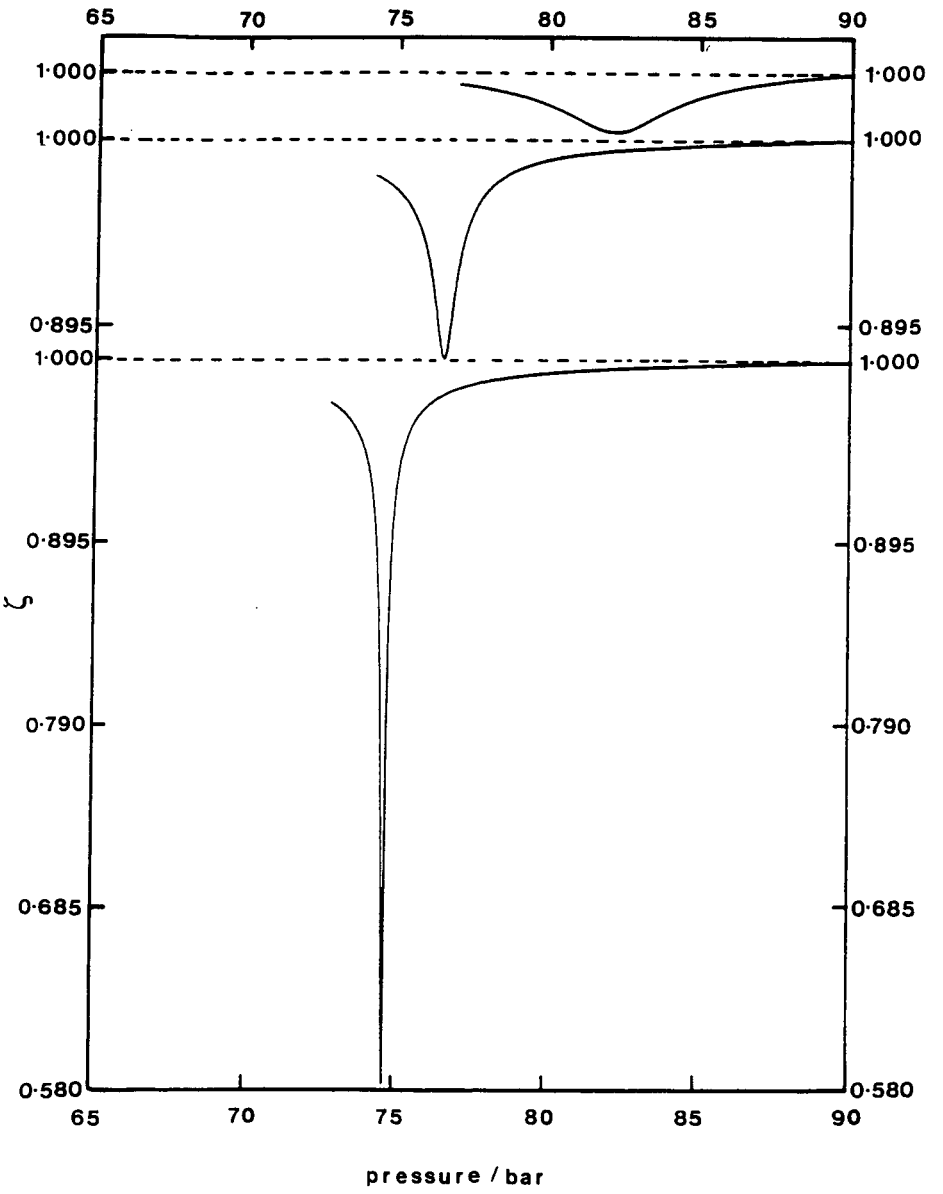

Fig. 6. Plots of ζ *versus* pressure, p, for solutions of naphthalene (mole fraction $4 \cdot 10^{-4}$) in carbon dioxide at temperatures 1, 3 and 9 K above the critical temperature of the pure solvent, calculated from the Van der Waals equation. The scale factor on the ζ axis is the same at all three temperatures.

Calculations show that V_2 is not sensitive to concentration below the solubility limit for naphthalene. Values are plotted for $x_2 = 4 \cdot 10^{-4}$ in Fig. 8. These demonstrate large negative values even at the highest temperature considered, and a value of -60 dm^3 mol^{-1} at 1 K above the critical temperature of carbon dioxide (this com-

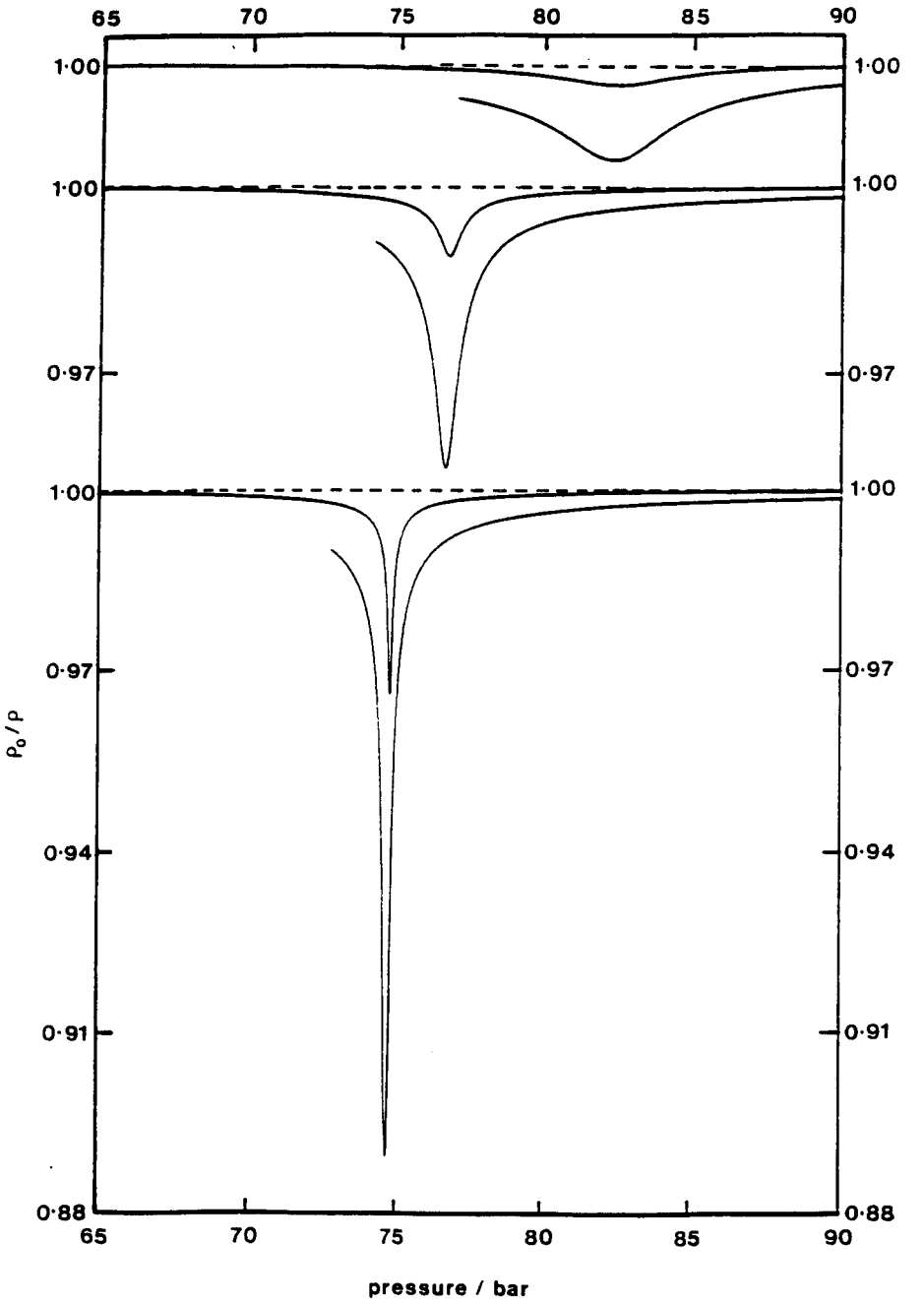

Fig. 7. Plots of ρ_0/ρ *versus* pressure, p, for solutions of naphthalene in carbon dioxide at temperatures 1, 3 and 9 K above the critical temperature of the pure solvent, calculated from the Van der Waals equation. ρ is the density of the mixture and ρ_0 that of the pure solvent at the same temperature and pressure. For the upper curves at each temperature $x_2 = 1 \cdot 10^{-4}$ and for the lower curves $x_2 = 4 \cdot 10^{-4}$. The scale factor on the ρ_0/ρ axis is the same at all three temperatures.

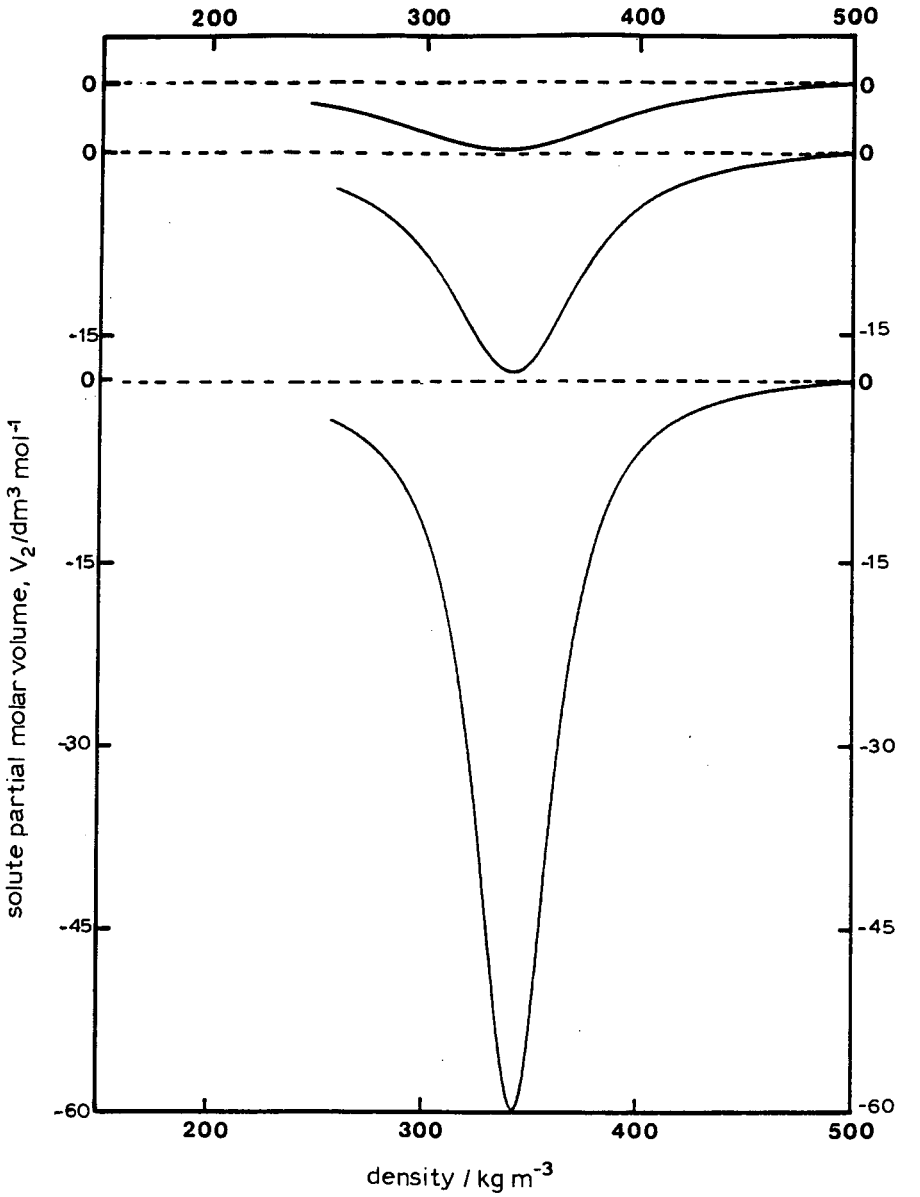

Fig. 8. Plots of the partial molar volume, V_2 of naphthalene of mole fraction $4 \cdot 10^{-4}$ in carbon dioxide at temperatures 1, 3 and 9 K above the critical temperature of the pure solvent, calculated from the Van der Waals equation. The scale factor on the V_2 axis is the same at all three temperatures.

pares with the molar volume of naphthalene of about $+0.2$ dm^3 mol^{-1}). Addition of naphthalene to carbon dioxide at its critical density and 1 K above the critical temperature, to form a solution of $4 \cdot 10^{-4}$ mole fraction (close to saturation), is predicted by the Van der Waals equation to reduce the volume to around half of its orginal value at the same pressure.

The results of calculations given above were obtained for naphthalene. For heavier solutes, the values of a_{22} and to a lesser extent a_{12}, which describe the attractive forces of solute–solute and solute–solvent interactions, respectively, will be greater. The consequence is, via eqns. 8 and 9, that the effects described above increase in magnitude.

CONCLUSIONS

From the calculations and experimental evidence above, it has been demonstrated that the effect of the anomaly in the diffusion coefficient on column efficiency in SFC can be avoided by starting a pressure programme some way above the critical pressure to avoid the region of critical density. The pressure yielding maximum peak broadening will increase from the critical pressure as the temperature is increased from the critical temperature, but the phenomenon diminishes in magnitude with this rise.

Even at 35°C, which is 4°C from the critical temperature, peak broadening was observed to be significant, particularly at a high mole fraction of injected solute, over part of the pressure range employed in the experimental study. Normally this effect should not be important in analytical SFC because of the low concentrations used; the calculations in the previous section show that the diffusion coefficient itself is not much affected with concentrations below mole fractions of 10^{-4} for naphthalene. If the mole fraction is below 10^{-5} the effect is negligible for naphthalene, and probably also for heavier solutes. The concentration limit above which solvent motion affects diffusion has not been quantified. If it is close to or more than that for the diffusion coefficient itself, then the arguments given in the next paragraph are valid. If not, then the limits given should be revised downwards.

In capillary SFC the solute is typically injected in a volume of *ca.* 0.1 μl to give a peak volume at the detector of *ca.* 1 μl. An approximate calculation shows that an injection of 10 ng or less of solute would, therefore, not bring about significant peak broadening in the critical region. For packed-column SFC the corresponding volumes are roughly an order of magnitude larger, and the injection limit would be *ca.* 100 ng. For preparative-scale SFC milligram amounts or higher are used, so the effects would be very significant, in spite of larger peak volumes.

ACKNOWLEDGEMENTS

The authors thank Mr. G. F. Shilstone for carrying out the calculations of naphthalene solubilities and Mr. D. G. Mills for drawing the figures. One of us (S.E.C.) thanks the Science and Engineering Research Council for a research studentship.

REFERENCES

1 J. V. Sengers, *Critical Phenomena: Varenna Lecture Courses L.I.*, Academic Press, New York, 1971.
2 P. R. Sassiat, P. Mourier and R. H. Rosset, *Anal. Chem.*, 59 (1987) 1164.
3 R. Feist and G. M. Schneider, *Sep. Sci. Technol.*, 17 (1982) 261.
4 H. H. Lauer, D. McManigill and R. D. Board, *Anal. Chem.*, 55 (1983) 1370.
5 T. Funazukuri, S. Hachisu and N. Wakao, *Anal. Chem.*, 61 (1989) 118.

6 E. Mack, *J. Am. Chem. Soc.*, 47 (1925) 2468.
7 S. Chapman and T. G. Cowling, *The Mathematical Theory of Nonuniform Gases*, Cambridge University Press, Cambridge, 3rd ed., 1979.
8 Yu. V. Tsekhanskaya, *Russ. J. Phys. Chem.*, 45 (1971) 744.
9 S. R. De Groot and P. Mazur, *Non-equilibrium Thermodynamics*, North-Holland, Amsterdam, 1962.
10 H. J. V. Tyrrell and K. R. Harris, *Diffusion in Liquids*, Butterworths, London, 1984.
11 J. G. Kirkwood, R. L. Baldwin, P. J. Dunlop, L. J. Gosting and G. Kegeles, *J. Chem. Phys.*, 33 (1960) 1505.
12 A. A. Clifford and S. E. Coleby, *Proc. R. Soc. London*, A433 (1991) 63.
13 M. J. E. Golay, in D.H. Desty (Editor), *Gas Chromatography*, Butterworths, London, 1958, pp. 36–55.
14 J. O. Hirshfelder, C. F. Curtiss and R. B. Bird, *The Molecular Theory of Liquids and Gases*, Wiley, New York, 1964.
15 K. D. Bartle, A. A. Clifford and G. F. Shilstone, *J. Supercrit. Fluids*, 2 (1988) 20.
16 D. Y. Peng and D. Y. Robinson, *Ind. Eng. Chem. Fundam.*, 15 (1955) 59.

Journal of Chromatography, 557 (1991) 85–97
Elsevier Science Publishers B.V., Amsterdam

CHROM. 23 372

Packed column supercritical fluid chromatography with carbon dioxide–polar modifiers

Influence of carbon dioxide density on retention

A. VILLERMET, D. THIÉBAUT*, M. CAUDE and R. ROSSET
Laboratoire de Chimie Analytique de l'ESPCI, 10 Rue Vauquelin, 75231 Paris Cedex 05 (France)

ABSTRACT

The influence of the CO_2 density in mixed mobile phases containing methanol, acetonitrile or carbon tetrachloride was investigated by packed column supercritical fluid chromatography. With bare silica and polystyrene–divinylbenzene (PRP1), the retention of model solutes was found to decrease with increase in the CO_2 density by the same order of magnitude as with neat CO_2 on bare silica. This is thought to be the result of variation in the solvation of the solutes in the mobile phase whereas the solvation of the stationary phase is governed by the amount of modifier in the mobile phase. The same relationship as with pure CO_2 was also found between retention and temperature on bare silica but the maximum retention depended on the boiling point of the solute. Liquid and gas chromatographic like behaviour occurred with silica and PRP1, respectively. Examples of density gradients for improving the separation time and selectivity are given.

INTRODUCTION

Since its revival in the 1980s, supercritical fluid chromatography (SFC) has been extensively studied and much progress has been made concerning the understanding of fundamentals and apparatus has been developed. However, only a few routine industrial applications have been published, despite the advantages of SFC over liquid chromatography (LC) (detection, faster separations) and gas chromatography (GC) (thermolabile compounds), because both LC and GC have reached a high level of sophistication.

With packed columns, SFC has been found to compete with LC for the separation of solutes in a wide polarity range by adding polar modifiers to the supercritical fluid. For example, carbohydrates [1], alkaloids [2], enantiomers [3] and polymers [4] have been successfully separated, generally under isocratic conditions. In contrast, with capillary columns, separations are often carried out with a CO_2 density gradient, because when GC detectors are used, polar modifiers are proscribed.

From the experience gained in our laboratory, we are convinced that SFC is easier to perform with conventional packed columns than capillary columns, essen-

0021-9673/91/$03.50

tially because more reliable devices exist for pressure control and LC injection valves can be used without modification. Unfortunately, the potential of SFC with packed columns will remain unrealized if one cannot take advantage of density programming in combination with complex mobile phases [5].

This paper demonstrates the usefulness of density gradients with carbon dioxide–polar modifier mixtures on packed columns. For complex mixtures, density and polar modifier gradients can be combined to enhance the selectivity.

EXPERIMENTAL

Apparatus

The SFC instrument consisted of a liquid chromatograph modified and commercialized for packed column SFC (Model 2500 M; Varian, Les Ulis, France). It consisted of two piston pumps (Model 2510), one with its head cooled to 0°C to deliver CO_2 and the other delivering modifiers without modification, a mixing chamber, a Valco injection valve with a 10-μl loop, a column oven, UV detector (Model 2550) and a Tescom back-pressure regulator thermoregulated at 30°C in order to avoid freezing during the expansion of the mobile phase. The pressure regulator was modified in the laboratory in order to apply pressure gradients. The knob of the Tescom valve was monitored by an electric motor taken from a Varian Model 4100 liquid chromatograph. The gradient controller of the Model 4100 chromatograph allowed monitoring of the rotation speed of the valve.

Columns

Two types of stationary phase were used: bare silica either LiChrosorb Si 60, 5 μm (15 × 0.46 cm I.D.) or Pecosphere 5C SI, 5 μm (15 × 0.41 cm I.D.) (Perkin-Elmer), and Polystyrene–divinylbenzene, PRP1, 10 μm (25 × 0.41 cm I.D.) (Touzart et Matignon, Vitry-sur-Seine, France). PRP1 was prefered over ODS silica because the retention mechanism has not been clearly elucidated on ODS silica and it has been shown that strong interactions occur between residual silanols and polar solutes. On PRP1, there is no silanol group and apolar partition and according to the solute structure, π–π interactions are responsible for the retention.

Mobile phases

Industrial carbon dioxide was purchased from L'Air Liquide (Paris, France). An increase in CO_2 density was obtained by closing the back-pressure regulator while the CO_2 was delivered at constant flow-rate by the pump. This means that the volumetric CO_2 flow-rate and the linear velocity of the mobile phase decreased slightly as the density increased.

Methanol (Prolabo, Paris, France), acetonitrile (Rathburn, obtained from Chromoptic, Montpellier, France) and carbon tetrachloride (Rathburn, obtained from Chromoptic) were used as modifiers in the mobile phase and were of HPLC grade.

It has been stated that one mechanism by which a polar modifier could influence retention is the density variation due to the amount added to the CO_2 [6]. In order to express the density of the mobile phase simply, in this paper only the CO_2 density will be considered because the percentage of polar modifiers in the mobile phase remained constant during the experiments.

Test solutes

Diphenyl phthalate and substituted polynuclear aromatic hydrocarbons (PAHs) were used as test solutes (Table I).

RESULTS AND DISCUSSION

Influence of density on retention

Bare silica. Fig. 1a and b shows the variation of the test solute capacity factors as a function of the CO_2 density for CO_2–methanol (94.4:5.6, mol/mol) and CO_2–acetonitrile (93.9:6.1, mol/mol) mixtures, respectively. A strong dependence of density on the retention is observed. Fig. 2a and b shows that log k' is a linear function of the density within the range investigated, as already reported for pure CO_2 [7–10]. Comparison of the present data with those reported by Mourier *et al.* [8] demonstrates that the retention decreases with increase in density by the same order of magnitude on bare silica with or without modifiers in the mobile phase. The k' value can be divided by a factor of *ca.* 2 by increasing the density from 0.56 to 0.77 g/cm^3.

These important results emphasize that the CO_2 density is a major parameter affecting retention in SFC with packed columns both with pure CO_2 and with CO_2–polar modifier mixtures. Hence, the influence of density, often neglected with packed columns, must be taken into account for monitoring solute retentions.

Polystyrene–divinylbenzene (PRP1). The variation of k' as a function of the CO_2 density in the mobile phase is shown with methanol (Fig. 3a), acetonitrile (Fig. 3b) and carbon tetrachloride (Fig. 3c) as modifiers.

Again, the solute retentions are strongly dependent on density and the higher the k' the greater is the slope of the line. This effect is much more important for diphenylphthalate, probably owing to the high density of π electrons in this solute. The extent of the variation of k' is of the same order of magnitude as with bare silica with methanol or acetonitrile as modifier. This suggests that the density of CO_2 governs the solute retention by modification of the solubility of the solute in the mobile phase [11]. In contrast, the stationary phase solvation would mostly depend on the modifier used with the CO_2. With carbon tetrachloride as modifier, the effect of CO_2 density is less pronounced.

TABLE I

TEST SOLUTES

Solute	pK_a	Boiling point (°C)
α-Naphthol	9.3	288
β-Naphthol	9.5	289
α-Naphthylamine	10.1	301
α-Naphthaldehyde		291
Benzoic acid	4.2	249
Indeno[1,2,3-*cd*]pyrene	–	–
Diphenylphthalate	–	–
Dodecylbenzene	–	331
Nonadecylbenzene	–	–

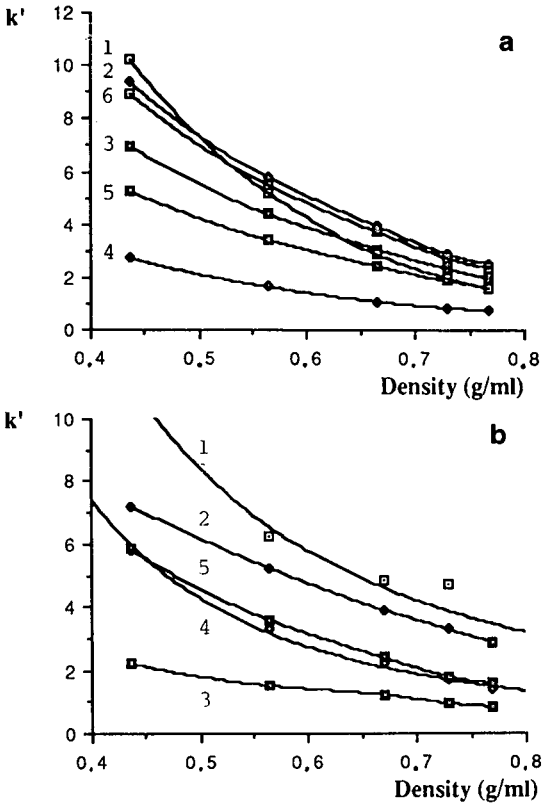

Fig. 1. Variation of solute capacity factors measured on bare silica with the CO_2 density in the mobile phase. Column, 150 × 4.6 mm I.D.; Stationary phase, 5-μm LiChrosorb Si 60; mobile phase, (a) CO_2–methanol (94.4:5.6, mol/mol) and (b) CO_2–acetonitrile (93.9:6.1, mol/mol); flow-rate (0°C), 5 ml/min; detection, UV at 254 nm. Solutes: (a) 1 = indeno[1,2,3-*cd*]pyrene; 2 = α-naphthol; 3 = α-napthylamine; 4 = α-naphthaldehyde; 5 = benzoic acid; 6 = β-naphthol; (b) 1 = β-naphthol; 2 = α-naphthylamine; 3 = α-naphthaldehyde; 4 = indeno[1,2,3-*cd*]pyrene; 5 = diphenyl phthalate.

In the investigated range of density, the retention on PRP1 can be expressed by

$$k' = a - b\rho \tag{1}$$

where a and b are constants. For the solutes studied, except diphenyl phthalate, a and b were found to be similar; consequently, for these solutes eqn. 1 becomes

$$k' = a(1-\rho) \tag{2}$$

This means that the selectivity should remain constant with variation in density (except when diphenyl phthalate is considered).

One must point out that the retentions were higher on PRP1 than silica because the test solutes contained aromatic rings, which strongly interact with those of the stationary phase to give π–π complexes.

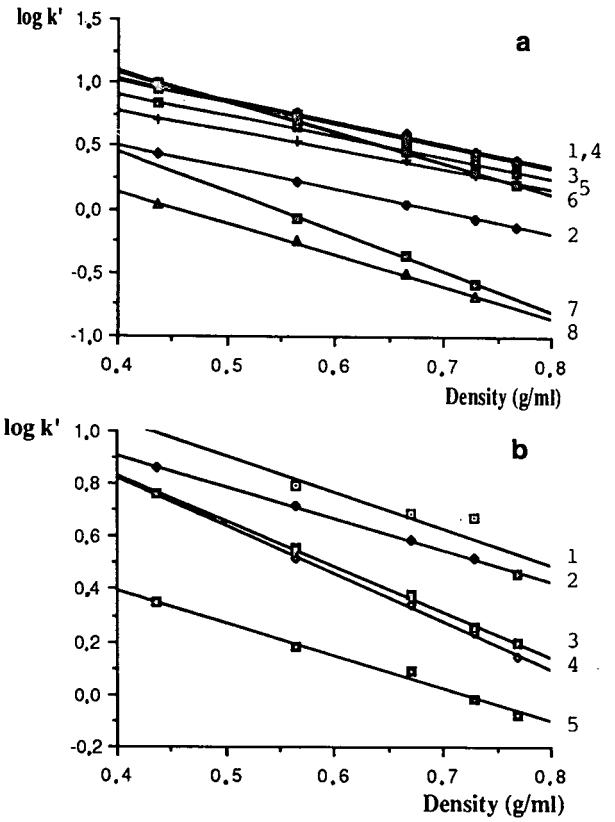

Fig. 2. Variation of logarithm of solute capacity factors on bare silica with the CO_2 density in the mobile phase. Conditions as in Figure 1. Solutes: (a) 1 = α-napthol; 2 = α-naphthaldehyde; 3 = α-napthylamine; 4 = β-naphthol; 5 = benzoic acid; 6 = indeno [1,2,3-*cd*]pyrene; 7 = nonadecylbenzene; 8 = dodecylbenzene; (b) 1 = β-naphthol; 2 = α-naphthylamine; 3 = α-naphthaldehyde; 4 = indeno[1,2,3-*cd*]pyrene; 5 = diphenyl phthalate.

Influence of density on selectivity

Bare silica. The plot of selectivity (α) *versus* CO_2 density in CO_2–methanol and CO_2–acetonitrile mobile phases is shown in Fig. 4. Straight lines are obtained but their slope is positive, negative or zero, meaning that the selectivity can increase, decrease or remain constant when the density increases. When α becomes lower than 1, the elution order of the solutes is reversed. These results are in good agreement with the behavior observed with neat CO_2 and Janicot's data [12] showing that the variation in selectivity occurred only for non-homologous families of compounds when the CO_2 density was increased.

Polystyrene–divinylbenzene. As one can deduce from the retention data shown in Fig. 3, on PRP1 the selectivity calculated for adjacent peaks varies with CO_2 density only when diphenyl phthalate is considered because its retention is strongly dependent on density. Otherwise, α can be considered as a constant for a given mobile phase (Fig. 5).

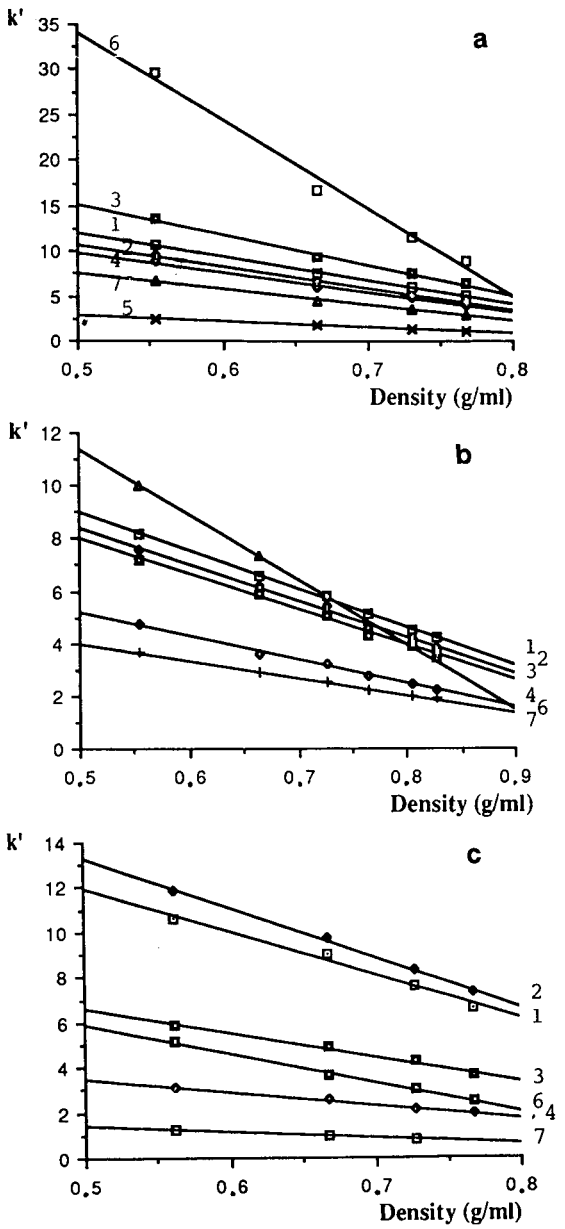

Fig. 3. Variation of solute capacity factors on PRP1 as a function of CO_2 density in the mobile phase. Column, 250 × 4.1 mm I.D.; stationary phase, 10-μm; mobile phase, (a) CO_2–methanol (94.4:5.6, mol/mol), (b) CO_2–acetonitrile (93.9:6.1, mol/mol) and (c) CO_2–carbon tetrachloride (94.4:5.6, mol/mol); Flow-rate (0°C), 5 ml/min; detection, UV at 254 nm. Solutes: 1 = α-naphthol; 2 = β-napthol; 3 = α-naphthylamine; 4 = α-naphthaldehyde; 5 = benzoic acid; 6 = diphenyl phthalate; 7 = dodecylbenzene.

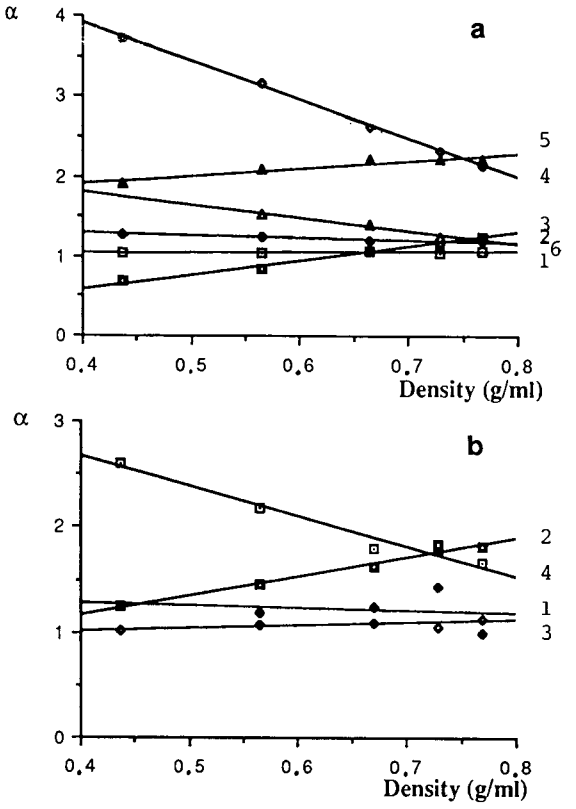

Fig. 4. Variation of solute selectivity on bare silica as a function of CO_2 density in the mobile phase. Conditions as in Figure 1. Solutes: (a) 1 = β-naphthol–α-naphthol; 2 = α-naphthol–α-naphthylamine; 3 = α-naphthylamine–indeno[1,2,3-*cd*]pyrene; 4 = indeno[1,2,3-*cd*]pyrene–α-naphthaldehyde; 5 = benzoic acid–α-naphthaldehyde; 6 = nonadecylbenzene–dodecylbenzene; (b) 1 = β-naphthol–α-naphthylamine; 2 = α-naphthylamine–diphenylphthalate; 3 = diphenylphthalate–indeno[1,2,3-*cd*]pyrene; 4 = indeno[1,2,3-*cd*]pyrene–dodecylbenzene.

Consequently, eqn. 2 cannot be valid for diphenyl phthalate. For the other solutes α can be expressed as follows:

$$\alpha = \frac{a(1-\rho)}{a'(1-\rho)} \tag{3}$$

meaning that α is a constant for pairs of solutes whose retention *versus* density can be expressed by eqn. 2.

Even when α does not vary with changes in CO_2 density, the use of CO_2 density programming can be very useful for decreasing the duration of analysis without a significant decrease in resolution (except the influence of k' on the resolution).

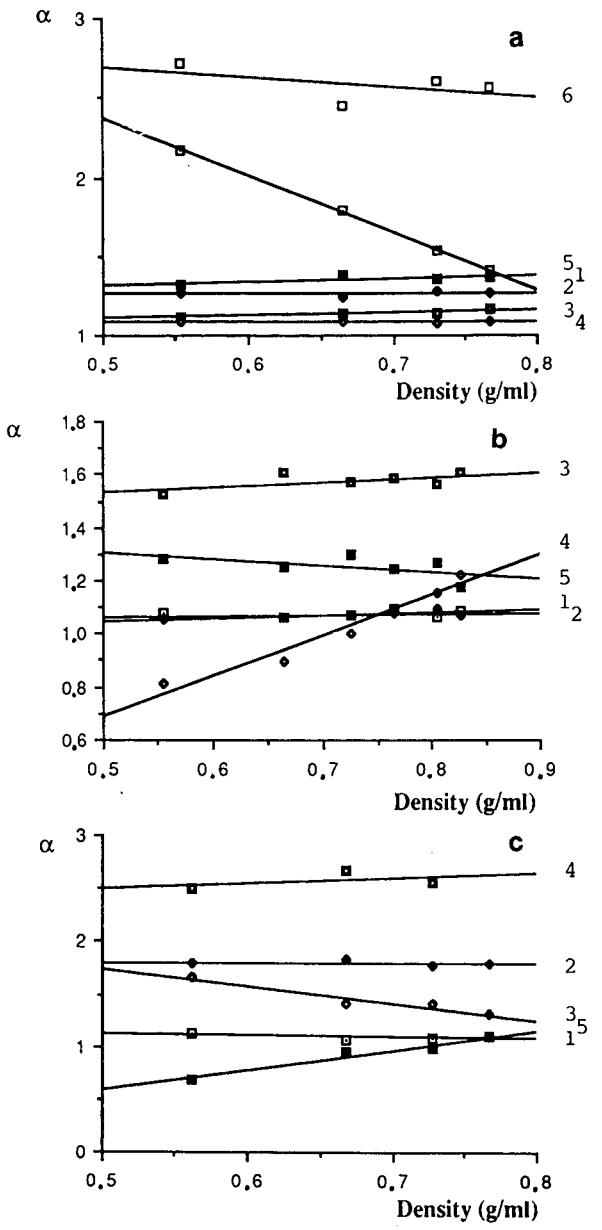

Fig. 5. Variation of solute selectivity on PRP1 as a function of CO_2 density in the mobile phase. Conditions as in Figure 2. Solutes: (a) 1 = diphenylphthalate–α-naphthylamine; 2 = α-naphthylamine–α-naphthol; 3 = α-naphthol–β-naphthol; 4 = β-naphthol–naphthaldehyde; 5 = α-naphthaldehyde–dodecylbenzene; 6 = dodecylbenzene–benzoic acid; (b) 1 = α-naphthol–β-naphthol; 2 = β-naphthol–α-naphthylamine; 3 = α-naphthylamine–naphthaldehyde; 4 = α-naphthol–diphenyl phthalate; 5 = α-naphthaldehyde–dodecylbenzene; (c) 1 = β-naphthol–α-naphthol; 2 = α-naphthol–α-naphthylamine; 3 = α-naphthylamine–naphthaldehyde; 4 = α-naphthaldehyde–dodecylbenzene; 5 = α-naphthylamine–diphenyl phthalate.

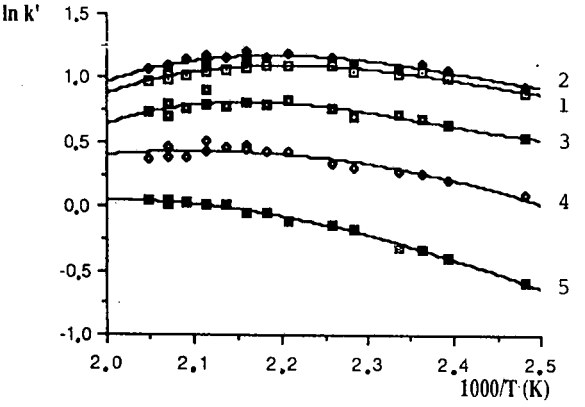

Fig. 6. Variation of logarithm of solute capacity factors on bare silica with reciprocal of mobile phase temperature. Conditions as in Fig. 1a. Solutes: 1 = α-naphthol; 2 = β-naphthol; 3 = α-naphthylamine; 4 = α-naphthaldehyde; 5 = dodecylbenzene.

Influence of temperature on retention

The influence of temperature on retention was studied on silica and PRP1. Fig. 6 shows the plot of the logarithm of the capacity factor *versus* the reciprocal of temperature for the test solutes on silica. The shape of the curve shows LC-like behaviour (increase in k' with increase in temperature) and a GC-like behaviour (decrease in k' with increase in temperature). It has been stated that the maximum k' is independent of the nature of the solute [13]. Fig. 6 shows that the position of the maximum (T_f) depends on the solute boiling point (b.p.) (Table I). For example, T_f for dodecylbenzene (b.p. = 331°C) is higher than that of α-naphthylamine and α-naphthaldehyde (b.p. = 301 and 291°C, respectively).

At a given temperature, the distance between the curves corresponds to the selectivity. From Fig. 6, selectivity variatons can be obtained by changing the temperature.

Using the equation [14]

$$\ln k' = \frac{-\Delta H_T^0}{RT} + \frac{\Delta S_T^0}{R} - \ln \beta \tag{4}$$

where ΔH_T^0 is the change in enthalpy of solute transfer, ΔS_T^0 is the change in entropy of solute transfer, β is the phase ratio of the column, T is temperature (K) and R is the gas constant, ΔH_T^0 can be deduced from the slope of the straight portion of the curves plotted in Fig. 6, assuming that the variation in density with temperature can be neglected within the studied range.

Because the slopes of the straight lines are negative, positive values of ΔH_T^0 are obtained (Table II). These values are intermediate between GC and LC. Similar results and T_f values reported by Chester and Innis [15] with neat CO_2 for derivatized oligomers of polysaccharides separated on a capillary column indicated that the affinity of the solutes for the mobile phase was high. Consequently, the mobile phase solvation was the main partitioning mechanism.

TABLE II

VARIATION OF TEST SOLUTE TRANSFER ENTHALPIES (ΔH_T^0) AND ENTROPIES (ΔS_T^0) DETERMINED ON SILICA

Solute	ΔH_T^0 (kJ mol^{-1})	ΔS_T^0 (J mol^{-1} K^{-1})
α-Naphthol	3.81	8.43
β-Naphthol	4.67	10.98
α-Naphthylamine	6.66	12.29
α-Naphthaldehyde	8.94	14.12
Dodecylbenzene	13.51	20.06

In contrast, on PRP1, solute retentions except for diphenyl phthalate were found to decrease with increase in temperature (between 20 and 70°C) for a constant pressure of 232 bar. No maximum occurred, indicating the strong influence of the stationary phase on the partition mechanism. Our results obtained with a modified mobile phase are in good agreement with previous results at constant density for model compounds on PRP1 with neat CO_2 and N_2O over the temperature range 20–60°C [16].

Use of simultaneous modifier and density gradients

The pressure programming device monitoring the pressure regulator allowed density gradients over a wide range from 5 to more than 100 bar/min. Such a high ramp is necessary because very fast separations can be done on packed columns, as shown in Fig. 7: the separation of twelve PAHs on bare silica was achieved in less than 3 min. It must be pointed out that the device used allows density gradients without an increase in the mobile phase velocity (in contrast, a slight decrease in the linear velocity of CO_2 occurs during the increase in the CO_2 density because the CO_2 is pumped at a constant mass flow-rate). Thus, to a first approximation, the operating conditions are maintained in the column while the column pressure drop will only depend on the changes in the mobile phase viscosity during density gradients. This increase in mobile phase viscosity can entail a mobile phase density gradient in the column and, therefore, peak broadening [17]. From a practical point of view, this negative effect has not often been observed [18,19].

Fig. 8 shows the separation of phenol derivatives. Addition of a modifier to the mobile phase is required to elute the more polar solutes, but the separation of *o*-cresol and 2,3-dimethylphenol needs simultaneously a low methanol content in the mobile phase (less than 2%) and a low CO_2 density (0.35 g/cm^3). In contrast, the density must be raised to 0.63 g/cm^3 and the methanol content to 3.3% in order to separate methylhydroquinone and resorcinol. Owing to the high polarity of phloroglucinol, its elution requires both a high CO_2 density and a high methanol content (8%). Consequently, the separation involved a methanol gradient (from 2 to 8%) and two pressure ramps, the first to elute compounds having two hydroxyl groups and the second one to elute phloroglucinol.

During high-ramp pressure gradients, a negative baseline drift occurred because the physical properties of the detection medium changed [20]. This effect can be attenuated by cooling (at 0°C) the connection tubing between the column and the

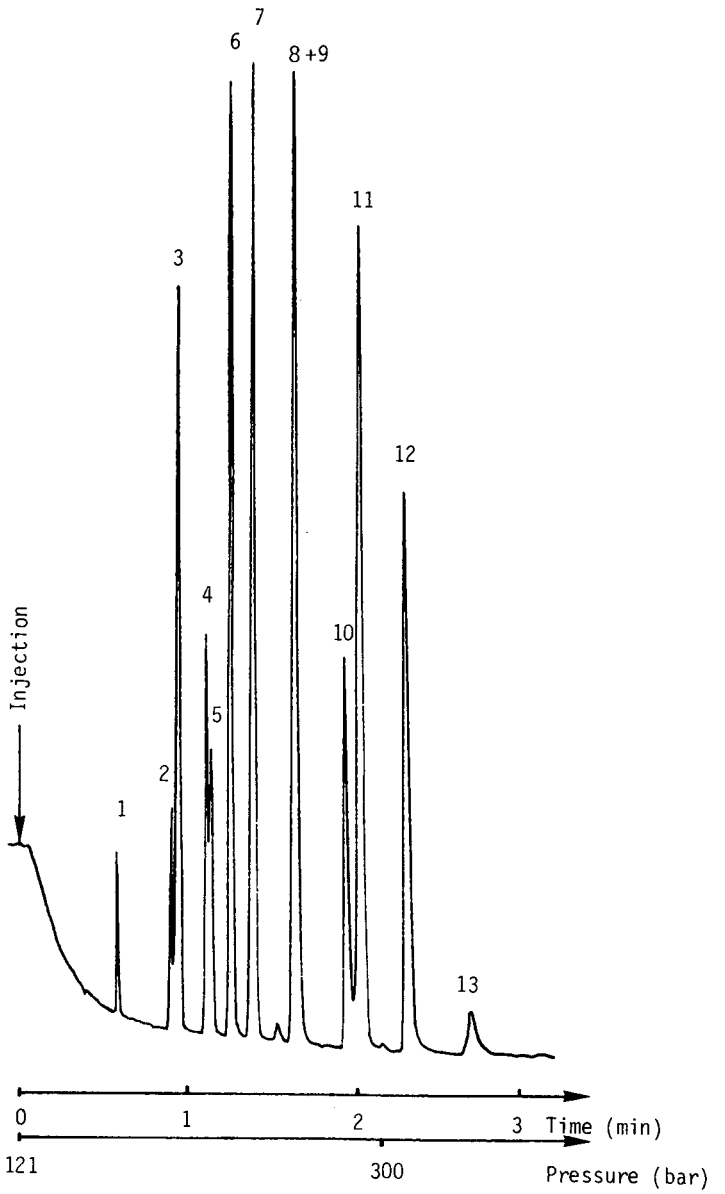

Fig. 7. Packed column SFC separation of PAHs using a fast pressure gradient. Column, 150 × 4.6 mm I.D.; stationary phase, 5-μm Pecosphere bare silica; mobile phase, CO_2; flow-rate (0°C), 4 ml/min; temperature, 85°C; detection, UV at 254 nm. Solutes: 1 = toluene; 2 = naphthalene; 3 = chloronaphthalene; 4 = acenaphthene; 5 = acenaphthylene; 6 = fluorene; 7 = phenanthrene; 8 = fluoranthene; 9 = pyrene; 10 = benzanthracene; 11 = triphenylene; 12 = benzopyrene; 13 = benzoperylene.

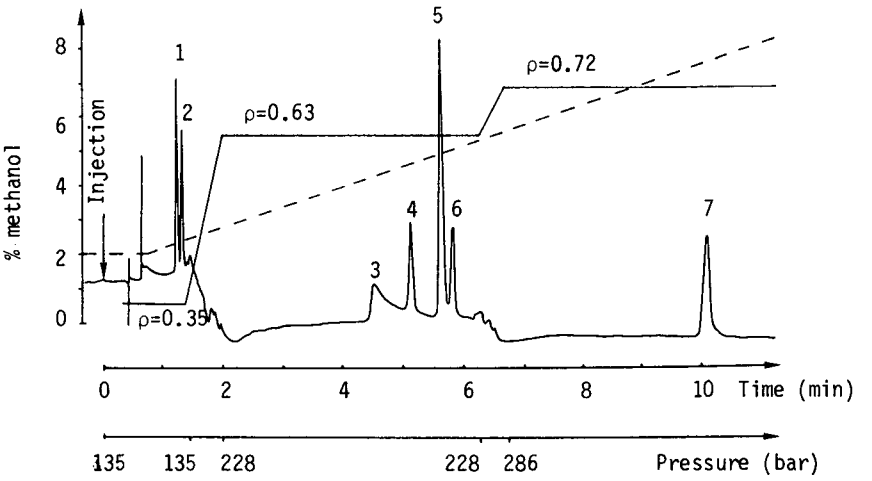

Fig. 8. Packed column SFC separation of phenol derivatives using pressure and modifier gradients. Column, 150 × 4.6 mm I.D.; stationary phase, 5-μm Pecosphere bare silica; mobile phase, CO_2–methanol; flow-rate (0°C) 4 ml/min; temperature, 85°C; detection, UV at 254 nm. Solutes: 1 = *o*-cresol; 2 = 2,3-dimethylphenol; 3 = resorcinol; 4 = methylhydroquinone; 5 = orcinol; 6 = hydroquinone; 7 = phloroglucinol.

detector. In that event, the CO_2 density does not vary greatly with the pressure and an LC-like behaviour is observed.

CONCLUSIONS

Mobile phase density programming in CO_2–polar modifier binary mixtures has often been a neglected parameter, particularly with packed columns. However, its influence on the solute chromatographic parameters is of the same order of magnitude as that with pure CO_2. Consequently, the physical parameters, temperature, CO_2 density and eluent composition (nature of the polar modifier), associated with the choice of the stationary phase (Table III) give general possibilities for improving the separation with respect to analysis time or resolution with multiple gradients. Among these, changes in the CO_2 density and polar modifier gradient result in large variations in the chromatographic parameters and must be taken into consideration in the future.

TABLE III

FUNDAMENTAL PARAMETERS AFFECTING SEPARATION IN GC, LC AND SFC

Parameter	GC	LC	SFC
Stationary phase	+	+	+
Mobile phase composition	−	+	+
Pressure	−	−	+
Temperature	+	±	+

REFERENCES

1 B. Hebreteau, M. Lafosse, L. Morin-Allory and M. Dreux, *J. Chromatogr.*, 505 (1990) 299.
2 J. L. Janicot, M. Caude and R. Rosset, *J. Chromatogr.*, 437 (1988) 351.
3 P. Macaudière, M. Lienne, M. Caude, R. Rosset and A. Tambuté, *J. Chromatogr.*, 467 (1989) 357.
4 A. Georgetti, N. Pericles, H. Widmer, K. Anton and P. Dätwyler, *J. Chromatogr. Sci.*, 27 (1989) 318.
5 F. P. Schmitz and E. Klesper, *J. Chromatogr.*, 388 (1987) 3.
6 J. G. M. Janssen, P. J. Schoenmakers and C. A. Cramers, *J. High Resolut. Chromatogr.*, 12 (1989) 645.
7 U. van Wasen and G. M. Schneider, *Chromatographia*, 8 (1975) 274.
8 P. Mourier, M. Caude and R. Rosset, *Analusis*, 13 (1985) 299.
9 P. J. Schoenmakers, *J. Chromatogr.*, 315 (1984) 1.
10 P. A. Peaden and M. L. Lee, *J. Liq. Chromatogr.*, 5 (1982) 179.
11 T. A. Berger and J. F. Deye, *Chromatographia*, 30 (1990) 57.
12 J. L. Janicot, *Thesis*, Université P. et M. Curie, Paris, 1990.
13 A. Munder, S. N. Chesler and S. A. Wise, *J. Chromatogr.*, 521 (1990) 63.
14 C. R. Yonker and R. D. Smith, *J. Chromatogr.*, 351 (1986) 211.
15 T. L. Chester and D. P. Innis, *J. High Resolut. Chromatogr. Chromatogr. Commun.*, 9 (1986) 209.
16 H. H. Lauer, D. McManigill and R. D. Board, *Anal. Chem.*, 55 (1983) 1370.
17 P. J. Schoenmakers and F. C. C. J. G. Verhoeven, *J. Chromatogr.*, 352 (1986) 15.
18 H. E. Schwartz. *LC · GC*, 5 (1987) 14.
19 D. R. Gere, R. D. Board and D. McManigill, *Anal. Chem.*, 54 (1982) 736.
20 D. J. Bornhop and J. G. Wansgaard, *J. Chromatogr. Sci.*, 27 (1989) 293.

Journal of Chromatography, 557 (1991) 99–111
Elsevier Science Publishers B.V., Amsterdam

CHROM. 23 307

Quantitative aspects of the determination of compounds with widely varying polarity using capillary supercritical fluid chromatography

LARS KARLSSON, LENNART MATHIASSON*, JENNY ÅKESSON and JAN ÅKE JÖNSSON
Department of Analytical Chemistry, University of Lund, S-221 00 Lund (Sweden)

ABSTRACT

The quantitative aspects of capillary supercritical fluid chromatography are discussed, focusing on the impact of the nature of the analytes and their chromatographic behaviour on quantification. In the experimental work model substances, mainly nitrogen containing, of varying polarity and basicity were chromatographed on a polar cyanopropyl–methyl- and a slightly polar phenyl–methyl-polysiloxane stationary phase using supercritical nitrous oxide as the mobile phase. Changes in the nature of the stationary phase were shown to decrease adsorption tendencies, resulting in improved peak shapes and thus better quantification. The precision of peak-area measurements using direct injection was 3–12% (relative standard deviation) in the concentration range 100–1000 ppm, the higher values being obtained for the non-optimum solute–stationary phase combinations, as indicated by the relative response plots. The detection limits obtained with a nitrogen-sensitive thermionic detector were in the range 2–29 ppm, corresponding to 0.1–1.4 ng. It was found that quantitative determinations of early eluting compounds is facilitated by using a precolumn-based injection system.

INTRODUCTION

Although the number of papers dealing with capillary supercritical fluid chromatography (SFC) is rapidly increasing, quantitative aspects are still rarely discussed. Table I lists papers on capillary SFC using the criterion that regression data were presented. In these papers, quantitative aspects are only briefly mentioned, and to our knowledge no paper has appeared in which quantification based on regression data is the main subject. Our previous paper [18] included a limited discussion on quantitative analysis, with a few model substances chromatographed on a slightly polar phenyl–methyl column. In this work we extended the number of model substances to include compounds of widely differing polarity and basicity. Their chromatographic behaviour was investigated on two capillary columns differing in polarity.

0021-9673/91/$03.50

TABLE I

QUANTITATIVE DETERMINATIONS REPORTED IN CAPILLARY SFC

Analyte[a]	Detection	Ref.
PAHs	Fluorimetric	1
PAHs (nitrated)	Thermionic	2
Benzothiophene	Flame photometric	3
Herbicides	UV absorbance; Flame ionization	4
PAHs	UV absorbance	5
PAHs	UV absorbance	6
Insecticides	Mass spectrometric	7
α-Keto acids	Thermionic	8
PAHs, hydrocarbons	UV absorbance; Flame ionization	9
Pesticides	UV absorbance	10
Caffeine	Fourier transform infrared spectrometric	11
Benzothiophene	Flame photometric	12
Trimyristin	Light scattering	13[b]
Thiols	Chemiluminescence	14
Pesticides	Radiofrequency plasma	15
Organosulphur compounds	Flame photometric	16
Steroids	Thermionic	17
Aromatic amines	Thermionic	18
Halogenated compounds	Electron capture	19
Mefloquine	Electron capture	20

[a] PAHs = polynuclear aromatic hydrocarbons.
[b] Packed capillary column.

EXPERIMENTAL

Equipment

The equipment has been described previously [18]. It consists of a syringe pump (Model 8500; Varian, Walnut Creek, CA, USA) and a gas chromatograph (Model 3710, Varian), equipped with either a thermionic nitrogen–phosphorus detector (Model TSD, Varian) or a flame ionization detector (Varian). The pump was modified to work under constant pressure, as described [21]. A digital voltmeter showed the pressure directly in bar, a digital pulse counter measured the flow-rate (3600 pulses correspond to 1 ml) and a table-top computer (ABC-80; Luxor, Motala, Sweden) equipped with a digital–analog converter was used for creating linear and parabolic pressure gradients. Samples were injected using a manual, 60-nl loop injector (Model C14W; Valco, Houston, TX, USA) or a precolumn injection system developed for trace analysis [22]. Collection and handling of chromatographic data were executed with a PC (Model V386A; Victor Svenska, Stockholm, Sweden) using the JCL6000 Chromatography Data System (Jones Chromatography, Hengoed, Mid-Glamorgan, UK). Chromatograms were also registered on a recorder (Model 1107; W + W Electronics, Basle, Switzerland).

The capillary columns were connected with a zero dead-volume union (Valco) to a 50- or 100-μm frit restrictor (Lee Scientific, Salt Lake City, UT, USA). The restrictor end was positioned 1–2 mm below the outlet of the detector tip and swept with make-up gas (25 ml/min of nitrogen) entering at the detector base.

Typical settings for the flame ionization detector were: hydrogen flow-rate 30 ml/min and air flow-rate 180 ml/min and for the thermionic detector 1.2 and 210 ml/min, respectively. For the thermionic detector the bead current was set at 3.27 A (580 scale divisions) and the bias voltage at 7 V. The optimization procedure of the thermionic detector has been described previously [18].

Nitrous oxide (medical grade, >99%; AGA, Stockholm, Sweden) was used as the mobile phase. Typical flow-rates from the pump (measured by the pulse counter) at room temperature and 100 bar were 6 μl/min.

Columns

The columns investigated were DB-17 (50% methyl–50% phenyl-polysiloxane), 10 m × 50 μm I.D., film thickness 0.10 μm (J&W Scientific, Folsom, CA, USA), SB-cyanopropyl-50 (50% methyl–50% cyanopropyl-polysiloxane), 10 m × 50 μm I.D., film thickness 0.25 μm (Lee Scientific) and SB-octyl-50 (50% *n*-octyl–50% methyl-polysiloxane), 10 m × 100 μm I.D., film thickness 0.5 μm (Lee Scientific).

Chemicals

All substances used as solutes in the direct injection mode are listed in Table II together with abbreviations.

2,6-TDA and MDA were obtained from Merck (Darmstadt, Germany). The carbamate derivatives 2,4-TDC and 2,6-TDC were prepared by reacting the corresponding diamine with ethyl chloromate (Sigma, St. Louis, MO, USA) according to the procedure described [23]. The amide derivative FMDA was prepared at the Department of Occupational Medicine (University Hospital of Lund). Methaqualone was a gift from R. Isaksson (Department of Organic Chemistry 3, University of Lund, Sweden). Cothinine was obtained from Pharmacia (Helsingborg, Sweden) and Raclopride from Astra (Södertälje, Sweden). Trioctylamine [>95% by gas chromatography (GC)] was obtained from Merck and dodecanoic acid dinitrile (purum) from Fluka (Buchs, Switzerland). Octadecane (Fluka) was used as a model substance in the precolumn injection experiments. Solvents were of the highest available purity.

RESULTS AND DISCUSSION

The analyte

In all quantitative work, the nature and concentration of the sample components must first be considered. In GC, a decision first is made between direct analysis or the development of a derivatization procedure. In SFC, the higher solubility of the solutes in the mobile phase compared with GC permits the direct analysis of more polar compounds. However, it must be stressed that the improved peak shapes that can be accomplished by derivatization give improved quantification possibilities also in SFC. The improved peak shape of, *e.g.*, MDA after derivatization to its amide derivative (Fig. 5 in ref. 18) resulted in an improvement in the precision [relative standard deviation (R.S.D.)] from *ca.* 13% to *ca.* 3% at concentrations of 25 ppm. Advantages of derivatization in SFC analysis have been recognized by others, *e.g.*, David and Novotny [8] in the determination of α-keto acids.

TABLE II

SURVEY OF COMPOUNDS TESTED

Compound	Abbreviation	Formula	Compound	Abbreviation	Formula
2,6-Toluenediamine	2,6-TDA	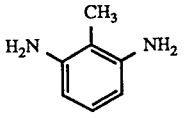	Methaqualone	MQ	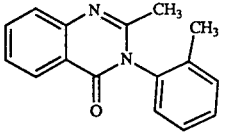
2,6-Toluenediethyldicarbamate	2,6-TDC	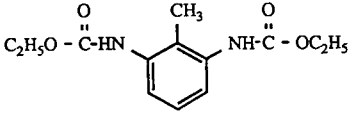	Cothinine	COTH	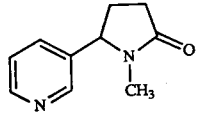
2,4-Toluenediethyldicarbamate	2,4-TDC	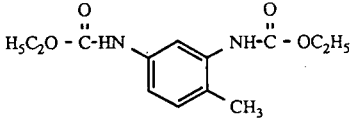	Raclopride	RP	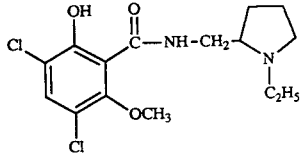
4,4′-Diaminodiphenylmethane	MDA	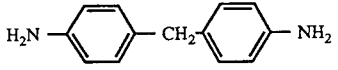	Trioctylamine	TOA	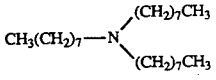
4,4′-Diaminodiphenylmethane (perfluorobutyro derivative)	FMDA	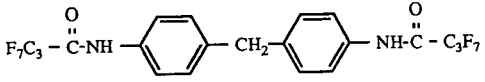	Dodecanoic acid dinitrile	DODN	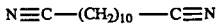

Chromatographic behaviour

A prerequisite for good quantification is a symmetric peak shape for the components of interest and a good separation between them. The peak shape, determined primarily by the mutual interactions between the analyte and the stationary phase, may be improved by changing the stationary phase polarity. Fig. 1 shows the improvement for the polar compound raclopride on changing from a slightly polar to a strongly polar stationary phase. Even though the peak heights differ considerably, the peak areas are the same. The accuracy of electronic integration will be considerably better in the case of peak shapes as in Fig. 1b.

The resolution, R_s, and the relative peak sizes, *i.e.*, the concentration ratio between two neighbouring peaks are also of considerable importance for quantitative accuracy and integrator performance. Both of these aspects have been discussed by Guiochon and Guillemin [24]. In SFC the resolution can be controlled by simultaneous variation of three parameters, namely temperature, pressure and mobile phase composition. This offers unique possibilities to tailor the separation. In practice, an optimization with respect to temperature and pressure is normally sufficient. With pressure programming normally little additional work is needed to improve the resolution greatly. For example, from an R_s value of 1.0 (at 120 bar and 150°C) the resolution was improved to 2.3 on applying a slightly concave parabolic pressure gradient for the pair MQ and COTH in a mixture of three model compounds (MQ, COTH and RP). This would decrease the error in the relative peak-area measurements from *ca.* 2% to virtually zero [24]. It should be noted that the elution order was changed when the pressure gradient was applied. The chromatograms in Fig. 2 illustrate the separation.

Instrumental aspects

Injection. In capillary SFC, a sample introduction system must be capable of introducing very small, repeatable sample volumes on the analytical column. We have used two different systems, manual direct valve injection of 60-nl samples and a device using precolumn enrichment and subsequent transfer of the analytes to the analytical column using the mobile phase. The sample solvent in this study was usually methanol, which was found [18] to give smaller solvent peaks than other solvents in the chromatographic system used.

With direct injections, no overloading effects were observed with analyte concentrations up to 2000 ppm (w/w) in methanol solution (*i.e*, injection of 95 ng), even at pressures as low as *ca.* 100 bar. The solubility of the solvent in the mobile phase and possible adsorption of the analyte in the injection valve determine the injection time needed to transfer the whole sample onto the analytical column. For example, we found previously that with 2,6-TDC in methanol at 90 bar, *ca.* ten loop volumes of mobile phase were needed, corresponding to an injection time of *ca.* 5 s [18]. The solubility can be improved and the adsorption tendency supressed by using higher mobile phase pressures, giving shorter injection times. On the other hand, too high pressures may destroy the separation between the compounds of interest, which is why a compromise must be chosen. However, the extra band broadening resulting from the longest injection time (5 s) needed in our experiments had no noticeable effects on the quantification.

In the precolumn injection mode, a solvent evaporation step reduces the size of

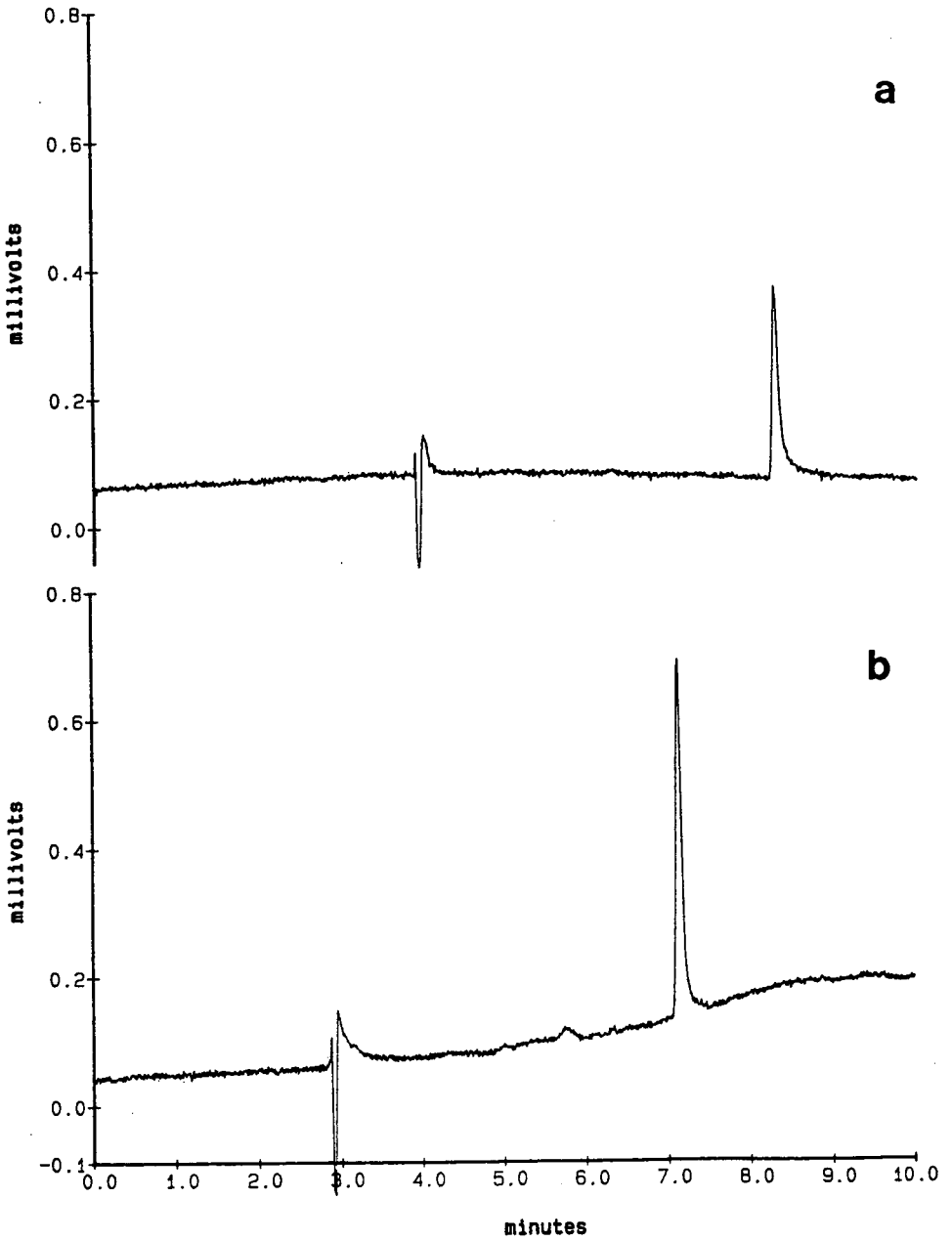

Fig. 1. Chromatograms of Raclopride. Columns, (a) DB-17, (b) SB-cyanopropyl-50; concentration, 250 ppm; sample solvent, methanol; injection volume, 60 nl; pressure programme: 100–180 bar at 10 bar/min; temperature, 150°C.

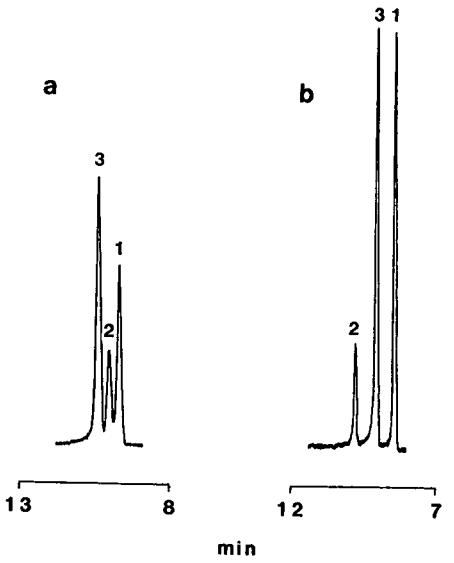

Fig. 2. Chromatograms of some model substances. Column: SB-cyanopropyl-50; concentration, 250 ppm; attenuation, (a) $4 \cdot 10^{-12}$ A f.s., (b) $2 \cdot 10^{-12}$ A f.s.; sample solvent, methanol; injection volume, 60 nl; system pressure, (a) 120 bar, (b) 120–180 bar, concave parabolic pressure gradient during for 10 min, 0.01 bar/min starting rate; temperature, (a) 150°C, (b) 115°C. Peaks: 1 = DODN; 2 = MQ; 3 = COTH (for abbreviations, see Table I).

the solvent peak in addition to giving a lower noise level during the entire chromatographic run. This permits determinations of early eluting analytes even at low concentrations. By increasing the sample size on the precolumn, enrichments are possible to the extent that analyses below 1 ppm are feasible. Fig. 3 shows a comparison between the two modes of injection, direct or via a precolumn, using flame ionization detection. The precolumn injection device is described in detail in a separate paper [22].

Detection. In this work, both flame ionization detection (FID) and nitrogen-sensitive thermionic detection (TID) were used, in both instances with nitrous oxide as the mobile phase.

In the precolumn experiments in which we have used nitrous oxide in combination with FID we found that the baseline increased linearly with increasing pressure, *i.e.*, increased flow-rate of nitrous oxide to the detector. The same behaviour was reported by Ashraf-Khorassani *et al.* [25], who attributed the baseline increase to the increase in oxidizing agent (nitrous oxide) in the flame. However, there is also a possibility that the increase may be due to hydrocarbon impurities in the nitrous oxide. A fact which may point in this direction is that the change in flame composition will be small as make-up gas (nitrogen) at 25 ml/min is used compared with a change in flow-rate from *ca.* 0.5 to *ca.* 1 ml/min during a pressure-programmed run. This problem will be investigated further. Fortunately, this does not seem to influence the linearity of the detector response. As the baseline is the same in different runs with the same set of experimental conditions, the baseline rise can be corrected for by using a chromatographic data system.

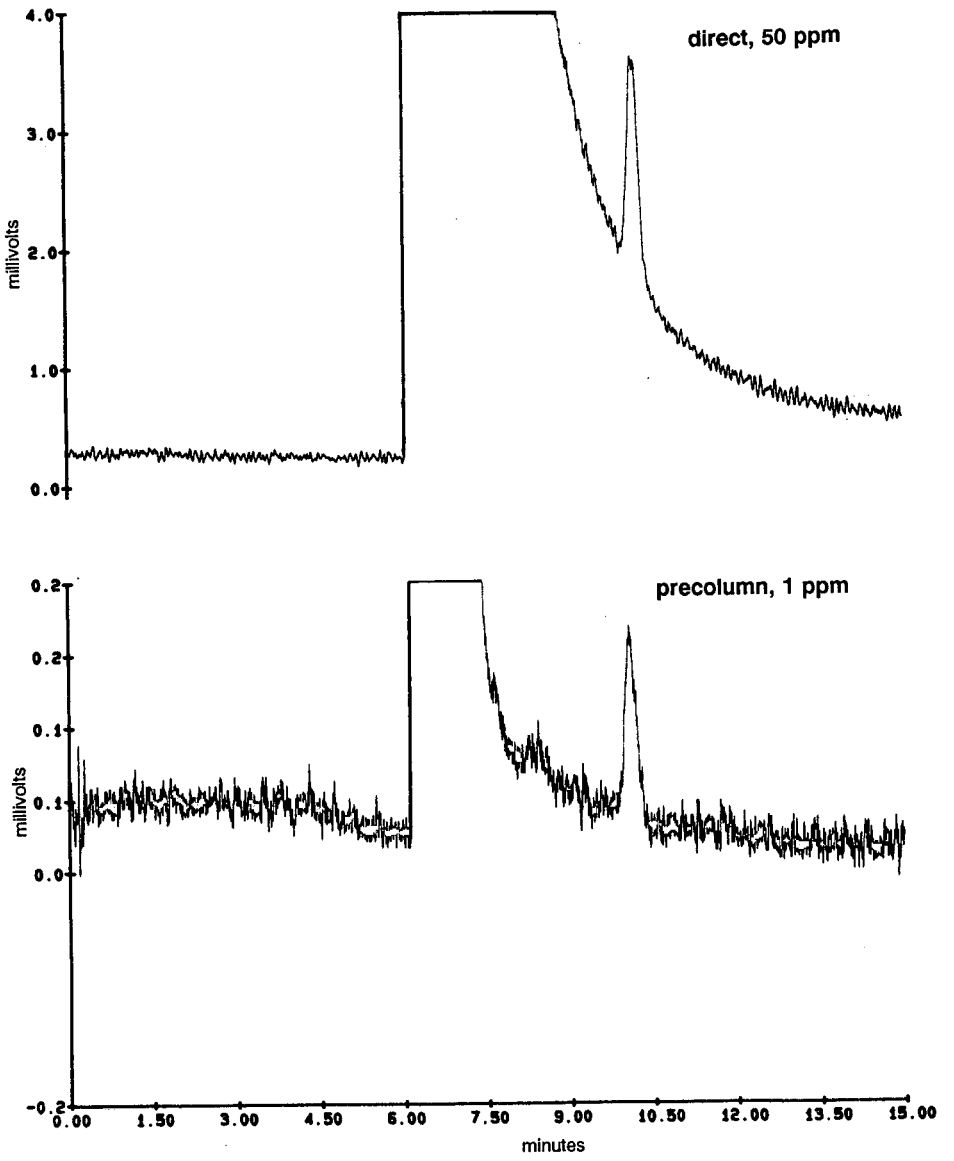

Fig. 3. Chromatograms of octadecane using direct and precolumn system injection. Column, SB-octyl-50; sample solvent, acetone; injection volume, 60 nl, direct injection; precolumn injection, 10 μl; system pressure, 100 bar, temperature, 170°C.

TID has been shown to give a linear response in the normal concentration range with nitrous oxide [8,17,18] as the mobile phase in both isobaric and pressure-programmed runs. As the TID response in general is linear, the occurrence of non-linear effects in some chromatographic systems is therefore attributed to the injection system or to the column.

It is advantageous to use a TID instead of FID, as the response with substances containing nitrogen is often about ten times higher and the selectivity is high towards hydrocarbons. This means that the separation of a nitrogen compound from a non-nitrogen-containing substance will not be as critical as when using FID. Further, bleeding of the stationary phase will generally be suppressed to a large extent, as will the signal from small amounts of hydrocarbon contaminants in the mobile phase. The stable baseline with TID also in pressure-programmed runs (see Fig. 2) is favourable compared with UV detection, where the changes in refractive index may result in baseline drift. Sometimes, however, we have found a small baseline drift with TID in pressure-programmed runs, especially on the cyanopropyl column (see Fig. 1b). This can probably be attributed to stationary phase bleeding or elution of compounds with very long retention times, as the situation is drastically improved after a reconditioning period at high operating pressure.

Quantification

Precision. Generally, the precision of peak-area measurements, using direct injection, was 3–12% (R.S.D.) in the concentration range 100–1000 ppm, corresponding to an injected amount of 5–50 ng (Fig. 4). As several non-optimum solute–stationary phase combinations were included in our investigations, extra band broadening, *e.g.*, due to adsorption, often occurs on the column. This means that the

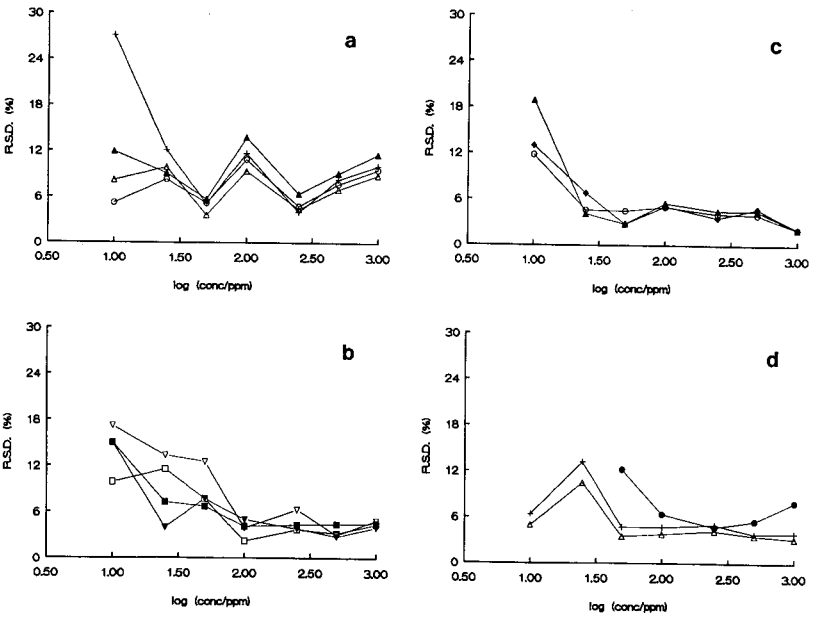

Fig. 4. Relative standard deviation *versus* logarithm of concentration. Columns, (a,b) DB-17, (c,d) SB-cyanopropyl-50; sample solvent, methanol; injection volume, 60 nl; pressure programme, (a) 100–180 bar at 8 bar/min, (b) 110–170 bar at 3 bar/min, (c) conditions as in Fig. 2b, (d) 90 bar isobaric for 3 min, 90–210 bar at 15 bar/min; temperature, (a,d) 150°C, (b) 135°C, (c) 115°C. (a) + = MQ, ▲ = COTH, △ = TOA, ○ = DODN; (b) ▽ = DMA, ▼ = FMDA, □ = 2,6-TDA, ■ = 2,6-TDC; (c) ▲ = COTH, ◆ = 2,4-TDC, ○ = DODN; (d) ● = RP, + = MQ, △ = TOA (for abbreviations, see Table I).

precision values obtained often contain significant contributions from this extra band broadening in the column and also from the injection procedure. The best precision (*ca.* 3%) was obtained, as expected, for near-optimum systems at high analyte concentrations. Automation of the direct injection procedure would probably further improve the precision.

When comparing the precision using manual direct injection with that using other sample introduction systems for capillary SFC, *viz.*, split injection [26,27], delayed split injection [28], time-split injection [28,31] and extraction injection [32], only time-split injection seems to be superior in this respect, capable of giving values lower than 2%. For example, Richter *et al.* [26] achieved an R.S.D. of 1.8–1.9% at concentrations of 200 ppm of C_{24}–C_{30} hydrocarbons, substances which ought to behave ideally on the column. For the precolumn injection system (still under development) [22], R.S.D. values of *ca.* 7% (five injections) at concentrations of 50 ppm have been obtained.

Detection limits. Detection limits, using direct injection, determined as twice the noise level for the model substances, are listed in table III. The results show, as expected, that the best precision in the low concentration range is obtained for the substances with the lowest detection limits; consider, *e.g.*, DODN in Fig. 4. However, the peak shape also has a large influence on precision. This can be seen for MDA and FMDA (also in Fig. 4). Although the detection limits for the two analytes are the same, the precision in the low concentration range is considerably worse for MDA, which gives a peak with marked tailing. With the precolumn injection system concentrations below 0.3 ppm can be determined. With a nitrogen-sensitive detector this value is expected to be *ca.* 10 times lower. Further work on these aspects is in progress.

Linearity. The merits of plotting normalized relative response *vs.* concentration instead of normal regression lines with response *vs.* concentration have been discussed previously [18]. The former approach, which gives more detailed information about possible adsorption effects in the low concentration range, was also used here.

Fig. 5 demonstrates the behaviour of different model substances at various concentrations on two columns with different polarity. All plots of response *vs.* con-

TABLE III

DETECTION LIMITS (ppm)

Compound	Columns	
	DB-17	SB-cyanopropyl-50
MQ	12	4.6
COTH	6.7	2.6
RP	–	29
TOA	7.1	6.4
DODN	3.0	1.8
2,6-TDA	2.1	–
2,6-TDC	5.6	–
2,4-TDC	–	9.1
MDA	5.3	–
FMDA	5.3	–

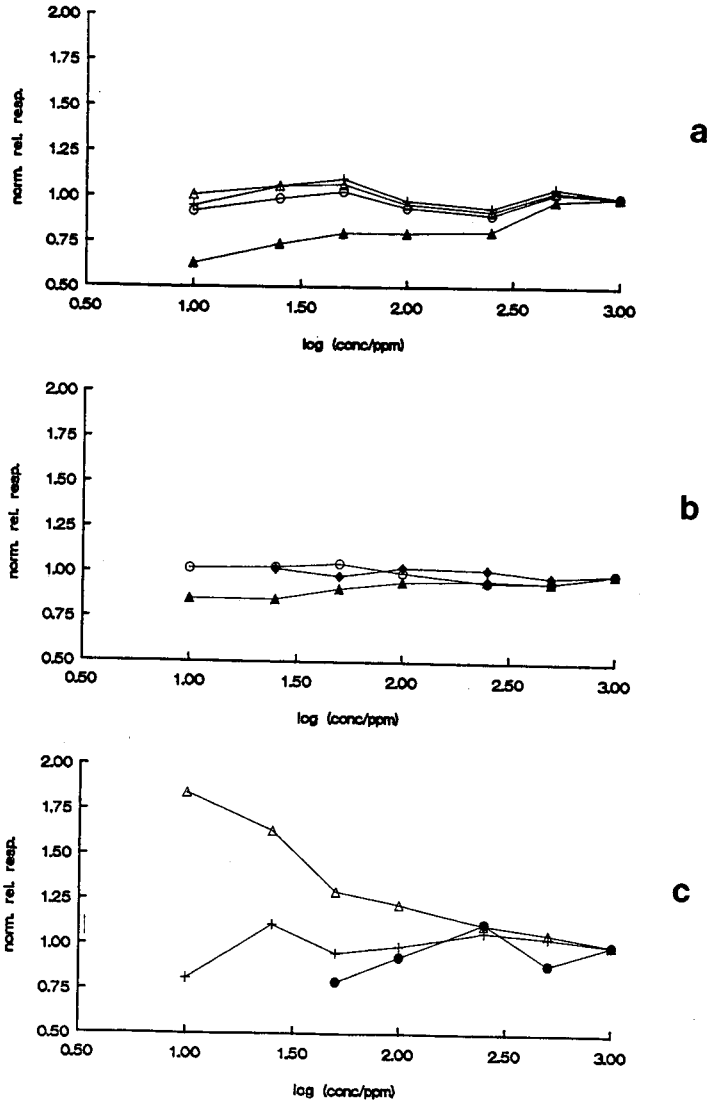

Fig. 5. Normalized relative response *versus* logarithm of concentration. Columns, (a) DB-17, (b,c) SB-cyanopropyl-50. Chromatographic conditions, (a) as in Fig. 4a, (b) as in Fig. 2b, (c) as in Fig. 4d. (a) + = MQ, ▲ = COTH, △ = TOA, ○ = DODN; (b) ▲ = COTH, ◆ = 2,4-TDC, ○ = DODN; (c) ● = RP, + = MQ, △ = TOA (for abbreviations, see Table I).

centration seem by visual inspection to be straigth lines and their linear correlation coefficients are all above 0.9995, except for COTH (0.9991) on the DB-17 column and RP (0.997) on the cyanopropyl column. In two of the systems considered, COTH on the DB-17 column and TOA on the cyanopropyl column, the regression lines deviate significantly from the origin at the 95% confidence level, indicating non-optimum behaviour. The sensitivity for RP is markedly lower compared with the other investigated substances. The noise therefore has a greater influence on the peak-area

determinations, which, not unexpectedly, resulted in this lower correlation coefficient.

Deviations from optimum behaviour are much more obvious in relative response plots. COTH has a low relative response in the low concentration range, indicating adsorption of this compound on the slightly polar DB-17 column (Fig. 5a), an effect which decreases considerably on the more polar cyanopropyl column (Fig. 5b).

TOA on the cyanopropyl column (Fig. 5c) illustrates the problem of quantification when the analyte elutes close to the solvent front. The positive error in the response of trioctylamine is more pronounced in relative terms at lower concentrations and results in a significant positive intercept of the normal regression line. A possible explanation for this behaviour may be a change in the detector sensitivity for substances coeluting with the solvent.

Apart from the deviations discussed above, fairly straight lines, parallel to the abscissa, were obtained for all other systems in the relative response plots. These straigth lines indicate near-optimum chromatographic behaviour, suggesting that quantitative determinations based on regression plots are possible in the concentration range considered.

Linear regression lines and calibration graphs for 2,6-TDA, 2,6-TDC, MDA and FMDA have been presented previously [18]. Two of the substances, the free amines 2,6-TDA and MDA, gave negative intercepts, indicating adsorption, but only with MDA was this deviation significant at the 95% confidence level.

CONCLUSIONS

We have shown that quantitative measurements using SFC with the conventional 60-nl injection loop in general are possible at concentrations above *ca.* 50 ppm, correponding to an injection of 2 ng in methanol. When analysing substances that elute early and are suitable for nitrogen-sensitive detection, accurate quantitative measurements can be performed at concentrations of a few ppm (*ca.* 100 pg). However, for trace analysis below this level, techniques for introduction of larger sample volumes still need to be improved.

REFERENCES

1 J. C. Gluckman, D. C. Shelly and M. Novotny, *Anal. Chem.*, 57 (1985) 1546.
2 K. E. Markides, E. D. Lee, R. Bolick and M. L. Lee, *Anal. Chem.*, 58 (1986) 740.
3 W. R. West and M. L. Lee, *J. High Resolut. Chromatogr. Chromatogr. Commun.*, 9 (1986) 161.
4 J. R. Wheeler and M. E. McNally, *J. Chromatogr.*, 410 (1987) 343.
5 J.C. Kuei, K. E. Markides and M. L. Lee, *J. High Resolut. Chromatogr. Chromatogr. Commun.*, 10 (1987) 257.
6 S. M. Fields, K. E. Markides and M. L. Lee, *Anal. Chem.*, 60 (1988) 802.
7 H. T. Kalnoski and R. D. Smith, *Anal. Chem.*, 60 (1988) 529.
8 P. A. David and M. Novotny, *J. Chromatogr.*, 452 (1988) 623.
9 D. J. Bornhop, S. Schmidt and N. L. Porter, *J. Chromatogr.*, 459 (1988) 193.
10 J. E. France and K. J. Voorhees, *J. High Resolut. Chromatogr. Chromatogr. Commun.*, 11 (1988) 692.
11 S. Shah, M. Ashraf-Khorassani and L. T. Taylor, *Chromatographia*, 25 (1988) 631.
12 S. V. Olesik, L. A. Pekay and E. A. Paliwoda, *Anal. Chem.*, 61 (1989) 58.
13 S. Hoffmann and T. Greibrokk, *J. Microcolumn Sep.*, 1 (1989) 35.
14 D. J. Bornhop, B. J. Murphy and L. Krieger-Jones, *Anal. Chem.*, 61 (1989) 797.
15 R. J. Skelton, P. B. Farnsworth, K. E. Markides and M. L. Lee, *Anal. Chem.*, 61 (1989) 1815.

16 L. A. Pekay and S. V. Olesik, *Anal. Chem.*, 61 (1989) 2616.
17 P. A. David and M. Novotny, *J. Chromatrogr.*, 461 (1989) 111.
18 L. Mathiasson, J. Å. Jönsson and L. Karlsson, *J. Chromatogr.*, 467 (1989) 61.
19 H.-C. K. Chang and L. T. Taylor, *J. Chromatogr. Sci.*, 28 (1990) 29.
20 D. L. Mount, L. C. Patchen and F. C. Churchill, *J. Chromatogr.*, 527 (1990) 51.
21 F. J. van Lenter and L. D. Rothman, *Anal. Chem.*, 48 (1976) 1430.
22 L. Karlsson, L. Mathiasson and J. Å. Jönsson, in preparation.
23 M. Dalene, L. Mathiasson, G. Skarping, C. Sangö and J. F. Sandström, *J. Chromatogr.*, 435 (1988) 469.
24 G. Guiochon and C. L. Guillemin, *Quantitative Gas Chromatography for Laboratory Analyses and On-Line Process Control*, Elsevier, Amsterdam, 1st ed., 1988, Ch. 15, pp. 646–650.
25 M. Ashraf-Khorassani, L. T. Taylor and P. Zimmermann, *Anal. Chem.*, 62 (1990) 1177.
26 B. E. Richter, D. E. Knowles, M. R. Andersen, N. L. Porter, E. R. Campbell and D. W. Later, *J. High Resolut. Chromatogr. Chromatogr. Commun.*, 11 (1988) 29.
27 J. Köhler, A. Rose and G. Schomburg, *J. High Resolut. Chromatogr. Chromatogr. Commun.*, 11 (1988) 191.
28 M. L. Lee, B. Xu, E. C. Huang, N. M. Djordevic, H-C. K. Chang and K. E. Markides, *J. Microcolumn Sep.*, 1 (1989) 7.
29 P. Sandra, F. David, F. Munari, G. Mapelli and S. Trestianu, in R. M. Smith (Editor), *Supercritical Fluid Chromatography*, Royal Society of Chemistry, London, 1st ed., 1988, Ch. 5, pp. 137–157.
30 S. B. Hawthorne and D. J. Miller, *J.Chromatogr. Sci.*, 27 (1989) 197.
31 B. E. Berg and T. Greibrokk, *J. High Resolut. Chromatogr.*, 12 (1989) 322.
32 W. P. Jackson, K. E. Markides and M. L. Lee, *J. High Resolut. Chromatogr. Chromatogr. Commun.*, 9 (1986) 213.

Journal of Chromatography, 557 (1991) 113–123
Elsevier Science Publishers B.V., Amsterdam

CHROM. 23 295

Bile salt surfactants in micellar electrokinetic capillary chromatography

Application to hydrophobic molecule separations

RODERIC O. COLE and MICHAEL J. SEPANIAK*
Department of Chemistry, University of Tennessee, Knoxville, TN 37996–1600 (USA)
WILLIE L. HINZE
Department of Chemistry, Laboratory for analytical Micellar Chemistry, Wake Forest University, Winston-Salem, NC 27109 (USA)
and
JOSEPH GORSE and KIMBERLY OLDIGES
Department of Chemistry, Baldwin-Wallace College, Berea, OH 44017 (USA)

ABSTRACT

Bile salt surfactants are used in the micellar electrokinetic capillary chromatography (MECC) separation of various hydrophobic compounds. The use of methanol in the mobile phase allows the separation of previously intractable compounds including polyaromatic hydrocarbons. The effects of methanol on critical micelle concentration is investigated for sodium dodecyl sulfate (SDS) and the bile salt sodium cholate. It is determined that the unique structure of the bile salt micelle is much more tolerant to the addition of organic solvents than SDS, thereby increasing the scope of applications of MECC to include hydrophobic compounds.

INTRODUCTION

Micellar electrokinetic capillary chromatography (MECC) is a form of capillary zone electrophoresis (CZE) which offers unique selectivities as well as the ability to separate neutral compounds. CZE separates charged solutes based on their migration rate in an electric field [1]. In the case of neutral compounds, no separation is usually observed for this separation mode. First reported in 1984 [2], MECC involves the addition of an ionic surfactant such as sodium dodecyl sulfate (SDS) to the mobile phase above the critical micelle concentration (CMC). The micelles are retarded in the electric field and move at a velocity slower than electroosmotic flow. In this situation, neutral solutes can partition between the micellar (pseudostationary) phase and the mobile phase, resulting in separation. Due to the fact that the micellar phase is moving toward the detector, an elution window is created that is bordered by a

0021-9673/91/$03.50

column void time (t_0) and a micelle migration time (t_m). As a result of this limited range, hydrophobic compounds (spending the bulk of the separation time associated with the micelle) tend to "stack up" (*i.e.*, coelute) near t_m. Since resolution in MECC is optimal for a capacity factor, k', in the range 1–5 [3], depending on the breadth of the elution window, the technique is limited to compounds that are relatively hydrophilic.

In an effort to extend the utility of the technique to more hydrophobic species, organic solvents such as methanol have been added to the mobile phase [4,5]. Organic solvents affect the MECC separation process in several ways. First, the organic solvent slows electroosmotic flow by interacting with the capillary wall and thereby extends the micelle migration time and thus the elution window [4]. Extension of the elution window is concomitant with an increase in peak capacity. Second, the partition ratio is altered by decreasing the overall polarity of the mobile phase. Solutes which are insoluble in water distribute more equitably between micellar and mobile phases (*i.e.*, k' is reduced). Moreover, this approach provides an element of selectivity [5]. These effects have allowed the development of step- and continuous-gradient elution techniques for MECC [6,7].

Relatively high concentrations of organic solvents degrade separation performance. At levels exceeding approximately 15% (v/v), efficiency begins to show significant reduction and analysis time becomes prohibitive [7]. Band broadening in this situation is attributed to micelle polydispersity [7]. Analysis time is dependent on the amount and type of organic solvent employed. Methanol and 2-propanol greatly extend the elution range, presumably due to strong wall interaction and thus significantly alter electroosmotic flow. In some cases, the flow can be reduced to a point where the electrophoretic mobility of the micelle exceeds electroosmotic flow and migrates toward the positive electrode, away from the detector [8]. Other solvents such as acetonitrile and dioxane reduce solute capacity without dramatically reducing flow, presumably due to less wall interaction.

When SDS is used as the pseudostationary phase, separations of extremely hydrophobic molecules such as polyaromatic hydrocarbons (PAHs) are often unsuccessful. Hydrophobic species usually coelute at t_m despite the addition of large ($\geqslant 20\%$) amounts of organic solvent to the mobile phase. Additives such as cyclodextrins have been used with SDS to separate compounds such as PAHs, chlorinated biphenyls and dioxins [9]. While successful, this approach is limited to solutes which can fit into the cyclodextrin cavity.

As an alternative surfactant system, the bile salts have found application in MECC. Bile salts exhibit several useful chromatographic properties such as the ability to recognize specific enantiomeric conformations [10–13] and increased micelle polarity [12,14]. Based on a hydroxyl-substituted steroid backbone, bile salts are important biological surfactants which possess both hydrophobic and hydrophilic "faces". Fig. 1 shows the structures of the bile salts used in this work. While the physical properties of bile salts have been extensively studied [15,16], there has been some controversy over the structure of their micelles. In 1968, Small [17] introduced a model in which the hydrophobic faces of the monomer units are proximal and the protruding hydroxyl groups face the bulk solution. This model, based on logical consideration of space-filling molecular models and interfacial behavior of the monomer units, has recently been expanded in light of more sophisticated experimentation.

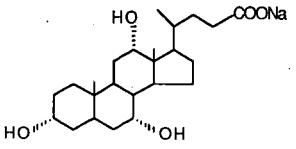

SODIUM CHOLATE

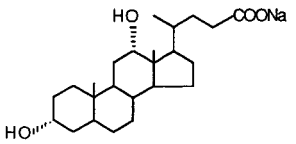

SODIUM DEOXYCHOLATE

Fig. 1. Bile salt structures.

Recent studies [18–20] suggest that the aggregates in question form helical micelles with the *hydrophobic* portions of the monomer facing the aqueous solution while the hydrophilic portions turn inward. Thus, in some respects, the bile salt micelle can be envisioned as an "inverted micelle". Studies with fluorescent and spin-label probe compounds lend further support to this argument [21,22].

The fact that the bile salt monomer is more polar than SDS leads to a general reduction of k' in MECC [12,14]. This is particularly advantageous in dealing with hydrophobic compounds, as separations which prove difficult with conventional SDS systems are more easily attained with bile salts. In addition, the unique inverted bile salt micelle appears to tolerate high concentrations of solvents such as methanol without drastic loss of efficiency or dramatic increase in analysis time. These desirable characteristics allow separations of compounds never before performed with MECC. This paper presents several separations of hydrophobic compounds using bile salt mobile phases with high organic modifier content. Investigations of the effects of methanol on the CMC for both SDS and sodium cholate, a trihydroxy bile salt, are also reported. Reasons for the tolerance of the bile salt micelles to organic solvent are discussed.

EXPERIMENTAL

Apparatus

Both absorbance and laser-based fluorescence detection were used in this study. Fluorescence excitation was provided by a Liconics (Sunnyvale, CA, USA) Model 423OMB helium–cadmium laser operated at 325 nm. Collection of fluorescence emission was as described elsewhere [12]. Parameters such as detection wavelengths, column length, mobile phase composition and applied voltage are given in the text.

Absorbance spectra were measured on a Perkin-Elmer Model Lambda 3B dual-beam spectrometer. The sample cuvette was maintained at 30°C with a Perkin-Elmer Model 0050405 temperature controller bath.

Chemicals

Sodium cholate (NaCh), sodium deoxycholate (NaDCh) and SDS were obtained from Sigma (St. Louis, MO, USA). Rhodamine 6G, amines and 7-chloro-4-nitrobenzo-2,1,3-oxadiazole (NBD-Cl) were purchased from Eastman Kodak (Kingsport, TN, USA). NBD-Cl derivatization of amines has been described previously [23]. All solvents were of high-performance liquid chromatography (HPLC) grade and were purchased from Baxter. PAHs and aflatoxins were obtained from Aldrich (Milwaukee, WI, USA). Benzo[*a*]pyrene (B[*a*]P) tetrol was obtained from Midwest Research Institute (Kansas City, MO, USA). Structures for compounds studied are depicted in Fig. 2.

Procedures

Injections were made by a common syphoning procedure [6]. Column pretreatment and equilibration was as described earlier [12]. Due to the very limited water solubility of some of the compounds studied, the samples were dissolved in methylene

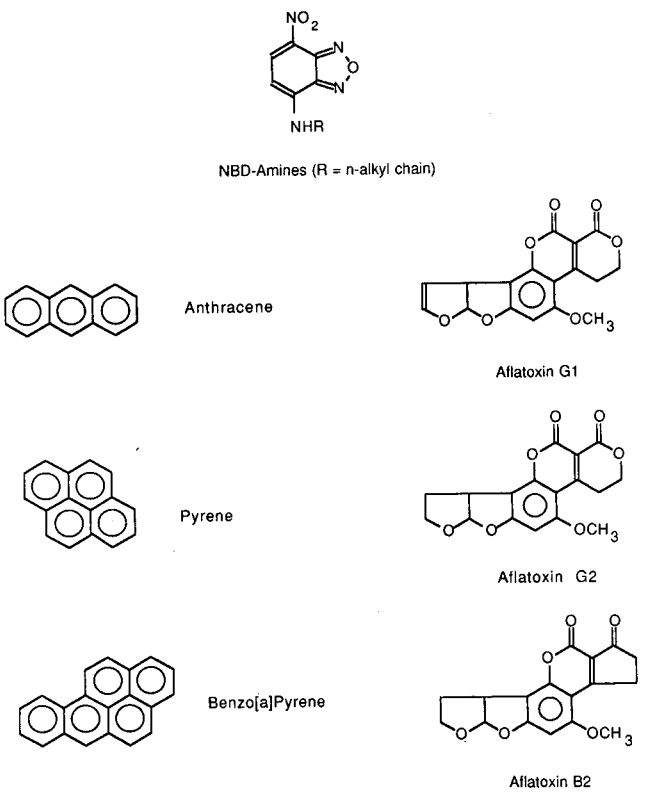

Fig. 2. Structures of compounds investigated in this work.

chloride and extracted into the mobile phase or further dissolved in methanol followed by dilution with an approximately 50% micellar solution. Injections from pure organic solvent were avoided to prevent problems with electric field distortions and loss of current.

CMC values were estimated via dye solubilization as described by Small and Carey [15]. This procedure consists of measuring the wavelength of maximum absorbance for a dye (Rhodamine 6G) under varying concentrations of bile salt and methanol. The wavelength of maximum absorbance (λ_{max}) is measured for each concentration and plotted against the logarithm of the surfactant concentration. All λ_{max} values are the average of three measurements.

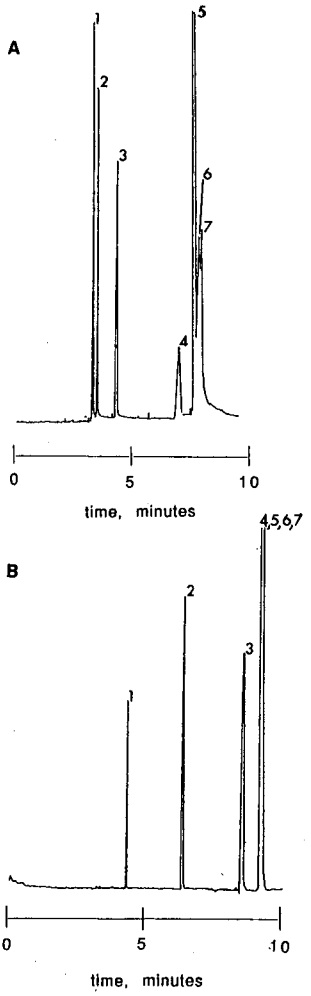

Fig. 3. Separation of NBD-derivatized amines in (A) NaCh and (B) SDS. Mobile phase, 0.05 *M* surfactant–0.01 *M* Na_2HPO_4–0.006 *M* $Na_2B_4O_7$; applied voltage, 15 kV; column length, 50 cm, 45 cm to window; detection, argon ion laser fluorescence, λ_{ex} 488 nm, λ_{em} 540 nm. Peaks: 1 = methylamine-NBD; 2 = propylamine-NBD; 3 = pentylamine-NBD; 4 = octylamine-NBD; 5 = decylamine-NBD; 6 = deodecylamine-NBD; 7 = quadradecylamine-NBD.

RESULTS AND DISCUSSION

In first evaluating the bile salts for hydrophobic separations, a well-characterized test mixture of derivatized *n*-alkyl amines were employed. To better estimate t_m and separation performance, a mixture of NBD derivatives was made: methyl, propyl, pentyl, octyl (C_8), decyl (C_{10}), dodecyl (C_{12}) and tetradecyl (C_{14}) amine were included. The late-eluting derivatives (C_8–C_{14}) serve to gauge hydrophobic compound separation performance as well as mark the micelle migration time. Fig. 3 shows the separation of these compounds with NaCh and SDS. Retention time increases linearly with increasing carbon chain length, so elution order is the same for both systems. Note that the late-eluting solutes are partially resolved with the NaCh. As mentioned above, the more polar micelle allows for k' values more near the optimum range.

A more significant example of the capabilities of MECC using bile salts is shown in Fig. 4; the separation of the aflatoxins G_1, G_2, and B_2 with a NaDCh pseudostationary phase. Aflatoxins are extremely toxic compounds found in spoiled foodstuffs [24]. Baseline separation of these compounds has been reported [25] with SDS, but only after addition of organic solvent. In this case baseline resolution is

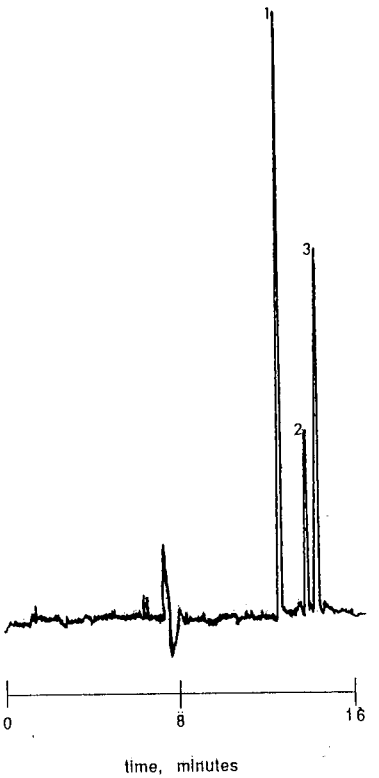

Fig. 4. Separation of aflatoxins. Peaks: 1 = G_2; 2 = G_1; 3 = B_2. Mobile phase, 0.05 *M* NaDCh–0.01 *M* Na_2HPO_4–0.006 *M* $Na_2B_4O_7$; applied voltage, 16 kV; column length, 53 cm, 50 cm to window; detection, HeCd laser fluorescence, λ_{ex} 325 nm, λ_{em} 450 nm.

obtained for all three compounds without the use of organic modifiers, thus saving analysis time. Coupled with the sensitivity of laser-based fluorescence, bile salt MECC offers a rapid assay for these toxins.

Further improvements in resolution are attained when methanol is added to the mobile phase. Fig. 5 shows the separation of the aforementioned NBD amines using a mobile phase containing 20% methanol. With the NaCh system (Fig. 5A), all of the more hydrophobic (C_8–C_{14}) amine derivatives are fully resolved, with reasonable efficiency. In contrast, the SDS system (Fig. 5B) allows resolution of only the C_8 from the C_{10}–C_{14} amine derivatives which coelute at t_m. In addition, analysis time for the SDS system is roughly three times that for the NaCh system. Efficiency is much poorer with the SDS system, presumably due to micelle polydispersity. Micelle polydispersity arises when the micelles have a range of aggregation numbers, leading to the formation of micelles with a possible range of electrophoretic mobilities. Solutes that associate with the micelles can experience a similar range of velocities and thereby become dispersed. This mechanism is thought to be a significant source of band dispersion in MECC [7,26]. The micelle polydispersity problem is most acute at or near the CMC [7,12]. Addition of organic solvent can lead to the onset of this problem at surfactant concentrations where this is usually not the case. When methanol is added to the mobile phase, the overall solution polarity is decreased. This presumably reduces the affinity of the hydrophobic tails of the SDS monomers for one another, causing an increase in CMC [27]. Conversely, the helical structure of the bile salt

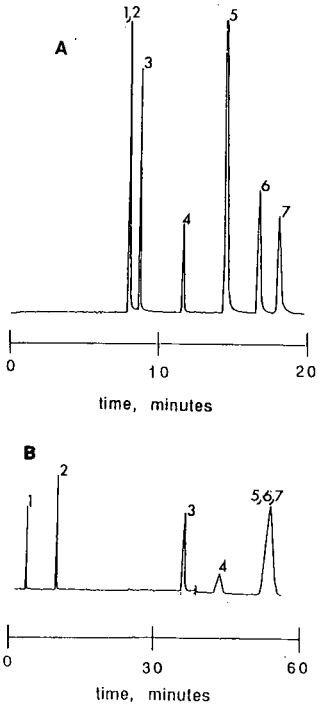

Fig. 5. Separation of NBD-derivatized amines. Conditons identical to Fig. 3 except mobile phase contains 20% methanol. (A) NaCh; (B) SDS.

micelle, since it resembles a reversed or inverted micelle, might be expected to be less vulnerable to disassociation by a reduction in the polarity of the bulk solution. The methanol-modified mobile phase might be favored by the hydrophobic face of the monomer, possibly stabilizing the micelle relative to SDS.

The impact of methanol content on micelle formation was studied by estimating the CMC for both SDS and NaCh under MECC mobile phase conditions. Dye solubilization was the method used in this study [15]. The wavelength of maximum absorbance was measured between 520 and 580 nm for Rhodamine 6G at several different NaCh concentrations. Plots of λ_{max} *vs.* log[NaCh] were constructed over a range of methanol concentrations. Fig. 6 shows a sample plot. The first shift in λ_{max} is taken as an estimate of the CMC. As the concentration of NaCh is increased past the CMC, λ_{max} continues to shift until a plateaus is reached. The shape of the plot is assumed to be the result of varying degrees of dye association with the micelle. As more micelles are formed, the dye interacts with increasing strength until a point is reached where the dye is completely micelle-solubilized, causing the wavelength shift to reach a maximum. The actual CMC could be taken as this plateau, the first shift, or the midpoint. We have arbitrarily chosen the first breakpoint after the work of Small and Carey [15]. It should therefore be emphasized that the CMC values presented here are arbitrary estimates of the true CMC. The dependence of the CMC for SDS and NaCh are shown in Fig. 7. The CMC for SDS begins to rise at methanol levels above approximately 10%, while NaCh stays nearly constant until 30% methanol. Chromatographic efficiency for SDS reflects these trends [7]. As mobile phase methanol content increases, the efficiency with the SDS system shows a steady decrease. The same peak in the NaCh system shows the same or even increased efficiency. Thus, the ability of NaCh to tolerate the presence of organic solvent without significant loss of efficiency enhances the capabilities of MECC with regard to the separation of hydrophobic compounds.

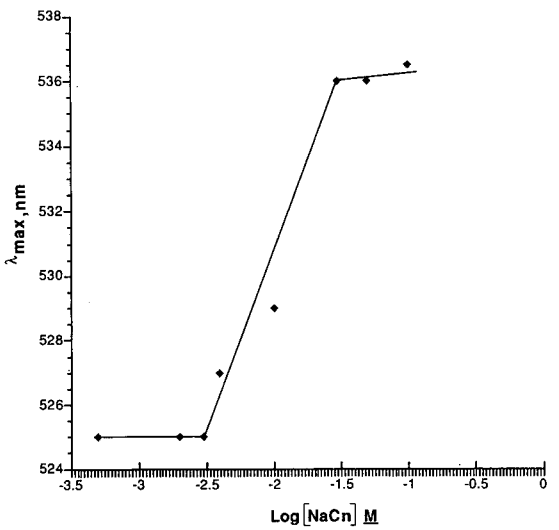

Fig. 6. Sample plot of wavelength of maximum absorbance *vs.* log[NaCh]. CMC is taken as first change in λ_{max}.

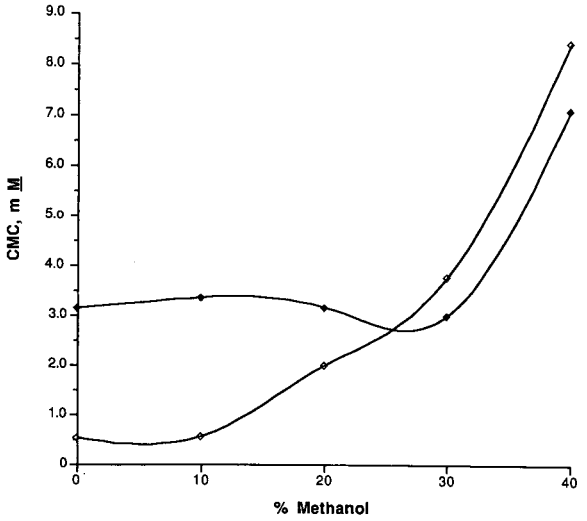

Fig. 7. Critical micelle concentration dependence on mobile phase methanol content for SDS and NaCh. Mobile phase contains 0.01 *M* Na_2HPO_4–0.006 *M* $Na_2B_4O_7$. ◆ = NaCh; ◇ = SDS.

One of the more challenging separation problems for MECC is that of PAHs. To date, there are only two reports of PAH separations with electrophoretic techniques. The earliest approach to hydrophobic neutrals was a CZE separation based on solvophobic interactions leading to charged complexes. Ionic PAH complexes were separated by the usual CZE mechanism [28]. A more recent approach involving micellar solutions and cyclodextrins has also been applied to the separation of certain relatively small molecules [9]. Bile salt MECC to date offers relatively efficient separations of PAHs as large as pyrene and B[*a*]P, and more general applicability than other electrokinetic-based approaches. Fig. 8 shows the separation of anthracene, pyrene and B[*a*]P with a NaCh system. PAHs larger than B[*a*]P can also be addressed by increasing the amount of organic modifier in the mobile phase. Baseline resolution is achieved at only 10% methanol, well in the efficient working range for NaCh. At 20% methanol, the resolution is further increased without drastic loss of efficiency, suggesting that PAHs larger than B[*a*]P might be separated.

Substituted PAHs such as hydroxy derivatives may also be separated with these systems. While more polar than unsubstituted PAHs, these compounds are difficult to address with SDS pseudostationary phases. Hydroxy-substituted PAHs play a critical part in determining the carcinogenity of PAHs, and metabolic pathways almost invariably terminate in hydroxy derivatives [29]. Fig. 9 shows the separation of B[*a*]P from B[*a*]P tetrol, one of the final forms in the metabolic pathway. This separation suggests that MECC could find application in monitoring ingestion and metabolic kinetics of PAHs in biological systems.

Bile salt surfactants clearly exhibit practical advantages over conventional *n*-alkyl surfactants. Selectivity and applicability of MECC is expanded by their use. Unique selectivity is achieved by the highly ordered nature of the micelles; chiral separations are possible. In addition, the polar interior allows increased resolution for

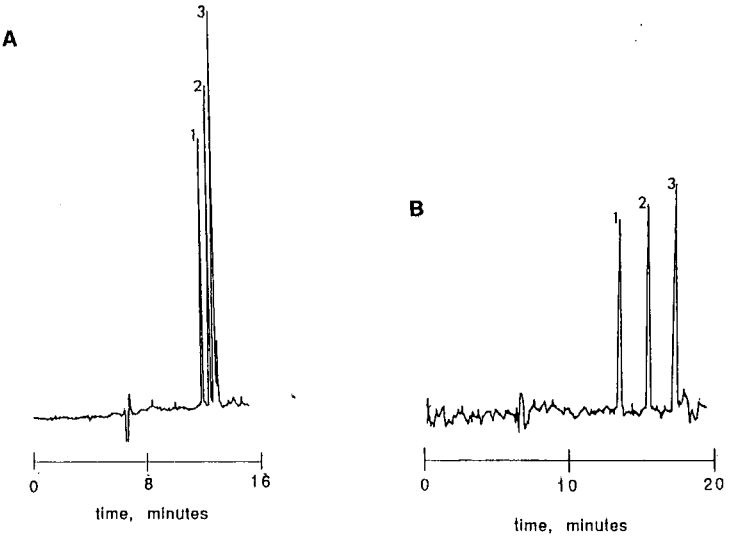

Fig. 8. Separation of polyaromatic hydrocarbons. Peaks: 1 = anthracene; 2 = pyrene; 3 benzo[*a*]pyrene. Mobile phase, 0.05 *M* NaCh–0.01 *M* Na_2HPO_4–0.006 *M* $Na_2B_4O_7$ with (A) 10% methanol and (B) 20% methanol; applied voltage, 20 kV; column length, 53 cm; detection, HeCd laser fluorescence, λ_{ex} 325 nm, λ_{em} 400 nm.

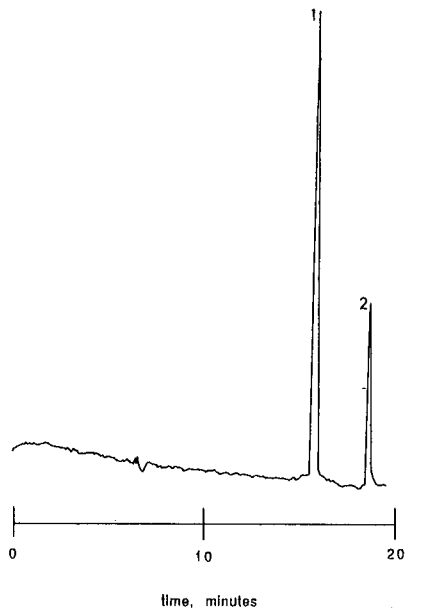

Fig. 9. Separation of (1) benzo[*a*]pyrene tetrol and (2) benzo[*a*]pyrene. Mobile phase, 0.05 *M* NaCh–0.01 *M* Na_2HPO_4–0.006 *M* $Na_2B_4O_7$; applied voltage, 16 kV; other conditions same as in Fig. 8.

hydrophobic compounds, extending the utility of the technique to previously intractable separation problems. The inverted structure of the aggregates appears to permit relatively undisturbed micelle formation in the presence of organic modifiers, thereby allowing greater peak capacity. The data presented herein also offer indirect support for the helical structure model of the bile salt micelle. It is evident that these surfactants will find application in many separation problems.

ACKNOWLEDGEMENT

This work was sponsored by The Division of Chemical Sciences, Office of Basic Energy Sciences, United States Department of Energy, under grant DE-FG05-86ER13613 with the University of Tennessee.

REFERENCES

1 J. W. Jorgenson and K. D. Lukacs, *Anal. Chem.*, 53 (1981) 1298–1302.
2 S. Terabe, K. Otsuka, K. Ichikawa, A. Tsuchiya and T. Ando, Anal. Chem., 56 (1984) 111–113.
3 S. Terabe, K. Otsuka and T. Ando, *Anal. Chem.*, 57 (1985) 834–841.
4 A. T. Balchunas and M. J. Sepaniak, *Anal. Chem.*, 59 (1987) 1466–1470.
5 J. Gorse, A. T. Balchunas, D. F. Swaile and M. J. Sepaniak, *J. High Resolut. Chromatogr. Chromatogr. Commun.*, 11 (1988) 554.
6 M. J. Sepaniak, D. F. Swaile and A. C. Powell, *J. Chromatogr.*, 480 (1989) 185–196.
7 A. T. Balchunas and M. J. Sepaniak, *Anal. Chem.*, 60 (1988) 617–621.
8 J. Jorgenson and M. Bushey, *J. Microcol. Separ.*, 1 (1989) 125–130.
9 S. Terabe, Y. Miyashita, O. Shibata, E. R. Barnhart, L. R. Alexander, D. G. Patterson, B. L. Karger, K. Hosoya and N. Tanaka, *J. Chromatogr.*, 516 (1990) 23–31.
10 S. Terabe, M. Shibata and Y. Miyashita, *J. Chromatogr.*, 480 (1989) 403–411.
11 H. Nishi, T. Fukuyama, M. Matsuo and S. Terabe, *J. Chromatogr.*, 515 (1990) 233–243.
12 R. O. Cole, M. J. Sepaniak and W. L. Hinze, *J. High Resolut. Chromatogr.*, 13 (1990) 579–582.
13 S. Terabe, H. Nishi, T. Fukuyama and M. Matsuo, *J. Microcol. Separ.*, 1 (1989) 234–242.
14 H. Nishi, T. Fukuyama, M. Matsuo and S. Terabe, *J. Chromatogr.*, 498 (1990) 313–323.
15 D. M. Small and M. G. Carey, *J. Colloid Interface Sci.*, 31 (1969) 382–395.
16 D. M. Small, in P. P. Nair and D. Kritchevsky (Editors), *The Bile Acids*, Plenum Press, New York, 1971, pp. 249–356.
17 D. M. Small, *Adv. Chem. Ser.*, 84 (1968) 31.
18 G. Conte, R. Di Blasi, E. Gigilo, A. Parretta and N. V. Pavel, *J. Phys. Chem.*, 88 (1984) 570–5724.
19 G. Esposito, E. Giglio, N. V. Pavel and A. Zanobi, *J. Phys. Chem.*, 91 (1987) 356–362.
20 A. R. Campanelli, C. De Sanctis, E. Chiessi, M. D'Alagni, E. Giglio and L. Scaramuzza, *J. Phys. Chem.*, 93 (1989) 1536–1542.
21 H. Kawamura, M. Manabe, T. Narikiyo, H. Igimi, Y. Murata, G. Sugihara and M. Tanaka, *J. Solution Chem.*, 16 (1987) 433–441.
22 L. Fisher and D. Oakenfall, *Aust. J. Chem.*, 32 (1979) 31–39.
23 G. M. Murray and M. J. Sepaniak, *J. Liq. Chromatogr.*, 6 (1983) 931–939.
24 R. D. Zare and G. J. Diebold, *Science (Washington, D.C.)*, 196 (1977) 1439–1441.
25 A. T. Balchunas, D. F. Swaile, A. C. Powell and M. J. Sepaniak, *Sep. Sci. Technol.*, 23 (1988) 1891–1904.
26 S. Terabe, K. Otsuka and T. Ando, *Anal. Chem.*, 61 (1989) 251–260.
27 L. Magid, in K. L. Mittal (Editor), *Solution Chemistry of Surfactants*, Plenum Press, New York, 1979, pp. 427–453.
28 J. Jorgenson and Y. Walbroehl, *Anal. Chem.*, 58 (1986) 479–481.
29 G. Becher and A. Bjørseth in A. Bjørseth and T. Ramdahl (Editors), *Handbook of Polycylic Aromatic Hydrocarbons*, Marcel Dekker, New York, 1985, pp. 237–252.

Journal of Chromatography, 557 (1991) 125–136
Elsevier Science Publishers B.V., Amsterdam

CHROM. 23 269

Electroosmotically driven electrochromatography of anions having similar electrophoretic mobilities by ion pairing

WILLIAM D. PFEFFER and EDWARD S. YEUNG*
Ames Laboratory–USDOE and Department of Chemistry, Iowa State University, Ames, IA 50011 (USA)

ABSTRACT

Anions of similar electrophoretic mobility are separated using an electrochromatographic technique which involves partitioning the anions, with the aid of the ion-pairing agent, tetrabutylammonium (TBA) cation, onto the surface of a reversed-phase open-tubular capillary liquid chromatographic (OTCLC) column. The anions separate based on differences in retention rather than differences in electrophoretic mobility. Resolution is easily controlled by varying the concentration of TBA in the buffer. Complete separation of anions having similar mobilities is achieved with as little as 600 μM TBA. Mass transfer broadening is inherently smaller for this electroosmotically driven system than that for pressure-driven OTCLC. The efficiency achieved for such a separation in a 40-cm column (N = 140 000) is twice that for a similar chromatographic separation and nearly equal to that for a similar, but poorly resolved, capillary zone electrophoretic separation.

INTRODUCTION

Recently, Everaerts *et al.* [1] discussed the concept of electrophoresis *versus* electrochromatography. They argued that for capillary zone electrophoresis (CZE), a pure electrophoretic separation can only be accomplished in capillaries of 200 μm I.D. or greater. Separations in capillaries of smaller I.D., especially those with I.D. < 50 μm and having electroosmotic flow (EO) as the major mode of solute transport, tend to exhibit behavior that is a hybrid between "purely" electrophoretic and "purely" chromatographic [1]. Nevertheless, in a typical CZE separation of ionic solutes, the separation will be predominantly based on the differential migration of the solutes. Highly efficient separations can be achieved in capillaries without the need for wall adsorption, which is essential for the complementary technique, open-tubular capillary liquid chromatography (OTCLC). In fact, for certain solutes, adsorption on the wall is viewed as disastrous to efficiency and to be avoided if possible [2,3]. However, narrow capillaries (I.D. < 200 μm) are desirable because they increase the surface area-to-volume ratio, which results in efficient heat dissipation.

In the typical CZE separation, the resolution between two solutes will be dependent on their electrophoretic mobility differences and also the EO flow. Increases in resolution are commonly achieved by changing the pH of the buffer, which can alter the degree of charge on the solutes, thereby altering their mobilities. At the same

0021-9673/91/$03.50

time, EO flow can be reduced, eliminated or reversed through buffer additives so that differences in mobility are better exhibited.

Achieving adequate resolution for ionic solutes whose mobilities are nearly identical and whose degrees of charge remain constant over a wide pH range, such as isomeric strong acids or bases, is an exceptionally difficult task. Increasing resolution based on varying pH or EO flow can be ineffective. In these instances, other methods to improve resolution must be adopted. These include the addition of an organic modifier to the buffer [4] and the use of electrokinetic chromatography [5,6].

Our approach to this problem is to take the mixed-mode behavior discussed earlier to an extreme by giving CZE separation a strong chromatographic component. Realizing that isomeric strong acids and bases are easily separated using reversed-phase ion-pair liquid chromatography, we decided to combine the high degree of analyte discrimination associated with the ion-pair technique with the ease and efficiency of a CZE separation. This is accomplished by replacing the CZE column with a reversed-phase OTCLC column of narrow I.D. (*ca.* 10 μm) and by including an ion-pairing agent in the buffer. Because narrow I.D. columns are used, and because the flow profile is flat (electroosmosis) rather than parabolic, the mass transfer contribution to zone broadening is minimized for partitioning solutes [7]. The ion-pairing agent is used to control the affinity of the anions for the stationary phase. We demonstrate the resulting technique, which can be called ion-pair electrochromatography, by separating a series of anions whose mobilities at the working pH are nearly identical.

EXPERIMENTAL

The buffer used throughout was 10 m*M* phosphate. A 0.1% hydroxypropylcellulose (HPC) (Aldrich, Milwaukee, WI, USA) solution was prepared from buffer and the final pH adjusted to 7.0. Ion-pairing solutions were prepared by diluting 40.0% (w/w) tetrabutylammonium hydroxide (TBA) (Aldrich) with the buffer and adjusting the final pH to 7.0. The anions 4-amino-1-naphthalenesulfonic acid (4A1N), 2-amino-1-naphthalenesulfonic acid (2A1N), 5-amino-2-naphthalenesulfonic acid (5A2N), 8-amino-2-naphthalenesulfonic acid (8A2N) (all from Aldrich) and 1-naphthol-4-sulfonic acid (1H4N) (Eastman Kodak, Rochester, NY, USA) were prepared in running buffer prior to their injection.

The fused-silica capillaries (Polymicro Technologies, Phoenix, AZ, USA) were 50 cm long and nominally of 10 μm I.D. These capillaries were used as supplied or coated, and the coating later cross-linked, with either 0.9% (w/v) PS-264 (Petrarch Systems, Bristol PA, USA) or 10.0% (w/w) OV-17v (Alltech, Deerfield, IL, USA) as described in ref. 8 or 9, respectively. The polyimide coating was burned off at one tip of the capillary to prevent analytes from possibly adsorbing to it during an injection. It was also burned off at 40 cm from this tip to facilitate on-column detection.

The CZE–electrochromatography system is similar to one described previously [10], except that a stationary phase is used in some instances. The electric field is supplied by either a positive or negative high-voltage supply (0–30 kV) (Glassman High Voltage, Whitehouse Station, NJ, USA; Model NJ30P0400-11 or MJ30N0400-11).

Chromatography was performed by disconnecting the CZE column from the

high-voltage isolation unit and attaching it to a solvent reservoir (Valco Instruments, Houston, TX, USA; Part No. ZU4L) which had a head pressure supplied by a regulated high-pressure helium tank.

Sample introduction for all three types of separations was accomplished by using hydrodynamic injection. The chromatographic solvent velocity and electroosmotic flow velocity were calculated from the baseline disturbance that resulted from the injection of running buffer containing *ca.* 10% of acetonitrile. Detection of the anions in all instances was accomplished by using a laser-based fluorescence detector described previously [7].

All data were either collected on a strip-chart recorder or subjected to analogue to digital conversion (Data Translation, Marlborough, MA, USA; Model DT2827, 5–10 Hz) and later stored on a personal computer (IBM PC-AT).

RESULTS AND DISCUSSION

When an anion in a buffer-filled capillary is subjected to an electric field, E, the anion will migrate with a velocity, v, described by

$$v = v_{ep} + v_{eo} = (\mu_{ep} + \mu_{eo})E \tag{1}$$

where v_{ep}, v_{eo}, μ_{ep} and μ_{eo} represent the electrophoretic velocity component, the electroosmotic velocity component, the electrophoretic mobility of the anion and the coefficient for electroosmotic flow, respectively. When two anions, 1 and 2, are subjected to these conditions, they will separate with a resolution, R, defined by

$$R = \frac{1}{4\sqrt{2}}(\mu_{ep_1} - \mu_{ep_2})\left[\frac{EL}{D(\bar{\mu}_{ep} - \mu_{eo})}\right] \tag{2}$$

where $\bar{\mu}_{ep}$ is their average mobility, D is their diffusion coefficient and L is the length of the column [11].

In a typical CZE separation of anions, μ_{ep} and μ_{eo} are of opposite sign; therefore, by reducing μ_{eo} in eqn. 2, the resolution between the two anions will be increased. In practice, this can be accomplished through the use of certain buffer additives, such as HPC. Fig. 1A represents an attempted separation of two anions using a buffer containing HPC. Although the EO flow has been nearly eliminated, the resolution between the two anions is still close to zero.

If these two anions were subjected to a separation using capillaries similar to those used in OTCLC, two results can be expected. First, owing to the stationary phase shielding the silanol groups, the EO flow will be drastically reduced; therefore, migration of the anions will be based on their mobility alone ($v \approx v_{ep}$). Second, if the anions have enough hydrophobic character, there is the possibility of the solutes partitioning onto the stationary phase. In such a case, an anion will travel with a velocity, v', which is related to v by

$$v' = \frac{v}{(1 + k)} \tag{3}$$

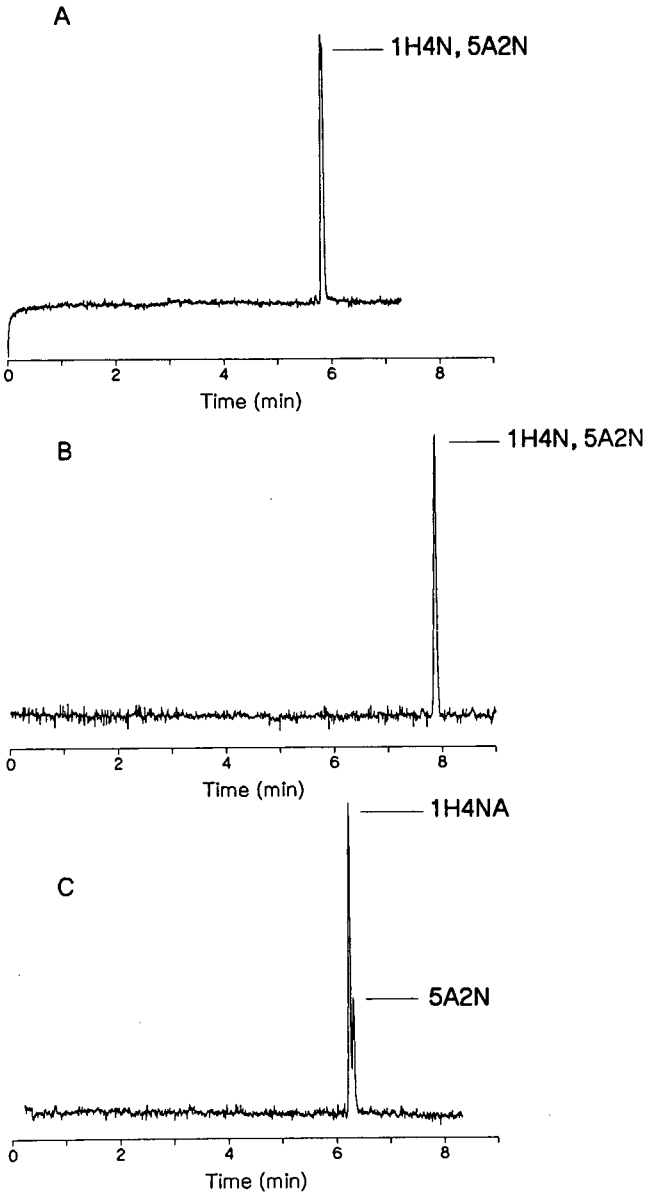

Fig. 1. (A) Elution profile of a CZE separation with reduced EO flow for 5A2N and 1H4N. Buffer conditions: 10 m*M* phosphate, 0.1% HPC, pH 7.0. The separation column is a 50 cm × 10 μm I.D. uncoated capillary having a 40 cm separation distance. Separation voltage, −21 kV. (B) Elution profile for an electrochromatographic separation of the same two anions. Buffer: 10 m*M* phosphate, pH 7.0. The column is a 50 cm × 10 μm I.D. capillary coated with PS-264 with a separating distance of 40 cm. Separation voltage, −21 kV. (C) Electrochromatographic elution profile for the same two anions using a column coated with OV-17v. Buffer, column dimensions and separation voltage are as in (B).

where k is the capacity factor of the anion. In the situation where two anions have similar mobilities but different capacity factors, they will elute with a velocity difference, $\Delta v'$, defined by

$$\Delta v' = \frac{v(k_2 - k_1)}{(1 + k_2)(1 + k_1)} \tag{4}$$

As $\Delta v'$ is proportional to the difference in the capacity coefficients, if a large enough difference exists, complete separation can be expected.

Using this rationale, we attempted to separate the two anions discussed earlier using a column coated with a polymer, PS-264. From Fig. 1B, it can be seen that the electroosmotic flow has been nearly eliminated but, as before, the resolution for the anions is near zero. An attempt to separate the two chromatographically in a pressure-driven system yielded the same results in that the anions were barely retained, if at all, and were inseparable under conditions similar to those in Fig. 1B.

We observe that as the individual capacity factors are small, increasing k for each anion may increase their difference and, hence, $\Delta v'$. The retention of a solute may be increased by modifying the stationary or the mobile phase. In the case of the stationary phase, an OTCLC column can be made more retentive by increasing the film thickness of the stationary phase. Because the column used in Fig. 1B is representative of the most retentive column that we are able to produce repeatedly using the method in ref. 8, we adopted a procedure developed by Dluzneski and Jorgenson [9]. They described a procedure for coating columns of similar I.D. using the polymer OV-17v. After preparing a column from conditions which produced the thickest polymer film in ref. 9, we again attempted to separate the two anions. It can be seen from Fig. 1C that, although incomplete, the beginning of a separation is present.

This approach has several drawbacks. The first is that changing columns to improve a separation is tedious and time consuming. The second, as Fig. 1C demonstrates, is that this technique will fail for many polar, ionic solutes. A similar problem existed in liquid chromatography, but the technique of ion pairing provided a useful solution. Therefore, to increase the retention of these anions through mobile phase modification, the principles of ion-pair chromatography were adopted.

It is well known in ion-pair chromatography that the addition to the eluent of a salt that contains a large organic cation will increase the affinity of an anion for the stationary phase. Although several models exist for reverse-phase ion-pair chromatography [12,13], many experimental results involving a bonded stationary phase have been described by the dynamic ion-exchange model [14–18]. An important requirement for the dynamic ion-exchange model is that the ion-pairing agent, in our case a cation, C^+, be partitioned onto the stationary phase. This can be described through the equilibrium

$$C_m^+ \overset{K_1}{\rightleftharpoons} C_s^+ \tag{5}$$

where the subscripts m and s denote the mobile and the stationary phase, respectively. The anion, A^-, is partitioned onto the column through the equilibrium

$$A_m^- + C_s^+ \overset{K_2}{\rightleftharpoons} (A^-C^+)_s \tag{6}$$

We have observed previously [7] that when a cationic surfactant is incorporated into an electrochromatographic system using a column similar to that in Fig. 1B, the EO flow is in the direction of the anode, and its velocity is dependent on the surfactant concentration. This is due to the surfactant partitioning itself between the mobile and stationary phases, which then modifies the charge on the surface. The EO velocity is directly proportional to this surface charge. Because of the equilibrium that exists, this charge, and hence EO velocity, are dependent on the cation concentration. For the same reason, it is evident from Fig. 2 that the cation, TBA, which is a common ion-pairing, agent, also partitions itself onto such a stationary phase. Based on this we assume that the dynamic ion-exchange model is the dominant retention mechanism. However, as it is unlikely that only one retention mechanism exists, we also take into account the formation of ion pairs.

For the model of ion-pair formation, the anion and the cation form an ion pair through

$$A_m^- + C_m^+ \overset{K_3}{\rightleftharpoons} (A^-C^+)_m \tag{7}$$

and this pair partitions onto the stationary phase through

$$(A^-C^+)_m \overset{K_4}{\rightleftharpoons} (A^-C^+)_s \tag{8}$$

In the absence of ion-pair formation, v' and $\Delta v'$ are described by eqns. 3 and 4, with v now being the sum of v_{ep} and v_{eo}. However, in the presence of ion-pair formation, the ion pair will have zero charge; therefore, it will be transported by EO flow alone. This makes v' and $\Delta v'$ more complicated. In this case, v' becomes

$$v' = \frac{Fv}{1 + k} + \frac{(1 - F)v_{eo}}{1 + k'} \tag{9}$$

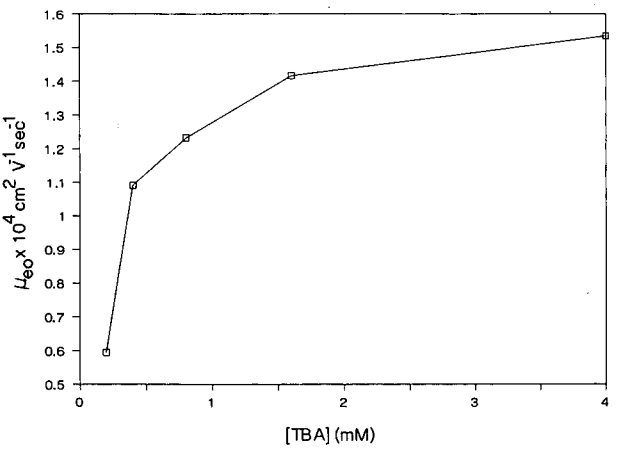

Fig. 2. Dependence of the coefficient for electroosmotic flow (μ_{eo}) on the concentration of TBA in a buffer of 10 mM phosphate, pH 7.0. Column and voltage conditions as in Fig. 1B.

and $\Delta v'$ becomes

$$\Delta v' = v\left[\frac{F_1 - F_2 + F_1k_2 - F_2k_1}{(1 + k_2)(1 + k_1)}\right] + v_{eo}\left[\frac{F_2 - F_1 + (1 - F_1)k'_2 - (1 - F_2)k'_1}{(1 + k'_2)(1 + k'_1)}\right] \quad (10)$$

where F is the fraction of free anion, k is the capacity factor for free ion and k' is the capacity factor of the ion pair. F can be determined from

$$F = \frac{[A_m^-]}{[A_m^-] + [A^-C_m^+] + [A^-C_s^+]} = \frac{1}{1 + K_3(1 + K_4)[C_m^+]} \quad (11)$$

We can illustrate the effect of the ion-paring agent on $\Delta v'$ using these equations for the case where the dynamic ion-exchange model is dominant ($K_1K_2 \gg K_3K_4$). At low concentrations of ion-pairing agent, F will be near unity and the second part of eqn. 10 can be neglected. In addition, if $F_1 \approx F_2$, eqn. 10 can be approximated by eqn. 4. With $k \propto K_1K_2[C_m^+]$ [19] and $\Delta v' \propto (k_1 - K_2)$, increasing retention via the ion-pairing agent will increase $\Delta v'$.

To demonstrate this, five anion were subjected to the same separation as in Fig. 1A. From the electropherogram in Fig. 3, it is observed that four of the five anions are unresolved because of similar mobilities. Next, the column was replaced with one identical with it, and equilibrated with a buffer containing 1.25 mM TBA. Separating the same five anions under these conditions resulted in no elution of any anion. To explain this, consider that when large, linear organic cations are incorporated into CZE buffers, the direction and magnitude of the EO flow becomes dependent on the

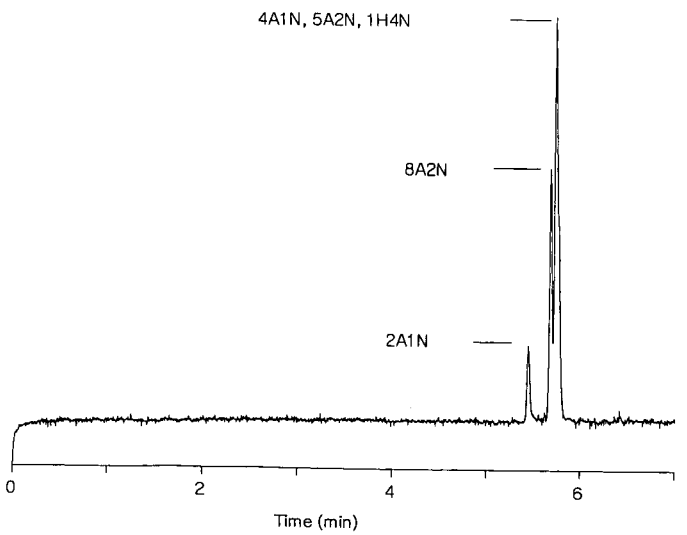

Fig. 3. CZE elution profile for five anions, four of which have similar electrophoretic mobilities. Column, buffer and voltage conditions as in Fig. 1A.

concentration of the cation. This has been discussed previously [20,21], but the effect in those reports is much less than that when a stationary phase is used [7]. In the case above, it was concluded that owing to the bulky nature of TBA, the amount adsorbed on the wall was ineffective at reducing the EO flow, which was later determined to be in the direction of the cathode (away from the detector). Attempting the same separation again, but with the polarity of the electric field reversed, resulted in the electropherogram shown in Fig. 4. Although the four anions with similar mobility are poorly resolved, the fact that 1H4N is separated from 5A2N is of interest. Under similar conditions (5 m*M* phosphate buffer, pH 7.0; +27 kV separating voltage), but with no TBA in the buffer, these two anions do not separate. As dynamic ion echange is unlikely owing to the poor column adsorption of TBA (stationary phase absent), this may be the result of ion-pair formation in the mobile phase.

The discussion above brings up a related point. The cations of salts such as cetyltrimethylammonium bromide and tetradecyltrimethylammonium bromide adsorb on uncoated capillary walls [20,21]. Therefore, CZE separations which have these or similar salts in the buffer may experience an ion-pairing effect. If such a separation is performed in a capillary with I.D. >> 10 μm and if the ion-pairing effect is significant, the bands may exhibit solute zone broadening owing to poor mass transfer.

To switch from CZE to electrochromatography, the CZE column was replaced with an OTCLC column similar to that used in Fig. 1B and equilibrated with a buffer containing 1.25 m*M* TBA. Subjecting the same five anions to a separation under these conditions resulted in the electrochromatogram shown in Fig. 5. Although the TBA concentration in Fig. 5 was 1.25 m*M*, the four anions of similar mobility can be separated completely using TBA even at 600 μM. At that concentration, however, the 2A1N peak is fused with the 1H4N peak. Note that the 2A1N, which was first to elute in Fig. 3, is now second from last. This is due to the amino group being adjacent to the

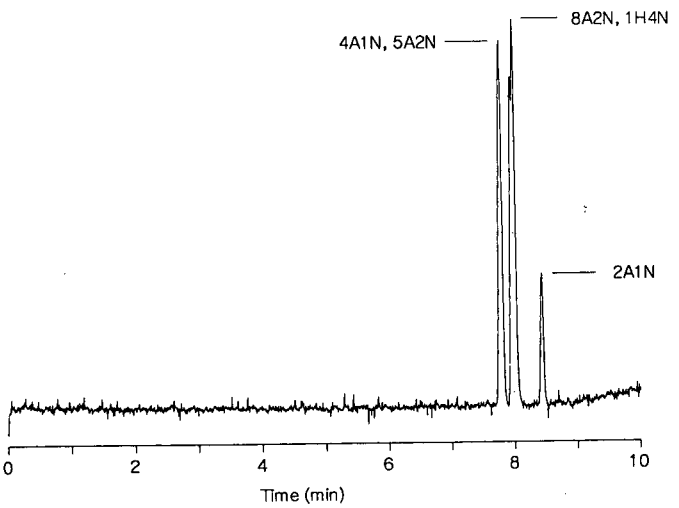

Fig. 4. CZE elution profile for the five anions using a 10 m*M* phosphate buffer, pH 7.0, containing 1.25 m*M* TBA. Column parameters as in Fig. 1A. Separation voltage, +21 kV.

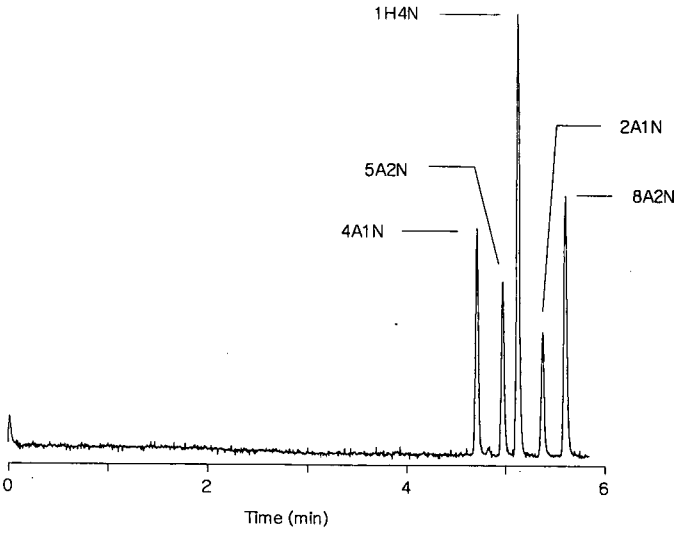

Fig. 5. Electrochromatographic separation of the five anions. Column conditions as in Fig. 1B and buffer conditions as in Fig. 4. Separation voltage, −21 kV.

sulfonic group for 2A1N, which results in a large k value in comparison with its isomers [22]. When TBA is at 7.5 mM, 2A1N becomes the last component to elute. Although not indicated in Fig. 5, all components elute with $v' > v_{eo}$; however, when TBA is at 7.5 mM, only 2A1N elutes with $v' < v_{eo}$. This illustrates the control of retention through $[C_m^+]$.

In order to compare this technique with ion-pair chromatography, the five anions were subjectd to a pressure-driven chromatographic separation using the same column and conditions as in Fig. 5. The result is shown in Fig. 6. For the four anions

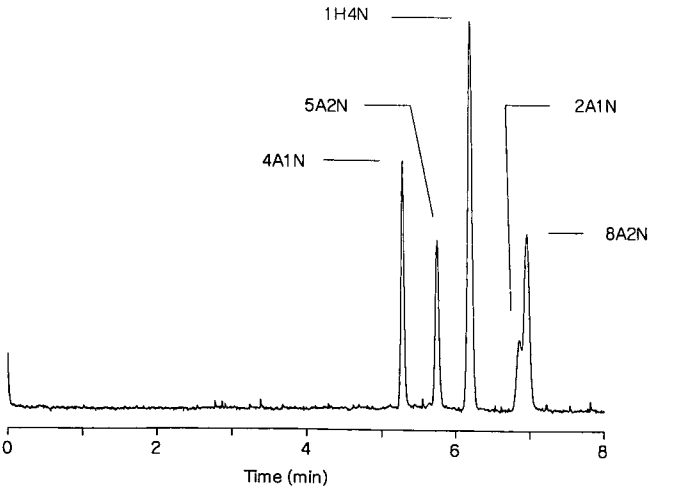

Fig. 6. Pressure-driven chromatographic separation of the five anions using the same buffer and column as in Fig. 5.

of similar mobility, the dominant separation factor present in Fig. 5 is their differences in column affinity, which is also the major separating factor in Fig. 6; hence the similarities in elution order and relative peak positions. As for the anions with different mobilities, the elution order and relative peak position will be a function of both mobility and column affinity, both of which are present only in the electrochromatographic technique. This explains the difference in peak position in Figs. 5 and 6 for the 2A1N peak relative to its neighbors.

The capacity factors for the anions in Fig. 6 are as follows: 4A1N 0.047, 5A2N 0.140, 1H4N 0.228, 2A1N 0.361 and 8A2N 0.380. The fact that these capacity factors are relatively small ($k < 1$) was expected because of the high separation efficiency observed in Fig. 5. The smallest number of theoretical plates, N, in Fig. 5 is for the 4A1N peak, with $N = 140\,000$. Comparing this value with those calculated for Fig. 6 reveals that this N is nearly twice that for the 4A1N peak and three times that for the 1H4N peak (smallest N). This is the result of the flat flow profile of electroosmotic and electrophoretic flow, contributing less to mass transfer broadening than the parabolic flow profile in pressure-driven systems [7,23–25]. Comparing the N value of 145 000 plates for the 2A1N peak in Fig. 5 with that in Fig. 3 or 4 reveals that they are nearly identical. Although no capacity factors were obtained, when TBA is at 7.5 mM 2A1N is eluted with $N = 50\,000$. Therefore, it can be seen that this technique will produce efficient separations only when k is kept small.

The resolution for each of the anion pairs in Fig. 5 was calculated and found to be >1 in all instances. As predicted, resolution can easily be controlled through the concentration of TBA, as shown in Fig. 7. The negative numbers in Fig. 7 results from the fact that the anion, 2A1N, changes elution order with 4A1N as the concentration of TBA is increased, *i.e.*, R actually becomes zero at some point in this range. The leveling off of the curves at high TBA concentration can be attributed to increased mass transfer broadening due to increased retention.

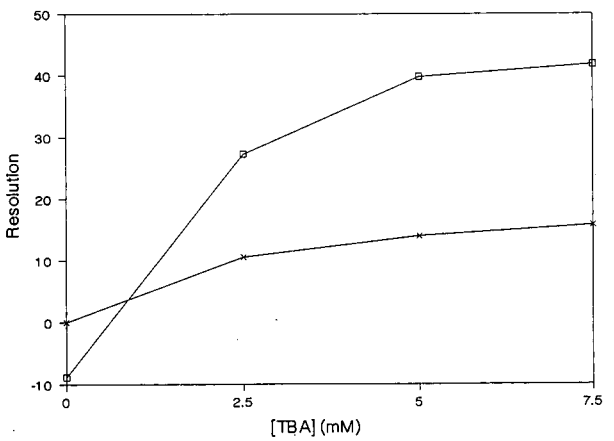

Fig. 7. Dependence of resolution on TBA concentration for ion-pair electrochromatography. Conditions as in Fig. 5. □ = 2A1N and 4A1N; × = 5A2N and 1H4N.

CONCLUSION

We have shown that anions that do not separate based on mobility differences in CZE can be made to separate electrochromatographically. The anions, which need no native affinity for the stationary phase, can be made to partition onto the column via an ion-pairing agent added to the buffer. In so doing, the anions now separate based on affinity differences for the column. Because mass transfer broadening is minimized by using columns of narrow I.D., by keeping the capacity factors small and by the flat flow profile which exists for electroosmotic flow, the efficiency of the resulting separation rivals that of a CZE separation. In addition, as there is a similarity between ion-pair electrochromatography and ion-pair chromatography, foundations for the separation of ionic solutes whose mobilities are similar can be derived from the vast amount of ion-pair chromatography literature. Finally, this technique is expected to be more sensitive than CZE to adjustments of such buffer parameters as pH, ionic strength and percentage of organic modifier, because not only will the electrophoretic component of the separation be affected, but also the chromatographic component.

ACKNOWLEDGEMENTS

The Ames Laboratory is operated by Iowa State University for the US Department of Energy under contract No. W-7405-Eng-82. This work is supported by the Director of Energy Research, Office of Basic Energy Sciences, Division of Chemical Sciences.

REFERENCES

1 F. M. Everaerts, A. A. A. M. Van de Goor, Th. P. E. M. Verheggen and J. L. Beckers, *J. High Resolut. Chromatogr.*, 12 (1989) 28.
2 S. Hjertén, *J. Chromatogr.*, 347 (1985) 191.
3 G. J. M. Bruin, J. P. Chang, R. H. Kuhlman, K.Zegers, J. C. Kraak and H. Poppe, *J. Chromatogr.*, 471 (1989) 429.
4 S. Fujiwara and S. Honda, *Anal. Chem.*, 59 (1987) 487.
5 E. Gassman, J. E. Kuo, and R. N. Zare, *Science*, 230 (1985) 813.
6 S. Terabe and T. Isemura, *Anal. Chem.*, 62 (1990) 652.
7 W. D. Pfeffer and E. S. Yeung, *Anal. Chem.*, 62 (1990) 2178.
8 W. D. Pfeffer and E. S. Yeung, *J. Chromatogr.*, 506 (1990) 401.
9 P. R. Dluzneski and J. W. Jorgenson, *J. High Resolut. Chromatogr. Chromatogr. Commun.*, 11 (1988) 332.
10 W. G. Kuhr and E. S. Yeung, *Anal. Chem.*, 60 (1988) 1832.
11 J. Jorgenson and K. D. Lukacs, *Anal. Chem.*, 53 (1981) 1298.
12 B. A. Bidlingmeyer, *J. Chromatogr. Sci.*, 18 (1980) 525.
13 H. Colin and G. J. Guiochon, *J. Chromatogr.*, 141 (1977) 289.
14 A. Zein and M. Baerns, *J. Chromatogr. Sci.*, 27 (1989) 249.
15 M. E. Del Rey and L. E. Vera-Avila, *J. Liq. Chromatogr.*, 11 (1988) 2885.
16 J. L. M. Van De Venne, J. L. H. M. Hendrix and R. S. Deelder, *J. Chromatogr.*, 167 (1978) 1.
17 P. T. Kissinger, *Anal. Chem.*, 49 (1977) 883.
18 N. E. Hoffman and J. C. Liao, *Anal.Chem.*, 49 (1977) 2231.
19 W. R. Melander and C. Horvathin, in M. T. W. Hearn (Editor), *Ion-Pair Chromatography*, Marcel Dekker, New Yok, 1985, Ch. 2.
20 T. Tsuda, *J. High Resolut. Chromatogr. Chromatogr. Commun.*, 10 (1987) 622.

21 X. Huang, J. A. Luckey, M. J. Gordon and R. N. Zare, *Anal. Chem.*, 61 (1989) 766.
22 C. Prandi and T. Venturini, *J. Chromatogr. Sci.*, 19 (1981) 308.
23 P. H. O'Farrell, *Science*, 227 (1987) 1587.
24 T. Tsuda and Y. Muramatsu, *Anal. Chem.*, 59 (1987) 521.
25 T. Tsuda, *Anal. Chem.*, 60 (1988) 1677.

Journal of Chromatography, 557 (1991) 137–153
Elsevier Science Publishers B.V., Amsterdam

CHROM. 23 253

Flip–flop elution concept in preparative liquid chromatography

HENRI COLIN* and PIERRE HILAIREAU
Prochrom, BP 9, 54250 Champigneulles (France)
and
MICHEL MARTIN
Ecole Supérieure de Physique et Chimie Industrielles, Laboratoire de Physique et Mécanique des Milieux Hétérogènes (URA CNRS 857), 10 Rue Vauquelin, 75231 Paris Cedex 05 (France)

ABSTRACT

A new concept is developed for improving the cycle time and the sample throughput in preparative liquid chromatography. In this flip–flop elution procedure, the direction of the mobile phase flow is reversed just after the compound of interest has been collected. The next sample injection is made at the other end of the column to the previous injection as the flow direction has been changed after a certain delay time. This time is determined in such a way that the compound of interest begins to elute (and can be collected) just after the end of the backflush peak of strongly retained components from the previous injection. In this way, no time is lost in separating and eluting the most strongly retained impurities. General expressions for the delay time and the cycle time (time between two consecutive injections) are given for diluted (Gaussian) as well as severely overloaded peaks. Similar expressions are also given for an optimized version of the normal elution procedure in which the direction of the flow of mobile phase remains unchanged. It is shown that the flip–flop operation gives a shorter cycle time than the optimized normal elution process when the time of the end of collection of the compound of interest is less than half the retention time of the last compound in the chromatogram. An experimental demonstration of the flip–flop elution concept is shown. It is emphasized that this concept can be extended to other separation techniques and to analytical separations where quantitative information is searched for only a fraction of the number of sample components.

INTRODUCTION

Recent years have seen rapid developments in high-performance preparative liquid chromatography (HPPLC), at both the theoretical and practical levels. HPPLC is now recognized as a powerful tool for industrial purifications, particularly in the pharmaceutical field. Whereas preparative liquid chromatography (PLC) was considered only few years ago to be a low-performance separation method based on the use of low-quality packing materials (large particle size and size distribution), the situation has changed dramatically recently and the present trend is to use high-quality packing materials with an average particle size in the range 10–20 μm and a narrow size distribution [1]. High efficiencies (more than 30 000 plates/m) can now be obtained

0021-9673/91/$03.50

routinely in large-size preparative columns (up to 45 cm I.D.). At the same time, important theoretical developments have occurred and the phenomena associated with intense overloading in non-linear chromatography are much better understood [2–5]. Economical aspects have also received much more attention in the recent past [6–8] and it has been demonstrated that when the purification conditions are properly optimized, the purification cost using HPPLC can be low enough to make this technique usable for products other than high added value materials.

Very high degrees of purity can be obtained by HPPLC. This, however, requires several conditions to be achieved at the same time. First, it is necessary to use high-quality solvents, otherwise solvent impurities would be concentrated in the purified product. Second, it is also necessary to use packing materials that do not release unwanted chemicals. Finally, contamination of collected material(s) by co-elution with the product(s) of interest of impurities coming from a previous injection must be avoided. This is a very important point, and potential users of HPPLC are often concerned by the fact that it is difficult to be sure that the column is clean before a new injection is made. Dealing with very strongly retained (late-eluted) compounds is thus an important issue. Before discussing the problems associated with such compounds, it is necessary to recall that their elution peaks are very broad and difficult to detect. In the best case, they only produce small baseline disturbances that can easily be ascribed to detector instability. It can also happen (not only with strongly retained products) that the detector is not sensitive to a particular compound and then its peak is not visible on the chromatogram.

There are several possibilities for handling late-eluted peaks, as follows. The most effective, but not necessarily the most convenient and economical, way is to unpack the column after the product of interest has been collected and repack the column with fresh material before a new injection is made. Some purifications in the pharmaceutical industry are made this way. It is also possible to continue elution until all the peaks have been eluted. This can require unacceptably large amounts of solvent, however, and, as indicate above, it is difficult (if possible) to know when everything has been eluted. It must be noted that the next injection can be made before the end of the actual run, provided that the peak of interest is not contaminated by co-eluted impurities. This optimized normal elution procedure is discussed later in this paper.

Another alternative is to find solvent conditions such that the compound of interest is the most retained. This is actually more a theoretical than a practical possibility, particularly since the optimization of the solvent conditions in preparative chromatography is primarily aimed at achieving a high selectivity between the peak of interest and its immediate neighbours.

Gradient elution can be used to clean the column after the product of interest has been eluted. It is an expensive approach, however, as it takes time and requires large amounts of solvent, not only for the cleaning step but also to regenerate the column before the next injection is made. At least three to five column volumes of solvent are typically required for this regeneration step. It must also be mentioned that the process of solvent regeneration (this is the best way to decrease HPPLC purification costs) is more complicated and expensive in gradient elution than isocratic elution. Last but not least, the purification process becomes more complicated, which is not desirable for industrial production conditions in which case as simple procedures as possible should be used.

A precolumn can be used to trap strongly retained impurities. This is a good strategy, but with some limitations. First, it requires an additional piece of hardware and thus increases the cost of the equipment. Second, it creates an additional source of band broadening. Third, the volume of the precolumn is necessarily much smaller than that of the column, and the precolumn is usually oversaturated with unpredictable retention effects. Fourth, the precolumn has to be regenerated (or changed) at some point.

Another possibility is to backflush the column. It will be seen in this paper that the flip–flop concept is an optimized backflush operation.

Finally, the flip–flop operation can be used.

THEORY

In order to describe the flip–flop concept, it is assumed that the mixture to be purified contains three compounds: the substance of interest (later called the "main peak") and two impurities, one eluted before and one after the main peak. The principle of flip–flop operation is illustrated in Fig. 1. In a first step the solvent flows from left to right and the first injection is made at the column left end (inlet). Elution proceeds and the first impurity is eluted, followed by the main product. Just after the collection of the main peak is completed, the flow direction is changed, the column inlet now being at the right end. The second impurity then starts to be backflushed. After a certain delay time (it is shown later how to calculate it), a second injection is made. The delay time is such that the end of the elution of the backflush peak from the strongly retained impurity of the previous injection corresponds to the beginning of the elution of the main peak of the actual injection. The weakly retained impurity of the actual injection can possibly interfere with the backflush peak of the strongly retained impurity from the previous injection, but this does not matter. The process is then repeated, the injections being made in turn at each end of the column. This mode of operation provides in some respect an answer to one of the frequently encountered objectives in preparative chromatography: the optimization of the isolation of the component of interest and the non-separation of the uninteresting components which are often impurities. Indeed, as these components are not to be collected, the optimization of the production throughput requires that no time is lost in separating them.

The critical point with the flip–flop operation is the column bed stability. With columns of regular design, it is often recommended to avoid reversing the flow of solvent (the direction must be what it was during the operation of packing the column), otherwise voids could be created and the column efficiency drastically reduced. This is particularly true with columns of large diameter. A solution to this problem is the technique of dynamic axial compression [9]. In addition to the technical aspect of column stability, the use of flip–flop elution requires the calculation of the delay time between the reversal of the flow direction and the next injection.

A typical preparative chromatogram is shown in Fig. 2. The horizontal lines under the chromatogram are an absolute and a reduced time axis. A reduced time is the ratio of an actual time to the dead time (t_0).

The following assumptions are made: (1) one product, the main component, has to be collected; (2) injection can be made in diluted as well as concentration overload

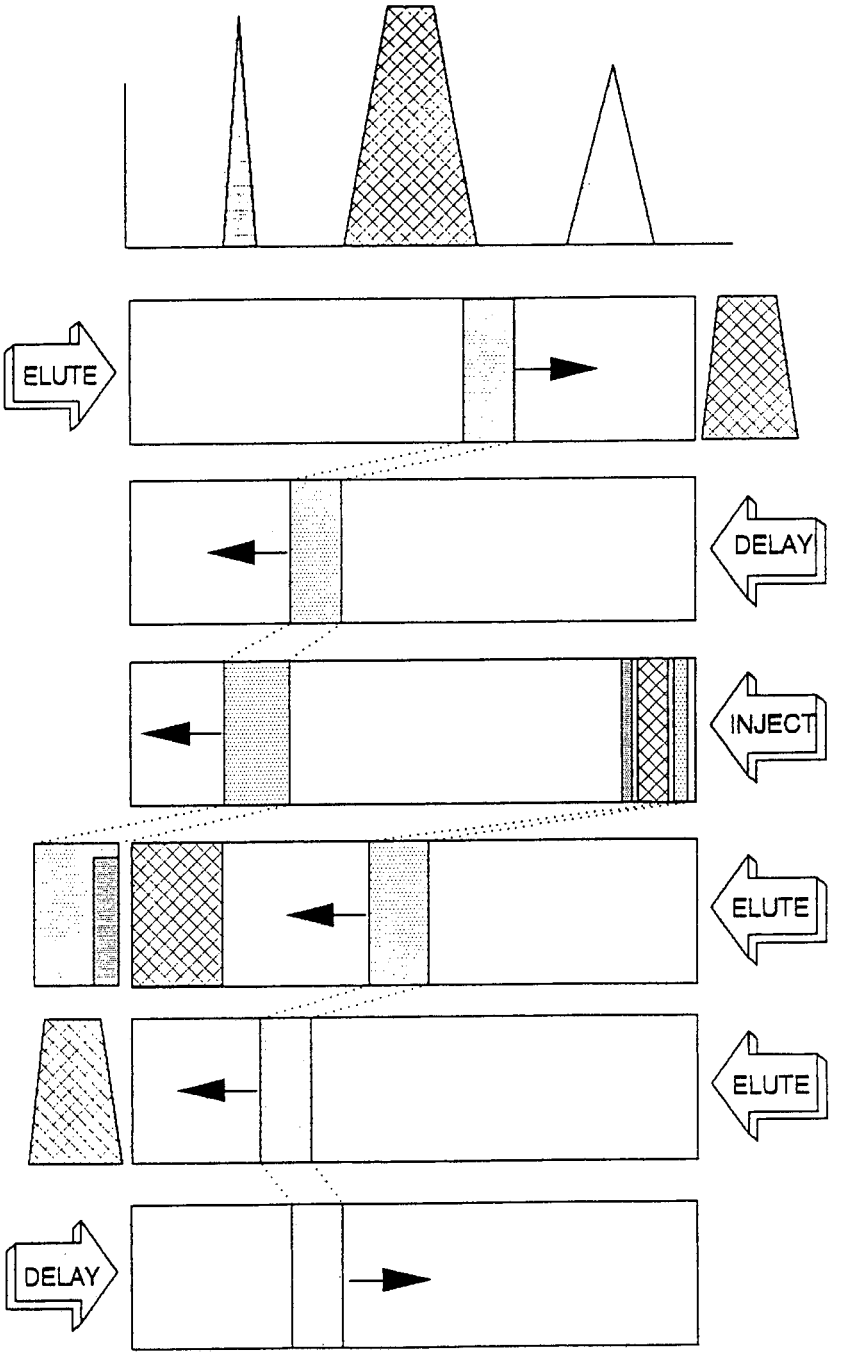

Fig. 1. Principle of flip–flop elution.

conditions; volume overloading can also take place but then in such a way that concentration overload is predominant, as recommended by Knox and Pyper [10]; (3) the possible amount of concentration overloading of the main peak and the start of the collection of this product are determined by the extent of interference with the impurity eluting immediately before this product; (4) whatever the extent of sample overloading, the end of the main peak appears at a constant time equal to the retention time in diluted conditions (*i.e.*, analytical injection) plus column band broadening (expressed in time units); this situation corresponds to a convex isotherm, such as a Langmuir isotherm; (5) no assumpton is made regarding the shape of the main peak (except for point 4).

The reduced times x_i and x_L (see Fig. 2) are given by

$$x_i = t_{Ri}/t_0 = 1 + k'_i \quad (1a)$$

$$x_L = t_{RL}/t_0 = 1 + k'_L \quad (1b)$$

where k' are the capacity factors.

The reduced cycle time is defined as the time between two consecutive injections relative to the time t_0. In flip–flop elution, this reduced time, *RFF*, is defined as

$$RFF = (t_s + DEL)/t_0 \quad (2)$$

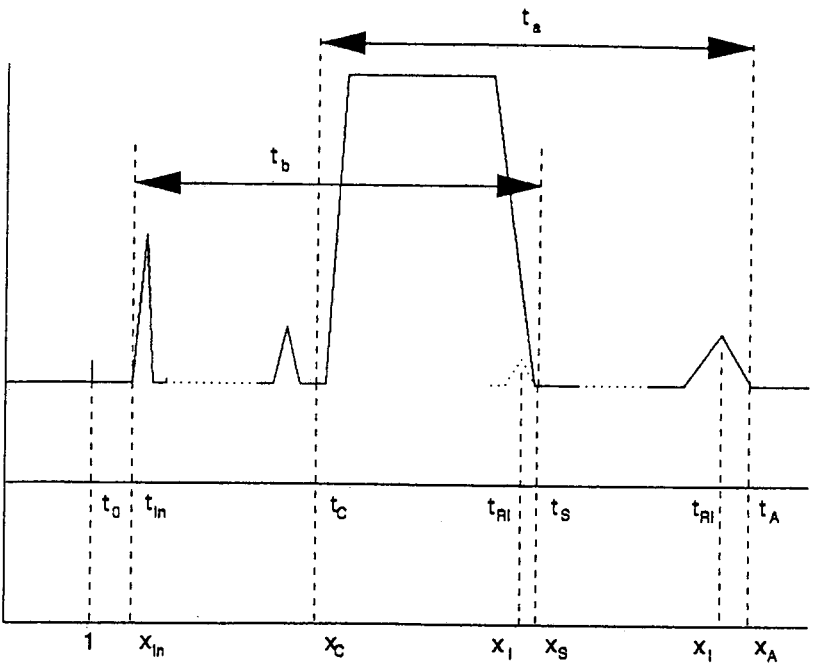

Fig. 2. Typical preparative chromatogram. t_0 = Dead time; t_{in} = retention time of the beginning of the first peak; t_c = time to start collecting the peak of interest; t_{Ri} = retention time of compound i; t_s = time of flow reversal (also end of collection); t_{RL} = retention time of the last compound; t_A = duration of the separation (return to baseline after the last peak). The x_i values correspond to the retention times t_i divided by the dead time t_0.

where t_s is the time elapsed between the injection and the switching of the flow direction and *DEL* is the delay time. It is recalled that *DEL* is such that the end of the peak of the most retained impurity from the previous injection (this peak is backflushed and is called in the following the "backflush peak") coincides with the beginning of the collection of the peak of interest in the actual injection.

The time spent in the column by the impurities more retained than the collected component is equal to $2t_s$. In order to calculate the end of the backflush peak, it is necessary to determine the standard deviation of the most retained component (in time units) as it contributes the most to the width of the backflush peak. This can be done using the plate height for this product and writing that this plate height is equal to the variance (in length units) divided by the distance travelled by the product. It is simple to derive the following equation in which the standard deviation (*SD*) is expressed in time units

$$SD = t_0 \sqrt{2x_L x_s/N} \tag{3}$$

where x_s is equal to t_s/t_0 and N is the plate number corresponding to one full passage through the column by the most retained impurity.

The reduced time corresponding to the end of the backflush peak is then defined as

$$x_{BF} = 2x_s + \lambda_L \sqrt{2x_L x_s/N} \tag{4}$$

where λ_L is a constant related to the peak shape of the last-eluted component and the desired level of purity of the collected peak. λ_L is usually between 2 and 3.

Writing that x_{BF} (associated with the previous injection) is equal to the reduced time of the beginning of the collection of the main peak from the actual injection (*i.e.*, $RFF + x_c$) and combining eqns. 2 and 4, allows the reduced delay time ($RDT = DEL/t_0$) and reduced cycle time to be calculated

$$RDT = x_s - x_c + \lambda_L \sqrt{2x_L x_s/N} \tag{5a}$$

$$RFF = 2x_s - x_c + \lambda_L \sqrt{2x_L x_s/N} \tag{5b}$$

Reduced times x_s, x_L and x_c can be calculated from the capacity factors and appropriate λ values similar to the λ_L parameter introduced in eqn. 4.

In order to evaluate the advantages of flip–flop elution, two cases are examined below. First, it is assumed that the main peak is not significantly overloaded and its shape is close to Gaussian. The total peak width, $x_s - x_c$, is assumed to be four times the standard deviation. Assuming that the column plate number is the same for the main peak and the last peak and taking $\lambda_L = 2$, one can then write eqn. 5a as

$$RDT = [4(1 + k'_i)/\sqrt{N}][1 + \sqrt{0.5(1 + 2/\sqrt{N})(1 + k'_L)/(1 + k'_i)}] \tag{6}$$

Figs. 3 and 4 show how *RDT* varies with k'_i, k'_L and N. The larger the column efficiency, the smaller is *RDT*. This is not surprising, as more efficient columns produce narrower peaks. As N is often larger than 2000, it is possible to neglect $2/\sqrt{N}$ compared with 1 in eqn. 6 and then it appears that *RDT* is inversely proportional to $\sqrt{N}$.

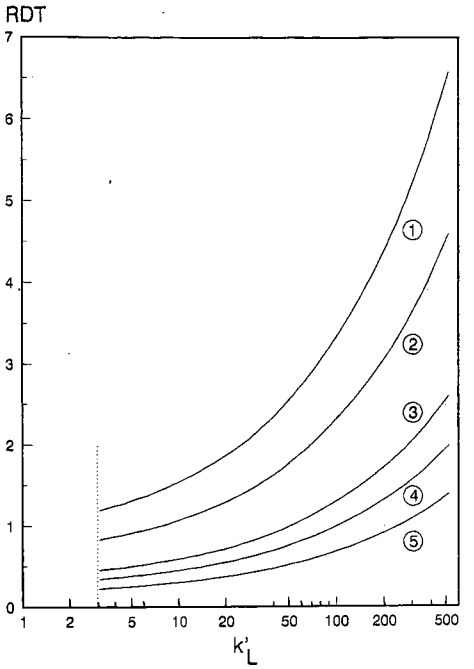

Fig. 3. Effect of the capacity factor of the most retained impurity (k'_L) on the reduced delay time (RDT) for different plate numbers (N). The capacity factor of the main product is assumed to be 3. The main peak is weakly overloaded (see text). N = (1) 500; (2) 1000; (3) 3000; (4) 5000; (5) 10 000.

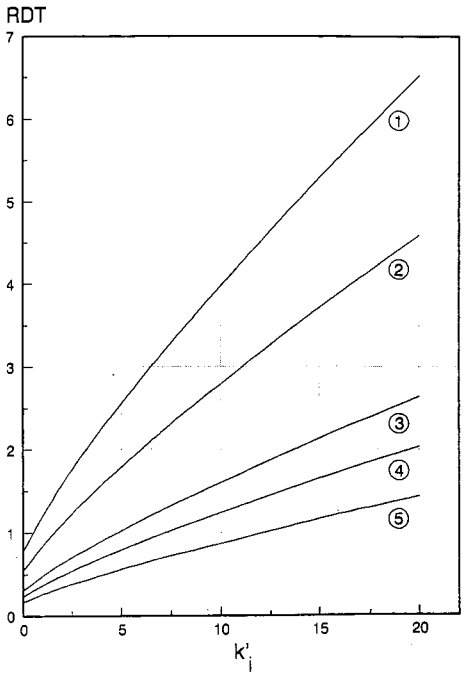

Fig. 4. Effect of the capacity factor of the main product (k'_i) on the reduced delay time (RDT) for different plate numbers (N). The capacity factor of the most retained impurity is assumed to be 20. The main peak is weakly overloaded (see text). N values as in Fig. 3.

For typical values of N and k'_i (3000 and 3, respectively), it can be seen that less than two column volumes of solvent have to be used in order to eliminate a strongly retained impurity with a capacity factor $k'_L = 100$. In such a case, about two times more solvent would be required to do normal backflusing and at least five times more to do gradient elution. If the column efficiency is increased to 5000 plates, then only one column volume of solvent is required to eliminate the same impurity. If the capacity factor of the most strongly retained impurity is more than 100, one can consider that the corresponding compound is almost irreversibly adsorbed (in the particular mobile phase selected) and a guard column can probably be used to eliminate the product.

The effect of k'_i on *RDT* is shown in Fig. 4 ($k'_L = 20$). The curves indicate that *RDT* increases almost linearly with k'_i, the rate of increase being smaller with larger column efficiency. When $k'_i = 5$, *RDT* increases from less than 1 for $N = 5000$ to 2.5 for $N = 500$. The advantage of a large column efficiency is also clearly seen here.

The previous discussion gives an optimistic view of flip–flop elution as it is assumed that the peak of interest is not overloaded. The most pessimistic situation corresponds to $x_c = 1$ (see eqn. 5a). In this case, the collection of the main peak starts immediately at time t_0. In other words, the main peak is so overloaded that its front is moved to the dead time. A real practical situation would be intermediate between this case and the previous one (no peak distorsion). Assuming that $x_c = 1$, eqn. 5a then becomes

$$RDT = k'_i + [2(1 + k'_i)/\sqrt{N}][1 + \sqrt{2(1 + 2/\sqrt{N})(1 + k'_L)/(1 + k'_i)}] \quad (7)$$

The most significant term on the right-hand side of eqn. 7 is k'_i. Because collection of the main peak starts much earlier than before, it is necessary to wait a longer time before the next injection can be made. The effects of k'_i, k'_L and N on *RDT* are shown in Figs. 5 and 6. The effect of the column efficiency is weaker than before. As shown in Fig. 6, at constant k'_L (= 20), *RDT* increases linearly with k'_i, at a rate which almost does not depend on the column plate number. To see a significant effect of N, it is necessary to reach large k'_L values (see Fig. 5).

The flip–flop concept described above corresponds to an improvement of the classical backflushing operation. In the latter, the next injection is made when the backflush peak is completely eluted. Then the cycle time in flip–flop operation is lower than in normal backflushing, the difference between the two reduced cycle times being equal to x_c. It is interesting to compare, on a reduced cycle time basis, flip–flop elution with "normal" (one-way) elution. For the comparison to be meaningful, normal elution has to be optimized in order to reduce the cycle time required for the satisfactory collection of the desired product. This can be done by injecting the next sample before the end of the elution of the last component from the previous injection [11]. The reduced cycle time in optimized normal elution, *ROE*, is then chosen so that the following two conditions are satisfied: (1) the beginning of the collection of the main peak for the actual injection happens simultaneously with (or just after) the end of the last peak from the previous injection (x_A); the corresponding *ROE* value is T_a (see Fig. 2); (2) the beginning of the first peak (x_{in}) from the actual injection happens simultaneously with (or just after) the end of the main peak from the previous injection; the corresponding *ROE* value is T_b.

It must be noted that the problem is actually more complex than described above

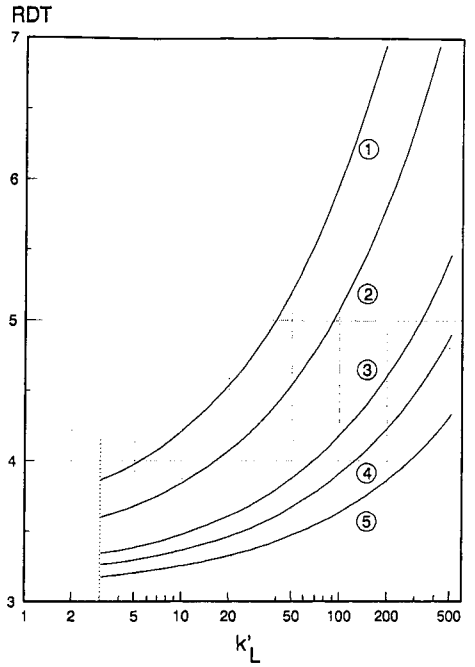

Fig. 5. Effect of the capacity factor of the most retained impurity (k'_L) on the reduced delay time (RDT) for different plate numbers (N). The capacity factor of the main product is assumed to be 3. The main peak is strongly overloaded and begins to elute at the void volume. N values as in Fig. 3.

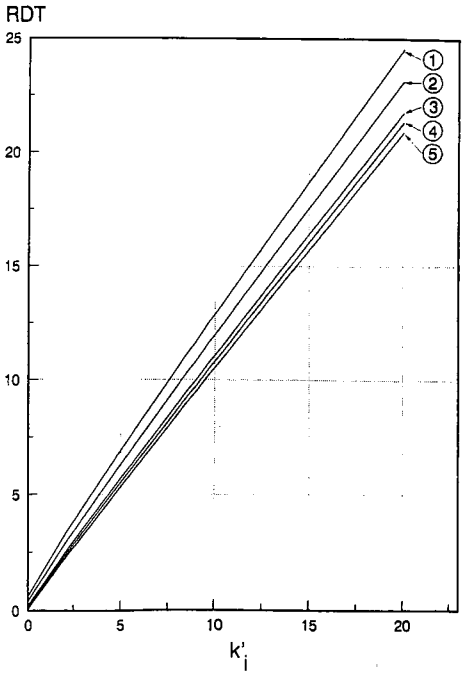

Fig. 6. Effect of the capacity factor of the main product (k'_i) on the reduced delay time (RDT) for different plate numbers (N). The capacity factor of the most retained impurity is assumed to be 20. The main peak is strongly overloaded and begins to elute at the void volume. N values as in Fig. 3.

because, in some particular situations where large gaps between some peaks are present, the injection sequence can be optimized so that the main peak is eluted in a window between adjacent impurities, involving more than two consecutive injections. Such cases are too specific, however, and cannot be included in the frame of a general discussion.

The value of *ROE* to be selected is equal to sup (T_a, T_b). Conditions 1 and 2 described above correspond to

$$T_a + x_c > x_A \tag{8a}$$
$$T_b + x_{in} > x_s \tag{8b}$$

In the following, optimized normal and flip–flop elution are compared. Two situations must be discussed depending on the relative values of T_a and T_b. It is first assumed that T_a is larger than T_b. This is equivalent to

$$x_s < x_A - x_c + x_{in} \tag{9}$$

Flip–flop elution will be better (shorter cycle time) than optimized elution when $RFF < ROE$, that is, according to eqns. 5b and 8a, when

$$2x_s - x_c + \lambda_L \sqrt{2x_L x_s/N} < x_A - x_c \tag{10}$$

or when

$$\sqrt{x_s} < 0.5[-\lambda_L \sqrt{x_L/2N} + \sqrt{\lambda_L^2 x_L/2N + 2x_A}] \tag{11}$$

Noting that x_A is equal to $x_L(1 + \lambda_L/\sqrt{N})$, condition 10 becomes after rearrangement

$$x_s < x_L/2 \qquad \text{or} \qquad t_s < t_{R,L}/2 \tag{12}$$

The condition has a very simple form: flip–flop elution is preferable to optimized normal elution when the switch time (end of collection of the main product) is less than half the retention time of the most retained impurity.

It can be shown that if T_b is less than T_a, *RFF* is always larger than *ROE*, and conversely that if x_s is less than $x_L/2$, then T_a is larger than T_b. Accordingly, the condition $x_s < x_L/2$ is necessary and sufficient for *RFF* to be lower than *ROE*.

If, as it has been assumed, the end of the main peak is not modified by overloading, then condition 12 can be rewritten as

$$k_i' < [0.5(1 + k_L')/(1 + \lambda_s/\sqrt{N_i})] - 1 \tag{13}$$

where N_i is the column efficiency for the main peak and λ_s a parameter which depends on the degree of interference accepted with the impurity eluted immediately after the main peak. This parameter is usually between 2 and 3.

Before discussing condition 13, the following comments should be made: the general condition described by relation 12 does not assume that the column efficiency

is the same for all peaks in the sample; in the previous discussion, the peak eluted just before the compound of interest does not play any role and, accordingly, condition 12 is valid even if the beginning of the collection of the main product does not correspond to the end of the peak of impurity eluted just before; and the general treatment developed above indicates that there is no need to make the assumption that only the main peak is overloaded, as other peaks can also be overloaded. Condition 12 is thus very general. It is the same whether the main peak is eluted in overloaded conditions or not.

In order to compare practically flip–flop and optimized elution, it is assumed that λ_s is equal to 2 and the column efficiency is larger than 2000 plates (the term $\lambda_s/\sqrt{N_i}$ can be neglected compared with 1). Under these conditions, relation 13 takes the simple form

$$k'_i < (k'_L - 1)/2 \tag{14}$$

The general conditions expressed by inequalities 12 or 14 for the cases where flip–flop operation is superior to optimized normal elution are in agreement with qualitative expectations. Indeed, backflush operation allows all components dispersed along the column at a given time to be combined in a single peak at one column extremity. Therefore, it is not surprising that flip–flop elution, which is an optimized version of backflushing, is especially useful when the unwanted impurities occupy an important fraction of the column length when the peak of interest is eluted, that is, when the main component elutes in the first part of the chromatogram.

It is interesting to calculate the relative gain in cycle time (relative time gain, *RTG*) when using flip–flop elution compared with optimized normal elution. *RTG* is given by

$$RTG = 1 - (RFF/ROE) \tag{15}$$

RFF is given by eqn. 5b and *ROE* is equal to $T_a = x_A - x_c$ (from eqn. 8a). From eqn. 15, it is simple to derive the ratio of the cycle times (*CTR*) in optimized normal elution to those in flip–flop elution

$$CTR = 1/(1 - RTG) \tag{16}$$

For the sake of simplicity, it is assumed in the following that λ_L is equal to 2 and the main peak is not significantly overloaded. It is then simple to derive the equation giving *RTG*

$$RTG = \frac{K - 2 - (4/\sqrt{N})(1 + \sqrt{K/2})}{K - 1 + 2/\sqrt{N}} \tag{17}$$

where K is defined as

$$K = (1 + 2/\sqrt{N})[(1 + k'_L)/(1 + k'_i)] \tag{18}$$

Some curves are shown in Figs. 7–9. They show the effect of k'_i on *RTG* and *CTR* for different k'_L values, assuming $N = 500$ (Fig. 7), 3000 (Fig. 8) and 10 000 (Fig. 9). The values of *RTG* and *CTR* are close to 0 and 1, respectively, when k'_i is close to $(k'_L - 1)/2$ (see eqn. 15). For larger k'_i values, optimized normal elution is preferable to flip–flop elution. The advantages of flip–flop elution over optimized normal elution clearly appear at large values of k'_L. For instance, when k'_i is 3 and k'_L is 50, the cycle time in flip–flop elution is about nine times shorter than it is in optimized normal elution.

It must be remembered that eqn. 17 and Figs. 7–9 are obtained assuming that the main product is not overloaded and that its width is equal to four times the standard deviation of the peak. In the case of strong overloading conditions for the main product, the advantage of flip–flop operation over optimized normal elution is less than that calculated in eqn. 17 and shown in Figs. 7–9. If RTG_{dil} represents the *RTG* calculated in eqn. 17, it is easy to show that the *RTG* value in overloaded conditions (RTG_{olc}) is given by

$$RTG_{olc} = RTG_{dil} \cdot \frac{x_A - x_i(1 - 2/\sqrt{N})}{x_A - x_c} \tag{19}$$

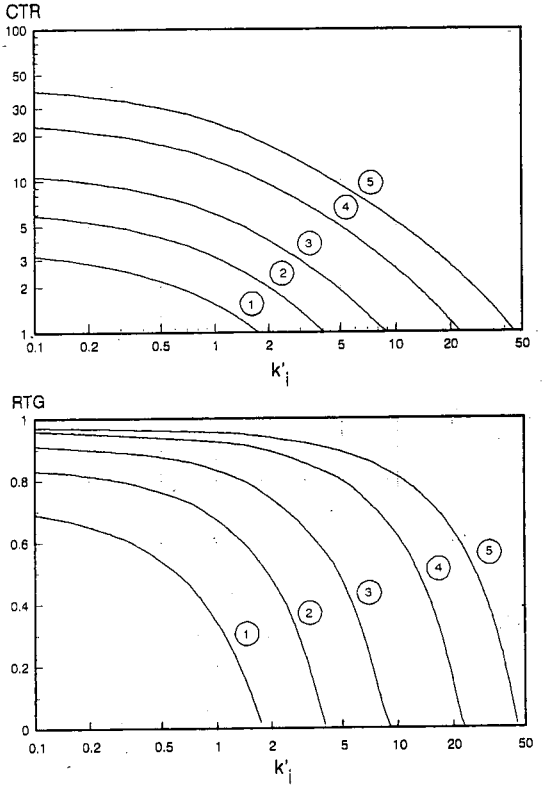

Fig. 7. Effect of the capacity factor of the main product (k'_i) on the reduced time gain (*RTG*) and the cycle time ratio (*CTR*) for different values of the capacity factor of the most strongly retained impurity (k'_L). The number of theoretical plates is $N = 500$. k'_L = (1) 5; (2) 10; (3) 20; (4) 50; (5) 100.

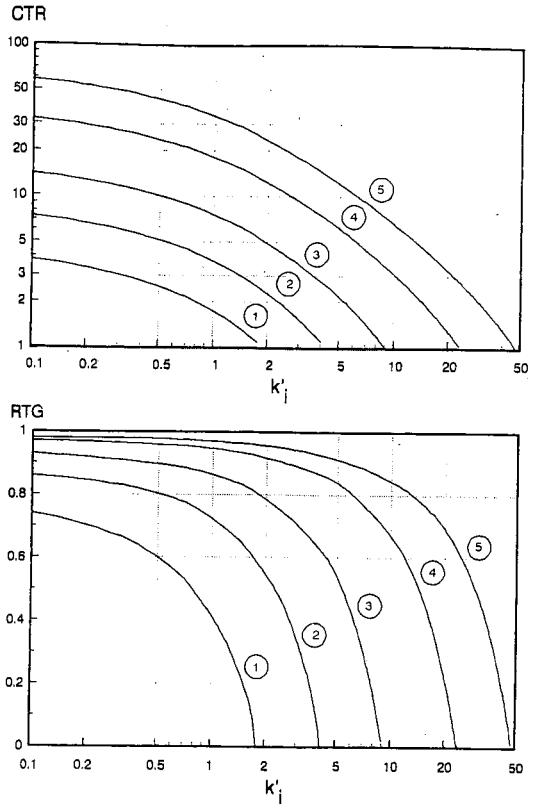

Fig. 8. Same as Fig. 7 but with $N = 3000$.

For instance, in the previous case ($k'_i = 3, k'_L = 50, N = 3000$), if the duration of collection of the main peak ($x_s - x_c$) is five or ten times larger than the width of the diluted peak, the cycle time in flip–flop elution is only 7.9 or 6.6 times shorter than that in optimized normal elution, respectively (instead of 9.4 times for a diluted peak). Nevertheless, this is still a definitive advantage of the flip–flop operation, particularly for medium- to large-scale preparative chromatography where the costs of solvent (proportional to the purification time) and labour are usually the most significant contributions to the cost of purification.

RESULTS AND DISCUSSION

An experimental demonstration of the flip–flop operation is shown in Figs. 10 and 11 for the separation of a natural extract of steroids by reversed-phase chromatography. The experiments were made using an analytical Zorbax C_{18} (10 μm) column (25 × 0.46 cm I.D.) (DuPont, Wilmington, DE, USA). The eluent was acetonitrile–water (50:50, v/v) at a flow-rate of 3 ml/min, with UV detection at 254 nm.

The chromatogram shown in Fig. 10A is for a normal run. The last visible peak is eluted at about 17 min. Actually, some other compounds are likely to be left on the

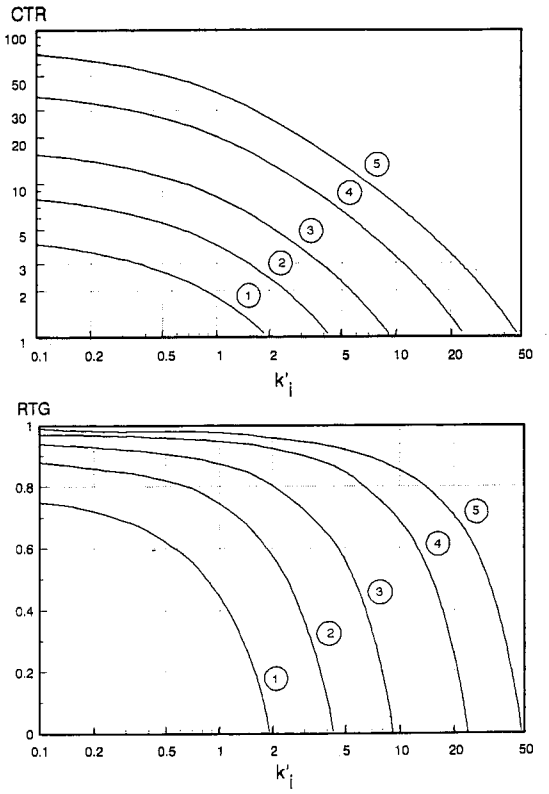

Fig. 9. Same as Fig. 7 but with $N = 10\,000$.

column at that time as continuation of elution over a longer time revealed that the baseline is not perfectly flat and shows some minor disturbances (not detected as peaks by the data processing system). The largest peak (shaded in Fig. 10A) is the compound of interest (about 60% pure based on relative peak areas). It is possible from the chromatogram to calculate the capacity factors of the main product ($k'_i = 3.4$) and the assumed last impurity ($k'_L = 15.8$), and the average column efficiency ($N = 2500$). In order to collect the main peak at the required purity, it is necessary to collect between times 4.0 and 4.8 min. At the latter time, the flow direction is changed and the late impurities are backflushed. This is shown in Fig. 10B and C. Fig. 10B shows the first part of the separation (collection of the main product) and Fig. 10C the backflushing of the late impurities. According to calculations, the end of the backflush peak should appear at 5.2 min (arrow in Fig. 10C) after the reversal of flow. In fact, the time is almost 6.7 min. Several factors can contribute to the difference between the calculated and experimental values. First, it is often observed that the column efficiency decreases with increasing k'. This increases the time when the backflush peak is observed (*e.g.*, see eqn. 3). Another possible explanation is the presence of strongly retained impurities (eluted after 17 min). Although such impurities do not modify the centre of gravity of the backflush peak, they do affect the end of this peak.

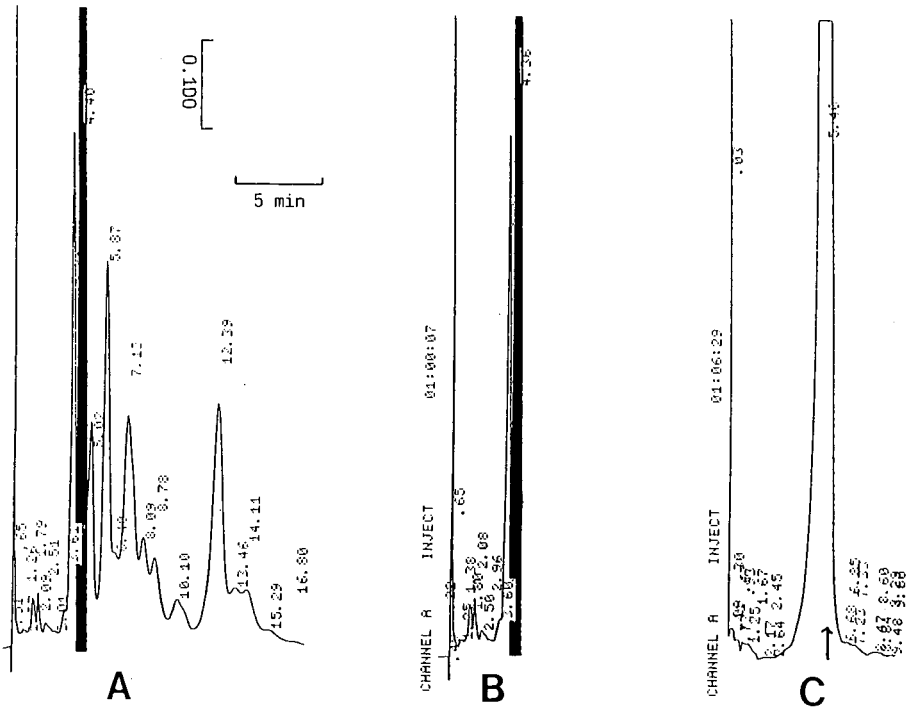

Fig. 10. Separation of a natural extract of steroids on an analytical C_{18} column with acetonitrile–water (50:50) as eluent. The abscissa is the separation time and the ordinate the detector signal. (A) Normal separation. (B) Collection of the main product. At the end of the main peak the flow direction is changed and the late impurities are being backflushed. (C) Backflush peak of the late impurities.

From the experimental value of the time of the end of the backflush peak, it is possible to select the proper parameters for flip–flop elution. A series of five injections is shown in Fig. 11. Since the beginning of collection is at time 4 min and the end of the backflush peak is at time 6.7 min, it is necessary to wait 2.7 min (about 2.7 column volumes) after reversing the flow direction and making the next injection. If normal optimized elution were applied, the cycle time would be about 13 min (total separation time = 17 min and beginning of collection = 4 min), compared with 7.3 min (4.8 + 2.7) in flip–flop elution. The corresponding savings in solvent consumption would be very significant in preparative work. As can be seen in Fig. 10C, the process is very stable, even though this case is difficult because of the large impurity eluted just before the main peak. For the last injection, the normal elution process was resumed and accordingly the end of the chromatogram is similar to that in Fig. 10A.

CONCLUSIONS

Flip–flop elution appears to be a simple yet powerful way to solve the problem of strongly retained components in PLC. When the time of the end of the collection of the main peak is less than half the retention time of the most strongly retained impurity, flip–flop elution gives shorter cycle times (and thus larger production capacities) than

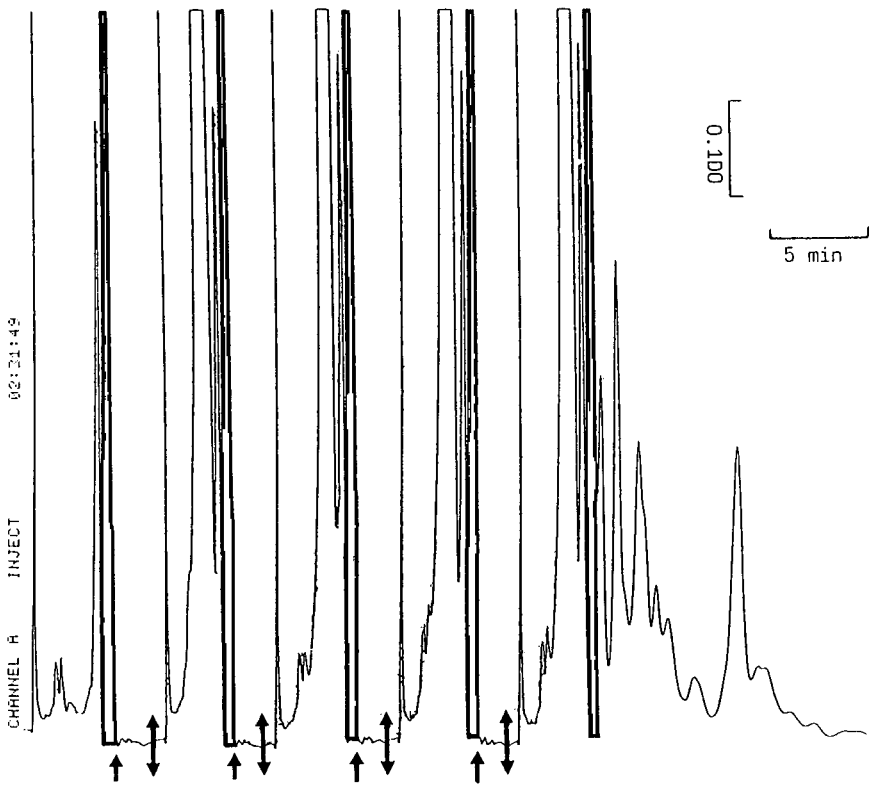

Fig. 11. Same conditions as for Fig. 10. Five injections are made in flip–flop conditions. The single-headed arrows on the baseline indicate when the flow direction is changed. The double-headed arrows indicate when a new injection is made. The abscissa is the separation time and the ordinate the detector signal.

optimized normal elution. In many instances, flip–flop elution is preferable to using a guard column or regenerating the purification column by gradient elution or simple backflushing. The advantages of flip–flop elution are particularly important when economics are considered.

The flip–flop concept has been described above while bearing in mind its application to PLC. It must be realized, however, that this concept is not restricted to PLC but can more generally be applied to gas as well as liquid chromatography, to analytical as well as preparative chromatography and to column chromatography as well as other elution separation techniques (electrophoresis, field-flow fractionation, etc.). Indeed, the flip–flop concept is useful when separation is required for only a fraction of the number of sample components. This is the case in preparative chromatography where generally the collection of one (often the major) component of the sample is sought. This can also be the case in application of analytical separation methods where quantitative information on only one or a few sample components is required (drug or forensic analysis, for instance). Then the mean routine analysis time per sample can be greatly reduced, compared with conventional procedures, by using flip–flop or optimized elution operation, depending on which one is the best.

The equations developed above for the specific case of preparative chromatography can be adapted directly to an analytical objective if the reduced times x_c and x_s correspond to the beginning of the elution of the first component of interest and the end of elution of the last component of interest, respectively. Making the difference between these two reduced times as small as possible, while maintaining a satisfactory resolution between the components of interest constitutes in that case the main challenge for the optimization of the separation conditions. In any case, the criterion expressed by eqn. 12 can be used to select the best of the two optimized processes, flip–flop or optimized normal elution.

REFERENCES

1 M. Verzele, *Anal. Chem.* 62 (1990) 265A.
2 G. Guiochon and S. Ghodbane, *J. Phys. Chem.* 92 (1988) 3682.
3 S. Ghodbane and G. Guiochon, *Anal. Chem.* 61 (1989) 1276.
4 S. Ghodbane and G. Guiochon, *Anal. Chem.* 61 (1989) 1368.
5 G. Guiochon and A. Katti, *Chromatographia*, 24 (1987) 165.
6 W. Skea, in P. R. Brown and R. A. Hartwick (Editors), *High Performance Liquid Chromatography*, Wiley, New York, 1989, p. 479–528.
7 I. Mazsaroff and F. E. Regnier, *J. Liq. Chromatogr.*, 9 (1986) 2583.
8 R. M. N. Nicoud and H. Colin, *LC · GC*, 8 (1990) 24.
9 H. Colin, P. Hilaireau and J. de Tournemire, *LC · GC*, 8 (1990) 302.
10 J. H. Knox and H. Pyper, *J. Chromatogr.*, 363 (1986) 1.
11 G. Mann, presented at the *7th International Symposium on Preparative Chromatography, Ghent, April 8–11, 1990.*

Journal of Chromatography, 557 (1991) 155–162
Elsevier Science Publishers B.V., Amsterdam

CHROM. 23 103

Simulated distillation of distillates on capillary columns: influence of the polarity of the stationary phase

M. DORBON*, S. LAMAISON and A. CHEVALIER
Institut Français du Pétrole, Centre d'Étude et de Developpement Industriel, B.P. 3, 69390 Vernaison (France)

ABSTRACT

Gas chromatographic-simulated distillation gives the boiling range of petroleum products. It has been shown that with capillary columns (as with packed columns), the simulated distillation results of aromatic samples change with the polarity of the stationary phase. Three columns of different politary, sufficiently thermostable to elute samples having boiling points as high as 600°C were tested. It has been shown that the more suitable column for simulated distillation of vacuum distillates is one with medium polarity.

INTRODUCTION

Simulated distillation is an analytical method widely used in the petroleum industry. It is a gas chromatographic (GC) method which gives the boiling range of complex petroleum mixtures and was first developed on packed columns because it did not require high resolution. More recently, with the development of macrobore columns, papers describing simulated distillation on capillary columns have been published [1–3]. Simultaneously, due to the development of temperature-resistant capillary columns, methods for simulated distillation of heavy petroleum fractions or crude oils have been described [4–8].

The methods previously published on macrobore capillary columns were developed on totally nonpolar columns which were coated with polymethylsilicone-type phases. On these phases, for a given boiling point, the aromatic compounds are eluted before the paraffins [9,10]. Since the calibration of the simulated distillation (transformation of the retention times into boiling points) is done using normal paraffins, the results of simulated distillation should depend on the phase polarity.

With the wide use in refineries of fluid catalytic and thermal cracking units, more and more samples with aromatic content up to 80% as light cycle oils (LCO) and heavy cycle oils (HCO) must be analysed. Consequently, this problem of simulated distillation of aromatic samples is important. In this article, we confirm, on capillary columns, the difference in retention times at a given boiling point between aromatics and paraffins on non-polar phases. It has been shown that on aromatic

0021-9673/91/$03.50

distillates the results depend on the polarity of the chromatographic column. Columns coated with phases of different polarity were tested in order to select a phase which is sufficiently polar to elute aromatics and paraffins of the same boiling point at almost the same retention time and which is sufficiently temperature-resistant to elute compounds with boiling points as high as 600°C. A compromise was found with a 1% vinyl, 7% cyanopropyl, 7% phenyl, 85% methylpolysiloxane chemically-bonded phase.

EXPERIMENTAL

Simulated distillation analysis was carried out using a Varian 3500 (Walnut Creek, CA, USA) gas chromatograph equipped with a temperature-programmable column injector.

The analytical columns were a 10 m × 0.53 mm I.D. wall-coated open-tubular (WCOT) fused-silica capillary column coated with a non-polar polydimethylsiloxane phase (wide-bore DB1; J & W, Folsom, CA, USA), a 10 m × 0.53 mm I.D. WCOT fused-silica capillary column coated with a 5% phenyl, 95% methyl polysiloxane phase (wide-bore CP-Sil8 CB; Chrompack, Middelburg, Netherlands) and a 10 m × 0.53 mm I.D. WCOT fused-silica capillary column coated with a 7% cyanopropyl, 7% phenyl, 85% methyl, 1% vinylpolysiloxane phase (wide-bore CP-Sil19 CB; Chrompack). All the phases were chemically bonded.

The carrier gas was helium and the operating conditions were as follows: from 0 to 330°C at 10°C/min for the oven and from 80 to 340°C at 200°C/min for the injector; the carrier gas flow-rate was 18 ml/min.

The principle of the simulated distillation calculation follows standard test method ASTM D2887-89 [10].

Integration was performed on a HP 1000 A 600 computer (Hewlett Packard, Palo Alto, CA, USA). The calculations of the boiling range of the samples were carried out on the same computer using an IFP developed Fortran software.

The samples analysed (A, B, C, D, E and F) were straight run or cracked middle or heavy distillates from different sources. The aromatic content of each sample is shown in Table I.

The pure aromatic compounds were commercially available (Interchim, Paris, France).

TABLE I

AMOUNTS IN WEIGHT PERCENT OF MONO-, DI- AND POLYAROMATICS IN SIX DIFFERENT DISTILLATES

Sample	Monoaromatics	Diaromatics	Polyaromatics	Total aromatics
A	11.1	5.0	0.8	16.9
B	12.2	5.1	4.1	21.4
C	22.4	6.5	3.1	32
D	24.2	41.0	8.7	73.9
E	31.9	25.2	25	82.1
F	33.4	28.8	36.6	98.8

RESULTS AND DISCUSSION

Thermostability of the columns

The three columns were used with temperature programming up to 330°C and a carrier gas flow-rate of 18 ml/min. With such operating conditions, *n*-C_{50}, which has a boiling point of 575°C, is eluted just at the end of the temperature programming. More than 100 analyses were performed on each column with no change of resolution, no increase of bleeding and no shift of retention times. Consequently, the three columns are sufficiently thermostable for the analyses of samples having a final boiling point up to 575°C. Thus the three types of columns are suitable for the analysis of vacuum distillates. At the moment, more polar columns cannot be used at temperatures higher than 300°C.

Retention of aromatics compared to n-paraffins as a function of the stationary phase

Thirty standard aromatic compounds were analysed on the three different column types. The simulated boiling points of those compounds were calculated by the formula

$$SBP_x = BP_n + (BP_{n+1} - BP_n) \times (RT_n - RT_x)/(RT_{n+1} - RT_n)$$

where SPB_x is the simulated boiling point of compound x; RT_x is the retention time of compound x; BP_n and BP_{n+1} are the boiling points of the *n*-paraffins eluted respectively just before and just after compound x; and RT_n and RT_{n+1} are the retention times of the *n*-paraffins eluted respectively just before and just after compound x.

Table II shows the actual boiling points of the aromatic compounds with their simulated boiling points and Fig. 1 shows the differences between the actual boiling points and the simulated boiling points of the aromatic compounds. The simulated boiling points on the DB1 and on the CP-Sil8 columns are of the same order of magnitude even if they are a little bit higher for the latter. They are higher by about 15°C on the CPSil19 column.

It can be seen that for compounds having boiling points between 80 and 300°C the differences between boiling points and simulated boiling points are between 20 and −20°C on the three columns. Between 300 and 450°C, this difference remains between 0 and 20°C for the CPSil19 column, but is between −20 and −40°C for the two other less polar columns. Beyond a boiling point of 450°C, this difference remains between −20 and −40°C for the more polar column but is around −60°C for the two less polar ones.

On the three columns, the analysis of pure aromatic compounds by simulated distillation shows that, at a given boiling point, the retention of aromatics is different from the retention of paraffins. However, this difference is lower on a medium polar phase such as 7% cyanopropyl, 7% phenyl, 85% methyl, 1% vinylpolysiloxane, mainly for a boiling point beyond 300°C. Since the calibration of the simulated distillation is done using *n*-paraffins, these differences would mean, for very aromatic samples, that the result of simulated distillation depends on the polarity of the column.

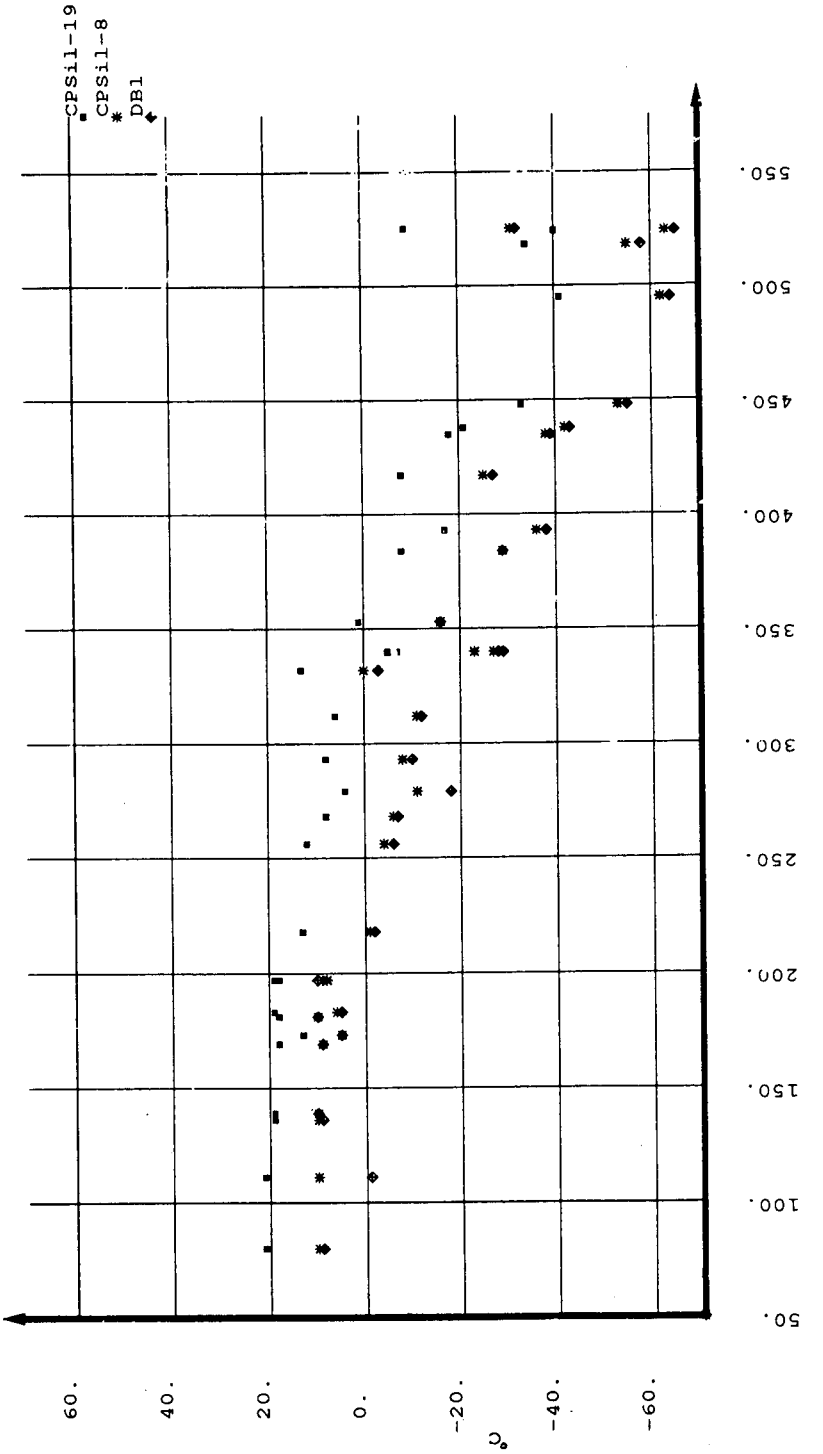

Fig. 1. Differences between boiling points and simulated boiling points on non-polar (DB1), slightly polar (CPSil8) and medium polar (CPSil19) columns for 30 different aromatic compounds having boiling points from 80 to 525°C. The aromatic compounds are those listed in Table II.

TABLE II

SURVEY OF THIRTY AROMATIC COMPOUNDS: BOILING POINTS (BP), SIMULATED BOILING POINTS (SBP) IN °C AND DIFFERENCE BETWEEN BP AND SBP ON THE THREE DIFFERENT CAPILLARY COLUMNS (DB1, CPSil8 AND CPSil19)

Compound	BP	DB1		CPSil8		CPSil19	
		SBP	Difference	SBP	Difference	SBP	Difference
Benzene	80	89	+ 9	90	+10	101	+21
Toluene	111	110	− 1	121	+10	132	+21
Ethylbenzene	136	145	+ 9	146	+10	155	+19
m-Xylene	139	149	+10	149	+10	158	+19
Trymethylbenzene	169	178	+ 9	178	+ 9	187	+18
Isobutylbenzene	173	178	+ 5	178	+ 5	186	+13
Metadiethylbenzene	181	191	+10	191	+10	199	+18
Idene	183	188	+ 5	189	+ 6	202	+19
Durene	197	207	+10	206	+ 9	216	+19
Tetramethylbenzene	197	207	+10	205	+ 8	215	+18
Naphthalene	218	216	− 2	217	− 1	231	+13
Diphenyl	256	250	− 6	252	− 4	268	+12
2,3-Dimethylnaphthalene	268	261	− 7	262	− 6	276	+ 8
Acenaphtalene	279	261	−18	268	−11	283	+ 4
Fluorene	293	283	−10	285	− 8	301	+ 8
9,10-Dihydroanthracene	312	300	−12	301	−11	318	+ 6
Ortoterphenyl	332	329	− 3	332	0	345	+13
Phenanthrene	340	311	−29	317	−23	335	− 5
Anthracene	340	312	−28	313	−27	333	− 7
4,5-Methylphenanthrene	353	337	−16	337	−16	354	+ 1
Fluoranthene	384	355	−29	355	−29	376	− 8
Pyrene	393	355	−38	357	−36	376	−17
9-Phenylanthracene	417	390	−27	392	−25	409	− 8
1,2-Benzanthracene	435	396	−39	397	−38	417	−18
Triphenylene	438	395	−43	396	−42	417	−21
Chrysene	448	393	−55	395	−53	415	−33
Benzo(*a*)pyrene	495	431	−64	433	−62	454	−41
1,2,3,4-dibenzanthracene	518	460	−58	463	−55	484	−34
1,2,5,6-dibenzanthracene	524	459	−65	461	−63	484	−40
Coronene	525	493	−32	494	−31	516	− 9

Influence of the stationary phase of the simulated distillation results

The simulated distillation of six different petroleum products was performed on the three columns. The samples were middle distillates having initial boiling points between ca. 200°C and 350°C, and final boiling points between ca. 400°C and 550°C. They have different percentages of aromatics as shown in Table I.

Fig. 2 shows the simulated distillation results of the three less aromatic samples (A, B and C). With two samples having an aromatic content of about 20% (A and B), the differences between the three columns are very small. Thus for these samples, the three columns are almost equivalent.

With the sample having 32% aromatics (C), the differences are more important. It can be noted that for the same content eluted, the higher boiling point is always with the more polar column, as expected. A small difference between the results

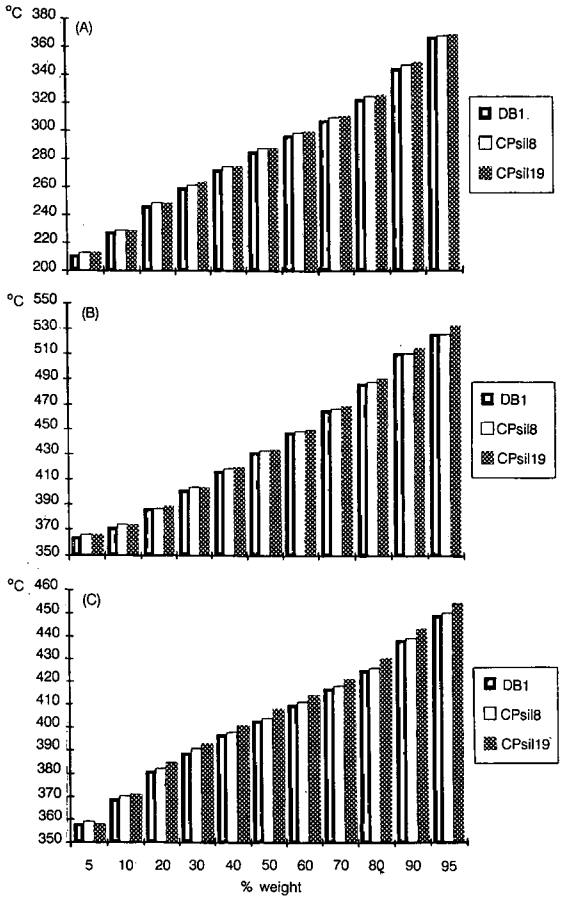

Fig. 2. Comparison of simulated distillation results carried out on non-polar (DB1), slightly polar (CPSil8) and medium polar (CPSil19) columns for three slightly aromatic distillates, A, B and C, the aromaticities of which are shown in Table I.

obtained on the two less polar columns can also be seen; it means that even for pure compounds the difference in retention times between the two columns is very low (Fig. 1), and thus the difference of polarity between the two phases can cause differences between simulated distillation results for mixtures.

For this sample, the boiling points at n% on CPSil19 are almost mid-way between the boiling points at n% and (n + 10)% on DB1; consequently, even for samples having about 30% aromatic content and more, the differences between the columns cannot be neglected.

On samples containing about 75% aromatic content (D and E), the difference between the three columns are very important (Fig. 3). The boiling points at n% on the CPSil19 column are almost the same as the boiling points at (n + 10)% on the less polar column DB1.

A very aromatic samples (F) was also studied (Fig. 3). On this sample, the difference between the three columns is higher. The boiling points at n% on the

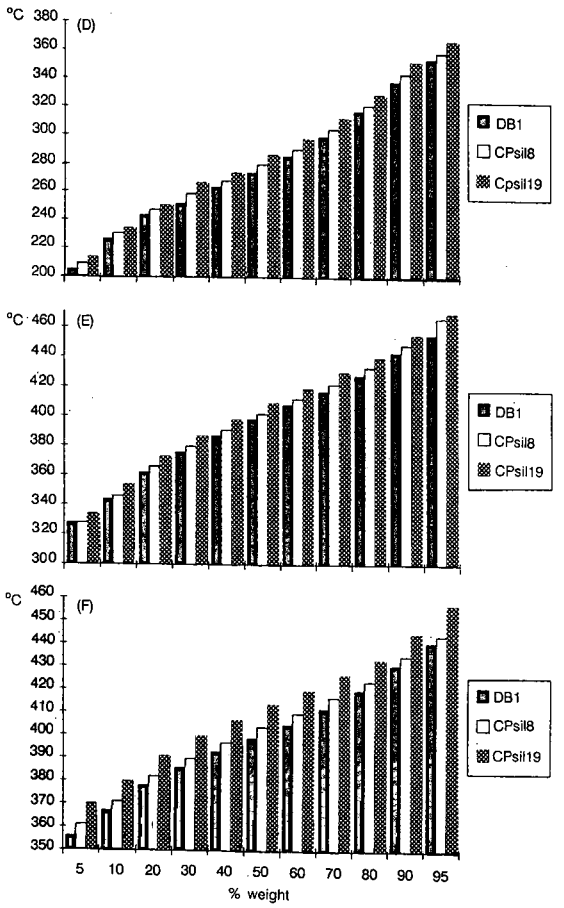

Fig. 3. Comparison of simulated distillation results carried out on non-polar (DB1), slightly polar (CPSil8) and medium polar (CPSil19) columns for three highly aromatic distillates, D, E and F, the aromaticities of which are shown in Table I.

CPSil19 column are almost equal and sometimes higher than the boiling point at (n + 20)% on the DB1 column; the boiling points at n% on CPSil8 are close to the boiling point at (n + 10)% on DB1.

Comparison between simulated distillation and true boiling point distillation (TBP)

The TBP analysis is both a time- and sample-consuming; this is the reason why this analysis was not performed for all the samples. On two of the samples, one with a low aromatic content and one with a high aromatic content, TBP was available. The results and the comparison with simulated distillation are shown in Tables III and IV. As expected, for the low aromatic sample, the TBP and the simulated distillation are very similar, whatever the column. But for the high aromatic sample, the results between the TBP and the simulated distillation on the CPSil19 column are close, but they are different from simulated distillation on the two other columns.

TABLE III

COMPARISON BETWEEN TBP AND SIMULATED DISTILLATION OF SAMPLE B WHICH CONTAINS 21.4% AROMATICS

Temperature (°C)	TBP (% weight)	DB1 (% weight)	CPSil8 (% weight)	CPSil19 (% weight)
399	25.5	28	27	25.5
448	57.5	60	59.5	58
499	84.5	85	85	84
524	93	94.5	94.5	93

TABLE IV

COMPARISON BETWEEN TBP AND SIMULATED DISTILLATION OF SAMPLE D WHICH CONTAINS 73.9% AROMATICS

Temperature (°C)	TBP (% weight)	DB1 (% weight)	CPSil8 (% weight)	CPSil19 (% weight)
247	16.5	22	21	17
298	58.5	68	65.5	60
347	86.5	93	91	88
374	95	98.5	98	96.5

CONCLUSION

The three columns tested, one non-polar, one slightly polar and one of medium polarity, were sufficiently thermostable to analyse petroleum products having boiling points up to 600°C. It has been shown that the difference in simulated distillation results between two columns depends on the aromatic content in the sample and on the polarity of the phase. For non-aromatic samples, the three columns are equivalent. But the difference increases with the aromatic content and is very high for samples having more than 70% aromatics. It appears that the medium polar column is the more suitable for simulated distillation of distillates. It is the one on which the difference in retention between aromatics and paraffins for a given boiling point is the lowest. Moreover, it has been shown for two samples of different aromatic content that it is with the medium polar column that the difference with TBP is the lowest.

REFERENCES

1 R. L. Firor, *Am. Lab.*, 21 (1989) 33–33.
2 F. Noel, *J. High Resolut. Chromatogr.*, 11 (1989) 837–839.
3 N. R. Warren and B. M. Lawrence, *Lab. Pract.*, 36 (1987) 80–81.
4 A. Rastogi, *J. High Resolut. Chromatogr.*, 10 (1987) 479–480.
5 J. Curvers and P. van den Engel, *J. High Resolut. Chromatogr.*, 12 (1989) 16–22.
6 R. L. Firor and R. J. Philips, *J. High Resolut. Chromatogr.*, 12 (1989) 181–183.
7 S.Trestianu, G. Zilioli, A. Sironi, C. Saravalle, F. Munari, M. Galli, G. Gaspar, J. M. Colin and J. L. Jovelin, *J. High Resolut. Chromatogr.*, 8 (1985) 771–781.
8 L. A. Luke and J. E. Ray, *J. High Resolut. Chromatogr.*, 8 (1985) 193–195.
9 N. Petroff, J. M. Colin, N. Feillens and G. Follain, *Rev. Inst. Fr. Petr.*, 36 (1981) 467–484.
10 *ASTM Standards*, Vol. 05-02, American Society for Testing and Materials, Philadelphia, PA, 1990, section 5, ASTM D2887-89, pp. 492–499.

Journal of Chromatography, 557 (1991) 163–171
Elsevier Science Publishers B.V., Amsterdam

CHROM. 23 390

Chiral π-donor stationary phases with (*R*)-N-pivaloylnaphthylethylamide groups for direct enantiomer separation by gas, liquid and supercritical fluid chromatography

RENE BRÜGGER, PETER KRÄHENBÜHL, ANDRE MARTI, ROLF STRAUB and HANS ARM*
Institute of Organic Chemistry, University of Berne, Freiestrasse 3, CH-3012 Berne (Switzerland)

ABSTRACT

Several monomeric and polymeric stationary phases, all with (*R*)-N-pivaloylnaphthylethylamide as the chiral selector group, were synthesized and tested for direct enantiomer separation by high-performance liquid, capillary gas, packed column supercritical and capillary supercritical chromatography.

INTRODUCTION

In the last 10 years there have been rapid developments in chromatographic methods for the direct separation of enantiomers. High-performance liquid chromatography (HPLC) is now very well established in this domain for both analytical [1,2] and preparative [3] separations and there is a wide choice of commercially available stationary phases [4]. Capillary gas chromatography (cGC) is developing very fast [5–7] and supercritical fluid chromatography (SFC) [8], either in packed (pSFC) or in capillary columns (cSFC) has profited from the theoretical and experimental knowledge in HPLC and GC.

The aim of this work was to synthesize different stationary phases for HPLC, cGC and SFC with packed and capillary columns, all with the same chiral group, and to investigate their chromatographic suitability. We chose for this purpose a derivative of (*R*)-N-pivaloylnaphthylethylamide ((*R*)-2,2-dimethyl-N-{1-[1-(4-amino) naphthylenyl]ethyl}propanamide, NH_2-PNEA; Fig. 1), the PNEA group having a

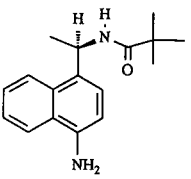

Fig. 1. Chiral group of all stationary phases, a derivative of (*R*)-N-pivaloylnaphthylethylamide: (*R*)-2,2-dimethyl-N-{1-[1-(4-amino)naphthalenyl]ethyl}propanamide, NH_2-PNEA.

0021-9673/91/$03.50

broad range of applications in HPLC [9]. It was outside the scope of this work to evaluate chiral separation mechanisms of the PNEA group with different kinds of samples (see, *e.g.* refs. 10 and 11) and for this reason elution orders were not determined.

LIQUID CHROMATOGRAPHY

Experimental

Three chiral stationary phases (CSPs) were synthesized: a monomeric bonded phase, CSP I (M) (Fig. 2), and two polymer-coated phases, CSP II (PG) and CSP III (G-Co) (Fig. 3). CSP I (M) contains 3-glycidoxypropyltrimethoxysilane as a spacer between the NH_2-PNEA groups and the silica matrix. In CSP II (PG), polyglycidoxypropylmethylsiloxane serves as a backbone carrying the chiral groups and the bonds to the aminopropylated silica matrix. In CSP III (G-Co), glycidoxypropylmethyldimethylsiloxane copolymer is used as a backbone.

Materials. LiChrospher Si 100 (Merck, Darmstadt, Germany) with a particle size of 5 μm and a specific surface area of S_{BET} = 264.4 ± 5.4 m^2/g was used. Polyglycidoxypropylmethylsiloxane and glycidoxypropylmethyl(45–55%)dimethylsiloxane copolymer were purchased from Petrarch Systems (Bristol, PA, USA) and all other chemicals either from Fluka (Buchs, Switzerland) or Merck (Zürich, Switzerland). For liquid chromatography, HPLC-grade solvents from Romil Chemicals (Shepsheed, UK) were used. The chiral selector NH_2-PNEA was available through a

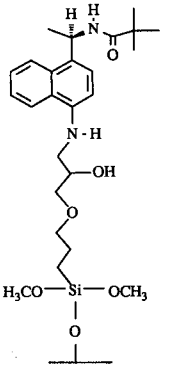

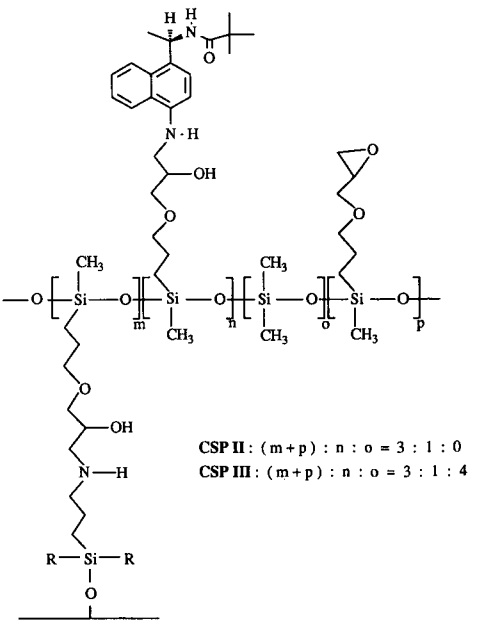

Fig. 2. Chiral stationary phase CSP I (M).

Fig. 3. Chiral stationary phases CSP II (PG) and CSP III (G-Co). For HPLC and pSFC, R = OC_2H_5; for cGC and cSFC, R = CH_3. m,n,o and p denote coefficients of indicated groups according to manufacturer and elemental analysis.

three-step reaction starting from (*R*)-(+)-1-(1-naphthyl)ethylamine. The general synthetic procedure has been reported previously [9,12].

CSP I (M). A 0.23 g (0.86 mmol) amount of NH_2-PNEA and 0.20 g (0.85 mmol) of 3-glycidoxypropyltrimethoxysilane were stirred in 20 ml of dry toluene (dried over Pb–Na alloy) during 1h. A 2.01 g amount of LiChrospher Si 100 [dried at 150°C and 1.3 Pa for 6 h] was added. The mixture was stirred slowly at 110°C for 6 h. After cooling, the derivatized silica was washed with toluene and methanol and dried at 90°C and 1.3 Pa for for 12 h. Weight increase: 0.18 g (8.99%). Analysis: found, C 6.99, H 1.51, N 0.69%; calculated, 0.23 mmol of (*R*)-amide per gram of stationary phase or about 0.60 groups/nm^2 (based on C), or 0.25 mmol of (*R*)-amide per gram of stationary phase or 0.63 groups/nm^2 (based on N).

Aminopropylated silica. A 6.97 g amount of LiChrospher Si 100 (dried at 150°C and 1.3 Pa for 8 h) was mixed with a solution of 4.42 g (20 mmol) of 3-aminopropyltriethoxysilane in 50 ml of dry toluene. The mixture was slowly stirred and refluxed under dry conditions for 24 h. After cooling, the derivatized silica was washed with toluene, methanol, diethyl ether and *n*-pentane and dried at 80°C and 10^{-2} Pa for 6 h. Weight increase: 0.88 g (12.7%). Analysis: found, C 4.78, H 1.43, N 1.61%; calculated, 0.57 mmol amine per gram of stationary phase or 1.5 groups/nm^2 (based on C).

CSP II (PG). A 0.18 g (0.68 mmol) amount of NH_2-PNEA and 0.37 g of polyglycidoxypropylmethylsiloxane (2.14 mmol of glycidoxy units) were dissolved in 25 ml of dry toluene and heated under nitrogen for 1 h at 70°C. Thereafter 1.97 g of aminopropylated silica were added and the suspension was slowly stirred at 110°C for 6 h. After cooling, the derivatized silica was washed with toluene, diethyl ether, ethanol and methanol and dried at 80°C and 1.3 Pa for 6 h. Weight increase: 0.21 g (10.6%). Analysis: found, C 10.67, H 2.28, N 1.43%.

CSP III (G-Co). A 2.02 g amount of aminopropylated silica was treated with 0.82 g of glycidoxypropyl(45–55%)dimethylsiloxane copolymer (2.36 mmol of glycidoxy units) and 0.22 g (0.82 mmol) of NH_2-PNEA in 25 ml of dry toluene under the same experimental conditions as with CSP II (PG). Weight increase after drying: 0.19 g (9.64%). Analysis: found, C 11.04, H 2.37, N 1.40%.

Procedures. The elemental analyses were done with a routine analyser in the Microanalytical Department of Ciba-Geigy (Basle, Switzerland).

To eliminate fines the CSPs were sedimented five times in methanol. Stainless-steel tubes (25 cm × 3.2 mm I.D.) were used as columns. A slurry prepared from about 1.9 g of the phase material and 30 ml of methanol–triethylene glycol (1:9) for CSP I and dibromomethane–*n*-hexane (8:2) for the other stationary phase was filled into the column with a Haskel air-driven fluid pump (Model 27486-4; Haskel Engineering and Supply, Burbank, CA, USA) at a pressure of 68 MPa. The columns were conditioned with methanol and *n*-hexane.

Chromatography was performed using an Altex (Berkeley, CA, USA) Model 110 solvent metering pump. A Hitachi Model 100-10 variable-wavelength UV detector (Kontron, Zürich, Switzerland) at 254 nm, a Rheodyne (Berkeley, CA, USA) Model 7125 syringe-loading sample injector with a 20-μl loop and as recording devices a Tarkan W & W Model 600 recorder (Kontron), a Servograph REA 310 pen drive (Radiometer, Copenhagen, Denmark) and an HP 3396 A integrator (Hewlett-Packard, Widen, Switzerland) were used.

The mobile phase used in the chromatographic experiments were *n*-hexane–2-propanol (78:22) and (90:10) at a flow-rate of 1 ml/min. The columns and the mobile phase container were maintained at 20°C (Assistant WTE var 3185 thermostat; R. C. Kuhn, Berne, Switzerland).

Toluene as a non-retained standard, dissolved in the appropriate mobile phase, was used to determine the dead time, t_0, and number of theoretical plates, N_0. The measured values were in the ranges $1.56 \leqslant t_0 \leqslant 1.66$ min and $6000 \leqslant N_0 \leqslant 8000$ for the three stationary phases tested.

The samples were synthesized according to common laboratory methods. Table I lists all samples used with the methods described below.

Results and discussion

Chromatography of the chiral α-phenylalkylamide derivatives DNB-PEA and DNB-PNA (Table II) shows different elution properties for the three stationary phas-

TABLE I

SAMPLES USED IN CHROMATOGRAPHIC EXPERIMENTS

DNB = 3,5-dinitrobenzoyl; TFA = trifluoroacetyl; HFB = heptafluorobutyryl.

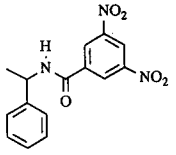

N-DNB-Phenylethylamine
(DNB-PEA)

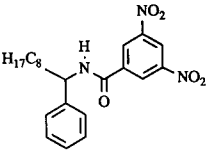

N-DNB-Phenylnonylamine
(DNB-PNA)

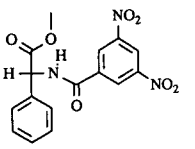

N-DNB-Phenylglycine methyl ester
(PG-ME)

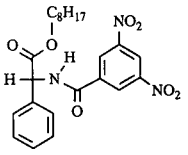

N-DNB-Phenylglycine octyl ester
(PG-OE)

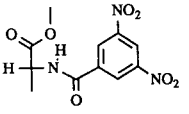

N-DNB-Alanine methyl ester
(DNB-Ala)

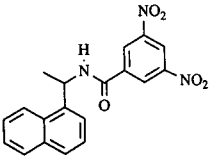

N-DNB-Naphthylethylamine
(DNB-NEA)

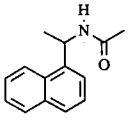

N-Acetylnaphthylethylamine
(Ac-NEA)

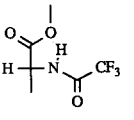

N-TFA-Alanine methyl ester
(TFA-Ala)

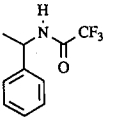

N-TFA-Phenylethylamine
(TFA-PEA)

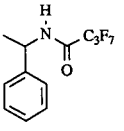

N-HFB-Phenylethylamine
(HFB-PEA)

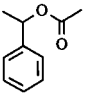

O-Acetylphenylethanol
(Ac-POH)

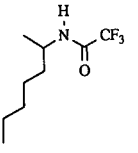

N-TFA-Heptylamine
(TFA-HAm)

TABLE II

RESOLUTION OF SOME 3,5-DINITROBENZOYLAMIDES BY LIQUID CHROMATOGRAPHY

HPLC conditions: mobile phase, (a) *n*-hexane–2-propanol (78:22) and (b) *n*-hexane–2-propanol (90:10); flow-rate, 1 ml/min; column, 25 cm × 3,2 mm I.D., 5 μm; detection, UV at 254 nm. k'_1 = Capacity factor of the first-eluted enantiomer; α = separation factor.

Compound	CSP I (M)[a]		CSP II (PG)[a]		CSP III (G-Co)[b]	
	k'_1	α	k'_1	α	k'_1	α
DNB-PEA	9.48	2.08	2.93	1.63	2.47	1.20
DNB-PNA	8.77	2.52	1.92	1.78	1.11	1.59
PG-ME	12.05	1.21	2.79	1.07		
PG-OE	5.21	1.23	1.22	1.09		

[a] Mobile phase a.
[b] Mobile phase b.

es. The glycidoxypropylmethyldimethylsiloxane copolymer, where about half of the epoxy-containing side-chains are replaced by methyl groups, together with a relatively low concentration of the chiral selector NH_2-PNEA, produces a non-polar separation quality of CSP III (G-Co). The DNB-PEA and DNB-PNA samples had to be separated with the less polar mobile phase hexane–2-propanol (90:10), because otherwise they would have been eluted in the dead time, t_0. CSP II (PG) contains more side-chains with epoxy groups and therefore a higher concentration of the chiral selector. The polarity of the phase is higher and the samples elute in a more polar mobile phase with higher capacity factors. For CSP I (M) these effects are even more pronounced. On all stationary phases the samples with longer alkyl chains elute before the corresponding homologues with shorter alkyl chains. CSP I (M) has the highest selectivity for the samples considered. This was also observed with other chiral aromatic samples. The separation factors decrease in the order CSP I (M) > CSP II (PG) > CSP III (G-Co). This behaviour is mainly due to the decrease in the surface concentration of the chiral selector. For the α-phenylalkylamide derivatives DNB-PEA and DNB-PNA, the separation factors increase on all the phases with increasing length of the alkyl chain. For the N-3,5-dinitrobenzoylphenylglycine derivatives PG-ME and PG-OE, the separation factors are scarcely influenced by the length of the alkyl chain.

CAPILLARY GAS CHROMATOGRAPHY

Experimental

Synthesis of stationary phase. The monomeric phase was prepared by heating NH_2-PNEA with an excess of butene oxide for 2 h at 60°C [CSP IV (M), Fig. 4]. The reaction of NH_2-PNEA with the glycidoxypolysiloxanes occurred after the coating in the capillaries during the conditioning process at 120°C.

Gas chromatography. Glass capillaries were drawn from Duran glass tubes with a modified Hupe & Busch capillary drawing machine. The capillaries (I.D. 0.3 mm)

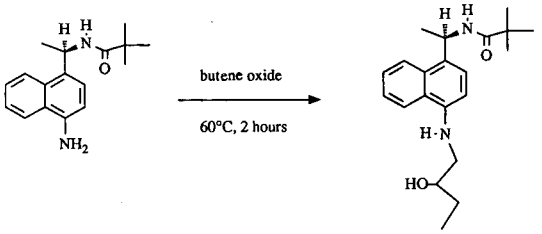

Fig. 4. Synthesis of chiral stationary phase CSP IV (M).

were leached according to Grob [13] at 170°C for 12 h. Deactivation was performed with aminopropyldimethylethoxysilane at 300 °C for 12 h. The deactivated capillaries were coated by the static method. The concentration of the monomeric phase CSP IV (M) was 1 mg/ml and the concentration of the polymeric phase CSP II (PG) was 1.3 mg of NH_2-PNEA and 3 mg of polyglycidoxypropylmethylsiloxane in 1 ml of dichloromethane. The concentration of the polymeric phase CSP III (G-Co) was 0.85 mg of NH_2-PNEA and 4.3 mg of glycidoxypropylmethyldimethylsiloxane copolymer in 1 ml of dichloromethane. The gas chromatograph (Hewlett-Packard, HP-5794A) used was equipped with a flame ionization detector and a split/splitless injector. Helium was used as the carrier gas at a velocity of 30 cm/s. The splitting ratio was set at 1:20.

Results and discussion

The stationary phases separate chiral amides and esters. The best separation factor (α) was obtained with the monomeric phase (Table III). However, the bleeding rate was high and the columns could be used only for short periods at temperatures higher than 100°C. The phase also formed droplets, even on non-deactivated surfaces. This caused a very low efficiency (maximum 650 plates/m).

The polymeric phases had some advantages over the monomeric phase. The wettability on the deactivated capillary surface was clearly better. This led to an improved efficiency (maximum 1500 plates/m). The thermal stability was also improved, but it was still lower than that with columns which were coated with polygly-

TABLE III

RESOLUTION OF SOME AMIDES AND ESTERS BY CAPILLARY GAS CHROMATOGRAPHY

GC conditions: carrier gas helium; injector temperature, 220°C; column, 10 m × 0.3 mm I.D.; flame ionization detection at 280°C. k'_1 = Capacity factor of the first-eluted enantiomer; α = separation factor.

Compound	Temperature (°C)	CSP IV (M)		CSP II (PG)		CSP III (G-Co)	
		k'_1	α	k'_1	α	k'_1	α
TFA-Ala	90	5.5	1.077	13.2	1.032	17.8	1.024
TFA-HAm	90	5.3	1.053	18.9	1.029	41.3	1.019
HFB-PEA	100			31.8	1.073	94.5	1.050
TFA-PEA	120	9.2	1.101	19.2	1.061	25.2	1.041
Ac-POH	90			14.9	1.025		

cidoxypropylmethylsiloxane and an achiral amine, *e.g.*, Jeffamine M-2070. The greatest advantage of the polymeric phases was the simple immobilization process during the conditioning. After rinsing with dichloromethane, more than 85% of the stationary phase remained in the column.

PACKED COLUMN SUPERCRITICAL FLUID CHROMATOGRAPHY

Experimental

The laboratory-constructed SFC apparatus [14] consisted of a System Gold 116 HPLC pump (Beckman Instruments, Basle, Switzerland) controlled by an NEC PC-8201A computer. The pump head was cooled by an ethanol cooling bath at −10°C. The cooling jacket was laboratory built. The sample was introduced by a Rheodyne Model 7125 HPLC injection valve with a 5-μl loop. Temperature control for the column was provided by an oven from a gas chromatograph (Sigma 2; Perkin-Elmer, Küsnacht, Switzerland). The outlet pressure was regulated at 40°C by a Tescom restrictor (Matkemi, Therwil, Switzerland). Inlet and outlet pressures were controlled by a laboratory-built pressure controller. A Uvikon 720 LC UV detector (Kontron) was used at 254 nm. The results were recorded with a Hewlett-Packard HP 3396A integrator. Carbon dioxide (40-grade with 5% of methanol) was obtained from Carbagas (Berne, Switzerland). Chromatography was performed with the CSPs used for HPLC.

Results and discussion

Some 3,5-dinitrobenzoylamides could be separated into the enantiomers with CSPs I–III by pSFC (Table IV).

The selectivities obtained with the SFC system are lower than those with the HPLC system, for different reasons. SFC separation was executed with another modifier (methanol) and at higher temperatures. On the other hand, the efficiency is much better with the SFC system because the solute diffusion coefficients are 5–10 times greater in SFC than in HPLC (Fig. 5).

TABLE IV

RESOLUTION OF SOME 3,5-DINITROBENZOYLAMIDES BY PACKED COLUMN SUPERCRITICAL FLUID CHROMATOGRAPHY

SFC conditions: mobile phase, carbon dioxide with 5% methanol; flow-rate, 1.8 ml/min; temperature, 40°C; column inlet pressure, 220 bar; column outlet pressure, 180 bar; column, 25 cm × 3.2 mm I.D., 5 μm; detection, UV at 254 nm. k'_1 = Capacity factor of the first-eluted enantiomer; α = separation factor.

Compound	CSP I (M)		CSP II (PG)		CSP III (G-Co)	
	k'_1	α	k'_1	α	k'_1	α
DNB-PEA	11.29	1.69	4.50	1.17	2.54	1.07
DNB-PNA	12.93	1.93	4.05	1.28	2.22	1.13
PG-ME	8.03	1.09	2.39	n.r.[a]	1.18	n.r.
DNB-NEA	17.97	3.21	7.30	1.51	4.41	1.23
DNB-Ala	4.86	1.45	2.17	1.09	1.26	n.r.

[a] Not resolved.

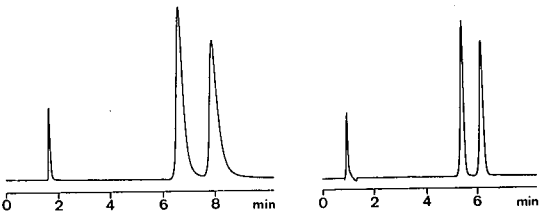

Fig. 5. Separation of N-DNB-phenylethylamine (DNB-PEA) on stationary phase CSP II (PG) in HPLC (left) and pSFC (right). Column, 25 cm × 3.2 mm I.D., 5 μm; UV detection at 254 nm. HPLC: mobile phase, hexane–2-propanol (80:20); flow-rate, 1 ml/min; temperature, 22°C. SFC: mobile phase, carbon dioxide with 5% methanol; flow-rate, 1.8 ml/min at −10°C; average column pressure, 200 bar; temperature, 40°C.

CAPILLARY SUPERCRITICAL FLUID CHROMATOGRAPHY

Experimental

The equipment was laboratory built [14]. The transport of the mobile phase (only carbon dioxide was used) was effected by a piston pump (ISCO SFC-500 Mikro flow pump with cooling jacket). Sampling was done with a four-way injection valve (Valco CI4W) with a 60-nl loop (Valco, Rotor 0.06). Temperature control for the column was provided by an oven from a gas chromatograph (Hewlett-Packard Model 5710A). The flame ionization detector (Hewlett-Packard Model 18710 A) was equipped with a capillary jet (Hewlett-Packard, part No. 18740-80230). A frit restrictor (Lee Scientific, batch No. 1028-1.4) was connected to the capillary column and situated in the capillary jet of the flame ionization detector. Chromatograms were recorded with a Model 3390A or 3396A integrator (Hewlett-Packard). The capillary column was made as described under capillary gas chromatography [15].

Results and discussion

Table V shows some of the results obtained. The efficiency of this column is very low, only 80 theoretical plates/m, and it seems that the stationary phase does not completely wet the capillary surface. In contrast to the separations in cGC, the capillary column was stable under the operating conditions.

TABLE V

RESOLUTION OF TWO SAMPLES BY CAPILLARY COLUMN SUPERCRITICAL FLUID CHROMATOGRAPHY

SFC conditions: mobile phase carbon dioxide (99.998%); temperature, 90°C; column, 5 m × 0.08 mm I.D.; flame ionization detection at 300°C; sample volume, 60 nl. k'_1 = Capacity factor of the first-eluted enantiomer; α = separation factor.

Compound	Pressure (bar)	Dead time, t_0 (min)	CSP II (PG)	
			k'_1	α
DNB-PEA	283	5.76	9.82	1.48
Ac-NEA	177	9.60	7.10	1.07

CONSLUSIONS

It is possible to use stationary phases with the same chiral selector group for direct enantiomer separations with different chromatographic methods. The synthesized phases are useful for the separation of enantiomeric mixtures of samples with π-acceptor groups. The monomeric and polymeric phases tested seem to be stable under the experimental conditions of HPLC and SFC in packed and capillary columns. Owing to wetting problems, the phases are not thermally stable in cGC and subject to bleeding; the stability of these immobilized columns towards organic solvents is good, which makes them suitable for cSFC.

ACKNOWLEDGEMENTS

We are indebted to Mr. W. Bolliger and the Apparatewerkstatt of the Theodor-Kocher-Institut, University of Berne, for the construction of several parts of the SFC apparatus, to Dr. J.-O. Bosset and the Eidgenössische Versuchsanstalt für Milchwirtschaft, Liebefeld-Berne, and Beckman Instruments, Basle, for providing equipment for SFC, and to Ciba-Geigy, Basle, for analytical service.

REFERENCES

1 Th. Jira, C. Vogt and T. Beyrich, *Pharmazie*, 43 (1986) 385.
2 W. Lindner and C. Pettersson, in I. W. Wainer (Editor) *Liquid Chromatography in Pharmaceutical Development*, Aster, Springfield, 1985, p. 63.
3 W. H. Pirkle and B. C. Hamper, in B. A. Bidlingmeyer (Editor), *Preparative Liquid Chromatography (Journal of Chromatography Library*, Vol. 38), Elsevier, Amsterdam, 1987, 235.
4 R. Däppen, H. Arm and V. R. Meyer, *J. Chromatogr.*, 373 (1986) 1.
5 V. Schurig, *Kontakte (Darmstadt)*, No. 1 (1986) 3.
6 W. A. König, S. Lutz and G. Wenz, *Angew. Chem.*, 101 (1989) 1744.
7 V. Schurig, M. Jung, D. Schmalzing, M. Schleimer, J. Duvekot, J. C. Buyten, J. A. Peene and P. Mussche, *J. High Resolut. Chromatogr.*, 13 (1990) 470.
8 P. Macaudière, M. Caude, R. Rosset and A. Tambuté, *J. Chromatogr. Sci.*, 27 (1989) 583.
9 R. Däppen, V. R. Meyer and H. Arm, *J. Chromatogr.*, 361 (1986) 93.
10 R. Däppen, H. Karfunkel and F. J. J. Leusen, *J. Chromatogr.*, 469 (1989) 101.
11 R. Däppen, H. Karfunkel and F. J. J. Leusen, *J. Comput. Chem.*, 11 (1990) 181.
12 R. Straub, *Dissertation*, University of Berne, Berne, 1990.
13 K. Grob, *Making and Manipulating Capillary Columns for Gas Chromatography*, Hüthig, Heidelberg, 1986.
14 P. Krähenbühl, *Dissertation*, University of Berne, Berne, 1990.
15 A. Marti, *Dissertation*, University of Berne, Berne, 1989.

Journal of Chromatography, 557 (1991) 173–185
Elsevier Science Publishers B.V., Amsterdam

CHROM. 23 268

Chiral stationary phase designed for β-blockers

W. H. PIRKLE* and J. A. BURKE, III
School of Chemical Sciences, University of Illinois, Urbana, IL 61801-3731 (USA)

ABSTRACT

A chiral stationary phase (CSP) derived from an N-3,5-dinitrobenzoyl-α-amino phosphonate was prepared for the direct separation of the enantiomers of underivatized β-blockers. Structure–chromatographic activity relationships for β-blockers and closely related analogues are reported for this CSP and are found to be consistent with the model used to design this CSP. The effect of temperature on the chromatographic behavior of β-blocker enantiomers is unusual. A reduction in temperature reduces the retention of the less retained enantiomer and increases the retention of the more retained enantiomer without appreciable band broadening.

INTRODUCTION

It is widely recognized that stereoisomers of pharmaceutical agents may have drastically different pharmacological potencies or actions [1,2]. For example, the so-called β-blockers, widely used in the treatment of angina pectoris and hypertension, differ considerably in the physiological responses that they elicit. Typically, the *S* enantiomers are 50-500 fold more active than their antipodes and may differ also in the nature of the elicited responses [3].

Owing to their importance, many potential β-blockers have been developed and tested and a number are now marketed. In the present scientific climate, all stereoisomers of a potential pharmaceutical must be evaluated individually. Consequently, methods for preparatively separating β-blocker stereoisomers and for ascertaining their stereochemical purity are of considerable current interest. Moreover, much effort continues to be expended by pharmacologists on the study of how β-blocker stereochemistry influences the extent and mode of their action. There are now a variety of liquid chromatographic methods which facilitate determinations of the stereochemical purity of β-blockers, studies of differences in the rate of metabolism of their enantiomers and studies of the stereochemical pathways of metabolism [4]. Although it is possible and often practical to derivatize enantiomers with a chiral reagent so as to obtain diastereomers which are separable on an achiral column, there are potential disadvantages to this approach. In some instances, the enantiomers of β-blockers have been separated on achiral columns through the use of chiral mobile phase additives [5,6]. However, the scope of this method remains undetermined and it too is disadvantageous in some applications. Instances of derivatization with an

0021-9673/91/$03.50

achiral reagent prior to enantiomer separation on a column containing chiral stationary phases (CSPs) have been reported [7,8]. Such derivatization, while requiring additional effort for sample preparation and validation, can aid in detection and help meet chiral recognition requitements. However, the need for derivatization and, in the case of preparative separations, de-derivatization, is an obstacle to be avoided if possible. The direct separation of underivatized enantiomers on a CSP is to be preferred but is neither always possible nor feasible.

Certain CSPs, notably those derived from chiral polymers, either natural or synthetic in origin, have shown the ability to separate the enantiomers of some underivatized β-blockers [9–13]. Such reports are typically fragmentary in that no indication is given of the ability of the phase to separate the enantiomers of β-blockers in general nor is any indication given of the mechanism(s) of chiral recognition employed by these CSPs. In the case of the protein and cellulosic CSPs, column lifetimes can be uncertain and band shapes are often unsatisfactory. A notable exception to this generalization is the recently reported cellulase-derived CSPs [14]. Protein CSPs, even though useful for analytical separations, are of limited utility for preparative separations owing to their extremely low sample capacities. To a great extent, the chiral recognition ability of polymeric CSPs depends on their secondary and tertiary structure, something difficult to understand and consequently harder to control. Extremely useful in certain applications, these polymeric CSPs must currently be regarded as empirical in their origin and application.

Several years ago, we undertook the design, based on mechanistic understanding, of a brush-type CSP intended to separate the enantiomers of underivatized β-blockers (Fig. 1). This paper reports the progress to date in this endeavor.

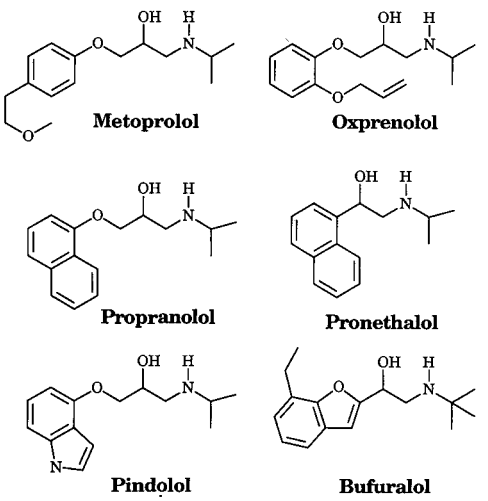

Fig. 1. Structures of β-blockers.

EXPERIMENTAL

Apparatus

Chromatography was performed using either of two systems. System one consisted of an Anspec–Bischoff Model 2200 isocratic high-performance liquid chromatographic (HPLC) pump, a Beckman Model 210 injector with a 20-μl sample loop, a Milton Roy LDC UV Monitor D fixed-wavelength detector operating at 254 nm and a Kipp and Zonen BD 41 dual-channel recorder. A Rudolph (Flanders, NJ, USA) Autopol III with a 20-cm flow cell was used to monitor the sign of $[\alpha]_D$. System two consisted of an Anspec–Bischoff Model 2200 isocratic HPLC pump, a Rheodyne Model 7125 injector with a 20-μl sample loop, two Milton Roy LDC UV Monitor D fixed-wavelength detectors connected in series operating at 254 and 280 nm and a Kipp and Zonen BD 41 dual-channel recorder. All HPLC equipment was purchased from Anspec (Ann Arbor, MI, USA). For variable-temperature experiments, *ca.* 1 m of 1/16-in. O.D. stainless-steel tubing was used between the injector and the column, the bulk of this tubing being coiled about the column as a heat exchanger. The entire column and heat exchanger were immersed in a Dewar flask containing the coolant. This experimental arrangement has given rise to linear Van 't Hoff plots for other columns and analytes.

Allyl alcohol, isobutyraldehyde and dimethyl phosphite were purchased from Aldrich (Milwaukee, WI, USA) and distilled prior to use. 2-Acetylbenzofuran was used as received from Aldrich. The N-(3,5-dinitrobenzoyl)phenylglycine column and the N-(2-naphthyl)alanine undecyl ester CSP were obtained from Regis Chemical (Morton Grove, IL, USA).

*Dimethyl N-(3,5-dinitrobenzoyl)-α-amino-2,2-dimethyl-4-pentenylphosphonate (**8**)*

A 100-ml oven-dried flask was charged with 2.20 g (12 mmol) of sodium hexamethyldisilamide and 50 ml of dry tetrahydrofuran (THF) followed by 1.75 g (12 mmol) of aldehyde **7** [15] and magnetically stirred under a nitrogen atmosphere at room temperature. After 1 h, 2.50 g (22.7 mmol) of dimethyl phosphite were added and the cloudy mixture was refluxed for 24 h. After cooling, the reaction mixture was diluted with 200 ml of diethyl ether followed by 100 ml of saturated sodium hydrogencarbonate solution and the resulting mixture was stirred for 1 h, then the phases were separated and the organic layer was washed with 50 ml of water then 50 ml of saturated sodium chloride solution. The combined aqueous layers were back-extracted with three 50-ml portions of dichloromethane. The combined organic layers are dried over sodium carbonate. After filtration, the solution of crude amino phosphonate was treated with 3.51 g (15 mmol) of 3,5-dinitrobenzoyl chloride and 100 ml of water–saturated sodium hydrogencarbonate solution (1:1). After strirring for 1 h, the aqueous layer was removed and replaced with 100 ml of the latter mixture. After stirring for a further 1 h, the layers were separated and the organic layer was washed with 50 ml of saturated sodium chloride solution, dried over magnesium sulphate and concentrated under reduced pressure. After column chromatography on silica using dichloromethane–diethyl ether (2:1) as eluent, (±)-**8** was obtained as a colorless oil (1.35 g, 25% yield). After recrystallization from methyl-*tert.*-butyl ether–hexane, ±-**8** melts at 128–129°C. Satisfactory analytical values for C, H, N and P were obtained. Thin-layer chromatography: R_F = 0.30 [silica gel plates with

dichloromethane–diethyl ether (1:1) as eluent]. ^{1}H NMR (C^2HCl_3): δ 1.15, 2 × s, 6H; 2.24, m, 1H; 2.32, m, 1H; 3.75, d (J = 16 Hz), 3H; 3.80, d (J = 16 Hz), 3H; 4.6–4.92, dd (J = 20, 10 Hz), 1H; 5.20, m, 2H; 5.90, m, 1H; 7.4, d (J = 10 Hz), 1H; 9.02, m, 2H; 9.19, m, 1H. $^{31}P\{^1H\}$ NMR (C^2HCl_3): δ 25.78 (ref. 85% H_3PO_4). IR (KBr, neat): 3248, 3098, 2961, 1734, 1670, 1630, 1541, 1344, 1284, 1234, 1035 cm^{-1}. Mass spectrum (70 eV): m/z 414 (0.8); 238 (18.0); 195 (100); 149 (81.5); 75 (76.7). High-resolution mass spectrum: m/z calculated for $C_{16}H_{22}N_3O_8P$, 415.1144; found, 415.1137.

Resolution of racemic ***8***

Enantiomer separation was accomplished by medium-pressure liquid chromatography on a 30 × 1 in. I.D. column packed with (+)-(*R*)-N-(2-naphthyl)alanine undecyl ester CSP bonded to 60-μm irregular silica. The mobile phase was isopropanol–hexane (2:98). Two chromatographic fractions were collected. The first was (+)-(*R*)-**8** of 98% enantiomeric purity, as judged by HPLC assay on a Regis (*R*)-N-(2-naphthyl)alanine column. The subsequently collected (−)-(*S*)-**8** was found to be of 99% enantiomeric purity. Each enantiomer was obtained as a colorless foam after drying *in vacuo*. The NMR spectrum of each enantiomer was identical with that of the racemate.

*Chiral stationary phase (R)-****6***

Mercaptopropylsilica (2.75 g), 0.60 g of enantiomerically pure (*R*)-**8** and 0.10 g of 2,2′-azobis(2-methylpropionitrile) were slurried in 30 ml of chloroform and heated to reflux [16]. After 36 h, the light-red mixture was cooled and the derivatized silica was collected by filtration. The silica was washed sequentially with 100 ml of methanol, 50 ml of ethyl acetate and 50 ml of diethyl ether. The modified silica was packed as a methanol slurry into a 120 × 4.6 mm I.D. column using conventional methods. Found: C 5.80, H 1.03, N 0.69%; calculated, 0.15 mmol/g (based on C); 0.16 mmol/g (based on N).

Analytes

The β-blocker samples were obtained as follows: pindolol from Sandoz, metoprolol from Ayerst Labs., proenthalol and propranolol from Imperial Chemical Industries, oxprenolol from Ciba-Giegy and bufuralol and its methylated analogues from Roche Products.

RESULTS AND DISCUSSION

Very early in the development of the CSPs, it became evident that basic amines are strongly retained by the π-acidic N-(3,5-dinitrobenzoyl)amino acid-derived phases. Consequently, basic primary and secondary amines are typically N-acylated prior to chromatography on these CSPs. The enantiomers of propranolol (as variously N-acylated derivatives, *e.g.*, the laurylamide) are modestly separated on an N-(3,5-dinitrobenzoyl)phenylglycine-derived CSP [17]. It is also known that the enantiomers of oxazolidones derived from β-blockers by treatment with phosgene are also separable on this CSP [18]. The need for derivatization arises from the basicity of the secondary amines. One way to reduce the basicity of an amine is through protonation, an easily reversed (and hence not undesirable) derivatization. Perhaps the ammonium

ion portion of a protonated β-blocker could be used as one of the essential interactions for chiral recognition.

During a sabbatical leave from Sumitomo Chemical, K. Moriguchi prepared several N-(3,5-dinitrobenzoyl)amino acid CSPs (**1–3**) in which the carboxylic acid group was left free (Fig. 2). By using a mobile phase containing ammonium acetate, it was expected that the carboxylic acid group of the CSP would be converted to a carboxylate group, which was intended to interact ionically with the ammonium ion portion of the protonated β-blocker. Propranolol, having a π-basic aromatic group, was expected additionally to undergo a strong π–π interaction with the CSP. Finally, the dinitrobenzamide N–H was expected to hydrogen bond to the hydroxy group of the β-blocker, affording a third bonding interaction. This *a priori* chiral recognition model predicts that CSPs **1–3**, if of the *R* configuration, should retain the *S* enantiomer of propranolol. NMR studies of mixtures of propranolol and a precursor to CSP **1** suggested that the expected interactions occur, although one cannot tell whether they occur simultaneously owing to time averaging.

When tested, CSP **1** was found to separate the enantiomers of propranolol with the expected elution order. Several other β-blockers are similarly resolved [19]. Satisfaction at having designed a CSP from mechanistic considerations which performs as expected was tempered by the observation that it led to long retention of the β-blockers and afforded undesirably broad bands and modest selectivity.

Chiral recognition typically stems from the weaker, not the stronger, of the essential interactions. The electrostatic interaction between the ammonium and carboxylate ions is sufficiently strong that, in order to keep retention at a reasonable level, a strong eluent has to be used. This interferes with the remaining weaker but

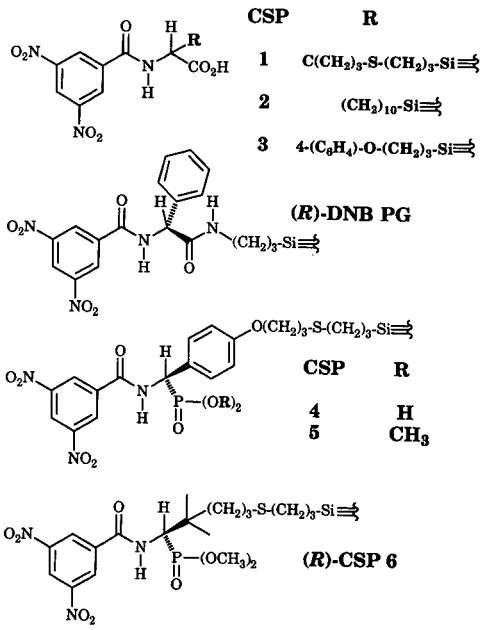

Fig. 2. Structures of chiral stationary phases.

essential interactions. To remedy this, phosphonic acid CSP **4** was prepared, the idea being that the charge on the phosphonate anion would be more diffuse and the ionic interaction would be weakened. Also considered was the possibility that the phosphonic acid group might be differently oriented (conformationally) and differently solvated, factors which might influence the strength of the electrostatic interaction. Indeed, CSP **4** does show improved enantioselectivity towards propranolol relative to CSPs **1–3**, but still shows undesirably strong retention.

Abandoning the use of a formal ionic interaction, phosphonate ester CSP **5** was prepared. Here, the intention is to have the amine (or ammonium ion) interact with the phosphonate ester through hydrogen bonding to the phosphinyl oxygen. The previously mentioned π–π and hydrogen bonding interactions were still expected to occur. Indeed, CSP **5**, the preparation of which has been described [20], does separate the enantiomers of propranolol and affords improved performance relative to its phosphonic acid analogue, **4**.

Being aware from other studies that phenyl substituents may serve as hydrogen bond sites [21], CSP **6** was prepared so as to avoid having a hydrogen bonding site on each face of the semi-rigid backbone of the CSP. In CSP **6**, the objectionable phenyl group has been replaced with a geminal dimethyl group which was expected to exert some conformational control and to provide a steric barrier projecting from one face of the chiral selector, thus controlling the preferred direction of approach by an analyte.

The synthetic sequence used to prepare CSP **6** is similar to that employed to prepare CSP **5** (Fig. 3). The route to CSP **6** begins with aldehyde **7**, readily available from the reaction of allyl alcohol and isobutyraldehyde [15]. This aldehyde has a terminal double bond (ultimately to be used to for attachment to silica) and is non-enolizable. Treatment of **7** with sodium hexamethyldisilamide affords the N-trimethylsilylimine, which adds dimethyl phosphite to give, after work-up, the α-amino phosphonate. The crude α-amino phosphonate was acylated with 3,5-dinitrobenzoyl chloride to afford racemic precursor **8**, resolvable on a variety of π-basic CSPs [22]. Preparative resolution of **8** was accomplished using a large column containing the N-2-(naphthyl)alanine-based CSP. The enantiomerically pure phosphonate was covalently bonded to 3-mercaptopropylsilanized silica using 2,2′-azobis(2-methylpropionitrile) as an initiator. The modified silica gel was slurry packed into a 120 ×

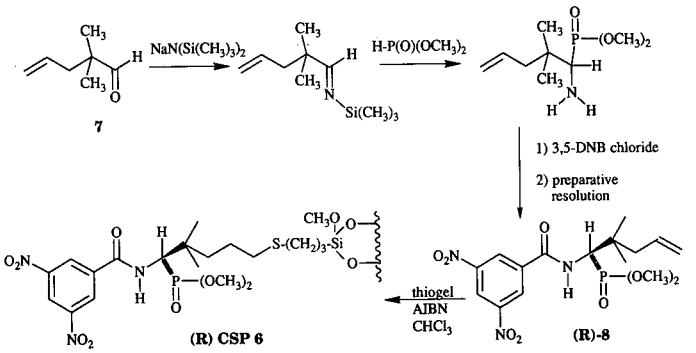

Fig. 3. Synthetic sequence for the preparation of CSP **6**.

4.6 mm I.D. stainless-steel column, end-capped with hexamethyldisilizane and evaluated for its ability to separate the enantiomers of an assortment of β-blockers and β-blocker analogues.

As mentioned earlier, the presence of a basic amino group in an analyte typically leads to long retention and peak tailing on silica-based π-acidic CSPs. Control of mobile phase pH and/or addition of amines to the mobile phase are frequently used cures for such peak tailing. Previous experience had shown that mobile phases consisting of halocarbons and lower molecular weight molecular alcohols and containing a low concentration of ammonium acetate allow the separation of enantiomers of propranolol on CSPs **1**–**3**. The ammonium acetate provides a means of protonating the amino group of the β-blockers and reduces peak tailing. In halocarbon–alcohol solvent mixtures, extensive formation of aggregated tight ion pairs is thought to occur. Increasing the concentration of the ammonium acetate in the mobile phase diminishes the retention of propranolol on CSP **6**, but does not drastically alter the enantioselectivity, thus suggesting that the ammonium acetate competes with the protonated β-blockers for absorption sites. This behavior is shown in Fig. 4, obtained using a chloroform–methanol mobile phase. In preparative separations, the volatility of the mobile phase components including ammonium acetate makes it possible to retrieve the β-blocker simply by evaporation of the mobile phase under vacuum.

For comparison of CSPs **5** and **6**, a mobile phase of dichloromethane–ethanol (19:1) containing 0.5 g/l (6.5 m*M*) of ammonium acetate was used. To improve the

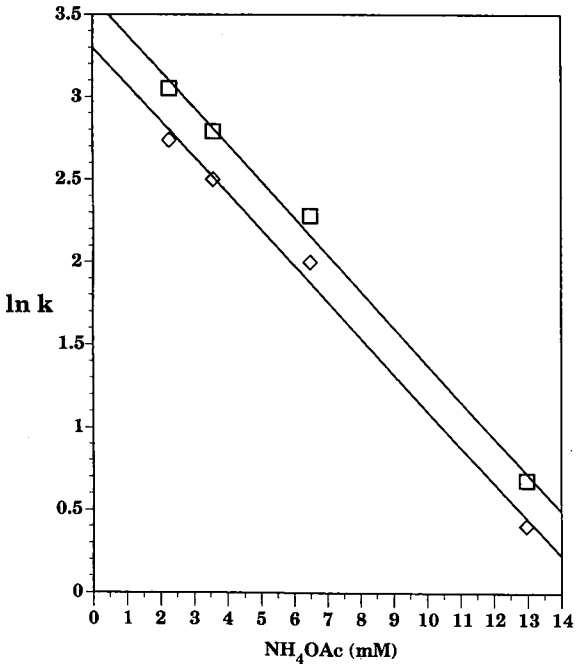

Fig. 4. Relationship between retention of propranolol enantiomers on CSP **6** and the amount of ammonium acetate (NH_4OAc) in chloroform–methanol (9:1) mobile phase. ◇ = ln k'_1; □ = ln k'_2.

TABLE I

SEPARATION OF THE ENANTIOMERS OF SOME β-BLOCKERS

Analyte	(*R*)-DNB PG			(*R*)-CSP **5**			(*R*)-CSP **6**		
	α^a	$k'_1{}^b$	$[\alpha]_D{}^c$	α^a	$k'_1{}^b$	$[\alpha]_D{}^c$	α^a	$k'_1{}^b$	$[\alpha]_D{}^c$
Metoprolol	1.05	9.86		1.15	6.57		1.16	2.57	
Oxprenolol	1.00	16.1		1.00	6.14		1.00	2.28	
Pronethalol	1.03	11.2		1.06	12.36		1.13	5.14	
Propranolol	1.00	12.8		1.34	13.4,	(+)-(*R*)-	1.39	4.36,	(+)-(*R*)-
Pindolol	1.12	45.1		1.12	50.1		1.30	15.0	
Bufuralol	1.16	4.94,	(+)-(*R*)-	1.22	6.67,	(+)-(*R*)-	1.93	2.79,	(+)-(*R*)-

[a] Chromatographic separation factor.

[b] The capacity factor for the first-eluted enantiomer using dichloromethane–ethanol (19:1) containing 0.5 g/l of ammonium acetate as the mobile phase at a flow-rate of 2 ml/min. The detector was operated at 254 nm.

[c] Sign of $[\alpha]_D$ of the more strongly retained enantiomer as determined using a polarimetric HPLC detector. The letter refers to the absolute configuration of the more strongly retained enantiomer.

reproducibility, a stock solution of ammonium acetate in absolute ethanol was prepared and diluted with dichloromethane as required. Comparative chromatographic data for six β-blockers obtained using a commercial covalent (*R*)-N-(3,5-dinitrobenzoyl)phenylglycine-derived phase (DNB PG), the (*R*)-phosphonate ester phase **5** and (*R*)-phosphonate ester phase **6** are presented in Table I. From these data, it is evident that the more π-basic β-blockers are the more strongly retained. However, enantioselectivity does not necessarily parallel retention. Note that bufuralol is one of the more weakly retained, judged by k'_1, of the β-blockers on CSP **6**, yet affords the largest separation factor in Table I.

The elution orders on CSP **5** and **6** can be explained using the aforementioned model, although this model is not in accord with the elution order noted on (*R*)-DNB PG. Owing to the Cahn–Ingold–Prelog priority sequence, (*R*)-CSPs **5** and **6** are stereochemically equivalent to (*S*)-DNB PG. To evaluate further the chiral recognition process, the effect of temperature on β-blocker retention by CSPs **5** and **6** was investigated. One generally expects a linear Van 't Hoff response (*i.e.*, a linear ln k' *versus* $1/T$ plot) with increases in retention, enantioselectivity and peak width as the column temperature is reduced. Using the CSP–mobile phase combination described, non-linear Van 't Hoff behavior is observed for an extended series of β-blockers and their analogues. As can be seen from the data in Table II, there are dramatic increases in enantioselectivity with comparatively little accompanying peak broadening (see Fig. 5). A reduction in temperature always decreases the retention of the less retained enantiomer and often slightly decreases that of the more retained enantiomer. For some analytes, the retention of the more retained enantiomer initially decreases then increases as the temperature is lowered further. In view of the number of equilibria possible in these complex systems, equilibria which may respond differently to temperature change, no rationalization of these observations is offered here.

It is not surprising that the enantiomers of bufuralol are better resolved than those of propranolol and pindolol. Unlike the later two, bufuralol lacks the methylene group between the π-basic aromatic group and the stereogenic center. Consequently, it

TABLE II

EFFECT OF TEMPERATURE ON RETENTION AND ENANTIOSELECTIVITY FOR SOME β-BLOCKERS AND ANALOGUES USING CSP **6**

Analyte	21°C			0°C			−24°C		
	α^a	$k'_1{}^b$	$k'_2{}^b$	α^a	$k'_1{}^b$	$k'_2{}^b$	α^a	$k'_1{}^b$	$k'_2{}^b$
Metoprolol	1.16	2.57	2.98	1.21	1.05	1.27	1.48	0.64	0.95
Oxprenolol	1.00	2.28	2.28	1.00	0.75	0.75	1.03	0.50	0.52
Pronethalol	1.13	5.14	5.81	1.21	2.21	2.67	1.31	1.50	1.97
Propranolol	1.39	4.36	6.06	1.63	1.86	3.03	2.11	1.28	2.70
Pindolol	1.30	15.0	19.5	1.43	7.29	10.4	1.72	6.71	11.5
Bufuralol	1.93	2.79	5.38	2.50	1.43	3.58	4.08	0.73	2.98
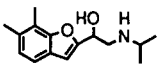	2.15	3.43	7.37	2.83	2.07	5.86	4.18	1.57	6.56
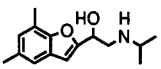	2.23	3.28	7.31	3.04	1.86	5.65	4.44	1.46	6.48
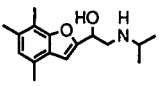	2.58	4.43	11.43	3.44	2.57	8.84	5.03	2.21	11.1
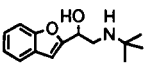	1.75	4.14	7.25	2.38	1.86	4.43	3.76	1.13	4.25
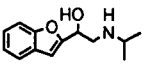	1.64	4.01	6.58	2.08	1.80	3.74	3.08	1.08	3.33
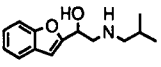	1.63	1.71	2.79	1.94	1.19	2.31	3.02	0.73	2.20

[a] Chromatographic separation factor.

[b] Capacity factors for the two enantiomers using dichloromethane–ethanol (19:1) containing 0.5 g/l of ammonium acetate as the mobile phase at a flow-rate of 2 ml/min. The detector was operated at 254 nm.

is more restricted conformationally, a circumstance often associated with appreciable degrees of enantioselectivity. Note that replacing the 7-ethyl substituent of bufuralol with two or, better, three methyl substituents on the benzofuran ring enhances enantioselectivity by increasing the π-basicity without adding polar sites for additional bonding interactions with the stationary phase (see Fig. 6) which increase retention but may possibly reduce enantioselectivity. The methyl substituents enhance enantioselectivity relative to bufuralol even though the analogues have N-isopropyl substituents, shown here to be inferior to N-*tert.*-butyl substituents in engendering enantioselectivity in bufuralol-like systems. For example, a series of bufuralol-like racemates were prepared by a synthetic route which allows variation of the N-alkyl substituent (Fig. 7). This sequence, similar to that reported for bufuralol [23], entails α-bromination of 2-acetylbenzofuran, reduction of the bromo ketone to the bromo alcohol with sodium tetrahydroborate and substitution of the desired *n*-alkylamine for the bromine. Fig. 8 shows the effect of the length of the N-alkyl substituent on α at 21, 0 and −24°C. As can be seen, alkyl groups longer than propyl have a negligible effect

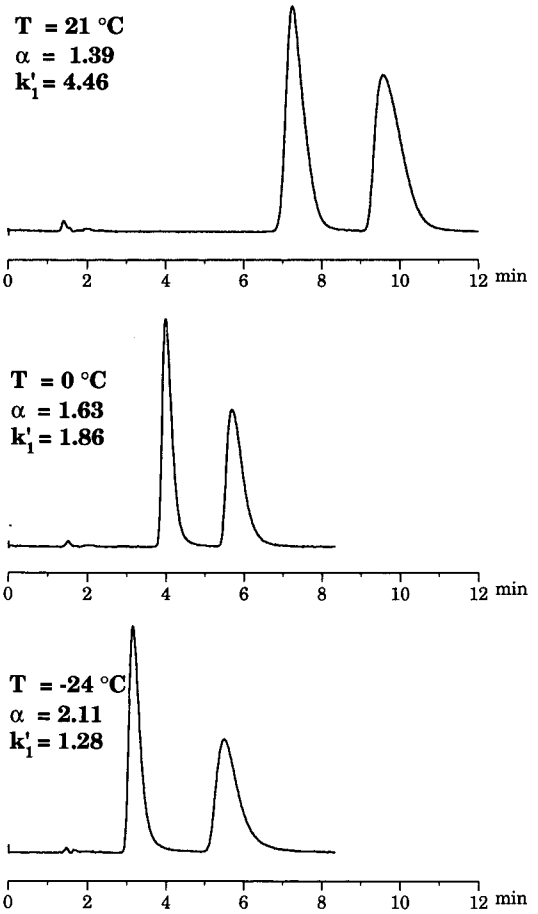

Fig. 5. Effect of temperature on retention and enantioselectivity of propranolol on CSP **6**. Mobile phase: chloroform–ethanol (19:1) containing 0.5 g/l of ammonium acetate.

on the magnitude of α, suggesting that the enantiomers show either no or little differential intercalation of the N-alkyl groups between strands of bonded phase [24,25].

In all instances, α increases dramatically as the temperature is diminished. The chromatographic response to temperature change of the bufuralol analogues having N-isopropyl, N-isobutyl and N-*tert.*-butyl substituents is shown in Table II. The N-isopropyl and N-isobutyl analogues show comparable levels of enantioselectivity at ambient temperature and are exceeded in this respect by the N-*tert.*-butyl analogue. This difference is accentuated at lower temperatures. All three analogues show lower selectivities than bufuralol, doubtless owing to the absence of a π-basicity-enhancing alkyl substituent on the benzofuran system.

Elution orders were rigorously established using β-blocker samples of known absolute configuration. In some instances, the signs of the rotation of the enantiomers were related to elution orders using a polarimetric detector in series with the ultraviolet

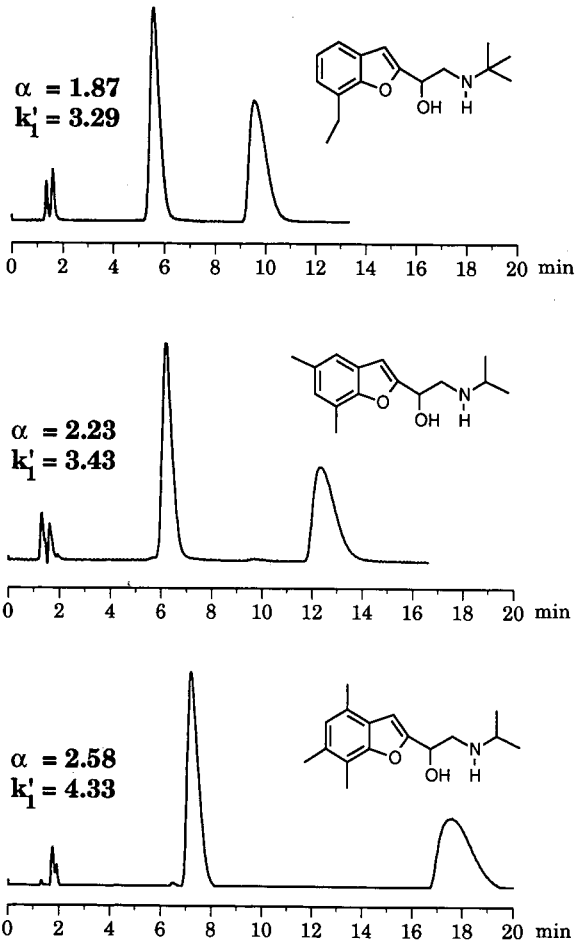

Fig. 6. Influence of ring methylation on the retention and enantioselectivity shown by several bufuralol analogues when chromatographed on CSP **6** using dichloromethane–ethanol (19:1) containing 0.5 g/l of ammonium acetate as the mobile phase.

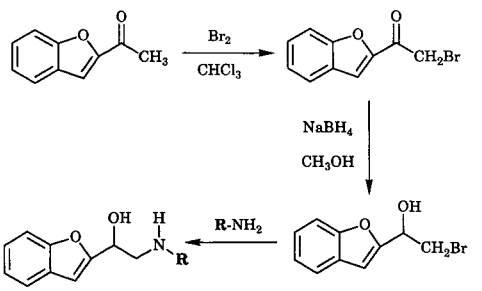

Fig. 7. Preparation of bufuralol-like racemates.

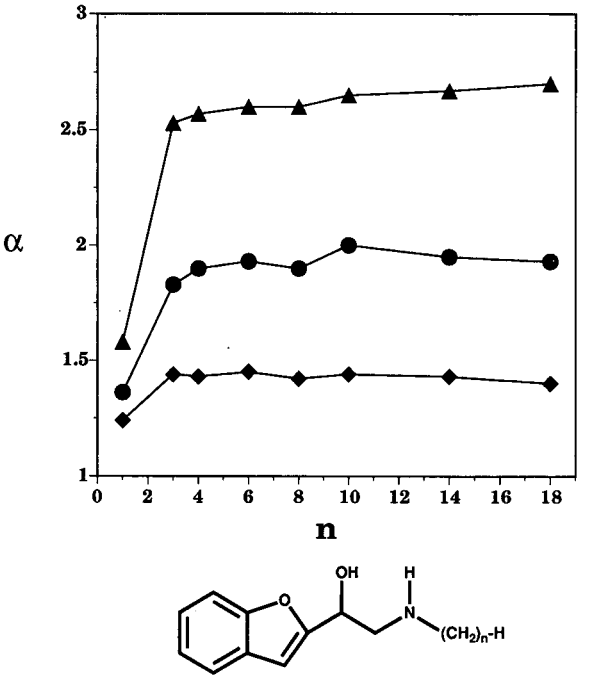

Fig. 8. Relationship between enantioselectivity on CSP **6** and *n*, the number of methylenes in the N-alkyl substituent, at three temperatures (◆ = 21; ● = 0; ▲ = −24°C) using dichloromethane–ethanol (19:1) containing 0.5 g/l of ammonium acetate as the mobile phase.

detectors. The observed elution orders on CSP **5** and **6** are consistent with the *a priori* formulated chiral recognition model, as are the structure–activity relationships noted. Although it is likely that further design changes will lead to CSPs that show greater scope and selectivity, it is evident that CSP **6** is useful for both analytical- and preparative-scale separations of a variety of β-blockers, no derivatization being required.

ACKNOWLEDGEMENTS

This work was supported by research grants from the National Science Foundation, Merck, Sharp and Dohme and Eli Lilly.

NOTE ADDED IN PROOF

Since submission of this paper, a comprehensive review ("Chromatography of β-adrenergic blocking agents") has appeared [26].

REFERENCES

1 E. J. Ariens, *Eur. J. Clin. Pharmacol.*, 26 (1984) 663.
2 D. Drayer, *Clin. Pharmacol. Ther.*, 40 (1986) 125.

3 W. Nelson and T. Burke, *J. Org. Chem.*, 43 (1978) 3641; and references cited therein.
4 W. Lough (Editor), *Chiral Liquid Chromatography*, Blackie, London, 1989; and references cited therein.
5 C. Pettersson, A. Karlsson and C. Gioeli, *J. Chromatogr.*, 407 (1987) 217.
6 C. Pettersson and G. Schill, *J. Chromatogr.*, 204 (1981) 179.
7 J. Hermansson, *J. Chromatogr.*, 325 (1985) 379.
8 W. König, K. Ernst and J. Vessman, *J. Chromatogr.*, 294 (1984) 423.
9 J. Hermansson, *Trends Anal. Chem.*, 8 (1989) 251.
10 A. Walhagen and L. Edholm, *J. Chromatogr.*, 473 (1989) 371.
11 Y. Okamoto, M. Kawashima, R. Abruratani, K. Hatada, T. Nishiyama and M. Masuda, *Chem. Lett.*, (1986) 1237.
12 H. Aboul-eneim and M. Islam, *Chirality*, 1 (1989) 301.
13 D. Armstrong, T. Ward, R. Armstrong and T. Beesley, *Science*, 232 (1986) 1132.
14 P. Erlandsson, I. Marle, L. Hannsson, R. Isaksson, G. Pettersson and C. Pettersson, *J. Am. Chem. Soc.*, 112 (1990) 4573.
15 R. Salomon and J. Ghosh, *Org. Synth.*, 63 (1984) 125.
16 C. Rosinin, C. Bertucci, D. Pini, P. Altemura and P. Salvadori, *Tetrahedron Lett.*, (1985) 3361.
17 W. H. Pirkle, J. Finn, J. Schriener and B. Hamper, *J. Am. Chem. Soc.*, 103 (1981) 3964.
18 I. Wainer, T. Doyle, K. Donn and J. Powell, *J. Chromatogr.*, 306 (1984) 405.
19 K. Moriguchi and W. H. Pirkle, presented at the *13th International Symposium on Column Liquid Chromatography, (CLC 1989), Stockholm, 1989*, paper M/TU-P017.
20 W. H. Pirkle and J. Burke, III, *Chirality*, 1 (1989) 57.
21 W. H. Pirkle, T. C. Pochapsky, G. S. Mahler, D. E. Corey, D. S. Reno and D. M. Alessi, *J. Am. Chem. Soc.*, 108 (1986) 5627.
22 J. A. Burke, III, unpublished results.
23 G. Fothergill, J. Osbond and J. Wicken, *Arzneim.-Forsch.*, 27 (1977) 978.
24 W. H. Pirkle, M. H. Hyun and G. A. Bank, *J. Chromatogr.*, 316 (1984) 585.
25 W. H. Pirkle and R. Dappen, *J. Chromatogr.*, 404 (1987) 107.
26 C. L. Davies, *J. Chromatogr.*, 531 (1990) 131.

Journal of Chromatography, 557 (1991) 187–197
Elsevier Science Publishers B.V., Amsterdam

CHROM. 23 271

Enantiomeric distribution and $^{13}C/^{12}C$ isotope ratio determination of γ-lactones: appropriate methods for the differentiation between natural and non-natural flavours?

SIEGFRIED NITZ*, HUBERT KOLLMANNSBERGER, BERND WEINREICH and FRIEDRICH DRAWERT

Institut für Lebensmitteltechnologie und Analytische Chemie, Technische Universität München, W-8050 Freising-Weihenstephan (Germany)

ABSTRACT

The quantitative and enantiomeric distribution of γ-lactones in certain fruits (strawberry, raspberry, pineapple, passion fruit, plum and coconut) compared with corresponding fruit concentrates and beverages was determined by multi-dimensional gas chromatography–mass spectrometry with an achiral–chiral column combination. It was found that significant variations in enantiomeric excess values of γ-lactones due to varieties and processing influences can occur. On-line multi-dimensional gas chromatographic–isotope ratio mass spectrometric $^{13}C/^{12}C$ isotope ratio measurements of γ-decalactone in vinous beverages and references (synthetic and microbial) were performed, in order to establish how far enantiomeric data in combination with additional $\delta^{13}C$ values can serve as a basis for the validation of the genuineness of flavours and flavoured products.

INTRODUCTION

The current trend toward natural foods and beverages and the differentiation of natural and non-natural flavouring substances required by legislation have increased the demand for appropriate analytical methods to ensure proper labelling and to identify the fraudulent use of synthetic compounds. Especially gas chromatographic (GC) methods such as enantioresolution on chiral capillary columns [1,2] and multi-dimensional GC (MDGC) with achiral–chiral column combinations [3–5] were developed for the determination to the fruit-specific distribution of optically active compounds, mainly γ-lactones. Because of their widespread occurrence in fruits and flavour compositions, they are believed to be useful indicators for the quality evaluation of flavours. Previously the chirality evaluation of natural γ-lactones revealed that especially in the case of deca- and dodecalactone, one enantiomeric from predominates [5–9]. Therefore, it was postulated that the occurrence of racemic lactones in processed foodstuffs and flavour formulations has to be associated with the addition of synthetic flavourings [4]. Consequently, the enantiomeric distribution is widely used as a criterion of genuineness.

0021-9673/91/$03.50

The exclusive use of the "typical" enantiomeric excess values corresponding to the different fruits without considering their natural range due to different varieties [9] and possible changes caused by processing influences may lead to erroneous conclusions. Therefore, in addition to the aforementioned aspects, the quantitative lactone distribution [10] can be regarded as a further criterion.

A particular problem arises when the enantiomeric ratio has been "tuned" using pure (*R*)- γ-decalactone of microbial origin. In this context, the determination of the natural abundance of stable isotopes by means of stable isotope ratio mass spectrometry (IRMS) offers a method for the assignment of the origin and treatment of foods and food ingredients [11–14]. Especially the recent developments in "on-line" GC–IRMS systems [15,16] and MDGC–IRMS [17] for measuring $^{13}C/^{12}C$ isotope ratios have extended its application to the analysis of complex mixtures such as flavour extracts.

The aim of this work was to delineate the limitations arising in the determination of naturalness, based on experimental data obtained by enantioresolution and/or GC–IRMS measurements.

EXPERIMENTAL

Materials

Fresh strawberries (var. Red Gauntlet); deep-frozen raspberries, freeze-dried raspberries (prepared in our laboratory), two commercial raspberry concentrates, fresh pineapples (from the Ivory Coast) [8], five pineapple concentrates [8], fresh yellow passion fruits (from Brazil) [6], fresh purple passion fruits (from Kenya) [6], five passion fruit concentrates (from Brazil) [6], fresh coconut, commercial coconut flakes, fresh plums (from northern Bavaria, frozen for 2 months), two plum wines (made in our laboratory from frozen plums by mash and juice fermentation, respectively), a sparkling strawberry wine, a vinous beverage ("weinhaltiges Getränk") with peach flavour and a vinous beverage named "piña colada" (labelled as a mixture of white wine, pineapple juice, flavour of coconut and other tropical fruits) were obtained from the local market or directly from manufacturers.

Sample preparation

Fruits (100–1000 g) were homogenized with methanol and the homogenates were centrifugated and diluted with water. Fruit concentrates (200–500 ml) were diluted with water. Plum wines, sparkling strawberry wine and alcoholic mixed-beverages (0.5–1 l) were used undiluted. After addition of a suitable proportion (1:5, v/v) of saturated potassium fluoride solution, all samples were extracted with pentane–dichloromethane (2:1).

The milk of one coconut (30 ml) was applied to an Extrelut column (Merck, Darmstadt, Germany) containing 14 g of Extrelut, and extracted with 60 ml of pentane–dichloromethane (2:1). One portion of the flesh (100 g) was homogenized in methanol, extracted with pentane–dichloromethane and the organic supernatant was decanted after freezing. Another 100-g portion was extracted by means of simultaneous distillation extraction (SDE) with diethyl ether. Commercial coconut flakes were extracted in the same way. Coconut fat obtained from flakes by Soxhlet extraction (46 g of fat from 100 g of flakes) was heated at 100–150°C for 3 h under a continuous

stream of oxygen, and flavour compounds were subsequently extracted by SDE with diethyl ether.

All extracts were dried over anhydrous sodium sulphate and concentrated to a final volume of 0.3–0.5 ml on a Vigreux column (40°C).

Enantioresolution of γ-lactones (MDGC–MS)

A Siemens SiChromat 2 dual-over gas chromatograph, equipped with a liquid injector (220°C, splitting ratio 1:11) and a total transfer device, was directly coupled with a Finnigan 4021 C quadrupole mass spectrometer. Preseparation of 2–5 μl of the samples was achieved on a wide-bore CW20M precolumn (G. Leupold, Weihenstephan, Germany) (30 m × 0.53 mm I.D.; film thickness 1.5 μm), programmed from 100 to 220°C at 5°C/min. The carrier gas was helium at 6 ml/min (100°C). At the corresponding retention ranges of γ-lactone reference substances, quantitative cuts into a precooled intermediate trap (liquid nitrogen; −150°C) were performed. On-line transfer of the enriched lactones into the chiral main column was achieved by heating the trap to 200°C, whilst the precolumn was backflushed. The enantiomers were separated on a chiral Lipodex B main column (Macherey, Nagel & Co., Düren, Germany) (50 m × 0.25 mm I.D.), programmed from 135°C (30 min) to 200°C at 3°C/min. The carrier gas was helium at 0.5 ml/min (135°C). Mass spectra were recorded at 70 eV in the mass range 50–150 u.

$^{13}C/^{12}C$ isotope ratio determination (MDGC–IRMS)

A Siemens SiChromat 2 dual-oven gaschromatograph, equipped with a liquid injector (220°C) and a "live-T" switching device, directly coupled with a VG Model Isochrom II GC–IRMS system [15,17], was used. Preseparation of 2–3 μl (splitless injection) of the samples was achieved on an SPB-5 precolumn (Supelco, Bellefonte, PA, USA) (30 m × 0.25 mm I.D.; film thickness 1.0 μm), programmed from 80 to 200°C (5 min) at 4°C/min and from 200 to 225°C at 2°C/min. The carrier gas was helium at 0.3 ml/min. After selective transfer of the γ-decalactone (cut: 37.3–41 min), the enantiomers were separated on a chiral Lipodex B fused-silica main column (Macherey, Nagel & Co.) (50 m × 0.25 mm I.D.), programmed from 140°C (60 min) to 150°C (20 min) at 1°C/min. Selective cuts of the chiral column effluent were introduced (transfer line temperature 180°C) into the combustion furnace filled with copper (II) oxide (operated at 800°C) by means of a Deans-type switching device (SGE, Ringwood, Australia). Water of reaction was removed continuously by a cryogenic trap (−100°C). The $^{13}C/^{12}C$ isotopic ratios are given in δ‰ relative to the values of PDB.

RESULTS

In the following some selected results of our recent studies on fruits and processed fruit products are presented. In additon to the determination of the total flavour composition, the quantitative distribution and enantiomeric ratios of γ-lactones were of particular interest. The data obtained were taken as a basis in order to establish their usefulness for the differentiation between natural and non-natural flavours.

Strawberry

As summarized in Table I, most of the lactones are predominantly in the *R* configuration. Small amounts of γ-heptalactone occur as a racemate, and for γ-hexalactone the *S* enantiomer preponderates. A similar enantiomeric distribution was observed in a commercially available sparkling strawberry wine.

TABLE I

ENANTIOMERIC COMPOSITION AND QUANTITATIVE DISTRIBUTION OF γ-LACTONES IN FRESH STRAWBERRIES AND A COMMERCIALLY AVAILABLE SPARKLING STRAWBERRY WINE

γ-Lactone	Strawberries			Sparkling strawberry wine		
	R (%)	*S* (%)	ppb	*R* (%)	*S* (%(	ppb
Hexa-	36	64	150	46	54	40
Hepta-	55	45	10	55	45	1
Octa-	85	15	120	68	32	15
Nona-	88	12	30	73	27	15
Deca-	99	1	10150	98	2	190
Dodeca-	100	0	1850	97	3	30

Raspberry

In addition to the small amounts of γ-lactones determined in raspberries, it is noticeable that the main component γ-octalactone and the higher homologous lactones may occur as racemates (Table II). One of the processed raspberry samples showed an obvious excess of (*R*)-γ-deca- and -dodecalactone, which might be caused by contamination during processing or due to varietal differences.

TABLE II

ENANTIOMERIC COMPOSITION AND QUANTITATIVE DISTRIBUTION OF γ-LACTONES IN DEEP-FROZEN AND PROCESSED RASPBERRY SAMPLES.

γ-Lactone	Deep-frozen raspberry			Processed raspberries	
	R (%)	*S* (%)	ppb	*R* (%)	Share (%)[a]
Hexa-	34	66	30	26–38	100
Hepta-	25	75	1	26–30	0–5
Octa-	44	56	65	40–55	50–150
Nona-	28	72	3	32–53	10–20
Deca-	49	51	2	54–68	5–10
Undeca-	55	45	1	51–55	0–5
Dodeca-	50	50	5	51–84	5–20

[a] Relative to γ-hexalactone as 100%.

TABLE III

ENANTIOMERIC COMPOSITION AND QUANTITATIVE DISTRIBUTION OF γ-LACTONES IN PINEAPPLE AND PINEAPPLE CONCENTRATES

γ-Lactone	Pineapple (9)[a]		Pineapple (5)[a] concentrates	
	R (%)	ppb	*R* (%)	Share (%)[b]
Hexa-	55–75	90–280	36–46	100
Hepta-	60–73	0–5		0
Octa-	67–75	40–190	52–76	6–20
Nona-	61–77	0–5		0
Deca-	63–91	1–10	65–84	1–4
Dodeca-	82–100	0–5	88	0–1

[a] No. of samples in parentheses.
[b] Relative to γ-hexalactone as 100%.

Pineapple

In contrast to the distribution in raspberries, the higher γ-lactones in fresh pineapple fruits exhibit a predominance of the *R* enantiomer, whereas for the major γ-hexalactone nearly equal amounts of *R* and *S* enantiomers could be determined (Table III). The shift towards higher *S* enantiomer contents for γ-hexa- and -octalactone in concentrates is assumed to be caused by cleavage of pineapple-typical acetoxy esters, mainly with *S* configuration [18]. In contrast to fresh fruits, only traces of the acetoxy esters were found in the concentrates [8].

The quantitative dominance of γ-hexalactone in the concentrates may be attributed to the concentration process. More water-soluble, short-chain γ-lactones remain in the fruit pulp, whereas less water-soluble, long-chain γ-lactones are released into the condensate [19].

Passion fruit

A preferred *R* configuration of the higher C_{10}- and C_{12}-lactones is also observed in yellow and purple passion fruits (Table IV). In yellow passion fruits γ-hep-

TABLE IV

ENANTIOMERIC COMPOSITION AND QUANTITATIVE DISTRIBUTION OF γ-LACTONES IN RED AND YELLOW PASSION FRUITS AND PASSION FRUIT CONCENTRATES

γ-Lactone	Yellow (3)[a]		Red (1)[a]		Passion fruit (5)[a] concentrates	
	R (%)	Share (%)[b]	*R* (%)	Share (%)[b]	*R* (%)	Share (%)[b]
Hexa-	79–89	100	73	100	79–87	100
Hepta-	56–65	0–3	75	3		0
Octa-	55–78	33–66	72	23	69–82	3–12
Nona-	50–56	13–66	66	3	53	0–1
Deca-	87–93	39–127	93	102	84–94	14–36
Dodeca-	99–100	73–151	100	270	100	10–27

[a] No. of samples in parentheses.
[b] Relative to γ-hexalactone as 100%.

ta-, γ-octa- and especially γ-nonalactone can also occur as racemic mixtures [6]. No significant differences in enantiomeric distribution could be detected on comparing fresh fruits with concentrates. The significant increase in the relative amount of γ-hexalactone is in accordance with our findings for pineapple concentrates.

Coconut

Based on the assumption that autoxidation of fatty acids leads to the formation of racemic γ-lactones, the effect of heating coconut fat was investigated. Neither in fresh coconut flesh and milk nor in commercially available coconut flakes could any γ-lactones be detected. As expected, considerable amounts of racemic γ-lactones were formed on heating extracted coconut fat under a continous stream of oxygen (see Fig. 1). The predominant formation of γ-octalactone corresponds with the fact that octanoic acid was found to be the major fatty acid in the extracted fat. This is in agreement with the findings of Pai *et al.* [20], who observed the preponderant production of γ-dodecalactone in autoxidized coconut fat consisting mainly of dodecanoic acid.

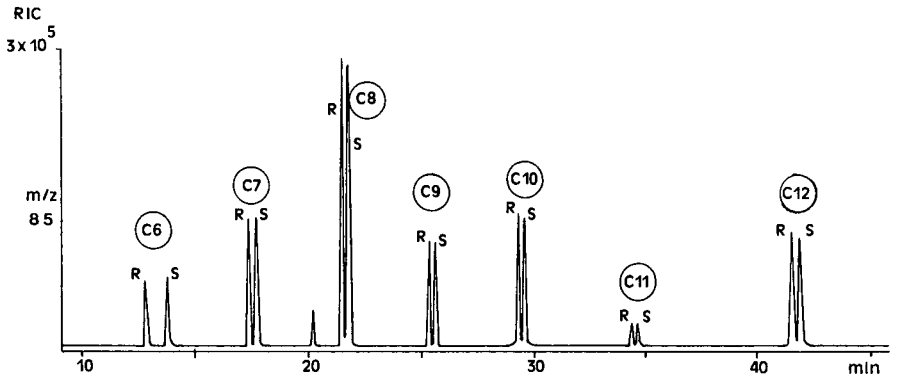

Fig. 1. Enantiomeric distribution of γ-lactones in heated coconut fat. Reconstructed ion chromatogram (*m/z* 85) of selected cuts from the precolumn on a Lipodex B column; see Experimental for details.

Plum

To evaluate the influence of fermentation processes on the lactone distribution, two plum wines fermented in different ways were investigated. As summarized in Table V, fermentation has no significant effect on the enantiomeric distribution, except for γ-nonalactone (Table V). As the content of the *R* enantiomer and the concentration of γ-nonalactone, relative to other γ-lactones, increased during fermentation, it is believed to be a fermentation product.

Similar results were achieved on investigating gooseberry wine and beer wort. The gooseberry concentrate exhibits only very small amounts of γ-decalactone (*R*:*S* = 78:22), which remain unchanged during fermentation. The fermented product additionally contains γ-nonalactone (*R*:*S* = 89:11).

In beer wort small amounts of racemic γ-hexa- and γ-nonalactone were identified. During fermentation γ-hexalactone remains racemic, whereas a twofold increase in the γ-nonalactone concentration, mainly with *R* configuration (γ-nonalactone in

TABLE V

ENANTIOMERIC COMPOSITION AND QUANTITATIVE DISTRIBUTION OF γ-LACTONES IN PLUMS AND TWO DIFFERENT PLUM WINES

γ-Lactone	Plum			Mash-fermented wine			Juice-fermented wine		
	R (%)	*S* (%)	ppb	*R* (%)	*S* (%)	ppb	*R* (%)	*S* (%)	ppb
Hexa-	88	12	100	86	14	10	89	11	8
Octa-	86	14	70	87	13	4	88	12	3
Nona-	70	30	20	84	16	4	81	19	4
Deca-	91	9	700	92	8	28	92	8	28
Dodeca-	100	0	1600	99	1	12	100	0	14

beer wort, *R*:*S* = 53:47; in beer, *R*:*S* = 74:26; see Fig. 2), indicates that (*R*)-nonalactone has to be regarded as a by-product of fermentation.

Vinous beverages (weinhaltige Getränke)

In Table VI the enantiomeric distribution of two beverages, containing wine and a mixture of fruit products (according to German legislation called "weinhaltige Getränke"), is shown. In both "vinous beverages" large amounts of (*R*)-γ-decalactone were found.

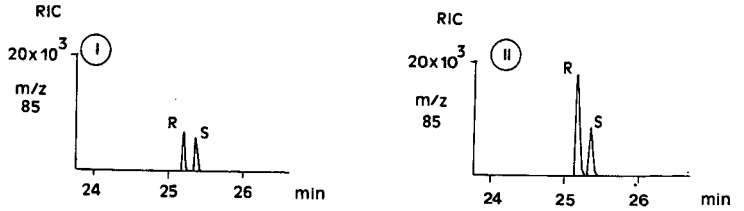

Fig. 2. Enantiomeric distribution of γ-nonalactone in (I) beer wort compared with (II) fermented beer. Reconstructed ion chromatograms (*m*/*z* 85) of selected cuts from the precolumn on a Lipodex B column; see Experimental for details.

TABLE VI

ENANTIOMERIC COMPOSITION AND QUANTITATIVE DISTRIBUTION OF γ-LACTONES IN TWO VINOUS BEVERAGES

γ-Lactone	Beverage I[a]			Beverage II[a]		
	R (%)	*S* (%)	ppb	*R* (%)	*S* (%)	ppb
Hexa-	70	30	10	40	60	15
Octa-			0	70	30	<5
Nona-	70	30	<5	70	30	5
Deca-	100	0	3300	98	2	2800

[a] I, with peach flavour; II, "piña colada".

TABLE VII

$^{13}C/^{12}C$ STABLE ISOTOPE RATIOS OF γ-DECALACTONES OF DIFFERENT ORIGIN

γ-Decalactone sample	$\delta^{13}C$ value (by MDGC–IRMS)		$\delta^{13}C$ value (conventional)		$\delta^{13}C$ ranges (literature data)	
	‰ (PDB)	n^a	‰ (PDB)	n^a	‰ (PDB)	Ref.
Synthetic	−28.7[b] ± 0.2	5	−28.7 ± 0.2	3	−24.4 to −28.3	7,21
Microbial	−30.3 ± 0.5	3	−30.2 ± 0.2	3	−30.1 to −31.2	7,21
Beverage I[c]	−30.2 ± 0.3	3				
Beverage II[c]	−30.3 ± 0.2	3				
Peach					−38.5 to −40.9	21
Strawberry					−26.0 to −30.5	16,21

[a] n = Number of samples.
[b] $\delta^{13}C$ values of *R* and *S* enantiomers are within the range of system specification (±0.3‰) and therefore not distinguishable.
[c] Vinous beverages: I, with peach flavour; II, "piña colada".

$^{13}C/^{12}C$ isotope ratio measurements

Owing to quantitative irregularities in the γ-decalactone content of the above-mentioned vinous beverages, their $\delta^{13}C$ values were determined and compared with data corresponding to γ-decalactone of synthetic and microbial origin (Table VII).

DISCUSSION

A direct chirospecific analysis of γ-lactones on chiral stationary phases is not recommended when dealing with complex flavour extracts, as co-eluting sunstances may interfere with the resolved enantiomers. Additionally, column overloading due to the main components in the sample can affect the column performance. These disadvantages can be avoided by MDGC, as the possibility of heart-cutting allows the selective transfer of the peak group of interest, after preseparation from other interfering constituents of the complex mixture. This is of special importance in the case of isotopic ratio determinations. Despite the high resolving power of MDGC, its application to IRMS measurements requires very careful adjustment of the cut parameters. Because of different elution rates of isotopic compounds (^{13}C compounds precede their ^{12}C counterparts by 10–100 ms), each peak must be integrated over its entire width to obtain the true isotopic ratio [16]. Therefore, partial heart-cutting of a component of interest has to be avoided. Overloading effects, especially with high injection volumes for the determination of trace amounts of lactones, are minimized if a precolumn with high capacity (*e.g.*, wide-bore columns with a 1–2-μm film thickness) is used. MS monitoring allows the control of the heart-cutting and separation efficiency and selective ion monitoring is capable of greater sensitivity for the determination of traces of lactones in enantiomeric ratio determination.

The potential of both methods for the determination of the naturalness of flavours is of particular interest. The legislation that regulates flavouring compounds is not uniform and has led to a differentiation between "natural", "artificial" and in some countries "nature-identical" substances [22].

Generally, the determination of qualitative and quantitative irregularities in the composition of main constituents can be used to detect adulterations due to the addition of single nature-identical and/or artificial flavouring substances. Frequently the determination of the "category" to which an aroma component belongs is difficult, especially if sensorial active traces have been used [22]. If chiral flavour-contributing compounds are detectable, the determination of the enantiomeric distribution is assumed to be an appropriate method to prove the authenticity of samples, as it is expected [4] that fruit-specific distributions with predominances of molecules with *R* or *S* configuration occur.

Our results clearly demonstrate that this assumption has no general validity, and therefore additional information apart from the enantiomeric distribution is necessary. Single-fruit products, *e.g.*, fruit wines, where German legislation does not allow any flavouring additives, are at first glance the easiest to asses. Chirality evaluation is thought to give valuable information with regard to the origin if, in addition to the typical distribution of volatiles due to fermentation, which should be known, the qualitative and quantitative composition shows no irregularities in comparison with data from fresh fruits. Whereas this holds for the strawberry wine analysed, which exhibits typical enantiomeric excesses for the higher γ-lactones (see Table I), it cannot be applied to raspberries, where apart from γ-hexa- and γ-heptalactone, racemic forms are observed (Table II). Similar findings for pineapple concentrates (Table III), yellow passion fruits (Table IV), coconut fat (Fig. 1) and mango [5,23] demonstrate that the presence of racemates cannot *a priori* be interpreted as evidence for adulteration. In such instances, in addition to the typical enantiomeric distribution in fresh fruits, shifts due to processing such as fermentation (Table V), hydrolytic cleavage of precursors and autoxidation of fats have to be considered.

According to the aforementioned considerations it might be stated that for strawberry wine no additives have been used, as data on the enantiomeric ratios and quantitative distribution (taking into account the dilution factor) in fresh fruits and wine are comparable (Table I). However, the dominant (*R*)-γ-decalactone could also be an additive of microbial origin. In this special case, the additional determination of the $\delta^{13}C$ isotopic abundance of γ-decalactone does not definitely enhance the capability to determine the authenticity of the sample. The scarce data available in the literature show that overlapping ranges of $\delta^{13}C$ values can be found for γ-decalactone from strawberries, of synthetic and microbial origin (see Table VII). More definite information for a reliable validation might be obtained if, instead of comparing single isolated $\delta^{13}C$ values, a related set of values in the form of a "fingerprint" is taken into consideration. However, up to now such information is not available. In combination with $\delta^{2}H$ values more possibilities for differentiation could be achieved [24].

A different situation was experienced with the peach-flavoured "vinous beverage" (see Table VI), containing large amounts of nearly exclusively (*R*)-γ-decalactone. Whereas the determination of the enantiomeric distribution gave no evidence for the use of a non-natural lactone, the $\delta^{13}C$ value seems to serve as a useful indicator for the determination of origin. According to literature data [7], γ-decalactone from peach has a $\delta^{13}C$ value of about $-40‰$. Instead, a value of $-30‰$ was found (Table VII), which so far on the basis of available data has to be considered as atypical for peach. A microbial origin of this γ-decalactone can be assumed. The large amount of nearly exclusively γ-decalactone supports this finding.

The importance of a comprehensive knowledge of the quantitative and enantiomeric composition of the ingredients of a mixed-fruit product can be illustrated with the results obtained for "piña colada", a vinous beverage labelled as a mixture of wine, pineapple juice and coconut flavour. The data for γ-hexa-, γ-octa- and γ-nonalactone can be attributed to pineapple and wine (see Table III and V), respectively, whereas the large amount of (*R*)-γ-decalactone does not correspond with the raw materials processed. Measurement of the carbon isotopic ratio revealed that this lactone ($\delta^{13}C$ value −30‰, see Table VII) might be of biotechnological origin.

These results are important, as German legislation does not allow the addition of "isolated flavour compounds" [10] or those isolated from natural sources (including microbial origin) to vinous beverages ("weinhaltige Getränke").

CONCLUSIONS

The exclusive use of the enantiomeric distribution of γ-lactones (occurrence of racemates or predominant *R* enantiomers) generally is not suitable for drawing conclusions about the authenticity or adulteration of samples.

Variations in the enantiomeric ratio due to varietal differences and technological influences, and also the quantitative lactone distribution, have to be considered as additional parameters in order to be able to make realiable statements.

Validation of naturalness based solely on isolated $^{13}C/^{12}C$ isotope ratio measurements of γ-lactones is not always reliable, as overlapping ranges of $\delta^{13}C$ values are encountered. The inclusion of additional $\delta^{13}C$ values for fruit typical components in form of "fingerprints" is recommended.

Comprehensive data on carbon isotope ratios of flavour compounds together with the consideration of possible variations due to external influences should be elaborated in order to permit a more definite evaluation of genuiness.

ACKNOWLEDGEMENTS

We thank Silesia G. Hanke for providing the GC–IRMS system, Mr. K. Kempe and A. Rossmann (Institut für Chemie, Weihenstephan, Germany) for measuring $\delta^{13}C$ values in the conventional way, Mrs. S. Kilb, R. Meier zu Farwig and A. Keller for technical assistance, Macherey, Nagel & Co. for kindly supplying a Lipodex B column and the Fonds der Chemischen Industrie for financial support.

REFERENCES

1 W. A. König, S. Lutz, C. Colberg, N. Schmidt, G. Wenz, E. von der Bey, A. Mosandl, C. Günther and A. Kustermann, *J. High Resolut. Chromatogr. Chromatogr. Commun.*, 11 (1988) 621.
2 D. W. Armstrong, C.-D. Chang and W. Y. Li, *J. Argic. Food Chem.*, 38 (1990) 1674.
3 S. Nitz, H. Kollmannsberger and F. Drawert, *Chem. Mikrobiol. Technol. Lebensm.*, 12 (1989) 75.
4 A. Mosandl, U. Hener, U. Hagenauer-Hener and A. Kustermann, *J. Agric. Food Chem.*, 38 (1990) 767.
5 A. Bernreuther, N. Christoph and P. Schreier, *J. Chromatogr.*, 481 (1989) 363.
6 S. Nitz, H. Kollmannsberger and F. Drawert, *Chem. Mikrobiol. Technol. Lebensm.*, 12 (1989) 105.
7 A. Bernreuther, J. Koziet, P. Brunerie, G. Krammer, N. Christoph and P. Schreier, *Z. Lebensm.-Unters.-Forsch.*, 191 (1990) 299.
8 H. Kollmannsberger, S. Nitz and F. Drawert, *Chem. Mikrobiol. Technol. Lebensm.*, 13 (1991) 58.
9 E. Guichard, A. Kustermann and A. Mosandl, *J. Chromatogr.*, 498 (1990) 396.

10 K. Hildenbrand, N. Christoph and A. Bernreuther, *Dtsch. Lebensm.-Rundsch.*, 86 (1990) 39.
11 F. J. Winkler and H.-L. Schmidt, *Z. Lebensm.-Unters.-Forsch.*, 171 (1980) 85.
12 J. Bricout, in H.-L. Schmidt, H. Förstel and K. Heinzinger (Editors), *Stable Isotopes, Proceedings of the 4th International Conference, Jülich, March 23–26, 1981*, Elsevier, Amsterdam, 1982, p. 483.
13 M. Butzenlechner, A. Rossmann and H.-L. Schmidt, *J. Agric. Food Chem.*, 37 (1989) 410.
14 R. A. Culp and J. E. Noakes, *J. Agric. Food Chem.*, 38 (1990) 1249.
15 P. A. Fredman, E. C. P. Gillyon and E. J. Jumeau, *Am. Lab.*, (1988).
16 W. A. Brand, M. Ricci and K. Habfast, *Finnigan MAT Delta S/GC Application Data Sheet No. 1*, Finnigan MAT, San Jose, CA, 1988.
17 S. Nitz, B. Weinreich and F. Drawert, *J. High Resolut. Chromatogr. Chromatogr. Commun.*, submitted for publication.
18 K.-H. Engel, J. Heidlas, W. Albrecht and R. Tressl, in R. Teranishi, R. G. Buttery and F. Shahidi (Editors), *Flavor Chemistry (ACS Symposium Series*, No. 388), American Chemical Society, Washington, DC, 1989, p. 8.
19 H. Kollmannsberger and S. Nitz, unpublished results.
20 J. S. Pai, S. S. Lomanno and W. W. Nawar, *J. Am. Oil Chem. Soc.*, 56 (1979) 494.
21 A. Mosandl, U. Hener, H.-G. Schmarr and M. Rautenschlein, *J. High Resolut. Chromatogr.*, 13 (1990) 528.
22 R. Tressl, K.-H. Engel and W. Albrecht, in S. Nagy, J. A. Attaway and M. E. Rhodes (Editors), *Adulteration of Fruit Juice Beverages*, Marcel Dekker, New York, 1988, p. 67.
23 R. Tressel and W. Albrecht, in T. H. Parliment and R. Croteau (Editors), *Biogeneration of Aromas (ACS Symposium Series*, No. 317), American Chemical Society, Washington, DC, 1986, p. 114.
24 H.-L. Schmidt, *Fresenius' Z. Anal. Chem.*, 324 (1986) 760.

Journal of Chromatography, 557 (1991) 199–213
Elsevier Science Publishers B.V., Amsterdam

CHROM. 23 251

Coupled column chromatography in chiral separations: systems employing β-cyclodextrin phases for chiral separation

ANDREAS M. RIZZI* and CHRISTINA PLANK
Institute of Analytical Chemistry, University of Vienna, Währingerstrasse 38, A-1090 Vienna (Austria)

ABSTRACT

Two-dimensional chromatographic systems were evaluated which combine a β-cyclodextrin (β-CD)-containing column for the optical resolution of enantiomers with a non-chiral column for the preseparation of these enantiomers from other solutes or impurities. β-CD is used either as a chemically bonded stationary phase or as a mobile phase additive. This multi-column system allows the accurate determination of the enantiomeric composition even in complex samples and improves the significance and reliability of the results. The system was evaluated with respect to peak dilation caused by the carry-over, the maximum carry-over volume up to which severe adverse effects on the resolution can be avoided, and the implications with regard to sensitivity.

INTRODUCTION

The use of coupled columns in high-performance liquid chromatography (HPLC) has attracted strong interest since its introduction more than 15 years ago [1]. This development was facilitated by the technical progress with HPLC apparatus and stimulated by the high demands required for analytical methods in biological analysis. The more complex the samples became, the more the advantages of coupled column chromatography (CCC) with column switching became important.

In recent years, coupled column chromatography has been introduced also in chiral separations [2–10]. The well known features of CCC with respect to matrix separation and its unique power for dramatically enhancing the peak capacity become especially important and decisive in the context of chiral separation problems: first, because any chiral separation increases the number of peaks to be resolved additionally; second, because several chiral recognition principles suffer from strong peak dispersion and thus from low peak capacity; and third, because the determination of the enantiomeric excess often has to be performed at a high level of accuracy although the analyte concentration is at the trace level, and as many samples become complex at very low concentration levels. In these respects the enhancement of peak capacity is often required, because the peak capacity determines the degree of

0021-9673/91/$03.50

significance and reliability with which the presence of other compounds can be excluded.

On the other hand, significant simplifications can be adopted under certain conditions: for the determination of the enantiomeric excess the quantification of the enantiomeric peaks relative to each other is sufficient, and for this purpose one needs to transfer only parts of the peak of unresolved enantiomers, if no chiral preseparation has occurred in the first column [3].

Chiral systems operated with aqueous mobile phases are of great interest in CCC as they are most appropriate for samples of biological origin. It is no surprise, therefore, that chiral separation techniques using aqueous mobile phases were first introduced in CCC: chiral ligand-exchange systems [2], immobilized protein columns [4–6], and immobilized cyclodextrin columns [3,8]. Even the swollen microcrystalline cellulose triacetate system, which is usually operated at high concentrations of alcohols in the mobile phase, can readily be combined with reversed-phase columns [10].

The consecutive order in which the columns are combined can be varied (non-chiral–chiral or chiral–non-chiral), and one can find good arguments for both types. Obviously, the decision as to which combination is to be preferred depends on the problem to be solved and on the main constraints. Such constraints may be low analyte concentrations, low sample amounts, complex sample matrices or a high degree of optical purity to be monitored.

This paper examines the possibilities and limitations of column switching in a coupled system of a non-chiral alkylsilica column and a subsequent chiral column involving β-cyclodextrin (β-CD) phases either as a bonded chiral stationary phase (CSP) or as a chiral mobile phase. The criteria are compatibility of the mobile phases with respect to deconditioning of the second column, degree of peak compression or dilation obtained and the potential loss (or gain) in sensitivity. Perspectives with respect to sensitivity are also given for the reverse column order.

EXPERIMENTAL

Instrumentation

Chromatographic experiments were carried out with two high-pressure liquid chromatographic pumps [(1) Model L-6200 intelligent pump (Merck–Hitachi, Tokyo, Japan) and (2) Solvent Module 116, System Gold (Beckman, San Ramon, CA, USA)], a syringe-valve injector (Model 7161; Rheodyne, Cotati, CA, USA) equipped with a 20-μl loop, two switching valves (Model 7030; Rheodyne), and a UV detector (Model L-4000; Merck–Hitachi) connected to an integrator (Model D-2000 chromato-integrator; Merck–Hitachi).

Columns

The following columns were used:

(1) Non-chiral columns for non-chiral separations or for chiral separations by use of β-CD as chiral mobile phase additive (CMA): prepacked stainless-steel columns (250 mm × 4.0 mm I.D.) filled with chemically bonded octylsilica (OS) or octadecyl-silica (ODS) material, particle diameter 5 μm. (LiChrosorb RP-8 or RP-18; Merck, Darmstadt, Germany).

(2) Chiral column: prepacked column (250 mm × 4.0 mm I.D.) filled with Cyclobond I (chemically bonded β-CD) (Astec, USA), mean particle diameter 5 μm.

Reagents and samples

Organic solvents (LiChrosolv grade) were obtained from Merck. Water was distilled twice from a quartz apparatus and additionally purified using an Elgastat UHQ apparatus (Elga, High Wycombe Bucks., UK). Cyclodextrin was purchased from Merck. Alcohol–water mixtures were partially premixed and degassed in an ultrasonic bath. All eluent mixtures were filtered before use through a nylon 66 membrane filter with 0.45-μm pore diameter (Supelco, Bellefonte, PA, USA).

Standard solutions of the racemic test analytes were used for the evaluation of the peak compression effect. Solutions of less pure standard analytes were employed for demonstrating the separation power of the column-switching set-up.

Chromatographic procedure

A schematic diagram of the instrumental set-up is given in Fig. 1. A general chromatographic elution and column switching protocol is described in Table I for the CCC system with an alkylsilica column and a subsequent β-CD-containing phase

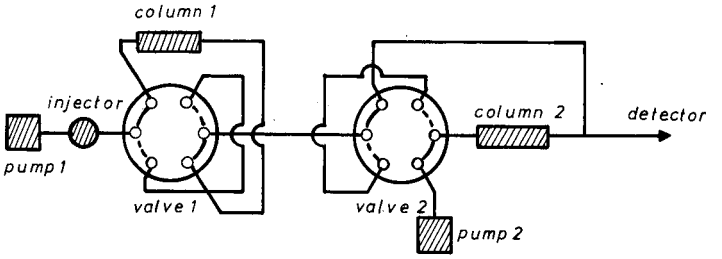

Fig. 1. Schematic diagram of the CCC system. Column 1 = alkylsilica (OS or ODS); column 2 = β-CD-CSP or a second alkylsilica column. Valves: rotor position A = solid lines; rotor position B = broken lines.

TABLE I

GENERAL ELUTION AND COLUMN-SWITCHING PROTOCOL

t_1 = Start of analyte transfer; t_2 = end of transfer; t_3 = end of the chromatogram at the RP column, change of eluent by changing the pump in operation; t_3–t_4 = elution of the chiral column. Rotor positions, A and B, of the switching valves refer to Fig. 1 (position A, solid lines; position B, broken lines). Column abbreviations: RP = reversed-phase (alkylsilica) column; β-CD = column with phase systems containing β-CD either as CSP or as CMA. Eluent 1 = eluent used for column 1 [*e.g.*, aqueous buffer with 40% (v/v) of methanol]; eluent 2 = eluent optimized for the separation at column 2 [*e.g.*, aqueous buffer with 20% (v/v) of methanol].

Time interval	Rotor position of valve		Columns in operation	Eluent	Comment
	1	2			
0–t_1	A	A	RP	1	Preseparation of the sample
t_1–t_2	A	B	RP + β-CD	1	Transfer of the racemic analyte
t_2–t_3	A	A	RP	1	Finishing of RP elution
t_3					Stopping of pump 1, starting of pump 2
t_3–t_4	A	A	β-CD	2	Chiral separation

system. Eluent 1 is delivered by pump 1 and eluent 2 by pump 2. By employing a second pump *ca.* 12–15 min (at a flow-rate of 0.5 ml/min) can be saved in one analysis cycle by avoiding repeated changing of the eluents. In principle, the same chromatograms can be obtained by using a single pump only and a capillary bypass according to the set-up described previously [10].

Ambient temperature was used for both columns, with UV detection at 254 nm. Flow-rates were 0.5 ml/min if not indicated otherwise.

RESULTS AND DISCUSSION

Retention characteristics in CCC systems as source of peak compression and dilation

Plots of logarithm of capacity factor (log k') *versus* alcohol concentration in the mobile phase are given in Figs. 2–4 for various analytes and different phase systems. The data in Fig. 2 were obtained with a simple octadecylsilica phase, those in Fig. 3 with the β-CD CSP and those in Fig. 4 with a system containing β-CD as CMA.

These data allow an approximate estimation of the main working range with respect to mobile phase composition (see broken lines). For the alkylsilica phase (column 1), this working range is determined mainly by the capacity factors of the analytes and lies between 30 and 60% (v/v) methanol (see Fig. 2) [corresponding to about 15–35% (v/v) ethanol]. The working range for the β-CD containing phases is mainly determined by the influence of the alcohol concentration on the enantioselectivity coefficients and lies near 20% (maximum 30%) (v/v) methanol for the CSP and near 20% (v/v) ethanol for the CMA system.

Assuming that the mobile phase composition employed is actually within these ranges, the capacity factor data given in the Figs. 2–4 allow an approximate estimation

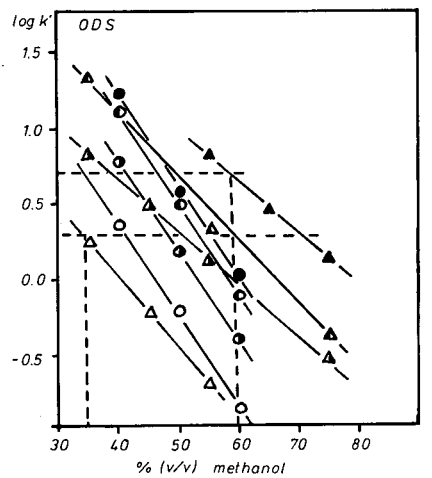

Fig. 2. Capacity factor, k', as a function of the alcohol concentration in the mobile phase for the ODS column. Mobile phase, aqueous buffer (10 m*M* ammonium acetate, pH 7) with varying content of methanol; temperature, 30°C. The horizontal broken lines indicate k' values of 3 and 5, respectively, and the vertical broken lines confine the working range with respect to the alcohol concentration in the mobile phase. △ = Chlorthalidone; ◭ = hexobarbital; ◮ = oxazepam; ▲ = nomifensin; ○ = Dns-Thr; ◑ = Dns-Val; ◐ = Dns-Leu; ● = Dns-Phe.

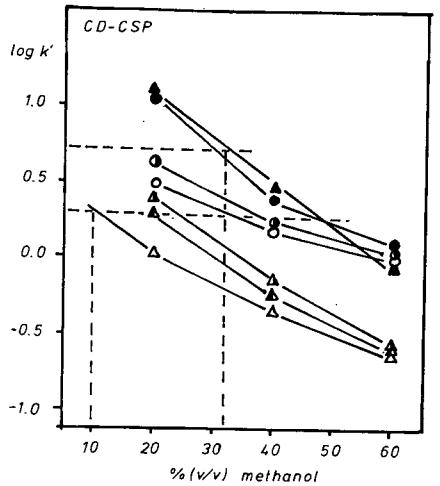

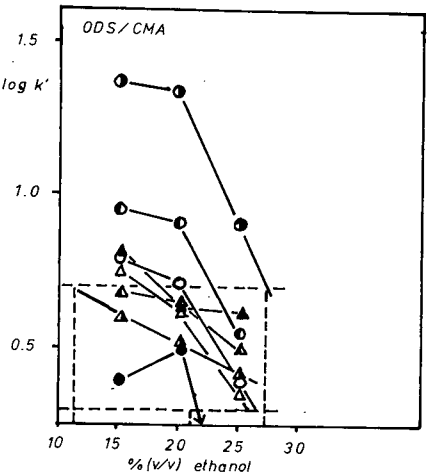

Fig. 3. Capacity factor, k', as a function of the alcohol concentration in the mobile phase for the β-CD-CSP column. Mobile phase, aqueous buffer (10 m*M* ammonium acetate, pH 7) with varying content of methanol; temperature, 30°C. Symbols as in Fig. 2.

Fig. 4. Capacity factor, k', as a function of the alcohol concentration in the mobile phase for the chiral phase system OS/β-CD-CMA. Mobile phase, aqueous buffer (25 m*M* ammonium acetate, pH 5.5–35 m*M* β-CD–1 *M* urea) with varying content of ethanol; temperature, 30°C. Symbols as in Fig. 2, except ◭ = ethylphenylhydantoin; ◐ = Dns-Ala; ● = Dns-Glu.

of the peak compression or peak dilation effects introduced by large carry-over volumes at the top of the second column. The thermodynamic peak compression effect for an analyte *i* caused by a step gradient is approximately calculated by the following equation [11–13]

$$pcf_i^{th} = \sigma_{v_i}(\text{before compr.})/\sigma_{v_i}(\text{after compr.}) = k'^{col.2}_{i_{co}}/k'^{col.2}_{i_{el.2}} \quad (1)$$

where pcf^{th} denotes the peak compression factor at the top of column 2, σ_v is the standard deviation of the peaks in volume units and the subscripts "co" and "el.2" denote the carry-over and the eluent employed for column 2, respectively.

Table II shows peak compression ($pcf > 1$) or dilation ($pcf < 1$) factors for various column combinations calculated according to eqn. 1. The given alcohol concentrations correspond to the actual working range. It is obvious from the $pcf < 1$ values that the column order alkylsilica–(β-CD-CSP) column is not very favourable from this point of view. The use of β-CD as CMA is superior in this respect, as the addition of β-CD to the mobile phase increases the solvation power of eluent 2, as indicated in Fig. 5. Peak compression factors near 1 or > 1 can thus be obtained in the optimum working range. The opposite situation is obtained with the reverse column order.

At least three observable effects are associated with deconditioning of the second column by the transfer of a carry-over with greater elution strength: peak broadening, distorsion of the peak shape (*cf.*, the computer simulation in ref. 14) and changes in (enantio)selectivity.

The degree of peak dilation given in Table II is found to be dependent on the

TABLE II

THEORETICAL PEAK COMPRESSION FACTORS, pcf^{th}, CALCULATED ACCORDING TO EQN. 1 FOR DIFFERENT COMPOSITIONS OF THE CARRY-OVER (ELUENT 1) AND ELUENT 2

Column sequence	Column I, ODS; column II, β-CD-CSP[a]					
Non-chiral–chiral	Analyte	Methanol in eluent 1 (%, v/v)[b]	pcf^{th}			
			Methanol in eluent 2 (%, v/v)[c]			
			10	20	30	40
	Dns-threonine	30		0.69[d]	1.00[d]	1.47
		40		0.47	0.68	1.00
	Hexobarbital	40		0.28[d]	0.49	
		50		0.18[d]	0.30	
		60		0.11	0.19	
	Chlorthalidone	20	0.55	1.00		
		30	0.36	0.66[d]		
		40	0.21	0.38		
	Column I, OS; column II, OS/β-CD-CMA[a]					
	Analyte	Ethanol in eluent 1 (%, v/v)[e]	pcf^{th}			
			Ethanol in eluent 2 (%, v/v)[f]			
			15	20	25	
	Dns-threonine	20	1.59	2.37[d]	4.09	
		25	0.62	0.93[d]	1.60	
		30	0.28	0.42	0.73	
	Hexobarbital	30	1.55	1.84[d]	2.31	
		40	0.53	0.63	0.79	
	Chlorthalidone	20	1.28	1.70[d]	3.28	
		25	0.48	0.64	1.23	
		30	0.20	0.27	0.53	
	Column I, β-CD-CSP; column II, ODS[a]					
Chiral–non-chiral	Analyte	Methanol in eluent 1 (%, v/v)[c]	pcf^{th}			
			Methanol in eluent 2 (%, v/v)[b]			
			20	30	40	50	60
	Dns-threonine	20		3.9	15.9	57.3	
		30		1.0	4.1	14.8	
		40		0.3	1.0	3.6	
	Hexobarbital	20			4.4	10.0	23.6
		30			2.0	4.6	10.8
	Chlorthalidone	10	3.0	8.5	25.3		
		20	1.0	2.8	8.4		

TABLE II (*continued*)

Column I, OS/β-CD-CMA; column II, OS[a]					
Analyte	Ethanol in eluent 1 (%, v/v)[f]	*pcf*[th]			
		Ethanol in eluent 2 (%, v/v)[e]			
		20	25	30	40
Dns-threonine	15	0.6	1.6	3.5	
	20	0.4	1.1	2.4	
	25	0.2	0.6	1.4	
Hexobarbital	15			0.6	1.9
	20			0.5	1.6
	25			0.4	1.3
Chlorthalidone	15	0.8	2.1	4.9	
	20	0.6	1.6	3.7	
	25	0.3	0.8	1.9	

[a] Column symbols: OS = octylsilica; ODS = octadecylsilica; β-CD-CSP = chiral stationary phase using immobilized β-cyclodextrin; OS/β-CD-CMA = octylsilica stationary phase, β-cyclodextrin employed as chiral mobile phase additive.

[b] Eluent composition: aqueous buffer solution (10 m*M* ammonium acetate, pH 7)–methanol; content of methanol as indicated.

[c] Eluent composition: aqueous buffer solution (10 m*M* ammonium acetate, pH 7)–methanol; content of methanol as indicated.

[d] Indicates the data obtained in the preferred working range of the eluents with respect to the alcohol concentration (working ranges are illustrated in Figs. 2–4).

[e] Eluent composition: aqueous buffer solution (25 m*M* ammonium acetate, pH 5.5)–ethanol; content of ethanol as indicated.

[f] Eluent composition: aqueous buffer solution (25 m*M* ammonium acetate, pH 5.5–35 m*M* β-CD–1 *M* urea)–ethanol; content of ethanol as indicated.

chemical structure of the analyte. The *pcf* values for hexobarbital are smaller than those for chlorthalidone and Dns-threonine in the optimum working range. The situation is changed when employing β-CD as CMA. In this instance peak dilation is smallest for hexobarbital.

The observable degree of peak broadening and distortion depends on the volume of the carry-over. Experimental data illustrating the influence of the carry-over volume on the σ_v values at the end of column 2 and the stereoselectivity data in this column are given in Table III. It can be seen that the enantioselectivity coefficient, α, is unaffected by the carry-over in all instances. The decrease in resolution observed in the chromatograms is always due to peak dilation (with CSP) or the absence of significant peak compression (with CMA). The effect of the carry-over volume on peak width and resolution is illustrated by the chromatograms in Fig. 6 for the β-CD-CSP and in Fig. 7 for the β-CD-CMA system.

The data in Table III allow the approximate evaluation of a critical carry-over volume, below which no significant adverse influence on the resolution is observed. For the β-CD-CSP system and the analytes hexobarbital and chlorthalidone this critical limit in the carry-over volume is near 50 μl and for Dns-threonine near 100 μl.

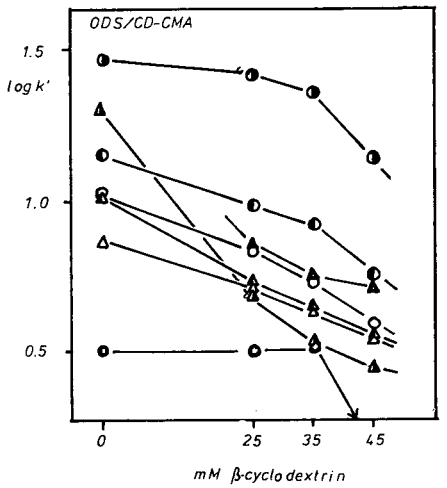

Fig. 5. Capacity factor, k', as a function of the concentration of β-CD in the mobile phase. Column, ODS; mobile phase, aqueous buffer (25 mM ammonium acetate, pH 5.5)–20% (v/v) ethanol, varying content of β-CD and urea (25 mM β-CD, no urea; 35 mM β-CD–1.0 M urea; 45 mM β-CD–1.7 M urea, respectively); temperature, 30°C. Symbols as in Fig. 4.

Above these values of the carry-over volume the apparent plate height values, H^{app}, increase dramatically. The critical carry-over volume is seen to depend on two parameters: first, the difference in the elution power of eluents 1 and 2, and second, the structure of the analytes. This influence is not yet well understood. Probably differences in the orientation of analytes during the inclusion in the β-CD ring play a major role.

For the β-CD-CMA system similar limits for the carry-over volume are obtained (50 μl for chlorthalidone and Dns-threonine and about 100 μl for hexobarbital). Hexobarbital, most strongly affected by high carry-over volumes with β-CD-CSPs, is the least affected in the β-CD-CMA system, which is the opposite of the situation with Dns-threonine.

Sensitivity obtainable with the column order non-chiral alkylsilica–chiral β-CD system

The sensitivities achievable by a particular column configuration can become a main factor in the selection of the consecutive order of columns. Three factors affect the obtainable sensitivity: (i) the percentage of analyte mass transferred between the columns, (ii) the degree of peak compression or dilation during transfer and (iii) the dispersion characteristics of the last column. These criteria will be referred to in evaluating the potential of different column configurations.

In the mentioned consecutive column order, peak dilation and distortion are often obtained as discussed before in detail. These adverse effects on the peak profile can be avoided by reducing the carry-over volume, if a consequent decrease in sensitivity can be accepted.

First, we consider this decrease in sensitivity by restricting the carry-over volume. To assess an approximate value for this loss, we assume a plate number of 9000 for the first column (alkylsilica, 250 mm × 4 mm I.D.) and a typical k' value of 4.

TABLE III

VOLUME STANDARD DEVIATION, σ_v, AT THE END OF COLUMN II, THE CORRESPONDING APPARENT THEORETICAL PLATE HEIGHT, H^{app}, AND THE ENANTIOSELECTIVITY COEFFICIENTS, α, AS A FUNCTION OF THE CARRY-OVER VOLUME

Column I, OS; column II, β-CD-CSP[a]

Analyte	Methanol in eluent (%, v/v)		Carry-over volume (μl)	σ_v (μl)	H^{app}[c]	α
	1[b]	2[b]				
Hexobarbital	40	20	50[d]	95	26	1.12
			100	125	(50)	1.12
Chlorthalidone	20	20	20	60	30	1.17
			40	65	34	1.17
	30	20	40	70	40	1.17
			100[d]	77	43	1.17
			200	127	(118)	1.17
	40	20	50[d]	80	44	1.18
			100	147	(150)	1.18
Dns-threonine	40	20	50	150	26	1.06
			100[d]	160	27	1.06

Column I, OS; column II, OS/β-CD-CMA[a]

Analyte	Methanol in eluent (%, v/v)		Carry-over volume (μl)	σ_v (μl)	H^{app}[c]	α
	1[e]	2[f]				
Hexobarbital	40	20	20	78	27	1.12
			50	60	29	1.12
			100[d]	70	(39)	1.12
			200	120	(90)	1.12
Chlorthalidone	30	20	20	75	30	1.21
			50[d]	80	35	1.21
			100	120	(66)	1.20
			200	220		1.21
Dns-threonine	30	20	20	95	29	1.19
			50	90	34	1.19
			100[d]	110	(62)	1.18
			200	170		1.19

[a] Column symbols as in Table II.

[b] Aqueous buffer solutions (10 m*M* ammonium acetate, pH 5.5)–methanol; content of methanol as indicated.

[c] Parentheses indicate H^{app} values strongly affected by the carry-over volume.

[d] Indicates values near the critical carry-over limit, above which the peak profile or resolution is significantly affected.

[e] Aqueous buffer solutions (25 m*M* ammonium acetate, pH 5.5)–ethanol; content of ethanol as indicated.

[f] Aqueous buffer solution (25 m*M* ammonium acetate, pH 5.5–35 m*M* β-CD–1 *M* urea)–ethanol; content of ethanol as indicated.

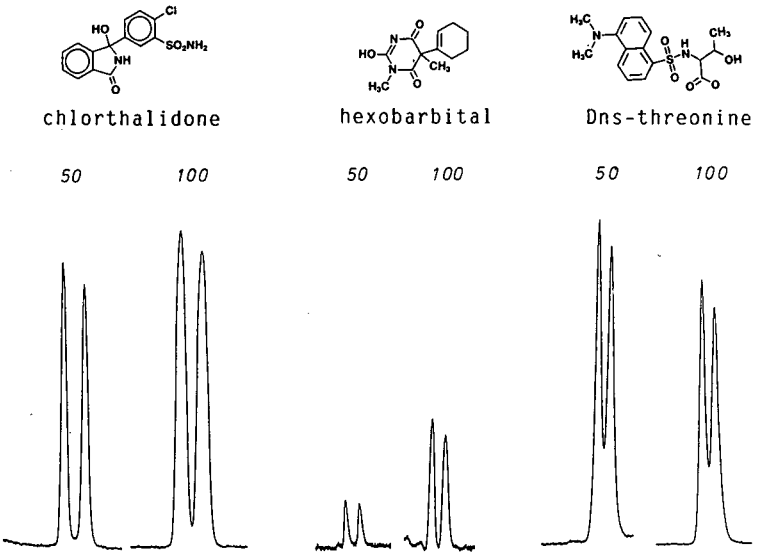

Fig. 6. Effect of the carry-over volume on the enantiomeric separations of the racemic analytes chlorthalidone, hexobarbital and Dns-threonine. CCC system: column 1, octylsilica; column 2, β-CD-CSP. Each pair of peaks represents the two separated enantiomers of the analytes indicated above. The peak pairs are small sections of the total chromatograms. Carry-over volumes: 50 or 100 μl as indicated. Mobile phases: aqueous buffer (0.1 *M* ammonium acetate, pH 5.5)–methanol (60:40, v/v) in eluent 1 and (80:20, v/v) in eluent 2.

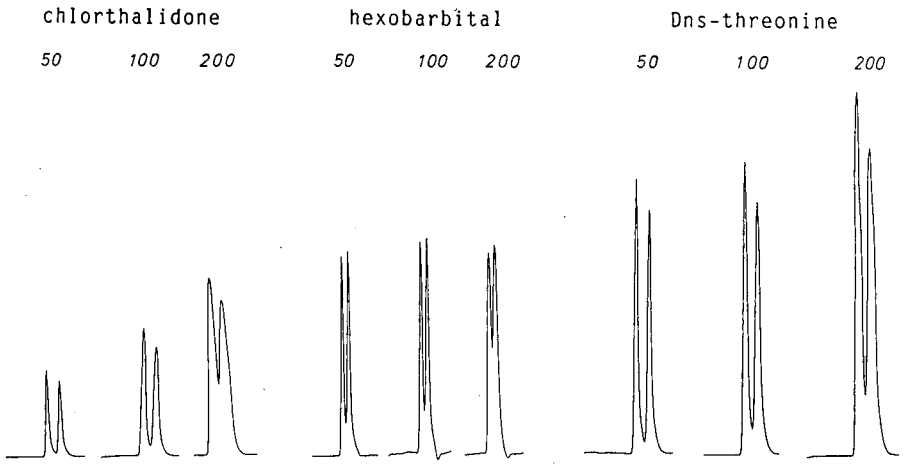

Fig. 7. Effect of the carry-over volume on the enantiomeric separations of the racemic analytes chlorthalidone, hexobarbital and Dns-threonine. CCC system: column 1, octadecylsilica; column 2, octylsilica with β-CD employed as chiral mobile phase additive. Each pair of peaks represents the two separated enantiomers of the analytes indicated above. The peak pairs are small sections of the total chromatograms. Carry-over volumes: 50, 100 or 200 μl as indicated. Eluent 1: aqueous buffer (0.1 *M* ammonium acetate, pH 5.5)–ethanol (60:40, v/v) for hexobarbital and Dns-threonine, (70:30, v/v) for chlorthalidone. Eluent 2: aqueous buffer (25 m*M* ammonium acetate, pH 5.5–35 m*M* β-CD–1 *M* urea)–ethanol (80:20, v/v).

A peak standard deviation at the end of column 1 of 126 μl is evaluated from these data. Assuming a maximum carry-over volume (up to which no influence on the enantiomeric resolution is practically observed) of about 100 μl, and transfer cuts symmetrical to the peak maximum of a Gaussian-type peak, one obtains a transfer yield of about 31% of the analyte mass, and thus a decrease in sensitivity of about 70%. This value may serve as an approximate guideline. It can be confirmed by calculating individual values of the sensitivity decrease for the single analytes, using the particular values of the maximum carry-over volume in Table III and experimentally obtained k' and plate-height data. These individual sensitivity decrease values are given in Table IV; most of them lie between 60 and 70%.

A means of reducing the decrease in analyte mass at constant carry-over volume is to lower the inner diameter of the first column. Such a reduction, however, lowers the sample volume which can be injected without affecting the resolution in the first column. Working with limited concentrations of analytes, the reduction in sample volume also reduces the injected analyte mass, and the overall sensitivity of the method

TABLE IV

ESTIMATED DECREASE IN SENSITIVITY ASSOCIATED WITH A RESTRICTION OF THE CARRY-OVER VOLUME

Values for the maximum carry-over-volume, V_{co}^{max} (μl), are approximate values obtained from the data in Table III. The standard deviation data for the analyte peak at the end of column 1, $\sigma_v^{col.1}$ (μl), were obtained by direct measurement. The percentage of mass transferred was evaluated by assuming a Gaussian distribution and transfer symmetric to the peak maximum.

Column I, OS; column II, β-CD-CSP[a]

Analyte	Methanol in eluent (%, v/v)		V_{co}^{max}	$\sigma_v^{col.1}$	$\frac{V_{co}^{max}}{\sigma_v^{col.1}}$	Mass transferred (%)	Decrease in sensitivity (%)
	1[b]	2[c]					
Hexobarbital	40	20	100	130	0.77	30	70
Dns-threonine	40	20	100	100	1.00	38	62
Chlorthalidone	30	20	150	100	1.50	54	46
	40	20	80	80	1.00	38	62

Column I, ODS; column II, OS/β-CD-CMA[a]

Analyte	Methanol in eluent (%, v/v)		V_{co}^{max}[c]	$\sigma_v^{col.1}$	$\frac{V_{co}^{max}}{\sigma_v^{col.1}}$	Mass transferred (%)	Decrease in sensitivity (%)
	1[d]	2[e]					
Hexobarbital	40	20	100	110	0.91	35	65
Dns-threonine	30	20	100	130	0.77	30	70
Chlorthalidone	30	20	100	80	1.25	48	52

[a] Column symbols as in Table II.
[b] Aqueous buffer (10 m*M* ammonium acetate, pH 5.5)–methanol, content of methanol as indicated.
[c] Aqueous buffer (10 m*M* ammonium acetate, pH 5.5)–methanol, content of methanol as indicated.
[d] Aqueous buffer (25 m*M* ammonium acetate, pH 5.5)–ethanol, content of ethanol as indicated.
[e] Aqueous buffer (25 m*M* ammonium acetate, pH 5.5–35 m*M* β-CD–1 *M* urea)–ethanol, content of ethanol as indicated.

is not improved in this instance. This drawback can be compensated for in principle via an enrichment step in the first column, applying a step gradient after sample injection, as has often been described for trace analysis.

Considering, finally, the efficiency of the two columns, it is noteworthy that the plate numbers employing a β-CD system are lower than those of alkylsilica columns, but not drastically: *ca.* 8000 plates in a 250-mm β-CD-CSP column and about 7000 in a column with the β-CD-CMA system. These data are approximate and average values obtained for the mentioned analytes under the experimental conditions described in the tables, *i.e.*, flow-rate 0.5 ml/min and ambient temperature.

TABLE V

THERMODYNAMIC PEAK COMPRESSION FACTORS, pcf^{th}, IN COLUMN 2 AND MAXIMUM EXPLOITABLE PEAK COMPRESSION EFFECT, pcf^{max}, AS A FUNCTION OF COLUMN DIAMETER FOR THE COLUMN ORDER CHIRAL–NON-CHIRAL

pcf^{th} calculated according to eqn. 1 and pcf^{max} according to eqn. 2, assuming $R_s^{(1+2)} = 0.90R_s^{(2)}$ (*i.e.*, the resolution in column 2 is affected by the peak profile of the transferred peak by not more than 10%). Column 1 I.D. = 4 mm, column 2 I.D. as specified under pcf^{max}.

Column I, β-CD-CSP; column II, OS[a]

Analyte	Methanol in eluent (%, v/v)		$\sigma_v^{col.1}$	$\sigma_v^{col.2}$	pcf^{th}	pcf^{max}			
						4 mm I.D.	3 mm I.D.	2 mm I.D.	1 mm I.D.
	1[b]	2[c]							
Hexobarbital	20	40	100	130	4.3	1.6	2.8	6.4	25
Dns-threonine	20	40	150	100	5.6	3.1	5.5	12	50
Chlorthalidone	20	30	60	100	2.0	1.2	2.2	5.0	20
	20	40	60	80	4.2	1.6	2.8	6.2	25

Column I, OS/β-CD-CMA; column II, ODS

Analyte	Ethanol in eluent (%, v/v)		$\sigma_v^{col.1}$	$\sigma_v^{col.2}$	pcf^{th}	pcf^{max}			
						4 mm I.D.	3 mm I.D.	2 mm I.D.	1 mm I.D.
	1[d]	2[e]							
Hexobarbital	20	30	70	230	3.2	0.6	1.1	2.5	10
	20	40	70	110	10.3	1.3	2.3	5.3	21
Dns-threonine	20	30	100	130	3.4	1.6	2.8	6.4	25
	20	40	100	70	16.6	3.0	5.2	12	47
Chlorthalidone	20	30	70	80	3.1	1.8	3.2	7.2	29
	20	40	70	60	14.4	2.4	4.3	9.6	39

[a] Column symbols as in Table II.
[b] Aqueous buffer (0.1 *M* ammonium acetate, pH 5.5)–methanol (80:20, v/v).
[c] Aqueous buffer (0.1 *M* ammonium acetate, pH 5.5)–methanol; content of methanol as indicated.
[d] Aqueous buffer (25 m*M* ammonium acetate, pH 5.5–35 m*M* β-CD–1 *M* urea)–ethanol (80:20, v/v).
[e] Aqueous buffer (25 m*M* ammonium acetate, pH 5.5)–ethanol; content of ethanol as indicated.

Perspectives for the column order chiral–non-chiral

The data given in Table II for the chiral–non-chiral column order show that strong peak compression is obtained for the β-CD-CSP column when choosing the working range shown in the Figs. 2 and 3. However, the whole peak compression effect at the top of column 2 cannot be exploited because of the peak dispersion taking place in the second column. The maximum exploitable peak compression factor, pcf^{max}, is calculated according to the following equation [10]

$$pcf^{max} = \frac{\sigma_v^{col.1}}{\sigma_v^{col.2}}\left[\left(\frac{R_s^{(2)}}{R_s^{(1+2)}}\right)^2 - 1\right]^{-1/2} \quad (2)$$

where $R_s^{(2)}$ is the chromatographic resolution obtained by use of column 2 and $R_s^{(1+2)}$ is that obtained by the use of a combination of both columns.

One can see from this equation that the peak compression at the top of column 2 has no practical (*i.e.* < 10%) effect on the resolution and peak height up to a carry-over volume equal to approximately half the volume standard deviation produced by column 2. One has to keep in mind that with this consecutive column order the complete peak has to be transferred, and that the carry-over volume therefore has to be at least six times $\sigma_v^{col.1}$.

Table V shows the theoretical peak compression factors, pcf^{th}, calculated according to eqn. 1 and the maximum exploitable values, pcf^{max}, calculated according to eqn. 2 for the CCC systems (β-CD-CSP)–OS and (OS/β-CD-CMA)–ODS. It can be seen that the theoretical peak compression effect achievable cannot be fully exploited by columns of equal (4 mm) inner diameter. This can be done more completely by reducing the peak dispersion (in volume units) in the second column by reducing its inner diameter. The calculation shows[a] that columns of 2 mm I.D. are best suited to exploit fully the peak compression obtained at top of column 2. On the other hand, the full potential of a column of 1 mm I.D. cannot be completely used owing to the given peak compression conditions. Depending on the phase systems employed, peak compression factors between 5 to 10 can be obtained and can be exploited by use of columns with reduced inner diameter, allowing in this way an increase in sensitivity by the same factor.

CONCLUSIONS

Retention data for several chiral compounds on alkylsilica- and cyclodextrin-containing phase systems are used as a basis for the evaluation of approximate peak compression or peak dilation effects, which are obtained at the top of the second column when choosing typical eluent compositions. Both types of consecutive column order are considered.

Peak compression factors smaller than 1, meaning peak dilation, are obtained in

[a] In the calculations of pcf^{max}, the plate number is assumed to be independent of the column inner diameter. This assumption implies that extra-column contributions can be kept small even with very small diameter columns. This is not very realistic for columns of 1–2 mm I.D. When accounting for extra-column dispersion, the pcf^{max} values are expected to be smaller in such instances in comparison with those given in Table V.

most instances with the column sequence alkylsilica–(β-CD-CSP). Less pronounced peak dilation or even small peak compression is obtained when using β-CD as CMA, owing to the additional solvation power of this mobile phase constituent.

The severity of the deconditioning effect observed depends on the volume of the carry-over. The volume up to which no adverse effect is observed is found experimentally to be between 50 and 100 μl, for both β-CD-CSP and β-CD-CMA systems. This result means that simple and straightforward column switching in the convenient column order alkylsilica–(β-CD) system can be successfully performed, when choosing sufficiently low carry-over volumes. Obviously, this method is restricted to instances where one can adopt the strategy of transferring only parts of the chiral analyte. The decrease in sensitivity associated with this strategy lies between 60 and 70% in most instances. A typical example for CCC with β-CD phases which illustrates the decrease in sensitivity is given in Fig. 8.

There are two alternative strategies, in principle, to overcome the adverse situation of higher elution power of the carry-over. First, the eluent dilution technique described and used by Lindner and co-workers [15,16], which reduces the elution strength of the carry-over by adding a weak eluent component, can be applied. This promising technique, however, needs an additional pump (a third pump if the analysis

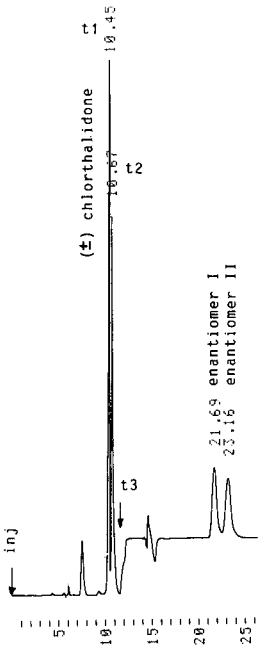

Fig. 8. Typical chromatogram obtained by CCC using octadecylsilica–octylsilica/β-CD-CMA columns. Analytes: enantiomers of chlorthalidone. Peaks (from the left): (±)-chlorthalidone with heart cut in the middle of the peak; first enantiomer of chlorthalidone eluted from column 2; and second enantiomer of chlorthalidone eluted from column 2. Chromatographic conditions: mobile phase, aqueous buffer (25 m*M* ammonium acetate, pH 5.5–35 m*M* β-CD–1 *M* urea)–30% (v/v) ethanol; temperature, 30°C; flow-rate, 0.5 ml/min. Times of switching events: t_1 = 10.40 min; t_2 = 10.60 min; t_3 = 11.50 min (for the definition of t_1, t_2 and t_3, see Table I). Bottom scale: time in minutes.

time should not be increased by repeated changes of eluents). This technique is being investigated further. Second, a small ion-exchange column can be inserted between the alkylsilica and the β-CD column for the retention of analytes which are charged at certain pH values. Peak compression can then be obtained by increasing the concentration of buffer ions, even if the alcohol concentration in the eluent is simultaneously reduced. Again, this set-up requires additional entities and is still being evaluated. We expect advantages especially for those chiral columns which cannot be used with higher concentrations of organic solvent components, such as some protein columns.

The reduction of the carry-over volume evaluated here is a possible means of using β-CD-containing phase systems within a multi-column set up of simple design.

For the reversed column order, β-CD–alkylsilica, values between 2 and 5 are calculated for the potential peak compression factors at the top of column 2. The actual value depends on the analyte structure and the separation problem. The use of columns with reduced inner diameter is required in order to exploit the full potential of peak compression achievable in this way and to enhance the sensitivity of determination by the same factors as mentioned above.

ACKNOWLEDGEMENT

This study was made possible by a grant from the Austrian Fond zur Förderung der Wissenschaftlichen Forschung (FWF). The authors are grateful for this support.

REFERENCES

1 J. F. K. Huber, R. van der Linden, E. Ecker and M. Oreans, *J. Chromatogr.*, 83 (1973) 267.
2 Y. Tapuhi, N. Miller and B. L. Karger, *J. Chromatogr.*, 205 (1981) 325.
3 L.-E. Edholm, C. Lindberg, J. Paulson and A. Walhagen, *J. Chromatogr.*, 424 (1988) 61.
4 I. W. Wainer and R. M. Stiffin, *J. Chromatogr.*, 424 (1988) 158.
5 Y.-Q. Chu and I. W. Wainer, *Pharm. Res.*, 5 (1988) 680.
6 A. Walhagen and L.-E. Edholm, *J. Chromatogr.*, 473 (1989) 371.
7 A. Walhagen, L.-E. Edholm, C. E. M. Heeremans, R. A. M. van der Hoeven, W. M. A. Niessen, U. R. Tjaden and J. van der Greef, *J. Chromatogr.*, 474 (1989) 257.
8 A. Walhagen, L.-E. Edholm, B. M. Kennedy and L. C. Viao, *Chirality*, 1 (1989) 20.
9 L. Silan, P. Jadaud, L. R. Witfield and I. W. Wainer, *14th International Symposium on Column Liquid Chromatography, Boston, May 1990*, poster 174.
10 A. M. Rizzi, *J. Chromatogr.*, 513 (1990) 195.
11 J. Lankelma and H. Poppe, *J. Chromatogr.*, 149 (1978) 587.
12 H. Poppe, J. Paanakker and M. Bronckhorst, *J. Chromatogr.*, 204 (1981) 77.
13 R. Hirz, *Thesis*, University of Vienna, 1982.
14 N. E. Hoffman and A. Rahman, *J. Chromatogr.*, 473 (1989) 260.
15 W. Lindner, H. Ruckendorfer, W. Lechner and W. Posch, *Int. J. Environ. Anal. Chem.*, 21 (1987) 235.
16 W. Lindner, W. Posch, O. S. Wolfbeis and P. Tritthart, *Chromatographia*, 20 (1985) 213.

Journal of Chromatography, 557 (1991) 215–226
Elsevier Science Publishers B.V., Amsterdam

CHROM. 23 240

Influence of counter-ion inclusion complexation on the quality of cyclodextrin-supported separations in isotachophoresis

IVAN JELÍNEK
Research Institute for Pharmacy and Biochemistry, Kouřimská 17, 130 60 Prague 3 (Czechoslovakia)
and
JIŘÍ SNOPEK and EVA SMOLKOVÁ-KEULEMANSOVÁ*
Department of Analytical Chemistry, Charles University, Albertov 2030, 128 40 Prague 2 (Czechoslovakia)

ABSTRACT

The effect of counter-ion inclusion complex formation on the separation efficiency in electrolyte systems modified with β-cyclodextrin and its methyl derivatives was studied. On the basis of the analysis of complex-forming equilibria established in the sample mixed zone, it was concluded that an increasing stability of the counter-ion inclusion complex results n a decreased efficiency of the separation process. This was verified experimentally on the set of eleven aliphatic and aromatic acids used as counter-ions in slightly acidic cationic electrolyte systems.

INTRODUCTION

The ability of cyclodextrins (CDs) and their derivatives to interact with various types of compounds and form inclusion complexes, according to the sizes and shapes of the molecules, has made possible a wide range of analytical applications, especially in chromatographic and related electromigration methods [1–3]. A number of reported applications have confirmed the possibility of using CDs as structural selectors in capillary isotachophoresis (ITP) [4]. It was proved experimentally that the modification of ITP electrolyte systems by CDs and their derivatives may substantially improve the resolution of structurally related compounds [5–8] and various types of isomers, including enantiomers [7–12].

Cyclodextrins and their derivatives have proved to have many exceptional properties making them unique structural selectors in ITP. From the practical point of view it is important that CDs form most stable inclusion complexes in aqueous solutions rather than in organic solvents. In the commonly used pH range of ITP electrolyte systems the CD molecule does not carry a significant electric charge and therefore it does not migrate under the influence of an applied electric field. An average velocity of CD molecules in the separation compartment is given only by complex-

0021-9673/91/$03.50

forming equilibria with charged species from an electrolyte system. Owing to the high molecular mass, the velocity of CD molecules is estimated to be many times lower than the migration velocities of charged species. Therefore, the role of CD molecules dispersed in the separation compartment of an ITP apparatus may be compared with the role of the stationary phase in chromatography.

Although in most instances the utilization of CDs leads to a significant improvement in resolution of structurally related compounds, it may fail in some applications because of small differences in the stabilities of sample component complexes. A possible role of two limiting CD–solute interactions, introduced as effective and non-effective complex formation, on the quality of ITP resolution has been studied and widely discussed [13].

The aim of this paper is to extend the proposed model of effective and non-effective complex formation, considering the influence of competitive inclusion complexation of the components of electrolyte systems on the quality of sample resolution.

THEORETICAL

In a first approximation, let us suppose that it is possible to neglect inclusion complex formation between cyclodextrin and minor components of electrolyte systems such as anti-convective additives and possible trace impurities. Only complexation of leading ions, terminating ions and counter ions will be involved in our considerations.

The components of electrolyte systems must satisfy at least two fundamental conditions in order to alter effectively the sample–CD complex-forming equilibria. It is essential that the requirements of proper size and shape of complexed molecules or ions fit well into the cavity of the CD used and form stable inclusion complexes. Another important requirement is continuous contact with separating components of the sample in the whole volume of the sample zone. The distribution of ionic species and CD molecules in leading, sample and terminating zones during the analysis is outlined schematically in Fig. 1.

As shown in Fig. 1, leading ions are not present in the sample zone during ITP analysis. The area of coexistence of leading and sample zones where competitive complex formation may occur is restricted to the boundary B1. Chlorides, the most commonly used leading ions in anionic electrolyte systems, do not form stable

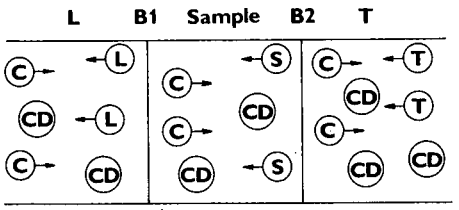

Fig. 1. Schematic distribution of ionic species and cyclodextrin molecules in leading, sample and terminating zones. C = Counter-ion; L = leading ion; T = terminating ion; CD = cyclodextrin molecule; B1 and B2 = zone boundaries.

inclusion complexes with β-CD and its methyl derivatives owing to their small ionic diameter and high charge density. Their contribution to complex-forming equilibria is considered to be negligible. For the same reasons it is not necessary to consider the complexation of NH_4^+ ions and the ions of alkali metals which are frequently used as leading ions in cationic electrolyte systems.

What is more significant is the complexation of CDs with ions of suitable size in the terminator. By using the correct injection technique ensuring minimum mixing of the sample with electrolyte system, the ions of the terminator are assumed not to be present in initial sample zone. As shown in Fig. 1, the area of competitive CD–terminator complex formation affecting the selective complexation of sample components is restricted to the moving boundary B2.

Critical for the quality of separation should be the competitive inclusion complexation of counter-ions. Many counter-ions used are able to fit well into the cavity of CDs and to form relatively strong inclusion complexes. From Fig. 1 it should be noted that the counter-ion–CD complex formation may occur in the whole volume of the sample zone during the analysis.

Simple considerations may be useful for characterizing the role of counter-ion inclusion complex formation in the ITP separation process. Let us suppose that three complex-forming equilibria with cyclodextrin are established in the mixed zone of two analyte components X and Y and the counter-ion.

$$X + CD \rightleftharpoons X\text{–}CD \quad \text{(I)}$$
$$Y + CD \rightleftharpoons Y\text{–}CD \quad \text{(II)}$$
$$C + CD \rightleftharpoons C\text{–}CD \quad \text{(III)}$$

The equilibrium reactions are characterized by conditional stability constants:

$$K'_X = \frac{[X\text{–}CD]}{[X][CD]_I} \qquad K'_Y = \frac{[Y\text{–}CD]}{[Y][CD]_{II}} \qquad K'_C = \frac{[C\text{–}CD]}{[C][CD]_{III}} \quad (1)$$

where [X–CD], [Y–CD] and [C–CD] are equilibrium molar concentrations of inclusion complexes, [X], [Y] and [C] are equilibrium molar concentrations of X, Y and C and $[CD]_I$, $[CD]_{II}$ and $[CD]_{III}$ are equilibrium molar concentrations of cyclodextrin not bound in inclusion complexes X–CD, Y–CD and C–CD.

The relationship between stability constant K and conditional stability constant K' is given by the equation

$$K'_{X(Y)} k_{X(Y)} = K_{X(Y)} \quad (2)$$

where $k_{X(Y)}$ is the coefficient of the side reaction for equilibrium I defined by

$$k_X = \frac{[CD]'}{[CD]} \quad (3)$$

The molar concentration of CD that is not bound in the X–CD complex, [CD]′, may be expressed as

$$[CD]' = [CD] + [Y\text{–}CD] + [C\text{–}CD] \quad (4)$$

Analogously the coefficient of side reactions for equilibrium II is defined by

$$k_Y = \frac{[CD]''}{[CD]} \tag{5}$$

where

$$[CD]'' = [CD] + [X\text{–}CD] + [C\text{–}CD] \tag{6}$$

The degree of complexation of the component X(Y) in the mixed zone, $\alpha_{X(Y)}$, is defined by

$$\alpha_{X(Y)} = \frac{[X(Y)\text{–}CD]}{[X(Y)] + [X(Y)\text{–}CD]} \tag{7}$$

Combining the defined expression for K'_X (eqn. 1), and eqns. 2, 3 and 7, we obtain

$$\alpha_X = \frac{K_X[CD]'/k_X}{1 + K_X[CD]'/k_X} \tag{8}$$

Analogously by substituting from the defined equation for K'_Y (eqn. 1), eqns. 2 and 5 into eqn. 7, α_Y could be expressed as

$$\alpha_Y = \frac{K_Y[CD]''/k_Y}{1 + K_Y[CD]''/k_Y} \tag{9}$$

With coexistence of complex forming equilibria I–III the following condition must be satisfied:

$$[CD]'/k_X = [CD]''/k_Y = [CD]_E \tag{10}$$

where $[CD]_E$ = equilibrium molar concentration of free CD in the mixed zone.

From eqns. 8 and 9 it should be noted that the degree of complex formation, $\alpha_{X(Y)}$, is expressed as a function of the corresponding stability constant $K_{X(Y)}$ and equilibrium concentration $[CD]_E$. It can be proved that with decreasing $[CD]_E$ the degree of complex formation $\alpha_{X(Y)}$ decreases. This fact is clearly visible from computer-simulated $\alpha_{X(Y)} = f([CD]_E)$ dependence (curves 1 and 2) given in Fig. 2.

Combining eqns. 7, 8 and 11 (see ref. 13), it is theoretically possible to determine effective mobilities of complexed solutes $(U_X)_C$ and $(U_Y)_C$ for given $[CD]_E$ and known molecular masses M_X, M_Y, effective charge Z, molecular mass of used cyclodextrin M_{CD} and empirical coefficients a and b:

$$(U_X)_C = a + b \cdot \frac{|Z + \alpha_X \Delta Z|}{M_X + \alpha_X \Delta M_{CD}}$$

$$(U_Y)_C = a + b \cdot \frac{|Z + \alpha_Y \Delta Z|}{M_Y + \alpha_Y \Delta M_{CD}} \tag{11}$$

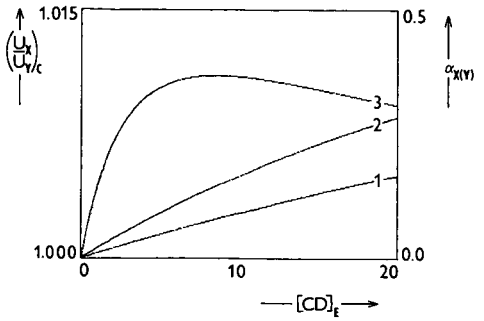

Fig. 2. Computer-simulated dependence of the degree of complexation $\alpha_{X(Y)}$ (curves 1 and 2) and of the ratio of effective mobilities $(U_X/U_Y)_C$ (curve 3) of complexed solutes X and Y on the molar concentration of free, uncomplexed cyclodextrin, $[CD]_E$ (mmol/l). Numerical values substituted in eqn. 11 (from ref. 13): $M_X = M_Y = 150$, $K_X = 10$, $K_Y = 20$, $Z = 0.5$, $M_{CD} = 1135$ (β-CD), $a = 69.85$, $b = 1558$.

The computer-simulated dependence of the ratio $(U_X/U_Y)_C$, characteristic for the separation quality, on changing the $[CD]_E$ value for the pair of enantiomers ($M_X = M_Y$) is shown in Fig. 2, curve 3. Characteristic for this dependence is the existence of a $(U_X/U_Y)_C$ maximum, a slight decrease in the mobility ratio for higher $[CD]_E$ values and a very fast decrease for low $[CD]_E$.

From eqns. 3–6 it results that $[CD]_E$ is a function of all considered stability constants and depends simultaneously on [X], [Y] and [C]. For a pair of components X and Y with given inclusion complex stability constants and concentrations in the mixed zone, the decrease in $[CD]_E$ value depends particularly on an increase in the stability of the C–CD complex caused by the choice of a counter-ion with a great affinity to the CD used. Even the simplified balance of the concentrations of components in the mixed zone during ITP separation confirms that the influence of counter-ion inclusion complex formation on the quality of CD-based separation is not marginal. In order to maintain electroneutrality, the molar concentration of counter-ions in the mixed zone must be equal to the sum of the molar concentrations of X and Y ions. Assuming similar values of the effective charges of counter-ion and sample molecules (*e.g.*, the case of enantiomers separated in a leading electrolyte buffered to a pH near to the numerical value of their dissociation constants), not only ionic but also their overall molar concentrations will be equal.

EXPERIMENTAL

Chemicals

Redistilled water was used in the preparation of the electrolyte and racemate solutions investigated. Hydroxyethylcellulose 4000 (HEC) (Serva, Heidelberg, Germany) was deionized by stirring its aqueous solution with Zerolit DM-F mixed-bed ion exchanger (BDH, Poole, UK). All other chemicals were of the highest quality commercially available and were used without any purification: hydrochloric acid (30%), acetic acid, propionic acid, butyric acid, valeric acid, caproic acid, trimethylacetic acid, 2-aminobenzoic acid, 4-aminobenzoic acid and 4-morpholinoethanesulphonic acid (MES) (Merck, Darmstadt, Germany); pyridine-2-carboxylic acid,

pyridine-3-carboxylic acid and pyridine-4-carboxylic acid (Fluka, Buchs, Switzerland); 6-aminocaproic acid (EACA) (Sigma, St. Louis, MO, USA); sodium hydrogenphosphate (Carlo Erba, Milan, Italy); and β-cyclodextrin (β-CD), heptakis(2,6-di-O-methyl)-β-cyclodextrin (diMe-β-CD) and heptakis(2,3,6-tri-O-methyl)-β-cyclodextrin (triMe-β-CD) (Chinoin, Budapest, Hungary).

The solutes of pseudoephedrine (ΨE) and *p*-hydroxynorpseudoephedrine (NHΨE) racemates were produced by the Research Institute of Antibiotics (Roztoky, Czechoslovakia).

Methods

Isotachophoretic experiments were performed with a Tachophor 2127 system (LKB, Bromma, Sweden) equipped with a conductivity detector and poly(tetrafluoroethylene) (PTFE) capillary. Injections were made with a 10-μl Hamilton syringe.

The pH of the electrolyte solutions was measured with a Metrohm (Herisau, Switzerland) Model 605 digital pH meter using a combined glass electrode.

All computations were made on a DS-15 data station (Varian, N. Springvale, Australia) using our own software.

RESULTS AND DISCUSSION

The possible role of competitive counter-ion complex formation in ITP separation processes was experimentally verified on a set of aliphatic and aromatic acids (Table I), that could be used as counter-ions for slightly acidic cationic electrolyte systems (pH 4.0–5.5). The stabilities of inclusion complexes of the chosen acids were studied in anionic electrolyte system 1 (Table II). The leading electrolyte was consecutively modified by β-CD, diME-β-CD and triMe-β-CD in amounts corresponding to concentrations of 0.5, 1.0, 2.0, 4.0, 6.0 and 8.0 mmol/l. Details of the experimental conditions, composition and injected amounts of the sample are given in Table III.

TABLE I

ORGANIC ACIDS AND THEIR DISSOCIATION CONSTANTS, pK_A [14], CHOSEN FOR EXPERIMENTAL VERIFICATION OF THE INFLUENCE OF COUNTER-ION COMPLEX FORMATION ON THE QUALITY OF ITP SEPARATION

No.	Acid	pK_A
1	Acetic	4.756
2	Propionic	4.874
3	Butyric	4.820
4	Valeric	4.842
5	Caproic	4.857
6	Trimethylacetic	5.037
7	2-Aminobenzoic	4.939
8	4-Aminobenzoic	4.853
9	Pyridine-2-carboxylic	4.9[a]
10	Pyridine-3-carboxylic	4.819
11	Pyridine-4-carboxylic	4.8[a]

[a] Determined by titration.

TABLE II

ELECTROLYTE SYSTEMS USED[a]

No.	Leading ion	Counter-ion	pH_{LE}	Terminating ion
Anionic electrolyte system				
1	Cl^- (5 mmol/l)	EACA	4.46	MES (10 mmol/l)
Cationic electrolyte systems				
1	Na^+ (5 mmol/l)	Acetate	4.00	EACA (10 mmol/l)
–		–	4.50	
–		–	5.00	
–		–	5.50	
2		Propionate	4.49	
3		Butyrate	4.51	
4		Valerate	4.48	
5		Capronate	4.49	
6		Trimethylacetate	4.47	
7		2-Aminobenzoate	4.50	
8		4-Aminobenzoate	4.51	
9		Pyridine-2-carboxylate	4.50	
10		Pyridine-3-carboxylate	4.51	
11		Pyridine-4-carboxylate	4.49	

[a] All the leading electrolytes used contained 0.08% of HEC.

The dependence of the relative step heights, $(h_i)_{rel}$, of the zones with increasing concentration of β-CD is shown in Fig. 3A. Sodium hydrogenphosphate, added to each solute injected, was used as an internal standard for the determination of $(h_i)_{rel}$ values. The experimental points obtained were interpolated by a polynomial function of suitable degree. The quality of approximation was controlled by the sum of square deviations from the experiment, ΣS^2. The computed first root of the selected polynomial function, r_1, which represents the slope of the interpolation curve at its beginning (where the molar concentration of cyclodextrin in the leading electrolyte $c_{CD} = 0$), was utilized advantageously as a value characterizing the stability of the corresponding inclusion complex. For better orientation, the acids in Fig. 3A are ordered according to increasing stability of their β-CD inclusion complexes characterized by increasing r_1 value. In agreement with the theory of inclusion complex

TABLE III

CONDITIONS FOR ITP MEASUREMENT

Parameter	Anionic mode	Cationic mode
Capillary	250 × 0.55 mm I.D.	300 × 0.55 mm I.D.
Detection	Conductivity	Conductivity
Current	100 μA (7 min), 50 μA det.[a]	150 μA (6 min), 50 μA det.[a]
Temperature	18°C	18°C
Injected sample	1 μl of aqueous solution of acid 1–11 (20 mmol/l) + $Na_2HPO_4 \cdot 2H_2O$ (4 mmol/l)	(i) 1, 2, 3 μl of ΨE (6.34 mmol/l); (ii) 1, 2, 3 μl of HNΨE (5.43 mmol/l)

[a] det. = for detection.

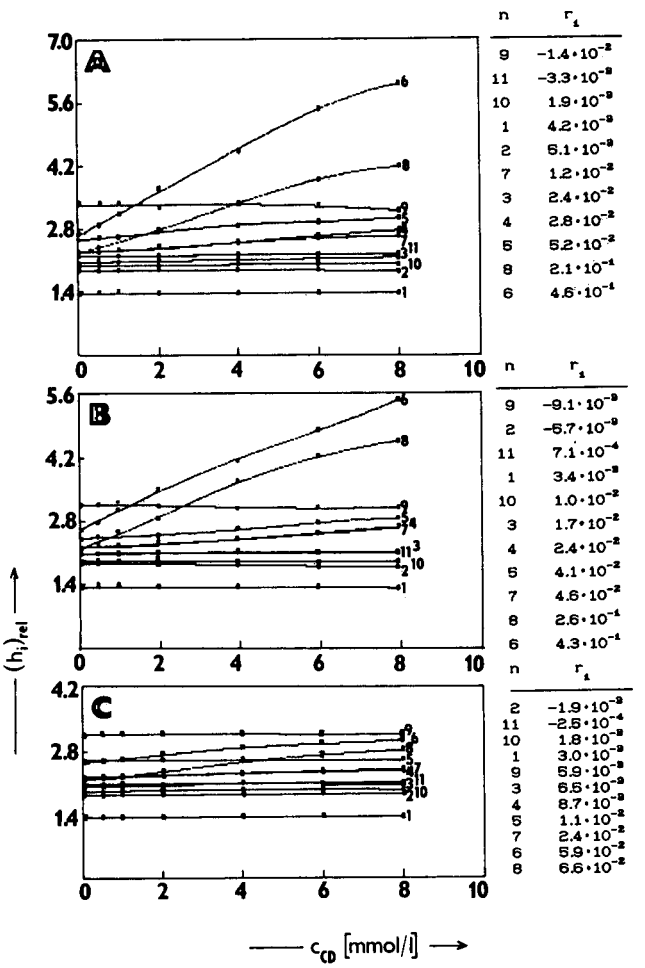

Fig. 3. Dependence of $(h_i)_{rel}$ values of acids 1–11 on increasing molar concentration, c_{CD}, of (A) β-CD, (B) diMe-β-CD and (C) triMe-β-CD in anionic electrolyte system 1. n = Index number of the acid according to Table I; r_1 = computed first root of approximating polynomial.

formation and known structural requirements on guest molecules, an increased stability of complexes may be observed for aliphatic acids with longer and especially branched chains (trimethylacetic acid). Also explained by theory is the observed difference in stability of *o*- and *p*-aminobenzoic acid complexes and the very low stability of β-CD complexes with all the studied pyridinecarboxylic acids.

The dependence of $(h_i)_{rel}$ values on increasing concentration of diMe-β-CD in the leading electrolyte, together with the list of studied acids ordered according to increasing stability of their complexes, are given in Fig. 3B. Unlike the above-mentioned complexation with β-CD, higher stabilities of *o*- and *p*-aminobenzoic acid complexes and lower stability of the trimethylacetic acid complex may be observed.

The complexation of the studied acids with triMe-β-CD is illustrated in Fig. 3C. From tabulated r_1 values it follows that only *o*-aminobenzoic, *p*-aminobenzoic, trimethylacetic and caproic acid are able to form more stable inclusion complexes.

After finishing the experiments in the anionic mode, which provided necessary data about the stabilities of inclusion complexes, the acids under examination were used as counter-ions in cationic electrolyte systems 1–11 (Table II). The racemates of ΨE and HNΨE were used as model samples for monitoring the effectiveness of the separation process with changing counter-ions. Both samples used are known to separate enantioselectively in a slightly acidic electrolyte system modified by β-CD or diMe-β-CD and, moreover, the HNΨE racemate could be resolved in the electrolyte system with triMe-β-CD [11].

In order to compare theoretical conclusions concerning the influence of counter-ion complex formation on the quality of separation with practical experiments, a suitable quantity characterizing the efficiency of the separation process must be chosen. The use of the maximum racemate load capacity, n_r [12], seems to be the most advantageous because of its availability from experiments.

The substitution of one counter-ion by another in the leading electrolyte induces changes in some experimental parameters. As follows from the theory of ITP, changes in the mobility of the counter-ion cause pH shifts in the sample mixed zone. This phenomenon may, however, alter the complex-forming equilibria with CD and change the separation capacity of the system without a contribution of competitive counter-ion complex formation. The role of changes in the pH of the leading electrolyte was verified experimentally by comparing the n_r values for ΨE obtained in β-CD-modified electrolyte system 1 and its analogues with leading electrolyte pH values ranging from 4.0 to 5.5. The slight and non-significant increase in n_r observed with increasing pH of the leading electrolyte indicates that the changes in pH in the mixed zone do not alter the quality of enantioselective resolution (Fig. 4). Therefore, all changes in n_r values in the following experiments should be assigned to the influence of competitive counter-ion complex formation.

The dependence of n_r values for ΨE and HNΨE on the increasing stability of counter-ion inclusion complexes (r_1 value) in cationic electrolyte systems 1–11 modified with β-CD (8 mmol/l) is shown in Fig. 5A. It is obvious that the best chiral resolution is achieved in electrolyte systems 1, 9, 10 and 11 containing acetate or

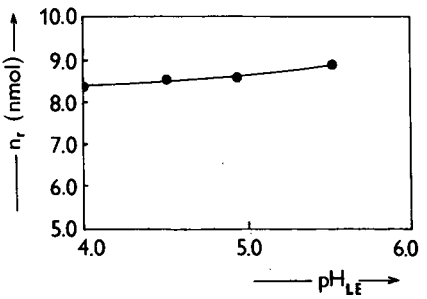

Fig. 4. Dependence of the maximum racemate load capacity n_r for ΨE on the pH of the leading electrolyte 1 modified with β-CD (8 mmol/l).

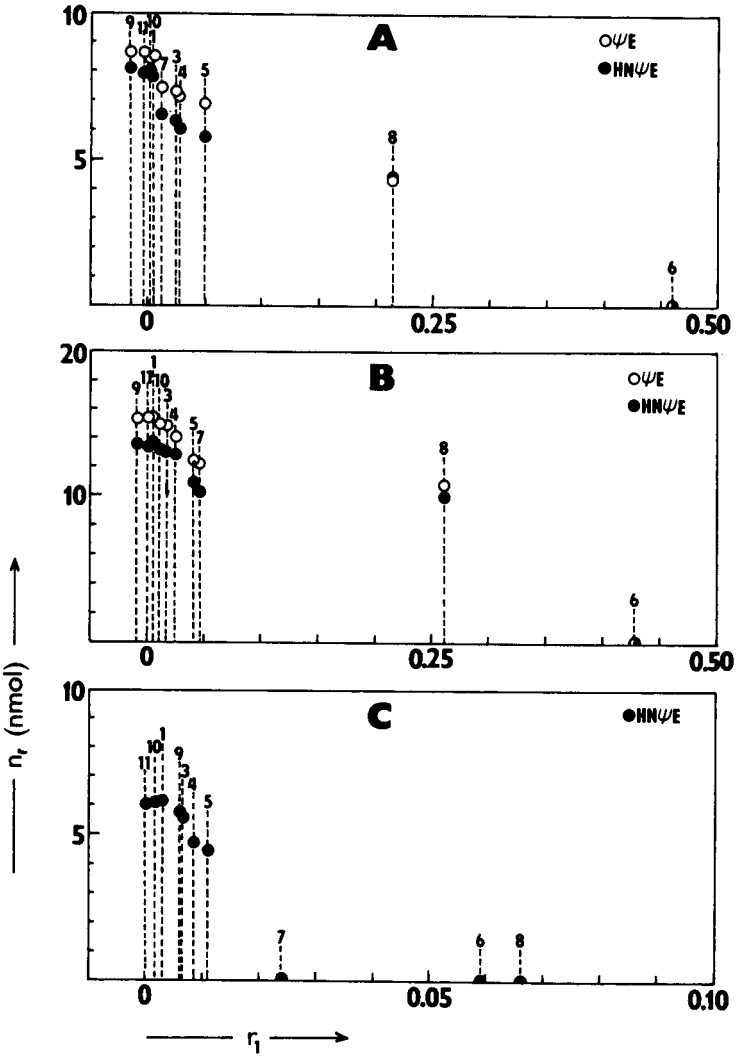

Fig. 5. Dependence of the maximum racemate load capacity n_r for ΨE and HNΨE on the stability of the counter-ion inclusion complex, characterized by the first root of the approximating polynomial function, r_1, in cationic electrolyte systems 1–11 modified with (A) β-CD, (B) diME-β-CD and (C) triMe-β-CD.

pyridinecarboxylate as the counter-ions with low affinity to β-CD. With increasing stability of the counter-ion inclusion complex, the maximum racemate load value steadily decreases. In electrolyte system 6 with the most complexed trimethylacetate, the chiral resolution of both racemates completely disappears.

The dependence of n_r for ΨE and HNΨE on the stability of counter-ion inclusion complexes, measured in electrolyte systems 1–11 modified with diMe-β-CD (8 mmol/l), is shown in Fig. 5B. As in the previously discussed example, the chiral resolution of both racemates deteriorates with increasing stability of the counter-ion

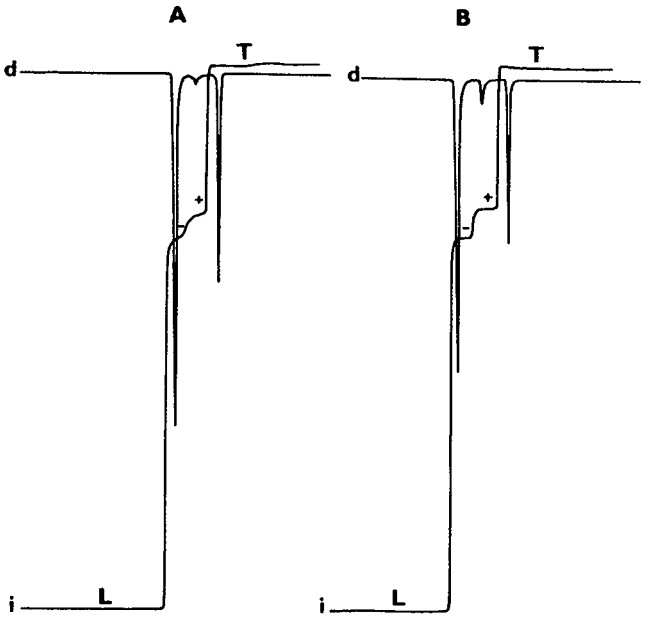

Fig. 6. Separation of ΨE enantiomers in cationic electrolyte systems (A) 9 and (B) 1 modified with β-CD (8 mmol/l). Conductivity detection.

inclusion complex. Similar conclusions may be drawn for th systems modified with triMe-β-CD (Fig. 5C). Critical is the decrease in n_r in electrolyte systems 6–8 containing the counter-ions significantly complexed by triMe-β-CD.

According to the n_r values obtained, the systems with aromatic and aliphatic uncomplexed or a few complexed counter-ions are nearly equal. By a more detailed study of the conductivity detector recordings obtained, it is possible, however, to find the differences in th boundary sharpness. As is shown in Fig. 6, the zone boundary between separated enantiomers is much sharper in an electrolyte system containing an aliphatic counter-ion than in a system with an aromatic counter-ion. The explanation of this phenomenon, which is probably connected with the decreased rate of sample inclusion complex formation in the presence of an aromatic counter-ion, must be found in the theory of kinetics of inclusion complex formation and decomposition [15].

CONCLUSIONS

On the basis of a theoretical analysis of complex-forming equilibria in the sample mixed zone and associated experiments, it was possible to demonstrate unambiguously the influence of counter-ion inclusion complex formation on the separation efficiency of the system modified with β-CD and its methyl derivatives.

The theoretically possible case when the separation in systems with more complexed counter-ions is more effective than in those with less complexed counter-ions [13], resulting from the existence of the maximum of $(U_X/U_Y)_C = f([CD]_E)$ (Fig. 2), was not confirmed experimentally. It is probable that in the range of optimized CD concentrations and possible stability constants of the sample inclusion complexes,

the $[CD]_E$ values are very low and only a significantly negative effect of counter-ion complex formation may be observed.

The measurements described made it possible to select the acids with a low affinity to β-CD and its methyl derivatives from the set examined, which could be used successfully as counter-ions in slightly acidic cationic electrolyte systems modified with β-CD and its methyl derivatives. According to the separation efficiency achieved and the sharpness of the zone boundaries, the most promising seems to be the use of electrolyte system 1 with acetate as counter-ion.

REFERENCES

1 E. Smolková-Keulemansová, *J. Chromatogr.*, 252 (1982) 17.
2 E. Smolková-Keulemansová, in D. Duchêne (Editor), *Cyclodextrins and Their Industrial Uses*, Editions de Santé, Paris, 1987, p. 259.
3 E. Smolková-Keulemansová, L. Feltl and J. Snopek, in D. Duchêne (Editor), *Proceedings of the 5th International Symposium on Cyclodextrins, Paris, 28–30 March, 1990*, Editions de Santé, Paris, 1990, p. 617.
4 J. Snopek, I. Jelínek and E. Smolková-Keulemansová, *J. Chromatogr.*, 452 (1988) 571.
5 M. Tazaki, T. Hayashita, Y. Fujino and M. Takagi, *Bull. Chem. Soc. Jpn.*, 59 (1986) 3459.
6 I. Jelínek, J. Snopek and E. Smolková-Keulemansová, *J. Chromatogr.*, 405 (1987) 379.
7 J. Snopek, E. Smolková-Keulemansová, I. Jelínek, J. Dohnal, J. Klinot and E. Klinotová, *J. Chromatogr.*, 450 (1988) 373.
8 I. Jelínek, J. Dohnal, J. Snopek and E. Smolková-Keulemansová, *J. Chromatogr.*, 464 (1989) 139.
9 J. Snopek, I. Jelínek and E. Smolková-Keulemansová, *J. Chromatogr.*, 411 (1987) 153.
10 I. Jelínek, J. Dohnal, J. Snopek and E. Smolková-Keulemansová, *J. Chromatogr.*, 435 (1988) 496.
11 J. Snopek, I. Jelínek and E. Smolková-Keulemansová, *J. Chromatogr.*, 438 (1988) 211.
12 I. Jelínek, J. Snopek and E. Smolková-Keulemansová, *J. Chromatogr.*, 439 (1988) 386.
13 I. Jelínek, J. Snopek and E. Smolková-Keulemansová, *J. Chromatogr.*, 470 (1989) 113.
14 T. Hirokawa, M. Nishino, N. Aoki and Y. Kiso, *J. Chromatogr.*, 271 (1983) D1.
15 A. Guarino, in J. L. Atwood, J. E. D. Davies and D. D. MacNicol (Editors), *Inclusion Compounds*, Vol. 3, Academic Press, New York, 1984, p. 156.

Journal of Chromatography, 557 (1991) 227–240
Elsevier Science Publishers B.V., Amsterdam

CHROM. 23 245

Enantiomer separation by chiral-phase liquid chromatography of urethane derivatives of natural diacylglycerols previously fractionated by reversed-phase liquid chromatography

B. G. SEMPORÉ* and J. A. BÉZARD
Laboratoire de Physiologie Animale et de la Nutrition, Université de Bourgogne, BP 138, 21004 Dijon Cédex (France)

ABSTRACT

Enantiomers of diacylglycerols such as 3,5-dinitrophenyl isocyanate (urethane) derivatives previously fractionated by reversed-phase high-performance liquid chromatography (HPLC) were separated by HPLC on a chiral phase column [N-(*R*)-1-(α-naphthyl)ethylamino-carbonyl-(*S*)-valine chemically bound to γ-aminopropylsilanized silica]. In addition to the separation of commercial monoacid–diacylglycerol isomers, separation of diacid–diacylglycerol isomers obtained from peanut oil and cottonseed oil triacylglycerols by chemical hydrolysis is reported. Hexane–ethylene dichloride–ethanol mixtures were used for elution of the diacylglycerol derivative isomers, which were detected by their refractive indices or their UV absorption. The *sn*-1,2- and *sn*-2,3-isomers of a racemic mixture were well separated whereas the *sn*-1,3- and *sn*-1,2-isomers were eluted together. In complex mixtures the elution order varies as a function of chain length and unsaturation of the constituent fatty acids, additionally to their positioning. The enantiomer compositions of mixtures calculated from peak areas are similar in both types of detection and are assumed to be representative. The method can be applied to compositional analysis of diacylglycerol optical isomers during studies of the stereospecific distribution of fatty acids in natural triacylglycerols.

INTRODUCTION

In the stereospecific analysis of triacylglycerols, diacylglycerol stereoisomers, especially *sn*-1,2- and *sn*-2,3-diacylglycerols, have to be separately studied for fatty acid distribution [1]. In Brockerhoff's method, the two stereoisomers are differentiated by the stereospecific action of the snake venon phospholipase on synthetic phospholipids derived from the *sn*-1,2(2,3)-diacylglycerol mixture to be studied [2,3]. The method is time consuming and to simplify it several workers have worked out chromatographic separations of enantiomers.

Michelsen and Odham [4] explored the possibility of using capillary gas chromatography (GC) coupled to mass spectrometry to separate (and identify) short-chain diacylglycerol diastereoisomers [*sn*-1,2(2,3)-diethanoyl-, -dibutylroyl- and -didecanoylglycerols]. They observed that the diethanoylglycerol enantiomers were almost completely separated, but the separation rapidly decreased with increasing

0021-9673/91/$03.50

chain length. They then used high-performance liquid chromatography (HPLC) [5] and partially separated *sn*-1,2(2,3)-dilauroyl, -dimyristoyl-, -dipalmitoyl- and -distearoylglycerols as derivatives with 1-(1-naphtyl)ethyl carbamate.

Recently, Laakso and Christie [6] succeeded in separating diacylglycerols as chiral derivatives using (*R*)- or (*S*)-1-(1-naphthyl)ethyl isocyanate by HPLC on a silica column. Separations were of very good quality but with relatively high retention times as a result of the column length. On the other hand, Ôi and Kitahara [7] developed different chiral phases for HPLC that showed characteristic enantioselectivity toward derivatized amino acids, carboxylic acids, alcools and other compounds. On a phase with the chiral selector N-(*S*)-2-(4-chlorophenyl)isovaleroyl-D-phenylglycine (Sumipax OA-2100 from Sumitomo, Osaka, Japan), Itabashi and Takagi [8] succeeded in separating dialkyl- and diacylglycerol enantiomers as 3,5-dinitrophenylurethane (DNPU) derivatives but with retention times of several hours. Another phase with the chiral selector N-(*R*)-1-(α-naphthyl)ethylaminocarbonyl-(*S*)-valine (Sumipax OA-4100 from Sumitomo) appeared more convenient [9], showing the same good separations as above but with much shorter retention times.

These previous studies described enantiomer separations of monoacid–diacylglycerols. On the same last chiral phase, Takagi and Suzuki [10] presented separations of synthetic saturated and unsaturated diacid–diacylglycerols, those more likely to be found in stereospecific analysis of natural triacylglycerols. For this purpose, however, extremely long elution times (several hours) were required. Recently, Itabashi *et al.* [11] resolved enantiomeric diacylglycerols derived from natural sources with very short elution times on an (*R*)-1-(1-naphthyl)ethylamine column. Additionally, after collection of the enantiomers and their GC analysis as trimethylsilyl ether derivatives, Itabashi *et al.* [12] deduced the composition of enantiomeric diacylglycerols issued from triacylglycerols of three oils. In this work the diacylglycerols were tentatively identified by their equivalent carbon number (*ECN*). However, in spite of the narrow range of component fatty acids of these oils, the enantiomer mixtures were still too complex to allow the complete composition of molecular species of the oil triacylglycerols to be calculated.

To obtain much simpler mixtures of enantiomeric diacylglycerols, we first isolated pure triacylglycerols from peanut oil by combined argentation thin-layer chromatography (TLC) and reversed-phase HPLC. The diacylglycerols formed by partial chemical deacylation of these triacylglycerols were fractionated as DNPU derivatives by reversed-phase HPLC [13]. This paper describes the HPLC resolution of the previously isolated enantiomeric *sn*-1,2(2,3)-diacylglycerol derivatives on an N-(*R*)-1-(α-naphthyl)ethylaminocarbonyl-(*S*)-valine phase. The results show that after previous fractionation by reversed-phase HPLC, enantiomers of diacylglycerols derived by Grignard degradation of individual peanut oil triacylglycerols can be readily identified and determined.

EXPERIMENTAL

Samples

The diacylglycerol samples used in this work were those reported in a previous study [13] dealing with their analysis by reversed-phase HPLC. They originated from two sources:

(i) Synthetic diacylglycerols were of commercial origin. They consisted of *rac*-1,2- and *sn*-1,3-dioleoylglycerols (18:1 18:1) from Serdary Research Labs. (London, Ontario, Canada); optically active *sn*-1,2-dioleoyl- and dipalmitoylglycerols (16:0 16:0) from Sigma (St. Louis, MO, USA). Prior to use the commercial *rac*-1,2-(18:1 18:1), partly isomerized, was separated into *rac*-1,2- and *sn*-1,3-(18:1 18:1), separately recovered, by TLC on borate-impregnated silica gel plates [14].

(ii) Natural-source diacylglycerols were prepared by Grignard deacylation [15] of triacylglycerols isolated from peanut and cottonseed oils by combined argentation TLC–reversed-phase HPLC [16]. These included palmitoyldioleoylglycerol (16:0 18:1 18:1), trioleoylglycerol (18:1 18:1 18:1), palmitoyloleoyllinoleoylglycerol (16:0 18:1 18:2), dioleoylinoleoylglycerol (18:1 18:1 18:2) and oleoyldilinoleoylglycerol (18:1 18:2 18:2) from peanut oil. The triacylglycerol 16:0 18:1 18:2 was also isolated from cottonseed oil for comparison. The *sn*-1,2(2,3)- and *sn*-1,3-diacylglycerols formed by hydrolysis were separated from the degradation products on borate-impregnated silica TLC [14].

Diacylglycerol derivatization

The commercial and natural-source diacylglycerols were analysed by reversed-phase and chiral-phase HPLC as urethane derivatives prepared as reported previously [13]. The acylglycerols reacted with 3,5-dinitrophenyl isocyanate (Sumitomo) in dry toluene in the presence of pyridine. The diacylglycerol derivatives were isolated from the reaction mixture either by TLC or by reversed-phase HPLC in a combined purification–fractionation procedure [13].

High-performance liquid chromatography

HPLC was used both to fractionate the diacylglycerol derivatives according to chain length, unsaturation and partly according to isomerism (reversed-phase HPLC) and to analyse the fractionated diacylglycerol derivatives according to positional isomerism (chiral-phase HPLC).

In both instances analyses were carried out using a Model 6000 A solvent-delivery system (Waters Assoc., Milford, MA, USA) connected either to a Model R 401 differential refractometer (Waters Assoc.) or to a Model 450 variable-wavelength UV detector (Waters Assoc.). The column and the conditions used in the reversed-phase HPLC analyses were as reported previously [13]. In the chiral-phase analyses, the column used was a Sumipax OA-4100 purchased from Sumitomo. The 250 mm × 4 mm I.D. stainless-steel column was packed with 5-μm particles of N-(*R*)-1-(α-naphthyl)ethylaminocarbonyl-(*S*)-valine chemically bound to γ-aminopropylsilanized silica. A LiChroCART 4-4 guard column filled with LiChrosorb Si 60 (Merck, Darmstadt, Germany) was attached to the column inlet.

The analyses were carried out isocratically at a constant flow-rate of either 0.9, 1.0 or 1.2 ml min^{-1} according to samples, at ambient temperature. The mobile phase was hexane–ethylene dichloride (or dichloromethane)–ethanol (80:20:1, v/v/v). Hexane of analytical-reagent grade was from SDS (Peypin, France). Ethylene dichloride (HPLC grade) was purchased from Fluka (Buchs, Switzerland). Dichloromethane (analytical-reagent grade) was obtained from Prolabo (Paris, France) and absolute ethanol from Carlo Erba (Rueil Malmaison, France). Solvents were filtered through a Millipore membrane (0.5 μm pore size) and the mobile phase mixtures were vacuum degassed for 2 min prior to use.

For quantitative determinations, peak areas were measured by means of an Enica 21 integrator–calculator (Delsi Instruments, Suresnes, France).

Gas chromatography

The fatty acid compositions of the diacylglycerols recovered from hydrolysis products and of the diacylglycerol derivatives fractionated by chiral-phase HPLC were determined by capillary GC of the methyl esters, as described previously [17]. The analyses were carried out on a Becker-Packard (Rungis, France) Model 417 gas chromatograph equipped with a laboratory-made 30 m × 0.4 mm I.D. glass capillary column, coated with Carbowax 20M (Applied Science Labs., State College, PA, USA), at a constant temperature of 195°C and a nitrogen flow-rate of 3 ml min^{-1}. The apparatus was fitted with a Ros injector [18] (Spiral, Dijon, France) and a flame-ionization detector (Becker-Packard). Peak areas were measured by means of an Enica 21 integrator–calculator (Delsi). Calibration factors for quantitative determinations were calculated using standard mixtures of fatty acids (Nu Chek Prep, Elysian, MN, USA).

Definitions

Different parameters were determined to characterize the chromatographic diacylglycerol separations. The partition number (*PN*) [1] or equivalent carbon number (*ECN*) [11] of the diacylglycerol fractions was calculated from the total acyl carbon number (*CN*) and the total number of double bonds (*DB*) of the two constituent fatty acids, according to the equation

$$PN = ECN = CN - 2\,DB$$

Peaks were characterized by their retention times, t_R (min), corrected from the column void volume and by their retention volumes, V_R (ml).

The separation between two peaks, 1 and 2 (in that elution order), was characterized by the separation factor, α [19], *i.e.* the ratio of their corrected retention times, t_{R2}/t_{R1}.

The resolution between two peaks, 1 and 2, was characterized by the resolution factor R_s calculated from the retention times t_R and the peak widths at the baseline (*W*) according to the equation [19]

$$R_s = 2\,(t_{R2} - t_{R1}) / (W_2 + W_1)$$

From $R_s = 1$ two peaks are reasonably well separated.

RESULTS AND DISCUSSION

Qualitative analysis

Fig. 1 shows four chromatograms registered during the analysis of dioleoylglycerol urethane derivatives by chiral-phase HPLC. The first (A) refers to a mixture of the three *sn*-1,2-, *sn*-2,3- and *sn*-1,3-dioleoylglycerol stereoisomers isolated after chemical deacylation of peanut oil trioleoylglycerol. Chromatograms B and D were obtained with the mixture of *sn*-1,2(2,3)- and *sn*-1,3-dioleoylglycerols, respectively,

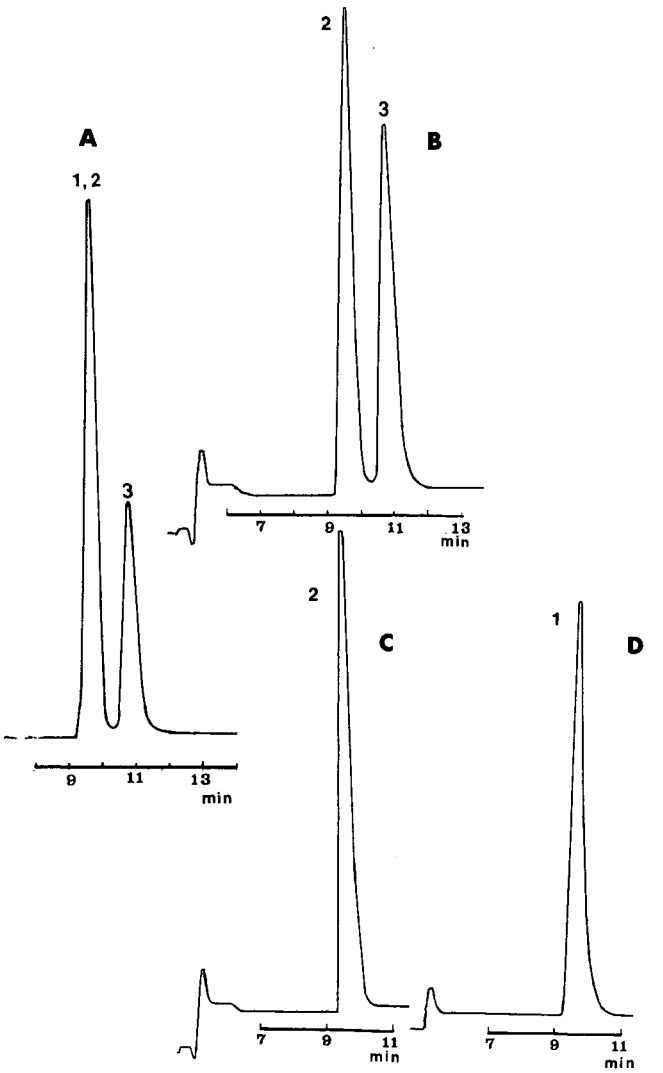

Fig. 1. Chiral-phase HPLC analysis as 3,5-dinitrophenyl isocyanate derivatives, of (1) *sn*-1,3-dioleoylglycerol (*sn*-1,3-18:1 18:1), (2) *sn*-1,2-18:1 18:1 and (3) *sn*-2,3-18:1 18:1. Mixture A contained the three isomers formed by partial chemical hydrolysis of peanut oil trioleoylglycerol. Mixture B was the enantiomeric *sn*-1,2(2,3)-dioleoylglycerol and D the *sn*-1,3-dioleoylglycerol isolated from mixture A. C was commercial *sn*-1,2-dioeoylglycerol. Mobile phase, hexane–ethylene dichloride–ethanol (80:20:1, v/v/v) at a flow-rate of 1 ml min^{-1}; analysis temperature, ambient (20.5°); detection, refractive index. Other HPLC conditions as in the text.

after separation by TLC on borate-impregnated silica plates of the mixture A diacylglycerols. Chromatogram C concerns the synthetic commercial *sn*-1,2-dioleoylglycerol. The mixture of the three stereoisomers (A) was resolved into two peaks with an approximate area ratio of 2:1. The mixture of *sn*-1,2(2,3)-isomers (B) was resolved

into two peaks with an area ratio of *ca.* 1:1. Comparison with chromatogram C shows that the retention time of the *sn*-1,2-dioloylglycerol corresponds to that of the first eluted peak in B, the second thus corresponding to *sn*-2,3-dioleoylglycerol. Comparison with chromatogram D demonstrates that, under the analytical conditions used, *sn*-1,3- and *sn*-1,2-dioleoylglycerol had approximately the same retention times (9,7 and 9.8 min from the injection point, respectively). They were not resolved. On the same chiral phase (Sumipax OA-4100), Takagi and Itabashi [9], using the same conditions as ours, partly separated *sn*-1,3- and *sn*-1,2-dioleoylglycerols (separation factor 1.04). The elution order was that which we observed, namely *sn*-1,3-, *sn*-1,2- and *sn*-2,3- according to increasing retention time. On another type of chiral phase, consisting of (*R*)-(+)-1-(1-naphthyl)ethylamine, which has a higher enantioselectivity, Itabashi *et al.* [11] obtained the complete resolution of *sn*-1,3- and *sn*-1,2-dioleoylglycerols (separation factor 1.23) with the same elution order as above.

As evident in chromatogram B, the two *sn*-1,2- and *sn*-2,3-stereoisomers of dioleoylglycerol were eluted as symmetrical and well separated peaks in less than 11 min after injection and with a resolution factor of 2.15. The observed elution order demonstrates that the *sn*-2,3-dioleoylglycerol showed a stronger diatereoisomeric interaction than the *sn*-1,2-isomer with the chiral stationary phase, in agreement with what was observed previously [11]. The earlier elution of the *sn*-1,3-dioleoylglycerol shows that this molecule is less polar than the other two, as was also shown by TLC on silica gel plates [20].

These results show that the analytical conditions used in this work were suitable for the separation of a mixture of enantiomers (*sn*-1,2- and *sn*-2,3-diacylglycerols) but not for the separation of the third possible *sn*-1,3-isomer. However, this drawback is not a problem in the stereospecific analysis of triacylglycerols as the two groups of diacylglycerols can be easily separated by TLC [14,21] or reversed-phase HPLC [13].

During their study on the separation of diacylglycerol enantiomers on the chiral column Sumipax OA-2100, Itabashi and Takagi [8] observed that the retention time of a diacylglycerol sample analysed consecutively several times varied over a range of 5–30 min. This situation could be due to a lack of equilibrium between the mobile phase and the chiral stationary phase, which may persist despite prolonged conditioning of the column. Moreover, the column stability is also influenced by the water content of the silica which binds the chiral compound and by the ambient temperature. Such variations were also observed in this work on another type of chiral column (Sumipax OA-4100). For example, with the dioleoylglycerol enantiomers the following extreme values of retention times were observed: for the *sn*-1,2-isomer 9.2 and 12.5 min and for the *sn*-2,3-isomer 10.3 and 14.0 min, under the same apparent analytical conditions. With other diacylglycerols the variations were more pronounced.

In spite of these difficulties, the analysis of a wide range of diacylglycerols produced by natural triacylglycerol hydrolysis could be performed and the elution order established by individual analyses of each molecular species.

In Table I are reported several characteristics observed in the analysis of twelve stereoisomers of mixed diacylglycerol urethane derivatives on the Sumipax OA-4100 chiral column. For each type of *sn*-1,2(2,3)-diacylglycerol the two enantiomers were well separated in less than 12 min from the injection time. The separation factor (α) between the two stereoisomers was identical (1.16) for the six diacylglycerols ana-

TABLE I

SOME CHROMATOGRAPHIC CHARACTERISTICS OBSERVED IN THE SEPARATION OF *sn*-1,2- AND *sn*-2,3-DIACYLGLYCEROL URETHANE DERIVATIVES BY CHIRAL-PHASE HPLC

Diacylglycerol[a]	Enantiomer[b]	*CN*[c]	*DB*[d]	*PN*[e]	t_R[f]	α[g]		R_s[h]	
						A	B	A	B
18:0 18:1	sn-1,2	36	1	34	6.9	1.16		2.09	
	sn-2,3				8.0				0.09[i]
16:0 18:1	sn-1,2	34	1	32	7.2	1.16	1.04	2.19	0.60
	sn-2,3				8.3		1.05		0.69
18:1 18:1	sn-1,2	36	2	32	7.2	1.16	1.00	2.15	0.05
	sn-2,3				8.4		1.01		0.09
16:0 18:2	sn-1,2	34	2	30	7.5	1.16	1.03	2.29	0.50
	sn-2,3				8.7		1.03		0.47
18:1 18:2	sn-1,2	36	3	30	7.6	1.16	1.02	1.97	0.31
	sn-2,3				8.8		1.02		0.25
18:2 18:2	sn-1,2	36	4	28	7.9	1.16	1.04	2.11	0.52
	sn-2,3				9.2		1.04		0.57

[a] *sn*-1,2(2,3)-Diacylglycerols represented by their two constituent fatty acids.
[b] *sn*-1,2- and *sn*-2,3-stereoisomers of the *sn*-1,2(2,3)-diacylglycerols.
[c] Carbon number = total acyl carbon atoms of the two constituent fatty acids.
[d] Total number of double bonds of the two constituent fatty acids.
[e] Partition number calculated according to $PN = CN - 2DB$.
[f] Retention time corrected for the column void volume.
[g] Separation factor between two peaks 1 and 2 represented by the ratio of their corrected retention times ($\alpha = t_{R2} / t_{R1}$); (A) between the two enantiomers *sn*-1,2 and *sn*-2,3 of the same diacylglycerol; (B) between the same enantiomer (*sn*-1,2 or *sn*-2,3) of two successive diacylglycerols as listed in the first column.
[h] Resolution factor between two peaks 1 and 2 according to $R_s = 2(t_{R2} - t_{R1}) / (w_2 + w_1)$, in which t_R represents the retention time (corrected or not) and w the peak width at the baseline.
[i] Resolution factor between *sn*-2,3-(18:0 18:1) and *sn*-1,2-(18:2 18:2).

lysed. Therefore, the separation efficiency was independent of the nature of the component fatty acids. Tagaki and Itabashi [9] also observed almost the same separation factor (1.15) between the *sn*-1,2- and *sn*-2,3-dioleoyl- and -dipalmitoylglycerols on the same chiral phase. On a more selective chiral phase, Itabashi *et al.* [11] observed a higher separation factor (1.44) but it was identical for dipalmitoyl- and dioleoylglycerols.

The resolution between the two optical isomers that we observed in this work varied from 1.97 to 2.29 according to the diacylglycerols, demonstrating very good resolution.

In addition to the separation between enantiomers due to the chiral selector, the separation of the different molecular species occurred according to chain length and unsaturation. This is due to the silica to which the chiral molecules are bound. The elution order was that of decreasing partition numbers (*PN*) or equivalent carbon number (*ECN*). When two isomers presented the same *PN* or *ECN*, the more unsaturated was eluted later. The observed elution order can be explained mainly by increasing polarity with increasing unsaturation and also by decreasing chain length.

Fig. 2 [log(retention volume) *versus* partition number] shows that for either type

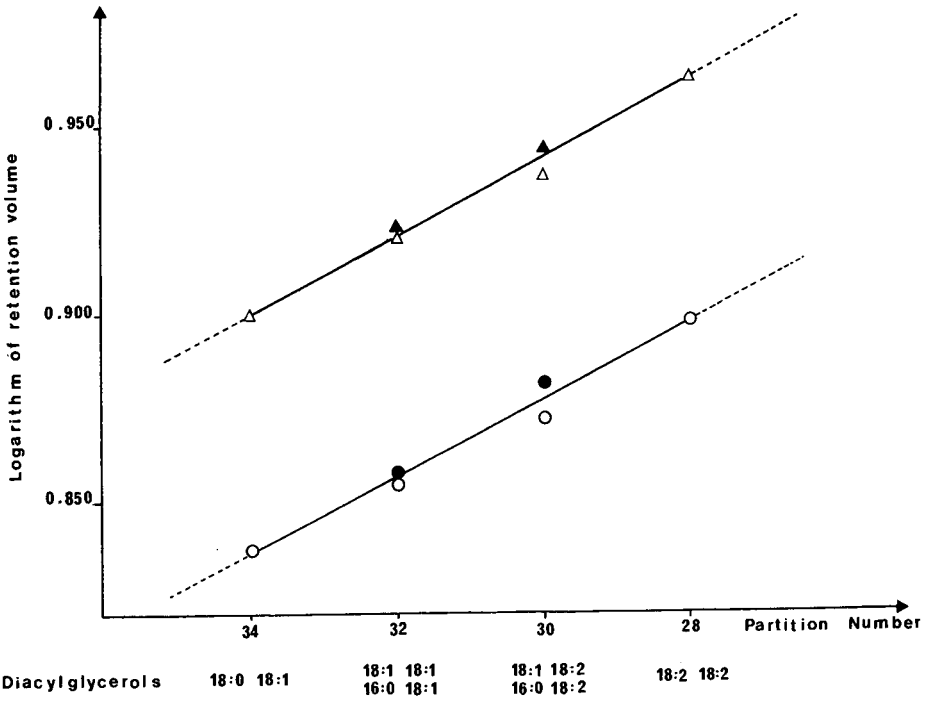

Fig. 2. Plot of logarithm of retention volume *versus* partition number of enantiomers of diacylglycerol urethane derivatives analysed by chiral-phase HPLC. Retention volume (ml) = retention time (min) corrected for the column void volume × solvent flow-rate (ml min^{-1}). Partition number: $PN = CN - 2DB$, where CN is the total number of acyl carbon atoms and DB the total number of double bonds of the two constituent fatty acids. △, *sn*-2,3-Enantiomer; ○, *sn*-1,2-enantiomer. Solid symbols for the more unsaturated and open symbols for the less unsaturated enantiomer (PN = 32 and 30).

of enantiomer an inverse proportionality was observed. A small variation was observed between the two critical pairs (16:0 18:1, 18:1 18:1 and 16:0 18:2, 18:1 18:2), the more unsaturated being eluted slightly later than the other (Table I). The two straight lines corresponding to the *sn*-1,2- and *sn*-2,3-isomers were parallel and related to each other by the equation

$$\log V_R \text{ (}sn\text{-2,3)} = \log V_R \text{ (}sn\text{-1,2)} + 0.065$$

where V_R is the retention volume. Extrapolation of the straight lines allows the retention volumes of known diacylglycerol isomers to be deduced or conversely the partition numbers of diacylglycerol isomers to be deduced from their retention volumes. Moreover, the above equation allows the retention volume of an enantiomer to be calculated when that of the other enantiomer is experimentally known.

The same observation was made by Itabashi and Takagi [8] in the separation of the enantiomers of dilauroyl-, dimyristoyl-, dipalmitoyl-, distearoyl- and dioleoylglycerols on Sumipax OA-2100 and OA-4100 chiral columns, and by Itabashi *et al.* [11] for natural diacylglycerols from linseed oil on a A-K03 chiral column (Sumitomo).

On a non-chiral silica column the same characteristics of elution were previously observed [22], indicating that it is a property of the silica support in the chiral columns.

Table I and Fig. 2 also show that the *sn*-1,2- and *sn*-2,3-enantiomers of two diacylglycerols exhibiting the same *PN* or *ECN* were virtually unseparated (separation factor $\approx$ 1 and resolution factor $\approx$ 0). Changing the mobile phase could possibly resolve the critical pairs by increasing the column efficiency, as was observed by Itabashi *et al.* [11] on another chiral phase.

For the *sn*-1,2- or *sn*-2,3-enantiomers differing by two carbon atoms (18:0 18:1 and 16:0 18:1) or by one double bond (16:0 18:1 and 16:0 18:2), the observed separation and resolution factors were low. The two molecular species were poorly separated. The same was true for the enantiomers showing an identical carbon number and an increasing degree of unsaturation (*e.g.*, 18:0 18:1, 18:1 18:1, 18:1 18:2 and 18:2 18:2 with respective *PN* or *ECN* of 34, 32, 30 and 28). Two molecular species differing in one double bond were poorly separated. In constrast when the *PN* differed by 4 units (four carbon atoms or two double bonds), the corresponding enantiomers were completely separated (*e.g.*, the two pairs 18:0 18:1, 18:1 18:2 and 18:1 18:1, 18:2 18:2 with respective resolution factors of 1.39 and 1.33 for the *sn*-1,2-isomers). The same was still more true when the molecular species differed by three double bonds (*e.g.*, the pair 18:0 18:1, 18:2 18:2 with respective resolution factors of 1.94 and 2.07 for the *sn*-1,2- and *sn*-2,3-isomers). These last values are very close to the average resolution factor observed between the two enantiomers of an *sn*-1,2(2,3)-diacylglycerol (between 1.97 and 2.29, as indicated in Table I). This means that the separation between two optical isomers *sn*-1,2- and *sn*-2,3- is identical with that between the *sn*-1,2- or the *sn*-2,3-enantiomers of two diacylglycerols differing by three double bonds. The same could probably be true with diacylglycerols differing by six carbon atoms or any combination of chain length and unsaturation to provide partition numbers differing by 6 units.

The different parameters calculated in the separation on the Sumipax OA-4100 chiral column of the twelve stereoisomers listed in Table I and partly reported in this table are different of those reported by Itabashi and Takagi [8] with the Sumipax OA-2100 chiral column. The chiral selector of this last column was adapted to the separation of monoacylglycerol enantiomers. However, the separation of diacylglycerol enantiomers required the use of three 25-cm columns in series and the retention times were increased. Recently, the same group [9] succeeded in separating diacylglycerol enantiomers on the same type of column as used in this work. With the more enantioselective A-K03 column Itabashi *et al.* [11] observed higher separation factors between enantiomers (1.23 compared with 1.16).

In Table II the twelve stereoisomers are listed according to their elution order and the separation and resolution factors between each peak and the preceding one are reported.

All the *sn*-1,2-enantiomers of the six diacylglycerols studied (Table I) were eluted earlier than their *sn*-2,3-isomers, a property also observed with still more complex mixtures of natural diacylglycerols [11]. In addition to the usual critical pairs whose enantiomers were eluted together (16:0 18:1, 18:1 18:1 and 16:0 18:2, 18:1 18:2), two stereoisomers were not easily separated, namely two different enantiomers, *sn*-1,2-(18:2 18:2) and *sn*-2,3-(18:0 18:1), with respective partition numbers of 28 and 34.

TABLE II

SEPARATION (α)[a] AND RESOLUTION FACTORS (R_s)[b] OF DIACYLGLYCEROL ENANTIOMER URETHANE DERIVATIVES ANALYSED BY CHIRAL-PHASE HPLC

Isomer	Parameter	Diacylglycerol[c]					
		18:0 18:1	16:0 18:1	18:1 18:1	16:0 18:2	18:1 18:2	18:2 18:2
sn-1,2-[d]	α		1.04	1.00	1.03	1.02	1.04
	R_s		0.60	0.05	0.50	0.31	0.52
sn-2,3-[d]	α	1.01	1.05	1.01	1.03	1.02	1.04
	R_s	0.09	0.69	0.09	0.47	0.25	0.57

[a] α = Separation factor between two successive peaks expressed as the ratio of their respective retention times corrected for the column void volume.

[b] R_s = resolution factor between two successive peaks 1 and 2 calculated from their respective retention times (t_R) and their widths (w) at the baseline according to $R_s = 2(t_{R2} - t_{R1}) / (w_2 + w_1)$.

[c] *sn*-1,2(2,3)-Diacylglycerols.

[d] *sn*-1,2- and sn-2,3-enantiomers of the diacylglycerols listed according to elution order.

Between two successive peaks, the separation factor was very low, hardly greater than 1, as was the resolution factor, which lay between 0.05 (peaks eluted together) and 0.60 (half-separated peaks). Stereospecific analysis of such a complex mixture of diacylglycerols cannot be correctly achieved on this type of column. This is generally also true for simpler mixtures of *sn*-1,2(2,3)-diacylglycerols produced by hydrolysis of natural oil triacylglycerols. When these triacylglycerols consist of three different fatty acids (*e.g.*, 16:0 18:1 18:2), six stereoisomers have to be properly separated to estimate their proportions accurately. When only two different fatty acids are present (*e.g.*, 18:1 18:1 18:2 or 18:1 18:2 18:2), four stereoisomers have to be separated.

We tried to analyse three mixtures of *sn*-1,2(2,3)-diacylglycerols formed by hydrolysis of the three peanut oil triacylglycerols cited above in parentheses. In the first instance (three different fatty acids) only two peaks (out of six) were readily distinguishable. Shoulders showed that minor peaks were partly separated. In the second instance (only two different fatty acids), two groups of two poorly separated peaks were registered on the chromatogram. Such poor resolutions preclude an accurate determination of enantiomer composition.

The resolution can probably be improved by varying the analytical conditions such as column length, solvent polarity and analysis temperature. However, the retention times probably increase considerably, as was observed by others [9]. The use of a chiral column with higher enantioselectivity can improve the resolution of enantiomers [11], although it was not evident when analysing complex mixtures of natural diacylglycerol enantiomers (from corn oil, linseed oil and menhaden oil). The alternative we preferred was to proceed to a previous fractionation (coupled with purification) of the diacylglycerol derivatives by reversed-phase HPLC to obtain much simpler mixtures with short retention times. These simple mixtures were easily resolved into their constituent enantiomers by chiral-phase HPLC, as shown in Fig. 3.

Quantitative analysis

Good separations between enantiomers such those reported in Fig. 3 are a

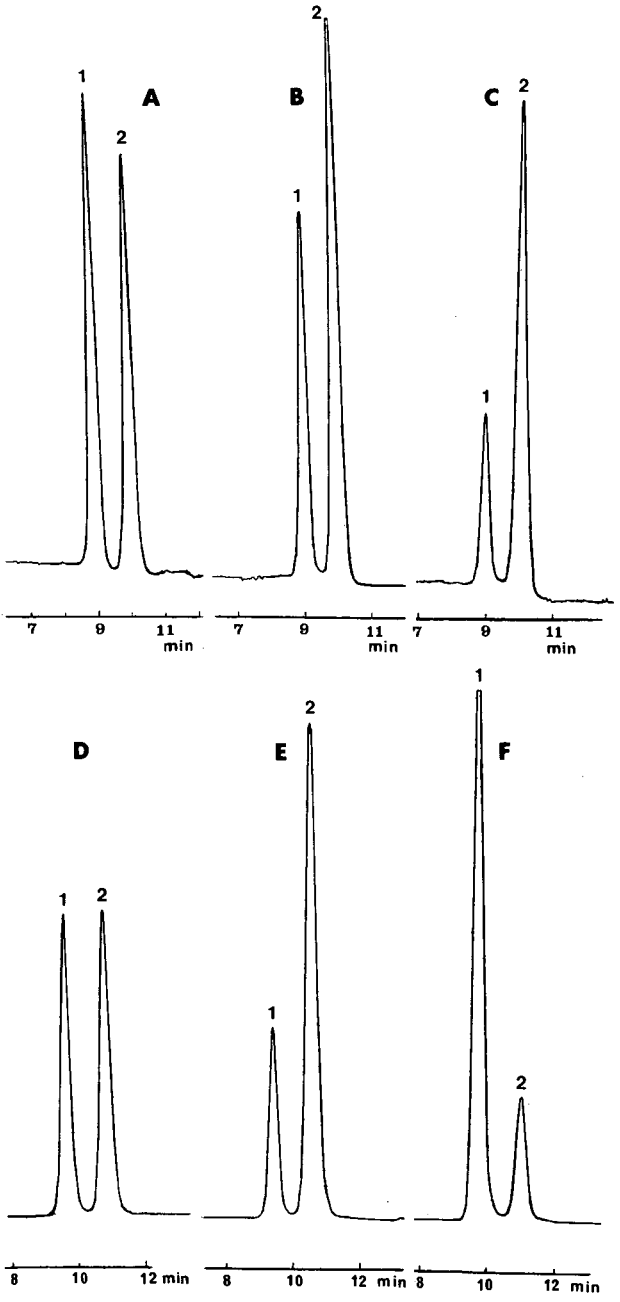

Fig. 3. HPLC separation of diacylglycerol enantiomers as 3,5-dinitrophenyl isocyanate derivatives on the chiral OA-4100 column. Diacylglycerols derived from peanut oil and cottonseed oil triacylglycerol by chemical (B, C, E and F) and enzymatic (A, D) hydrolysis. They were previously fractionated by reversed-phase HPLC. (A) 18:0 18:1; (B) 16:0 18:1; (C) 18:1 18:1; (D) 16:0 18:2; (E) 18:1 18:2; (F) 18:2 18:2. Peaks: 1 = *sn*-1,2-Enantiomer and 2 = *sn*-2,3-enantiomers in each chromatogram. Chromatograms B, C, E and F correspond to enantiomeric diacylglycerols B, C, E and F reported in Table III. Detection, UV absorption (254 nm). Other conditions as in Fig. 1.

prerequisite for compositional analysis. The second condition is quantitative detection of the molecules eluted by HPLC. This could be checked with commercial standard mixtures. As commercial standards of diacylglycerol urethane derivatives were not available, the quantitative aspects of their detection were studied in another way. The diacylglycerol derivatives analysed by chiral-phase HPLC are generally detected by their UV absorption [8,9,11], a very sensitive mode of detection. As these derivatives were quantitatively detected by their refractive indices when previously separated by reversed-phase HPLC [13], we compared, in the present enantiomer analysis, peak areas registered after detection by a variable-wavelength UV detector and a

TABLE III

QUANTITATIVE ANALYSIS OF ENANTIOMERS OF *sn*-1,2(2,3)-DIACYLGLYCEROL URETHANE DERIVATIVES BY CHIRAL-PHASE HPLC DETECTED BY THEIR REFRACTIVE INDICES OR UV ABSORPTION

Oil	Hydrolysed triacylglycerol[a]	*sn*-1,2(2,3)-Diacylglycerol[b]	Enantiomer[c]	Peak area (%)[d]		Variation (%)[e]
				RI	UV	
Peanut	16:0 18:1 18:1	18:1 18:1	*sn*-1,2-	37.6	38.2	1.6
			sn-2,3-	62.4	61.8	
		16:0 18:1	*sn*-1,2-	58.9	59.0	0.2
			sn-2,3-	41.1	41.0	
	18:1 18:1 18:1	18:1 18:1	*sn*-1,2-	50.1	49.6	1.0
			sn-2,3-	49.9	50.4	
	16:0 18:1 18:2	18:1 18:2	*sn*-1,2-	38.0	39.0	2.6
			sn-2,3-	62.0	61.0	
		16:0 18:2	*sn*-1,2-	68.5	66.0	7.3
			sn-2,3-	31.5	34.0	
		16:0 18:1 (B)[f]	*sn*-1,2-	37.3	35.5	5.1
			sn-2,3-	62.7	64.5	
	18:1 18:1 18:2	18:1 18:2	*sn*-1,2-	57.6	55.8	4.3
			sn-2,3-	42.4	44.3	
		18:1 18:1 (C)[f]	*sn*-1,2-	22.9	23.6	3.0
			sn-2,3-	77.1	76.4	
	18:1 18:2 18:2	18:2 18:2 (F)[f]	*sn*-1,2-	82.2	81.8	2.2
			sn-2,3-	17.8	18.2	
		18:1 18:2 (E)[f]	*sn*-1,2-	22.3	24.3	4.1
			sn-2,3-	77.7	75.7	
Cottonseed	16:0 18:1 18:2	18:1 18:2	*sn*-1,2-	48.2	47.6	1.3
			sn-2,3-	51.8	52.4	
		16:0 18:2	*sn*-1,2-	49.9	50.1	0.4
			sn-2,3-	50.1	49.9	
		16:0 18:1	*sn*-1,2-	53.8	53.2	1.3
			sn-2,3-	46.2	46.8	

[a] Triacylglycerols isolated from peanut oil and cottonseed oil by coupled argentation TLC–reversed-phase HPLC and deacylated by Grignard reagent.

[b] *sn*-1,2(2,3)-Diacylglycerols isolated from hydrolysis products by borate-impregnated silica TLC and fractionated by reversed-phase HPLC as urethane derivatives.

[c] *sn*-1,2- and *sn*-2,3-diacylglycerol derivatives separated by chiral-phase HPLC.

[d] Peak areas (%) of the two enantiomers detected by their refractive indices (RI) or UV absorption (UV).

[e] Maximum % variation between the two series of figures.

[f] The enantiomeric diacylglycerols B, C, E and F correspond to chromatograms B, C, E and F in Fig. 3.

differential refractometer. Samples were prepared from chemical hydrolysis products of peanut oil and cottonseed oil triacylglycerols. The *sn*-1,2(2,3)-diacylglycerols isolated by TLC were derivatized and fractionated by reversed-phase HPLC [13] according to chain length and unsaturation. The two enantiomers of the diacylglycerol derivatives were separated by chiral-phase HPLC, first detected by means of the differential refractometer (sensitivity 25–50 μg per peak, attenuation 8), and then detected, under strictly the same analytical conditions, by the UV detector (sensitivity 1 μg per peak, attenuation 2 a.u.f.s.).

The percentages of the two enantiomers were calculated from the peak areas. The two series of values reported in Table III were compared and the maximum percentage variation was calculated from the difference observed for the lower percentages. In most instances the variation between the two figures was very low (< 5%). The average variation was 2.6%. Relatively high variations were observed in the analysis of the three diacylglycerol mixtures formed by deacylation of peanut oil 16:0 18:1 18:2 (7.3% maximum). This is probably due to a defective peak integration in this instance, as the same three diacylglycerol mixtures formed by deacylation of the same triacylglycerol but isolated from cottonseed oil (last column) exhibited much smaller differences (1.3% maximum).

As detection by refractometry was found to be quantitative, at least for the enantiomer mixtures and in the range of the diacylglycerols checked [13], we can reasonably conclude that detection of the separate enantiomers by the UV detector, comparable to that by refractometry, is also quantitative. Peak areas so determined can be used to calculate the percentages of the two enantiomers in the mixture. As the two enantiomers contain the same two fatty acids, peak-area percentages also represent weight or molar percentages.

Another proof of the accuracy of the enantiomer determination can be found in the analysis of the *sn*-1,2(2,3)-diacylglycerols formed by chemical deacylation of trioleoylglycerol (18:1 18:1 18:1) whose racemic character is obligatory. The values found with both types of detection were very close to the expected values of 50:50.

Another sample was unexpectedly found to be racemic in these analyses. This was the diacylglycerol 16:0 18:2 produced by hydrolysis of the cottonseed oil 16:0 18:1 18:2, whereas this did not occur with the identical triacylglycerol isolated from peanut oil, whose enantiomer proportion was close to 2:1. This shows that depending on its origin, a given triacylglycerol can present different stereospecific distributions of the same three fatty acids between the three positions of the glycerol moiety. These differences probably reflect species specificity in triacylglycerol biosynthesis in seeds.

The results obtained with cottonseed oil 16:0 18:1 18:2 in this work were different from those obtained in another study using Brockerhoff's method [23]. The percentages of the two 16:0 18:2 diacylglycerol enantiomers were found to be *ca.* 40 and 60 instead of *ca.* 50 and 50 in this work. Several features may be responsible for this difference. First, the cottonseed oil sample used to prepare the triacylglycerol was not the same in both studies. This could mean that in the same vegetable species, stereospecific distribution of fatty acids in the glycerol molecules can vary according to particular factors. Second, the method used for stereospecific analysis of the triacylglycerols was different in the two instances. Comparison between the two methods would be of great interest.

The results obtained in this work with a relatively wide range of mixed di-

acylglycerols confirm and extend those reported by Takagi and Itabashi [9] for racemic simple diacylglycerols, by Tagaki and Suzuki [10] for synthetic mixed diacylglycerols and by Itabashi *et al.* [11] for natural complex diacylglycerol mixtures. They show that accurate stereospecific analyses of natural triacylglycerols can be achieved by chiral-phase HPLC provided that the original complex diacylglycerol mixtures were divided into simpler mixtures by reversed-phase HPLC fractionation [13].

ACKNOWLEDGEMENT

We are grateful to J. Gresti for his skilful assistance in the GC and HPLC analyses and in the chromatogram reproduction.

REFERENCES

1 C. Litchfield, *Analysis of Triglycerides*, Academic Press, New York, London, 1972.
2 H. Brockerhoff, *J. Lipid Res.*, 6 (1965) 10.
3 H. Brockerhoff, *J. Lipid Res.*, 8 (1967) 167.
4 P. Michelsen and G. Odham, *J. Chromatogr.*, 331 (1985) 295.
5 P. Michelsen, E. Aronsson, G. Odham and B. Akesson, *J. Chromatogr.*, 350 (1985) 417.
6 P. Laakso and W. W. Christie, *Lipids*, 25 (1990) 349.
7 N. Ôi and H. Kitahara, *J. Liq. Chromatogr.*, 9 (1986) 511.
8 Y. Itabashi and T. Takagi, *J. Chromatogr.*, 402 (1987) 257.
9 T. Takagi and Y. Itabashi, *Lipids*, 22 (1987) 596.
10 T. Tagaki and T. Suzuki, *J. Chromatogr.*, 519 (1990) 237.
11 Y. Itabashi, A. Kuksis, L. Marai and T. Tagaki, *J. Lipid Res.*, 31 (1990) 1711.
12 Y. Itabashi, A. Kuksis and J. J. Myher, *J. Lipid Res.*, 31 (1990) 2119.
13 B. G. Semporé and J. A. Bézard, *J. Chromatogr.*, 547 (1991) 89.
14 M. Yurkowski and H. Brockerhoff, *Biochim. Biophys. Acta*, 125 (1966) 55.
15 W. W. Christie and J. H. Moore, *Biochim. Biophys. Acta*, 176 (1969) 445.
14 J. Krüger, H. Rabe, G. Reichmann and B. Rüstow, *J. Chromatogr.*, 307 (1984) 387.
15 P. J. Ryan and T. W. Honeyman, *J.Chromatogr.*, 331 (1985) 177.
16 J. A. Bézard and M. A. Ouédraogo, *J. Chromatogr.*, 196 (1980) 279.
17 H. T. Slover and E. Lanza, *J. Am. Oil Chem.Soc.*, 58 (1979) 933.
18 A. Ros, *J. Gas Chromatogr.*, 3 (1965) 252.
19 L. R. Snyder and J. J. Kirkland, *Introduction to Modern Liquid Chromatography*, Wiley, New York, 2nd ed. 1979.
20 A. Kuksis, in H. K. Mangold (Editor), *CRC Handbook of Chromatography*, Vol. I, CRC Press, Boca Raton, FL, 1984, p. 381.
21 A. E. Thomas, III, J. E. Scharoun and H. Ralston, *J. Am. Oil Chem. Soc.*, 42 (1965) 789.
22 R. D. Plattner, G. F. Spencer and R. Kleiman, *J. Am. Oil Chem. Soc.*, 54 (1977) 511.
23 J. Bézard, M. A. Ouédraogo and G. Semporé, *Rev. Fr. Corps Gras*, 37 (1990) 171.

Journal of Chromatography, 557 (1991) 241–253
Elsevier Science Publishers B.V., Amsterdam

CHROM. 23 411

Capillary gas chromatography of C_5–C_{13} branched alkynes on squalane and liquid crystal stationary phases

LADISLAV SOJÁK*
Chemical Institute, Comenius University, 842 15 Bratislava (Czechoslovakia)
PAVEL FARKAŠ
Food Research Institute, 825 09 Bratislava (Czechoslovakia)
IVAN OSTROVSKÝ
Chemical Institute, Comenius University, 842 15 Bratislava (Czechoslovakia)
JAROSLAV JANÁK
Institute of Analytical Chemistry, Czechoslovak Academy of Sciences, 642 11 Brno (Czechoslovakia)
and
JACQUES R. CHRÉTIEN
Laboratoire de Chimiométrie, Université d'Orléans, 45067 Orléans Cedex 2, and Institut de Topologie et de Dynamique des Systèmes, Université Paris VII, associé au CNRS, 75005 Paris (France)

ABSTRACT

The retention behaviour of 49 C_5–C_{13} branched alkynes, including all 36 methyl- and dimethylalkynes up to C_8, were studied by capillary gas chromatography on squalane and 4-*n*-pentylacetophenone-O-(4-*n*-pentyloxybenzoyl)oxime liquid crystal as stationary phases. An additive method of retention increments based on the analogy of retention in homologous series of the corresponding branched alkynes and alkenes, showing an average precision of 1 index unit, was suggested for the calculation of retention indices of branched alkynes and alkynes with a methyl group on the α-carbon in particular. Both regularities and anomalies in the retention behaviour of branched alkynes are discussed with regard to retention–structures correlations. The advantages of liquid crystals as stationary phases for the separation of isomers with close physico-chemical characteristics are pointed out.

INTRODUCTION

Alkynes are intermediates in a number of organic syntheses. They are produced at low concentrations as the by-products of processes of catalytic and thermal conversions of hydrocarbons and, owing to their high reactivity, they can affect further processing of the products.

Capillary gas chromatography of straight-chain alkynes has been studied in considerable detail for compounds with a wide range of carbon numbers, up to C_{20} [1–9]. However, the retention behaviour of branched-chain alkynes has not been studied. Only Hively and Hinton [1] have published, among the retention indices of other hydrocarbons, also those of 4-methyl-1-pentyne and 5-methyl-1-hexyne on

0021-9673/91/$03.50

squalane. Starting from previous studies of the retention behaviour of hydrocarbons of various types, the aim of this work was to characterize the retention behaviour of branched alkynes on squalane and 4-*n*-pentylacetophenone(O-4-*n*-pentyloxybenzoyl) oxime (PBO) liquid crystal, *i.e.*, in systems in which we earlier studied retention behaviour of straight-chain alkynes [2].

EXPERIMENTAL

The PBO nematic liquid crystal, having a mesophase range of 63–94°C and possible supercooling to 27°C, was synthesized by Dr. W. Weissflog, Martin Luther University (Halle, Germany).

Model mixtures of branched alkynes were prepared from 24 different C_5–C_{13} branched alkynes which were prepared by acetylene alkylation in liquid ammonia for the less crowded compounds or donated by Dr. L. Miginiac (University of Poitiers, France). A further fifteen C_7 and C_8 branched alkynes were prepared as mixed standards by the methylene group insertion reaction (MIR) [10] in molecules of *n*-alkynes and branched alkynes.

Model mixtures of alkynes were separated on a 107 m × 0.25 mm I.D. glass capillary column coated with squalane with a film thickness of 0.40 μm at an inlet pressure of 0.26 MPa and a linear velocity of hydrogen carrier gas of 36 cm s^{-1}, with an efficiency $n = 360\,000$, or $n_{eff} = 260\,000$ plates for 1-nonyne with $k = 5.4$ at 80°C. The parameters of the capillary column with the PBO liquid crystal were 106 m × 0.25 mm I.D. inlet pressure of hydrogen carrier gas 0.20 MPa and linear velocity was 21 cm s^{-1}, with an efficiency $n = 360\,000$ or $n_{eff} = 214\,000$ plates for 1-nonyne with $k = 1.5$ at 80°C.

An adapted Perkin-Elmer F-11 gas chromatograph and a Fractovap 4200 (Carlo Erba) with flame ionization detectors were used to measure retention characteristics. The thermostat temperature was maintained with a precision of ±0.1°C with a calibrated glass thermometer. Samples were injected onto the column with a 1-μl syringe with the aid of a splitter with a splitting ratio of 1:100 so that a sample size range of 10^{-9}–10^{-10} g for of each component could be obtained. Retention times were measured from the methane peak maximum with a precision of 0.1 s. The measurement repeatability of retention indices expressed in terms of the standard deviation of the arithmetic mean was ±0.03 index unit (i.u.) on squalane and ±0.05 i.u. on PBO.

RESULTS AND DISCUSSION

Table I shows the retention indices of C_5–C_{13} branched alkynes and their temperature dependence measured on squalane and PBO liquid crystal with synthesized individual standards (denoted s) or mixed products from MIR (r). Table I also gives the retention indices of alkynes up to C_8 calculated for a temperature of 40°C (c). Table I is supplemented with retention indices of C_6–C_{13} straight-chain alkynes measured under the same conditions as those used previously [2]. They serve for comparison of the retention data of branched- and straight-chain alkynes or were used to calculate the retentions of branched alkynes.

The comparison of the measured and published [1] retention indices for 4-

TABLE I

RETENTION INDICES AND THEIR TEMPERATURE COEFFICIENTS dI/dT FOR C_5–C_{13} ALKYNES ON SQUALANE (SQ) AND PBO LIQUID CRYSTAL

The calculated values of retention indices of branched alkynes (c) are valid for the temperature of 40°C. dI^{SQ}/dT values of C_5–C_8 alkynes were measured in the temperature range 40–60°C and those of C_9–C_{13} alkynes at 70–90°C; dI^{PBO}/dT values of C_5–C_8 alkynes were measured at 40–60°C, those of C_9–C_{13} alkynes at 80–90°C.

Alkyne		I_{80}^{SQ}	dI^{SQ}/dT	I_{80}^{PBO}	dI^{PBO}/dT	ΔI^{PBO-SQ}
3-Methyl-1-butyne	s	435.5	0.00	512.8	−0.07	77.6
3,3-Dimethyl-1-butyne	s	467.1	0.00	525.9	0.01	58.9
3-Methyl-1-pentyne	c	539.4	–	–	–	–
4-Methyl-1-pentyne	s	550.3	0.02	633.2	0.04	82.9
1-Hexyne	s	583.4	0.01	678.0	0.08	94.6
3,3-Dimethyl-1-pentyne	c	589.3	–	–	–	–
4-Methyl-2-pentyne	c	594.2	–	–	–	–
4,4-Dimethyl-1-pentyne	r	600.3	0.09	–	–	–
4,4-Dimethyl-2-pentyne	s	611.6	−0.12	658.4	0.20	46.8
3-Hexyne	s	623.1	−0.09	692.8	0.05	69.7
3,4-Dimethyl-1-pentyne	r	623.5	0.07	–	–	–
3-Methyl-1-hexyne	r	634.3	0.02	–	–	–
2-Hexyne	s	640.3	−0.04	718.9	0.05	78.6
5-Methyl-1-hexyne	r	653.6	0.05	–	–	–
4-Methyl-1-hexyne	r	659.3	0.07	–	–	–
2-Methyl-3-hexyne	s	660.2	−0.12	713.2	0.15	53.0
2,2-Dimethyl-3-hexyne	s	674.6	−0.15	707.1	0.17	32.5
3,3-Dimethyl-1-hexyne	c	678.8	–	–	–	–
1-Heptyne	s	683.6	0.01	779.1	0.06	95.5
2,5-Dimethyl-3-hexyne	s	688.9	−0.16	723.2	0.10	34.2
3,5-Dimethyl-1-hexyne	c	689.6	–	–	–	–
4-Methyl-2-hexyne	c	689.8	–	–	–	–
2,2,5-Trimethyl-3-hexyne	s	695.6	−0.18	707.8	0.05	12.3
5,5-Dimethyl-1-hexyne	c	699.6	–	–	–	–
5-Methyl-2-hexyne	s	701.2	−0.03	771.0	0.22	69.8
3-Heptyne	s	717.3	−0.07	782.4	0.09	65.1
4.4-Dimethyl-1-hexyne	c	717.9	–	–	–	–
4,4-Dimethyl-2-hexyne	s	719.5	−0.09	767.1	0.32	47.7
3,4-Dimethyl-1-hexyne	c	726.7	–	–	–	–
3-Methyl-1-heptyne	r	730.1	0.01	–	–	–
4,5-Dimethyl-1-hexyne	c	735.1	–	–	–	–
5,5-Dimethyl-2-hexyne	r	740.0	0.00	–	–	–
2-Heptyne	s	743.0	−0.03	820.4	0.16	77.4
4-Methyl-1-heptyne	r	749.9	0.05	–	–	–
6-Methyl-1-heptyne	r	749.9	0.03	–	–	–
2-Methyl-3-heptyne	s	752.6	−0.10	800.3	0.12	47.7
5-Methyl-1-heptyne	r	759.7	0.07	–	–	–
5-Methyl-3-heptyne	r	756.9	−0.07	–	–	–
4,5-Dimethyl-2-hexyne	r	760.4	−0.03	–	–	–
6-Methyl-3-heptyne	s	776.7	−0.04	833.4	0.22	55.9
4-Methyl-2-heptyne	r	780.6	−0.07	–	–	–
1-Octyne	s	783.0	0.02	879.4	0.06	96.4
4,4,5-Trimethyl-2-hexyne	s	806.01	−0.02	849.7	0.38	43.6
4,4-Dimethyl-2-heptyne	s	806.5	−0.12	850.4	0.31	43.9
6-Methyl-2-heptyne	r	807.8	−0.02	–	–	–
5-Methyl-2-heptyne	r	811.1	0.00	–	–	–

(*Continued on p. 244*)

TABLE I (*continued*)

Alkyne		I_{80}^{SQ}	dI^{SQ}/dT	I_{80}^{PBO}	dI^{PBO}/dT	ΔI^{PBO-SQ}
4-Octyne	s	811.3	−0.05	872.1	0.14	60.8
6,6-Dimethyl-3-heptyne	s	813.6	−0.01	856.6	0.35	43.0
5,5,4-Trimethyl-2-hexyne	s	816.5	0.01	863.2	0.45	46.7
3-Octyne	s	818.0	−0.06	880.5	0.17	62.5
2,2,6-Trimethyl-3-heptyne	s	822.7	−0.09	838.6	0.30	15.9
4-Ethyl-4-methyl-2-hexyne	s	825.3	−0.06	873.1	0.40	47.8
2-Octyne	s	842.3	−0.04	920.7	0.18	68.4
2,2,6,6-Tetramethyl-3-heptyne	s	857.4	−0.03	861.6	0.41	4.3
1-Nonyne	s	883.3	0.02	980.2	0.08	96.9
2,2,5-Trimethyl-5-ethyl-3-heptyne	s	905.8	−0.06	896.0	0.26	−9.8
4-Nonyne	s	910.4	−0.04	967.7	0.20	57.3
2,2,5,6,6-Pentamethyl-3-heptyne	s	914.4	−0.01	908.8	0.41	−5.6
3-Nonyne	s	916.0	−0.06	980.2	0.18	64.2
2,7-Dimethyl-4-octyne	s	929.6	0.00	973.5	0.38	43.9
2-Nonyne	s	941.0	−0.03	1019.1	0.20	78.1
2,2,5,5,6,6-Hexamethyl-3-heptyne	s	956.4	0.04	938.7	0.47	−17.7
1-Decyne	s	983.2	0.02	1080.8	0.18	97.6
2,2,7,7-Tetramethyl-4-octyne	s	1003.4	0.08	1024.5	0.52	21.1
4-Decyne	s	1007.3	−0.03	1067.5	0.41	60.2
5-Decyne	s	1008.2	−0.02	1064.9	0.48	56.7
3-Decyne	s	1014.3	−0.05	1079.0	0.36	64.7
2-Decyne	s	1041.1	−0.03	1120.6	0.34	79.5
1-Undecyne	s	1083.3	0.02	1181.4	0.14	98.1
5-Undecyne	s	1104.2	−0.01	1161.5	0.53	57.3
4-Undecune	s	1104.8	−0.02	1164.7	0.48	59.9
3-Undecyne	s	1113.5	−0.04	1178.3	0.44	64.8
2-Undecyne	s	1140.9	−0.02	1220.7	0.35	79.8
1-Dodecyne	s	1183.3	0.02	1282.2	0.15	98.9
6-Dodecyne	s	1199.6	0.00	1258.2	0.58	58.6
5-Dodecyne	s	1201.1	−0.02	1258.2	0.58	57.1
4-Dodecyne	s	1203.3	−0.03	1263.1	0.50	59.8
3-Dodecyne	s	1212.5	−0.05	1277.6	0.44	65.1
2-Dodecyne	s	1240.8	−0.03	1321.0	0.36	80.2
1-Tridecyne	s	1283.4	0.02	1382.9	0.15	99.5
6-Tridecyne	s	1295.6	0.01	1353.4	0.64	57.8
5-Tridecyne	s	1298.5	0.01	1355.8	0.62	57.3
4-Tridecyne	s	1301.5	−0.01	1361.6	0.53	60.1
3-Tridecyne	s	1311.9	−0.04	1377.1	0.44	65.2
2-Tridecyne	s	1340.6	−0.02	1421.2	0.38	80.6

methyl-1-pentyne and 5-methyl-1-hexyne on squalane suggests that the retention indices measured by us are lower by 2.6 and 2.1 i.u., respectively. This is in accord with our previous finding that for unsaturated hydrocarbons the retention indices from ref. 1 are systematically higher, *e.g.*, for C_6–C_8 aromatic hydrocarbons by 3.3 i.u. on average.

Retention of branched alkynes on squalane

As we had only a limited number of standard alkynes at our disposal for characterizing the retention behaviour of branched alkynes, we studied the possibility of calculating their retentions. As far as the compounds with more functional groups in

their molecules such as branched alkynes are concerned, their retention indices may be calculated from the sum of contributions of homomorphic factors of separate functional groups under the assumption that they do not affect one another [11]. The measured values of retention indices of branched alkynes were used to investigate the additivity of contributions of functional groups of branched alkynes, *i.e.*, of triple bond and methyl branching, on the basis of known retention indices of *n*-alkynes [2] and of branched alkanes [12] on squalane. We started from the concept that the branched alkyne molecule consists of structural elements of the coresponding *n*-alkyne and branched alkane. The homomorphic factor which characterizes the contribution of the functional groups to the retention index is defined as follows [12]:

$$H = I_i - I_z \tag{1}$$

where I_i is the retention index of sample compound i and I_z is the retention index of the corresponding *n*-alkane with the same carbon skeleton on the given stationary phase and at the given temperature. H values for branched alkynes are given by

$$H_{\text{alkyne}} = \mathrm{H}_{n\text{-alkyne}} + H_{\text{branched alkane}} \tag{2}$$

On the basis of eqns. 1 and 2, the calculated values of the retention indices for 36 C_5–C_8 branched alkynes agreed with those measured on squalane in the range from −64.7 to +2.3 i.u. The difference between the measured and the calculated retention indices of branched alkynes on squalane, $\sigma I = I_m - I_c$, depends on the position of the methyl group with respect to the triple bond, on the position of the triple bond in the chain and on the number of carbon atoms in the molecule of the particular alkyne.

Fig. 1 illustrates the dependences of σI on the position of one and two methyls

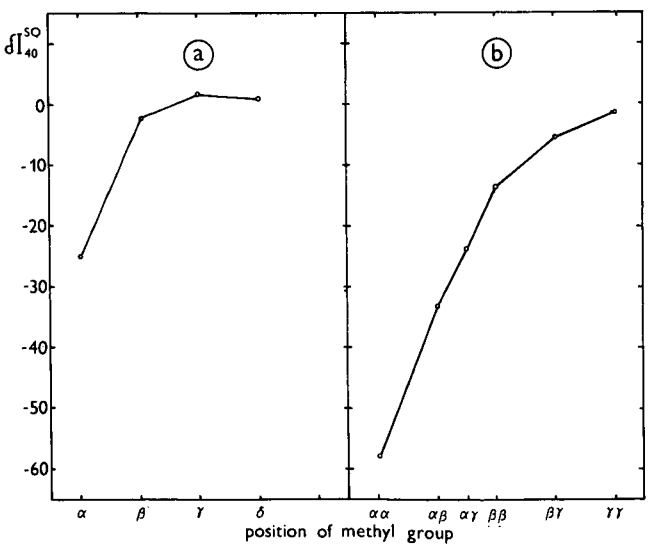

Fig. 1. Dependence of difference between measured and calculated retention indices of (a) methyl- and (b) dimethylalkynes on squalane at 40°C on the position of the methyl groups with respect to the triple bond.

with respect to the triple bond. For the methyl groups on the carbon atom neighbouring the triple bond, the calculated retention indices of alkynes are higher by 25 and 58 i.u. than the measured values. As the distance of the methyl group from the triple bond increases, the value of σI approaches zero. The dependence of σI on the position of the triple bond for methylheptynes and dimethylhexynes in Fig. 2 illustrates a characteristic increase in negative σI values with shift of the triple bond towards the centre of the alkyne molecule. The influence of the number of carbon atoms on σI in Fig. 3 illustrates the decrease in negative σI values with increasing number of carbon atom in 3,3-dimethyl-1-alkynes.

The retention indices calculated for monomethylalkynes according to eqns. 1 and 2 agree with the measured values within few units if methyl branching is separated from the triple bond by at least one CH_2 group, but the agreement diminishes with shift of the triple bond towards the chain centre (Fig. 2). For dimethylalkynes the agreement of σI is within a few units if both methyl groups are separated from the triple bond by at least two CH_2 groups (Fig. 1b). Limits of the calculation of retention indices of branched alkynes by eqns. 1 and 2 are illustrated by the fact that the calculation does not differentiate 3-methyl-1-hexyne and 4-methyl-1-hexyne although their retention indices on squalane differ by 23 i.u.

On the basis of this evaluation, we propose a different procedure based on the similarity of retention in homologous series of the corresponding branched alkynes and alkenes (whose retention indices on squalane up to C_8 are known [11–16], for calculation of the retentions of branched alkynes up to C_8 with methyl branching on the carbon atom neighbouring the triple bond (and also for other alkynes). The homomorphic factor of an alkyne was calculated from the relationship

$$H_{\text{alkyne}} = H_{\text{alkene}} + \delta H_1 + \delta H_2 \tag{3}$$

where H is the homomorphic factor of the branched alkyne or alkene with the same carbon atom skeleton on squalane at the given temperature. σH_1 expresses the difference between the homomorphic factors for *n*-alkyne and *n*-alkene with the same position of the multiple bond and with the same number of carbon atoms as in the main chain of the branched hydrocarbon:

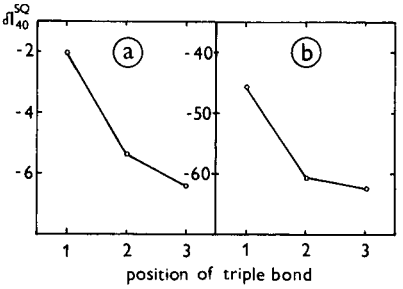

Fig. 2. Dependence of difference between measured and calculated retention indices on squalane at 40°C for (a) methylheptynes with the methyl group on the β-carbon and (b) dimethylhexynes with two methyl groups on the α-carbon.

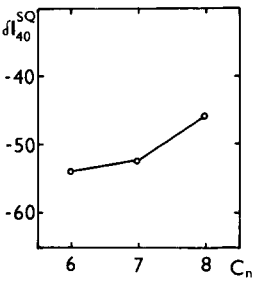

Fig. 3. Dependence of difference between measured and calculated retention indices on squalane at 40°C on the number of carbon atoms for 3,3-dimethyl-1-alkynes.

$$\delta H_1 = H_{n\text{-alkyne}} - H_{n\text{-alkene}} \quad (4)$$

σH_2 expresses different effect of an alkyl group in the side chain in the molecule of the branched alkyne on retention in comparison with the corresponding alkene. It may be calculated from the known values of retention indices of branched alkynes and alkenes with the same carbon atom skeleton and with the same position of the multiple bond:

$$\delta H_2 = H_{\text{alkyne}} - H_{\text{alkene}} - \delta H_1 \quad (5)$$

σH_2 values characterize the given structure in the given homologous series similarly to σH_1 values. Therefore, for the calculation of σH_2 it is sufficient to know the retention of one member of the given homologous series of alkynes.

For the homologous series of 3-methyl-1-alkynes we only measured the retention index of 3-methyl-1-butyne. On the basis of eqn. 3, from the known retention indices of 3-methyl-1-alkynes we calculated the retention indices of further 3-methyl-1-alkynes up to C_8. The σH_1 value was considered for the 1-butyne–1-butene pair to be $\sigma H_1^{SQ} = -2.9$ i.u. and the value of $\sigma H_2^{SQ} = -11.7$ i.u. was calculated from the homomorphic factors for 3-methyl-1-butyne (−64.5) and 3-methyl-1-butene (−49.9). We compared the retention indices for 3-methyl-1-hexyne and 3-methyl-1-heptyne calculated in this way with those measured experimentally in the case of products from the reaction of methylene group insertion into the molecule of corresponding 1-alkynes. The agreement of 0.5 i.u. suggests a high precision of the calculation of retention by this procedure for structures with methyl branching on the carbon atom neighbouring the triple bond.

Retention indices of other branched alkynes up to C_8 for which the retention index of only one member of the homologous series was known, *i.e.* of 4-methyl-1-alkynes, 5-methyl-1-alkynes, 5-methyl-2-alkynes, 3,3-dimethyl-1-alkynes and 4,4-dimethyl-1-alkynes, were calculated in a similar way.

For 6-methyl-1-heptyne, where no retention index was available for any of the members of the homologous series, in the calculation of its retention index we started from the σH_2 value which we obtained by extrapolation of the dependence of σH_2 on the position of the methyl group in the side chain in relation to the multiple bond in position 1. For this we started from the assumption that σH_2 would approach zero as the methyl group became increasingly isolated from the multiple bond. The value of the retention index of 6-methyl-1-heptyne calculated in this way was 1.6 i.u. higher than that measured for the product of MIR (according to eqn. 2 the retention index was lower by 1.0 i.u.).

For 6-methyl-2-heptyne we also derived the contribution of σH_2 to retention in a similar way to 6-methyl-1-heptyne by extrapolating the dependence of σH_2 values for methyl-2-alkynes and -alkenes with increasing distance of the methyl group from the multiple bond. The retention index calculated in this way was 2.3 i.u. higher than the measured value (according to eqn. 2 higher by 0.5 i.u.).

The contribution of σH_2 to the retention of 4-methyl-2-alkynes (α-methyl-2-alkynes) was found by interpolating σH_2 values for α-methyl-1-alkynes and α-methyl-3-alkynes. The calculated retention index for 4-methyl-2-heptyne was 1 i.u. lower than the measured value (the calculated value according to eqn. 2 is 27.9 i.u. higher than the measured value.

The contribution of σH_2 to the retention of 3,4-dimethyl-1-pentyne (α,β-dimethyl-1-alkyne) was calculated as the sum of the contributions of σH_2 for 3-methyl-1-pentyne (α-methyl-1-alkyne) and 4-methyl-1-pentyne (β-methyl-1-alkyne). The calculated retention index for 3,4-dimethyl-1-pentyne is 3.8 i.u. higher than the measured value for the MIT product (according to eqn. 2 higher by 34.4 i.u.). The value of σH_2 back-calculated for α,β-dimethyl-1-alkynes was used to calculate the retention index of 3,4-dimethyl-1-hexyne (the retention index calculated by eqn. 2 was higher by 25.0 i.u.).

For 4,4-dimethyl-1-pentyne, 5,5-dimethyl-2-hexyne and 5-methyl-3-heptyne none of the procedures based on eqn. 3 could be used to calculate their retention indices with acceptable precision. As they are alkynes in which dimethyl branching is separated from the triple bond by one CH_2 group and methyl branching occurs on the carbon atom neighbouring the triple bond, calculation of their retention indices according to eqn. 2 is not precise enough. Their retention indices were measured experimentally from peaks of the MIR mixture if all other reaction products were identified (retention indices calculated according to eqn. 2 were 12.6, 20.8 and 32.4 i.u., respectively, higher).

Of 44 possible isomers of branched alkynes up to C_8, all 36 methyl- and dimethylalkynes were thus characterized (26 by the measurements and 10 by calculation of retention indices). Retention indices of ethylalkynes and trimethylalkynes could neither be calculated by the above procedures according to eqn. 3 nor, because of a lack of starting substances, be obtained by MIR reaction. As their structures contain ethyl and methyl branching in the neighbourhood of the triple bond, the calculation of their retention indices by eqn. 2 is not sufficiently precise.

Values of homomorphic factors of branched alkynes up to C_8 on squalane at 40°C depending on the number of carbon atoms in various homologous series for monomethyl- and dimethylalkynes are illustrated in Figs. 4 and 5. In comparison with straight-chain alkynes, branching of the carbon chain causes a considerable decrease in retention depending on the degree of branching, position of the methyl group with respect to the triple bond and the number of carbon atoms in the alkyne molecule. Isomers of branched alkynes with the methyl group on the α-carbon next to the triple bond show the lowest retention. With increasing distance of the methyl from the triple bond the retentions of individual isomers increase.

In contrast to *n*-alkynes for which the first members of their homologous series show higher *H* values, the first members of the series of branched alkynes often have relatively lower *H* values. This lower retention can be observed, *e.g.*, for 3-methyl-1-butyne and 5-methyl-2-hexyne (Fig. 4), 3,3-dimethylbutyne and 4,4-dimethyl-2-pentyne (Fig. 5) and other alkynes. A common structural feature of the branched alkynes showing such behaviour is the presence of a quaternary or tertiary carbon at the end of the chain, *i.e.*, the following structures:

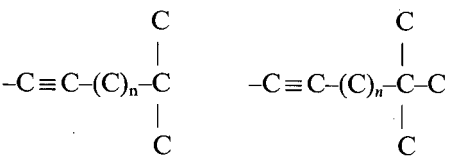

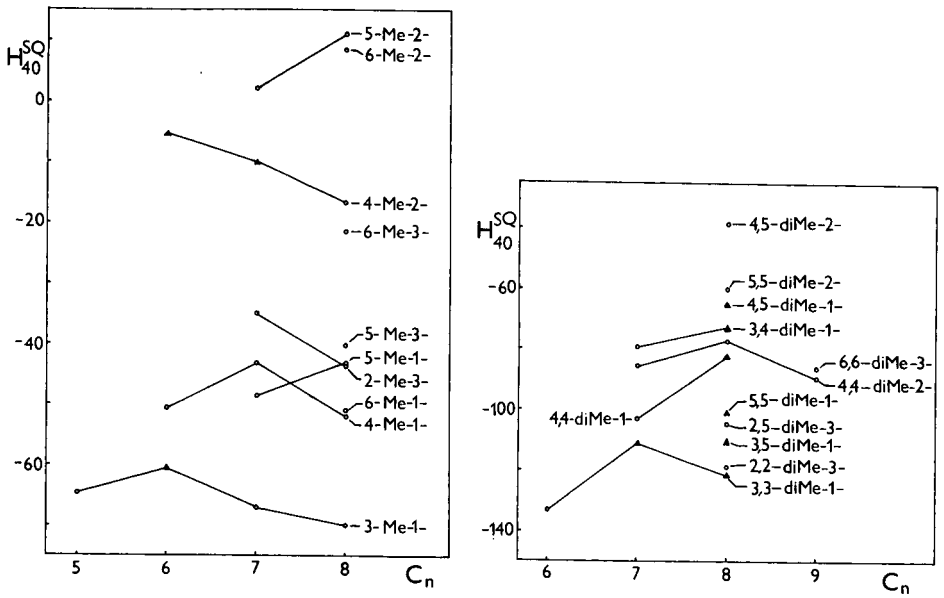

Fig. 4. Dependence of H_{40}^{SQ} on the number of carbon atoms for homologous series of C_5–C_8 monomethylalkynes on squalane at 40°C. 4-Me-1 = 4-Methyl-1-alkyne, etc. ○ = Measured values; △ = calculated values.

Fig. 5. Dependence of H_{40}^{SQ} on the number of carbon atoms for homologous series of C_6–C_9 dimethylalkynes on squalane at 40°C. 3,3-diMe-1- = 3,3-Dimethyl-1-alkyne, etc. ○ = Measured values; △ = calculated values.

A higher symmetry of the molecule and hence also lower polarizability and weaker solute–solvent interactions are characteristic of these structures. In accord with this, the retention for 5-methyl-1-hexyne is anomalously lower than that for 4-methyl-1-hexyne and similarly for 6-methyl-1-heptyne in comparison with 5-methyl-1-heptyne. A similar effect was found previously [17] also for branched alkanes, which suggests its general validity also for other branched hydrocarbons.

The dependence of the temperature coefficients of retention indices, dI/dT, on the number of hydrocarbon atoms for C_5–C_8 monomethylalkynes on squalane is shown in Fig. 6. It is obvious that the dI/dT values for monomethyl-1-alkynes are positive, similarly to those for linear 1-alkynes, in the range 0.00–0.07 i.u./°C. Similarly to linear alkynes, the dI/dT values for monomethylalkynes with the triple bond situated inside the chain are negative, in the range 0.00 to −0.12 i.u./°C.

Comparing the dependences dI/dT (C_z) and H (C_z) for homologous series of monomethylalkynes, we can observe a certain similarity. In both instances the values mentioned above reach more positive values as the distance of the methyl group in the side-chain from the triple bond increases. Anomalously lower are also the dI/dT values for structures with a quaternary or tertiary carbon atom at the end of the chain. These results agree with the fact that more symmetrical structures have lower dI/dT values. Similarly to straight-chain alkynes, the dI/dT values become more negative as the triple bond moves along the carbon chain of branched alkynes from position 1 to 3. Similar dependences between structure and dI/dT values were also found for C_6–C_9 dimethylalkynes.

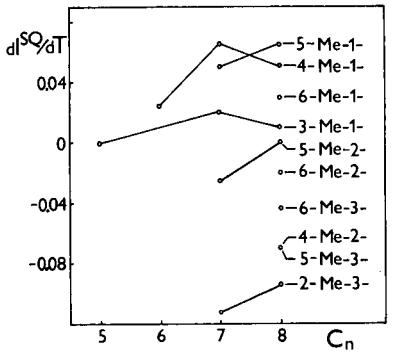

Fig. 6. Dependence of dI^{SQ}/dT on the number of carbon atoms for C_5–C_8 monomethylalkynes on squalane.

Retention of branched alkynes on PBO

The previous study [2] of the retention behaviour of straight-chain alkynes on PBO illustrated the advantage of liquid crystals as stationary phases for the separation of isomeric *n*-alkynes, particularly those with a central position of triple bond. For instance, for a quantitative separation of the pairs 5-and 4-decyne and 5- and 4-undecyne on squalane, 875 000 and 1 200 000 plates, respectively, are required, but on PBO the required plate numbers were an order of magnitude lower. The selectivity of the liquid crystal for isomeric *n*-alkynes increases with the shift of the triple bond from the centre of the molecule towards end of the carbon chain, hence in the same direction in which the isomers are eluted. Therefore, the conditions for their separation are also milder on the liquid crystal. In the separation of isomers with a central position of the triple bond from their neighbouring positional isomers, the different orientations of the ends of the zig-zag carbon chain in the molecules of the two types of isomer have a marked effect. The isomer that has the end of the zig-zag chain oriented in the direction of the molecular axis, which leads to a more stretched molecule (a greater molecular length-to-width ratio) has an increased retention on the liquid crystal. This is manifested, for instance, with *n*-decynes as a reversed retention sequence of 5- and 4-decynes on PBO in comparison with that on squalane.

Retention indices of various synthesized C_5–C_{13} branched alkynes on PBO liquid crystal are listed in Table I. For the calculation of retention indices of other branched alkynes according to eqns. 2 and 3 the required retention indices of corresponding alkanes and alkenes on PBO are missing.

The retention of branched alkynes on PBO, owing to its selectivity for the length-to-width ratio of the solute molecule, is, in comparison with retention on squalane, determined more markedly by the degree of alkyne branching. At the same time, as result of the polarity of PBO, dipole–dipole interactions also appear. With increasing branching of the alkyne molecule as result of decreasing molecule length-to-width ratio and with increasing shielding of the triple bond, the retentions of alkynes on PBO decrease in comparison with those on squalane in a corresponding way. This is demonstrated by the difference in retention indices, ΔI_{80}^{PBO-SQ}, of alkyl-3-heptynes in Table II. The shielding effect of methyl groups and the decrease in linearity of the molecules of strongly branched alkynes manifests itself in a lower value of

TABLE II

VALUES OF ΔI^{PBO-SQ} FOR 3-HEPTYNE AND METHYL-3-HEPTYNE AT 80°C

Alkyne	ΔI_{80}^{PBO-SQ}
3-Heptyne	65.1
2-Methyl-3-heptyne	47.7
6,6-Dimethyl-3-heptyne	43.0
2,2,6-Trimethyl-3-heptyne	15.9
2,2,6,6-Tetramethyl-3-heptyne	4.3
2,2,5,6,6-Pentamethyl-3-heptyne	−5.6
2,2,5,5,6,6-Hexamethyl-3-heptyne	−17.7

their retention indices on PBO in comparison with those on squalane: *e.g.*, for 2,2,5,5,6,6-hexamethyl-3-heptyne $\Delta I^{PBO-SQ} = -17.7$ i.u.

The contribution of the methyl group in the alkyne side-chain to retention on PBO depends, in the first place, on the position with respect to the triple bond. The methyl group closer to the triple bond has a stronger shielding effect on the triple bond and hence also on the dipole–dipole interaction, which is reflected in lower values of ΔI^{PBO-SQ} (Table III). However, as shown by retention measurements on isomeric methylalkanes on PBO, the contribution of the shape of the molecule to the retention on the liquid crystal also decreases in the same direction.

The contribution of the methyl group in the alkyne side-chain to the retention on PBO depends, in comparison with squalane, on the position of the triple bond in the chain and on the number of carbon atoms in the molecule to a relatively smaller extent. This is proved by the values of $\Delta\Delta I^{PBO-SQ}$ (Table IV), calculated as

$$\Delta\Delta I^{PBO-SQ} = \Delta I_b - \Delta I_n \tag{6}$$

where

$$\Delta I_b = I_b^{PBO} - I_b^{SQ}$$

b being the branched alkyne and

$$\Delta I_n = I_b^{PBO} - I_n^{SQ}$$

n being the straight-chain alkyne with the same number of carbon atoms and with the same position of the triple bond as in the main chain of the branched alkyne.

TABLE III

VALUES OF ΔI^{PBO-SQ} FOR ALKYL-3-HEPTYNES AND 3-HEXYNE AT 80°C

Alkyne	ΔI_{80}^{PBO-SQ}
2-Methyl-3-heptyne	47.7
6-Methyl-3-heptyne	55.9
2,2-Dimethyl-3-hexyne	32.5
6,6-Dimethyl-3-heptyne	43.0

TABLE IV

THE VALUES OF $\Delta\Delta I^{PBO-SQ}$ FOR BRANCHED ALKYNES WITH THE SAME POSITION OF METHYL GROUPS TOWARDS THE TRIPLE BOND AT 80°C

Alkyne	Number of C atoms	Position of methyl group	$\Delta\Delta I_{80}^{PBO-SQ}$
3-Methyl-1-butyne	5	α	−15.0
2-Methyl-3-hexyne	6	α	−16.7
2-Methyl-3-heptyne	7	α	−17.4
5-Methyl-2-hexyne	7	β	−8.8
6-Methyl-3-heptyne	8	β	−9.2
3,3-Dimethyl-1-butyne	6	α,α	−33.7
4,4-Dimethyl-2-pentyne	7	α,α	−31.2
4,4-Dimethyl-2-hexyne	8	α,α	−30.9
4,4-Dimethyl-2-heptyne	9	α,α	−33.5

It is obvious from Table IV that the values of $\Delta\Delta^{PBO-SQ}$ for alkynes with the methyl group on the α-carbon are approximately double those for alkynes with the methyl group on the β-carbon and for alkynes with two methyl groups on the α-carbon, and they are approximately double those for alkynes with one methyl group on the α-carbon.

On the basis of the above correlations, it is possible, to a certain extent, to predict the retention indices of branched alkynes on PBO from the measured retention indices of straight-chain alkynes on PBO and squalane, and from those for branched alkynes on squalane.

The temperature coefficients of the retention indices of C_5–C_{13} branched alkynes on PBO are positive (3-methyl-1-butyne is an exception with −0.07 i.u./°C) in the range 0.01–0.52 i.u./°C, and are higher than those on squalane. Positional 1-alkynes show the lowest dI/dT values. The dI/dT values of other branched alkynes change as a function of the position of the triple bond in the main chain, on the degree of branching and on the positions of methyl groups in side-chain with respect to the triple bond.

The selectivity of liquid crystal stationary phases for the separation of isomeric branched alkynes was used in the separation of 6-methyl-1-heptyne and 4-methyl-1-

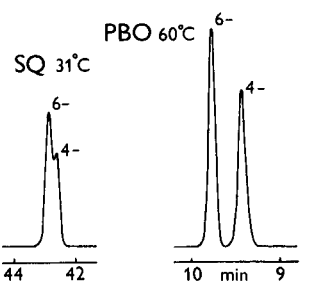

Fig. 7. Separation of 4-methyl-1-heptyne (4-) and 6-methyl-1-heptyne (6-) on a capillary column with squalane and PBO liquid crystal.

heptyne, which have similar retentions on squalane ($\sigma I_{40}^{SQ} = 0.8$ i.u.). As can be seen from Fig. 7, the separation of these isomers is substantially easier on the liquid crystal and the sequence remains unchanged, which suggests a more selective retention of 6-methyl-1-heptyne, in accordance with the above expectations.

The knowledge obtained in the separation and characterization of alkynes was used for the analysis of alkynes in the C_5 fraction from the pyrolysis of higher hydrocarbons and from catalytic dehydrogenation of *n*-heptane.

ACKNOWLEDGEMENT

The authors are grateful to Dr. L. Miginiac, University of Poitiers (France), for the gift of some of the alkynes.

REFERENCES

1 R. A. Hively and R. E. Hinton, *J. Gas Chromatogr.*, 6 (1968) 203.
2 L. Soják, P. Farkaš, J. Janák, S. Rang and O. Eisen, *J. Chromatogr.*, 287 (1984) 271.
3 W. Meltzov, S. Warwel and B. Fell, *Chromatographia*, 6 (1973) 183.
4 R. Riedo, D. Fritz, G. Tarján and E. Kováts, *J. Chromatogr.*, 126 (1976) 63.
5 S. Rang, K. Kuningas, A. Orav and O. Eisen, *J. Chromatogr.*, 119 (1976) 451.
6 S. Rang, K. Kuningas, A. Orav and O. Eisen, *J. Chromatogr.*, 128 (1976) 53 and 59.
7 G. Dielmann, *Dissertation*, Ruhr-Universität, Bochum, 1977.
8 Th. Welsch, W. Engewald and P. Berger, *Chromatographia*, 1 (1978) 5.
9 S. Rang, O. Eisen, A. V. Kiselev, A. E. Meister and K. D. Scherbakova, *Chromatographia*, 7 (1979) 327.
10 I. Dvoretzky, D. B. Richardson and L. R. Durret, *Anal. Chem.*, 4 (1963) 545.
11 G. Schomburg, *J. Chromatogr.*, 23 (1966) 1.
12 J. A. Rijks and C. A. Cramers, *Chromatographia*, 7 (1974) 215.
13 D. A. Tourres, *J. Gas Chromatogr.*, 5 (1967) 35.
14 J. C. Loewenguth and D. A. Tourres, *Fresenius' Z. Anal. Chem.*, 236 (1968) 170.
15 A. Matukuma, in C. L. A. Harbourn (Editor), *Gas Chromatography 1968*, Institute of Petroleum, London, 1969, p. 55.
16 L. Soják and A. Bučinská, *J. Chromatogr.*, 51 (1970) 75.
17 L. Soják, unpublished results.

Journal of Chromatography, 557 (1991) 255–270
Elsevier Science Publishers B.V., Amsterdam

CHROM. 23 412

Gas chromatography and gas chromatography–mass spectrometry study of hydrocarbons in Vlasta oil (Adriatic Basin) as the basis for geochemical interpretation

A. ALAJBEG*, A. TODORIĆ and S. ŠVEL-CEROVEČKI
INA-Oil Industry, Research and Development, Zagreb (Yugoslavia)
and
M. ŠUŠTERČIĆ
Naftaplin, Zagreb (Yugoslavia)

ABSTRACT

In order to elucidate the chemistry and geochemistry of Vlasta oil (central Adriatic Basin) a gas chromatography and gas chromatography–mass spectrometry study of hydrocarbon composition and structure was performed, as well as some global geochemical characterization. Twenty-one components of the light end of the oil, 83 components of the whole-oil sample and 17 components of the heavy end of the oil were identified by gas chromatography and by a gas chromatography–mass spectrometry coupled system. The light components are represented by straight and branched alkanes, cycloalkanes and aromatics, whereas thioethers are found to be whole-oil components. The heavy components are represented by pentacyclic triterpanes. The obtained results have shown algal and bacterial biomass to be the most probable origin of the Vlasta oil, which was deposited in anoxic hypersaline in carbonate beds during the Triassic period. Oil was released from related kerogen in the early stage of maturity. It underwent no significant biodegradation.

INTRODUCTION

The composition of an oil (petroleum) reflects the origin and deposition of precursors, the stage of maturation of the related source rock and the history of oil migration and trapping in geological strata [1,2]. In studying oils, modern analytical chemistry offers the possibility of detailed investigation at the level of interest.

In order to obtain global composition characteristics, oils are investigated by NMR [3,4], liquid chromatography, thin-layer chromatography [5] and other techniques for group analysis. Many valuable geochemical parameters depend upon individual constituents.

Many efforts have been made to indentify oil components [6,7], and many geochemical rules enable the conversion of analytical data into geochemical parameters, which are important in studying oils and oil basins.

Oil constituents can be identified by gas chromatographic–mass spectrometric (GC–MS) analysis of whole oil [8] as well as of oil fractions. In addition to full mass

0021-9673/91/$03.50

spectra, mass fragmentograms help to discriminate between compounds classes and improve individual component identification [9–12].

Biomarkers [13], which are important molecular geochemical indicators, are frequently studied by fragmentograms, such as m/z 191 for terpenoids and m/z 177 for biodegraded terpenoids [14]. Terpenoids, as well as some other important classes of biomarkers, are present in oils as complex mixtures of isomers and homologues in very low concentration and elute at the heavy end of the gas chromatogram.

In order to increase the concentration, some separation procedures may help [1], *e.g.* asphaltene precipitation and maltene fractionation into saturated and non-

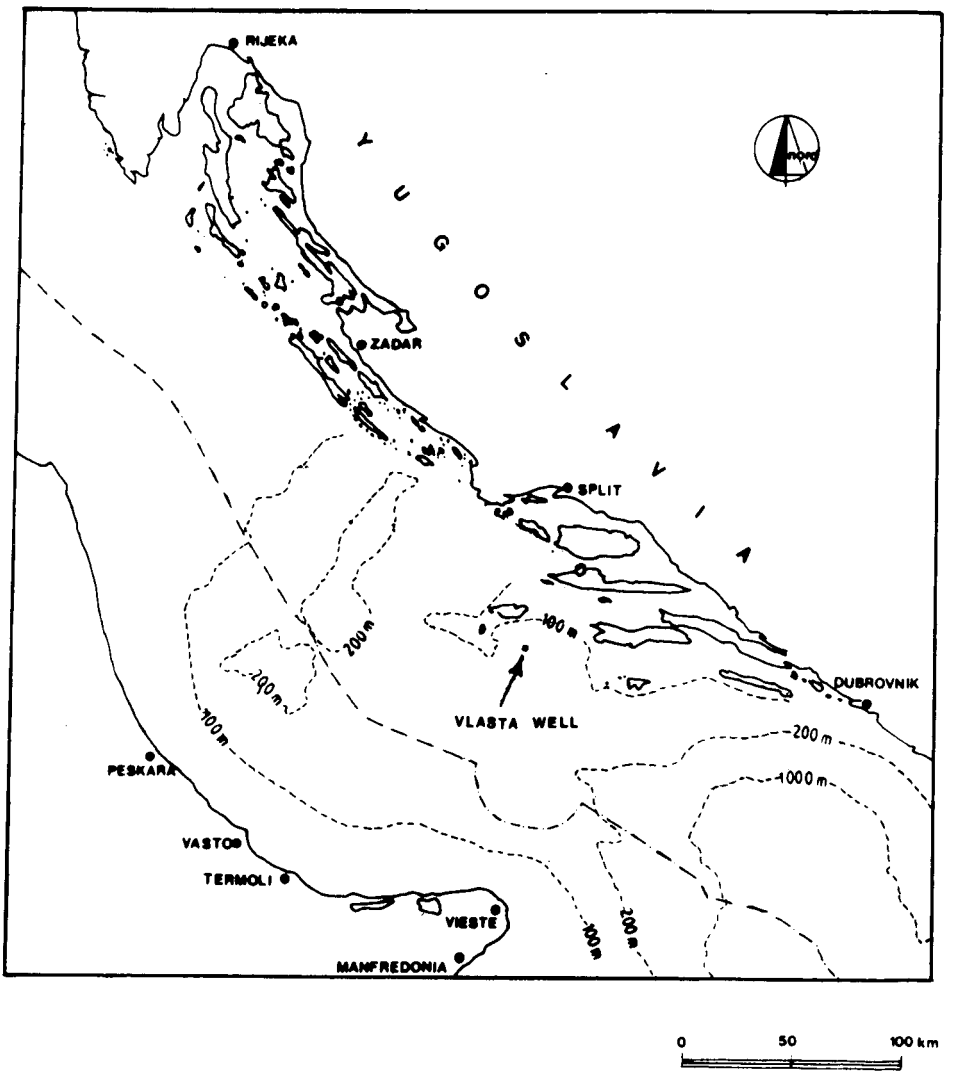

Fig. 1. Sample location (central Adriatic Basin).

saturated components. The former could be used to prepare samples for a terpenoid study.

To avoid a loss of information caused by the overlapping of light-component peaks during whole-oil analysis (under reasonable working conditions), the light-oil fraction may be studied separately.

In order to facilitate the geochemical oil classification, some global properties, such as elemental composition, stable isotope depletion and aliphatic to aromatic ratio, may provide useful complementary data in a hydrocarbon study.

A geochemical study of Croatian oils started recently [15–20]. The oils from the Adriatic Basin are rarely studied in detail. This paper is a study of Vlasta oil. Its aim is to determine the origin, precursor deposition environment, kerogen maturation level and biodegradation rank of oils in the central part of the Adriatic Basin.

EXPERIMENTAL

Vlasta oil originates from the central Adriatic Basin (Fig. 1). It was brought with the well mud from the Triassic layers in the interval between 5200 and 5500 m. During collection and transportation the sample may have suffered some loss of light components. The oil was dewatered and mineral particles removed. It then underwent an analytical procedure (Fig. 2), which involved GC and GC–MS analyses, as well as some complementary global geochemical characterization, such as elemental analysis

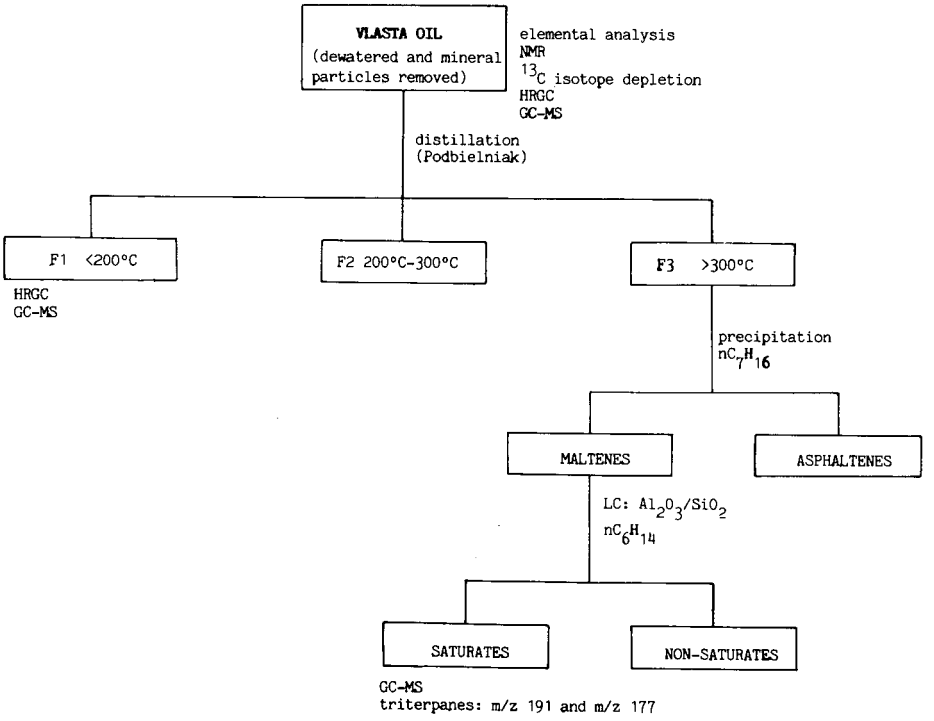

Fig. 2. Analytical procedure scheme.

TABLE I

EXPERIMENTAL CONDITIONS FOR GC AND GC–MS ANALYSIS

(A) For whole oil	
(I) GC conditions	
Gas chromatograph	Pye Unicam 304
Column	Fused-silica, non-polar DB1, 30 m
Temperature	50°C for 5 min, 4°C/min to 300°C
Carrier gas	Hydrogen
Pressure	0.21 MPa
Flow-rate	About 1.2 ml/min
Sample size	1 μl of ca. 10% oil solution in nC_6H_{14}
Injection mode	Splitless, 30 s
Detection	Flame ionization
(II) GC–MS conditions	
Gas chromatograph	Varian 3700
Column, column temperature, flow, sample size and injection mode as in AI	
Carrier gas	Helium
GC–MS coupling	Open split
Mass spectrometer	Varian MAT 112S
Scanning rate	1 s/decade
Interscan time	0.2 s
Resolution	1:500
Ionization	Electron impact
Electron energy	70 eV
Emission current	0.7 mA
Ion source temperature	250°C
Ion source pressure	10^{-5} Pa
(B) For light end	
(I) GC conditions	
Gas chromatograph, column, carrier gas, pressure, flow and detection as in AI	
Column temperature	30°C, Isothermal
Sample size	0.1 μl
Injection mode	Splitting 50:1
(II) GC–MS conditions	
Column, flow, sample size and injection mode as in BI	
Column temperature	Room temperature
GC chromatograph, carrier gas, GC–MS coupling and mass spectrometer conditions as in AII	
(C) For heavy end	
GC–MS conditions	
Column	Fused-silica, non-polar, DB1, 60 m
Temperature	150°C, 10°C/min to 300°C
Flow-rate	About 1 ml/min
Sample size	1 μl of *ca.* 10% solution of saturates in nC_6H_{14}
Injection mode	Splitless, 30 s
The other conditions as in AII	
Full-scan and mass fragmentograms (m/z 191 and m/z 177) were taken.	

(ASTM D-1551), aliphatic to aromatic ratio (NMR [3]) and ^{13}C isotope depletion [21].

^{1}H-NMR analysis was performed on a Varian EM 390 using tetramethylsilane (TMS) (Merck, Darmstadt, Germany) as standard. ^{13}C isotope depletion was measured by a Finnigan MAT 250 mass spectrometer, using NBS 22 (NBS, Washington, USA) standard.

The oil was cut by Podbielniak distillation (ASTM D-2892) into fractions: F1 up to 200°C, F2 between 200°C and 300°C, and F3 above 300°C. F1 was analysed by GC–MS as well as by GC co-injection of reference compounds such as 2-methylpentane, 3-methylpentane, 2,4-dimethylpentane, 2-methylhexane, 2,3-dimethylpentane, 3-methylhexane, 1,3-dimethylcyclopentane (*cis*), 1,3-dimethylcyclopentane (*trans*) and 1,2-dimethylcyclopentane (trans) (all from PolyScience, IL, USA), under the conditions listed in Table IB.

Maltenes were isolated from the F3 fraction by precipitation of asphaltenes in *n*-heptane (and *n*-heptane evaporation). The concentrate of high-molecular weight saturates (normal- + iso- + cycloalkanes with boiling point above 300°C) was separated from maltenes by column chromatography with aluminium oxide–silicon oxide (Kemika, Zagreb, Yugoslavia), with *n*-hexane as eluent.

The concentrate of saturates was taken for a study of pentacyclic triterpanes (biomarkers) by GC–MS (under the conditions listed in Table IC). Full spectra and mass fragmentograms (*m/z* 191 and *m/z* 177) were used for identification of triterpanes.

The heights of GC or GC–MS or mass fragmentogram peaks were used for calculation of geochemical parameters, with no correction factors.

RESULTS AND DISCUSSION

Global geochemical characterization points to the prevailing aliphatic character of Vlasta oil. NMR analysis showed not more than 3% of hydrogen atom to be bonded to aromatic rings. One-third of them were found to belong to phenyl groups, while two-thirds are attached to fused aromatic rings. Also, an average of 1.8 hydrogen atoms are attached to one carbon atom (elemental analysis).

Carbon isotope depletion, $\delta\ ^{13}C$, for whole oil was $-30.3‰$ and classifies the Vlasta oil sample as belonging to the Triassic group of Adriatic oils [20].

The gas chromatogram of the oil (Fig. 3; peak labels 1W to 83W relate to the same labels in Table II) shows that most of the prominent peaks belong to *n*- and isoalkanes. In the gas chromatograms of whole oil, *n*-alkanes are recognizable in the range from *n*-C_8H_{18} (1W) up to *n*-$C_{30}H_{62}$ (83W) (the light end covered by a solvent added for splitless type of GC injection). Their distribution reaches a maximum at $C_{15}H_{32}$ (59W), with still reasonable *n*-$C_{17}H_{36}$ (68W). After reaching the maximum the *n*-alkane distribution rapidly diminishes in concentration, being rather low and constant after *n*-$C_{19}H_{40}$ (72W). This type of chromatogram is an indication for the marine algal origin of the oil [22]. There is a slight preponderance of *n*-alkanes with an even number of carbon atoms over those with an odd number carbon preference index [23] = 0.96), which might indicate that the biomass was deposited as oil precursor in a carbonate environment [22].

Besides the prominent *n*-alkane homologues series, pristane (69W) and phytane

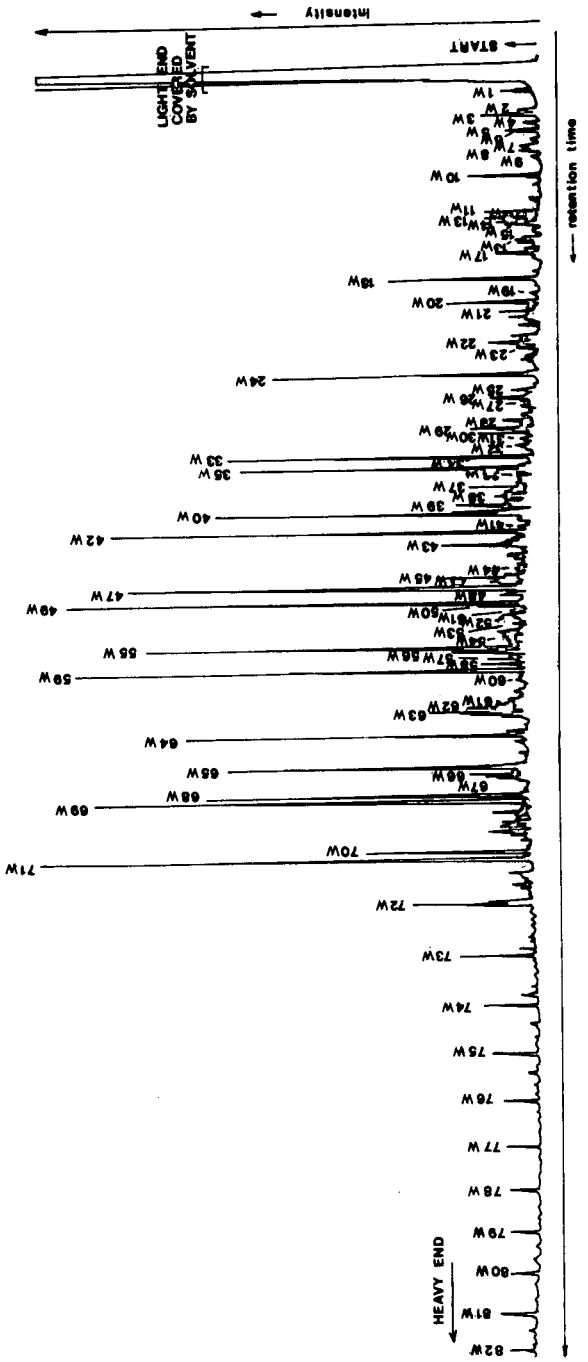

Fig. 3. Gas chromatogram of Vlasta oil. (GC conditions as in Table IA).

TABLE II

COMPONENTS IDENTIFIED IN OIL SAMPLE

Label (as in Fig. 3)	Component	
1W	*n*-Octane	$n\text{-}C_8H_{18}$
2W	2,6-Dimethylheptane	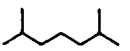
3W	Isononane	$iso\text{-}C_9H_{20}$
4W	Ethylbenzene	
5W	*m*-Xylene	
6W	*p*-Xylene	
7W	4-Methyloctane	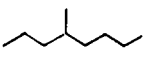
8W	*o*-Xylene	
9W	Cyclohexylpropane	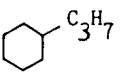
10W	*n*-Nonane	$n\text{-}C_9H_{20}$
11W	Isodecane	$iso\text{-}C_{10}H_{22}$
12W	Propylbenzene	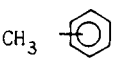
13W	Cyclohexylbutane	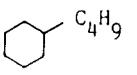
14W	1-Methyl-3-ethylbenzene	
15W	1-Methyl-4-ethylbenzene	
16W	1,3,5-Trimethylbenzene	
17W	1,2,4-Trimethylbenzene	

(*Continued on p. 262*)

TABLE II (*continued*)

Label (as in Fig. 3)	Component	
18W	*n*-Decane	*n*-$C_{10}H_{22}$
19W	1,2,3-Trimethylbenzene	
20W	Isodecane	Iso-$C_{10}H_{22}$
21W	1-Methyl-3-sec-propylbenzene	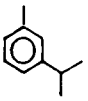
22W	Butylbenzene	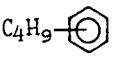
23W	Isoundecane	iso-$C_{11}H_{24}$
24W	*n*-Undecane	*n*-$C_{11}H_{24}$
25W	Cyclohexylpentane	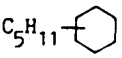
26W	Pentylbenzene	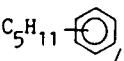
27W	Diethylbenzene/sec-butylbenzene	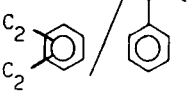
28W	Pentylbenzene	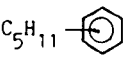
29W	Naphthalene	
30W	Methylthioheptane	C_7H_{15}–S–CH_3
31W	Pentylbenzene	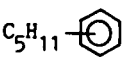
32W	Methylthioheptane	C_7H_{15}–S–CH_3
33W	Pentylbenzene	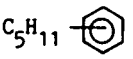
34W	Cyclohexylheptane	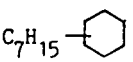
35W	*n*-Dodecane	*n*-$C_{12}H_{26}$
36W	Isotridecane	iso-$C_{13}H_{28}$
37W	Cyclohexylheptane	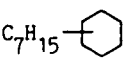
38W	Methylthioheptane	C_7H_{15}–S–CH_3

TABLE II (*continued*)

Label (as in Fig. 3)	Component	
39W	Cyclohexyloctane	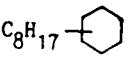
40W	Isotetradecane (isoprenoid)	iso-$C_{14}H_{30}$
41W	Cyclohexyloctane	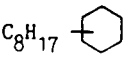
42W	*n*-Tridecane	*n*-$C_{13}H_{28}$
43W	Methylthiooctane	C_8H_{17}–S–CH_3
44W	Heptylbenzene	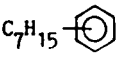
45W	Cyclohexylnonane	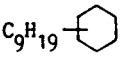
46W	Ethylthiooctane	C_8H_{17}–S–C_2H_5
47W	Isopentadecane (isoprenoid)	iso-$C_{15}H_{32}$
48W	Cyclohexylnonane	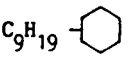
49W	*n*-Tetradecane	*n*-$C_{14}H_{30}$
50W	Hexylbenzene	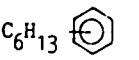
51W	Ethylnaphthalene	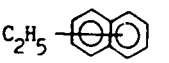
52W	Ethylthiooctane	C_8H_{17}–SS–C_2H_5
53W	Ethylthiooctane	C_8H_{17}–S–C_2H_5
54W	Cyclohexyldecane	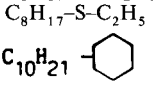
55W	Isohexadecane (isoprenoid)	iso-$C_{16}H_{34}$
56W	Ethylthiooctane	C_8H_{17}–S–C_2H_5
57W	Cyclohexyldecane	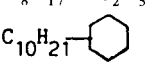
58W	Isotetradecane	$C_{14}H_{30}$
59W	*n*-Pentadecane	*n*-$C_{15}H_{32}$
60W	Methylthiodecane	$C_{10}H_{21}$–S–CH_3
61W	Methylethylnaphthalene	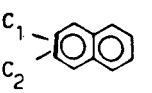
62W	Isohexadecane	iso-$C_{16}H_{34}$
63W	Isopentadecane	iso-$C_{15}H_{32}$
64W	*n*-Hexadecane	*n*-$C_{16}H_{34}$

(*Continued on p. 264*)

TABLE II (*continued*)

Label (as in Fig. 3)	Component	
65W	Cyclohexylundecane	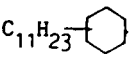
66W	Isohexadecane	iso-$C_{16}H_{34}$
67W	Cyclohexylundecane	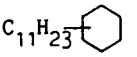
68W	*n*-Heptadecane	*n*-$C_{17}H_{36}$
69W	Pristane	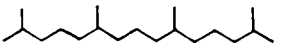
70W	*n*-Octadecane	*n*-$C_{18}H_{38}$
71W	Phytane	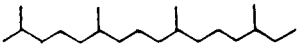
72W–83W	*n*-Alkane homologues from nonadecane to triacontane	*n*-$C_{19}H_{40}$–*n*-$C_{30}H_{62}$

(71W) also appear in a comparatively high concentration. These two isoprenoids, thought to be the fragments released from chlorophyll and/or from archae-bacterial lipids, are thought to be dependent on the concentration and on redox potential of the oil precursors' deposition environment [23]. The pristane–phytane ratio, which does not exceed 0.81, might be an indication that oil precursors were deposited mainly in anoxic conditions.

Regarding MS spectra (taken by GC–MS), isoprenoidal structure may be related to one tetradecane (40W), one pentadecane (47W) and one hexadecane (55W). For positive structure determination (head-to-head, tail-to-tail, head-to-tail), co-injection of the reference compounds is necessary. The nature of component 2W was confirmed (2,6-dimethylheptane, Aldrich, Milwaukee, WI, USA).

Isoprenoids in oils are the remnants of terpanes originating from biomass, which were partly preserved during their geological history. Partly cyclized terpane structures may be mirrored in fragments composed of cyclic and alkyl counterparts. The alkylcyclohexanes found in Vlasta oil (9W, 13W, 25W, 34W, 37W, 39W, 41W, 45W, 48W, 54W, 57W, 65W and 67W), may be related to them.

The relatively high concentration of the isoalkanes and cyclohexyl alkanes cannot be definitely attributed to biodegradation, which in preference destroys *n*-alkanes [1,2]. The explanation may be found at an early stage of the kerogen maturity at the time when the release of Vlasta oil occurred. At an early stage of maturation, the kerogen (cross-linked macromolecular oil and gas precursor) may have had a better yield of fragments by cracking the bonds related to the tertiary carbon atoms, since they appear to be weaker, than the bonds between secondary carbon atoms.

Aromatic compounds are found in low concentration. In the sample of whole

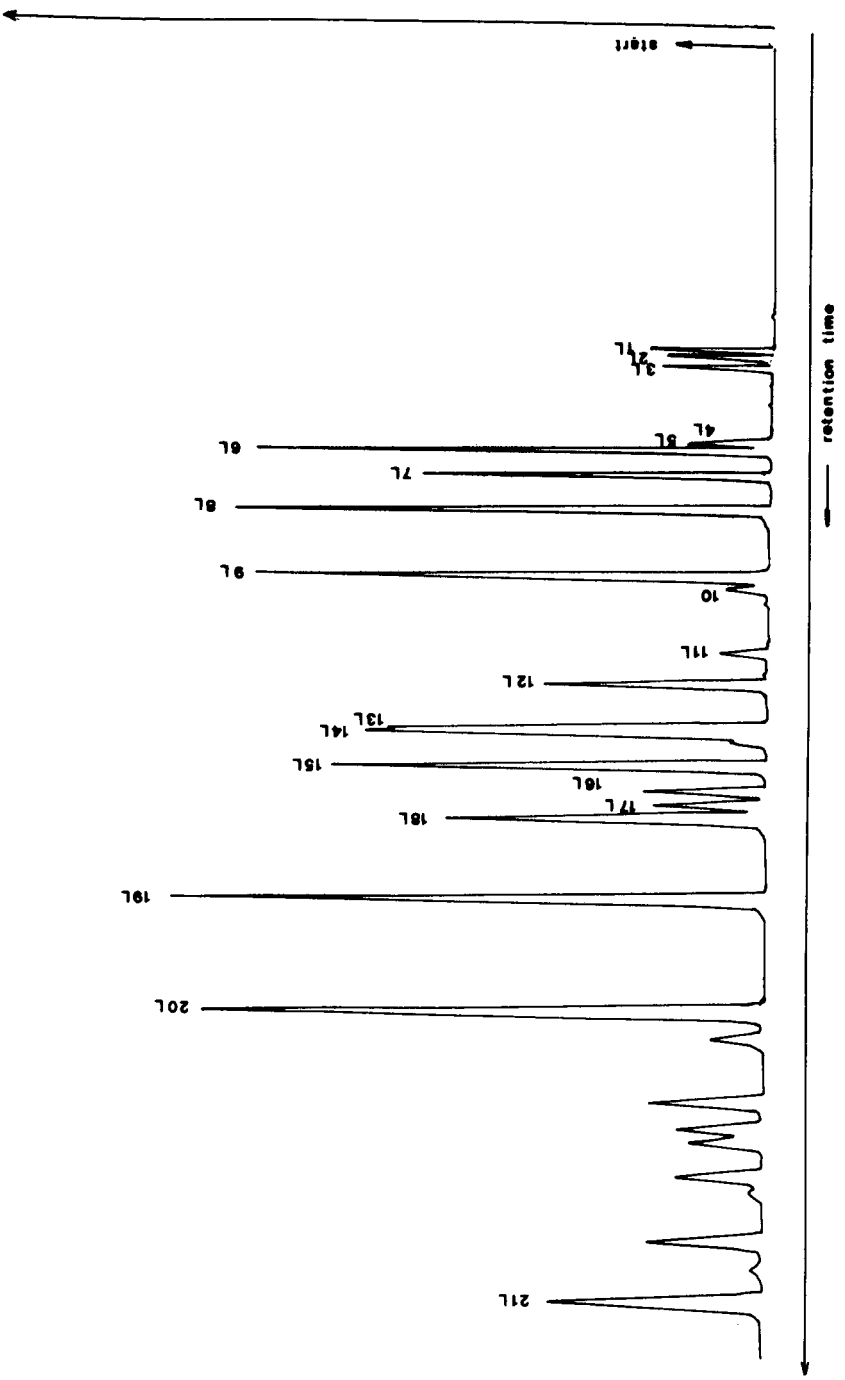

Fig. 4. Light-end chromatogram (GC conditions as in Table IB).

TABLE III

LIGHT-END COMPONENTS

Label (as in Fig. 4)	Components	
1L	*n*-Butane	
2L	Isopentane	iso-C_5H_{12}
3L	*n*-Pentane	
4L	Cyclopentane	
5L	2,3-Dimethylbutane	
6L	2-Methylpentane	
7L	3-Methylpentane	
8L	*n*-Hexane	
9L	Methylcyclopentane	
10L	2,4-Dimethylpentane	
11L	Benzene	
12L	Cyclohexane	
13L	2-Methylhexane	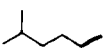
14L	2,3-Dimethylpentane	
15L	3-Methylhexane	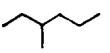

TABLE III (*continued*)

Label (as in Fig. 4)	Components	
16L	1,3-Dimethylcyclopentane (*cis*)	
17L	1,3-Dimethylcyclopentane (*trans*)	
18L	1,2-Dimethylcyclopentane (*trans*)	
19L	*n*-Heptane	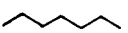
20L	Methylcyclohexane	
21L	Toluene	

oil alkylbenzenes ranging up to heptylbenzene (44W) were found. Among them mono-, di- and trialkylbenzenes were identified. Besides naphthalene (29W), alkylnaphthalenes with two (51W) and three (61W) aliphatic carbon atoms were found in the mixture, as complex as oil is. Sulphur compounds such as methyl- and ethylthioethers were identified (30W, 32W. 38W, 43W, 46W, 52W, 53W, 56W and 60W). They reflect the highly reducing environment of the precursor depostion in which anaerobic microbial reduction of (inorganic) sulphate to sulphite took place [24]. In the case of a lack of heavy metal ions, S^{2-} groups are incorporated within kerogen before entering the early-maturity stage. (According to elemental analysis sulphur comprises 2.5% of the mass of the oil.)

At the light end of the Vlasta oil (F1 analysed under the conditions shown in Table IB), 21 components were identified by mass spectra and/or reference compound(s) co-injection (components shown in Fig. 4 and Table III, labelled 1L to 21L). They are *n*-alkanes (1L, 3L, 8L and 19L) starting from *n*-butane; isoalkanes (2L, 5L-7L, 10L, 13L–15L); cycloalkanes including cyclopentane (4L), cyclohexane (12L) and their alkyl- and dialkyl homologues (9L, 16L–18L and 20L), as well as two aromatics: benzene (11L) and toluene (21L).

The components in Vlasta whole oil, including the light end, represent the majority of the oil (*e.g.* the oil portion which is able to pass through the GC column under conditions as shown in Table I).

The heavy end of the Vlasta oil consists of components which dramatically diminish in concentration. Among the components, terpenoids were studied, as they can serve as biomarkers of oil source [13], precursor deposition environment [22],

TABLE IV

PENTACYCLIC TRITERPANE BIOMARKERS

m/z 191 = pentacyclic triterpanes, for example C_{30} hopane

Label (as in Fig. 5)	Component
1t	22,29,30-Trisnorneohopane, Ts
2t	22,29,30-Trisnorneohopane, Tm
3t	17α(H),21β(H),30-Norhopane
4t	C_{30}-Cheilantane
5t	17α(H),21β(H)-Hopane
6t	17α(H),21β(H)-Hopane (moretane)
7t	17α(H),21β(H),29-Homohopane 22S
8t	17α(H),21β(H),29-Homohopane 22R
9t	Gammacerane
10t	17α(H),21β(H),29-Bishomohopane 22S
11t	17α(H),21β(H),29-Bishomohopane 22R
12t	17α(H),21β(H),29-Trishomohopane 22S
13t	17α(H),21β(H),29-Trishomohopane 22R
14t	17α(H),21β(H),29-Tetrakishomohopane 22S
15t	17α(H),21β(H),29-Tetrakishomohopane 22R
16t	17α(H),21β(H),29-Pentakishomohopane 22S
17t	17α(H),21β(H),29-Pentakishomohopane 22R

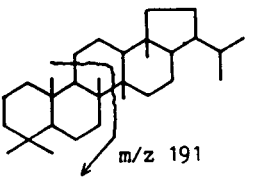

m/z 177 = 25-Norhopane (10-desmethylhopane), no significance

C_{29} 25-Nor-17α(H)-hopane (10-desmethylhopane)

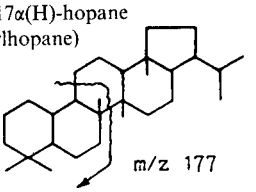

maturity stage [25], and aerobic biodegradation of oil [20]. Since they are present in a very low concentration in the complex mixture, a fragmentogram *m/z* 191 was taken to study pentacyclic triterpanes (hopanes) and *m/z* 177 for their biodegraded derivatives (Fig. 5, Table IV, components labelled 1t to 15t).

Hopanes are supposed [26] to be derived from bacteriohopanetetrol (origin from prokaryotes) as a result of anaerobic bacterial activity. The more anoxic the environment, the higher the preservation, *i.e.* the relative concentration of tetra- and pentakishomohopanes as the largest derivatives. Higher homohopanes were well preserved in hypersaline conditions [27]. In the fragmentogram, homohopanes gradually decrease in concentration until tetrakishomohopanes (14t and 15t), suggesting low redox potential in the geochemical environment during and immediately after the deposition of the Vlasta oil source.

The presence of gammacerane (9t) as a highly specific biomarker [22] supports the idea of the hypersaline deposition environment prevailing in the Vlasta oil precursor. The ratio between Ts and Tm is (regardless of the influence of depostion environment [28] a relevant maturity parameter [22], since Tm is found to diminish in concentration as a result of maturation, while Ts is rather stable. Expressed as Ts/

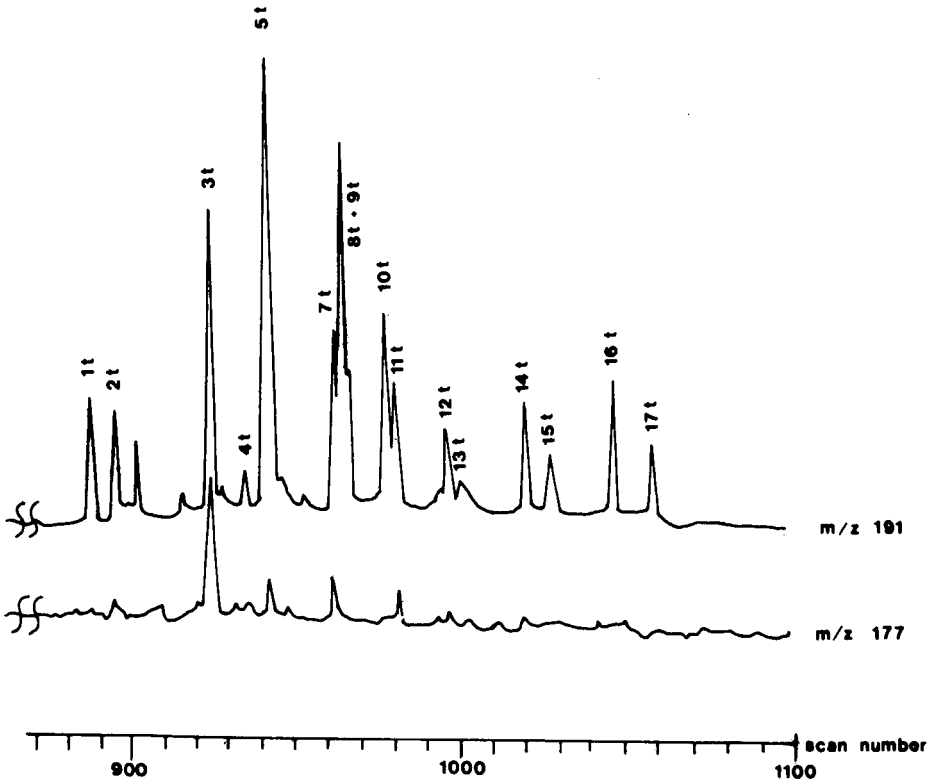

Fig. 5. Mass fragmentograms (GC–MS conditions as in Table IC): m/z 191 = pentacyclic triterpanes; m/z 177 = 10-desmethylhopanes.

(Ts + Tm) this parameter reaches 0.50 during an early stage of maturity. For Vlasta oil it is found to be 0.55. The additional support for maturity level is the ratio of 22*S*/22*S* + 22*R*) diastereoisomers of homohopanes. This parameter reaches an equilibrium of 0.62 at an early maturity stage [25]. For the Vlasta oil it is recorded at 0.60 for bishomohopanes (10t and 11t).

Oleanane, which suggests the terrestrial source input [22], has not been identified in the Vlasta oil.

Masses m/z 177 may indicate the presence of 25-norhopanes (10-desmethylhopanes) which were the result of aerobic biodegradation of oils [29]. In Vlasta oil C_{29}-25-nor-17α(H) hopane, the anticipated representative of 25-norhopanes, was not detected, and neither were its homologues. This suggests that Vlasta oil was very well preserved in a geological reservoir and that no apparent biodegradation took place.

CONCLUSIONS

The study of hydrocarbons in the Vlasta oil (121 components identified or characterized) offered a good insight into structural composition, as well as a reasonable basis for the study of its origin, deposition environment, maturity level and biodegradation rank.

The identified components indicate that Vlasta oil is composed of straight and branched alkanes, cycloalkanes and polycyclics, often with their aliphatic counterpart(s), and aromatics and thioethers. In terms of content, alkanes are found to prevail, while aromatic and sulphur compounds are found in low proportions.

Vlasta oil originates from marine organic matter, probably algae and/or bacteria. The biomass was deposited during the Triassic period in an anoxic hypersaline environment in a carbonate mineral matrix. Vlasta oil appears to be released from the related kerogen at its early maturation stage. The oil shows no significant biodegradation.

ACKNOWLEDGEMENTS

The authors are grateful to colleagues from INA, R&D Zagreb, and The Institute J. Štefan, Ljubljana, Yugoslavia, for analytical support.

REFERENCES

1 B. P. Tissot and D. H. Welte, *Petroleum Formation and Occurrence*. Springer, Berlin, 2nd ed., 1984.
2 J. M. Hunt, *Petroleum Geochemistry and Geology*, Freeman, San Francisco, CA, 1979.
3 J. Mühl, V. Scricá, G. Car and J. Jakopović, *Editions Technip, Collection Coloque et Seminaires*, 40 (1984) 340.
4 O. M. Kvalheim and N. Telnaes, *Anal. Chem.*, 57 (1985) 2858.
5 B. J. Fuhr, L. R. Holloway and C. Reicher, *J. Chromatogr. Sci.*, 26 (1988) 55.
6 H. M. Smith, *U.S. Bureau of Mines Bull.*, 642 (1968).
7 J. G. Erdman and D. A. Morris, *Am. Assoc. Petr. Geol. Bull.*, 58 (1974) 2326.
8 S. Zadro, J. K. Haken and W. V. Pinczewski, *J. Chromatogr.*, 323 (1985) 305.
9 E. J. Gallegos, in T. R. Ashe and K. V. Woods (Editors), *Nobel Techniques in Fossil Fuels Mass Spectrometry*, ASTM STP 1019. ASTM, Philadelphia, 1989, p. 94.
10 S. Derenne, C. Largeau, E. Casadevall, J. S. Sinninghe Damste, E. W. Tegelaar and J. W. De Leeuw, *Org. Geochem.*, 16 (1990) 873.
11 A. Jenisch, H. Richnow and W. Michaelis, *Org. Geochm.*, 16 (1990) 917.
12 P. G. Hatcher, *Org. Geochm.*, 16 (1990) 959.
13 G. Eglinton and M. Kalvin, *Sci. Am.*, 261 (1967) 32.
14 A. S. Mackenzie, S. C. Brassel, G. Eglinton and J. R. Maxwell, *Science*, 217 (1982) 491.
15 A. Alajbeg, J. Mühl, S. Marin-Mudrovčić and A. Putniković, *Org. Geochem.*, 13 (1988) 81.
16 A. Alajbeg, S. Švel-Cerovečki, A. Todorić, K. Horvat, A. Putniković and Š. Runjić, *Nafta*, 40 (1989) 393.
17 A. Alajbeg, V. Britvić, S. Švel-Cerovečki, Ch. Cornford, A. Todorić, J. Rajković, G. Barić and A. Putniković, *Org. Geochem.*, 16 (1990) 339.
18 G. Barić, *Nafta*, 39 (1988) 527.
19 G. Barić, J. Mesić, M. Jungwirth and D. Španić, *Nafta*, 41 (1990) 71.
20 J. M. Moldowan, C. Y. Lee, P. Sundararaman, T. Salvadori, A. Alajbeg, B. Gjukić and G. J. Demaison, *J.Am. Chem. Soc.; Prep. Am. Chem. Soc., Div. Pet. Chem.*, 34 (1989) 112.
21 M. Schoell, in J. Brooks and d. H. Welte (Editors), *Advances in Petroleum Geochemistry*, Academic Press, London, 1984, p. 21.
22 J. M. Moldowan, W. K. Seifert and E. J. Gallegos, *AAPG Bull*, 69 (1985), 1255.
23 E. E, Bray and E. D. Evans, *Geochem. Cosmochem. Acta*, 22 (1961) 2.
24 D. Payzant, D. S. Montgomery and O. P. Strausz, *Org. Geochem.*, 9 (1986) 357.
25 A. S. Mackenzie, in J. Brooks and D. H. Welte (Editors), *Advances in Petroleum Geochemistry*, Academic Press, London, 1984, p. 115.
26 G. Ourisson, P. Albrecht and M. Rohmer, *Pure Appl. Chem.*, 51 (1979) 709.
27 J. M. Moldowan, P. Sundararaman, And M. Schoell, in D. Leyhauser and J. Rullkotter (Editors) *Advances in Organic Geochemistry 1985*. Pergamon, Oxford, Vol. 10, 1986, p. 915.
28 J. J. Boon, H. Hines, A. L. Burlingame, J. Klok, W. I. C. Rijpstra, J. W. De Leeuw, K. E. Edmunds and G. Eglinton, in M. Bjorøy (Editor), *Advances in Organic Geochemistry 1981*. Wiley, Chichester, 1983, p. 207.
29 W. K. Seifert, J. M. Moldowan and G. J. Demaison, *Org. Geochem.*, 6 (1984) 633.

Journal of Chromatography, 557 (1991) 271–288
Elsevier Science Publishers B.V., Amsterdam

CHROM. 23 313

Identification of chlorophyll transformation products in a lake sediment by combined liquid chromatography–mass spectrometry

C. B. ECKARDT, B. J. KEELY and J. R. MAXWELL*
School of Chemistry, Organic Geochemistry Unit, University of Bristol, Cantock's Close, Bristol BS8 1TS (UK)

ABSTRACT

Negative-ion liquid chromatographic–mass spectrometric analysis of the pigment composition of the bottom sediment (15–20 cm) of a eutrophic lake revealed the presence of a novel series of chlorophyll transformation products, in which a series of C_{27}–C_{30} sterols and stanols are esterified to a pyrophaeophorbide *a* nucleus of algal origin. The major components are algal-derived chlorophyll *a* and *b* degradation products, and the presence of a bacteriochlorophyll-related phaeophytin indicates the presence of anoxic conditions extending into the photic zone when the sediment was laid down.

INTRODUCTION

Since the first report of the high-performance liquid chromatographic (HPLC) separation of chlorophyll transformation products [1], the technique has been developed further and been widely applied in the analysis of chlorophyll pigments, their degradation products and co-occurring carotenoid pigments. For example, the approach has been used to separate higher plant chlorophylls and carotenoids [2], bacteriochlorophylls of green photosynthetic bacteria [3], algal pigments [4–6] and sedimentary chlorins [7,8] and carotenoids [9]. The most widely used conditions have typically involved reversed-phase columns employing mixtures of aqueous and organic mobile phases, and using an ion-pair or buffer system to effect the separation of free acid pigments [5,6].

These studies have relied on a variety of approaches for the assignment of components, *inter alia* (i) retention time comparison with standards or with known distributions of components in selected organisms, (ii) single- [2] or dual-wavelength [4] detection by UV–VIS spectrophotometry, fluorescence detection [7,8], or a combination of both [10], (iii) stop-flow scanning [5] or diode-array detection [11]. Such approaches have proved adequate for pigment identification when the distributions are relatively simple, *e.g.*, from a single organism, or when the interest lies only in the assignment of the major components. In other circumstances, they may, however, be insufficiently precise for compound identification, as follows: (i) the mixtures are

0021-9673/91/$03.50

complex, *e.g.*, in surface sediments where the chlorophylls, their degradation products and the carotenoids have arisen from a variety of organisms and transformation pathways [8,12]; (ii) minor key components are of interest; (iii) novel compounds are present, *e.g.*, the recently identified bacteriochlorophyll *e* [13] or chlorophyll c_3 [14]. In these circumstances, the direct coupling of liquid chromatography with mass spectrometry (LC–MS), without a significant loss of chromatographic resolution, offers a means of obtaining structural information from consideration of the mass spectra of the individual compounds, and of detecting co-elution of components. Recently, we have demonstrated [15] that such an approach had the potential for application in the investigation of the transformations of chlorophylls in aquatic environments and for recognizing in bottom sediments components which could be markers for inputs from particular classes of organisms in the primary producer community. For example, bacteriochlorophyll *c*, *d* and *e* and their transformation products in sediments would be markers for the occurrence of anaerobic photosynthetic bacteria in the water column, and would, therefore, provide indirect evidence for the extension of anoxic conditions into the photic zone. Likewise, the occurrence of bacteriochlorophyll *e* in the water column of the Black Sea provides direct molecular evidence for such conditions [13].

In this study we describe the application of LC–MS to a further investigation of the tetrapyrrole assemblage of a Recent lake sediment which has previously been shown to contain a number of chlorophyll *a* and *b* transformation products [16,17]. Priest Pot (Cumbria, UK) is a small eutrophic lake [18,19] which becomes stratified owing to the development of a thermocline during the summer months. The phytoplankton periodicity is complex although, in general, species of Chlorophyta (green algae) dominate. Blooms of diatoms and of chlorococcales (green algae) and of volvocales (green algae) occur in the spring and summer, respectively, and blue-green algae are common. In addition, the presence of photosynthetic bacteria (Chlorobiacea e) has been reported [18,19].

EXPERIMENTAL

Sample extraction and fractionation

A frozen sediment sample (section 15–20 cm), obtained from a 1-m core of the bottom sediment from Priest Pot Lake [20], was allowed to thaw and excess water was removed by centrifugation (MSE, Crawley, UK; Centaur 1 with four-place swing-out No. 43124-126; 10 min at 3000 rpm). The sediment was extracted by sonication in acetone (*ca.* 1.5 ml g^{-1} sediment). Following centrifugation (as above) the supernatant was decanted and the extraction procedure repeated twice. The combined extracts were filtered and an aliquot for LC–MS analysis (Fig. 1a) was methylated using diazomethane. The remainder of the extract was fractionated by gel permeation chromatography (GPC) on a Polymer Labs. (Church Stretton, UK) PL-Gel (50 Å) column (600 mm × 7.5 mm I.D.) using a Spectra-Physics (Hemel Hempsted, UK) SP8000 ternary delivery HPLC system, fitted with a Rheodyne (Cotati, CA, USA) Model 7125 injection valve. HPLC chromatograms were obtained by monitoring the absorbance at 400 nm. Using methanol–dichloromethane (51:49, v/v) at a flow-rate of 1.5 ml min^{-1}, six fractions were collected (1–6 in Fig. 1b). Each was analysed by UV–VIS spectrophotometry (see below) and aliquots for LC–MS analysis were methylated using diazomethane.

Preparation of standards

Tetrapyrrole standards (see below) were prepared from chlorophyll *a* and *b*, according to previously published methods [21–23], and, after purification by reversed-phase HPLC, were characterized using fast atom bombardment (FAB) MS and ^{1}H NMR spectroscopic techniques [20]. Carotenoid standards were obtained Dr. H. Kjøsen (University of Trondheim, Norway) (isorenieratene **1**) and Dr. G. Britton (Biogeochemical Department, University of Liverpool, UK) (zeaxanthin, **2**). Standards used for relative retention time and mass spectral comparisons are listed in Table I.

To determine their detection limits in LC–MS analysis, injected quantities of pyrophaeophorbide *a* methyl ester (**4**) and phaeophytin *a* (**7**) were calculated by measuring the absorbance in acetone at 662 nm and using molar absorptivities of 0.146 and 0.061 l mol^{-1} cm^{-1}, respectively [20].

LC–MS

Instrumentation. LC–MS coupling was carried out using a Waters Assoc. (Watford, UK) MS 600 Silk quaternary delivery HPLC system and a Finnigan MAT (Hemel Hempsted, UK) TSQ 70 quadrupole mass spectrometer, linked via a Finnigan MAT TSP-2 thermospray interface [15]. Prior to entering the ion source, the HPLC effluent was passed through a variable-wavelength absorbance detector (Waters Model 484), to allow monitoring of the chromatographic separation. Sample injection was performed using a Rheodyne model 7125 injection valve, equipped with a 20-μl injection loop. The injector and the detector cell were chosen to withstand back-pressures up to 4000 p.s.i. The detector was linked to a VG (Altringham, UK) Minichrom data acquisition system, to allow UV–VIS-monitored chromatograms to be obtained.

HPLC conditions. Analyses were carried out under reversed-phase conditions, using two Waters Nova-Pak C_{18} radial compression cartridges (each 100 mm × 5 mm I.D.) in-line with a precolumn containing the same phase (Waters Guard-Pak C_{18}; 10 mm × 5 mm I.D.) and operated at a flow-rate of 1.0 ml min^{-1}, using a linear gradient

TABLE I

STANDARDS USED FOR RELATIVE RETENTION TIME AND MASS SPECTRAL COMPARISONS

Standard (structure)[a]	t_R (min)[b]
Phaeophorbide *a* methyl ester (**3**)	20.3
Zeaxanthin (**2**)	20.7
Pyrophaeophorbide a methyl ester (**4**)	23.1
Isorenieratene (**1**)	39.3
Phaeophytin *b* (**5**)	40.5
Pyrophaeophytin *b* (**6**)	43.5
Phaeophytin *a* (**7**)	44.0
Pyrophaeophytin *a* (**8**)	47.2

[a] For structures see Fig. 6.

[b] Reversed-phase HPLC (see Experimental).

TABLE II

SOLVENT ELUTION PROGRAMME FOR HPLC

Time (min)	Acetone (%)	Methanol (%)	Water (%)
0	0	90	10
5	0	90	10
15	70	15	15
40	90	5	5
75	90	5	5
85	0	90	10
95	0	90	10

programme (Table II). Typical back-pressures using the HPLC system off-line were *ca.* 1600 psi at 1.0 ml min^{-1} methanol–water (90:10, v/v). Conventional chromatograms were obtained by monitoring the absorbance at 400 nm. Prior to injection, samples were filtered through Millex GV_{13} 0.22-μm membrane filters (Millipore, Watford, UK).

Interface and MS conditions. The LC effluent was ionized in the discharge ionization mode, using the following source conditions: discharge voltage, 1200 V; vaporizer temperature, 65°C; source temperature, 250°C; repeller electrode, 0 V. Typical back-pressures were *ca.* 1900 p.s.i. with methanol–water (90:10, v/v) at 1.0 ml min^{-1}. Mass spectral information was obtained in the negative-ion mode, with scanning from m/z 300 to 1000 in 1.5 s.

UV–VIS spectrophotometry

Spectra (750–350 nm) were recorded in acetone (1 cm path length) using a Shimadzu (Duisburg, Germany) UV-180 spectrophotometer at a scan speed of 120 nm min^{-1} and a slit width of 2 nm.

Solvents

In general, doubly distilled solvents were used. For HPLC and LC–MS analyses HPLC-grade solvents, filtered through 0.2-μm membrane filters, were used.

RESULTS AND DISCUSSION

Fractionation of total extract

In earlier studies of the pigments of the surface sediment (0–5 cm) of Priest Pot [20], GPC was used to separate the carotenoid pigments (early eluting fraction) from the chlorophylls and their degradation products using dichloromethane as eluent, according to the method of Repeta [24]. Under these conditions, phaeophytins (*e.g.*, phaeophytin *a*, **7**) were separated (as a discrete fraction) from phaeophorbide methyl esters (*e.g.*, phaeophorbide *a*, **3**), and there was some separation within the latter fraction [20]. However, HPLC analysis of the tetrapyrroles revealed the presence of a complex mixture of components, particularly within the phaeophorbide-containing fraction.

In the present LC–MS study of the pigments from 15–20 cm depth, it was decided to use dichloromethane–methanol as GPC eluent, in an attempt (i) to improve

the separation within the phaeophorbide to allow more detailed fractionation and (ii) to allow a search for minor porphyrin transformation products from the chlorophylls *c*, which would be markers for the presence of diatoms and/or dinoflagellates in the water column when the sediment was laid down *ca*, 25–35 years ago. Under these conditions, however, true size-exclusion behaviour was not observed within the tetrapyrroles. Hence, the phaeophorbide methyl esters eluted before the phaeophytins and novel high-molecular-weight pyrophaeophorbide esters (see below). On the other hand, the conditions did allow these minor high-molecular-weight chlorins to be concentrated within one fraction, six fractions being collected (Fig. 1b). Assignment of

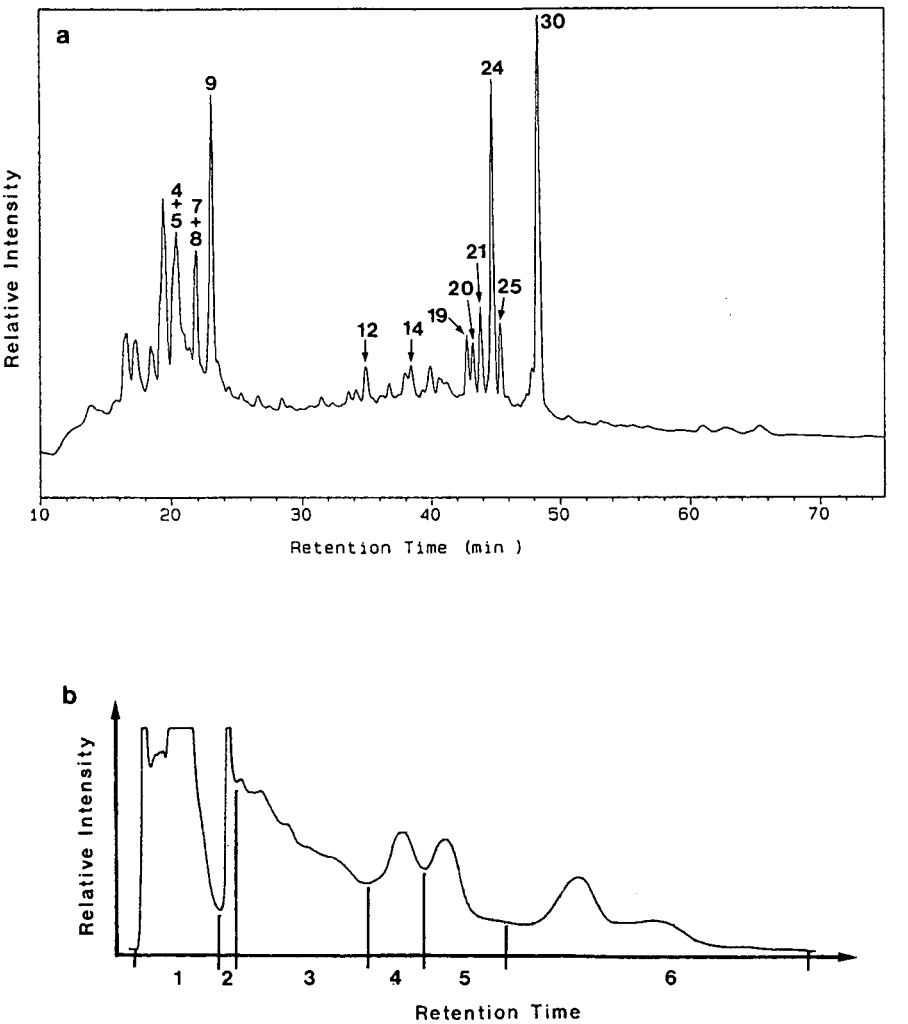

Fig. 1. (a) UV–VIS-detected chromatogram (400 nm) from the LC–MS analysis of the total methylated extract from the Priest Pot lake bottom sediment (15–20 cm). For peak identification see Table III; for HPLC and MS conditions see Experimental. (b) Gel permeation chromatogram (UV–VIS, 400 nm) from the separation of the total extract into GPC fractions 1–6. For conditions see Experimental.

components in the fractions was based on comparison of their negative-ion mass spectra and retention times with those of standards, or by mass spectral interpretation based on the fragmentation behaviour of the standards.

LC-MS spectra of phaeophytins and phaeophorbide methyl esters

As observed previously [15] for a number of chlorophyll *a*-derived standards, the chlorophyll *b*-derived standards used here show abundant $M^{-\cdot}$ species (Fig. 2). Also,

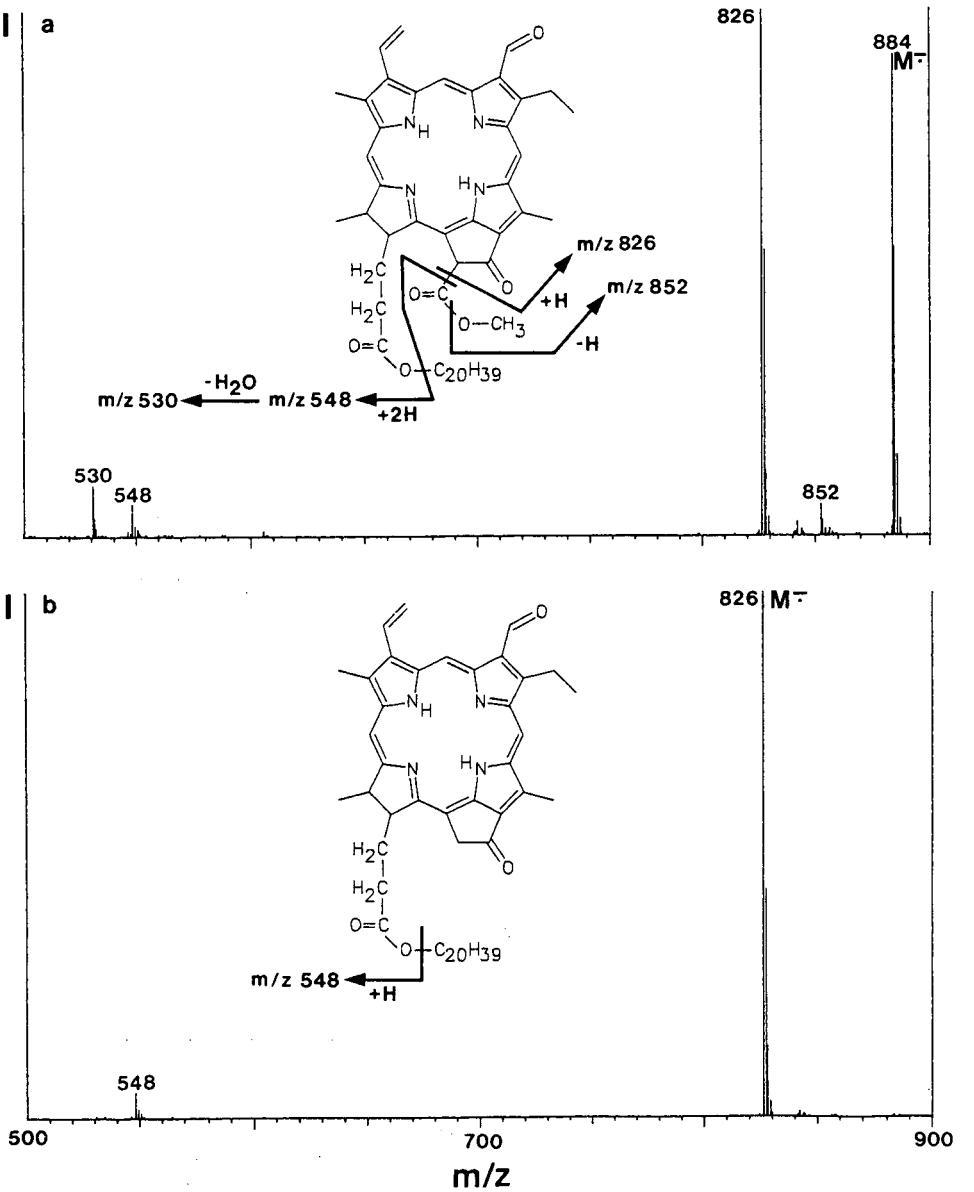

Fig. 2.

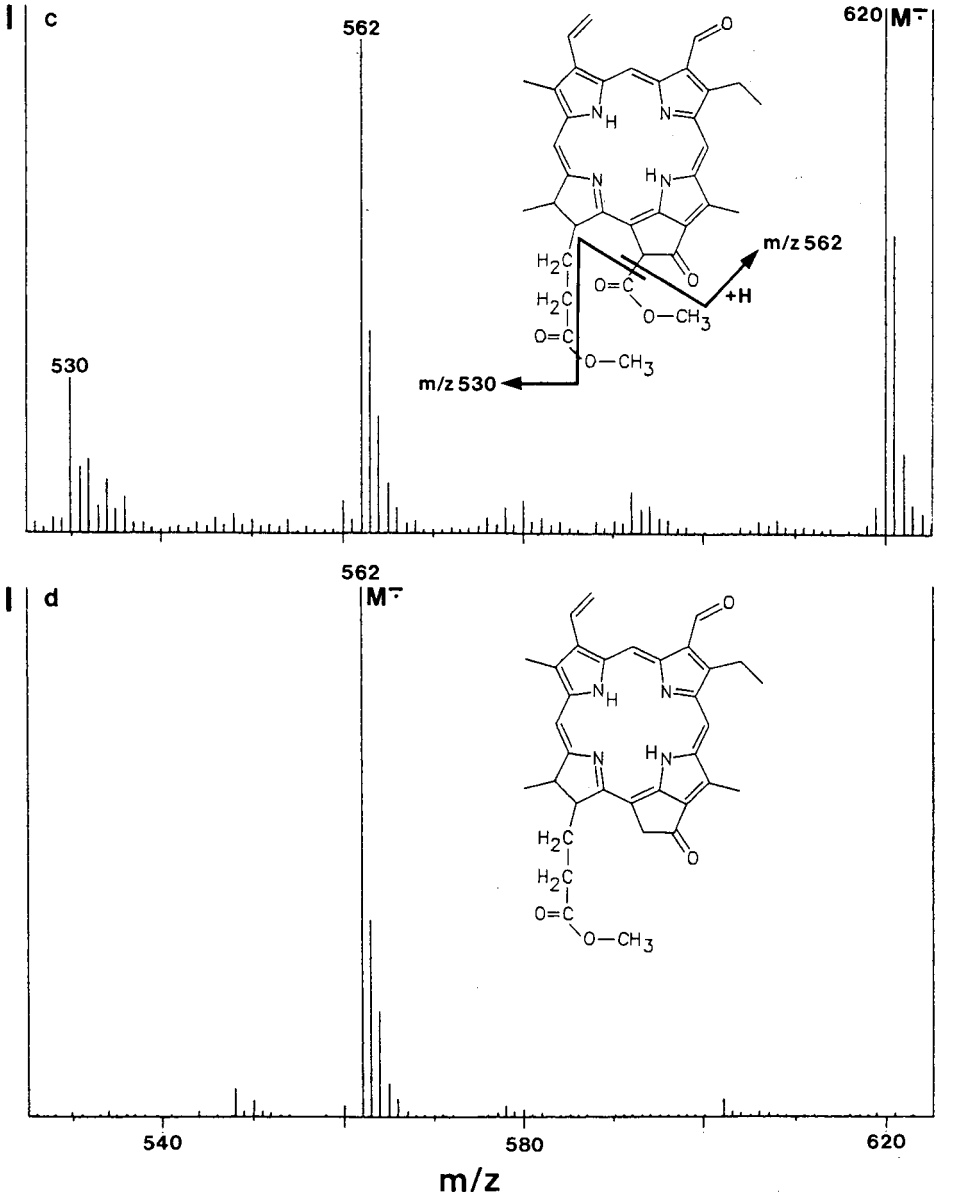

Fig. 2. Mass spectra of standards of (a) phaeophytin *b*, (b) pyrophaeophytin *b* and (c) phaeophorbide *b* methyl ester and (d) of peak 8 (*cf.*, Table III) in GPC fraction 3, obtained by negative-ion LC–MS with discharge ionization. Source conditions: source temperature, 250°C; discharge, 1200 V; vaporizer temperature, 65°C; repeller, 0 V. For HPLC conditions see Experimental.

the fragmentation (where observed) is explicable in terms of that seen under positive-ion FAB-MS conditions [25]. Hence, the spectrum of phaeophytin *b* (**5**), apart from $M^{-\cdot}$ at *m/z* 884 (Fig. 2a) and a minor ion at *m/z* 852, from loss of CH_3OH from

the C-13^2 carbomethoxy substituent, is dominated by *m/z* 826, corresponding to loss of the whole C-13^2 substituent with hydrogen transfer. The ion at *m/z* 548 results from additional loss of the phytyl side-chain (as $C_{20}H_{38}$), with *m/z* 530 representing additional loss of H_2O. In the spectrum of pyrophaeophytin *b* (Fig. 2b), lacking the C-13^2 carbomethoxy substituent, the only fragment ion occurs at *m/z* 548, again from loss of the phytyl substituent as $C_{20}H_{38}$. Perhaps surprisingly, no additional loss of H_2O was observed to give *m/z* 530, although this fragmentation is seen in the negative-ion mass spectrum of pyrophaeophytin *a* (**8**) [15]. The presence of the C-13^2

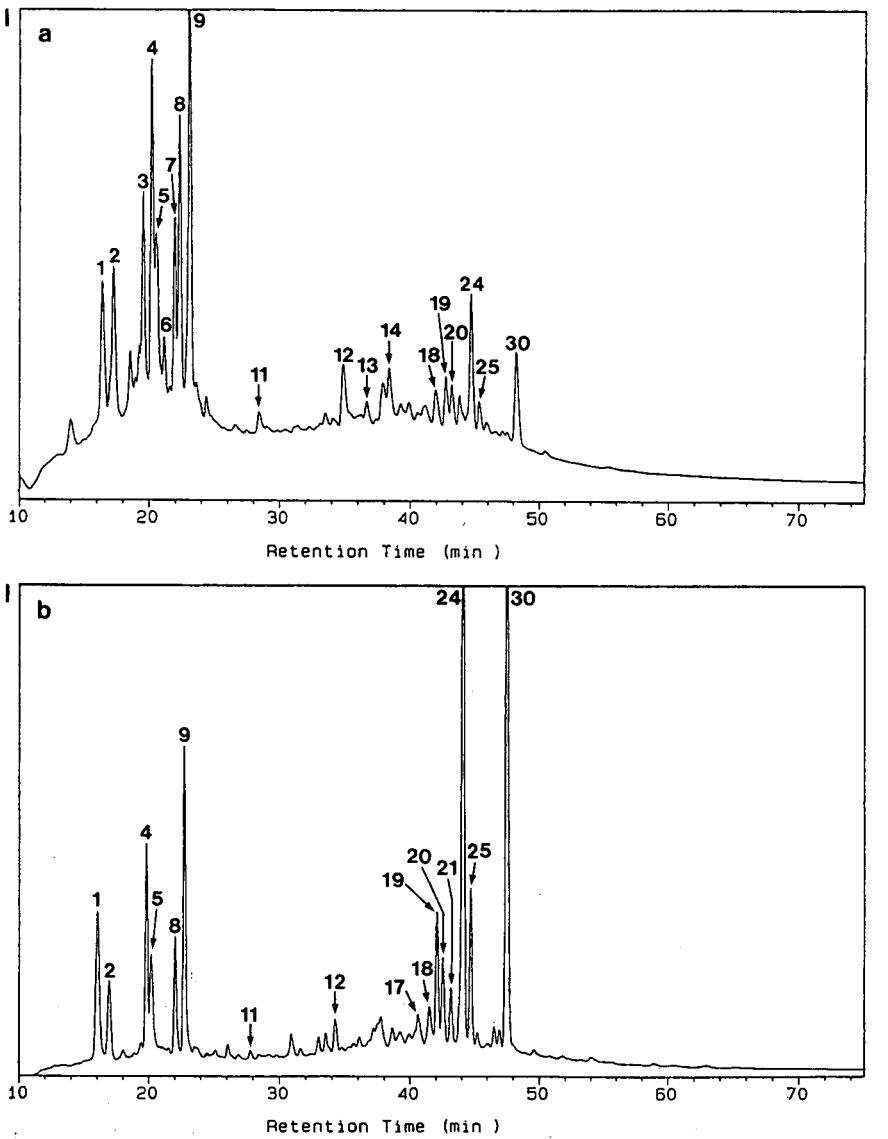

Fig. 3.

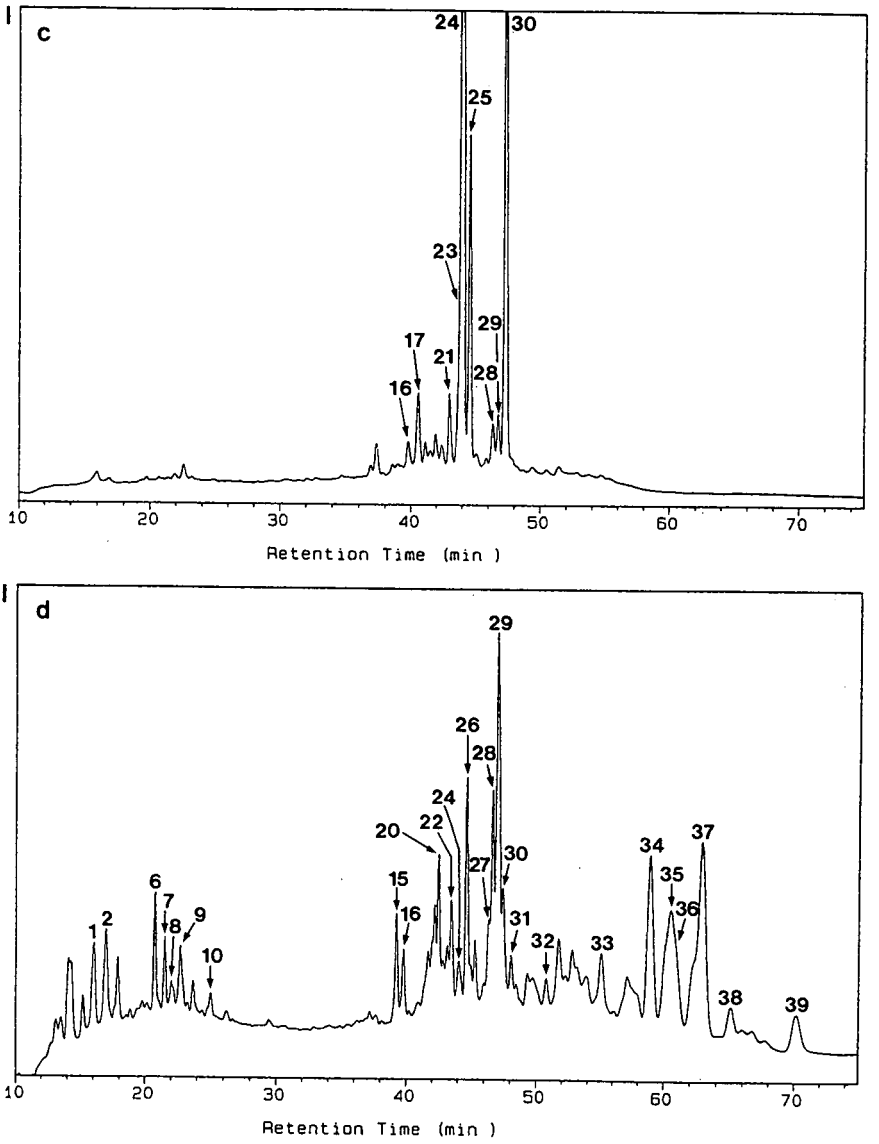

Fig. 3. UV–VIS-detected chromatograms (400 nm) from the LC–MS analyses of (a) GPC fraction 1, (b) GPC fraction 3, (c) GPC fraction 4 and (d) GPC fraction 6. For peak identification see Table III. For HPLC and MS conditions see Experimental.

carbomethoxy substituent in the spectrum of phaeophorbide *b* methyl ester (**9**, Fig. 2c) is readily observed by the presence of an abundant ion at *m/z* 562 (*cf.*, Fig. 2a, *m/z* 826), with the ion at *m/z* 530 corresponding to additional loss of CH_3OH within the C-17 propionic substituent. A standard of pyrophaeophorbide *b* methyl ester (**10**) was not available. The spectrum of peak 8 in gel fraction 1 (Fig. 3a) is shown in Fig. 2d. By

TABLE III
CHLOROPHYLL DEGRADATION PRODUCTS IN PRIEST POT SEDIMENT[a]

Peak	Fig.	$M^{-\cdot}$[b] (m/z)	Prominent ions[c] (m/z)	Assignment of major component(s)	Esterifying alcohol	Structure[d]
1[e]	3, 5		532, 516	Unidentified carotenoid		
2[e]	3, 5	622	532, 516	Unidentified carotenoid		
3[e]	3	564	562	Unidentified carotenoid		
4	1, 3, 5	606	566, *548*, *516*	Phaeophorbide *a*[f]	Methanol[g]	**3**
5[e]	1, 3, 5	606	582, 566, 562, *548*,	Phaeophorbide *a* epimer	Methanol[g]	**3**
		568	532, 518, *516*	Zeaxanthin[f]		**2**
6	3	564		Unidentified carotenoid		
7	1, 3	564		Unidentified carotenoid		
8	1, 3, 5	562		Pyrophaeophorbide *b*[h]	Methanol[g]	**10**
9[e]	3, 5	548	*516*	Pyrophaeophorbide *a*[f]	Methanol[g]	**4**
10	3		530, 516	Unidentified carotenoid(s)		
11	3, 5	770	566, 548, 516	Bacteriophaeophytin[h,i]	Farnesol	**11**
12[e]	1, 3, 5	788	594	Unknown phaeophytin		
		762		Unknown phaeophytin		
13[e]	3	802		Unknown phaeophytin		
		776		Unknown phaeophytin		
14[e]	1, 3	854	816, 564, 562	Unknown phaeophytin		
15	3	528		Isorenieratene[f]		**1**
16	3	528		Renieratene[h,i]		**16**
17[e]	3, 5	884	*826*, 814, *548*, *530*, 516	Phaeophytin *b*[f]	Phytol	**5**
		872		Pyrophaeophytin *b* methoxylactone[h]	Phytol	**14**
18[e]	3, 5	884	*826*, 814, *548*, *530*, 516	Phaeophytin *b* epimer	Phytol	**5**
		872		Pyrophaeophytin *b* methoxylactone epimer[h]	Phytol	**14**
19[e]	1, 3, 5	886	816, 758, 740, 552, 534, 530, 518, 516	Phaeophytin *a* allomer[j]	Phytol	
20	1, 3, 5	566		Unidentified carotenoid		
21[e]	1, 3, 5	916	886, 828, 812, 530, 516	Phaeophytin *a* methoxylactone[h]	Phytol	**15**
22[e]	3	598	534, 516	Unidentified carotenoid		
		566		Unidentified carotenoid		
23	3	826	812, 730, 548, *530*, 516	Pyrophaeophytin *b*[f]	Phytol	**6**
24	1, 3, 5	870	838, 826, 814, *812*, 794, *534*, *516*	Phaeophytin *a*[f]	Phytol	**7**

25	3, 5	870	838, 814, *812*, 794, 548, *534, 516*	Phaeophytin *a* epimer	Phytol	**7**
26	3	598	516	Unidentified carotenoid		
27	3	536	516	Carotenes[h,i]		
28	3	536	516	Carotenes[h,i]		
29	3	536	516	Carotenes[h,i]		
30[e]	1, 3, 5	812	*534, 516*	Pyrophaeophytin *a*[f]	Phytol	**8**
31[e]	3	868	812, 580, 536, 516	Unknown		
32[e]	3	902	716, 536, 516	Unknown		
		812		Unknown		
33[e]	3	944	812, 534[k], 530, 516	Pyrophaeophorbide *a* ester	C_{30} sterol *l*	
		930		Pyrophaeophorbide *a* ester	C_{29} sterol *l*	
		914		Pyrophaeophorbide *a* ester	C_{28} sterol *m*	
		900		Pyrophaeophorbide *a* ester	C_{27} sterol *m*	
34[e]	3	928	534[k], 516	Pyrophaeophorbide *a* ester	C_{29} sterol *m*	
		916		Pyrophaeophorbide *a* ester	C_{28} sterol *l*	
		902		Pyrophaeophorbide *a* ester	C_{27} sterol *l*	
35[e]	3	928	534[k], 516	Pyrophaeophorbide *a* ester	C_{29} sterol *m*	
		916		Pyrophaeophorbide *a* ester	C_{28} sterol *l*	
36[e]	3	930	534[k], 516	Pyrophaeophorbide *a* ester	C_{29} sterol *l*	
		928		Pyrophaeophorbide *a* ester	C_{29} sterol *m*	
		916		Pyrophaeophorbide *a* ester	C_{28} sterol *l*	
37[e]	3	930	534[k], 516	Pyrophaeophorbide *a* ester	C_{29} sterol *l*	
38[e]	3	930	788, 534[k], 516	Pyrophaeophorbide *a* ester	C_{29} sterol *l*	
		918		Pyrophaeophorbide *a* ester	C_{28} stanol	
39[e]	3	946	866, 534[k], 516	Pyrophaeophorbide *a* ester	C_{30} stanol	

[a] Based on spectral interpretation or comparison with spectra and relative retention times of standards.
[b] Molecular ion of major component(s).
[c] Other ions in mass spectrum. Fragment ions in spectra of standards given in italics.
[d] See Fig. 6.
[e] Co-elution.
[f] t_R and mass spectrum compared with authentic standard.
[g] Due to esterification prior to analysis.
[h] Tentative assignment.
[i] One of several possible structural isomers.
[j] Single-oxygen allomer.
[k] Fragment ion assigned to macrocycle.
[l] One double bond.
[m] Two double bonds.

comparison with the spectra in Fig. 2a–c, peak 8 was assigned as this component (Table III), although no ion at *m/z* 530 was apparent (*cf.*, Fig. 2c). The assignment remains, however, tentative, as the spectrum (not shown) of pyrophaeophorbide *a* methyl ester (**4**) does contain a low-intensity ion at *m/z* 516, corresponding to loss of CH_3OH from $M^{-\cdot}$.

Consideration of the spectra in Fig. 2 and of those of their chlorophyll *a*-derived counterparts allowed the assignment of several phaeophytins and phaeophorbide methyl esters on the gel fractions.

Gel fractions 1 and 2

The UV–VIS spectra (not shown) of fraction 1 (major, Fig. 3a) and fraction 2 (minor) showed them to be dominated by carotenoids. Hence, the Soret band of free base chlorins (*ca.* 400 nm) was obscured and any absorbance bands in the region of 664 nm, which would be typical of functionalized chlorins, were present only at very low relative intensities. The absorbance chromatograms obtained during LC–MS analysis showed, however, similar distributions of components at the wavelength monitored (400 nm), particularly within the tetrapyrroles. The spectrum of peak 5 indicated the presence of co-eluting components. One of these was shown to be the bicyclic carotenoid diol zeaxanthin (**2**), from comparison with the spectrum of a standard ($M^{-\cdot}$ = *m/z* 568 and little fragmentation) and with its retention time. A co-eluting tetrapyrrole was assigned as the C-13^2 epimer of phaeophorbide *a* methyl ester (**3**), based on retention time and mass spectral comparison with the epimer present in the standard of phaeophorbide *a* (*cf.*, peak 4 in Table III). The other tetrapyrroles assigned in fractions 1 and 2 are discussed in relation to fractions 3 and 4 where they are present in greater abundance.

Gel fraction 3

All of the phaeophorbide methyl esters in fractions 1 and 2 were present in fraction 3, the UV–VIS spectrum showing a dominance of chlorin components (λ_{max} 664 nm). Apart from the epimeric phaeophorbide *a* methyl esters (**3**, peaks 4 and 5), and pyrophaeophorbide *b* methyl ester (**10**, peak 8), the only other phaeophorbide was pyrophaeophorbide *a* methyl ester (**4**, peak 9).

The spectrum of a minor component (peak 11) showed $M^{-\cdot}$ at *m/z* 770 (Fig. 4a) and was tentatively assigned as a bacteriophaeophytin (**11**) derived from one of the bacteriochlorophylls *c* (**12**) or two of the bacteriochlorophylls *d* (**13**) from spectral interpretation. The absence of an abundant ion at *m/z* 712 confirms the absence of a C-13^2 carbomethoxy substituent (*cf.*, Fig. 2a and b). From comparison of the spectra of phaeophytin *a* (**7**) the ion at *m/z* 566 would correspond to loss of $C_{15}H_{24}$, indicating that the esterifying alcohol is farnesol, which would be lost as the tetraene (*cf.*, phytyl chain as phytadiene [15]). Similarly, *m/z* 548 is explicable in terms of additional loss of H_2O, as observed in the spectrum of phaeopthytin *a* [15]. The ions at *m/z* 516 and 530 are more difficult to explain in the absence of an appropriate standard. They may indicate the presence of a co-eluting tetrapyrrole component, although *m/z* 530 could result from an additional loss of H_2O from the C-3 secondary alcohol substituent (Fig. 4a). The presence of a bacteriochlorophyll transformation product, albeit in very low relative abundance, provides molecular evidence for the presence of anaerobic photosynthetic bacteria (see above) in the water column when the sediment was laid

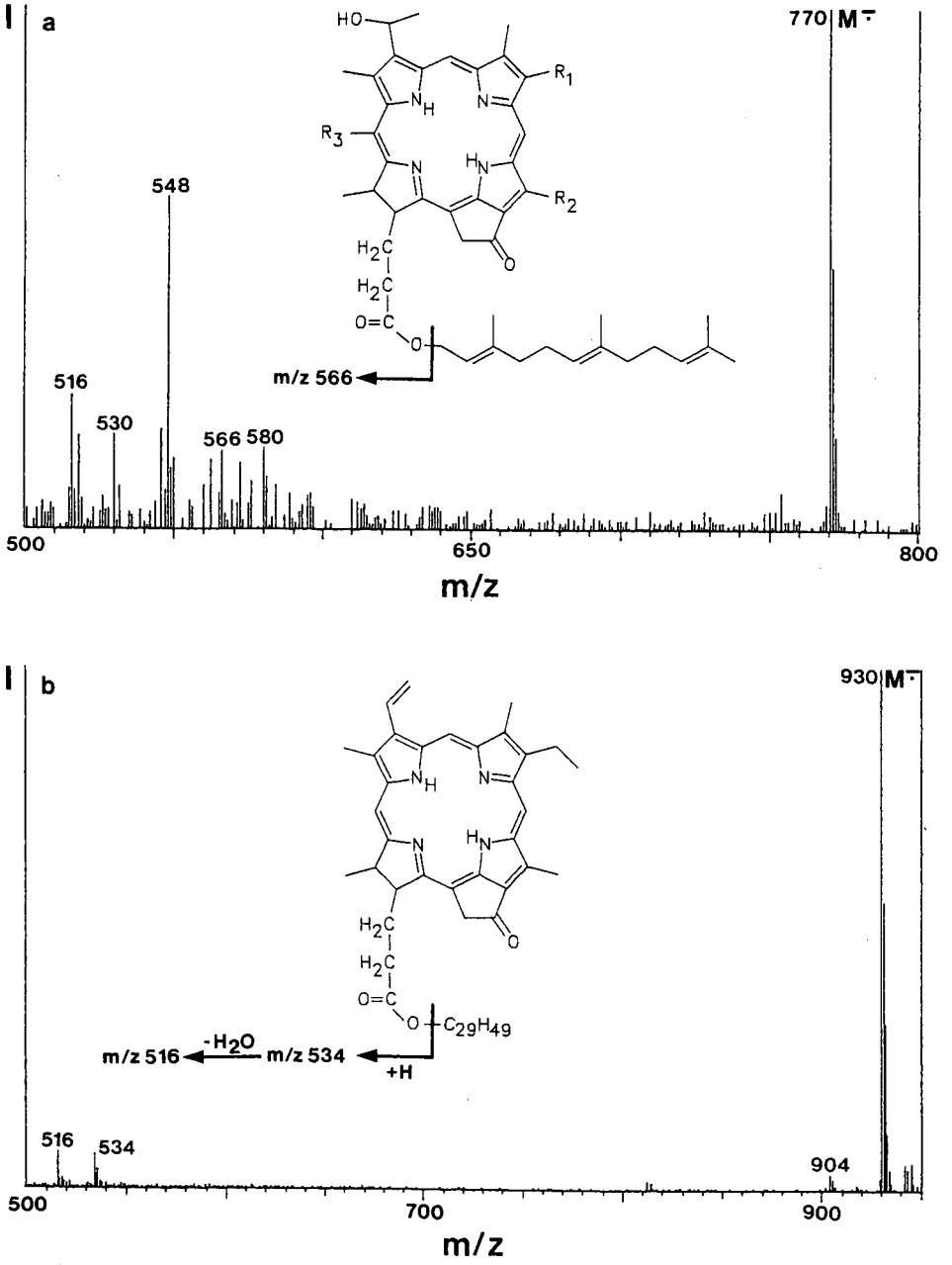

Fig. 4. Mass spectra of (a) peak 11 (*cf.*, Table III) and (b) major component in peak 37 (*cf.*, Table III), obtained by negative-ion LC–MS. Source conditions as in Fig. 2. For HPLC conditions see Experimental.

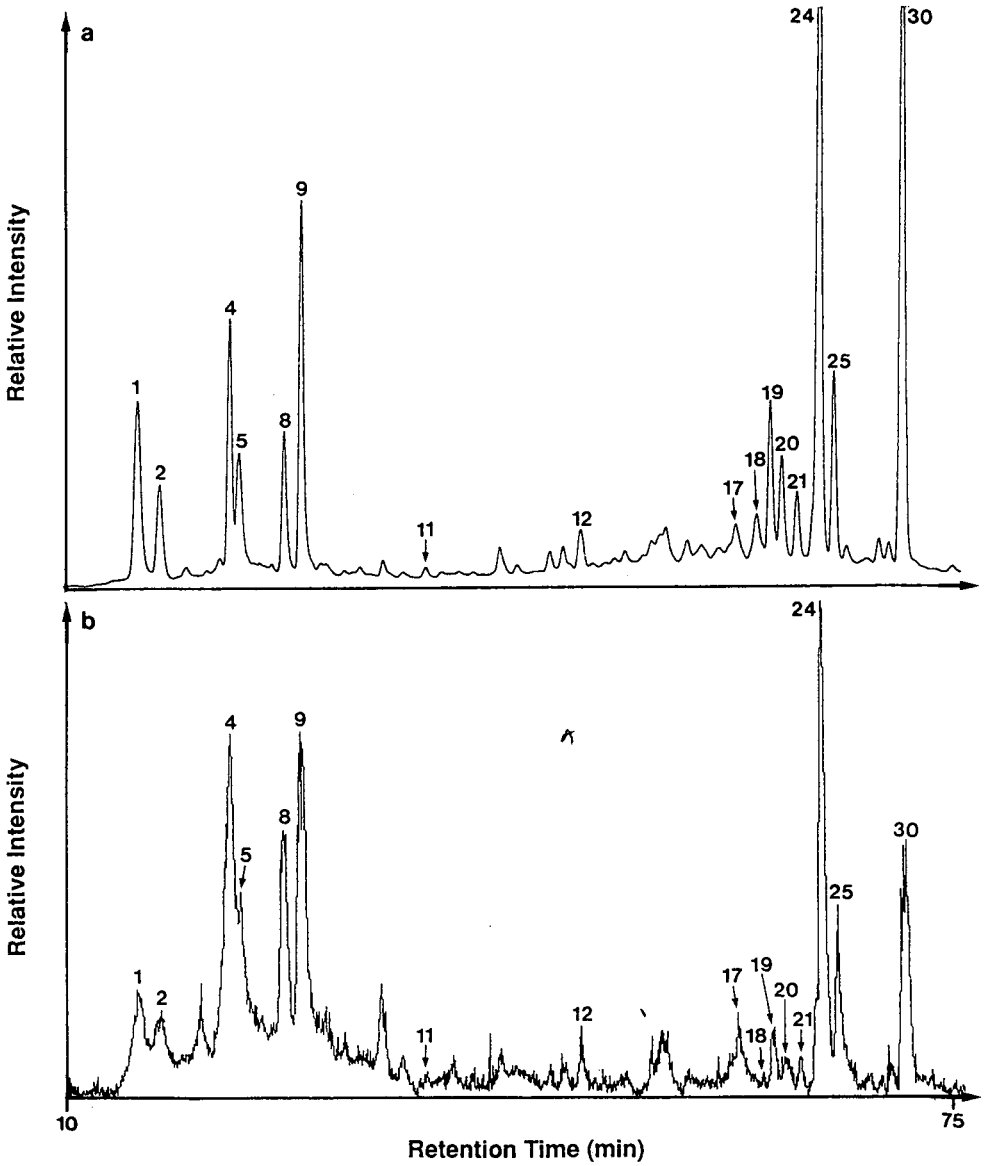

Fig. 5. Partial (10–75 min) (a) UV–VIS and (b) RIC chromatograms from negative-ion LC–MS analysis of GPC fraction 3. For peak identification see Table III. For HPLC and MS conditions see Experimental.

down *ca.* 25–35 years ago, although the dominance of chlorophyll *a*- and *b*-derived products in the sediment indicates that the major tetrapyrrole input was algal in origin.

Peak 12 appears to contain two other co-eluting phaeophytins ($M^{-\cdot}$ = *m/z* 788 and 762, Table III) with major components (peaks 24, 25 and 30) being the phaeophytin *a* epimers (**7**, $M^{-\cdot}$ = *m/z* 870) and pyrophaeophytin *a* (**8**, $M^{-\cdot}$ = *m/z* 812), as shown by comparison with standards.

Peak 17, as well as containing phaeophytin *b* (**5**), showed an abundant $M^{-\cdot}$ at *m/z* 872, which, based on its retention position, could correspond to the methoxylactone of pyrophaeophytin *b* (**14**), an autoxidation product formed in the presence of a nucleophilic solvent, *e.g.*, methanol [26]. Likewise, peak 18 appears to contain the C-13[2] epimer of this component, co-eluting with the phaeophytin *b* epimer (**5**). Similarly, peak 21, with $M^{-\cdot}$ at *m/z* 916, appears to contain the methoxylactone autoxidation product of phaeophytin *a* (**15**).

A comparison between the UV–VIS -monitored chromatogram of fraction 3 and the recontructed ion current chromatogram (RIC) is shown in Fig. 5, indicating only a slight loss of chromatographic resolution between the HPLC detector and the ion source. The differences in the relative abundances of the components are thought to result from differences in (i) absorption at 400 nm and (ii) ionization efficiencies [15]. From injection of a known amount (see Experimental) of pyrophaeophorbide *a* methyl ester (**4**) and of phaeophytin *a* (**7**), peaks 9 and 24 correspond to *ca.* 560 nmol and 880 nmol of these components. The detection limits of **4** and **7** to give an acceptable mass spectrum and a 3:1 signal-to-noise ratio in the mass chromatograms of *m/z* 548 (for **4**) and 870 (for **7**) were 15–25 nmol (10–20 μg).

Gel fractions 4 and 5

The UV–VIS spectra of fractions 4 (Fig. 3c) and 5 (minor) indicated them to contain predominantly tetrapyrrole pigments. The tetrapyrrole distributions are very similar and are dominated by phaeophytins (peaks 23–25 and 30, Table III) of the chlorophyll *a* and *b* series.

Gel fraction 6

This minor fraction showed a number of components found in earlier fractions, presumably as a result of "tailing" in the gel permeation chromatogram. Peaks 15 and 16 (Table III) were assigned as the aromatic carotenoid hydrocarbons isorenieratene (**1**, peak 15) and renieratene (**16**) or renierapurpurin (**17**) from comparison with a standard of isorenieratene. The occurrence of isorenieratene provides further molecular evidence for the presence of anaerobic photosynthetic bacteria in the water column when the sediment was laid down, as it has been reported as a major carotenoid in some species of the Chlorobiaceae [27], such bacteria having been reported to occur in the water column of Priest Pot (see above).

Peaks 33–39 showed a series of $M^{-\cdot}$ species which had unexpectedly high *m/z* values in comparison with the other tetrapyrroles observed. The spectrum of the major component in peak 37 (Fig. 4b) showed significant fragment ions at *m/z* 534 and 516. From direct comparison with the spectrum of pyrophaeophytin *a* [15], *m/z* 534 would indicate loss of the esterifying side-chain as $C_{29}H_{48}$ by way of a rearrangement with hydrogen transfer, *i.e.*, that the esterifying alcohol is a C_{29} monounsaturated sterol, as $C_{29}H_{48}$ corresponds formally to a C_{29} steroid diene. The ion at *m/z* 516 corresponds to an additional loss of H_2O [15]. The spectra from peaks 33–36 and 38–39 all showed similar characteristics, with *m/z* 534 and 516 as significant fragment ions (Table III), the differences being attributable to different C_{27}–C_{30} sterol or stanol esterifying moieties. On this basis, the chlorin nucleus appears to be the same as in pyrophaeophytin *a* (**8**). In this context, the two major esterified chlorins in an ancient lacustrine sediment of Miocene age, which were characterized after isolation of the

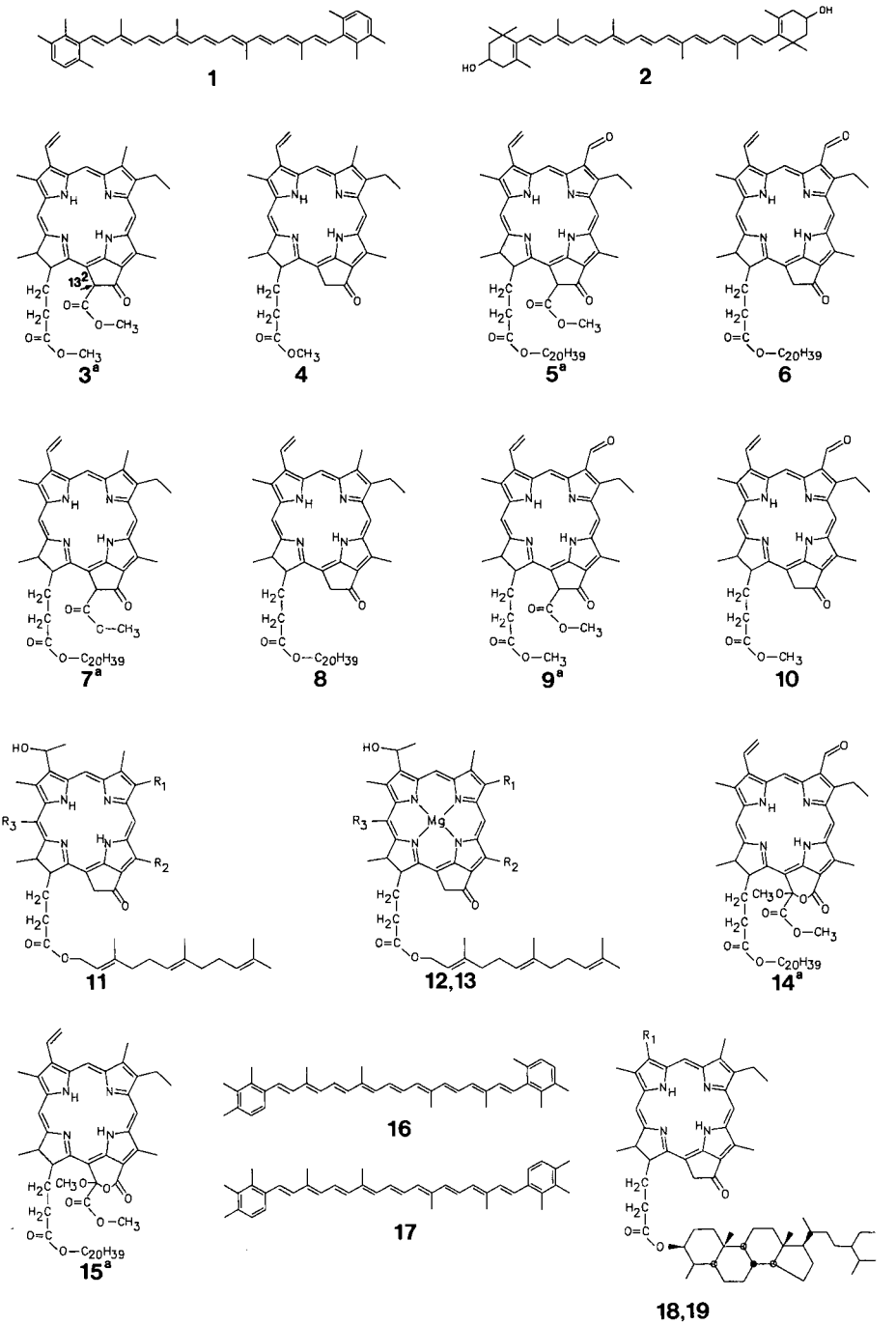

Fig. 6. Structures of compounds. **1** = Isorenieratene; **2** = zeaxanthin; **3**^{a} = phaeophorbide *a* methyl ester; **4** = pyrophaeophorbide *a* methyl ester; **5**^{a} = phaeophytin *b*; **6** = pyrophaeophytin *b*; **7** = phaeophytin *a*; **8** = pyrophaeophytin *a*; **9**^{a} = phaeophorbide *b* methyl ester; **10** = pyrophaeophorbide *b* methyl ester; **11** = major component in peak 11 (*cf.*, Fig. 3a and b), R_1 = Et, $R_{2,3}$ = Me or R_1 = *n*-Pr, R_2 = Me, R_3 = H or $R_{1,2}$ = Et, R_3 = H; **12** = bacteriochlorophyll *c*, R_1 = Et, $R_{2,3}$ = Me; **13** = bacteriochlorophyll *d*, R_1 = *n*-Pr, R_2 = Me, R_3 = H or $R_{1,2}$ = Et, R_3 = H; **14**^{a} = phaeophytin *b* methoxylactone; **15**^{a} = phaeophytin *a* methoxylactone; **16** = renieratene; **17** = renierapurpurin; **18** = pyrophaeophorbide *a* sterol ester (*cf.*, [28]), R_1 = vinyl; **19** = mesopyrophaeophorbide *a* sterol ester (*cf.*, [28]), R_1 = Et. [Me = methyl, Et = ethyl, Pr = propyl. ^{a} Epimeric at C-13^2 (*cf.*, **3**)].

individual components, are the novel sterol esters **18** and **19** [28]. In that case, since no chlorophylls with sterol side-chains are known, it was concluded that the components were of algal origin, with the esterification being a biological reaction occurring at the time of sediment deposition. This study provides further evidence for this hypothesis, as components of this type are present in a bottom sediment from a present-day lake, and suggests that esterification of phaeophorbides with algal sterols is a novel and widespread transformation of chlorophyll degradation products in the aquatic environment. Further studies involving full identification of the Priest Pot components are in progress.

CONCLUSIONS

Negative-ion LC–MS provides a valuable approach in the investigation of the complex degradative pathways of chlorophylls in aquatic environments, can assist in providing structural information about novel transformation products and readily reveals the presence of co-eluting components.

The major chlorins of the bottom sediment (15–20 cm) of Priest Pot lake are transformation products of chlorophylls *a* and *b* of algal origin. Despite the incomplete separation on 50 Å Styragel of the pigment classes, resulting from a change in elution solvent from dichloromethane to dichloromethane–methanol, LC–MS analysis of the fractions has revealed the presence of (i) marker compounds (**1** and **11**) indicative of the presence of photosynthetic bacteria in the water column when the sediment was laid down *ca.* 25–35 years ago, and (ii) an unexpected suite of chlorins esterified with a range of C_{27}–C_{30} sterols and stanols.

ACKNOWLEDGEMENTS

We thank the Deutsche Forschungsgemeinschaft (Ec 95/1-1) and the Natural Environment Research Council (GR3/6619) for financial support. Dr. P. A. Cranwell and Mr. P. V. Allen of the Freshwater Biological Association, Sawrey, are thanked for obtaining the sediment core. Mr. J. F. Carter is acknowledged for mass spectrometric assistance.

REFERENCES

1 N. Evans, D. E. Games, A. H. Jackson and S. A. Matlin, *J. Chromatogr.*, 115 (1975) 325.
2 K. Eskins, C. R. Scholfield and H. J. Dutton, *J. Chromatogr.*, 135 (1977) 217.
3 M. B. Caple, H. Chow and C. E. Strouse, *J. Biol. Chem.*, 253 (1978) 6730.
4 S. W. Wright and J. D. Shearer, *J. Chromatogr.*, 294 (1984) 281.
5 R. F. C. Mantuora and C. C. Llewellyn, *Anal. Chim. Acta*, 151 (1983) 297.
6 M. Zapata, A. M. Ayala, J. M. Franco and J. L. Garrido, *Chromatographia*, 23 (1987) 26.
7 L. M. Brown, B. T. Hargrave and M. D. Mackinnon, *Can. J. Fish. Aquat. Sci.*, 38 (1981) 205.
8 G. Liebezeit and J. Bartel, *J. High Resolut. Chromatogr. Chromatogr. Commun.*, 6 (1983) 573.
9 S. K. Hajibrahim, P. C. Tibbetts, C. D. Watts, J. R. Maxwell, G. Eglinton, H. Colin and G. Guiochon, *Anal. Chem.*, 50 (1978) 549.
10 W. W. Gieskes and G. W. Kraay, *Mar. Biol.*, 92 (1986) 45.
11 R. F. C. Mantuora and C. C. Llewellyn, *J. High Resolut. Chromatogr. Chromatogr. Commun.*, 7 (1984) 632.
12 D. J. Repeta and R. B. Gagosian, *Nature (London)*, 295 (1982) 51.
13 D. J. Repeta, *Nature (London)*, 342 (1989) 69.

14 C. J. R. Fookes and S. W. Geoffrey, *J. Chem. Soc., Chem. Commun.*, (1989) 1827.
15 C. B. Eckardt, J. F. Carter and J. R. Maxwell, *Energy Fuels*, 4 (1991) 741.
16 B. J. Keely and R. G. Brereton, *Org. Geochem.*, 10 (1986) 975.
17 B. J. Keely, R. G. Brereton and J. R. Maxwell, *Org. Geochem.*, 13 (1988) 801.
18 N. Robinson, *Ph.D. Thesis, University of Bristol*, Bristol 1984.
19 N. Robinson, P. A. Cranwell, B. J. Finlay and G. Eglinton, *Org. Geochem.*, 6 (1984) 143.
20 B. J. Keely, *Ph.D. Thesis*, University of Bristol, Bristol 1989.
21 F. C. Pennington, H. H. Strain, W. A. Svec and J. J. Katz, *J. Am. Chem. Soc.*, 86 (1964) 1418.
22 P. H. Hynninen, *Acta Chem. Scand.*, 27 (1973) 1771.
23 G. W. Kenner, S. W. McCombie and K. M. Smith, *J. Chem. Soc., Perkin Trans. 1*, (1973) 2517.
24 D. J. Repeta, *Ph.D. Thesis*, Massachusetts Institute of Technology, Woods Hole, 1982.
25 B. J. Keely and J. R. Maxwell, *Energy Fuels*, 4 (1991) 737.
26 P. M. Schaber, J. E. Hunt, R. Fries and J. J. Katz, *J. Chromatogr.*, 316 (1984) 25.
27 S. Liaaen-Jensen, E. Hegge and L. M. Jackman, *Acta Chem. Scand.*, 18 (1964) 1703.
28 W. G. Prowse and J. R. Maxwell, *Org. Geochem.*, in press.

Journal of Chromatography, 557 (1991) 289–305
Elsevier Science Publishers B.V., Amsterdam

CHROM. 23 276

Characterization of a tryptic digest by high-performance displacement chromatography and mass spectrometry[a]

JOHN FRENZ*, CYNTHIA P. QUAN and WILLIAM S. HANCOCK
Department of Medicinal and Analytical Chemistry, Genentech, Inc., 460 Point San Bruno Blvd., South San Francisco, CA 94080 (USA)
and
JAMES BOURELL
Department of Protein Chemistry, Genentech, Inc., 460 Point San Bruno Blvd., South San Francisco, CA 94080 (USA)

ABSTRACT

High-performance displacement chromatography (HPDC) provides a means of increasing the capacity of a chromatographic column, while maintaining the resolution afforded by high-performance liquid chromatographic (HPLC) instruments. The high capacity and high resolution of HPDC can be exploited in tryptic mapping to facilitate the characterization of a protein preparation. In this manner, minor constituents of the mixture, which may be difficult to isolate by conventional chromatographic methods, can be obtained in sufficient amounts to permit chemical characterization by established techniques. The isolation by HPDC of peptides obtained by digestion of recombinant human growth hormone (rhGH) and the subsequent characterization of the peptides are described. The identification of certain of these peptides revealed information on the specificity of trypsin for the substrate, rhGH, and for autolysis. Fractions from the HPDC tryptic map were collected and analyzed by electrospray ionization mass spectrometry (ESI-MS) either directly or following further separation by gradient elution HPLC. Fragment ions observed in the ESI mass spectra facilitated identification of peptides obtained by HPDC tryptic mapping.

INTRODUCTION

Displacement chromatography is a mode of operating a chromatographic separation that significantly increases the feed loading capacity of the column while maintaining high resolution and high speed. The enhanced capacity attainable in displacement chromatography has prompted studies of its feasibility for preparative- and process-scale purification [1–6]. While the main features of displacement chromatography were described by Tiselius almost 50 years ago [7], it has recently been re-established as a convenient means of increasing the capacity of preparative high-

[a] Presented at the *14th International Symposium on Column Liquid Chromatography (HPLC '90), Boston, May 20–25, 1990*, under the title "HPDC–MS: Chromatography for the Masses". The majority of the papers presented at this symposium have been published in *J. Chromatogr.*, Vols. 535 (1990) and 536 (1991).

0021-9673/91/$03.50

performance liquid chromatography (HPLC). The resulting approach to preparative separations on high-efficiency analytical instrumentation has been termed high-performance displacement chromatography (HPDC) [8,9]. This approach has been shown to increase by one to two orders of magnitude the amount of a feed mixture that can be purified in a single run on analytical chromatographic equipment [10–12].

The feature that distinguishes displacement from elution chromatography is that rather than being washed (eluted) from the column, the feed components are displaced from the surface by a solution of a strongly retained substance that follows the feed into the column. In elution chromatography the eluent contains a modifier, whether an organic solvent in reversed-phase chromatography or a salt in ion-exchange chromatography, that is less strongly retained than the feed components to be separated. The modifier is employed at a sufficiently high concentration that it washes the feed components from the surface and as a result the separated bands of the feed mixture leave the column mixed with the eluent modifier. In displacement chromatography, on the other hand, the displacer is more strongly retained than the feed components, it is pumped into the column only after the feed mixture has been loaded and the separated bands leave the column just *ahead* of the displacer, rather than mixed with it. As described more fully below, the separated feed components leave the column as adjacent, rectangular bands, rather than as discrete peaks as in elution chromatography. The concentrations of the bands containing individual purified feed components are fixed, independent of the amount of the feed [13], so the volume occupied by a component as it leaves the column is uncoupled from its resolution from other feed components, unlike peak width in elution chromatography. In the latter instance, resolution suffers as the peak width and loading increase [14], so the column capacity is governed by the band-broadening characteristics of the separation conditions. The added control over the concentration and volume of the separated bands afforded by operating the column in the displacement mode increases the capacity of the chromatographic equipment and accounts for the advantages of this approach for large-scale, high-performance separations [15].

The high capacity and control over the concentrations of bands in displacement chromatography also have potential advantages for enhancing the sensitivity of analytical and micro-preparative applications of HPDC. One factor determining the detectability of a component of a mixture is the amount of that component in the sample, so increasing the feed capacity in an analytical system increases the detectability of minor components of a complex mixture. In addition, as noted above, the concentration of a band in displacement chromatography is controlled by the operating conditions, so even a minor component will be focused into a narrow, concentrated band in the fully developed displacement chromatogram. This focusing effect can be exploited to enhance significantly the detectability of trace mixture components, as has been argued by Guiochon and co-workers [16,17].

The displacement mode has previously been applied to the analysis of a tryptic mixture by capillary liquid chromatography coupled with continuous-flow fast atom bombardment mass spectrometry [18]. In that application, the flow-rate and column dimensions were constrained by the high-vacuum requirements of the mass spectrometer, so HPDC permitted enhanced column capacity and increased detectability of minor components of the mixture. Those findings also revealed that the mass spectrometer is a nearly ideal detector for displacement chromatography of peptides as it

rapidly and selectively monitors the composition of the displacement train leaving the column.

The high column capacity and focusing of minor components of a mixture can be applied to effect the preparative isolation of useable amounts of minor components of a mixture for characterization by a variety of techniques. In this paper, the isolation of components of a tryptic digest of recombinant human growth hormone (rhGH) is demonstrated on conventional analytical-scale columns and instrumentation. Off-line approaches to coupled displacement chromatography and mass spectrometry and sequential displacement chromatography with separation of fractions by elution liquid chromatography and identification of peptides by mass spectrometry were used to confirm the identity of peptides identified previously by directly coupled DC–MS [18]. The coupling of DC with LC analysis of fractions was employed to provide quantitative assessment of the amounts of peptides identified by MS. Fragmentation information has been obtained from spectra of peptides analyzed on an electrospray ionization mass spectrometer. This additional information confirmed the amino acid sequence for certain of the peptide molecular ions [19,20].

THEORY

Displacement chromatography, as described originally by Tiselius [7], is the mode of chromatography in which a solution of a substance, the displacer, with a stronger affinity for the stationary phase than any of the feed components, is made to flow into the column behind the feed. The operating conditions are chosen so that the displacer saturates the column and drives the feed mixture ahead of it. The concentration of the displacer is constant at the column inlet, so the saturation front moves with constant velocity as a step increase in concentration down the column. Ahead of the displacer, the feed components arrange themselves into rectangular bands that move together, in sequence, according to their relative affinities for the stationary phase, in a "displacement train" down the column. Despite the similarities in terminology, displacement chromatography is distinct from affinity chromatography [21], as no specific interaction between a feed component and a bound ligand is exploited in HPDC. Rather, *relative* affinities among the feed components and displacer are exploited to achieve separation, and the HPDC operating mode can be carried out on non-specific sorbents such as those used in reversed-phase and ion-exchange chromatography.

Feed components arrange themselves into rectangular bands in the displacement train under the influence of the displacer front, which moves the feed mixture forward at constant velocity, and the adsorption isotherms that govern the equilibrium between the mobile and stationary phases. In many adsorptive processes the adsorption isotherms for individual components are concave downward, such as are shown in Fig. 1 for four different species. The concave downward isotherm is characteristic of a saturable stationary phase surface. The adsorption isotherm governs the phase equilibrium of a substance and, concomitantly, governs the velocity of the substance in the chromatographic column. The speed of the displacer front as it moves down the column is given by the expression [22]

$$v_d = \frac{v_o}{1 + \Phi q_d / c_d} \quad (1)$$

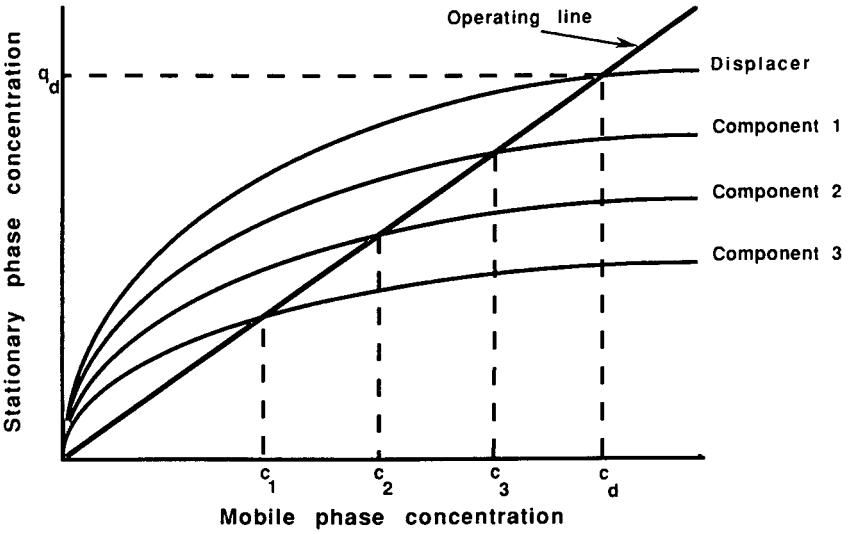

Fig. 1. Schematic diagram of individual adsorption isotherms illustrating the relationships among feed component concentrations and the displacer concentration in the displacement train. The operating line connects the point on the isotherm corresponding to the displacer concentration, c_d, with the origin. c_1, c_2 and c_3 are the isotachic concentrations of the feed components and c_d is the displacer concentration.

where v_o is the velocity of the mobile phase through the column, q_d is the stationary phase concentration of the displacer in equilibrium with a mobile phase concentration c_d and Φ is the phase ratio of the column. The ratio $q_d c_d$ which, from eqn. 1, determines the speed at which the displacer moves down the column, can be represented graphically by the chord to the displacer isotherm in Fig. 1. In the fully developed displacement train, each separated component of the feed moves at the same speed as the displacer front, and the velocity of the individual bands in the train can be described by equations exactly analogous to eqn. 1. Hence, the velocities of the individual species in the train are also governed by the ratio q_i/c_i, where i represents a single component of the feed mixture. As the velocities of all components of the mixture are equal to that of the displacer front in the fully developed train, then

$$q_d/c_d = q_i/c_i \tag{2}$$

for all components of the mixture. Graphically, this is represented in Fig. 1 by the intersection of the chord to the displacer concentration with each individual isotherm of the feed components. The chord thus governs the speed of the displacer front and of the bands in the displacement train, and has been termed the "operating line" [23]. The point at which the operating line intersects its isotherm governs the speed of the zone of an individual component through the column and fixes the concentration of the zone in the displacement train. This accounts for the rectangular bands characteristic of displacement chromatography, as individual components are thermodynamically contrained to move through the column at the concentration established by the relationship in eqn. 2. As the concentration of a band in the displacement train is

fixed, the volume occupied by a given component of the mixture is variable, and depends on the amount of that component present in the feed mixture. Hence a major constituent of the mixture will form a relatively wide band in the displacement train whereas a trace component of the mixture will form a relatively narrow band [16,17].

These features account for certain of the advantages of the displacement mode over conventional elution chromatography in both preparative and analytical separations. In elution chromatography, the relationship between band height and width (*i.e.*, a solute's concentration and volume) is more complex than in HPDC. When the column is underloaded, all peaks have roughly the same width, so that peak height is dependent on the amount of a component present in the feed mixture and retention times are constant. This simple, predictable relationship accounts for the broad acceptance of linear elution chromatography since its inception 40 year ago [24]. On overloading the column, the peaks of the major constituents of the mixture will be overloaded, with both high concentrations at the apex and broadening due to the skewing effect of saturating the stationary phase [22]. Minor components of the mixture, on the other hand, form small peaks, which may also be skewed owing to interference effects from the major components of the mixture [25]. The complex behavior of overloaded elution chromatography limits its utility in analytical applications.

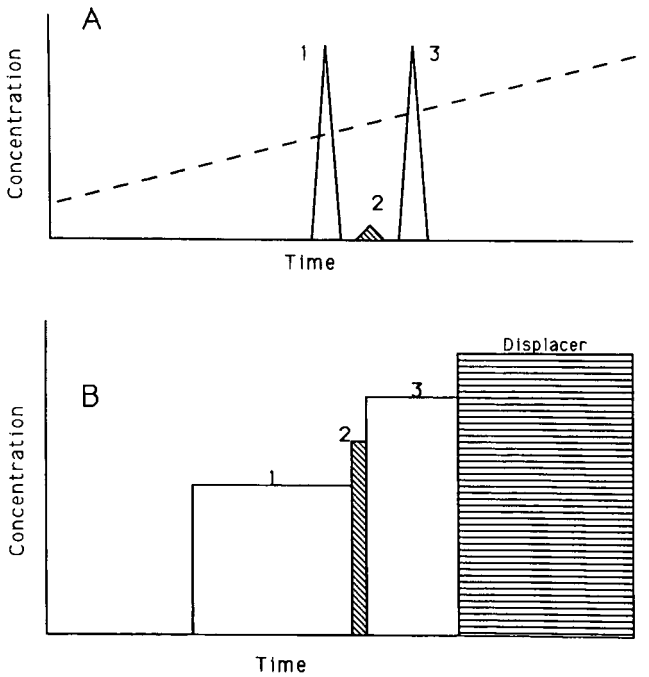

Fig. 2. Comparison of (A) elution and (B) displacement chromatograms of a mixture consisting of two major components (1 and 3) and one trace component (2). The dashed line in (A) illustrates the increase in eluent modifier concentration in the mobile phase in gradient elution chromatography. The larger feed load and focusing effect afforded by operating in the displacement mode are illustrated in (B), and account for the advantages of HPDC for the analysis of minor components of a mixture.

The analysis of minor components of a mixture can be facilitated by using the displacement mode of chromatography, in which all bands within the displacement train form relatively concentrated bands, as described above. The minor components are thus focused between bands of major components of the mixture, as shown schematically in Fig. 2, which compares chromatograms obtained in linear elution and displacement chromatography. The linear elution profile (Fig. 2A) shows the minor component of the mixture as a small peak between two larger peaks that represent major components. In the displacement chromatogram (Fig. 2B), the minor component is represented as a tall narrow band focused between two larger, broad rectangular bands of the major components of the mixture. Fig. 2 illustrates the two advantages expected from analytical displacement chromatography: first, the minor components of the mixture are focused into narrow bands, and second, a larger feed can be separated in a single run, permitting a larger loading of trace components. The larger load and focusing of minor components by displacement chromatography have been advanced as a powerful means of enhancing the detectability of these species [16–18].

EXPERIMENTAL

Materials

Trifluoroacetic acid (TFA) was obtained from Pierce (Rockford, IL, USA). L-1-Tosylamide-2-phenylethyl chloromethyl ketone (TPCK)-treated bovine trypsin was obtained from Worthington (Freehold, NJ, USA). Water was purified with a Milli-Q system from Millipore (Bedford, MA, USA). Hydrochloric acid and cetyltrimethylammonium bromide (CTAB) were from Aldrich (St. Louis, MO, USA) and HPLC-grade acetonitrile (ACN) from Burdick & Jackson (Muskegon, MI, USA). Recombinant human growth hormone was expressed in *E. coli* at Genentech. All other chemicals were of ACS grade or better.

Methods

Tryptic digest. Digestion with trypsin was carried out by reconstituting 10 mg of rhGH in 4 ml of 100 m*M* Tris–acetate buffer (pH 8.3), warming the sample to 37°C and adding 100 μg of trypsin. After 2 h, a second aliquot of 100 μg of trypsin was added. Digestion was stopped 2 h later by lowering the pH of the solution below 3 with 1 *M* hydrochloric acid. The digest mixture was stored at 5°C until analyzed.

HPLC analyses. Tryptic maps were produced by reversed-phase HPLC on a Hewlett-Packard (Palo Alto, CA, USA) Model 1090M system equipped with a Nucleosil C_{18} (Alltech, Deerfield, IL, USA) column. An aliquot of the tryptic digest mixture was injected into the column equilibrated at 35°C with 0.1% aqueous TFA at a flow-rate of 1 ml/min. A linear gradient to 40% ACN over 20 min was started upon injection. At the end of the gradient, the ACN content was increased to 70% over 1 min. The column effluent was monitored at 214 nm. Peaks were identified by comparison of retention times with previously characterized maps [26]. Analyses of fractions collected from the displacement separation were carried out under the same conditions. Peaks analyzed off-line by mass spectrometry were collected manually from separations carried out under identical conditions, except on an HP 1050 instrument equipped with a FIatron Laboratory Systems (Oconomowoc, WI, USA) Model CH-30 column heater.

HPDC tryptic map. The displacement separations were carried out on the Hewlett-Packard 1090M HPLC instrument with two 150 mm × 0.46 mm (I.D.) Nucleosil C_{18} columns connected in series. A 9-mg aliquot of the digest mixture was injected into the column, equilibrated with a carrier solvent consisting of 0.1% TFA in water. After a 5-min hold, the displacer solution consisting of CTAB and 0.1% TFA in water was pumped into the column at a flow-rate of 1 ml/min. The switch from starting eluent to displacer solution occurred within a 1-min period. Fractions were collected at 1-min intervals. The absorbance detector monitored the column effluent at 214, 254 and 280 nm.

Mass spectrometry. Mass spectra were acquired with a Sciex (Thornhill, ON, Canada) API-III triple quadrupole mass spectrometer equipped with an ionspray interface. Peptides were infused in a solution of 50% acetonitrile and 1% formic acid in water at a flow-rate of 10 μl/min. The orifice voltage was set to 80 V and the ionspray potential to 4500–5000 V.

RESULTS AND DISCUSSION

The rationale for adopting HPDC for mapping the peptides formed by tryptic digestion of a protein is to characterize the minor components of the mixture whose presence conveys information about the composition of the protein preparation digested and also about the specificity of the enzymatic digestion and side-reactions occurring in the digestion. Chief among the objectives of examining the "fine structure" in the enzymatic map is to identify the tell-tale peptides indicating the presence of protein variants in the preparation. These variants can arise from degradative processes acting on the protein, such as deamidation, oxidation and proteolysis, from incorrect folding and disulfide rearrangement, from errors in translation by the host cell [27], from chemical modifications to the protein caused by processing conditions used, for example, to cleave the target protein from a larger fusion construct, or from the heterogeneity conferred on a glycoprotein by the covalently linked carbohydrate structures. Other peptides occurring at low levels in the tryptic map may arise as artifacts of the digestion process, resulting either from autoproteolysis of trypsin [28] or from non-specific cleavages of the protein that are observed even in highly purified preparations of proteolytic enzymes. Finally, host cell proteins may also contribute to the low-level contaminants found in the peptide mixture, although in a pharmaceutical-grade protein these contaminants are expected to be present at undetectable levels [29]. Hence, the information content of the minor components of a mixture can be sufficient to warrant development of methods, such as HPDC, for closer examination of the trace level components of the mixture.

A chromatogram of the tryptic digest mixture of rhGH run under conventional gradient elution conditions is shown in Fig. 3A. Table I shows the identities and masses of the major peptides expected from the map, designated numerically according to the position of the peptide in the linear sequence of the protein [26]. The peptides labelled $T10c_1$ and $T10c_2$ are fragments resulting from a chymotryptic-like clip in the T10 peptide that is one example of the non-specificity of the cleavage observed with trypsin. Fig. 3B is an enlargement of the baseline of Fig. 3A, showing the presence of numerous small peaks that presumably convey certain of the information described above. As the small peaks are present at such low levels, they are not readily characterized from the tryptic map to extract this information.

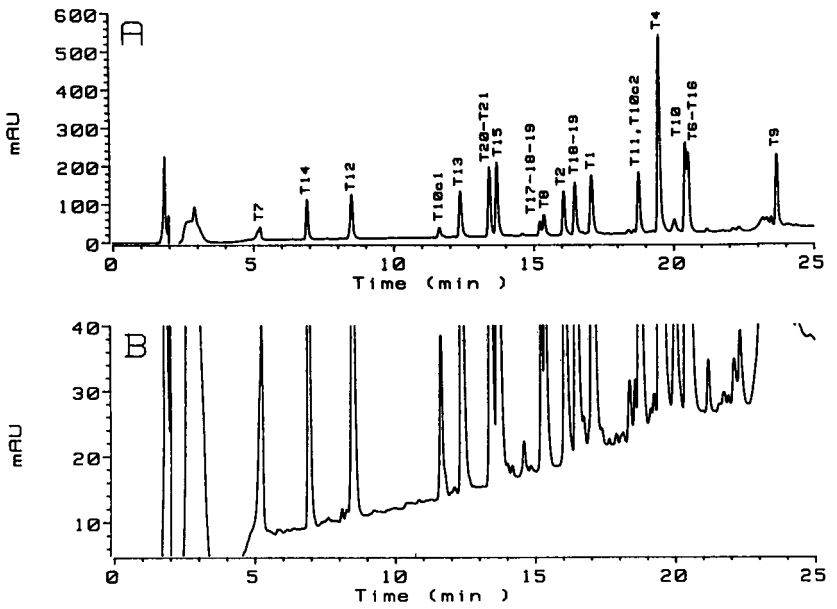

Fig. 3. (A) Absorbance profile of the tryptic map of rhGH obtained by gradient elution chromatography. (B) The same chromatogram at lower attenuation, showing the minor component peaks occuring in the tryptic map.

TABLE I

PEPTIDES PRODUCED BY DIGESTION OF HUMAN GROWTH HORMONE WITH TRYPSIN

$[M+H]^+$ is the calculated molecular weight for the most abundant monoisotopic species.

Identifier	Residues	$[M+H]^+$	Sequence[a]
TI	1–8	930.54	FPTIPLSR
T2	9–16	979.50	LFDNAMLR
T3	17–19	383.21	AHR
T4	20–38	2342.14	LHQLAFDTYQEFEEAYIPK
T5	39–41	404.22	EQK
T6[b]	42–64	2616.24	YSFLQNPQTSLCFSESIPTPSNR
T7	65–70	762.36	EETQQK
T8	71–77	844.49	SNLELLR
T9	78–94	2055.20	ISLLLIQSWLEPVQFLR
T10	95–115	2262.13	SVFANSLVYGASDSNVYDLLK
$TIOc_1$	96–99	537.27	SVFAN
$TIOc_2$	100–115	1743.90	LWGASDSNVYDLLK
TII	116–127	1361.67	DLEEGIQTLMGR
T12	128–134	773.38	LEDGSPR
T13	135–140	693.39	TGQIFK
T14	141–145	626.32	QTYSK
T15	146–158	1489.69	FDTNSHNDDALLK
T16[b]	159–167	1148.55	NYGLLYCFR
T17–T18–TI9	168–178	1381.71	KDMDKVETFLR
T18–T19	171–178	1253.62	DMDKVETFLR
T20[c]	179–183	618.34	IVQCR
T21[c]	184–191	785.31	SVEGSCGF

[a] Single-letter coding for amino acids used.

[b] T6 and T16 are disulfide-linked, with a total $[M+H]^+$ of 3762.8.

[c] T20 and T21 are disulfide-linked, with a total $[M+H]^+$ of 1401.4.

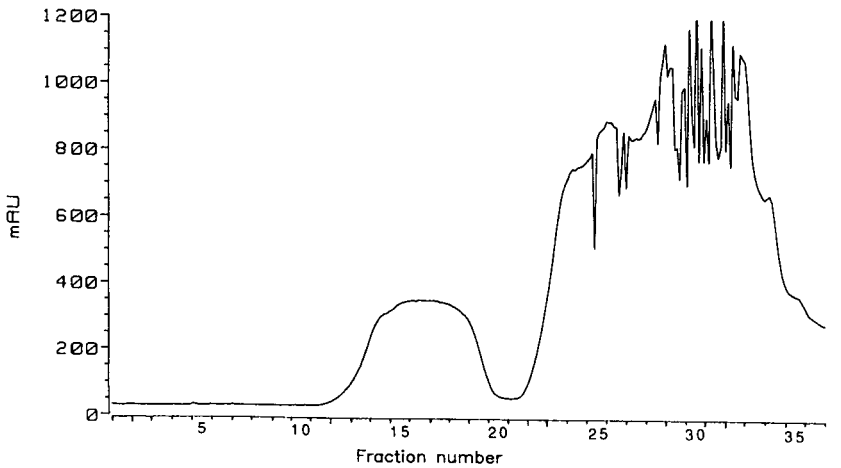

Fig. 4. Displacement chromatogram of 9 mg of rhGH tryptic peptides. The displacer concentration was 3 mg/ml. Fraction collection commenced at 309 min, and 1-min fractions were collected. The chromatogram shown was produced by summing the absorbance profiles obtained at 214, 254 and 280 nm.

In order to develop HPDC tryptic mapping conditions, an essential requirement is to identify a substance suited to displacement of the peptide mixture. The required characteristics of a displacer have been described [9], and several potential displacers of peptides have been reported [1–6]. One of these displacers, CTAB, has been employed as a displacer in this application [18] and so was used here to displace a feed consisting of 9 mg of the tryptic peptide mixture. The resulting displacement train is shown in Fig. 4. The angular shape of the profile suggests that the components of the mixture have formed a classical displacement train, although non-ideal effects at these concentrations disturbed the absorbance detection. The HPLC analyses of fractions collected during the displacement separation are shown in Fig. 5. Roughly

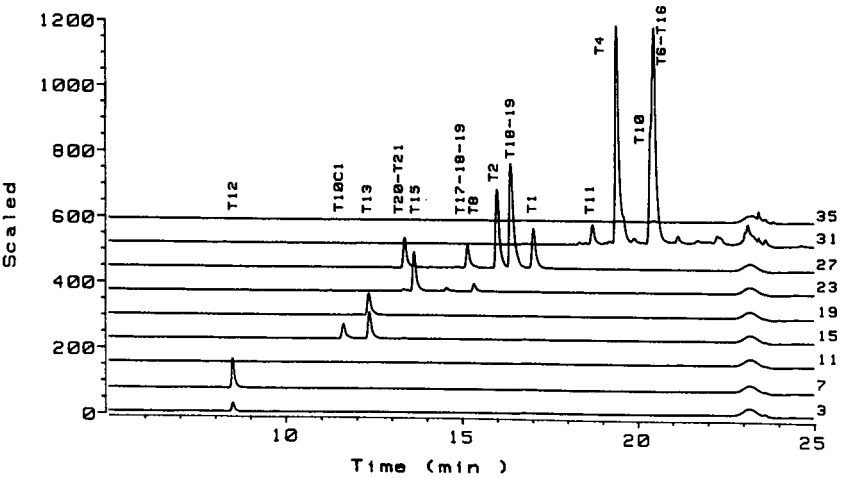

Fig. 5. HPLC of the fractions collected during the displacement separation shown in Fig. 4. The fraction number is indicated adjacent to each chromatogram.

similar trends are observed in the relative retention behavior of peptides in elution chromatography, employed for the analyses of fractions, and in the HPDC separation. Thus, the peptides that elute early in the tryptic map are also those which occur early in the displacement train. There are exceptions to the parallelism of relative retention in the two modes. One example is the peptide identified as T20–T21 in Fig. 5, which elutes ahead of T15 in the linear elution tryptic map, but occurs behind T15 in the displacement train, as indicated by its appearance in fraction 27 and absence from fraction 23. The later fractions in Fig. 5 are seen to contain a considerable number of peptides, indicating that bands in this part of the displacement train are highly concentrated and narrow, relative to the 1-ml volume of the fractions. As expected, the rear of the displacement train contains the most strongly retained peptides and these form the most concentrated bands. This portion of the chromatogram also reveals that essentially all of the peptides through T6–T16 are effectively displaced by CTAB, and the only major peptide absent from the displacement train is the most hydrophobic, T9, which is poorly soluble in aqueous buffers. The absence of peptides from fraction 35 indicates that the displacement train components did not tail into the displacer zone, which lends support to the conclusion that CTAB efficiently displaced the peptide mixture under these conditions.

Mass spectrometry offers an alternative approach for the rapid analysis of the fractions collected in the HPDC analysis and has the additional benefit of providing mass information that can aid in identification of peptides in the mixture. Aliquots of fractions 15 and 23 were analysed by electrospray MS, yielding the spectra shown in Fig. 6 and 7, respectively. In each of the mass spectra the masses corresponding to major constituents of the digest mixture are identified. The chromatogram of fraction 15 shown in Fig. 5 reveals the presence of two main constituents, the peptides $T10c_1$ and T13, which also dominate the spectrum in Fig. 6 by their molecular ions with m/z 537 and 693, respectively. In addition to these molecular ions, the doubly charged T13

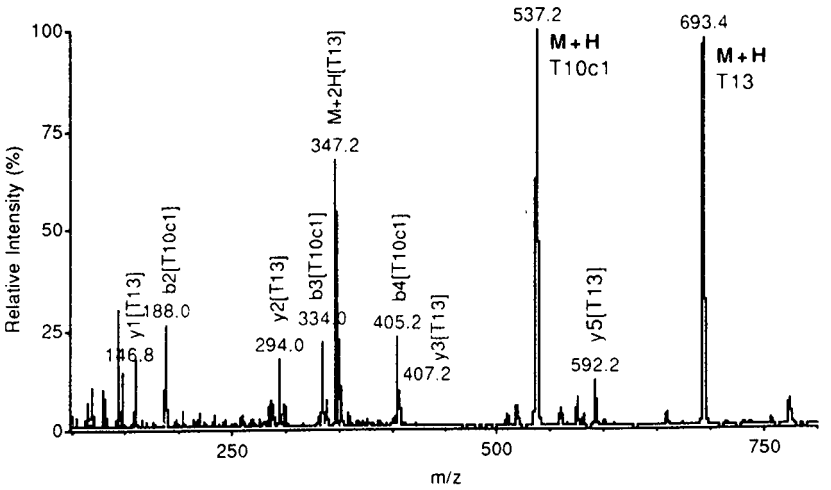

Fig. 6. Mass spectrum of fraction 15. Ions arising from $T10c_1$ and T13, including fragment ions, are identified.

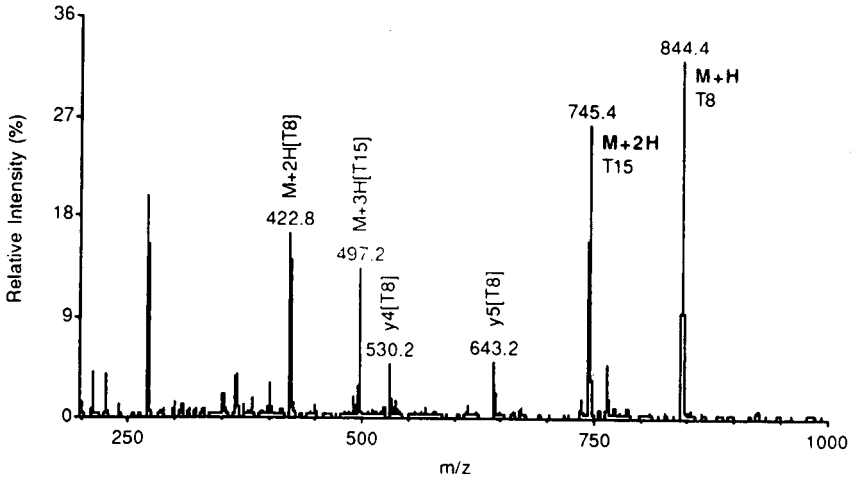

Fig. 7. Mass spectrum of fraction 23. Ions arising from T15 and T8, including fragment ions, are identified.

ion (m/z = 347) is apparent along with several ions that are products of collision-induced dissociation in the electrospray interface [19,20]. Such fragmentation is an artifact of the electrospray ionization mechanism even at the low orifice potential employed in these analyses and can provide additional sequence information to aid in the identification of the molecular ion, as discussed further below. In addition to the ions derived from the two major peptides in this mixture, there are ions present at

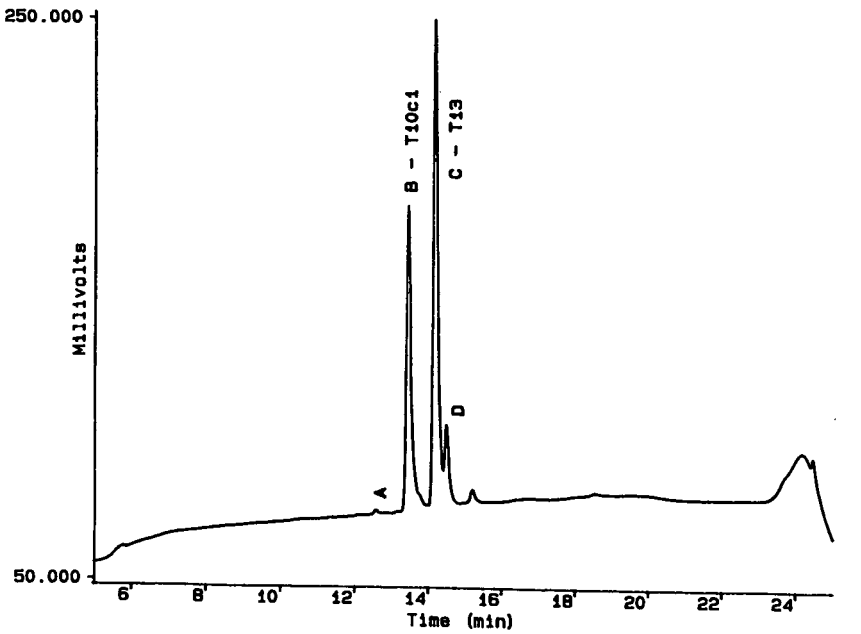

Fig. 8. Reversed-phase HPLC of fraction 15 of the HPDC tryptic map. Peptides collected for identification by mass spectrometry are labelled to correspond with the appropriate spectrum in Fig. 9.

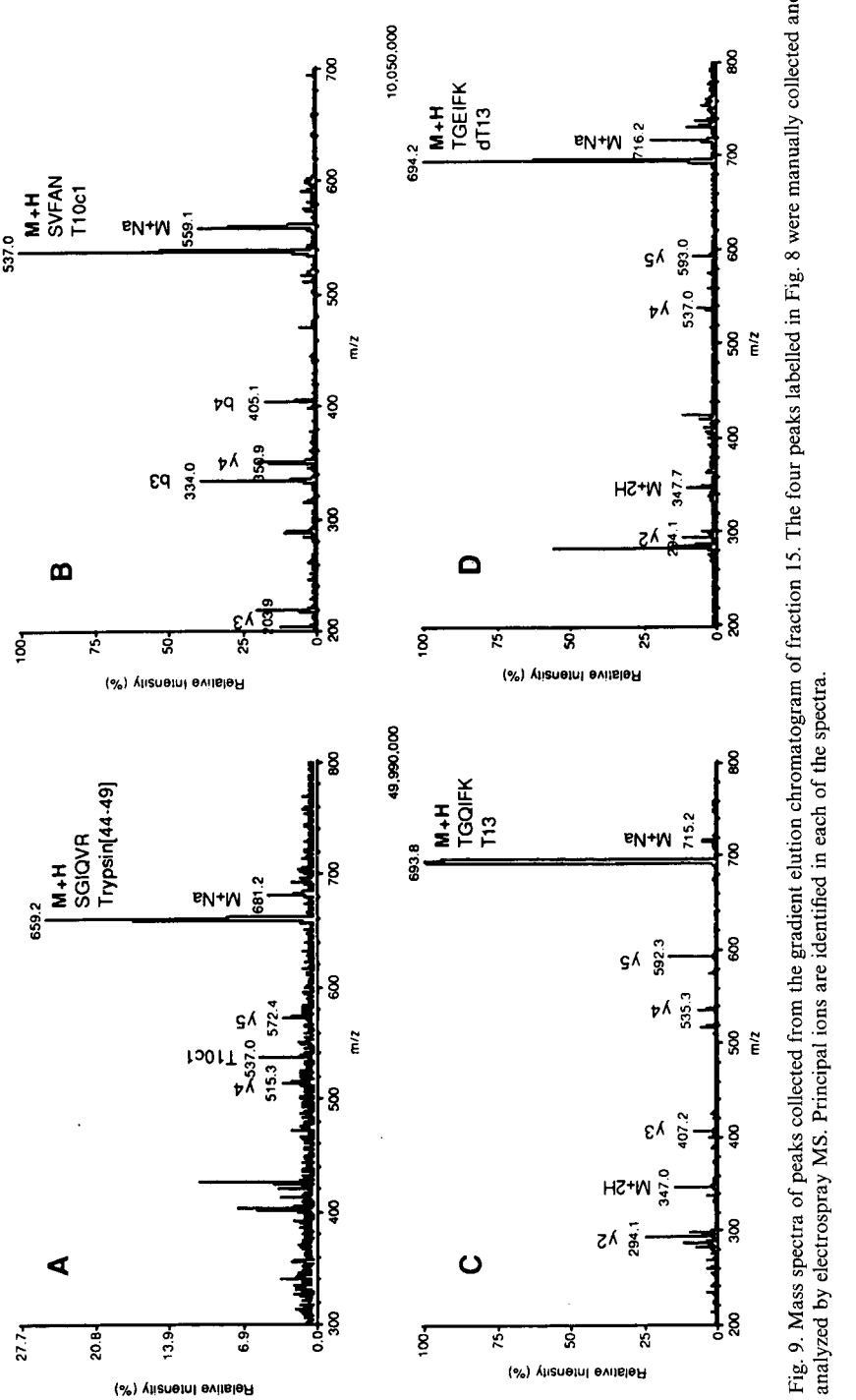

Fig. 9. Mass spectra of peaks collected from the gradient elution chromatogram of fraction 15. The four peaks labelled in Fig. 8 were manually collected and analyzed by electrospray MS. Principal ions are identified in each of the spectra.

much lower abundances that presumably represent components of the fraction present at low concentrations, including peptides present as minor peaks in the chromatogram of the mixture in Fig. 5. The mass spectrum of fraction 23 shown in Fig. 7 yields an analogous picture. The chromatogram of fraction 23 shown in Fig. 5 contains the two tryptic peptides, T15 and T8. The mass spectrum of the mixture is likewise dominated by molecular and fragment ions of these two peptides. Also present, as in Fig. 6, are ions that are not readily associated with peptides expected to arise from typtic mapping of rhGH, and whose identification may warrant further investigation.

As the fractions themselves represent relatively complex mixtures, this investigation is hampered by limitations on the interpretation of mass spectral data such as described above. Therefore, the identification of these minor components requires further purification and isolation of individual species. As argued above, identification of the peptides corresponding to these peaks is expected to yield information about the composition of the protein preparation and about the trypsin digestion process. To illustrate the isolation by HPDC of useful amounts of minor components of the peptide digest, individual fractions from the separations shown in Fig. 5 were rechromatographed by gradient elution HPLC and the resulting peaks were manually collected for subsequent analysis by electrospray mass spectrometry. Figure 8 shows the four peaks collected by gradient elution HPLC analysis of fraction 15 of the displacement separation. The mass spectra of the individual peaks are shown in Fig. 9. Certain of the assignments of peaks in Fig. 8 correspond to peptides already identified from the conventional tryptic map shown in Fig. 3. Thus, T10c$_1$ (m/z = 537) and

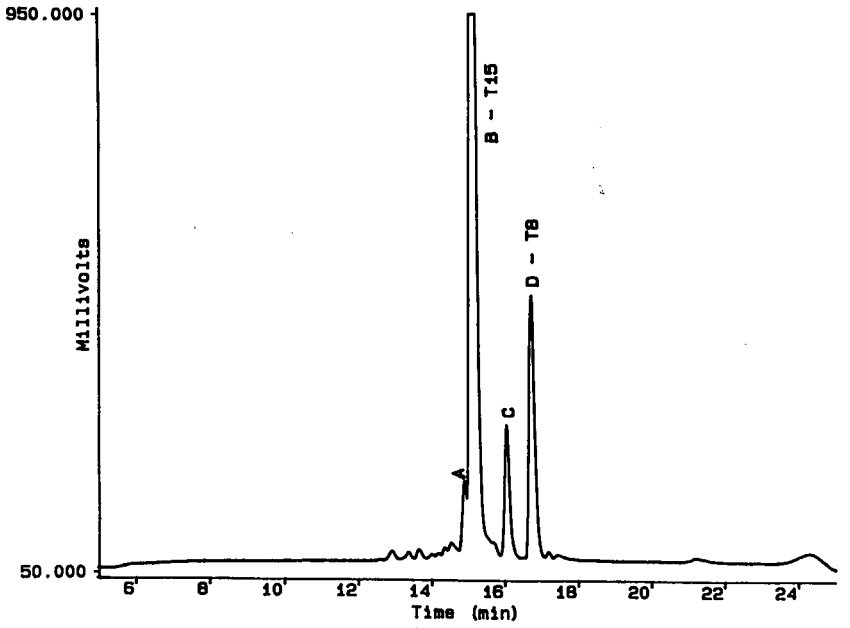

Fig. 10. Reversed-phase HPLC of fraction 23 of the HPDC tryptic map. Peptides collected for identification by mass spectrometry are labelled to correspond with the appropriate spectrum in Fig. 11.

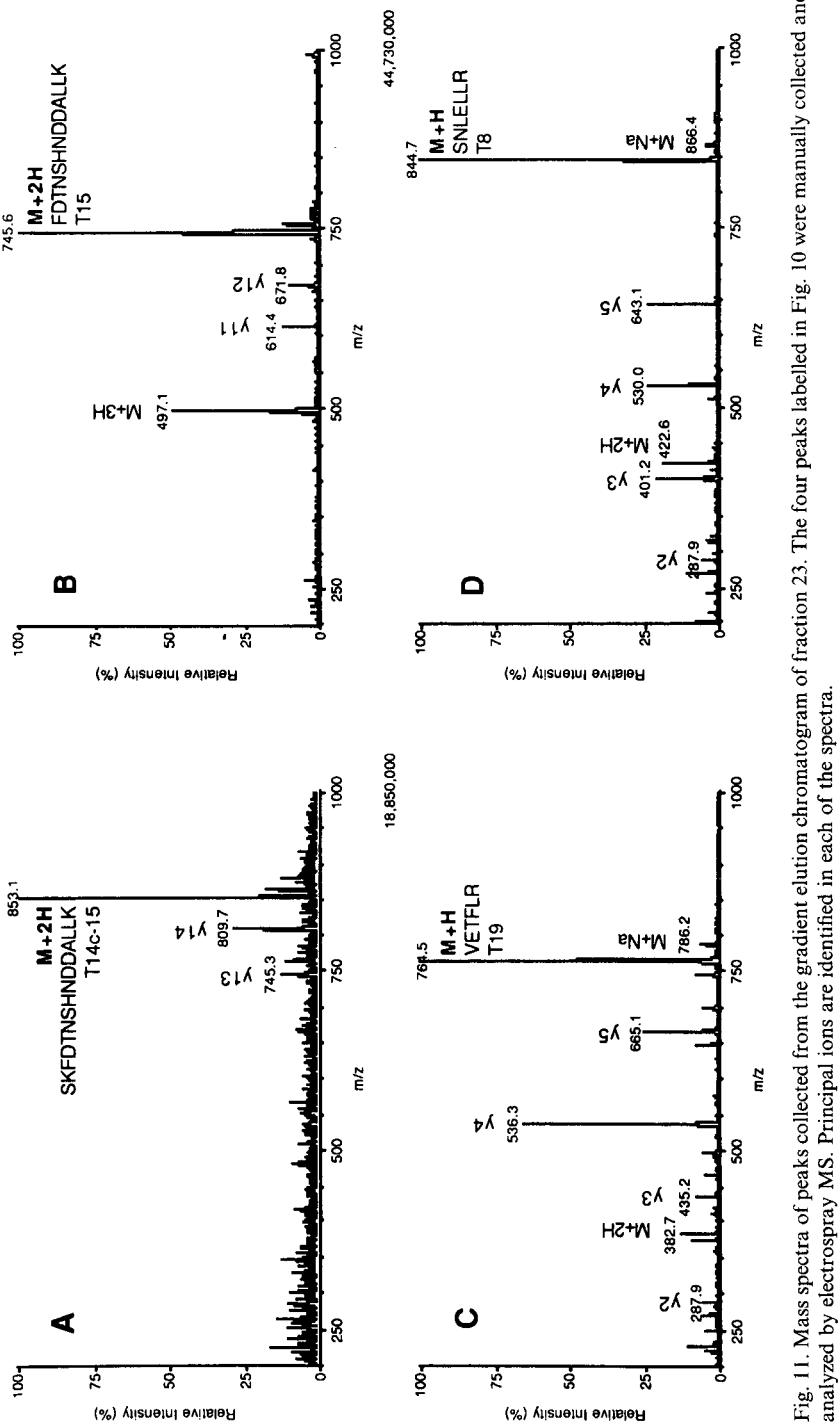

Fig. 11. Mass spectra of peaks collected from the gradient elution chromatogram of fraction 23. The four peaks labelled in Fig. 10 were manually collected and analyzed by electrospray MS. Principal ions are identified in each of the spectra.

T13 (m/z = 693) are readily identified by molecular ion information and confirmed by fragment ion identification.

The assignments of fragment ions for these purified peptides is less tentative than in the spectrum shown in Fig. 6, which is the mass spectrum obtained by analysis of a mixture. The fragment ions observed are related to the parent ion peptide sequence with, for instance, predominantly *y*-series ions, in the standard nomenclature [30], observed in the T13 spectrum. *y*-Series ions are C-terminal fragments, and arise from maintenance of the positive charge on the C-terminal lysine of this tryptic peptide. Conversely, the spectrum of $T10c_1$, which lacks a C-terminal basic residue, contains predominantly *b*-series ions, *i.e.*, N-terminal fragments, which occur owing to maintenance of the positive charge at the N-terminus of the fragmented peptide. The other peptides in fraction 15 are relatively minor components of the tryptic digest mixture. Among these is a deamidated variant of the T13 peptide (m/z = 694). T13 contains a single glutamine residue that can undergo deamidation to a relatively small extent under the alkaline conditions employed for digestion with trypsin. Deamidation converts the glutamine residue to glutamic acid, resulting in a unit increase in the mass of the deamidated peptide that can be resolved with the mass spectrometer. Comparison of the fragment ions arising from the deamidated T13 with those of the native T13 peptide confirms that the unit increase in mass is associated with the glutamine residue in the peptide, as can be seen by comparing Fig. 9C and D. The deamidated peptide is resolved from the native T13 peptide in the reversed-phase chromatogram, but was not resolved in the mass spectrum of the mixture, as seen in Fig. 6. Thus, identification of this important degradation product is best carried out by sequential chromatographic separation and mass spectral analysis, rather than by MS alone.

Also contained in fraction 15 is a peptide arising from autolysis of the trypsin employed for digestion of the protein. The spectrum of the trypsin-derived peptide (m/z = 659) is shown in Fig. 9A and corresponds to residues 44–49 of the sequence of bovine pancreatic typsin [28]. This assignment of the molecular ion is supported by sequence data obtained by assignment of the fragment ions arising from collision-induced dissociation in the electrospray interface [19,20]. Hence, the molecular ion with m/z 659 corresponds to the peptide with sequence SGIQVR, using the single-letter code, in trypsin. Accompanying the molecular ion are fragment ions with m/z 572 (corresponding to the y_5 fragment ion), 515 (y_4) and 402 (y_3). The coincidence of these ions with the molecular ion confirms the identification of this peak as a peptide arising from autolysis of trypsin.

Fig. 10 shows the peaks collected from the chromatogram of fraction 23. The identifications of the major peaks as the doubly charged T15 (m/z = 745) and the singly charged T8 (m/z 844) were confirmed by their mass spectra, as shown in Fig. 11B and D. Two minor peaks were also identified, and corresponded to cleavages that are not commonly seen in trypsin digestion of rhGH. The earlier eluting of these peaks, with m/z 853, was identified by MS as a doubly charged peptide constituting residues 144–158 of hGH, and represents a chymotryptic-like clip between Tyr-143 and Ser-144 in what would be the T14 peptide. Residue 145 is a lysine, but no cleavage occurred after this residue, suggesting that this amide bond, occurring near the clipped portion of T14, is a poor substrate for trypsin. The fragmentation pattern discerned for this peptide and shown in Fig. 11A confirms the identification of this

relatively unusual product of tryptic digestion. Analysis of all the fractions collected idicates that this peptide constitutes *ca.* 0.9% of the T15 residues in the digest mixture, demonstrating the high resolving power of HPDC for minor components of a complex misture. The other minor peptide identified in fraction 23 is T19, which is usually not cleaved from T18 by trypsin, as indicated in Fig. 3 and Table I. The fragmentation pattern observed in Fig. 11D confirms that this peptide is present in the digest of hGH. Integration of the chromatograms of fractions containing this peptide shows that it occurs at a level of *ca.* 1.5% of the T19 residues in the protein, compared with *ca.* 26.5% present in the T18-19 peptide and the balance in the T17–18–19 peptide.

CONCLUSIONS

HPDC permits the recovery of useful amounts of minor components of the peptide mixture produced by digestion of a protein with trypsin. Characterization of these trace component peptides can provide information on the enzymatic properties of trypsin and on the detailed nature of the protein substrate. HPDC tryptic mapping can be employed to identify variants constituting less than 1% of the protein preparation. Hence, tryptic mapping by HPDC has a comparable sensitivity to successful analytical methods involving chromatography of the intact protein, and significantly improved sensitivity compared with conventional gradient elution tryptic mapping. Mass spectrometry is a rapid and efficient means of identifying the minor peptides isolated by HPDC tryptic mapping. Molecular ion fragmentation patterns occurring during electrospray ionization MS provide compelling additional support for the identification of peptides in a mass spectrum.

ACKNOWLEDGEMENT

The authors acknowledge with gratitude the enthusiasm and interest of Professor Guiochon and stimulating discussions on the topic of HPDC.

REFERENCES

1 Cs. Horváth, in F. Bruner (Editor), *The Science of Chromatography*, Elsevier, Amsterdam, 1985, pp. 179–203.
2 A. R. Torres, S. C. Edberg and E. A. Peterson, *J.Chromatogr.*, 389 (1987) 177.
3 G. Vigh, Z. Varga-Puchony, G. Szepesi and M. Gazdag, *J.Chromatogr.*, 386 (1987) 353.
4 A. M. Katti and G. A. Guiochon, *J. Chromatogr.*, 449 (1988) 25.
5 D. J. Sawyer, J. E. Powell and H. R. Burkholder, *J. Chromatogr.*, 455 (1988) 193.
6 G. Subramanian, M. W. Phillips, G. Jayaraman and S. Cramer, *J. Chromatogr.*, 484 (1989) 225.
7 A. Tiselius, *Ark. Kemi Mineral. Geol.*, 16A (1943) 1.
8 Cs. Horváth, A. Nahum and J. H. Frenz, *J. Chromatogr.*, 218 (1981) 365.
9 J. Frenz and Cs. Horváth, in Cs. Horváth (Editor), *HPLC—Advances and Perspectives*, Vol. 5, Academic Press, New York, 1989, p. 212.
10 H. Kalász and Cs. Horváth, *J. Chromatogr.*, 215 (1981) 295.
11 Cs. Horváth, J. Frenz and Z. El Rassi, *J. Chromatogr.*, 255 (1985) 273.
12 J. Frenz, Ph. van der Schrieck and Cs. Horváth, *J. Chromatogr.*, 330 (1985) 1.
13 J. Frenz and Cs. Horváth, *AIChE J.*, 31 (1985) 400.
14 P. C. Wankat, *Large Scale Adsorption and Chromatography*, Vol. II, CRC Press, Boca Raton, FL, 1986, p. 1.

15 J. Jacobson and J. Frenz, in preparation.
16 A. M. Katti and G. Guiochon, *C.R. Acad. Sci., Ser. II,* 309 (1989) 1557.
17 R. Ramsey, A. M. Katti and G. Guiochon, *Anal. Chem.*, 62 (1990) 2557.
18 J. Frenz, J. Bourell and W. S. Hancock, *J. Chromatogr.*, 512 (1990) 299.
19 R. D. Smith, J. A. Loo, C. J. Barinaga, C. G. Egmonds and H. R. Udseth, *J. Am. Soc. Mass Spectrom.*, 1 (1990) 53.
20 V. Katta, S. K. Chowdhury and B. T. Chait, *Anal. Chem.*, 63 (1991) 174.
21 A. F. Bergold, D. A. Hanggi, A. J. Muller and P. W. Carr, in Cs. Horváth (Editor), *HPLC–Advances and Perspectives*, Vol. 5, Academic Press, New York, 1989, p. 95.
22 D. DeVault, *J. Am. Chem. Soc.*, 65 (1943) 532.
23 L. Hagdahl, in E. Heftmann (Editor), *Chromatography*, Reinhold, New York, 1961, p. 70.
24 F. Helfferich and G. Klein, *Multicomponent Chromatography—Theory of Interference*, Marcel Dekker, New York, 1970.
25 A. T. James and A. J. P. Martin, *Biochem. J.*, 50, (1952) 679.
26 W. J. Kohr, R. Keck and R. N. Harkins, *Anal. Biochem.*, 122 (1982) 348.
27 G. Bogosian, B. N. Violand, E. J. Dorward-King, W. E. Workman, P. E. Jung and J. F. Kane, *J. Biol. Chem.*, 264 (1989) 531.
28 M. M. Vestling, C. M. Murphy and C. Fenselau, *Anal. Chem.*, 62 (1990) 2391.
29 S. E. Builder and W. S. Hancock, *Chem. Eng. Prog.*, August (1988) 42.
30 P. Roepstorff and J. Fohlman, *Biomed. Mass Spectrom.*, 11 (1984) 601.

Journal of Chromatography, 557 (1991) 307–313
Elsevier Science Publishers B.V., Amsterdam

CHROM. 23 286

Application of capillary zone electrophoresis to the characterization of multiple antigen peptides

ANTONELLO PESSI[a], ELISABETTA BIANCHI[a] and LORELLA CHIAPPINELLI
Peptide Synthesis Unit, Sclavo SpA, 00015 Monterotondo, Rome (Italy)
and
ANNALISA NARDI and SALVATORE FANALI*
Istituto di Cromatografia del CNR, Area della Ricerca di Roma, C.P. 10, 00016 Monterotondo Scalo, Rome (Italy)

ABSTRACT

Capillary zone electrophoresis (CZE) was applied to the analysis of a recently described class of synthetic branched peptides, multiple antigen peptides (MAPs). In comparison with high-performance liquid chromatography (HPLC), CZE showed superior resolution of minor impurities in samples of MAPs obtained by preparative chromatography. MAPs that differed only in the substitution of uncharged residues (Ala–Ser) could be separated by the addition of organic solvents (acetonitrile, methanol, ethanol) to the aqueous background electrolyte.

INTRODUCTION

Multiple antigen peptides (MAPs) are branched molecules in which a branching core of lysine residues, with both α- and ε-amide bonds between themselves, form the skeleton for the assembly of multiple copies of a given peptide sequence (see Fig. 1). These peptides, first described by Tam [1], are finding widespread application as candidate synthetic vaccines [2–4], as antigens for solid-phase immunoassays [5,6] and to raise antibodies for immunocytochemistry [7]. Moreover, a MAP-like structure has recently been described as a prototype synthetic enzyme [8].

MAPs are assembled by solid-phase synthesis [9] either by the Boc–polystyrene strategy [1] or by the flow polyamide method [10].

Until now analytical characterization of MAPs has been performed by high-performance size-exclusion chromatography (SEC) [1,2,5,10] and reversed-phase high-performance liquid chromatography (RP-HPLC) [5,8,10]. SEC has also been used for the purification of the MAPs [1,2,5,8].

Capillary zone electrophoresis (CZE) has been recently applied to the separation of protein and peptide mixtures [11–18]. Some desirable features of this tech-

[a] Present address: Instituto di Ricerche di Biologia Molecolare, Via Pontina, Km 30,600 Pomezia, Rome, Italy.

0021-9673/91/$03.50

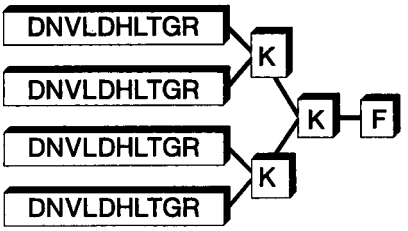

Fig. 1. Structure of MAPs. The figure depicts the structure of MAP^4 (DNVLDHLTGR), *i.e.*, compound 1 in Table I. In MAP nomenclature, the superscript refers to the number of branches and the sequence in parentheses is that assembled on each amino group of the lysine residues. The one-letter code for the amino acids is used throughout (D = Asp, N = Asn, V = Val, L = Leu, T = Thr, H = His, G = Gly, R = Arg, P = Pro, A = Ala, S = Ser).

nique, namely high efficiency and resolution and short analysis time, suggested that it should be well suited for the analytical characterization of MAPs. In this paper we describe the application of CZE to the analysis of a series of MAPs produced by the flowpolyamide method.

EXPERIMENTAL

Apparatus and procedures

The electrophoretic experiments were performed in a Bio-Rad Lab. (Richmond, CA, USA) HPE 100 unit equipped with an on-column UV detector. The separations were done in a 20 cm × 0.025 mm I.D. coated fused-silica capillary (Bio-Rad) at room temperature. The sample was introduced into the capillary by electromigration. The capillary was washed after each run with the appropriate background electrolyte. Lyophilized peptides were dissolved in doubly distilled water, filtered through a 0.45-μm filter and used without further treatment. Electropherograms were recorded with an LKB Model 2210 line recorder at a chart speed of 10 mm/min.

For analytical HPLC, a Merck–Hitachi Model 655A liquid chromatograph was used equipped with a Rheodyne Model 7161 injection valve, a Jasco Model 875 UV detector and a Merck–Hitachi Model D-2000 integrator. Other conditions are given in the legend to Fig. 3.

Chemicals

Sodium dihydrogenphosphate, ammonium acetate, acetic acid and methanol were purchased from Carlo Erba (Milan, Italy) and phosphoric acid, ethanol and acetonitrile (ACN) from Merck (Darmstadt, Germany); trifluoroacetic acid (TFA), also from Merck, was distilled before use. The background electrolytes (BGE) used were a 0.1 *M* solution of phosphate buffer (pH 2.5 and 3.5) and a 0.1 *M* solution of acetate buffer (pH 4.5). For the separations in aqueous–organic mixtures, a stock solution of 0.1 *M* phosphate buffer (pH 2.5) was mixed with the appropriate amounts of organic solvent and water; the final concentration of the electrolyte was 0.05 *M*.

Peptides

The peptides used were prepared by the flow polyamide method as described

[10]. Details of the synthesis and of the purification of MAP 1 in Table I have been reported elsewhere [19].

RESULTS AND DISCUSSION

The peptides used are listed in Table I. Compound 1 is a well characterized molecule, whose synthesis, purification and 2D-NMR conformational analysis have been reported [19]. Preparative purification by reversed-phase sample displacement chromatography (SDC) [20] had made available the purified main product in the crude mixture (fraction A), and a pool of the more closely related impurities (fraction B). Therefore, this product was an ideal test case to compare the resolving power of CZE, when applied to MAPs, with that of HPLC. Compounds 2 and 3 represent another difficult test case: the sequences of these high-molecular-weight MAPs differ only by an uncharged amino acid. As the antigenic sequence is a tandem repeated dimer, $(PGTHLPA/SLP)_2$, the substitution takes place twice.

Moreover, to examine how the multi-branched structure affects the electrophoretic behaviour, these MAPs were compared with the corresponding linear peptides (compounds 4 and 5 in Table I).

The CZE experiments were carried out in a relatively short, coated capillary tube (Bio-Rad); this allowed short analysis time and minimized adsorption of the analytes on the capillary walls.

The synthetic peptides studied all possess positive charge at acidic pH. Therefore, various BGEs at pH 2.5, 3.5 and 4.5 were tested to find the optimum separation conditions, which must be established for each peptide.

The migration time of all the components in the mixture increased with increase in pH, and the BGE at pH 3.5 represents the optimum compromise between selectivity, efficiency and duration of the analysis. Fig. 2 shows the electropherogram of compound 1, fraction B at pH 3.5.

Fig. 3 shows the RP-HPLC of the crude mixture of compound 1 (Fig. 3a), fraction A (purified product, Fig. 3b) and fraction B (more closely related impurities,

TABLE I

PEPTIDES USED IN THIS STUDY

The MAP nomenclature is explained in the legend to Fig. 1.

Peptide	Sequence	Sample
1	MAP^4 (DNVLDHLTGR)	Crude[a]
		Fraction A[b]
		Fraction B[c]
2	MAP^8 $(PGTHLPALP)_2$	Crude
3	MAP^8 $(PGTHLPSLP)_2$	Crude
4	$(PGTHLPALP)_2$-NH_2	Crude
5	$(PGTHLPSLP)_2$-NH_2	Crude

[a] Crude means peptide cleaved from the resin after the solid-phase synthesis without further purification, apart from desalting (Sephadex G-10).

[b] Purified main product from SDC (see text).

[c] Pool of the more related impurities, also from SDC (see text).

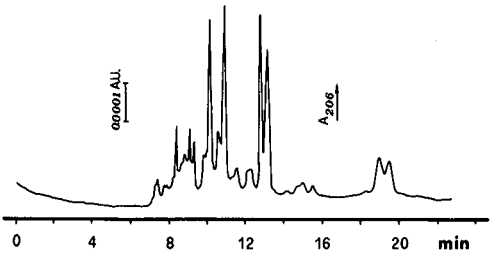

Fig. 2. Electropherogram of MAP[4] (DNVLDHLTGR), fraction B, using BGE at pH 3.5. Sampling, 4 kV, 5 s; sample concentration, 0.6 mg/ml; electrophoresis at 8 kV (constant), 16–20 μA.

Fig. 3c). The corresponding electropherograms of these peptides are reported in Figs. 2 (fraction B), 4a (crude mixture) and 4b (fraction A). HPLC was performed at 230 nm, to minimize drifting of the baseline during gradient elution, due to the organic phase modifier (TFA). This is common with peptide samples, and does not alter the qualitative picture, as absorption in the range 206–230 nm is mainly due to the amide chromophore. The absorption maximum of the peptide chromophore at 206 nm was instead chosen for CZE.

The overall pictures given by the two techniques are very similar, indicating the successful purification of the main peak from several impurities. CZE reveals, however, that at least ten minor peaks are present in the "pure" preparation (fraction A), which HPLC shows as essentially a single peak. The impurities collectively account for only a small fraction of the total material present in the sample, which can be classified as >90% pure; this is consistent with a series of deleted and truncated sequences, each one present in a very small amount, as often found in peptides prepared by solid-phase synthesis [21]. The multi-chain nature of the MAP may explain the difficulty encountered in their separation from the desired sequence. It therefore

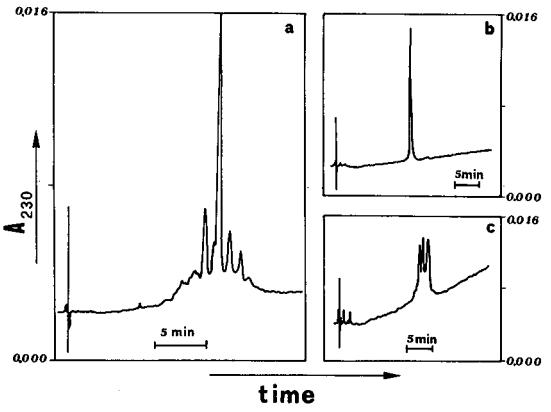

Fig. 3. Analytical HPLC of MAP[4] (DNVLDHLTGR). (a) Crude mixture from solid-phase synthesis; (b) purified main product; (c) pool of the more closely related impurities. Column, Vydac 218TP (5 μm); eluent A, 0.1% TFA in water; eluent B, 0.1% TFA in acetonitrile; linear gradient from 25 to 40% B over 20 min; flow-rate 1.5 ml/min; injection, 5 μl; sample concentration, 1 mg/ml.

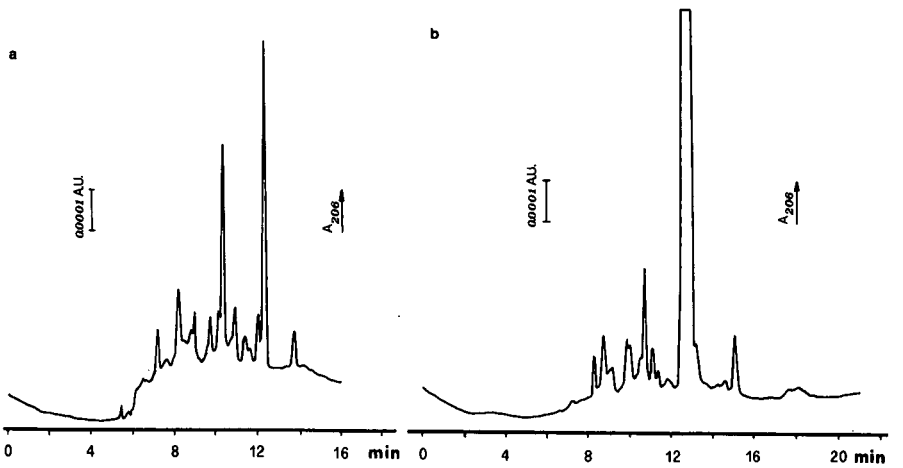

Fig. 4. Electropherograms of MAP[4] (DNVLDHLTGR). (a) Crude; (b) fraction A. Sampling: (a) 6 kV, 7 s; (b) 4 kV, 5 s. BGE pH, 3.5. Electrophoresis at 17 μA (constant), 8.5 kV. Sample concentration: (a) 0.6 mg ml; (b) 0.6 mg/ml.

seems necessary to include CZE among the routine controls applied to this class of peptide.

Samples 2–5 were injected separately and electrophoresis was performed at pH 2.5, 3.5 and 4.5. With all the BGEs used, a short migration time (less than 5 min) of the peptides was complemented by a good separation of several minor impurities from the main peak. For these compounds, the best results were obtained with the BGE at pH 2.5. At every pH, the mobility of each MAP was higher than that of the corresponding linear peptide.

However, no variation in BGE led to the separation of the pairs of compounds that differ only in the Ala–Ser substitution (*i.e.*, compounds 2 and 3 and compounds 4 and 5).

It has been reported that the addition of organic solvents to an aqueous BGE can influence the effective mobility of the analytes [22,23]. Therefore, we studied the influence of various organic solvents (methanol, ethanol and acetonitrile) on the resolution of mixtures 2–3 and 4–5.

Methanol, ethanol and acetonitrile were added, separately, to the BGE at different concentrations ranging from 10 to 50% (v/v) and these aqueous–organic mixtures were used for the separation of peptide mixtures 2–3 and 4–5. With all the aqueous–organic BGEs used the migration times of all the four peptides analysed increased owing to a decrease in their effective electrophoretic mobilities. For all solvents an optimum percentage could be found that maximized the separation of the two components. For both mixtures, acetonitrile yielded the best resolution, albeit at different percentages: 40% (v/v) for mixture 2–3 and 50% (v/v) for mixture 4–5.

Fig. 5a and b show the separation obtained by using the same BGE in aqueous and aqueous–acetonitrile mixture, respectively.

Grossman *et al.* [13] recently observed that in a series of short, linear peptides that differed in a single neutral amino acid, the electrophoretic mobility in an aqueous

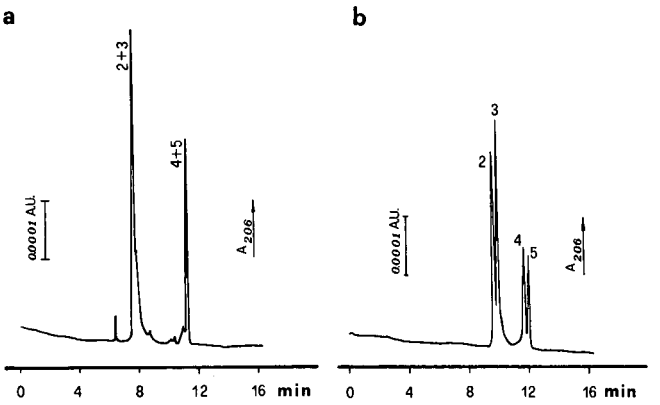

Fig. 5. Electrophoretic separation of peptides differing only in the Ala–Ser substitution. Sample: mixture of compounds 2, 3, 4 and 5, 0.1 mg/ml each. (a) BGE, 50 m*M* phosphate buffer (pH 2.5); sampling, 4 kV, 6 s; electrophoresis at 7 kV (constant), 11 μA; (b) BGE, 40% ACN in 50 m*M* phosphate buffer (pH 2.5); electrophoresis at 7 kV (constant), 7 μA.

solvent decreased with increase in the hydrophobicity index of the amino acid. In our case the Ser peptides (3 and 5) always moved towards the cathode with lower velocity than the Ala peptides, despite the lower hydrophobicity of Ser. The influence of the organic solvents, which appeared to be the same for the linear and the branched compounds, was probably due to the different solvation of the peptide chains. Further studies are planned to ascertain whether this is a general effect.

CONCLUSIONS

The results indicate that CZE is a powerful technique for the characterization of MAPs. The known advantages of CZE, *e.g.*, short analysis time, low electrolyte consumption and high sensitivity, are complemented by the superior resolution and efficiency with respect to HPLC. By addition of organic solvents to the BGE, it is possible to separate MAPs that differ only in neutral amino acids, such as the Ala–Ser pair. The combined use of preparative HPLC and analytical CZE therefore offers a good potential to solve the purification problems with this important class of pharmaceutical peptides.

REFERENCES

1 J. Tam, *Proc. Natl. Acad. Sci. U.S.A.*, 85 (1988) 5409.
2 J. Tam and Y.-A. Lu, *Proc. Natl. Acad. Sci. U.S.A.*, 86 (1989) 9884.
3 J. Tam, P. Clavijo, Y.-A. Lu, V. Nussenzweig and F. Zavala, *Exp. Med.*, 171 (1990) 299.
4 G. Del Giudice, C. Tougne, J. Louis, P. H. Lambert, E. Bianchi, F. Bonelli, L. Chiappinelli and A. Pessi, *Eur. J. Immunol.*, 20 (1990) 1619.
5 J. Tam and F. Zavala, *J. Immunol. Methods*, 124 (1989) 53.
6 F. Troalen, A. Razafindratsita, A. Puisieux, T. Voeltzel, C. Bohuon, D. Bellet and J. M. Bidart, *Mol. Immunol.*, 27 (1990) 363.
7 K. J. Hang, W. Pugh, S. G. Blanchard, J. McDermed and J. Tam, *Proc. Natl. Acad. Sci. U.S.A.*, 85 (1988) 4929.
8 K. W. Hahan, W. A. Klis and J. M. Stewart, *Science*, 248 (1990) 1544.

9 R. B. Merrifield, *J. Am. Chem. Soc.*, 85 (1963) 2149.
10 A. Pessi, E. Bianchi, F. Bonelli and L. Chiappinelli, *J. Chem. Soc., Chem. Commun.*, (1990) 8.
11 F. Foret and P. Bocek, in A. Chrambach, M. J. Dunn and B. J. Radola (Editors), *Advances Electrophoresis*, VCH, Weinheim, 1989, p. 273.
12 J. W. Jorgenson and K. D. Lukacs, *Science*, 222 (1983) 266.
13 P. D. Grossman, K. J. Wilson, G. Petrie and H. H. Lauer, *Anal. Biochem.*, 173 (1988) 265.
14 B. L. Karger, A. S. Cohen and A. Guttman, *J. Chromatogr.*, 492 (1989) 585.
15 S. Hjerten and M. D. Zhu, *Protides Biol. Fluids, Proc. Colloq.*, 33 (1985) 537.
16 V. Rohlicek and Z. Deyl, *J. Chromatogr.*, 494 (1989),87.
17 K. A. Cobb and M. Novotny, *Anal. Chem.*, 61 (1989) 2226.
18 F. Foret, S. Fanali and P. Bocek, *J. Chromatogr.*, 516 (1990) 219.
19 G. Esposito, L. Chiappinelli, M. T. De Magistris and A. Pessi, *Biopolymers*, submitted; a preliminary account of this work was presented at the *2nd Naples Workshop on Bioactive Peptides, Capri, May 21–23, 1990.*
20 T. W. Lorne Burke, C. T. Mant and R. S. Hodges, *J. Liq. Chromatogr.*, 11 (1988) 1229.
21 C. Birr, *Aspects of the Merrified Peptide Synthesis*, Springer, Heidelberg, 1978.
22 J. Gorse, A. T. Balchunas, D. F. Swaile and M. J. Sepaniak, *J. High Resolut. Chromatogr. Chromatogr. Commun.*, 11 (1988) 554.
23 T. Hirokawa, T. Tsuyoshi and Y. Kiso, *J. Chromatogr.*, 408 (1987) 27.

Journal of Chromatography, 557 (1991) 315–324
Elsevier Science Publishers B.V., Amsterdam

CHROM. 23 289

Separation and indirect detection of amino acids as acetylated derivatives

DONGXING YUAN and DONALD J. PIETRZYK*
Department of Chemistry, University of Iowa, Iowa City, IA 52242 (USA)

ABSTRACT

Iron(II)–1,10-phenanthroline [$Fe(phen)_3^{2+}$] salts are used as mobile phase additives for the separation and indirect photometric detection (IPD) of N-acetylated amino acid (N-Ac-AA) derivatives on a reversed stationary phase. Mobile phase $Fe(phen)_3^{2+}$ concentration, pH, organic modifier concentration and counter anion affect retention and IPD. Disodium-1,5-naphthalene disulfonate and sodium benzoate as counter anions and buffer anion, respectively, are optimum because of their contribution to eluent strength, pH and location of their system peaks. The retention order of N-Ac-AA derivatives is influenced by AA side-chain structure. Mixtures of AA can also be separated, detected by IPD and determined after conversion of the AA to the N-Ac-AA derivatives via acetylation. The detection limit depends on the AA side-chain. For N-Ac-Val and derivatives of similar types of AA the detection limit was 0.5 nmol for a 10-μl injection. A similar detection limit was found for Val when the acetylation step was included in the procedure.

INTRODUCTION

Modern liquid chromatographic (LC) procedures for the separation and detection of complex mixtures of amino acids (AA) generally involve a derivatization step prior to or following the separation [1–5]. In the latter strategy free AA are separated on a cation or an anion exchanger [4], on a reversed stationary phase [1–3,5] or on a reversed stationary phase using an ion interaction (ion-pairing) reagent in the mobile phase [5–7]. The sole purpose of the derivatization step is to allow detection of the AA with low detection limits. If a precolumn derivatization strategy is used in the separation of AA the chromatographic mobile and stationary phase conditions are optimized according to the AA derivative structure. Thus, in this case, derivatization is used to influence both the separation and the detection. The more common derivatization reagents that are used are ninhydrin [1–5,8], *o*-phthalaldehyde [3,8,9] dansyl chloride [3,10] and phenyl isothiocyanate [3,11,12]. The former two can be employed with either absorbance or fluorescence detection while the third requires an absorbance detector.

We have previously shown that inorganic [13,14] and organic analyte anions can be separated and detected by an indirect detection strategy at favorable detection limits using iron(II)– or ruthenium(II)–1,10-phenanthroline or –2,2′-bipyridyl complexes as mobile phase additives. In a basic mobile phase AA are also anionic and

0021-9673/91/$03.50

they can be separated and indirectly detected without derivatization by using a Ru(phen)$_3^{2+}$ salt as the additive [15,16]. The Ru(phen)$_3^{2+}$ salts being chromophoric and fluorescent permit either an indirect photomeric (IPD) [13] or indirect fluorometric (IFD) detection [14] strategy to be used for detection of the resolved AA. A limitation in the separation from a basic mobile phase is that several AA analyte peaks overlap with the OH^- and HCO_3^-–CO_3^{2-} (due to dissolved CO_2) system peaks. As a basic mobile phase is required to convert the AA into anions, modifications of the mobile phase to move system peaks to a region of less interferences is not possible.

This paper describes a procedure for the separation of N-acetylated amino acids (N-Ac-AA) on a reversed stationary phase using an iron(II)–1,10-phenanthroline [Fe(phen)$_3^{2+}$] salt as a mobile phase additive. The contribution of the amine group to dissociation is significantly reduced when the amine group is converted into an acetylated derivative. Thus, the N-Ac-AA derivatives are converted into anions at a much lower pH than is possible for free AA. This allows the N-Ac-AA derivatives to be separated and detected by the IPD strategy at favorable detection limits without interference from OH^- and HCO_3^-–CO_3^{2-} system peaks as a basic mobile phase is no longer required. The procedure described here can be used for the separation and determination of naturally occurring N-Ac-AA. Furthermore, complex mixtures of AA can also be determined using this same separation and indirect detection strategy by first acetylating the AA mixture to form the N-Ac-AA derivatives, as by controlling the conditions it is possible to obtain a reproducible and quantitative acetylation.

EXPERIMENTAL

Materials

The Fe(phen)$_3^{2+}$ salts were synthesized and converted to a specific counter anion form by anion exchange [13,16]. Amino acids and N-Ac-AA derivatives were purchased from Sigma and disodium 1,5-naphthalenedisulfonate (1,5-NDS) from Eastman Kodak. Ionic strength and buffer salts were of analytical-reagent grade, organic solvents were of liquid chromatographic quality and distilled water was purified by a Sybron/Barnsted unit. Hamilton PRP-1 polystyrene–divinylbenzene (10-μm) columns (150 mm × 4.1 mm I.D.; and DuPont Zorbax ODS (5-μm) columns (150 mm × 4.6 mm I.D.) were used. The LC instrumentation used is described elsewhere [15,16].

Procedures

Aqueous solutions of N-Ac-AA derivative standards (1 mg/ml) and mixtures of standards were injected by syringe (10 μl). Preparations of acetylated derivatives were based on AA weight. Mobile phase solvent mixtures are expressed as percent by volume. Buffer, ionic strength and counter-anion salts, prepared as standard solutions, and Fe(phen)$_3^{2+}$ salts by weight were added to mobile phase solvent prior to dilution to volume. The procedure for column conditioning was described previously [13,16]. The flow-rate was 1.0 ml/min, the column temperature was 30°C, the inlet pressure was varied from 600 to 1000 p.s.i., depending on the column and mobile phase, the column void volume was 1.1–1.3 ml, IPD was at 510 nm, the background absorbance, which was always less than 0.7, was electronically offset to zero and the equilibrium amount of Fe(phen)$_3^{2+}$ salt maintained on the column (column and mo-

bile phase dependent), which was determined from column breakthrough data [13,16], was *ca.* 60–75 μmol per column. For an aqueous 0.10 m*M* $Fe(phen)_3$(1,5-NDS)–0.10 m*M* 1,5-NDS (pH 6) mobile phase and a Zorbax ODS column, the equilibrium amount of $Fe(phen)_3^{2+}$ maintained on the column was 71 μmol per column.

Amino acid N-acetylation

A weighed amount (about 0.1 mmol) of each AA was transferred into a 25 ml beaker. The AA were dissolved with stirring with small amounts of water and 0.50 *M* NaOH (pH 9.0). Excess of NaOH should be avoided because it increases the hydrolysis of the acetylating reagent and the total volume should be small so as to maintain an AA concentration as high as possible. The acetylating reagent was added so that the mole ratio of AA to acetic anhydride was in the range 1:1.5 to 1:5. The acetylating reagent was made by diluting 6.5 ml of acetic anhydride (Eastman Kodak) to 25.0 ml with acetonitrile. The solution, which was refrigerated when not in use, was stable for about 3 weeks. After 1 min of reaction the mixture was carefully heated at about 70°C until all the liquid had evaporated. (Excess of acetic anhydride should be removed in this step). The residue was dissolved in water, tranferred into a volumetric flask (10 ml) and diluted to volume with water. Aliquots (10 μl) of this solution were injected as samples.

RESULTS AND DISCUSSION

The $Fe(phen)_3^{2+}$ salt serves a dual role when used as a mobile phase additive. Its presence, depending on mobile phase composition, maintains an equilibrium amount of the $Fe(phen)_3C_2$, where C is a counter anion, on the reversed stationary phase surface as a double layer and provides the sites for interaction with analyte anions [14] such as the anionic form of an N-Ac-AA derivative. Second, the amount of Fe $(phen)_3^{2+}$ in the N-Ac-AA analyte band differs from the amount of $Fe(phen)_3^{2+}$ in the mobile phase background in proportion to the amount of analyte present, hence sensitive indirect detection of the analyte is possible by monitoring the effluent where $Fe(phen)_3^{2+}$ absorbs [13]. The peak can be either positive or negative depending on whether the amount of $Fe(phen)_3^{2+}$ increases or decreases in the analyte band relative to the amount of $Fe(phen)_3^{2+}$ in the background due to the mobile phase.

All N-Ac-AA derivatives, **I** where R is the AA side-chain, will dissociate as follows:

$$\underset{\mathbf{I}}{CH_3C(O)NHCHRCO_2H} + H_2O \rightleftarrows CH_3C(O)NHCHRCO_2^- + H_3O^+ \quad (1)$$

The acetyl group significantly diminishes the basicity of the amine group and its effects on dissociation. Thus, the N-Ac-AA derivatives have ionization constants (carboxyl group) at $pK_a \approx 5$ and will be appreciably anionic in a mobile phase with a pH larger than this value. The advantage of the intermediate mobile phase pH is twofold: the $Fe(phen)_3^{2+}$ salts are stable in this pH region [13] and interfering OH^- and HCO_3^-–CO_3^{2-} system peaks that are present when using a basic mobile phase are absent.

TABLE I

COMPARISON OF RETENTION OF NA-Ac-AA DERIVATIVES ON REVERSED STATIONARY PHASE

Mobile phase: 0.10 m*M* $Fe(phen)_3(ClO_4)_2$–0.10 m*M* 1,5-NDS–5:95 acetonitrile–water (pH 7.5).

Analyte	Column			
	Capacity factor, k'		Plate number, 10^3/m	
	PRP-1	Zorbax	PRP-1	Zorbax
N-Ac-Ser	2.23	1.09	14.8	29.6
N-Ac-Asn	2.23	1.12	14.0	45.2
N-Ac-Gln	2.41	1.31	12.0	45.2
N-Ac-Gly	2.41	1.23	10.9	29.0
N-Ac-Ala	2.77	1.65	11.4	29.6
Analyte pair	Selectivity, α		Resolution, R_s	
	PRP-1	Zorbax	PRP-1	Zorbax
N-Ac-Asn/N-Ac-Ser	1.00	1.03	0	0.82
N-Ac-Gly/N-Ac-Asn	1.08	1.10	1.37	2.13
N-Ac-Gln/N-Ac-Gly	1.00	1.07	0	1.97
N-Ac-Ala/N-Ac-Gln	1.15	1.26	2.56	5.53

Table I shows that N-Ac-AA derivatives are retained on reversed stationary phases from a mobile phase of pH 7.5 containing a $Fe(phen)_3^{2+}$ salt as a mobile phase additive. Further, the retention differs for the derivatives according to the structure of the AA side-chain. The more non-polar the side-chain, the higher is the retention. Retention is also higher for acidic side-chains which are dissociated at pH 7.5. In all instances the derivatives were detected as positive peaks by the IPD strategy. As the N-Ac-AA derivatives are readily retained at an intermediate pH, silica-based reversed phases can be used, unlike in the separation and detection of free AA [15,16] where a basic mobile phase is required to convert the AA into anions. Table I also compares the column efficiency, selectivity and resolution obtained for the retention of several N-Ac-AA derivatives on the polymeric PRP-1 and silica-based C_{18} Zorbax columns. Retention is higher on the PRP-1 because the equilibrium amount of the $Fe(phen)_3^{2+}$ maintained on PRP-1 at the given mobile phase condition is larger than on the Zorbax column. However, selectivity is more favorable on the Zorbax column, as is resolution, because of the improved efficiency. For these reasons all the studies reported here are for the Zorbax column.

The N-Ac-AA derivatives with their increased hydrophobic character and size will be more highly retained than the underiviatized AA. Thus, stronger eluents are required for the successful elution of the N-Ac-AA derivatives. Disodium 1,5-naphthalenedisulfonate was shown to be an eluent counter anion of high enough selectivity to elute the N-Ac-AA derivatives in a reasonable time while producing an eluent counter anion system peak that occurs at a high retention time that does not interfere with the analyte peaks. For example, for the mobile phase conditions used in Fig. 3 the 1,5-NDS system peak is observed at a retention time exceeding 3 h. Buffer

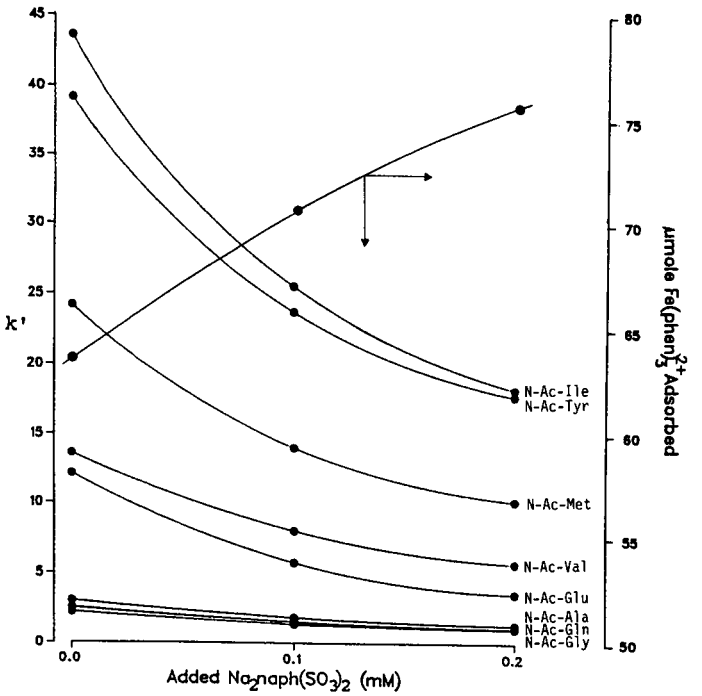

Fig. 1. Retention of N-Ac-AA and equilibrium amount of $Fe(phen)_3^{2+}$ salt on the stationary phase as a function of 1,5-NDS mobile phase concentration. Mobile phase: aqueous 0.10 m*M* $Fe(phen)_3$(1,5-NDS)–1,5-NDS (pH 6).

anions, such as citrate, phthalate and benzoate, which are weaker counter anions than 1,5-NDS, were evaluated. The benzoate salt was selected because its system peak, which occurs within the range of the N-Ac-AA derivative chromatographic peaks, does not overlap with any of the N-Ac-AA derivative peaks.

Increasing the amount of organic solvent in the mobile phase decreases the equilibrium amount of $Fe(phen)_3^{2+}$ salt maintained on the stationary phase surface, which results in a decreased retention of the N-Ac-AA derivatives. When the ionic strength of the 1,5-NDS mobile phase concentration is increased, the equilibrium amount of $Fe(phen)_3^{2+}$ maintained on the stationary phase increases; however, the analyte retention decreases because of the mass action effect of 1,5-NDS as a counter anion. This is illustrated in Fig. 1 where both the retention data for several N-Ac-AA derivatives and the stationary phase surface loading of $Fe(phen)_3^{2+}$ are plotted as a function of mobile phase 1,5-NDS concentration. When the mobile phase pH is increased the retention of the N-Ac-AA derivatives increases as dissociation increases. This is illustrated in Fig. 2 for several derivatives and indicates that a mobile phase pH of about 5 is optimum. The presence of an acidic side-chain in the AA will also influence retention because of additional dissociation as pH is increased. For example, at pH < 5.0 the elution order is N-Ac-Asp $<$ N-Ac-Glu $<$ N-Ac-Val, whereas at pH > 5.4 N-Ac-Val is eluted first. The higher pH value increases the mole ratio of N-Ac-AA as a divalent anion because of additional dissociation at the side-chain

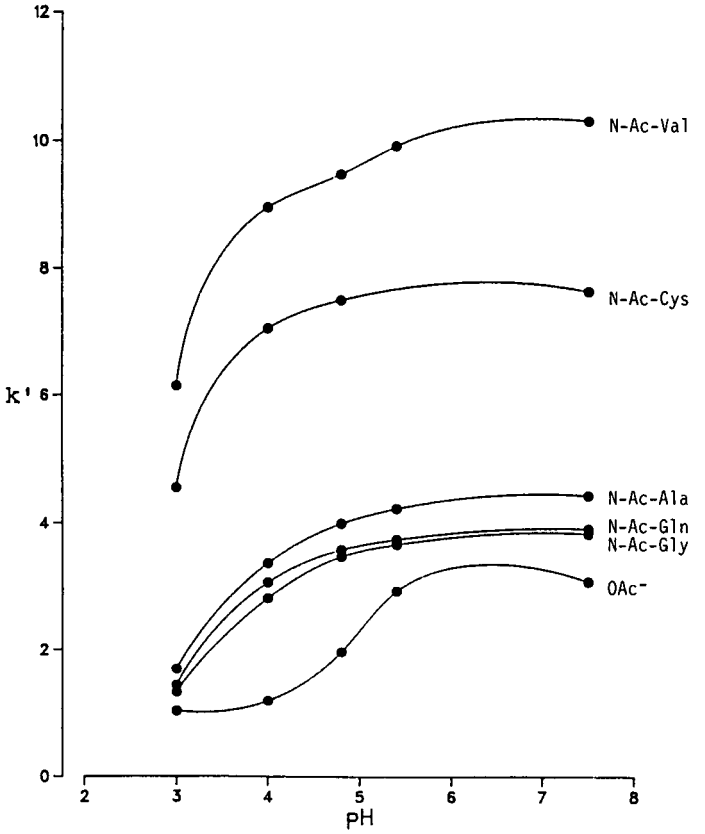

Fig. 2. Effect of pH on N-Ac-AA retention. Mobile phase: 0.10 m*M* $Fe(phen)_3(ClO_4)_2$–0.10 m*M* $NaClO_4$–5:95 acetonitrile–water (pH 3–7.5).

carboxyl group for the Asp and Glu derivatives compared with the monovalent anion that is present when the sample is the Val derivative.

Fig. 3 illustrates a typical separation of a mixture of N-Ac-AA standards using isocratic elution and indirect detection at 510 nm. All analyte peaks are positive peaks for the mobile phase conditions used. The Phe and Trp derivatives, which are not included in Fig. 3, are more highly retained and a stronger eluent is required to elute these derivatives. The benzoate system peak occurs at about 38 min and does ot interfere with the N-Ac-AA derivative peaks while the 1,5-NDS system peak occurs at >3 h. A double peak was found for the N-Ac-Pro standard that was used, which may be due to a sample that contained derivatives where acetylation has occurred at the ring or terminal amine group or both. For the separation of simpler mixtures of N-Ac-AA derivatives the analysis time can be adjusted by altering the mobile phase organic solvent and/or 1,5-NDS concentration.

Fig. 4 shows a calibration graph that was obtained when using N-Ac-Val as a standard. A fixed-loop 10-μl aliquot was used with indirect detection at 510 nm. No attempt was made to determine the upper limit of linearity. For the conditions and instrumentation used the detection limit using a 3:1 signal-to-noise ratio was *ca.* 0.5

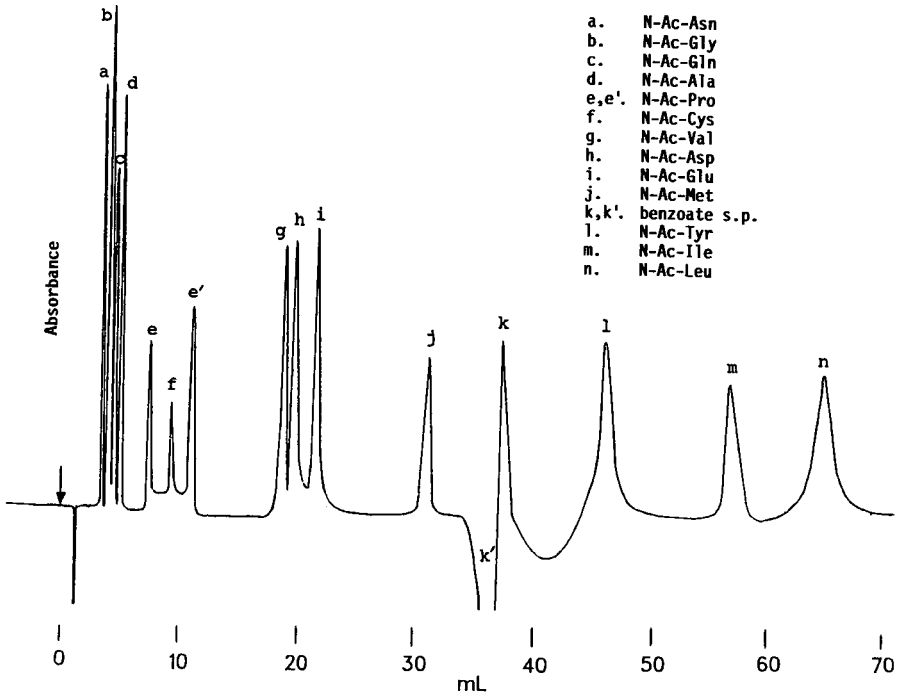

Fig. 3. Separation of a mixture of N-Ac-AA standards. Mobile phase: aqueous 0.050 m*M* $Fe(phen)_3$(1,5-NDS)–0.050 m*M* $Fe(phen)_3$ $(benzoate)_2$ (pH 5.4). s.p. = System peak.

nmol of N-Ac-Val injected as a 10-μl sample. The equation describing the calibration graph is nmol N-Ac-Val (peak area $\times$ 10^5) = $-0.325 + 1.89$ (nmol), with a linear correlation coefficient of 1.00.

Amines can be determined using either acid- [17] or base-catalyzed [18,19] acetylation with acetic anhydride as the acetylating reagent. In general, water is avoided in these procedures because acetylating reagents such as acetic anhydride or acetyl chloride hydrolyze quickly in water, particularly in the presence of the catalyst.

When the water concentration was kept low, the AA concentration was high and the acetylating reagent-to-AA ratio was 1:1.5 to 1:5 in the acetylating mixture, it was shown that AA N-acetylation will occur at a faster rate than hydrolysis of acetic anhydride. The effect of each of these parameters on acetylation *versus* hydrolysis was established by systematically changing each parameter while the others were held constant. Thus, N-acetylation of an aqueous AA sample is not only possible but is also a simple and rapid method that provides excellent conversion to the acetylated derivative.

In the presence of OH^-, acetylation of Val:

$$H_2NCHCH_3CO_2H + (CH_3CO)_2O \overset{OH^-}{\rightleftharpoons} CH_3C(O)NHCHCH_3CO_2^- + CH_3CO_2^- \quad (2)$$

yields 98% N-Ac-Val. The reaction is complete in seconds, and the following step of

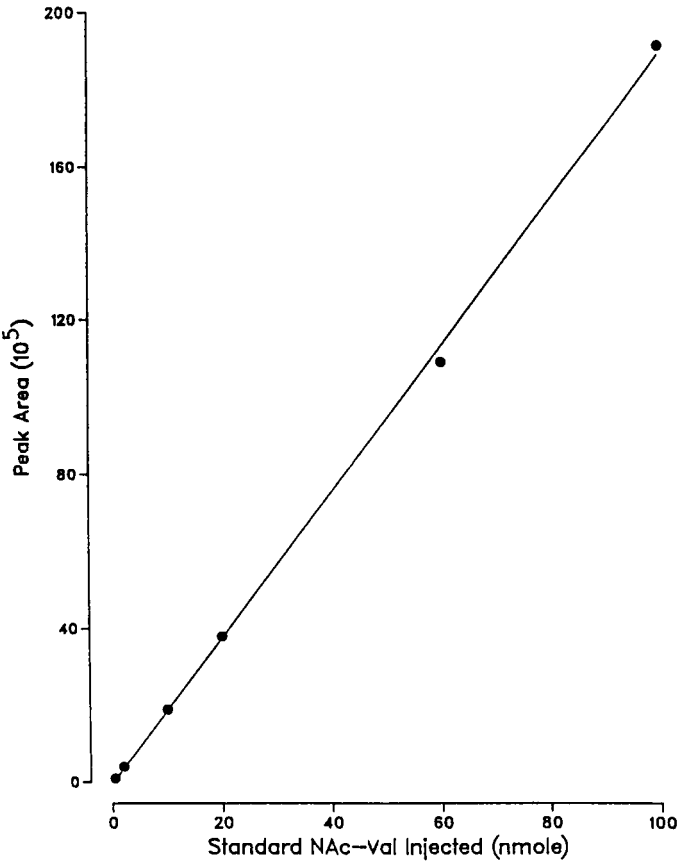

Fig. 4. Calibration graph for N-Ac-AA as a standard. Mobile phase as in Fig. 3 except with acetate in place of benzoate.

solvent anhydride removal and product drying takes only a few minutes. The AA N-acetylation method provides a rapid, simple, and convenient way to convert free AA to N-Ac-AA derivatives which can then be separated: (1) at an intermediate mobile phase pH without interference from the OH^- and CO_3^{2-}–HCO_3^- system peaks and (2) with a high-efficiency silica-bonded stationary phase. The effects of pH, AA concentration, acetylating reagent concentration and buffer concentration were established [16] using Val as a standard by determining the N-Ac-Val chromatographic peak area as a function of the conditions. Using the procedure outlined under Experimental the acetylation was shown to be reproducible, quantitative for the AA tested and provided chromatography identical with N-Ac-AA standards. A calibration graph was prepared for synthesized N-Ac-Val based on Val weight as the sample followed by the acetylation step. The calibration graph, which was almost identical with Fig. 4, corresponded to the equation nmol N-Ac-Val (or Val) (peak area x 10^5) = 1.05 = 1.86 nmol, with a linear correlation coefficient of 1.00. The linear range, like the standard N-Ac-Val calibration graph shown in Fig. 3, is over two orders of magnitude and the detection limit using a 3:1 signal-to-noise ratio is *ca.* 0.5 nmol

calculated as Val. When repeated five times the yield for the derivatization step was reproducible at about 98% acetylation compared with a standard N-Ac-Val calibration graph. Similar results were found when using Ala, Pro and Ile. Hence, it should be possible also to determine free AA after conversion to their acetylated derivatives. Only for AA with reactive side-chains was acetylation found to be low. For example, Glu yielded about 70% acetylation when using the outlined acetylation procedure. Also, AA containing alcoholic or side-chain amine groups will be acetylated at these groups [17–19].

A 0.2 *M* AA solution containing 0.1 nmol each of twelve AA was taken and its pH was adjusted to 9.0 with NaOH solution. A 2-ml volume of acetylating reagent was added and the acetylation and work-up were carried out as outlined under Experimental. The chromatogram for this mixture of synthesized N-Ac-AA derivatives is shown in Fig. 5 using the same mobile phase conditions as shown in Fig. 3 except that the mobile phase pH was 6.0. This mobile phase pH was used in order to improve the separation of N-Ac–N′-Ac-Lys, N-Ac-Asp, N-Ac-Glu. As indicated in Fig. 5, side-chain acetylation can occur in those cases where AA contain an amine or hydroxyl side-chain. The acetateO^-, which is formed in the acetylation (and hydrolysis of acetic anhydride) (see eqn. 2) is not highly retained for the chromatographic conditions used and only partially interferes with the chromatographic peak for the least retained derivative, N-Ac-Gly. Residues of the acetylating reagent do not cause any other interferences of the N-Ac-AA derivatives. If acid catalysis is used, which also

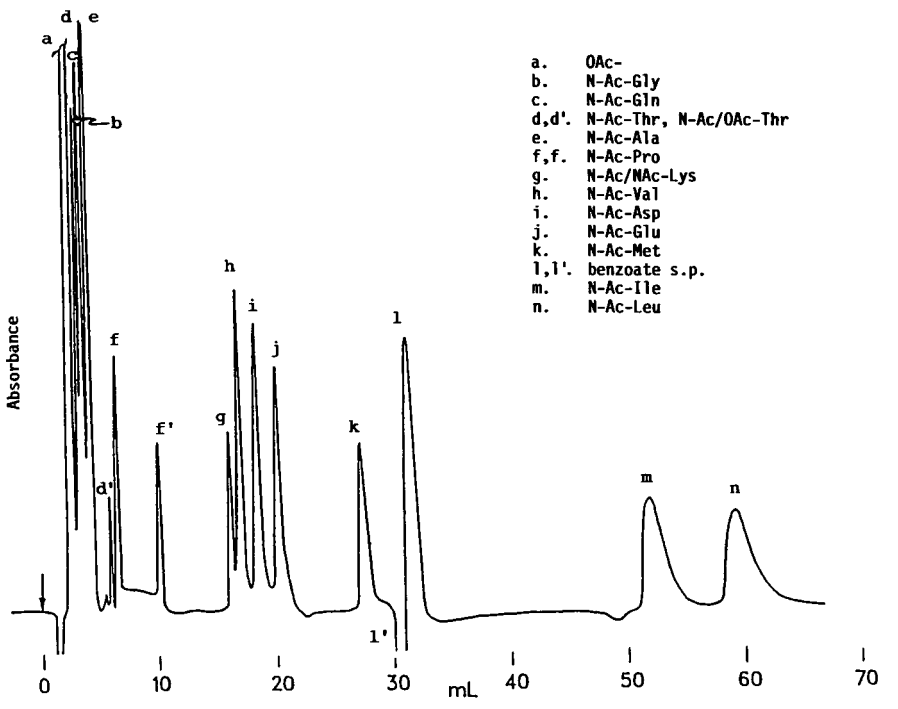

Fig. 5. Separation of an amino acid mixture after acetylation. Mobile phase as in Fig. 3 except pH = 6.0.

leads to quantitative acetylation, the counter anion from the strong acid catalysts that are usually used in acid-catalyzed acetylation [17], such as Cl^- or SO_4^{2-}, will provide a peak that interferes with several AA derivative peaks depending on the counter anion. For this reason base-catalyzed acetylation is preferred.

CONCLUSIONS

Naturally occurring N-acetylated amino acids can be separated and determined with a favorable detection limit using an indirect photometric detection strategy in the visible region where the iron(II)–1,10-phenanthroline complex absorbs. Indirect photometric and fluorimetric detection are also possible if the ruthenium(II) complex [13] is used. It is possible to determine amino acids after acetylation to form the N-acetylated amino acid derivative. Formation of the derivative is not used to enhance the detection limit but rather to block the contribution of the amine group to dissociation, thus allowing the derivatives to be separated as anions at a lower pH. The advantage of the low pH is that system peaks due to OH^- and CO_3^{2-}–HCO_3^- are eliminated. Acetylation of amino acids under a based-catalyzed controlled condition is rapid and quantitative and does not contribute system peaks to the separation.

REFERENCES

1 S. Blackburn, in G. Zweig and J. Sherman (Editors), *CRC Handbook of Chromatography: Amino Acids and Amines*, Vols. I and II CRC Press, Boca Raton, FL, 1983.
2 W. S. Hancock, *CRC Handbook of HPLC for the Separation of Amino Acids, Peptides, and Proteins*, Vol. I, CRC Press, Boca Raton, FL, 1984.
3 Z. Deyl, J. Hyanek and M. Horakova, *J. Chromatogr.*, 379 (1986) 177–250.
4 R. F. Pfeifer and D. W. Hill, *Adv. Chromatogr.*, 22 (1983) 37.
5 M. T. W. Hearn and W. S. Hancock, in G. L. Hawk (Editor), *Biological/Biochemical Applications of Liquid Chromatography*, Vol. 2, Marcel Dekker, New York, 1979, p. 243.
6 Z. Iskandarani, R. L. Smith and D. J. Pietrzyk, *J. Liq. Chromatogr.*, 7 (1984) 111–150.
7 T. A. Walker and D. J. Pietrzyk, *J. Liq. Chromatogr.*, 10 (1987) 161–174.
8 R. L. Cunico and T. Schlabach, *J. Chromatogr.*, 266 (1983) 461–470.
9 J. D. Cooper, M. T. Lewis and D. C. Turnell, *J. Chromatogr.*, 285 (1984) 484–489.
10 C. DeJong, G. J. Hughes, E. Van Wieringen and K. J. Wilson, *J. Chromatogr.*, 241 (1982) 345–359.
11 S. M. Kim, *J. Chromatogr.*, 247 (1982) 103–110.
12 B. A. Bidlingmeyer, S. A. Cohen and T. L. Tarvin, *J. Chromatogr.*, 336 (1984) 93–104.
13 P. G. Rigas and D. J. Pietrzyk, *Anal. Chem.*, 60 (1988) 454–459.
14 P. G. Rigas and D. J. Pietrzyk, *Anal. Chem.*, 60 (1988) 1650–1654.
15 D. J. PIetrzyk, D. Yuan and P. G. Simonson, presented at the *Tenth International Symposium on HPLC of Proteins, Peptides and Polynucleotides, Wiesbaden (Germany), October 29–31, 1990*, paper no. 621.
16 D. Yuan, *Ph. D. Thesis*, University of Iowa, 1988.
17 G. H. Schenk and J. S. Fritz, *Anal. Chem.*, 32 (1960) 987–990.
18 C. L. Ogg, W. L. Porter and C. O. Willits, *Ind. Eng. Chem., Anal. Ed.*, 17 (1945) 394–397.
19 G. H. Schenk, P. Wines and P. Mojzis, *Anal. Chem.*, 36 (1964) 914–919.

Journal of Chromatography, 557 (1991) 325–334
Elsevier Science Publishers B.V., Amsterdam

CHROM. 23 389

Dye–ligand affinity partitioning of lactate dehydrogenase isoenzymes

J. KIRCHBERGER and G. KOPPERSCHLÄGER*
Institute of Biochemistry, University of Leipzig, Liebigstrasse 16, 7010 Leipzig (Germany)
and
M. A. VIJAYALAKSHMI
Laboratoire de Technologie des Separations, Université de Technologie de Compiègne, B.P. 649, 60206 Compiègne Cedex (France)

ABSTRACT

Aqueous two-phase systems consisting of dextran and polyethylene glycol (PEG) were used to study the partition behaviour of isoenzymes of lactate dehydrogenase (LDH; E.C. 1.1.1.27) from rabbit tissues in the presence and absence of a series of triazine dyes covalently coupled to PEG. The variations in the primary structures of LDH1(H_4) and LDH5(M_4) are reflected by significantly different partition coefficients. A class of dyes exhibiting defined structural elements is able to distinguish between both of these isoenzymes. This may be based on differences in the binding affinity to the catalytic site of the enzyme. The difference in the relative affinities of LDH1 and LDH5 to Procion Blue H-5R, as estimated by affinity partitioning, were corroborated by chromatographic experiments. Affinity partitioning in aqueous two-phase systems can be used to predict and to optimize conditions for the fast and simple chromatographic separation of isoenzymes.

INTRODUCTION

The importance of the determination of isoenzymes is a result of their emergence throughout evolution and their functional significance in existing species. Isoenzymes are linked with cell differentiation and development, and with metabolic regulation and tumour growth. The detection of tissue-specific forms of human isoenzymes improves the specificity and sensitivity of enzyme diagnostic methods [1].

Many approaches are available for the determination of isoenzymes, either by using separation techniques based on differences in the charge of the enzymes and in the affinity to specific immobilized ligands, or by applying non-separating methods based on alterations in the kinetics and physico-chemical and immunological properties of the isoenzymes.

For the separation of lactate dehydrogenase (LDH) isoenzymes, electrophoretic methods [2], anion-exchange chromatography [3] and affinity chromatography using diverse affinity ligands (adenosine-5'-mono-phosphate, oxomate or Cibacron Blue F3G-A) have been described [4–6].

0021-9673/91/$03.50

Non-separating detection methods for LDH isoenzymes are based on differences in the stability, kinetic behaviour or immunological properties of the H and M type of the LDH subunits [7].

It is well established that dye–ligand affinity partitioning in aqueous two-phase systems is an attractive approach for studying dye–protein interactions in more detail. The high sensitivity in the recognition of even weak ligand–protein interactions and simple handling particulary favour this method [8–10].

For characterizing the behaviour of enzymes in affinity partitioning, the difference in the logarithms of the partition coefficients in systems with and without the ligand ($\Delta\log K$) is a valuable parameter. The dependence of $\Delta\log K$ on the ligand concentration in a two-phase system generally follows a saturation curve from which two parameters, namely, the maximum partition effect ($\Delta\log K_{max}$) and the relative affinity of the ligand to the protein ($0.5\ \Delta\log K_{max}$) can be calculated [11]. The change in the partition coefficient of an enzyme in the presence of a ligand polymer and competing effectors gives information on the specificity and mode of interaction of the ligand–protein binding [8].

In this work affinity partitoning in aqueous two-phase systems consisting of polyethylene glycol (PEG) and dextran was used to study the binding behaviour of LDH isoenzymes to different triazine dyes covalently coupled to PEG. The aim of this work was to prove the potential of dye–ligands to recognize differences in the properties between isoenzymes determined by individual gene loci.

EXPERIMENTAL

Materials

Lactate dehydrogenase (E.C. 1.1.1.27) from rabbit muscle (LDH5, M_4-isoenzyme) and rabbit heart (LDH1, H_4-isoenzyme), nicotinamide–adenine dinucleotide, oxidized (NAD^+), nicotinamide–adenine dinucleotide, reduced (NADH) and pyruvate were obtained from Sigma (France). PEG 6000, dextran 500 and 2-oxobutyric acid were purchased from Serva (Germany). The dyes were obtained from ICI Organics Division (Blackley, UK) and Ciba-Geigy (Basle, Switzerland). The Vilmax Dye I and Vilmax Dye II were a generous gift from Dr. Mazza, Vilmax (Buenos Aires, Argentina). All other biochemicals were of analytical-reagent grade.

Methods

Preparation of the dye derivatives. The triazine dyes were coupled to PEG 6000 under aqueous alkaline conditions and the reaction product was purified by extraction with chloroform and ion-exchange chromatography on DEAE–cellulose (Serva) according to the method of Johansson [9]. The purity of the conjugates was determined by thin-layer chromatography on silica plates G 60 (Merck, Germany) in butan-1-ol–propan-2-ol–ethylacetate–water (20:35:10:35). Procion Blue H-5R and Procion Red HE-3B were coupled to Sepharose 4B (Pharmacia, Sweden), as described by Hughes *et al.* [12].

Enzyme assay. The activities of LDH1 and LDH5 were assayed at 25°C as described by Bergmeyer [13] in 50 m*M* sodium phosphate buffer solution, pH 7.5, using 0.6 m*M* pyruvate and 0.18 m*M* NADH as substrates. The 2-hydroxybutyrate dehydrogenase (HBDH) activity of the LDH isoenzymes was determined in 50 m*M*

sodium phosphate buffer, pH 7.5, with 3.3 m*M* 2-oxobutyrate and 0.2 m*M* NADH at 25°C. One unit of the activity is defined as the amount of the enzyme catalysing the conversion of 1 μmol/min of the respective substrate at 25°C.

Aqueous two-phase partitioning. The two-phase systems were prepared from stock solutions of PEG 6000 (20% w/w), dextran 500 (30% w/w), sodium phosphate buffer, pH 0.5 (0.5 *M*) and NAD^+ (15 m*M*) by weighing the respective amounts to obtain systems of total mass 2 g with compositions as indicated in the figure legends.

The content of the dye–ligand PEG expressed as percentage is related to the total mass of PEG present in the system. A sample of 2 g of a two-phase system containing about 5 units of LDH was maintained at 25°C and equilibrated by gentle mixing for 30 s. After centrifugation at 1500 × g for 5 min, the samples were withdrawn from both phases and diluted with the test buffer. An inhibition of the enzyme in the assay mixture by the dye–PEG was avoided by dilution of the samples.

The partition coefficient, *K*, is defined as the ratio of the enzyme activity per unit volume in the top and bottom phases.

Affinity chromatography. Disposable columns (8 mm × 30 mm I.D.) from Bio-Rad Labs. (France) containing a 5-ml bed volume of dye–ligand Sepharose 4B were equilibrated with 50 m*M* sodium phosphate buffer, pH 7.5, at 25°C. The dialysed enzymes were applied successively to the column. The unbound protein was removed by washing with equilibration buffer at a flow-rate of 10 ml/h. The bound isoenzymes were eluted from the column by a linear gradient of NAD^+ (0–3 m*M*). Fractions of 1 ml were collected and assayed for LDH and HBDH activity.

The concentration of NAD^+ in the fractions was determined by measuring the absorbance at 260 nm using a molar absorption coefficient of 17.6 l mol^{-1} cm^{-1}.

RESULTS

Affinity partitioning

Affinity partitioning of LDH1 and LDH5 was screened with a series of dyes and the results are listed in Table I. In the absence of the dye–ligand PEG both isoenzymes partition in favour of the dextan-rich bottom phase ($K < 0.5$), but with different extents. After the addition of 2% dye–PEG to the systems, the partition of the isoenzymes changes depending on the nature of the dye–ligand and isoenzyme, as shown in Table I.

The greatest difference in the affinity partitioning effect ($\Delta \log K$) for LDH5 and LDH1 calculated from the data in Table I was found with Procion Blue H-5R, followed by Cibacron Red 3BA, Cibacron Blue F3G-A and Vilmax Dye I. The structures of these dyes are shown in Fig. 1.

To study these dye–LDH interactions in more detail, the partition of LDH1 and LDH5 was studied as a function of the concentration of the dye–PEG. Hyperbolic curves were obtained for both isoenzymes, as exemplified in Fig. 2 with Procion Blue H-5R and Procion Red HE-3B.

The maximum effect of the affinity partitioning ($\Delta \log K_{max}$) and the relative affinity (aff_R at 0.5 $\Delta \log K_{max}$) determined from double reciprocal plots of $\Delta \log K$ *versus* the dye concentration are listed for selected dyes in Table II. In general, higher $\Delta \log K_{max}$ values were obtained with LDH5 compared to LDH1. For LDH5 the highest $\Delta \log K_{max}$ was determined for Procion Blue H-5R. Cibacron Blue F-3GA

TABLE I

AFFINITY PARTITIONING OF LDH ISOENZYMES

Systems (2 g) containing 9% (w/w) dextran 500, 6% (w/w) PEG 6000 (2% dye–PEG), 50 m*M* sodium phosphate buffer, pH 7.5, and 5 units of LDH1 and LDH5, respectively, were equilibrated at 25°C.

Dye–PEG	Log *K*	
	LDH1	LDH5
Procion Red HE-3B	+0.894	+1.195
Procion Red MX-8B	−0.353	−0.213
Procion Red H-3B	−0.109	+0.095
Procion Red H-8BN	−0.299	+0.180
Procion Red MX-5B	−0.113	+0.216
Cibacron Red 3BA	+0.146	+1.185
Procion Scarlet MX-G	−0.061	−0.010
Procion Blue MX-G	+0.985	+1.528
Procion Blue MX-3G	+0.320	+0.532
Procion Blue H-5R	+0.786	+2.008
Procion Blue MX-2G	+0.199	+0.548
Cibacron Blue F3G-A	+0.605	+1.430
Procion Navy HE-R	+1.196	+1.557
Procion Navy MX-RB	+0.146	+0.471
Procion Yellow HE-3G	+1.379	+1.445
Procion Yellow H-ER	+0.843	+1.133
Procion Yellow H-A	−0.343	−0.775
Procion Orange MX-G	−0.401	−0.651
Procion Orange MX-2R	−0.135	+0.323
Procion Orange H-2R	−0.124	+0.161
Procion Brown H4-GR	+0.162	+0.126
Procion Green H-4G	+1.603	+1.780
Vilmax Dye I	+0.455	+1.327
PEG alone	−0.411	−0.990

generated the highest $\Delta\log K_{max}$ with LDH1. With the exception of Procion Red HE-3B, all the other dyes show a significantly higher relative affinity to LDH5 compared to LDH1. The greatest difference in the relative affinity (ten-fold) was found for Procion Blue H-5R.

To analyse the relationship between the enzyme–dye interaction and the binding specificity, the competitive effect of NAD^+ on the affinity partitioning of LDH isoenzymes was studied.

The coenzyme partitions in the aqueous two-phase system used with a *K*-value of 0.85, independent of the presence or absence of the dye–ligand. As a result of the different affinities of the dye–ligand to both isoenzymes the competition of NAD^+ must be related to a definite concentration of dye–PEG which was defined as the two-fold concentration of the dye–PEG generating 0.5 $\Delta\log K_{max}$.

With increasing concentrations of NAD^+ the $\Delta\log K$ value for both isoenzymes decreased, as shown for Procion Blue H-5R and Procion Red HE-3B in Fig. 3. In contrast to the result with Procion Red HE-3B-PEG, significant differences in the extent of the decrease of $\Delta\log K$ for LDH1 and LDH5 were observed using Procion Blue H-5R-PEG.

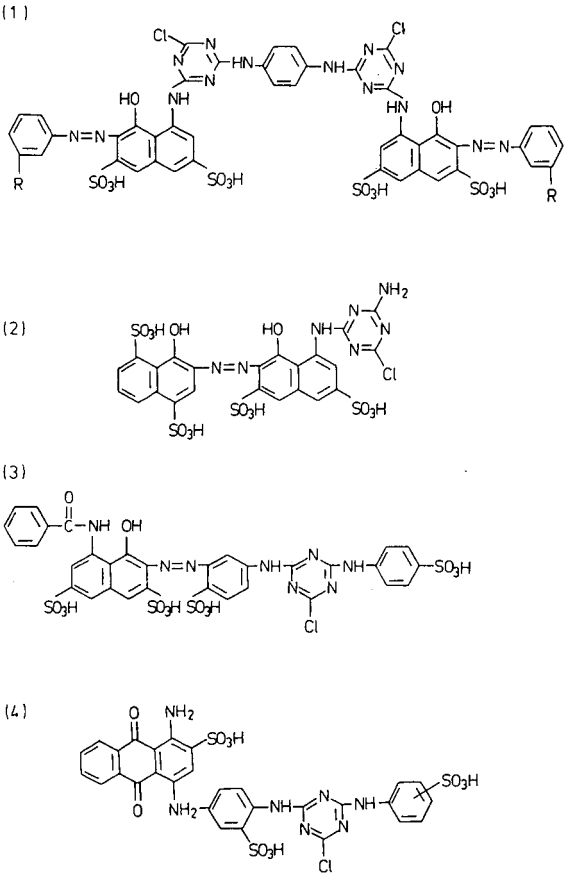

Fig. 1. Structures of triazine dyes: 1 = Procion Red HE-3B (R = SO_3H); Vilmax Dye I (R = H); 2 = Procion Blue H-5R; 3 = Cibacron Red 3BA; 4 = Cibacron Blue F3G-A.

In Table III the data for the effect of NAD^+ on the affinity partitioning of the LDH isoenzymes in the presence of several dyes are listed. In the case of LDH1, NAD^+ competes most effectively with Vilmax Dye I and Cibacron Red 3BA. With LDH5 the competitive effect of NAD^+ was less pronounced for all dyes tested and showed, with the exception of Procion Blue H-5R at 2 m*M* NAD^+, negligible differences between all dye–ligands.

Affinity chromatography

Applying the results of affinity partitioning in affinity chromatography, a separation of LDH isoenzymes (LDH1 and LDH5) should be realized under certain conditions. In Fig. 4 the elution profile of a mixture of LDH1 and LDH5 on Procion Blue H-5R–Sepharose with increasing concentration of NAD^+ is shown. Two distinct fractions with LDH and HBDH activity appeared. By comparing the ratio of the HBDH:LDH activity in fractions 1 and 2 (0.51 and 0.09, respectively) with those of the individual enzymes it becomes evident that fraction 1 contains LDH1 and fraction 2

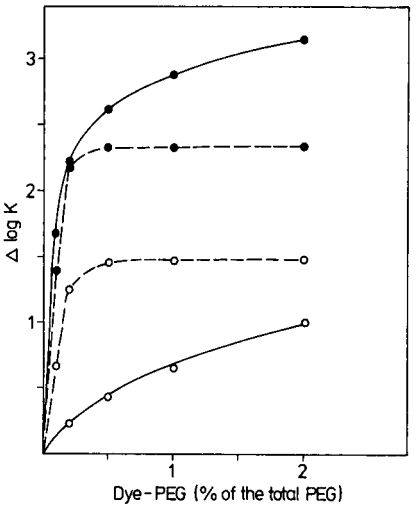

Fig. 2. Affinity partitioning of LDH1 (○) and LDH5 (●) as a function of the concentration of Procion Red HE-3B–PEG (– – –) and Procion Blue H-5R–PEG (———). The systems (2 g) contained 9% (w/w) dextran 500, 6% (w/w) PEG 6000 (partially replaced by dye–PEG), 50 m*M* sodium phosphate buffer, pH 7.5, and 5 units of the respective isoenzyme. The systems were equilibrated at 25°C.

LDH5 in the pure state. The concentration of NAD^+ in the main fraction of peak 1 and peak 2 was 0.35 and 1.45 m*M*, respectively. The overall recovery of the LDH and the HBDH activity was 90%.

In accordance with the results of affinity partitioning the affinity chromatography of LDH1 and LDH5 on immobilized Procion Red HE-3B and NAD^+ as eluting effector revealed only one peak containing 91% of the overall LDH and HBDH activity applied. The concentration of NAD^+ in the main fraction was 0.67 m*M* (Fig. 5).

TABLE II

AFFINITY PARTITIONING OF LDH ISOENZYMES AS A FUNCTION OF THE AMOUNT OF DYE–PEG IN THE SYSTEM

Systems (2 g) containing 9% (w/w) dextran 500, 6% (w/w) PEG 6000, 50 m*M* sodium phosphate buffer, pH 7.5, and 5 units of enzyme were equilibrated at 25°C.

Dye–PEG	LDH1		LDH5	
	$\Delta\log K_{max}$	aff_R[a]	$\Delta\log K_{max}$	aff_R[a]
Procion Red HE-3B	1.47	0.15	2.34	0.10
Procion Blue H-5R	1.33	1.02	3.33	0.10
Cibacron Blue F3G-A	1.61	0.65	2.45	0.12
Cibacron Red 3BA	1.43	2.38	2.86	0.44
Vilmax Dye I	1.25	0.92	2.86	0.31

[a] The term relative affinity (aff_R) is defined as that dye–PEG concentration (expressed as % of total PEG) which generates affinity partitioning of 0.5 $\Delta\log K_{max}$.

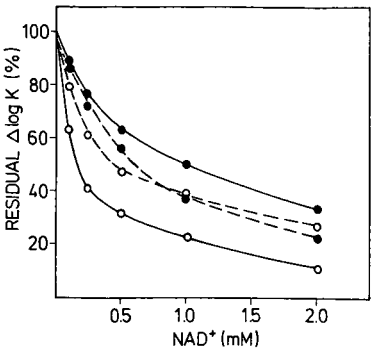

Fig. 3. Affinity partitioning of LDH isoenzymes as a function of the amount of NAD^+ added to the system. The systems (2 g) contained 9% (w/w) dextran 500, 6% (w/w) PEG 6000, including 0.3% Procion Red HE-3B–PEG (– – –) and 2% Procion Blue H-5R–PEG (———) for LDH1 (○) and 0.2% Procion Red HE-3B–PEG and 0.2% Procion Blue H-5R–PEG for LDH5 (●), 50 m*M* sodium phosphate buffer, pH 7.5, and 5 units of the respective isoenzyme. The systems were equilibrated at 25°C.

DISCUSSION

Aqueous two-phase systems consisting of dextran and PEG are able to recognize differences in the primary structures of both LDH isoenzymes. The higher log K value for LDH1 in comparison to LDH5 may be caused by different surface properties (a larger negative net charge or degree of hydrophobicity) of this isoenzyme, which is also indicated by the existence of different epitopes on LDH1 and LDH5 [6].

The interaction of triazine dyes with multiple forms of enzymes, including isoenzymes, as shown for alkaline phosphatase, collagenase, creatine kinase and LDH, is preferentially studied by kinetic and chromatographic methods [14–17].

The applicability of dye–ligand affinity partitioning for this study was restricted.

TABLE III

INFLUENCE OF NAD^+ ON THE AFFINITY PARTITIONING OF LDH ISOENZYMES

Systems (2 g) containing 9% (w/w) dextran 500, 6% (w/w) PEG 6000, 50 m*M* sodium phosphate buffer, pH 7.5, and 5 units of enzyme were equilibrated at 25°C.

Dye–PEG	Residual $\Delta\log K$ (%)			
	LDH1		LDH5	
	NAD^+ (m*M*)		NAD^+ (m*M*)	
	0.25	2.00	0.25	2.00
Procion Red HE-3B	62	28	73	22
Procion Blue H-5R	41	11	78	35
Cibacron Blue F3G-A	38	13	64	21
Cibacron Red 3BA	27	0	64	26
Vilmax Dye I	23	0	64	21

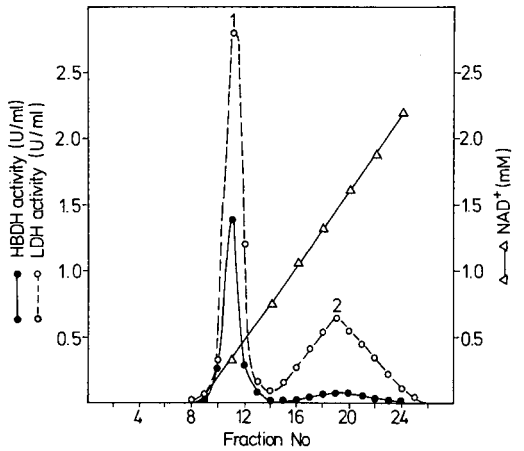

Fig. 4. Affinity chromatography of lactate dehydrogenase isoenzymes on Procion Blue H-5R–Sepharose 4B. The column (1.5 cm × 3.0 cm) was equilibrated with 50 m*M* phosphate buffer, pH 7.5, at 25°C. The dialysed isoenzymes (5 units of LDH activity each) were applied. The enzymes were desorbed by a linear gradient of NAD^+ (0–3 m*M*) in equilibration buffer. The LDH activity (○- - -○) and the HBDH activity (●—●) were determined in all fractions (1 ml).

Ligands such as Cibacron Red 3BA, Procion Blue H-5R, Cibacron Blue F3G-A and Vilmax Dye II covalently coupled to PEG lead to an increase on the difference in the partition coefficients of both isoenzymes, whereas other dyes such as Procion Scarlet MX-G and Procion Yellow HE-3G reduce the difference. Other dyes such as Procion Yellow H-A and Procion Orange MX-G do not show any interaction with either isoenzyme.

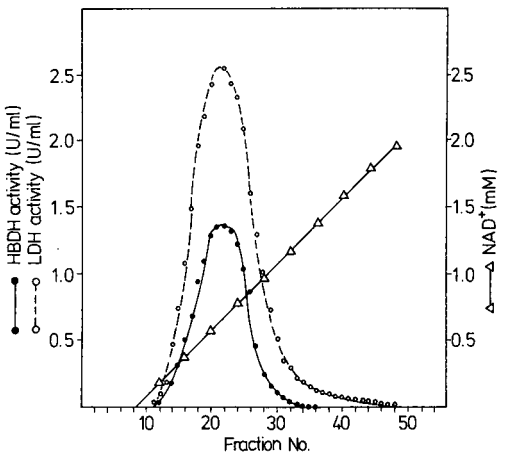

Fig. 5. Affinity chromatography of lactate dehydrogenase isoenzymes on Procion Red HE-3B–Sepharose 4B. The column (1.5 cm × 3.0 cm) was equilibrated with 50 m*M* phosphate buffer, pH 7.5, at 25°C. The dialysed isoenzymes (13 units of LDH activity each) were applied. The enzymes were desorbed by a linear gradient of NAD^+ (0–3 m*M*) in equilibration buffer. The LDH activity (○- - -○) and the HBDH activity (●---●) was determined in all fractions (1 ml).

By comparing the structure of all the dyes investigated with the results obtained, one common feature can be suggested. Only polysulphonated dyes containing 1-amino-8-naphthol-3,6-disulphonic acid rings or 1-amino-4-(4′-aminophenylamino)-anthraquinone-2,3′-disulphonic acid moieties are able to distinguish between both isoenzymes.

For a deeper insight, only dyes which generate high differences in the $\Delta \log K$ values of both isoenzymes have been selected to compare their relative affinity to LDH1 and LDH5. These data have additionally been compared with results obtained with Procion Red HE-3B, a well characterized pseudo-biospecific ligand of LDH from rabbit muscle [6,18]. Generally, LDH5 possesses a higher relative affinity to the dye–ligands selected than LDH1. Only Procion Red HE-3B showed a similar high relative affinity to both isoenzymes. As shown in the competitive experiments with NAD^+, the partition of the isoenzymes in the presence of Procion Red HE-3B, Procion Blue H-5R, Cibacron Red 3BA, Cibacron Blue F3G-A and Vilmax Dye I is based on pseudo-biospecific interactions. The hydrophobic nicotinamide pocket and arginine residues of the substrate binding site are probably involved in the binding of dyes such as Cibacron Blue F3G-A and Procion Red HE-3B with such a high affinity [18,19].

As no exact data about the structural differences in the active centre of LDH1 and LDH5 from rabbit tissues are available at present, the differences in the relative affinity of the dyes to the LDH isoenzymes cannot be discussed on the basis of the specific interaction of amino acid residues with structural elements of the dyes.

From kinetic analysis it becomes obvious that LDH isoenzymes exhibit different catalytic properties. As already published and corroborated by these authors' experiments (data not shown), both LDH isoenzymes possess a higher affinity to NADH than to NAD^+. The differences in the affinity of LDH5 to NAD^+ and NADH are more pronounced than for LDH1. The K_m values for NAD^+ of LDH1 and LDH5 are very similar [13,20]. Consequently, the differences in the decrease of $\Delta \log K$ with increasing concentrations of NAD^+ is more affected by the different affinity of the isoenzymes to the dye–ligand (Procion Blue H-5R and Procion Red HE-3B, respectively) than by the differences in the affinity to NAD^+.

The affinity chromatographic separation of isoenzymes depends on differences in: (1) the affinity between the ligand and the enzymes; (2) the affinity between the enzymes and the competitive effector; and (3) the classes of binding sites. Considering these features and the results of affinity partitioning, only Procion Blue H-5R in combination with NAD^+ as a competitive effector should be a good biomimetic ligand for the chromatographic separation of LDH isoenzymes. This is demonstrated by the results obtained here.

The separation of LDH isoenzymes by using high-performance liquid chromatography with immobilized Cibacron Blue F3G-A, as reported by Lowe *et al.* [21], can be explained by the results reported in this paper. The difference in the relative affinities of LDH1 and LDH5 to the dye–ligand seems to be sufficient to separate both isoenzymes with increasing concentration of NADH.

In summary, affinity partitioning in aqueous two-phase systems is a sensitive and simple method of studying ligand–isoenzyme interactions. The parameters obtained allow determination of the conditions for the chromatographic separation of isoenzymes with high efficiency.

ACKNOWLEDGEMENT

This work was supported by the France–German Democratic Republic scientific exchange programme under the auspices of the Ministry of External Affairs and Cooperation.

REFERENCES

1 C. C. Rider and C. B. Taylor (Editors), *Outline Studies in Biology, Isoenzymes*, Chapman & Hall, London, New York, 1980.
2 S. L. Kowalewski, in G. Weitzel and N. Zollner (Editors), *Biochemie und Klinik*, Thieme Verlag, Stuttgart, 1972.
3 E. D. Wachsmuth and G. Pfleiderer, *Biochem. Z.*, 336 (1963) 556.
4 S. Ohlson, L. Hansson, P. O. Larsson and K. Mosbach, *FEBS Lett.*, 93 (1978) 5.
5 P. O'Carra and S. Barry, *Methods Enzymol.*, 34 (1977) 598.
6 G. Kopperschläger, H.-J. Böhme and E. Hofmann, in T. K. Ghose, A. Fiechter and N. Blakebrough (Editors), *Advances in Biochemical Engineering*, Springer, Heidelberg, 1982, p. 101.
7 M. Maekawa, *J. Chromatogr.*, 429 (1988) 373.
8 G. Kopperschläger, G. Lorenz and E. Usbeck, *J. Chromatogr.*, 259 (1983) 97.
9 G. Johansson, *Methods Enzymol.*, 104C (1984) 356.
10 G. Birkenmeier, G. Kopperschläger and G. Johansson, *Biomed. Chromatogr.*, 1 (1986) 64.
11 G. Johansson, G. Kopperschläger and P.-A. Albertsson, *Eur. J. Biochem.*, 131 (1983) 589.
12 P. Hughes, C. R. Lowe and R. F. Sherwood, *Biochim. Biophys. Acta*, 700 (1982) 90.
13 H. U. Bergmeyer (Editor), *Methods of Enzymatic Analysis*, Vol. 2, Academic Press, New York, 1974, p. 574.
14 D. G. Williams, P. G. H. Byfield and D. W. Moss, *Enzyme*, 33 (1985) 70.
15 H. Yamamoto, M. Tanaka, T. Okochi and S. Kishimoto, *Biochem. Biophys. Res. Commun.*, 111 (1983) 36.
16 M. D. Bond and H. E. Van Wart, *Biochemistry*, 23 (1984) 3077.
17 T. Wallimann, B. Zurbriggen and H. M. Eppenberger, *Enzyme*, 33 (1985) 226.
18 J. Kirchberger, F. Cadelis, G. Kopperschläger and M. A. Vijayalakshmi, *J. Chromatogr.*, 483 (1989) 289.
19 S. T. Thompson and E. Stellwagen, *Proc. Natl. Acad. Sci. U.S.A.*, 73 (1976) 361.
20 *Biochemica Information*, Boehringer Mannheim, Mannheim, 1987, p. 46.
21 C. R. Lowe, M. Glad, P.-O. Larsson, S. Ohlson, T. Atkinson and K. Mosbach, *J. Chromatogr.*, 215 (1981) 303.

Journal of Chromatography, 557 (1991) 335–358
Elsevier Science Publishers B.V., Amsterdam

CHROM. 23 274

High-performance liquid chromatography of amino acids, peptides and proteins

CXIV[a]. Protein interactions with porous coulombic sorbents: comparison of experimental findings with predictions of several adsorption models

A. JOHNSTON and M. T. W. HEARN*

Department of Biochemistry and Centre of Bioprocess Technology, Monash University, Clayton, Victoria 3168 (Australia)

ABSTRACT

The adsorption behaviour of three anion-exchange sorbents, DEAE Trisacryl M, DEAE Sepharose FF and DEAE Fractogel 650 M has been investigated for proteins of different size and charge distribution. The maximum capacity, q_m, and the dissociation constant, K_d, were found to be protein size dependent. Protein loadings with carbonic anhydrase infer unhindered access to the pores of these three sorbents and thus high capacities. Kinetic profiles, monitoring protein uptake from solution, indicated that the rate of adsorption was fast for small proteins. Mathematical models, derived by others, were adopted to extract values for the interaction rate, k_1, and the effective diffusion, D_p. The simplest model of Horstmann *et al.* [*J. Chromatogr.*, 361 (1986) 179] gave high values for k_1, confirming that this model lumped together the resistances to mass transfer. Correlation between theory and experiment was best when using the most sophisticated model, that of Arve and Liapis [*AIChE. J.*, 33 (1987) 179] where the resulting values for k_1 were larger. Diffusion for the smaller proteins agreed well with bulk diffusion, indicating little restriction to mass transfer through the pores. Contrary to this, values of D_p for the largest protein, ferritin, were 1/40th of the free diffusivities, further highlighting the influence of protein size on pore accessibility.

INTRODUCTION

The structural diversity and dynamic nature of proteins give rise to a plethora of species that differ widely in physical, chemical and biological properties. For a particular protein, microheterogeneity can arise from natural evolution, during transcription and post-translational modifications, or from misoccurances during isolation. With the onsurge of recombinant DNA technology, biosynthetically derived protein heterogeneity has become increasingly more prevalent and of greater concern at both the recovery and quality control stages of product manufacture. The existence

[a] For Part CXIII, see ref. 45.

0021-9673/91/$03.50

of isoforms of proteins, differing in a number of properties such as charge distribution, apparent size and three dimensional structure, has thus fostered the need for careful and highly tuned separation techniques that selectively purify the desired protein from its contaminants, and in particular contaminants that are closely related structurally.

In laboratory-scale purifications, affinity chromatography is one such technique used, despite its relative cost per cycle. However, the increasing demand for recombinant proteins with human therapeutic, industrial, diagnostic or other commercial uses has necessitated the need to process large quantities of source material. Further steps other than immuno-affinity or other forms of biospecific chromatographic procedures are therefore essential in the overall mass separation at the preparative process scale. In particular, tandem steps are usually chosen to maximize the throughput of the source material to minimize time and to achieve a high level of purity. This last criterion becomes more important when the protein is designated for human therapeutic use. As an example of this strategy, the scheme chosen for the extraction of serum albumin from human plasma entailed taking a volume reduction step first, namely ion-exchange chromatography, whilst the most expensive step, affinity chromatography, was used last, to ensure 99% purity at minimum cost [1]. This scheme thus follows two of the six cardinal rules in the heuristics of process design [2].

Positive chromatographic purification can be simply visualised as entailing three operational steps. (1) The starting material is loaded onto a column packed with adsorbent resin and the target protein is specifically adsorbed; (2) the column is washed with running buffer to remove unwanted, unadsorbed components; (3) the target protein, having adsorbed to the resin during step (1) is desorbed with an appropriate elution buffer. These steps are fundamental to all modes of process chromatography, and are widely used in practice today to purify important therapeutic protein substances from biological fluids and fermentation broths. Optimization of these steps has up till now concentrated on the process parameters, such as flow-rate and loadability. However, it has recently been shown that the mechanism of protein interaction needs to be considered as an integral part of the process optimisation [3]. For example, the performance of the resin with respect to its interactive properties can affect the stability of the protein and its purification. At a process level, effects such as slow diffusion of the protein through the porous network, tortuosity, non-specific adsorption onto heterogeneous sites and rotational masking can become detrimental to process efficiency. In addition, adsorption of the target protein to the chromatographic resin may cause undesirable structural changes to the protein. With reversed-phase sorbents, for instance, the highly hydrophobic surface has been found to promote unfolding of the protein [4–7]. Reorientation of immunoglobulin G (IgG) bound to an ion-exchange sorbent has also been observed [8]. Essentially, the hydrophobic and coulombic forces that are important in maintaining protein structure are the same forces often used to affect chromatographic separations. In conjunction with the adverse effects of interaction with the resin, the elution buffers used to desorb the protein, such as organic solvents in the case of reversed-phase, or high salt concentrations in ion-exchange chromatography, can also promote conformational change or aggregation of the protein molecules [8–10]. Thus, exposure of the protein to buffers vastly different in composition to those it experiences in its natural physiological environment may cause a perturbance in the protein's integrity and ultimately result in a loss of activity.

It is therefore clear that the time the protein takes to pass down the column (the column residence time) interacting with the resin along its path, desorbing and resorbing from buffer to resin is crucial [11]. Residence time depends upon the kinetic rate and strength of the interaction, as well as the rate at which the protein diffuses to the functional groups distributed on the surface of the resin. Porous resins, offering a high surface area and high capacity, are commonly used in chromatographic separations. In preparative procedures, the choice of large macroporous resins is preferred over non-porous sorbents due to higher productivity without sacrificing resolution and column back pressure. Protein diffusion through the porous matrix of the resin then becomes an additionally important time-dependent factor. The rate constant, indicative of the kinetics of adsorption, and the effective diffusivity of the protein are thus two physicochemical parameters that characterize retention and hence are important parameters governing process performance. Unfortunately these two parameters cannot be measured directly from experimental work. Recent research has been directed towards developing mathematical models that describe the adsorption process from which these physicochemical parameters can be calculated. The applicability and adequacy of each of these models will depend upon the complexity of the crude source mixture, the integrity of the target protein and the homogeneity of the resin's macro- and micro-structure.

In this paper, the adsorption behaviour of several proteins in the ion-exchange mode has therefore been examined, in order to assess the adequacy of several models prominent in literature. Two ion-exchange resins, in industrial employment and a new synthetic ion-exchange resin are evaluated both in terms of the kinetic rate constant and the apparent rate of protein diffusion through the porous resins.

THEORY

Langmuir isotherms

The adsorption of protein to interactive resins was initially perceived as being similar to the adsorption of gases and small molecules to surfaces. The adsorbent is visualized as having a number of identical, non-cooperative sites, upon which a monolayer coverage of the protein adsorbs. The dependence of the amount of the protein that adsorbs (at constant temperature and after a certain time interval) at a particular solution concentration is called the adsorption isotherm. The simplest type of isotherm, the Langmuir isotherm, is based on the principles of stoichiometry, with one protein molecule interacting with one specific functional site. The expression thus derived takes the form

$$q^* = \frac{K_a\, q_m\, c^*}{1 + K_a\, c^*} \tag{1}$$

The parameters K_a and q_m can be calculated from a double reciprocal plot of eqn. 1 ($1/c^*$ against $1/q^*$) where under ideal operational criteria, this plot is predicted to be linear. This Langmuir isotherm has been found to adequately describe, for example, the affinity adsorption of IgG to immobilized Protein A on Superose [12], and of bovine serum albumin to Cibacron Blue Sepharose CL-6B [23]. Reports based on low concentration loading onto a non-porous sorbent also demonstrate that the Langmuir

approach provides a realistic interpretation of other types of adsorption processes [14]. The adsorption behaviour of other affinity systems have also been tailored to fit empirical relationships, like the Freundlich isotherm. Yang *et al.* [15] have demonstrated this correlation with the binding of trypsin to trypsin inhibitor immobilized to Sepharose 4B.

The utility of the Langmuir isotherm is however limiting. The association constant, K_a, reflecting the strength of the interaction, and the maximum capacity, q_m, are *equilibrium* parameters and shed no light on the *rate* of interaction. The adsorption of the protein to the functional groups on the sorbent is a dynamic process requiring the movement of the protein from the bulk mobile phase to the stationary phase. In process chromatography, where large volumes of dilute protein concentrations are processed, the time taken for equilibrium to be achieved is significant. It is therefore inappropriate to use a model equation that assumes that equilibrium is established instantaneously at all points surrounding the particle's external and internal surface. Thus a model describing the time-dependency of the protein concentration should be used.

The model according to Horstmann et al. [16]

Horstmann *et al.* [16] have therefore proposed that the protein adsorbs to a porous resin at a rate k_1, and that this rate is equal to the rate of disappearance of the protein from solution less the rate of desorption from the resin. The concentration of the protein in solution at any time can then be described by,

$$C(t) = C_0 - v\frac{(b+a)\left\{1 - \exp\left[-2a\left(\frac{v}{V}\right)k_1\, t\right]\right\}}{\left(\frac{b+a}{b-a}\right) - \exp\left[-2a\left(\frac{v}{V}\right)k_1\, t\right]} \tag{2}$$

In the derivation Horstmann *et al.* [16] have assumed the concentration in the bulk solution is constant, that is there is no stagnant film layer surrounding the resin particles, so that there is no film mass transfer resistance. In addition, there is no concentration gradient within the pores of the particles, and no diffusional restrictions to the protein movement, so that the diffusion of protein is assumed to be equal to the bulk diffusivity. Thus, this model uses a single mass transfer parameter, k_1, to describe the adsorption of protein to sorbent. The equation is based on a bimolecular-type second order reversible interaction, and in the limit of high k_1, the adsorption process can be assumed to be irreversible (that is, desorption from the resin is negligible).

The model according to Arnold et al. [17]

Arnold *et al.* [17] have found, however, that if the protein is large and the pore openings of the sorbent small, then the rate at which the protein diffuses into the pores of the resin is significantly retarded. In the case of high affinity adsorption such as ion-exchange chromatography, the rate of interaction is concomitantly fast, and its contribution to the overall rate of adsorption considered negligible. In this case, the overall rate of protein uptake from bulk solution is said to be limited by protein

diffusion into the pores of the particles. The interactive process in this situation can be represented by the expression,

$$D_p \frac{(1-e)\,t}{r_p^2 e} = \frac{1}{3}\ln\left|\frac{\alpha^3+\omega^3}{\alpha^3+1}\right| + \frac{1}{6\alpha}\ln\left[\frac{(\alpha^2-\alpha+1)(\alpha+\omega)^2}{(\alpha^2-\alpha\omega+\omega^2)(\alpha+1)^2}\right] + \frac{1}{3^{1/3}\alpha}\left[\arctan\left(\frac{2-\alpha}{3^{1/3}\alpha}\right) - \arctan\left(\frac{2\omega-\alpha}{3^{1/3}\alpha}\right)\right] \quad (3)$$

This equation may be applied to any batch adsorption process that has essentially a fast irreversible rate of adsorption. The above expression assumes that the bulk concentration at the pore entrance and the intraporous concentration are equivalent, that is, there are no film diffusion effects contributing to the protein movement into the pores. In addition the volume held in the pore volume is small compared with the volume of the bulk volume. These assumptions are similar to those adopted by Horstmann *et al.* [16], except that in deriving eqn. 3 it is assumed that the pore diffusivity is the rate determining step, whilst the dynamics of the interaction are ignored, since for an irreversible adsorption, $k_2 \rightarrow 0$ and $k_1 \rightarrow \infty$.

The model according to Tsou and Graham [18]

Distribution of the protein in the bulk solution surrounding the resin particle, however, may not necessarily be uniform due to concentration gradients. These may be minimized or eliminated by adequate agitation. Moderately high agitation, however, may still not eliminate these gradients in the neighbourhood of the particles, rendering a resistance to mass transfer which is manifested by a film layer. Tsou and Graham [18] have developed a model equation based on the two phase diffusion model, which allows for two effective resistances, one dependent on the film mass transfer of the protein through the film layer and the other related to the diffusion of the protein into the porous resin. The overall rate is then defined as being proportional to an overall mass transfer coefficient, K, and an equilibrium parameter, m'', which are both assumed to remain constant over the range of protein concentration usually encountered in adsorption processes. This implies that the adsorption is limited to the linear part of the adsorption isotherm, so that the kinetic solution becomes,

$$\ln(1 - F(t)) = \frac{-3\,K\,t}{r_p}\left(\frac{v}{V} + \frac{1}{m''}\right) \quad (4)$$

Eqn. 4 is simplified by considering situations where the film mass transfer is infinitely fast and under these conditions it can be assumed that $1/m'' \ll v/V$ and the mass transfer coefficient, K, is governed by pore diffusion, D_p, thus establishing a simple linear relationship between $\ln(1 - F(t))$ and D_p. Like eqn. 3, eqn. 4 implies that the overall rate of adsorption is solely proportional to the rate at which the protein diffuses through the resin, and that the rate of interaction is negligible, that is the dynamics of the interaction are again ignored.

The model according to Arve and Liapis [19]

From theoretical consideration many cases of protein adsorption can be contemplated where the rates of interaction, diffusion and mass transfer across the film are comparable, such that eqns. 2, 3 and 4 do not adequately describe the adsorption process. Indeed from practical considerations this may always be the circumstance. Discrimination between the rates has always been a difficult task experimentally, hence the need to make certain assumptions about which step is the rate limiting step. Various investigators [20–23] and most recently, Arve and Liapis [19], have taken on the formidable task of developing sophisticated models that incorporate parameters which describe three mass transfer resistances. The fundamental mass balance equations, such as those given in eqn. 5 have yet to be solved analytically, but by making various assumptions, one can arrive at solutions, such as those given by Horstmann *et al.* [16], Tsou and Graham [18] and Arnold *et al.* [17]. Arve and Liapis [19], amongst others, have adopted numerical techniques, to arrive at solutions to the equations, that take into account three mass transfer resistances. The bulk phase concentration is taken to be uniform, except for a small film layer around the particle surface, and once equilibrium is achieved the concentration adsorbed to the resin can be described by the Langmuir isotherm, eqn. 1. The batch adsorption model presented by Arve and Liapis [19] for the protein–ligand interaction of an irreversible process (presumed to incorporate very high affinity interactions, like ion-exchange) has been evaluated here, in which k_1 represents an irreversible rate constant. According to their numerical solution, the overall rate is assumed to be dictated by a combination of the film mass transfer coefficient, K_f, the pore diffusivity, D_p, and the interaction rate, k_1. A detailed description of the coupled partial differential equations can be found in the literature [19], but for the purpose of reference, eqn. 5 is given here to represent the rate of change of the bulk concentration as proposed by Arve and Liapis [19], thus,

$$\frac{\partial C(t)}{\partial t} = \mathrm{f}\,(K_f, D_p, k_1, e, r_p, e_p, q_m, C_0) \tag{5}$$

These models, represented by eqns. 2–5, have been developed to quantify the physicochemical parameters associated with batch adsorption. Equilibrium isotherms, designed to reflect the static performance of a sorbent, have been used over the last decade in protein adsorption studies. However, the information from the isotherm alone cannot yield estimates of the rates at which protein adsorbs, and indeed for an irreversible adsorption process such as ion-exchange, in which the isotherms are often rectangular in shape, very little information can be extracted. Therefore kinetic equations, such as eqns. 2–5, which describe the mechanism of adsorption in terms of rate limiting steps have been selected to illucidate the dynamic nature of adsorption behaviour. The models reported above make the same assumptions with regard to parameter independence on protein concentration and bulk diffusivity in batch systems, with the following differences. (1) The model of Horstmann *et al.* [16] which is based on a kinetically controlled batch adsorption. (2) The model of Arnold *et al.* [17] which assumes an irreversible adsorption with pore diffusion controlling the rate of adsorption. (3) The model of Tsou and Graham [18] which consider both film and pore diffusion to be rate controlling. (4) The model of Arve and Liapis [19] which

incorporates film and pore diffusion, as well as the kinetic rate into the overall rate of adsorption.

The models to date have neglected to discriminate secondary equilibrium effects, such as protein–protein interactions, protein-ion equilibrium and non-equilibrium effects. This is because of the increased complexity involved in solving mass balance equations that describe non-ideality. This neglect may be acceptable if one is to predict and optimize the purification of a "well behaved" and "well characterized" protein. The manufacture of novel macroporous packing materials, that have minimal diffusional restrictions and improved flow properties, also assists in ensuring near ideal adsorption. On the other hand, the discovery of more synthetic and natural protein variants, proof of multiple orientation and conformational changes during adsorption, and requirement for extreme levels of protein purity, places more demand on better parameter estimation during process optimization.

EXPERIMENTAL

Proteins with low isoelectric points have been selected, so that adsorption to anion-exchange media at near neutral pH is possible. Human serum albumin (HSA), as a 21% solution, was kindly donated by Commonwealth Serum Laboratories (C.S.L.) (Melbourne, Australia). Carbonic anhydrase, from *Saccharomyces cerevisiae*, and ferritin, from horse liver (chromatographically isolated) were purchased from Sigma (St. Louis, MO, USA). A 5 m*M* disodium–dihydrogen orthophosphate buffer was chosen, with a pH corresponding to 1 to 2 units above the p*I* of the target protein, in the case of ferritin and HSA (pH 6), whilst pH 11.5 was necessary for carbonic anhydrase. Buffer salts were obtained from Aldrich (Milwaukee, WI, USA). Three weak ion-exchange resins were used: a polymethacrylate resin, DEAE Trisacryl M, purchased from Australia Chemical Company (Melbourne, Australia), DEAE Fast Flow Sepharose, an industrially important agarose resin and a gift from C.S.L., and the polymeric DEAE Fractogel 650 M, from Merck (Darmstadt, Germany). Experimental apparatus for batch adsorption, included a Model 2238 UV Spectrophotometer and a Model 2210 two pen chart recorder from Pharmacia (Uppsala, Sweden). Pascal and Fortran programs were written on an IBM PC with linkage to a VAX mainframe, to generate theoretical solutions outlined in the theory section. Experimental data was also analysed using the IBM PC. Each experiment for measuring the isotherm was performed a minimum of three times to ensure reproducibility, and three kinetic profiles were used to extract the physicochemical parameters associated with eqns. 2–5, using linear regression or a least square determination. Thus the values listed in Tables IV and V are average values of three separate experimental runs.

Values for the film mass transfer coefficient, K_f, were taken from the correlation of Ohashi *et al.* [24] whilst an initial estimate for the pore diffusivity, D_p, was taken to be the value for the mobile free diffusivity determined from the correlation given by Young *et al.* [25].

RESULTS AND DISCUSSION

In the present study, the three proteins (HSA, ferritin and carbonic anhydrase)

TABLE I

PROPERTIES OF THE ANION-EXCHANGE RESINS

Resin	Particle size (μm)[a]	Capacity; albumin (mg/ml)	Ionic capacity (meq/ml)	Exclusion limit (relative molecular mass)
DEAE Sepharose FF	45–165	110[b]	100	4 000 000
DEAE Fractogel 650 M	45–90	20–30[c]	100	5 000 000
DEAE Trisacryl M	40–80	100–110[d]	300	10 000 000

[a] Wet bead diameter.
[b] Determined in 0.05 *M* phosphate buffer pH 9.0, Pharmacia specification.
[c] Determined in 0.05 *M* phosphate buffer pH 7.0, Merck specification.
[d] Determined in 0.05 *M* Tris–HCl buffer pH 8.0, LKB-Pharmacia specification.

were selected on the basis of size and isoelectric point, to principally assess the affect of protein hydrodynamic volume on (1) the capacity of the anion-exchange resins and (2) the rate of adsorption to the functional groups on the resins. Table I lists the physical properties of the proteins, in terms of their molecular masses, their hydrodynamic radii, derived from correlation data [26], their p*I* and their free or bulk diffusivity in solution, also derived from correlated data [25]. The resins are all weak anion exchangers, with the functional group being diethylaminoethyl (DEAE), and vary in their physical properties and their adsorption capacities, see Table II. According to the manufacturer's specifications, and others [27], the Trisacryl M and the Sepharose FF resins have similar capacity for HSA, although Trisacryl M has a higher ionic capacity in terms of meq/ml resin, as well as having a smaller mean particle size (hence larger surface area) and a greater exclusion limit (larger pore size). Fractogel 650 M, like Sepharose FF has a high ionic capacity, however, this sorbent has been specified by the manufacturers to have a low capacity for HSA, with a low exclusion limit.

In this study, the dynamic capacity of these resins was measured using a bath system as previously described [28] whereby a protein solution was injected into a well mixed bath containing buffer and resin and the uptake of the protein was monitored continuously. Serial injections were carried out until the resin no longer adsorbed the protein from solution, this being exhibited by a steady-state UV absorbance reading of the on-line spectrophotometer. The total protein adsorbed was calculated from the difference between the total amount added to the bath and that remaining in solution. From the experimental results of each injection, adsorption isotherms were thus constructed, reflecting the equilibrium capacity of the sorbent at a particular concentration of the protein in solution.

TABLE II

PROPERTIES OF THE PROTEINS

Protein	Molecular mass	Radius (nm)	p*I*	Bulk diffusivity ($\times 10^{-11}$ m^2/s)
Ferritin	440 000	8.4	4.0	3.2
Human serum albumin	67 000	4.5	4.9	6.1
Carbonic anhydrase	30 000	3.5	6.0	7.9

Equilibrium studies

Fig. 1a and b shows the experimental data for the adsorption of HSA and ferritin to the various weak ion-exchange resins. Fig. 1a shows that the Trisacryl M and Sepharose FF have high capacities for HSA, whilst Fractogel 650 M exhibits a lower value, as expected from the reported values in Table I. The opposite trend is true for ferritin, where the maximum capacity found experimentally, q_m, for Trisacryl M is 3-fold lower than Fractogel 650 M, despite the fact that Trisacryl M has a higher ligand density, and larger exclusion limit. This trend has previously been documented by Kato *et al.* [27] in an extensive study of the protein capacity of commercial anion exchangers. This result suggests that mechanisms other than simple point surface charge interactions are dominating the adsorption of ferritin to these weak ion exchangers. It is well known that proteins form dimers and trimers in solution, and that protein stacking onto affinity adsorption sorbents can occur [29]. Multilayering of the protein onto the ion-exchange resin is thus a possible explanation for this observed trend.

Adsorption isotherms were also obtained for the smallest protein, carbonic anhydrase. The values of q_m found experimentally and q_m and K_a obtained from double reciprocal plots ($1/q^*$ *versus* $1/c^*$, refer eqn. 1) for this protein, together with those for HSA and ferritin are given in Table III. This table clearly shows that the capacity of a particular resin is dependent on the size of the protein. Comparing the protein capacity of the Trisacryl M, that for the smallest protein, carbonic anhydrase (radius = 3.5 nm) was the greatest, $q_m = 2.7$ μmol/ml, compared to $q_m = 0.05$ μmol/ml for ferritin (radius = 8.4 nm), consistent with carbonic anhydrase having the greatest accessibility to the functional groups in the interior of the resin. Porous particles have

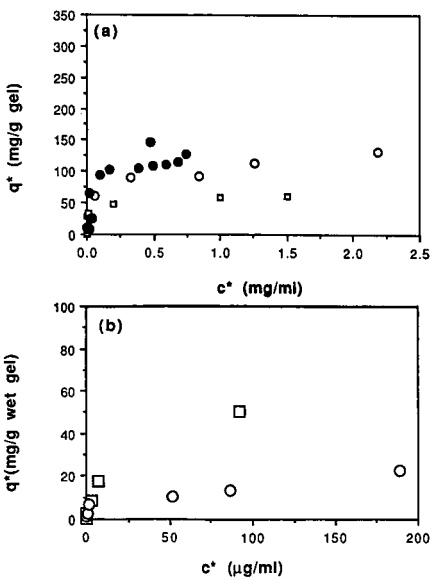

Fig. 1. Adsorption isotherms for the binding to the weak anion-exchange resins. (a) HSA, (b) ferritin. ○ = DEAE Trisacryl M; ● = DEAE Sepharose FF; □ = DEAE Fractogel 650 M.

TABLE III

VALUES OBTAINED FROM THE EQUILIBRIUM EXPERIMENTS

Resin	q_m (mg/g)		q_m (μmol/ml) Experimental	K_a		Coefficient of regression
	Theoretical	Experimental		ml/mg	$\times 10^6\ M^{-1}$	
HSA						
Trisacryl M	99.7	140	2.1	56	3.8	0.978
Sepharose FF	64.0	110	1.6	12	0.8	0.999
Fractogel 650 M	48.9	55	0.8	40	2.7	0.933
Ferritin						
Trisacryl M	19	–	0.04	377	165	0.997
Fractogel 650 M	75	–	0.18	95	40	0.999
Carbonic anhydrase						
Trisacryl M	35.1	35	2.7	140	4.2	0.991

an appreciable portion of these ligand groups within the particle. The same trend is apparent for Fractogel 650 M where q_m is 5-fold greater for the smaller HSA than for ferritin. It should be kept in mind, however, that the capacity of an ion-exchange resin depends on the extent of ionization of the functional groups on the resin as well as the apparent charge of the protein, both of which are a function of the pH and ionic strength of the buffer. Therefore the high capacity for carbonic anhydrase may be indicative of the higher pH of the buffer (pH 11.0) rather than solely due to the relatively small size of the protein. Irrespectively, the relationship between capacity, accessibility and pore restriction has been confirmed by these results, as well as substantially documented by a number of other investigators [18,30–33].

For the conditions shown in Fig. 1 and in other cases not plotted here, the isotherms are rectangular in shape and the data do not fit the Langmuir equation, eqn. 1. However, in order to fit the theoretical models, it has been necessary to use eqn. 1 to calculate the association constant K_a, the results of which are given in Table III. For further discussion of the relationship of K_a in the "irreversible" adsorption of proteins in ion-exchange chromatography, see Horstmann *et al.* [16]. The rectangular nature of the experimental isotherms of Fig. 1a and b indicates very high association constants (where the initial slopes of the isotherms are proportional to this constant) which is to be expected since the interaction is dominated by strong electrostatic forces. The high values for K_a, 10^6–$10^7\ M^{-1}$, compare well with values reported in the literature, for example the association constant for bovine serum albumin binding to Sephadex A50 [18] was $K_a = 2.2 \cdot 10^6\ M^{-1}$. These K_a values are an order of magnitude greater than the association constants for biospecific affinity adsorption, for example the adsorption of the protein α-chymotrypsin to proflavin immobilised to Lichrospher 500 has reported [34] to be $0.15 \cdot 10^6\ M^{-1}$. These calculated association constants, like the capacity, also appear to be protein size dependent. The largest protein, ferritin, shows K_a values of the order of $10^7\ M^{-1}$, whilst that for carbonic anhydrase is only $10^6\ M^{-1}$. Results from zonal elution chromatography of carbonic anhydrase onto Mono Q, reporting a low retention coefficient and early elution in gradient elution, confirm the weak interaction exhibited

by carbonic anhydrase with anion-exchange sorbents [35]. Multiple factors underly the relationship between K_a and molecular size and it is not possible in these preliminary results to ascribe a particular molecular or physical feature as the sole origin of this effect. The association of the protein with the ionic resin is predominantly electrostatic, the strength of this association is dictated by the charge anisotropy of the protein, the number and spatial arrangement of the charges and its distance from the resin. Whilst models, such as the net charge model [36], have been introduced to predict the retention characteristics of proteins in high-performance ion-exchange chromatography, it has been found that proteins do adsorb to anion-exchange resins below their p*I* value [35,37–39] because of a non-uniform distribution of surface charge. Thus, the interaction is more complex than one charged species adsorbing to an ionic surface, and hence the strength of this interaction, K_a, is not predictable from an analysis solely based on net charge considerations or size criteria.

Although the parameters, q_m and K_a, are equilibrium parameters, and give no indication of the rate at which the protein adsorbs to the resin, they nevertheless represent the adsorption condition after extended periods of time. Using these static equilibrium parameters, one can therefore predict time-averages of the dynamic adsorption parameters. Eqn. 2 of the model of Horstmann *et al.* [16] and the numerical solution of the model of Arve and Liapis [19], for example, use these equilibrium values in the calculation of the interaction rate constant. The dynamic adsorption of protein to ion-exchange resin was therefore investigated for the three proteins, HSA, ferritin and carbonic anhydrase by measuring the rate of protein uptake from solution, the results of which are presented below. The shape of the curve reflects, amongst other things, the strength of the interaction and the overall rate of interaction. Its curvature will vary according to the level of saturation of the sorbent. At low concentrations, for example <0.1 mg/ml of HSA, the three resins studied here will not be near saturation (see the isotherms of Fig. 1) and uptake of the protein from solution will generally be fast in the case of an ion-exchange interaction. The ionic adsorption at this level is also irreversible, with $C(t)/C_0$ approaching zero. This pattern is in contrast to affinity adsorption, in which the interaction is not as strong, the adsorption is incomplete, and equilibrium is established after longer periods of time. Kinetic adsorption curves of HSA binding to Cibacron Blue F3GA-Fractogel HW75 [33] and IgG to Protein A-Superose B [16] have shown figures of $C(t)/C_0$ asymptoting to 0.45 and 0.3, respectively. At high concentrations, >0.5 mg/ml of HSA for example, the resins used in this study are near saturation and the kinetic curve should therefore reflect this by asymptoting to a non zero $C(t)/C_0$.

Kinetic studies

Fig. 2 compares the dimensionless concentrations of HSA, ferritin and carbonic anhydrase adsorbing to the weak anion resins Trisacryl M, Sepharose FF and Fractogel 650 M as a function of time. These plots show that the resins Trisacryl M and Fractogel 650 M exhibit similar kinetic profiles, whilst those of Sepharose FF are different. In addition, it can be seen that the adsorption of the small protein, carbonic anhydrase, yields kinetic profiles that approach zero quickly (steady-state time is 10 min) indicating that the protein is irreversibly bound to the resin and that the resin is far from saturation. Adsorption of HSA to Trisacryl M and Fractogel 650 M also show similar behaviour. Binding of HSA to the Sepharose FF, however, is indicative of

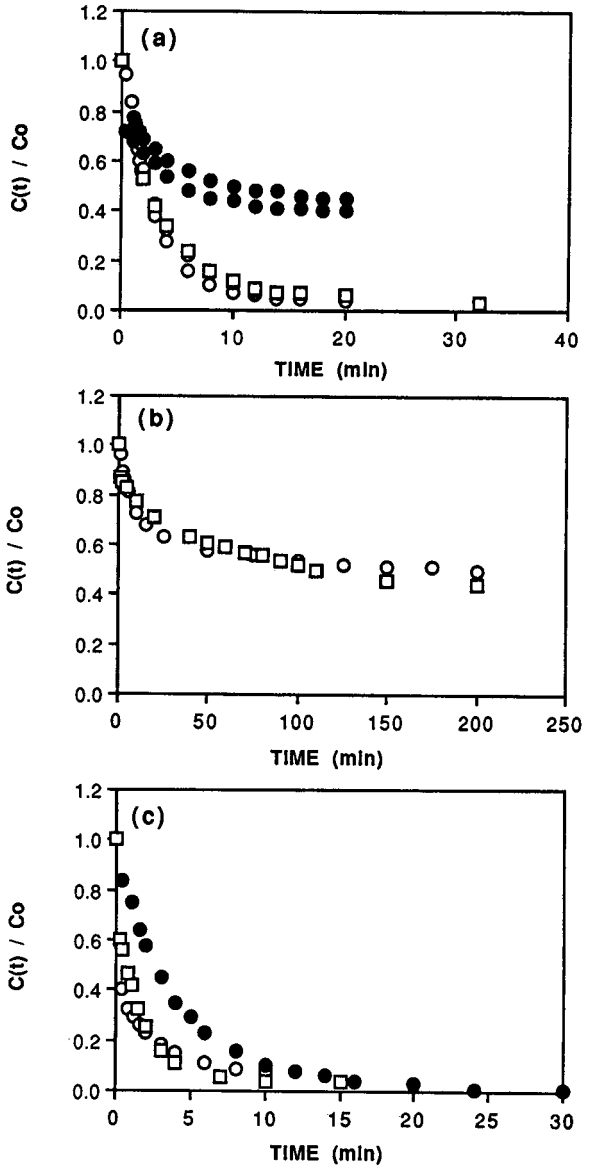

Fig. 2. Kinetic profiles for the adsorption to the weak anion-exchange resins. (a) HSA, (b) ferritin, (c) carbonic anhydrase. ○ = DEAE Trisacryl M; ● = DEAE Sepharose FF; □ = DEAE Fractogel 650 M.

a reversible interaction, with $C(t)/C_0$ approaching 0.4. The association constant found from serial injections, is also lower than that for Trisacryl M and Fractogel 650 M which concurs with a lower affinity. The adsorption of ferritin to all the resins also does not approach zero, $C(t)/C_0 = 0.4$, see Fig. 2b, and this might be attributed to the high concentration of protein initially injected into the bath, C_0 here being 0.1 mg/ml, with

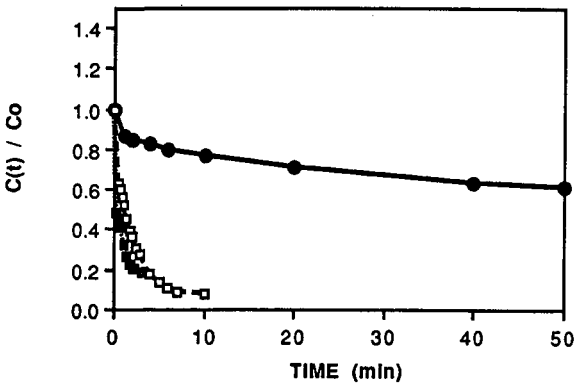

Fig. 3. Kinetic profiles for the adsorption of the proteins to DEAE Trisacryl M. ● = Ferritin; □ = HSA; ■ = carbonic anhydrase.

the equilibrium concentration, c^*, becoming 0.04 mg/ml, which is near saturation of the resins (see Fig. 1b).

Fig. 3 compares, at constant molar concentration, the adsorption behaviour of the three different proteins to Trisacryl M. These results directly relate how the size of the protein influences the overall rate of the adsorption. Interaction with an ion-exchange resin, is influenced by a combination of things, of which the contact area of the protein–ligand interaction is just one. It can be expected, however, that a large protein with a large global surface area may have a stronger interaction with the charged resin, and hence larger K_a value. However, from unit cell packing considerations, the number of proteins able to interact per unit adsorption area of the sorbent will be limited because of steric hindrance. It is thus not surprising then that the adsorption profiles of Fig. 3, shows $C(t)/C_0$ approaching 0.4 for the large protein ferritin, and that in the experimental system studied, equilibration time was greater than 50 min.

Modelling studies

The kinetic profiles presented above illustrate qualitative differences in the adsorption behaviour of different weak ion-exchange resins with three proteins of different molecular masses and different surface charge distribution. However, in order to extract quantitative values for the rate of interaction, and the diffusion coefficient, an iteration procedure and regression analysis involving the theoretical equations presented in the theory section is required. Utilising the models of Horstmann *et al.* [16], Arnold *et al.* [17], Tsou and Graham [18] and Arve and Liapis [19], the results of the adsorption experiments have been compared with predictions of these four models. The findings are given below.

Data evaluation using the model of Horstmann et al. [16]. Eqn. 2 of Horstmann *et al.* [16] has been used to generate the theoretical profiles illustrated in Fig. 4. Non-linear regression has been used to determine the value of k_1 for the curve of best fit. Fig. 4a is an example of a case where sum of squares of variances (representing the goodness of fit) is low, of the order of 10^{-4}. The adsorption of low concentrations of HSA (<0.1 mg/ml) to all of the resins studied showed good correlation between

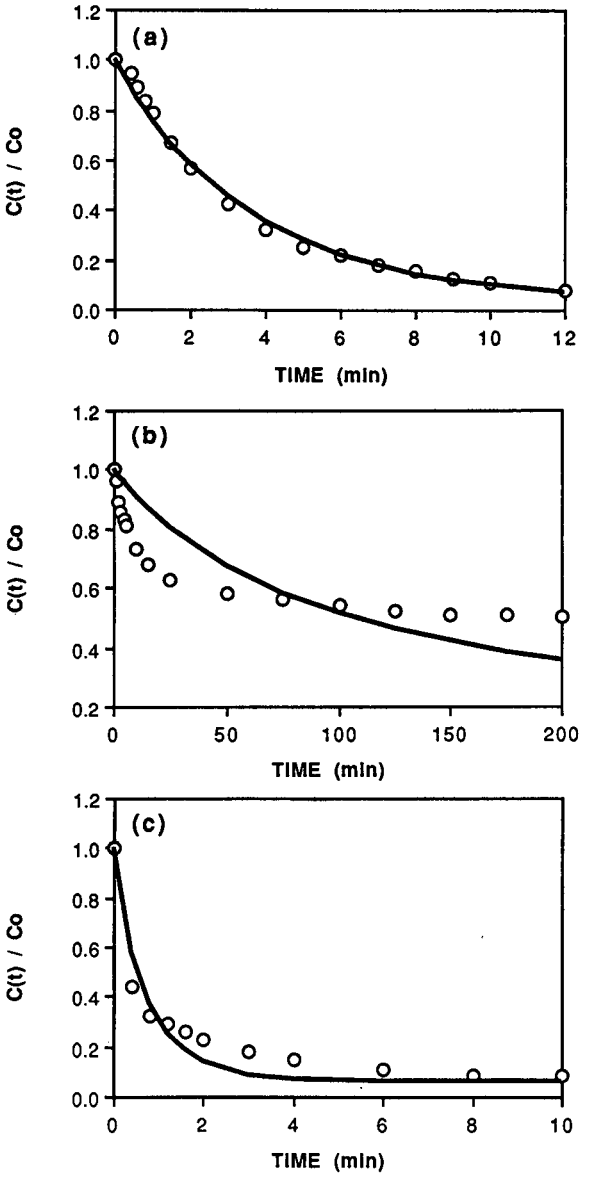

Fig. 4. Typical kinetic profiles for the adsorption to DEAE Trisacryl M. C_0 = 104 μg/ml. (a) HSA, k_1 = 0.007 ml/mg s; (b) ferritin, k_1 = 0.002 ml/mg s; (c) carbonic anhydrase, k_1 = 0.127 ml/mg s. ○ = Experimental; — = eqn. 2.

experiment and theory. Converse to this, at higher concentrations (>0.5 mg/ml), and for the large protein, ferritin, the fit was poor, with the sum of squares being 10^{-2}, Fig. 4b. In all cases the regression analysis was designed to provide the minimum sum of residuals, such that the best fit in the case of Fig. 4b gave a theoretical curve that crossed the experimental curve. In retrospect, it may have been more appropriate to fit

the last part of the curve, so that the theoretical and experimental curves attained the same equilibrium position. However, it should be kept in mind that the model of Horstmann *et al.* [16] has not been developed for ion-exchange adsorption. This model has been derived from a stoichiometric assumption that one protein molecule adsorbs to one functional group on the resin. In its derivation, it has also inherently assumed that the rate of adsorption is the rate limiting step. For large proteins, diffusional restrictions into small pores will be significant, so that the predicted equilibrium position, or $C(t = \infty)$ of ferritin in Fig. 4b is likely to be lower than that attained experimentally.

Data evaluation using the model of Arnold et al. [17]. The parameters g, (proportional to the maximum capacity) and $D_p(1 - e)/(r_p^2 e)$ as defined by the model of Arnold *et al.* [17], eqn. 3, were varied to generate curves of best fit for the experimental profiles, shown as Fig. 5. The theoretical curve of Fig. 5a appears to fit the experimental curve best near equilibrium, whilst Fig. 5b, HSA binding to Sepharose FF, is illustrative of the case where the correlation between theory and experimental is poor at all times. As has been already shown, the Sepharose FF resin behaves differently from the other resins (see Figs. 2, 5b and 6a). The observed behaviour might be attributed to the heterogeneity of the resin, due to a large size

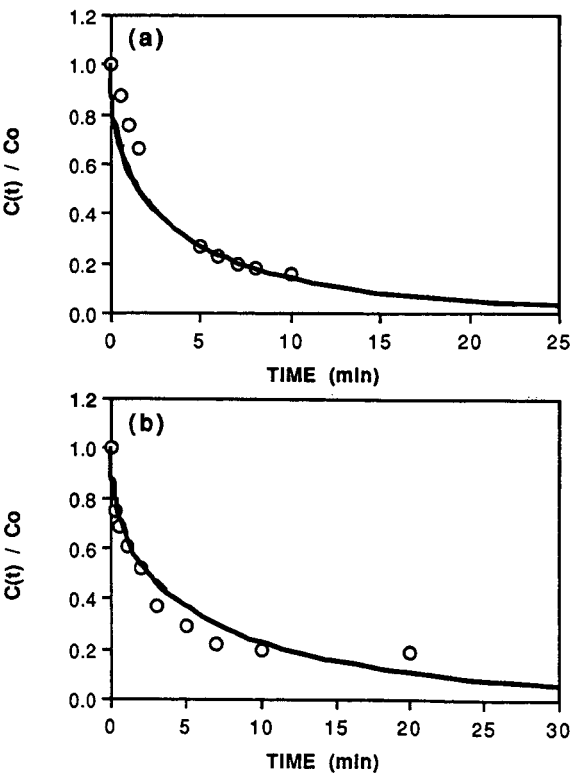

Fig. 5. Typical kinetic profiles for the adsorption of HSA to weak anion-exchange resins. (a) DEAE Trisacryl M, $C_0 = 65$ μg/ml, $D_p = 0.5 \cdot 10^{-11}$ m²/s. (b) DEAE Sepharose FF, $C_0 = 93$ μg/ml, $D_p = 1.3 \cdot 10^{-11}$ m²/s. ○ = Experimental; — = eqn. 3.

distribution (45–165 μm) and a large pore size distribution. In addition, eqn. 3 has been derived for the case of irreversible adsorption, which means that all the protein from solution should be adsorbed to the resin until the resin itself becomes completely saturated. Thus the model predicts each time that $C(t)/C_0$ approaches zero, although experimentally this is not always the case. Hence the parameters extracted from this model may not have any real physical significance.

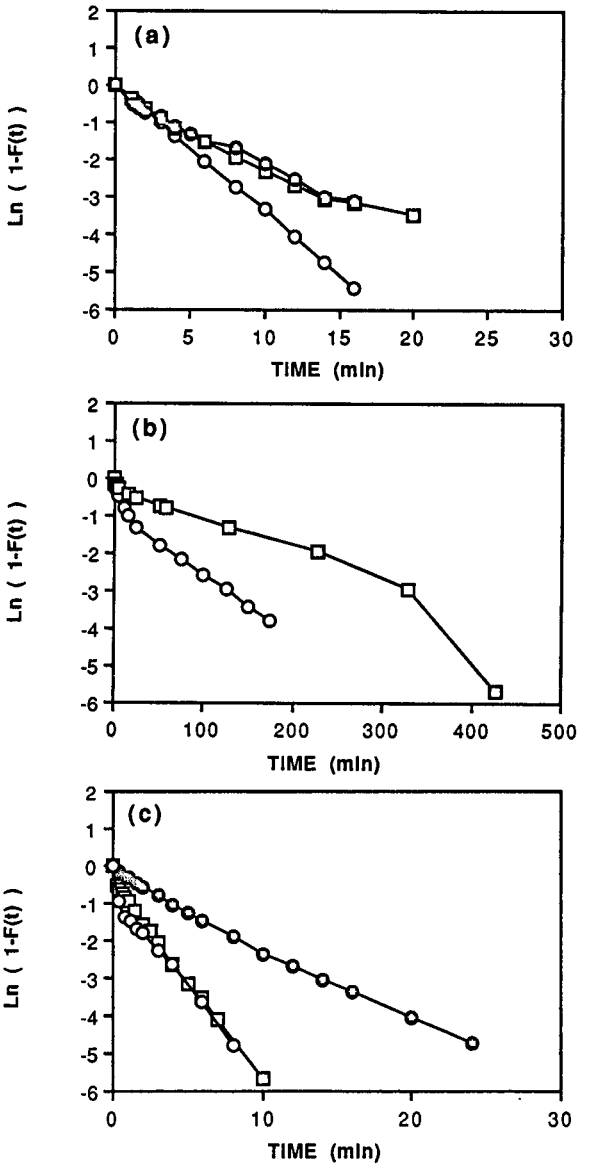

Fig. 6. Typical logarithmic transformations from eqn. 4. C_0 = 104 μg/ml. (a) HSA, (b) ferritin, (c) carbonic anhydrase. ○ = DEAE Trisacryl M; ● = DEAE Sepharose FF; □ = Fractogel 650 M.

Data evaluation using the model of Tsou and Graham [18]. Logarithmic transformations of the adsorption profiles, according to eqn. 4, are illustrated in Fig. 6. According to Tsou and Graham [18], if the adsorption is governed by pore diffusion, then these plots should be linear. Straight lines were seen to occur for low concentrations of the smaller proteins, HSA and carbonic anhydrase adsorbing to all resins studied, although two slopes were evident for ferritin (Fig. 6a). Similarly, at high concentrations (> 1 mg/ml) near saturation of the sorbent, there is a significant change in the slope of the plots of ln $[1 - F(t)]$ *versus* time, t, and biphasic behaviour is apparent. This change in the slope of the logarithmic plots might correspond to the transfer of protein mobility from film diffusion to pore diffusion, according to eqn. 4. At low concentrations, a component of the initial slope corresponding to the film diffusion may be so small that it is not detected, with the apparent slope reflecting the pore diffusion. Use of this model may therefore be limited, since at high concentration of the protein the adsorption isotherm is no longer linear, and the slope of the operating line, m'', changes with the concentration. The concentration of protein within the pores may also be significant, establishing concentration gradients, that may have some effect on the linearity of the plots of ln $[1 - F(t)]$ *versus* time.

Despite the divergence from linearity, the plots of Fig. 6 illustrate differences between the resins. The Sepharose FF resin demonstrates slower rates, manifested in these logarithmic plots as smaller slopes, and the faster binding of ferritin to Trisacryl M than to Fractogel 650 M is clearly evident.

Data evaluation using the model of Arve and Liapis [19]. A 20% deviation of the film mass transfer coefficient, K_f, (varying in the radius of the resin particle, the porosity, and the bulk diffusivity) was found to have little affect on the shape of the concentration profile, allowing only a two parameter curve fitting exercise for the model of Arve and Liapis [19]. Thus, iteration of the parameters D_p and k_1 according to this model led to the theoretical curves of Fig. 7. The curve of ferritin binding to Fractogel 650 M, Fig. 7b, is indicative of low concentration profiles, with the theoretical curve agreeing well with the experimental profile. This has found to be the case for the majority of the experimental curves of low concentrations of HSA adsorbing to the Trisacryl M and Fractogel 650 M resins, with the coefficient of regression being greater than 0.9 in all cases. At low concentrations, adsorption is not at saturation levels and the mechanism of interaction is likely to be less complex. Lower regression coefficients, 0.7–0.8, were calculated for the experiments with high concentrations of HSA, where the system is at or near saturation of the sorbent, and non-equilibrium effects, such as protein–protein interaction, and other non-ideal effects such as steric hindrance may be more significant. Other theoretical predictions, given in Fig. 7b, designed to provide the best fit to the adsorption of HSA to Sepharose FF, also showed a poor correlation between theory and experimental. In Fig. 7b, the model of Arve and Liapis predicts that all the protein adsorbs to the resin, $C(t)/C_0 = 0.0$, whereas, as Figs. 2a and 5b show, this is not the case. Poor fits were also apparent for adsorption of carbonic anhydrase, yet good fits were obtained for all the ferritin experiments.

In terms of interpretation of the experimental data, this model appears to be the most useful of those previously described, for it takes into account the mass transfer resistance, represented as K_f, and the diffusive restrictions of the protein into the interior of the particles, D_p, in the determination of the interaction rate constant, k_1.

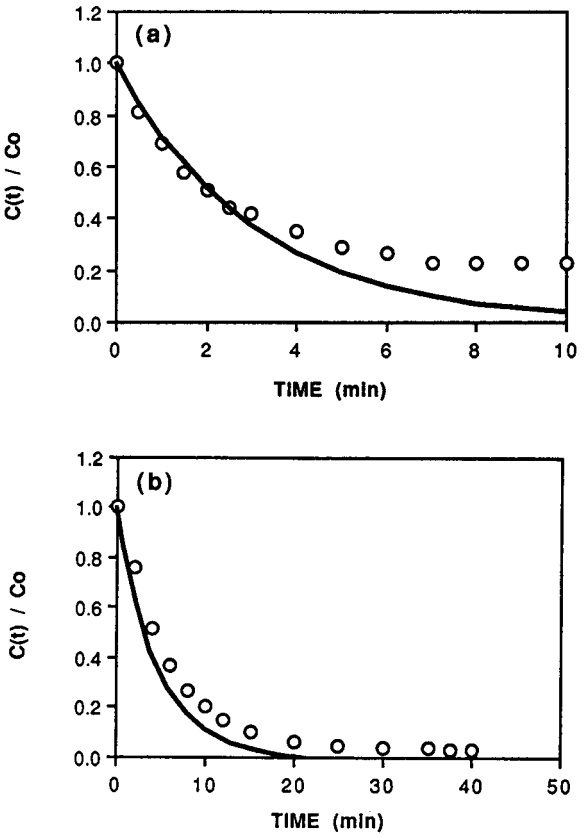

Fig. 7. Typical kinetic profiles for the adsorption to weak anion-exchange resins. (a) HSA binding to DEAE Sepharose FF, $C_0 = 56\,\mu g/ml$, $K_f = 5 \cdot 10^{-6}$ m/s, $r_p = 52.5\,\mu m$, $D_p = 6.1 \cdot 10^{-11}$ m^2/s, $k_1 = 1.0$ ml/mg s. (b) Ferritin binding to DEAE Fractogel 650 M, $C_0 = 248\,\mu g/ml$, $K_f = 2.5 \cdot 10^{-6}$ m/s, $r_p = 34\,\mu m$, $D_p = 0.9 \cdot 10^{-12}$ m^2/s, $k_1 = 0.5$ ml/mg s. ○ = Experimental; — = eqn. 5.

The theoretical profiles therefore represent the sum contribution of the series of resistances to the overall rate of adsorption.

Comparison of the kinetic data. In Fig. 8, direct comparison is made of the theoretical profiles of Horstmann *et al.* [16], Arnold *et al.* [17] and the numerical calculation of Arve and Liapis [19]. The model of Tsou and Graham (eqn. 4) cannot be easily transformed into a kinetic profile of concentration with time. The experimental conditions of the adsorption of a 0.1 mg/ml solution of HSA to the resins Trisacryl M, Fig. 8a, and Fractogel 650 M, Fig. 8b, and of ferritin to Fractogel 650 M, Fig. 8c), are given also. The shape of the curves generated from the model of Arve and Liapis show the best fit to the experimental profiles, and this was found to be the case in the majority of experiments undertaken. In these cases, the plots asymptote to zero, and are not as steep at the onset of adsorption. This is not surprising since a two parameter curve fit is possible.

From the theoretical curves presented in the Figs. 1–8 and other experimental data, the relevant physicochemical parameters, D_p and k_1, have been calculated and

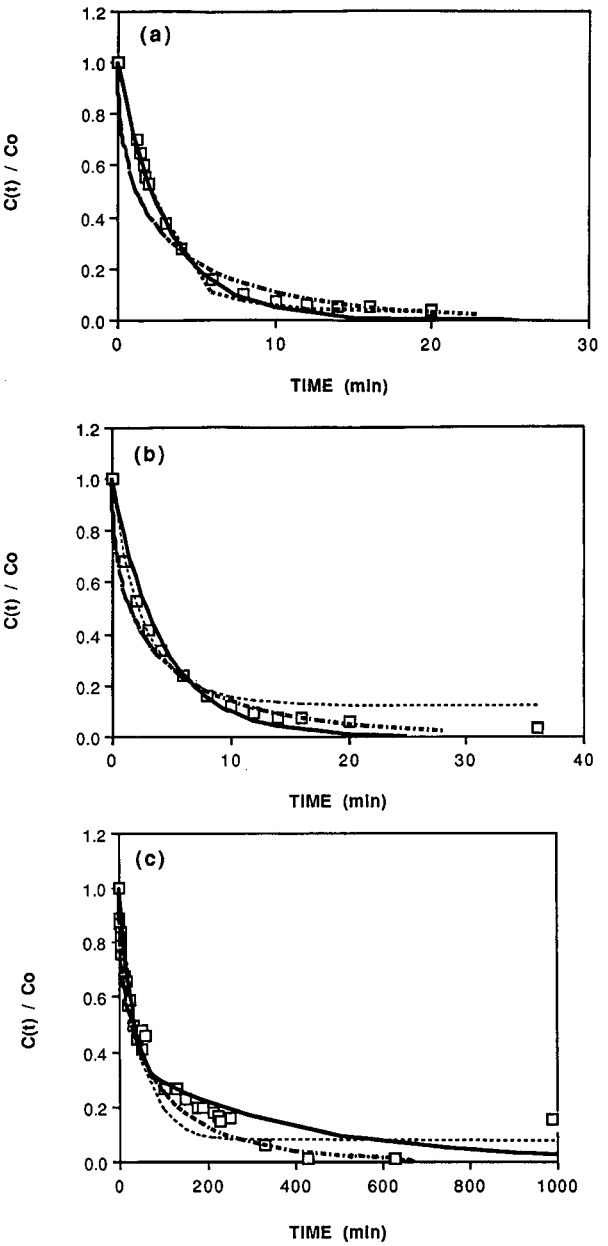

Fig. 8. Comparison of the theoretical curves obtained from eqns. 2–5. C_0 = 104 μg/ml. (a) □ = HSA binding to DEAE Trisacryl M, ------ = eqn. 2 of Horstmann *et al.* [16], k_1 = 0.008 ml/mg s, -·-·- = eqn. 3 of Arnold *et al.* [17], $D_p = 0.6 \cdot 10^{-11}$ m²/s, ——— = simulation of Arve and Liapis [19], k_1 = 0.5 ml/mg s, $D_p = 6.1 \cdot 10^{-11}$ m²/s. (b) □ = HSA binding to DEAE Fractogel 650 M, ------ = eqn. 2 of Horstmann *et al.* [16], k_1 = 0.002 ml/mg s, -·-·- = eqn. 3 of Arnold *et al.* [17], $D_p = 0.13 \cdot 10^{-11}$ m²/s, ——— = simulation of Arve and Liapis [19], k_1 = 0.5 ml/mg s, $D_p = 6.1 \cdot 10^{-11}$ m²/s. (c) □ = Ferritin binding to DEAE Fractogel 650 M, ------ = eqn. 2 of Horstmann *et al.* [16], k_1 = 0.001 ml/mg s, -·-·- = eqn. 3 of Arnold *et al.* [17], $D_p = 4.7 \cdot 10^{-11}$ m²/s, ——— = simulation of Arve and Liapis [19], k_1 = 0.1 ml/mg s, $D_p = 0.3 \cdot 10^{-11}$ m²/s.

TABLE IV

KINETIC PARAMETERS FROM THE MODEL EQUATIONS

Resin	C_0 (μg/ml)	k_1 (ml/mg s)		D_p ($\times 10^{-11}$ m^2/s)			
		Eqn. 2	Eqn. 5	Eqn. 2	Eqn. 4	Eqn. 5	Eqn. 3
Trisacryl M	56 ± 7	0.012 ± 0.033	0.02	6.1	7.3 ± 0.2	6.1	0.9 ± 0.2
	104 ± 1	0.007 ± 0.001	0.01	6.1	5.2 ± 0.3	6.1	0.9 ± 0.2
Sepharose FF	55 ± 12	0.011 ± 0.002	1.0	6.1	18 ± 5	6.1	3.12 ± 1.8
	104	Not found	0.3	6.1	11	6.1	2.59
Fractogel 650 M	51	0.120 ± 0.039	0.3	6.1	8.4	6.1	2.4
	104	0.002	0.5	6.1	5.1 ± 0.5	6.1	1.3

the results are listed in Tables IV and V. Table IV shows a comparison of the adsorption parameters from the binding of HSA to the three resins, Trisacryl M, Sepharose FF and Fractogel 650 M, at two different concentrations. Table V compares the parameters for the three different proteins.

(i) Examination of k_1. It has been previously reported [33] that the values obtained from the model of Horstmann *et al.* [16] overestimate the value for k_1, as the model does not discriminate between the other steps involved with the overall adsorption rate. Use of this model may only be appropriate and physically consistent in the case where the protein to pore size ratio is small, as in the adsorption of carbonic anhydrase to the Trisacryl M resin. Furthermore, Arve and Liapis [19] have provided evidence that the model of Horstmann *et al.* [16] is thermodynamically inconsistent. Therefore, if this model equation is used in estimating the interaction rate, k_1, in other cases, for example HSA binding to Fractogel 650 M or ferritin to Trisacryl M, the value may be up to an order of magnitude too low [k_1 (Horstmann *et al.*) = 0.067, k_1 (Arve and Liapis) = 0.014]. This has been found to be the case in previous work [33]. The interaction rates k_1 from the model of Horstmann *et al.* [16] for the different proteins, Table V, show a decrease with increasing molecular weight and size, k_1 for ferritin being 10-fold smaller than k_1 for carbonic anhydrase. In contrast, k_1 calculated from Arve and Liapis [19], shows an increase. Clearly this interaction rate is a reflection of the retention mechanisms dominating adsorption. As different proteins have different sizes, charge distribution and density, this difference is not necessarily

TABLE V

KINETIC PARAMETERS FOR THE ADSORPTION OF PROTEIN TO TRISACRYL M

Protein	k_1 (ml/mol s)		D_p ($\times 10^{-11}$ m^2/s)			
	Eqn. 2	Eqn. 5	Eqn. 2	Eqn. 4	Eqn. 5	Eqn. 3
Carbonic anhydrase	2000	420	7.9	16.2	7.9	14.7
HSA	737	2010	6.1	8.4	6.1	0.90
Ferritin	880	30 800–220 000	3.1	0.3	0.1	0.08

surprising. Similarly high values for the kinetic rates of adsorption have been reported in literature. For example [40], bovine serum albumin adsorbing to the hydrophobic sorbent Hp-70, k_1 was given as 3350 $M^{-1}s^{-1}$, and for IgG binding to the bioaffinity resin [41], Protein A-Lichrospher Si 500, k_1 was 17 000 $M^{-1}s^{-1}$.

(ii) Examination of D_p. Table IV also serves to illustrate the differences in the diffusivities calculated from the various equations. In studies on affinity adsorption, Horstmann *et al.* [16] assumes there is no restriction on the movement of the protein within the particles interior, hence the diffusivities listed are the protein diffusivity in free solution, calculated from a correlation derived from the Stokes–Einstein equation [25], see Table I. The effective diffusivities of HSA as calculated from the model of Tsou and Graham [18] are similar in magnitude to the free diffusivity, that is, although the model is based on pore diffusion, it predicts that the diffusion restrictions are negligible. Assuming that the pore sizes of all of the resins studied are at least an order of magnitude larger than the hydrodynamic radii of HSA, that is, if the molecular cut-off ranges of the resins and the dimensions of the near elipsodal shape of the monomeric albumin molecules [9] are considered, it is likely that the protein effectively diffuses through the porous network at a rate comparable to the rate it diffuses in free solution. These effective diffusivities, calculated from the models of Arnold *et al.* [17] and Tsou and Graham [18] also show a slight concentration dependency. At higher concentrations the protein has less freedom to move about because of the increased number of molecules in solution and also because of possible lateral interactions with increasing amounts of adsorbed protein (the adsorbed protein is likely, also, to hinder accessibility of the free protein into the pores of the resin). These diffusivities also reflect the differences in the performance of the resins, as shown in Figs. 2–8. The value obtained for the Sepharose FF resin is higher than the other resins, and in fact the diffusivity as calculated by the model of Tsou and Graham [18] is twice what it is in free solution. It is important to note here that the standard deviation for the values of D_p shown in Table IV was 30% indicating scatter in the data, possibly due to the heterogeneity of the resin.

Table V lists results of the adsorption behaviour of different proteins to the Trisacryl M resin at a constant concentration. The models of Tsou and Graham [18] and Arnold *et al.* [17] give similarly high estimates of the diffusivity of carbonic anhydrase, and low estimates for the largest protein ferritin, whilst the model of Arve and Liapis [19] also predicts that there is no restriction to movement of the small proteins, and that the pore diffusion of ferritin is 1/40th that of the free diffusivity. Similar phenomena of pore restrictions resulting in low diffusivities has been repeatedly reported in affinity [28,33], reversed-phase [31,42] and ion-exchange chromatography [17,18,30,33,43,44]. The molecular quantification of this phenomenon still requires systematic description if the full predictive capabilities of adsorption models are to routinely aid process scale-up in ion-exchange chromatography.

CONCLUSIONS

The adsorption of proteins to ion-exchange sorbents is a complex process that has yet to be well defined in terms of molecular kinetic mechanisms. From a physical and chemical viewpoint, it is known that electrostatic forces steer the protein towards the charged resin, yet other associated forces, for example hydrophobic interactions,

may also be contributing factors. It has been shown that if the pores of the resin are typically of the same order of magnitude as the diffusing protein [33], then they will restrict mass transfer and adsorption, the ramifications of which may be a low capacity and/or slow kinetics. Furthermore, it can be postulated that molecular docking, protein masking and multiple and dynamic orientation of protein isoforms may effect the efficiency of the process in terms of purity levels and throughput. Interpretation of these non-ideal, non-equilibrium phenomena from observed adsorption behaviour is a taxing task. Most mathematical models derived to predict true adsorption behaviour, have neglected these detrimental effects because of the complexity of the associated mass balance equations. Indeed no analytical solution to even the idealised mass balance equation of eqn. 5 has been forthcoming.

The results presented here, however, have provided further insight into the validity of the various models outlined in the theory section. Firstly, the Langmuir isotherm, although a very poor fit to the high affinity ion-exchange process, yields useful qualitative information about the association constants and the protein capacities. Variation between different anion resins with the same functional group can be seen through the association constant, which also shows protein size dependency. The maximum capacity of each resin studied has also been shown, via the Langmuir treatment to be dependent on the hydrodynamic size of the protein. Secondly, the kinetic equations, although derived using different assumptions, indicate conclusively, that there were no restrictions to the diffusion of the small proteins such as carbonic anhydrase, upon binding to each of the resins examined; the extracted values for the effective diffusivities were of the same order of magnitude as the correlated free diffusivity. Adsorption of the largest protein, ferritin, was found to be pore restricted, with the diffusivity calculated using the models of Tsou and Graham [18], Arnold *et al.* [17] and Arve and Liapis [19] being up to 1/40th that in solution. With the use of the models of Horstmann *et al.* [16] and Arve and Liapis [19], no definite trend was apparent for the values of the rate of interaction for the protein binding to the charged functional groups. The model of Arve and Liapis [19] gave rate values that were independent of concentration, high for large proteins and low for smaller proteins. The model of Horstmann *et al.* [16], on the contrary, yielded lower rates at higher concentrations, and higher rates for the smallest protein. All the rates extracted from this model were also lower than those predicted from the model of Arve and Liapis [19]. The values for these experimentally and theoretically derived parameters, q_m, K_a, D_p and k_1, concur well with those reported in the literature [14,16–19,28,33]. High protein capacity and high association constant are indicative of ion-exchange adsorption, whilst the kinetic parameters, D_p and k_1 correlate well considering the ratio of protein to pore size.

The applicability of these data in preparative scale-up, has yet to be ascertained, where the equilibrium isotherm is unlikely to be linear, and operation will invariably be at high protein concentrations, at the saturation level of the isotherm. The premise of Langmuir behaviour is also dubious. Furthermore, the assumptions of restricted pore diffusion events or kinetic rate dominance are unlikely to be valid, whilst protein–protein and protein–ion interactions are anticipated to be far more complex than what occurs in these batch experiments. The experiments in the study have been performed with pure protein solutions, and in a batch mode of operation. In preparative chromatography, packed column configuration is usually adopted and the feed stock

is a cocktail of proteins, each varying in their abundance, charge distribution, size and sorption behaviour. In addition, heterogeneity of the resins in terms of particle to pore size and ligand distribution may become more pronounced in preparative operation, and this heterogeneity will require attention during optimization and prediction studies. Details of such practical and modelling applications with packed beds will be reported subsequently.

SYMBOLS

a^2 $\quad b^2 - \dfrac{C_0 V}{q_m v}$

b $\quad \dfrac{1}{2}\left[C_0\left(\dfrac{v}{V}\right) + q_m + K_d\left(\dfrac{v}{V}\right)\right]$

C_0 initial protein concentration in the bulk fluid

$C(t)$ concentration of protein at any time, t

c^* equilibrium concentration of protein in solution

D_p effective (pore) diffusivity

e batch void fraction

e_p porosity of the resin

$F(t)$ fractional obtainment to equilibrium, $\dfrac{q^* - q(t)}{q^* - q_0}$

K overall mass transfer coefficient

k_1 the first order rate constant, forward rate constant

k_2 the reverse rate constant

K_a the association constant, $\dfrac{k_1}{k_2}$

K_d the dissociation constant, $\dfrac{1}{K_a}$

m'' $\quad \dfrac{q^* - q(t)}{C(t) - C_0}$

q_m maximum protein capacity of the resin

q_0 initial concentration of protein adsorbed to the resin

$q(t)$ concentration of protein adsorbed at any time t

q^* concentration of protein adsorbed to the resin in equilibrium with c^*

r_p radius of resin particle

V volume of buffer in the bath

v volume of resin

α $\quad \begin{cases} (\gamma - 1)^{1/3} & \gamma > 1 \\ 0 & \gamma = 1 \\ -(1 - \gamma)^{1/3} & \gamma < 1 \end{cases}$

γ $\quad \dfrac{e\, C_0}{q_0\, r_p}$

ω $\quad \left[1 - \gamma\left(1 - \dfrac{C(t)}{C_0}\right)\right]^{1/3}$

REFERENCES

1 J. Saint-Blanchard, J. M. Kirzin, P. Riberon, F. Deht, J. Fourcant, P. Girot and E. Boschett, in T. C. J. Gribnau, J. Visse and R. J. F. Nivard (Editors), *Affinity Chromatography and Related Techniques*, Elsevier, Amsterdam, 1982, pp. 200–300.
2 S. M. Wheelwright, *Bio/Technology*, 5 (1987) 789.
3 M. T. W. Hearn, in J. A. Asenjo (Editor), *Isolation and Purification Separation Processes in Biotechnology*, Marcel Decker, New York, 1990, pp. 17–66.
4 J. Luiken, R. Van der Zee and G. W. Welling, *J. Chromatogr.*, 284 (1984) 482.
5 M. T. W. Hearn, A. N. Hodder, P. G. Stanton and M. I. Aguilar, *Chromatographia*, 24 (1987) 769.
6 F. E. Regnier, *Science (Washington, D.C.)*, 238 (1987) 317.
7 P. Oroszlan, R. Blanco. X.-M. Lu, D. Yarmush and B. L. Karger, *J. Chromatogr.*, 500 (1990) 481.
8 S. Mazsaroff, S. Cook and F. E. Regnier, *J. Chromatogr.*, 443 (1988) 119.
9 P. G. Squire, P. Moser and C. T. O. Konski, *Biochemistry*, 7 (1968) 4261.
10 P. Strop, V. Zizkovsky, J. Korcakova, M. Havranova and F. Mikes, *Int. J. Biochem.*, 16 (1984) 805.
11 M. T. W. Hearn, A. N. Hodder and M. I. Aguilar, *J. Chromatogr.*, 327 (1985) 47.
12 B. J. Horstmann and H. A. Chase, *Chem. Eng. Res. Des.*, 67 (1989) 243.
13 H. A. Chase, *J. Chromatogr.*, 297 (1984) 179.
14 F. B. Anspach, A. Johnston, H.-J. Wirth, K. K. Unger and M. T. W. Hearn, *J. Chromatogr.*, 499 (1990) 103.
15 B. L. Yang, M. Goto and S. Goto, *J. Chem. Eng. Japan*, 22 (1989) 532.
16 B. J. Horstmann, C. N. Kenney and H. A. Chase, *J. Chromatogr.*, 361 (1986) 179.
17 F. H. Arnold, H. W. Blanche and C. R. Wilke, *Chem. Eng. J.*, 30 (1985) B9.
18 H. S. Tsou and E. E. Graham, *AIChE J.*, 31 (1985) 1959.
19 B. H. Arve and A. I. Liapis, *AIChE J.*, 33 (1987) 179.
20 C. Delisi, H. W. Hethcote and J. W. Brettler, *J. Chromatogr.*, 240 (1982) 283.
21 R. D. Fleck, D. J. Kirwan and K. R. Hall, *Ind. Eng. Fundam.*, 12 (1973) 95.
22 G. H. Cowan, I. S. Gosling, J. F. Laws and W. P. Sweetenham, *J. Chromatogr.*, 363 (1986) 37.
23 S. C. Nigam and H. Y. Wang, in J. A. Asenjo and J. Hong (Editors), *Separations, Purification and Recovery in Biotechnology: Recent Advances and Mathematical Modeling*, (*ACS Symposium Series*, No. 314), American Chemical Society, Washington, DC, 1986, pp. 153–168.
24 H. Ohashi, T. Sugawar, K. Kikuchi and K. Konno, *J. Chem. Eng. Japan*, 14 (1981) 433.
25 M. E. Young, P. A. Carroad and R. L. Bell, *Biotech. Bioeng.*, 12 (1980) 947.
26 R. C. Travers and F. C. Church, *Int. J. Peptide Prot. Res.*, 26 (1985) 539.
27 Y. Kato, K. Nakamura and T. Hashimo, *J. Chromatogr.*, 253 (1982) 219.
28 F. B. Anspach, A. Johnston, H.-J. Wirth, K. K. Unger and M. T. W. Hearn, *J. Chromatogr.*, 476 (1989) 205.
29 R. Janzen, K. K. Unger, W. Muller and M. T. W. Hearn, *J. Chromatogr.*, 522 (1990) 77.
30 E. E. Graham and C. F. Fook, *AIChE J.*, 28 (1982) 245.
31 W. Kopaciewicz, S. Fulton and S. Y. Lee, *J. Chromatogr.*, 409 (1987) 111.
32 B. F. Ghrist, M. A. Stadalius and L. R. Snyder, *J. Chromatogr.*, 387 (1987) 1.
33 A. Johnston and M. T. W. Hearn, *J. Chromatogr.*, 512 (1990) 101.
34 A. Fersht, in A. Fersht (Editor), *Enzyme Structure and Mechanism*, W. H. Freeman, Reading, UK, 1977, pp. 130–131.
35 M. I. Aguilar, A. N. Hodder and M. T. W. Hearn, *J. Chromatogr.*, 327 (1984) 115.
36 N. K. Boardman and S. M. Partridge, *Biochem. J.*, 59 (1955) 543.
37 R. A. Barford, B. J. Sliwinski and H. L. Rothbart, *J. Chromatogr.*, 185 (1979) 393.
38 W. Kopaciewicz, M. A. Rounds, J. Fausnaught and F. E. Regnier, *J. Chromatogr.*, 266 (1983) 3.
39 M. A. Rounds and F. E. Regnier, *J. Chromatogr.*, 283 (1984) 37.
40 K. Nakamura, Y. Hirai, H. Kitana and N. Ise, *Biotech. Bioeng.*, 30 (1987) 216.
41 D. S. Hage and R. R. Walter, *Anal. Biochem.*, 58 (1986) 274.
42 C. K. Colton, G. N. Satterfield and C. J. Lai, *AIChE J.*, 21 (1975) 289.
43 K. Yamamoto, R. Nakanishi, R. Matsuno and T. Kamikubo, *Biotech./Bioeng.*, 225 (1983) 1465.
44 E. Furuya, Y. Takeuchi and K. E. Noll, *J. Chem. Eng. Japan*, 22 (1989) 670.
45 Q. M. Mao, A. Johnston, I. Prince and M. T. W. Hearn, *J. Chromatogr.*, 548 (1991) 147.

Journal of Chromatography, 557 (1991) 359–368
Elsevier Science Publishers B.V., Amsterdam

CHROM. 23 376

Performances and limits of plasma desorption mass spectrometry in the primary structure determination of proteins

JEAN-MARIE SCHMITTER
Laboratoire de Biochimie, URA 240 CNRS, École Polytechnique, Route de Saclay, 91128 Palaiseau Cedex (France)

ABSTRACT

The resolution, sensitivity, matrix effect, cationization and spectral suppression in plasma desorption mass spectrometry (PD-MS) were investigated in the context of peptide analysis. Excessive cationization may be avoided by the addition of citric acid on the target. The importance of the relative net charge of peptides in PD-MS spectra suppression was confirmed. Esterification of peptides is shown to be an easy way to overcome spectral suppression. Provided that cationization and spectral suppression of peptides are under control, PD-MS is an excellent tool for protein sequence analysis, affording the necessary complement to automated Edman degradation.

INTRODUCTION

Primary structure determination of proteins consisting of several hundred amino acids is a delicate and lengthy task, even with the help of modern automated stepwise Edman degradation [1]. Indeed, it requires a careful piecing together of peptides generated by various cleavage techniques, and subsequently purified to homogeneity. Thus, the sequence of a large protein is preferably deduced from an alternative approach, by sequencing the gene encoding this protein. This then implies verifying the deduced sequence and identifying possible post-translational modifications and sequence heterogeneities [2,3]. Automated Edman degradation may be used for this purpose, after having generated and purified a set of peptides. However, in addition to the fact that this sequencing technique is time consuming, it cannot handle peptides having blocked N-termini and does not lead in a direct way to a complete identification of all possible post-translational structure modifications. The best choice is then to use mass spectrometry.

Recent advances in desorption–ionization techniques have opened the way to high mass measurements [4–7], and several instrumental combinations allow the analysis of peptides by mass spectrometry. Among low-resolution instruments, spectrometers based on a ^{252}Cf plasma desorption source and a time-of-flight (TOF) analyser offer several attractive features for this type of application [8–11]. In addition to a

0021-9673/91/$03.50

simple-to-operate instrumental combination, the sensitivity of this technique matches that of automated sequencing based on Edman degradation. Further, an analysis by plasma desorption mass spectrometry (PD-MS) destroys less than 1% of a sample deposited on the target; this allows the use of subsequent *in situ* chemical derivatizations and proteolytic digestions. Further structural information may then be obtained by reanalysing the same target [12,13].

The capabilities of such an instrument are presented in the context of protein structure determination, focusing on the aspects of resolution and sensitivity. As a complement to Edman degradation, it was important to evaluate the potential of PD-MS to handle peptide mixtures. Therefore, the effects of matrix, cationization and spectral suppression on peptide molecular ion signals were investigated.

EXPERIMENTAL

Mass spectrometer

The ^{252}Cf fission fragment ionization TOF mass spectrometer (Depil-X) was constructed at the Institut de Physique Nucléaire (Orsay, France) and has been described elsewhere [14–16]. An electrostatic mirror allows both an increase in resolution and access to metastable ion studies [15,16]. Spectra were acquired with an acceleration voltage of 10 kV. When the electrostatic mirror was used, a 13 kV voltage was applied to the mirror in order to reflect ions to an axial annular stop detector [14].

Mass calibration of spectra was based on the flight times of H^+ and Na^+ for positive ions and of H^- and CN^- for negative ions.

Sample probes

Aluminized Mylar was used as the primary sample support. In most instances, a thin nitrocellulose (NC) film was produced on this support by electrospraying 25 μl of a 2 mg/ml solution of NC in acetone [17].

Peptides samples were dissolved at a concentration of 0.1–1 m*M*. Various solvents were used, with the following compositions: water–methanol (1:4 or 1:1, v/v); 0.05 *M* sucrose octaacetate in methanol–water (1:1); 0.05 *M* citric acid in methanol–water (1:1); 0.05 *M* glutathione in methanol–water (1:1); and 0.05 *M* citric acid–0.05 *M* glutathione in methanol–water (1:1). A 1–3-μl volume of sample was usually applied on the NC layer and allowed to dry on the probe.

Peptides were obtained from Serva (Heidelberg, Germany), except tryptic peptides from *E. coli* thioredoxin, which were a gift from Dr. P. Decottignies (Orsay, France). The single letter code is used for amino acids.

Methanolic hydrochloric acid (3 *M*) was used for the esterification of peptides. After reaction for 1 h at room temperature, this reagent was removed under a stream of nitrogen and peptides were taken up in methanol–water (1:1).

RESULTS AND DISCUSSION

Influence of the sample matrix

Peptide samples may be directly electrosprayed onto an aluminized Mylar surface and analysed by PD-MS. Most often, this results in a difficult control of alkali

metal ion concentration on the target, and the $[M + H]^+$ ion may almost disappear to the benefit of pseudomolecular ions cationized with sodium or potassium, such as $[M + Na]^+$ and $[M + 2Na - H]^+$ (Fig. 1A). Another drawback of direct electrospraying on aluminized Mylar is that only a few solvents are suitable for this technique, those with a high water content being prohibited. For these reasons, nitrocellulose (NC), which can be electrosprayed on aluminized Mylar from a solution in acetone [17], has gained wide acceptance for peptide analysis by PD-MS. Aqueous solutions may be easily used to adsorb peptides on NC, and the amount of alkali metal ions on the target is much lower than that observed with direct electrospraying on aluminized Mylar. This is illustrated by the analysis of the tripeptide GPA on an NC backing (Fig. 1B). Various combinations of aqueous solvents, including methanol–water and acetonitrile–water, with or without the presence of 0.1% of trifluoroacetic acid, may be used in order to load peptides on the probe without altering the uniformity of the NC layer. Methanol–water (1:1) always gave good results when a 1–3-μl sample volume was allowed to dry on the target.

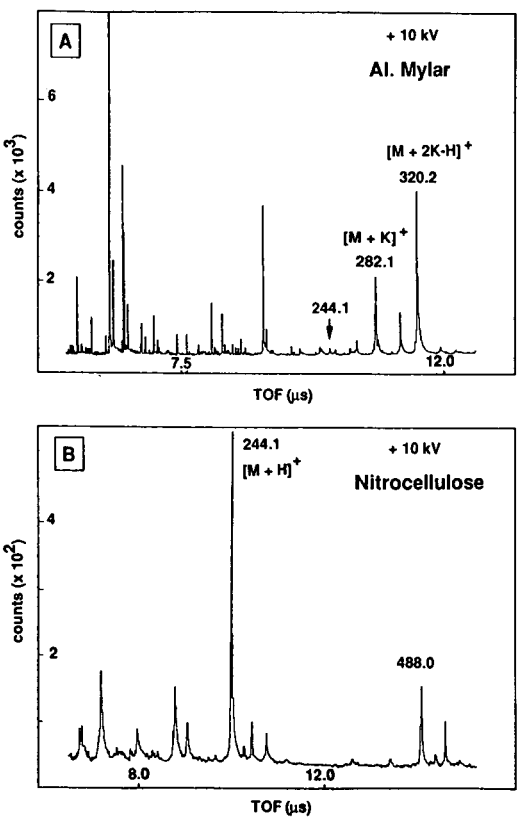

Fig. 1. (A) When the tripeptide GPA (single-letter coding for amino acids is used) is electrosprayed on aluminized Mylar from a methanol–water (4:1, v/v) solution, the $[M + H]^+$ ion (m/z 244.1) hardly appears, and major pseudomolecular ion species result from cationization with potassium. (B) By drying the tripeptide solution (same solvent) on a previously electrosprayed nitrocellulose layer, the $[M + H]^+$ ion dominates all cationized species.

Using NC as a matrix, fragmentation of peptides occurs only to a very minor extent, and only information on molecular mass is usually obtained from the spectra. This behaviour differs from that of peptides electrosprayed on Mylar, which sometimes leads to the formation of fragment ions [18].

A gain in sensitivity of 1–2 orders of magnitude is obtained with NC backings as compared with aluminized Mylar. Therefore, for all these reasons, subsequent analyses were performed with an NC matrix.

Resolution and sensitivity

A TOF mass spectrometer equipped with an electrostatic mirror allows access to the study of metastable ions, als already outlined [14–16]. Reflecting ions toward an annular stop detector with about twice the length of the initial flight path, and partly removing neutral species, results in a significant increase in resolution. This is illustrated with the analysis of an eleven-residue-long peptide (Fig. 2). With the electrostatic mirror in operation (reflex mode), the resolution reaches about 3000. This feature is of major interest when accurate mass measurements are required; such is

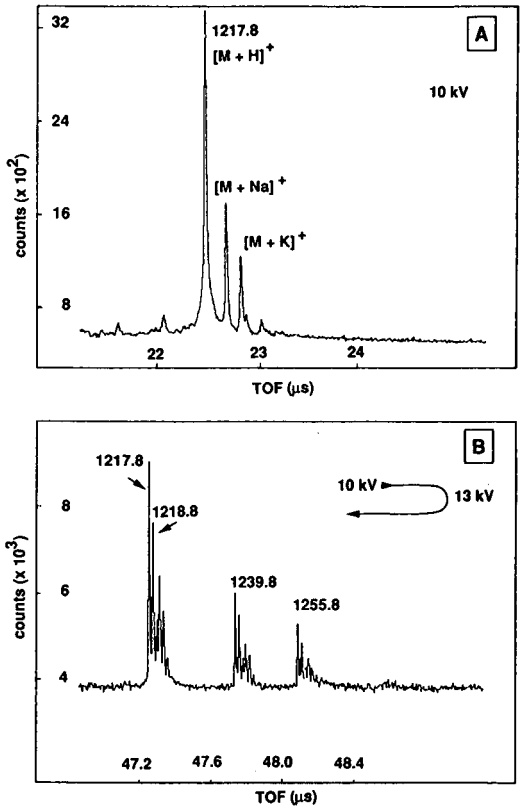

Fig. 2. Improvement in resolution achieved with the electrostatic mirror. (A) An undecapeptide (calculated relative molecular mass 1216.7, 300 pmol) loaded on an NC layer [methanol–water (4:1, v/v) solution] is analysed with a 10 kV acceleration voltage. (B) By applying 13 kV to the mirror, ions are reflected and detected after about twice their initial flight time [14], and the isotopic cluster is resolved.

the case when a normal (–COOH) peptide C-terminus must be distinguished from an amidated one, with only 1 u difference.

However, the use of the electrostatic mirror is limited by the sensitivity that can be achieved. With the 80-cm long flight tube of the Depil-X instrument, a clear molecular ion signal of a peptide of relative molecular mass below 2000 can be obtained in the direct mode with less than 100 pmol of sample, and this within a few minutes of spectral accumulation time. This amount of sample has to be multiplied by a factor of about ten when relative molecular masses in the range 2000–5000 are to be measured; above 5000 successful results are strongly dependent on sample preparation and the nature of the peptide itself. In the reflex mode, the sensitivity drops by a factor of about ten. This can be partly compensated for by using longer spectral accumulation times, but the use of the electrostatic mirror in PD-MS is very limited for relative molecular masses above 3000–5000.

Control of cationization

As already evidenced with the analysis of a tripeptide presented in Fig. 1, the presence on the target of a large amount of alkali metal ions may lead to very weak signals of $[M + H]^+$ ions, and possibly result in a wrong attribution of molecular ions. Indeed, dealing with peptides of unknown sequences, strong cationization by sodium may lead to the absence of the $[M + H]^+$ ion, and to the presence of abundant $[M + Na]^+$ and $[M + 2Na - H]^+$. As these two latter ions differ by 22 u, the $[M + Na]^+$ ion may then be wrongly identified as the $[M + H]^+$ ion.

When analysing peptides of unknown sequences, cationization should therefore be kept as low as possible. After a preliminary analysis, it is safe to reanalyse the sample after having treated nitrocellulose-bound peptides in order to reduce the amount of sodium and potassium ions susceptible to form adducts with peptides.

As a first possibility, the target may be washed with deionized water or with a dilute acid solution. As already outlined by other workers [10,17], we observed that this treatment may result in important losses of peptides having relative molecular masses below 1000–1500. Another possibility consists in treatment of peptide solutions with an ion-exchange resin prior to sample adsorption on the NC layer, but losses cannot be excluded when this procedure is applied to subnanomolar amounts of peptides.

Thus, adding on the target a solution of a non-volatile carboxylic acid was found to be more generally applicable. Excellent results were obtained with solutions of citric acid (0.05–0.1 *M*), as shown in Fig. 3. This treatment was found to reduce considerably or even abolish cationization by sodium and potassium, but also to increase slightly the overall sensitivity for pseudomolecular ion species.

The addition of sucrose octaacetate to NC-bound peptides also results in a decrease in cationization, but this time to the detriment of sensitivity. As a practical rule, less than 10 nmol of this sugar derivative should be added to the target in order not to quench $[M + H]^+$ ions when subnanomolar amounts of peptides are analysed. Unfortunately, this amount is then too low to trap alkali metal ions efficiently.

It is worth mentioning that glutathione, which has been used as an additive to improve the desorption of polypeptides [19], also leads to a strong decrease in cationization of NC-bound peptides. This was experienced by adding 1–2 μl of a 0.05 *M* solution of glutathione (reduced form) to peptides adsorbed on NC. Glutathione was

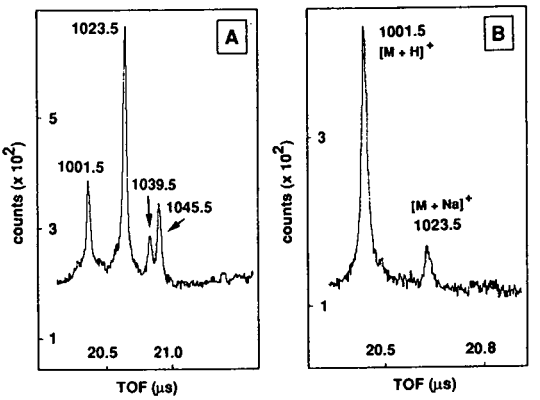

Fig. 3. Analysis in the positive-ion mode on an NC backing (10 kV acceleration voltage) of peptide GIPTLLLFK (from *E. coli* thioredoxin, calculated relative molecular mass 1000.6, 1 nmol). (A) The sample has been dissolved in methanol–water (4:1, v/v); (B) the target has been treated by drying 1 μl of a 0.1 *M* solution of citric acid on the surface and reanalysed.

found to be less efficient than citric acid for cationization removal, but for a large variety of peptides the overall sensitivity was improved after this treatment (data not shown).

As a general result for routine laboratory PD-MS analysis, peptides are now dissolved in a solution of 0.05 *M* citric acid–0.05 *M* glutathione in methanol–water (1:1). However, when subsequent enzymatic cleavages are planned to be performed on the target, peptides are dissolved in methanol–water (1:1).

Control of spectral suppression

The potential of peptide mapping by means of mass spectrometry is of particular interest for protein primary structure analysis. Indeed, in order to speed up a sequence verification, the effort on peptide purification should be kept to a minimum. However, it was experienced, with the hitherto most often used fast atom bombardment (FAB) mapping technique, that the analysis of peptide mixtures rarely led to complete peptide maps [4,20,21]. The spectral suppression phenomenon observed with FAB mapping can be related to strong differences in hydrophobicity, missing peptides being the most hydrophilic ones [20–22].

PD-MS has also been proposed as a tool for peptide mapping [12]. Spectral suppression effects were sometimes observed with this desorption–ionization mode, but were not well documented untill a recent study by Nielsen and Roepstorff [22]. According to them, spectral suppression of peptides in PD-MS is related to their relative net charge and not to their relative hydrophobicity.

An investigation of the applicability of PD-MS for both quantitative analysis and mapping of peptides was therefore undertaken, aimed at the design of optimum conditions for obtaining complete peptide maps.

Spectral suppression may not be observed at all when studying ^{252}Cf desorption of peptides. This technique has been used to characterize a carboxypeptidase Y (CPD-Y) catalysed transpeptidation of peptides [23]. Under certain conditions, this exopeptidase is able to catalyse the replacement of the carboxyl-terminal amino acid

of a peptide by an exogeneous amino acid. By analysing a transpeptidation reaction mixture, one may thus find starting material, together with hydrolysis and transpeptidation products. If the N-terminal amino acid bears an aromatic residue, such as tyrosine, a reversed-phase chromatographic system can easily lead to the quantification of the various constituents of the mixture. In the case of CPD-Y catalysed transpeptidation of peptide YPFPGPI with methionine, quantitative analysis of the reaction mixture by both high-performance liquid chromatography (HPLC) and PD-MS gave nearly identical results, *i.e.*, no spectral suppression was observed (Fig. 4).

In order to probe the relationship between the relative net charge of peptides and the spectral suppression effect in PD-MS, an equimolecular mixture of peptides YPFVEPI (net charge −1 at pH 7) and LWMRFA (net charge +1 at pH 7) was prepared. When analysed separately using an NC target in the positive-ion mode, each peptide desorbs in excellent yield. When using methanol–water (1:1) as a solvent and loading the mixture of the two peptides on NC, the spectrum shown in Fig. 5 was obtained. The signal of peptide YPFVEPI is strongly suppressed compared with LWMRFA. Also, the $[M + H]^+$ ion of YPFVEPI is very weak, this peptide being more cationized than LWMRFA by sodium. This result confirms the important role of the relative net charge of peptides in PD-MS analysis. The next step was to investigate possible ways to overcome spectral suppression effects.

By dissolving the previous equimolecular mixture of LWMRFA and YPFVEPI in methanol–water (1:1) in the presence of 0.05 *M* citric acid and 0.05 *M* glutathione, cationization disappears as expected, and spectral suppression of YPFVEPI also

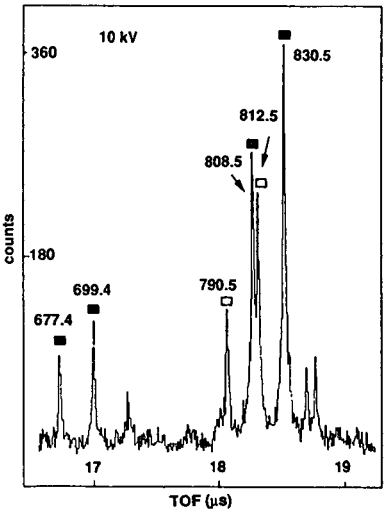

Fig. 4. Analysis of a reaction mixture resulting from carboxypeptidase Y-catalysed transpeptidation of the peptide YPFPGPI, with methionine added as exogenous nucleophile. Peak areas of the hydrolysis product YPFPGP (closed squares, $[M + H]^+$ at m/z 667.4), starting peptide (open squares, $[M + H]^+$ at m/z 790.5) and transpeptidation product YPFPGPM (shaded squares, $[M + H]^+$ at m/z 808.5) were found to be in good agreement with those measured by HPLC (absorbance of tyrosine at 280 nm [23]). The solvent used for loading on the NC target was methanol–water (4:1, v/v). Cationization by sodium affects the three peptides in the same proportion.

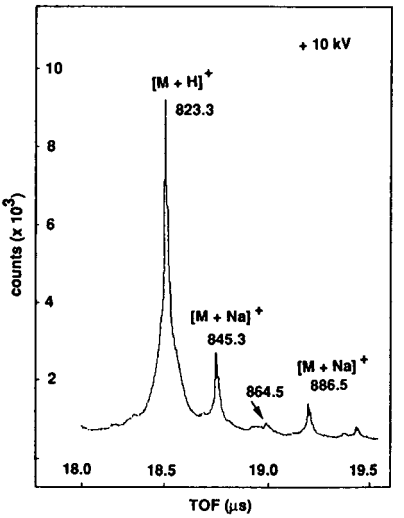

Fig. 5. Equimolecular mixture of peptides LWMRFA ($[M + H]^+$ at m/z 823.3) and YPFVEPI ($[M + H]^+$ expected at m/z 864.5) analysed with a 10 kV acceleration voltage after adsorption on an NC layer from methanol–water (1:1, v/v).

slightly diminishes in the positive-ion mode (Fig. 6A). The situation is more favourable in the negative-ion mode, but at the expense of a lower sensitivity (Fig. 6B).

Taking into account the hypothesis of the important role of the relative net charge of peptides [22], changing this net charge by derivatization of carboxylic acid groups should reduce the spectral suppression of peptides having negative net charg-

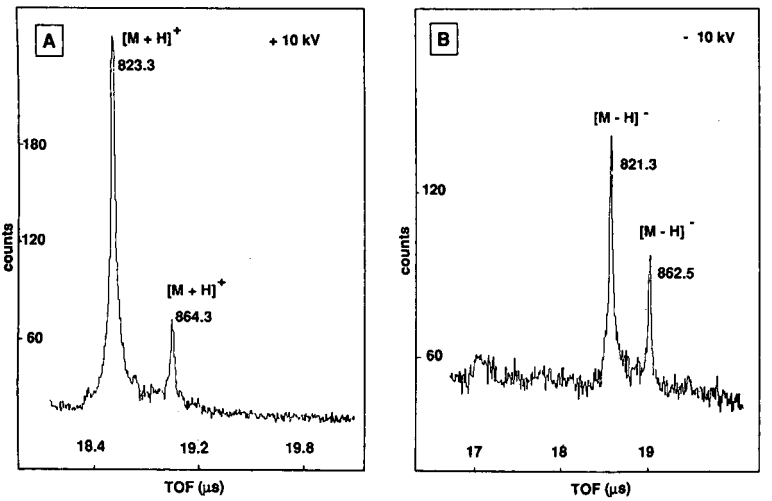

Fig. 6. Equimolecular mixture of peptides LWMRFA and YPFVEPI dissolved in 0.05 *M* citric acid–0.05 *M* glutathione in methanol–water (1:1). After loading on an NC layer, the analysis in both (A) positive-ion (+10 kV) and (B) negative-ion (−10 kV) modes shows that both cationization and spectral suppression have strongly decreased in comparison with the conditions used to obtain Fig. 5.

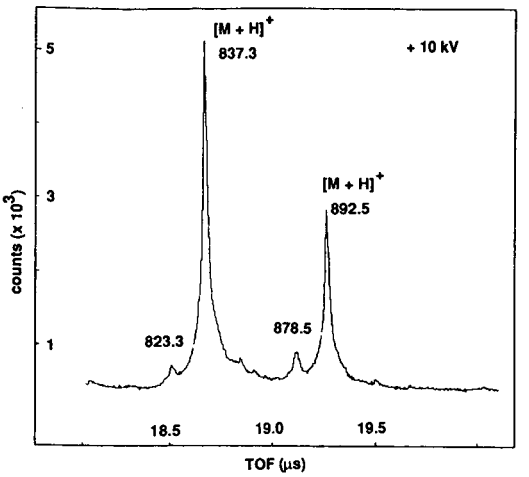

Fig. 7. Spectral suppression of peptide YPFVEPI almost disappears after esterification. An equimolecular mixture of LWMRFA and YPFVEPI, treated with methanolic hydrochloric acid, was dissolved in methanol–water (1:1) solvent mixture and loaded on an NC backing. Two methyl groups have been added for YPFVEPI ($[M + H]^+$ at m/z 892.5); this peptide is also present with a single function esterified ($[M + H]^+$ at m/z 878.5).

es. Thus, the same equimolecular mixture of YPFVEPI and LWMRFA was first esterified by means of methanolic hydrochloric acid. After evaporation to dryness, the sample was dissolved in methanol–water (1:1), adsorbed on NC and analysed in the positive-ion mode (same conditions as in Fig. 5). As shown in Fig. 7, spectral suppression almost disappeared. This single derivatization step is thus of great help in the sequence analysis of proteins, as it is an easy way to solve the problem posed by spectral suppression in PD-MS, and simultaneously provides the additional information of the number of carboxyl groups present in peptides.

As a result of this work, a general strategy for PD-MS mapping was designed. If enough peptidic material is available, the peptide mixture to be analysed is divided into two equal parts. One part is analysed in both positive- and negative-ion modes, using glutathione and citric acid as additives on the NC backing. The second part is first esterified, and subsequently analysed in the same way, in order to detect peptides suppressed under the first set of analytical conditions. In this way, PD-MS really is a valuable tool for protein sequence analysis, *i.e.*, an excellent technique to be used in combination with automated microsequencing.

ACKNOWLEDGEMENTS

The author thanks Bertrand Platel for assistance with the mass spectrometric analysis, Pierre-François Berne for providing the transpeptidation reaction mixture and Dr. Paulette Decottignies for providing tryptic peptides from *E. coli* thioredoxin. The constant interest of Professor Sylvain Blanquet in this work, and his efforts, together with those of Dr. Henri Audier, to develop this research programme are gratefully acknowledged. The Depil-X spectrometer was purchased with the financial support of INSERM and the École Polytechnique.

REFERENCES

1 R. M. Hewick, M. W. Hunkapiller, L. E. Hood and W. J. Dryer, *J. Biol. Chem.*, 256 (1981) 7990.
2 B. W. Gibson and K. Biemann, *Proc. Natl. Acad. Sci. U.S.A.*, 81 (1984) 1956.
3 K. Biemann and H. A. Scoble, *Science, (Washington, D.C.)*, 237 (1987) 992.
4 K. Biemann and S. A. Martin, *Mass Spectrom. Rev.*, 6 (1987) 1.
5 T. R. Covey, R. F. Bonner, B. I. Shushan and J. Henion, *Rapid Commun. Mass Spectrom.*, 2 (1988) 249.
6 F. Hillenkamp, *Adv. Mass Spectrom.*, 11A (1989) 354.
7 K. D. Henry, E. R. Williams, B. H. Wang, F. W. McLafferty, J. Shabanowitz and D. F. Hunt, *Proc. Natl. Acad. Sci. U.S.A.*, 86 (1989) 9075.
8 R. D. McFarlane and D. F. Torgerson, *Science, (Washington, D.C.)*, 191 (1976) 920.
9 R. D. McFarlane, J. C. Hill, D. L. Jacobs and P. W. Geno, *Adv. Mass Spectrom.*, 11A (1989) 3.
10 P. Roepstorff and B. Sundqvist, in S. J. Gaskell (Editor), *Mass Spectrometry in Biomedical Research*, Wiley, New York, 1986, Ch. 15, p. 269.
11 S. K. Chowdhury and B. T. Chait, *Anal. Biochem.*, 180 (1989) 387.
12 A. Tsarbopoulos, G. W. Becker, J. L. Occolowitz and I. Jardine, *Anal. Biochem.*, 171 (1988) 113.
13 K. Klarskov, K. Breddam and P. Roepstorff, *Anal. Biochem.*, 180 (1989) 28.
14 S. Della Negra and Y. Le Beyec, *Int. J. Mass Spectrom. Ion Processes*, 61 (1984) 21.
15 S. Della Negra and Y. Le Beyec, *Anal. Chem.*, 57 (1985) 2035.
16 Y. Le Beyec, *Adv. Mass Spectrom.*, 11A (1989) 126.
17 G. P. Jonsson, A. B. Hedin, P. L. Hakansson, B. U. R. Sundqvist, B. G. S. Säve, P. F. Nielsen, P. Roepstorff, K.-E. Johansson, I. Kamensky and M. S. L. Lindberg, *Anal. Chem.*, 58 (1986) 1084.
18 J. Fohlman, P. A. Petersson, P. Roepstorff, P. Højrup, I. Kamensky, B. G. S. Säve, P. L. Hakansson, B. U. R. Sundqvist, *Biomed. Mass Spectrom.*, 12 (1985) 380.
19 M. Alai, P. Demirev, C. Fenselau and R. J. Cotter, *Anal. Chem.*, 58 (1986) 1303.
20 S. Naylor, A. F. Findeis, B. W. Gibson and D. H. Williams, *J. Am. Chem. Soc.*, 108 (1986) 6359.
21 R. M. Caprioli, W. T. Moore and T. Fan, *Rapid Commun. Mass Spectrom.*, 1 (1987) 15.
22 P. F. Nielsen and P. Roepstorff, *Biomed. Environ. Mass Spectrom.*, 18 (1989) 131.
23 P. F. Berne, J. M. Schmitter and S. Blanquet, *J. Biol. Chem.*, 265 (1990) 19551.

Journal of Chromatography, 557 (1991) 369–382
Elsevier Science Publishers B.V., Amsterdam

CHROM. 23 308

Adsorption–desorption isotherm hysteresis of β-lactoglobulin A with a weakly hydrophobic surface

SHIWEN LIN, RIGOBERTO BLANCO and BARRY L. KARGER*
Barnett Institute, Northeastern University, Boston, MA 02115 (USA)

ABSTRACT

Adsorption–desorption isotherms of bovine β-lactoglobulin A (β-lact A) on a weakly hydrophobic stationary phase (C_1-ether) were measured by frontal analysis. The adsorption isotherms obtained at different pH were found to be dramatically different in shape, column capacity and desorption reversibility. At pH 4.5, an S-shaped adsorption isotherm was observed whereas at pH 6.0 a Langmuir isotherm was found. In addition, the desorption isotherm at pH 6.0 was found to overlap with the adsorption isotherm, and the adsorption–desorption process of β-lact A under this condition could be characterized by a fully reversible Langmuir model. The desorption isotherm at pH 4.5, however, did not retrace the adsorption isotherm, resulting in hysteresis loops. A higher aggregate (tetramer) of β-lact A is shown to be in an equilibrium with the β-lact A protomer (dimer) at pH 4.5 whereas the dimer alone is predominant at pH 6.0. It is further shown that changes in the adsorption coefficient between the adsorption and the desorption cycles for the tetramer at pH 4.5 can account for the hysteresis. The results demonstrate that pH can be a sensitive parameter in protein adsorption isotherm behavior and ultimately the behavior of species in preparative-scale chromatography.

INTRODUCTION

The investigation of protein adsorption at liquid–solid interfaces is of great importance in many fields, including the chromatographic separation of proteins and the design of biomaterials and biosensors [1–3]. The measurement of the adsorption isotherm can provide important information on the adsorption process: for example, adsorption isotherms can be used as a tool in the prediction of elution behavior in the preparative-scale chromatography of proteins [4]. In preparative-scale liquid chromatography, loading of relatively high concentrations of substances is a common practice, and protein–protein interaction leading to association or aggregation can be an important consideration at such high concentrations [5]. Multiple equilibria between oligomers open up a new dimension of complexity in such systems, and significant effects on adsorption behavior can be expected [6]. An understanding and control of such behavior can be important in chromatography, as well as in general protein adsorption phenomena.

β-Lactoglobulin A (β-lact A) is a classical example of a protein aggregating system, in which self-association can occur to different extents, depending on the pH

0021-9673/91/$03.50

and other conditions of the system [7]. Below pH 3.5, the dimeric β-lact A (molecular weight, MW 36 800) tends to dissociate to a nearly spherical monomer (MW 18 400). Between pH 3.7 and 5.2 (pI = 5.2), dimers can associate to form higher order aggregates, with the distribution depending on the total concentration and with a maximum extent of self-association occurring at pH 4.5 and 4°C [8]. Above pH 5.2, species larger than dimer decrease in relative amount and the stable dimeric form is predominant at pH 6.0 [7].

Previously, we have demonstrated the separation of three aggregated species of β-lact A, a tetramer, octamer and dodecamer, by hydrophobic interaction chromatography on a C_1-ether phase column with a gradient from 3 to 0 M ammonium sulfate (pH 4.5) at 4°C [5]. On the other hand, a single species was eluted at pH 6.0. More recently, we reported an S-shaped adsorption isotherm of β-lact A on the C_1-ether phase with 0.85 and 1.0 M ammonium sulfate at pH 4.5 [6]. The S-shaped isotherm was interpreted in terms of two species, a protomer and a higher order stronger adsorbing species in the stoichiometric ratio of 1:2, and an explicit adsorption isotherm equation was developed for the aggregating system. We also noted that adsorption hysteresis occurred in this system.

Although other hysteresis phenomena involving proteins, such as enzymatic activity hysteresis and thermal sol–gel hysteresis, have been known for decades, protein adsorption hysteresis has drawn increasing attention only recently [9]. Hysteresis is a characteristic phenomenon in protein adsorption where, for example, conformational or reorientational changes on the hydrophobic adsorbent surface (alkyl-derivatized agarose beads) can result in altered species which bind more strongly to the surface [9–11]. In addition, a recent study on the adsorption isotherm of albumin on a TSK-DEAE anion exchanger also pointed to a probable desorption hysteresis because of non-specific hydrophobic adsorption and possible conformational alerations leading to stronger binding [12].

In this paper, as a continuation of our previous work, both the adsorption and desorption isotherms of β-lact A on a weakly hydrophobic surface at pH 4.5 and 6.0 are examined in depth. Adsorption–desorption isotherms of β-lact A at pH 4.5 again revealed hysteresis loops, with an S-shaped adsorption isotherm and a series of Langmuir-shaped desorption isotherms. The behavior is shown to result from an increase in the adsorption coefficient of the aggregate in the desorption cycle relative to the adsorption cycle. At pH 6.0, on the other hand, both the adsorption and desorption isotherms were found to be Langmuirian in shape and fully reversible. The results point to the dramatic changes in adsorption–desorption behavior that can result when the mobile phase conditions are altered.

EXPERIMENTAL

Equipment

Fig. 1 depicts schematically the apparatus used for isotherm measurements. Frontal chromatography was conducted on a system consisting of an Altex 110A microflow pump with an Altex 420 system controller (Beckman, San Ramon, CA, USA), two Model 7125 syringe-loading sample injection valves (Rheodyne, Cotati, CA, USA) with two 1-ml loops, and a photodiode-array detector (Hewlett-Packard, Palo Alto, CA, USA). The photodiode-array detector was used specifically to mon-

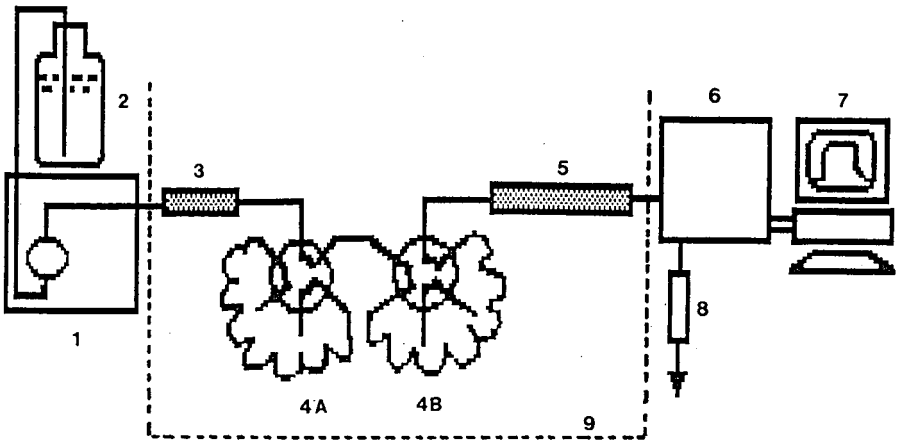

Fig. 1. Instrument for isotherm measurements. 1 = Pump; 2 = mobile phase reservoir; 3 = precolumn; 4A = loop A, 1 ml; 4B = loop B, 1 ml; 5 = analytical column; 6 = photodiode-array detector; 7 = workstation; 8 = flow-rate monitor; 9 = thermostated water-bath.

itor the UV spectra of the protein solute during the breakthrough curve and in the plateau region to search for any structural alteration of the protein in the frontal analysis [13]. The chromatograms and spectra were collected and stored in an HP 9 000 workstation through HP 7996A operating software (Hewlett-Packard).

The column packing consisted of Vydac silica (Separation Group, Hesperia, C A, USA) bonded with a methyl polyether (C_1-ether) phase (particle size 5 μm, pore diameter 300 Å, specific surface area 72 m^2/g) and prepared as described elsewhere [14]. The surface coverage was 6.3 $\mu mol/m^2$, as determined by elemental analysis (ass uming a bonding stoichometry of two ethoxy groups of the silane to silica). The 28 mm × 2.9 mm I.D. column was slurry packed under pressure in carbon tetrachloride–methanol (70:30, v/v) with methanol as driving solvent. The temperature of the column, sample loop and tubing connecting the pump to the injector was regulated at 5 ± 0.5°C by a thermostated water-bath (Neslab, Portsmouth, NH, USA).

Reagents

HPLC-grade water, analytical-reagent grade acetic acid and ammonia solution were purchased from J. T. Baker (Phillipsburg, NJ, USA). 4-(2-Hydroxyethyl)-1-piperazineethanesulfonic acid (HEPES) and 2-(N-morpholino)ethanesulfonic acid (MES) buffer were obtained from Research Organics (Cleveland, OH, USA). High-purity ammonium sulfate (treated to reduce the content of heavy metals) and electrophoretically pure bovine β-lactoglobulin A were purchased from Sigma (St. Louis, MO, USA).

Procedures

The mobile phase solutions were prepared by dissolving the correct weight of salt (0.85 *M* ammonium sulfate) and buffer (20 m*M* HEPES–20 m*M* MES–20 m*M* acetic acid) in HPLC water, adjusting the pH to 4.5 or 6.0 with either acetic acid or

ammonia solution, transferring the solution to a volumetric flask and diluting to volume with water. Mobile phase solutions were filtered and degassed under vacuum before use. Protein samples were freshly prepared in the mobile phase buffer and filtered through a 0.45-μm membrane immediately before each injection.

Adsorption isotherm determination

The column was first equilibrated with at least 100 column volumes of the mobile phase buffer, followed by loading of the protein solution through loop B (Fig. 1). At 23 min after the outlet UV absorbance of the eluent had reached a plateau in frontal development, the pure mobile phase buffer (*i.e.*, without protein dissolved) was switched into the column to elute the adsorbed protein and to regenerate the surface for the next loading. Protein concentration was monitored at 310 nm. Calibration graphs at this wavelength showed a linear relationship between the concentration used and the absorbance response. The adsorbed amount per unit volume of stationary phase (Q) equilibrated with a given concentration of protein in solution was derived from the breakthrough curve as follows:

$$Q = FA_a/\varepsilon V_s \tag{1}$$

where F is the flow-rate, A_a is the area of the retained portion of the breakthrough curve, as described previously [6], ε is the molar absorptivity in mAU ml/mg of β-lact A in the mobile phase buffer measured from the calibration graph at 310 nm and V_s is the volume of stationary phase determined by a standard weight difference method, using methanol and carbon tetrachloride [15,16].

The recovery derived from the ratio of the rear boundary area to the front boundary area after each elution with the pure mobile phase was 98 ± 3% (three runs). This means that each loading run began with a clean regenerated surface. The flow-rate was measured periodically at the detector outlet by using a buret and an electronic timer. The outlet flow-rate was determined to be constant (± 1 μl/min) during the injection of the sample, uptake of the protein and in the plateau region. The adsorbed amount was found to be constant within 5% over a 10-fold range of flow-rate (10, 20, 50 and 100 μl/min) for a given solution concentration of protein, indicating that the mass transfer inside and outside the pores of the adsorbent was rapid in the present system.

Desorption isotherm determination

Protein sample was first loaded into the column through loop B as above. Instead of switching to pure mobile phase buffer at 20 min, after a stable plateau had developed, a sample of lower concentration was introduced into the column through loop A to elute a portion of the adsorbed protein. Loop A was loaded with a lower concentration of sample and the valve was rotated to the injection position while loop B was still in the injection position. After the sample solution passed through the connecting tubing between the loops, loop B was switched back to the loading position to allow the lower concentration sample in loop A to pass onto the column. After a lower plateau had developed, the pure mobile phase buffer was switched into the column to elute the remainder of the adsorbed protein.

The desorption isotherms were constructed by using the adsorbed amount of protein on the stationary phase derived as follows:

$$Q(C) = Q_0(C_0) - \frac{F}{\varepsilon V_S} \cdot A_d \tag{2}$$

where $Q(C)$ is the amount of adsorbed protein on the stationary phase in mg/ml equilibrated with a solution concentration C, $Q_0(C_0)$ is the initial amount of adsorbed protein equilibrated with the solution concentration C_0 and A_d denotes the area in mAU min under each elution breakthrough curve (see Fig. 2). Each desorption was initiated from the same adsorbed state $Q(C_0)$. Two initial states (C_0 = 10.0 and 15.0 mg/ml) were used to obtained two separate desorption isotherms.

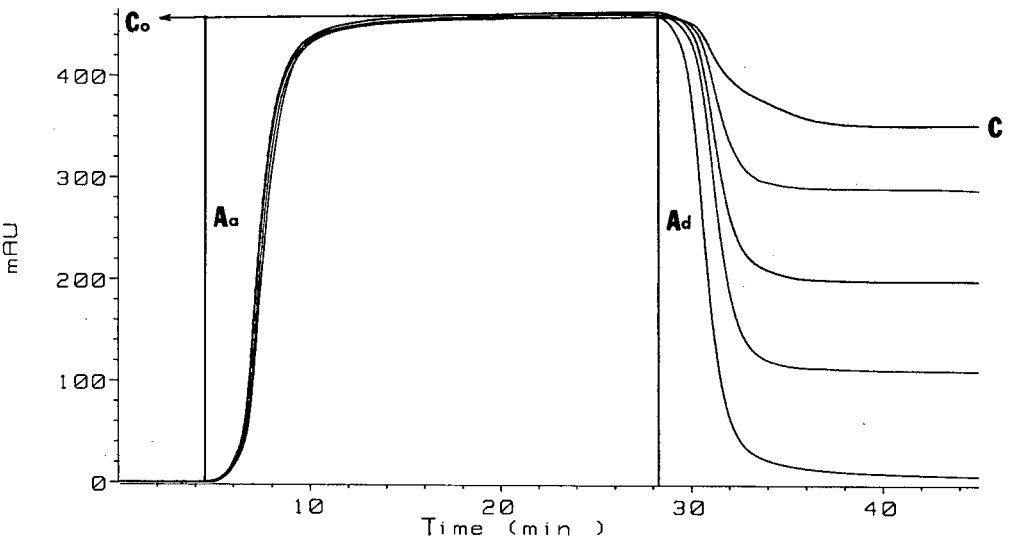

Fig. 2. Frontal chromatograms for the determination of the desorption isotherms. Column, C_1-ether (28 mm × 2.9 mm I.D.); sample, β-lact A in mobile phase buffer, 530-μl injection; mobile phase, 0.85 *M* ammonium sulfate–0.02 *M* HEPES–0.02 *M* MES–0.02 *M* acetic acid, pH adjusted to 4.5 or 6.0 with acetic acid or ammonia solution; flow-rate, 23.0 μl/min; pure mobile phase was switched into the column at 23 min; temperature, 5°C.

RESULTS AND DISCUSSION

Frontal analysis and elution chromatography

Frontal analysis breakthrough curves and slopes (first derivative) for β-lact A at pH 4.5 and 6.0 are shown in Fig. 3. At pH 4.5 both the front and rear boundaries appear more diffuse compared with those at pH 6.0, owing to the relatively shallow first-derivative trace. This is an unusual behavior because in general the front and rear boundaries are alternatively diffuse and self-sharpening, exhibiting either a Langmuir or an anti-Langmuir shape. The diffuse front and rear boundaries for the present system of β-lact A adsorption on the C_1-ether phase at pH 4.5 suggest changes in the

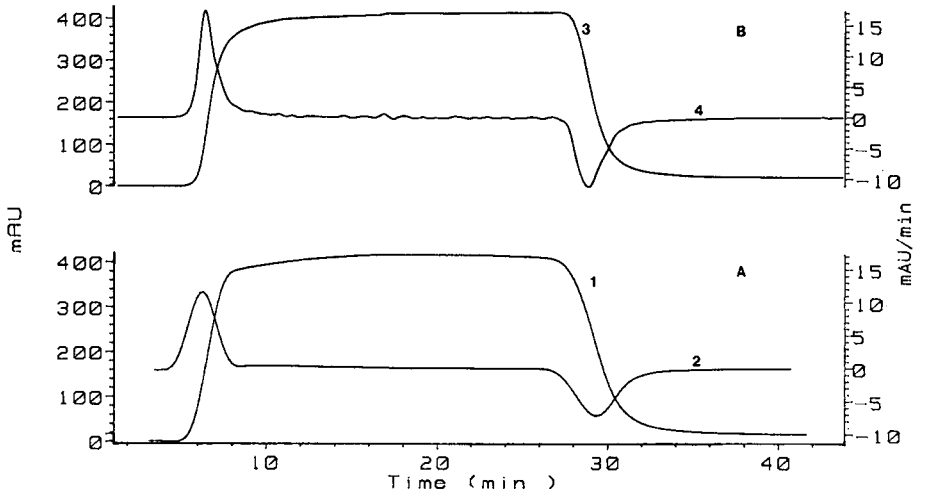

Fig. 3. Frontal chromatograms of β-lact A on the C_1-ether column at pH (A) 4.5 and (B) 6.0. Detection wavelength, 310 nm; curves 1 and 3, frontal chromatograms; curves 2 and 4, slope of frontal chromatograms. Other conditions as in Fig. 2.

adsorption–desorption process. At pH 6.0, on the other hand, the sharper front boundary compared with the rear boundary as identified by the derivative trace indicates a Langmuirian isotherm.

The broader band spreading at pH 4.5 relative to that at pH 6.0 can also be seen from the isocratic elution chromatograms in Fig. 4. The slightly longer retention of

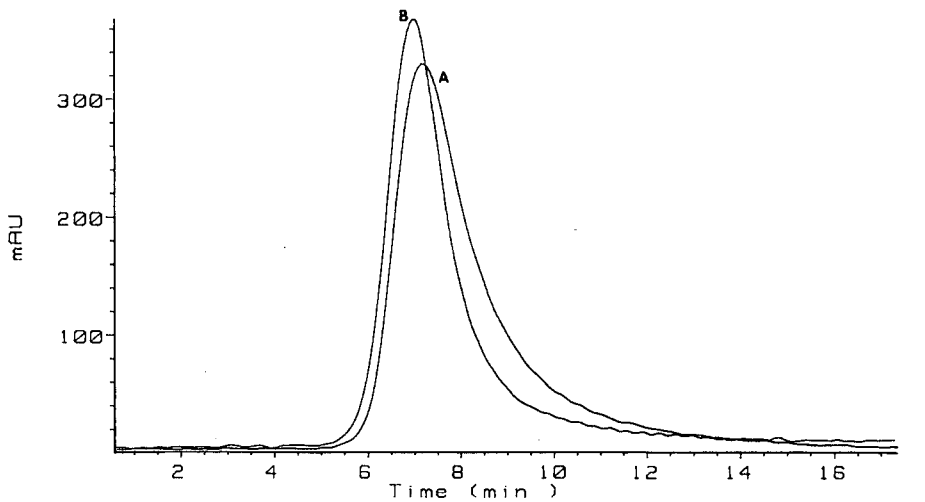

Fig. 4. Isocratic elution chromatograms of β-lact A on the C_1-ether column at pH (A) 4.5 and (B) 6.0. Conditions as in Fig. 2, except that 5.0 mg/ml of β-lact A in mobile phase buffer and 20 μl injections were used.

β-lact A at pH 4.5 indicated a stronger interaction. The band broadening may be a result of the presence of multiple species at pH 4.5 which co-elute under the present conditions [6], whereas these species could be resolved by other conditions [5].

The adsorbed amount of protein, Q, was determined from the retained portion of the breakthrough curves from eqn. 1. By definition, the adsorbed amount Q at equilibrium or at the steady state should be independent of the mobile phase flow-rate used for the measurements. Indeed, as already noted, Q was found to be constant within 5% over a tenfold range of flow-rate (10–100 μl/min), for a given solution concentration of protein.

The desorption isotherm was derived from the frontal analysis as depicted in Fig. 2. As already noted, each desorption step began with the same amount of adsorbed protein corresponding to a specific solution concentration $Q(C_0)$. After the elution with a protein solution of lower concentration, the amount of protein left in the stationary phase was derived from eqn. 2. These results were used to construct the desorption isotherm. The amount of desorbed protein during the elution experiments was also found to be independent of flow-rate in the range 10–100 μl/min.

The UV spectra during the frontal analysis were collected by the photodiode-array detector. As in the plateau region the absorbance at the maximum wavelength (280 nm) was not in the linear range of the detector, only the spectra taken at the beginning of the front boundary and at the end of the rear boundary were compared. No differences were found betweeen the normalized spectra or the second-derivative spectra, indicating no major unfolding of the protein during the adsorption and desorption processes. This result, however, does not exclude the association of β-lact A during the frontal analysis, as the UV spectra for different oligomers are similar [6].

Adsorption–desorption isotherms

In principle, binding equilibria of a solute to an adsorbent from a liquid phase can be obtained by either adsorption or desorption. In a thermodynamically reversible system, the equilibria obtained by the two procedures will be identical, *i.e.*, the adsorption isotherm will be retraced by the desorption isotherm. This is the case for the adsorption of β-lact A at pH 6.0 on the C_1-ether phase.

At pH 6.0, the Langmuir adsorption and desorption isotherms of β-lact A on the C_1-ether phase overlap each other, as shown in Fig. 5. This result suggests full reversibility in the adsorption and desorption steps. In addition, a linear relationship ($r^2 = 0.990$) of Q/C *vs.* Q was observed in the Scatchard plot for the isotherms at pH 6.0, as shown in the inset in Fig. 5. The adsorption–desorption process at pH 6.0 can thus be characterized by the Langmuir model (*i.e.*, single species, uniform adsorption site, no lateral interaction or association on the surface). This result can be easily understood, as β-lact A in solution at pH 6.0 is a stable dimeric species (MW 36 800) [7]. Our previous gradient chromatographic results on the C_1-ether phase column [5] also demonstrated that β-lact A exists as a single species on the C_1-ether phase surface at pH 6.0 during the chromatographic process.

In contrast, at pH 4.5 the adsorption isotherm of β-lact A on the C_1-ether phase was not retraced by the desorption isotherm, resulting in hysteresis. Fig. 6 depicts the adsorption and desorption isotherms and the hysteresis loops at pH 4.5. As previously, an S-shaped isotherm [6] was obtained for the adsorption (or loading) process. The

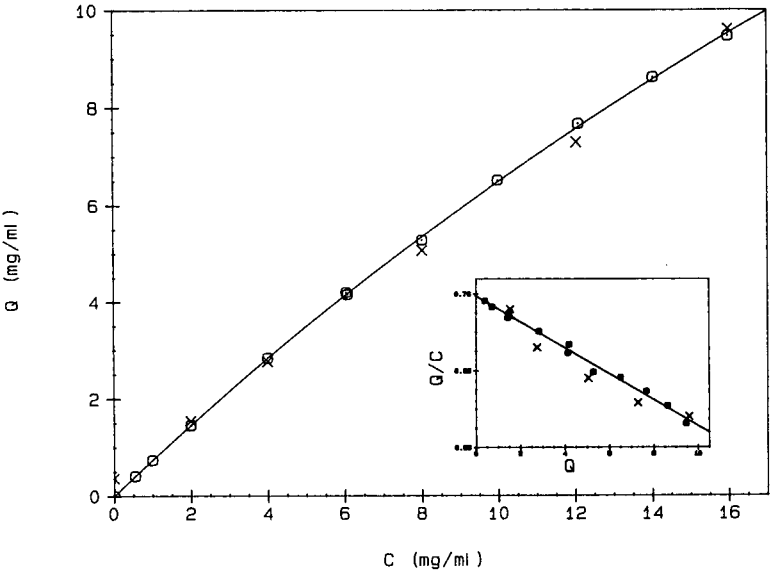

Fig. 5. Adsorption–desorption isotherm of β-lact A on C_1-ether phase at pH 6.0. (○) Adsorption; (×) desorption. Inset: Scatchard plot of the adsorption–desorption isotherm.

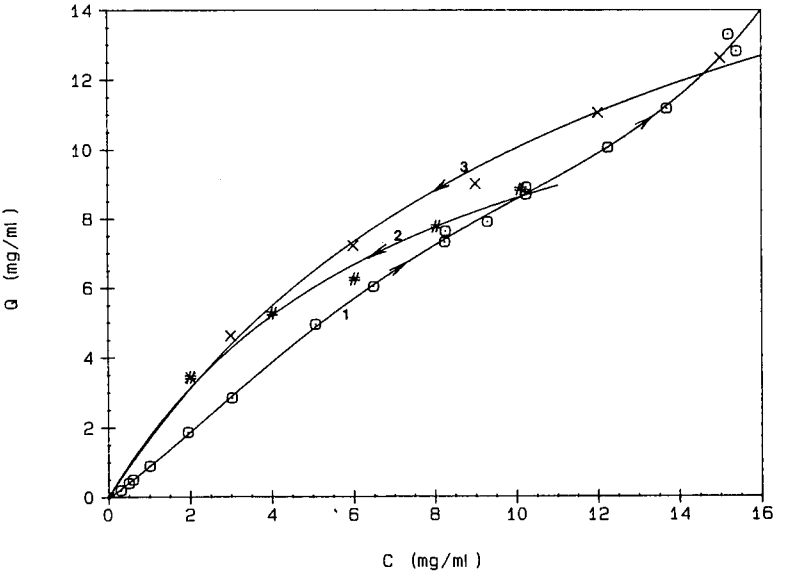

Fig. 6. Adsorption–desorption isotherms of β-lact A on C_1-ether phase at pH 4.5 (1) Adsorption isotherm; (2) desorption isotherm from 15.0 mg/ml of β-lact A equilibrated stationary phase; (3) desorption isotherm from 10.0 mg/ml of β-lact A equilibrated stationary phase. Other conditions as in Fig. 2.

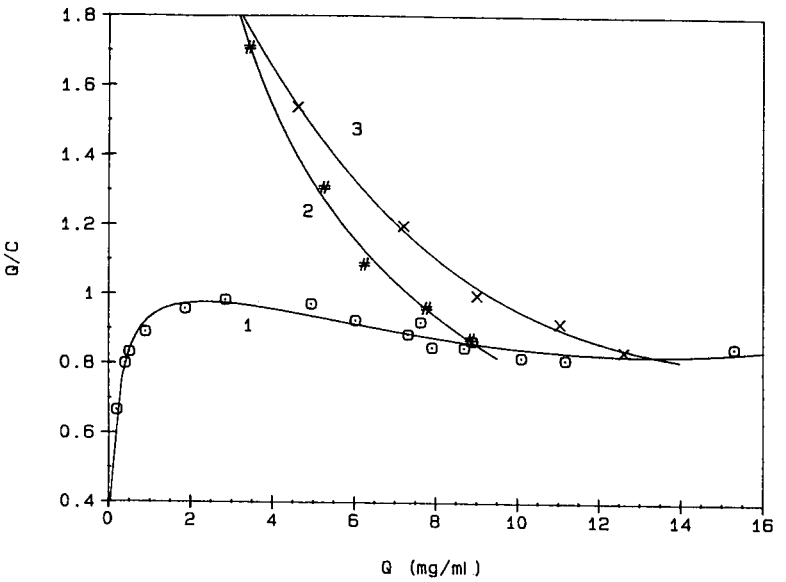

Fig. 7. Scatchard plots of the adsorption–desorption isotherms of β-lact A on the C_1-ether phase at pH 4.5. Conditions as in Fig. 2.

S-shape is indicative of positive cooperativity of protein adsorbate in which either association between molecules in solution [6] or lateral interaction or association between the adsorbed molecules on the surface can occur. The desorption isotherms, however, are Langmuir shaped. These isotherms form closed loops which can only be traced in one direction (see arrows in Fig. 6) as imposed by adsorption or desorption, respectively, The size of the hysteresis loop depends on the original amount of adsorbed protein. Changes in affinity and the shape of the isotherm between the adsorption and desorption branch indicate a change in the adsorbed state of the protein from the loading to the desorption steps.

The Scatchard plot is one of the most widely used methods to obtain a macroscopic indication of the type of cooperativity in the binding reaction. Fig. 7 presents Scatchard plots derived from the adsorption and desorption isotherms. A positive initial slope, characteristic of positive cooperativity in the low protein concentration region, was obtained for the adsorption process, while convex downwards Scatchard plots were observed for the desorption isotherms. Such convex downwards Scatchard plots reveal negative cooperativity in the process represented by the desorption isotherm.

Model for adsorption–desorption hysteresis

Positive cooperativity in the adsorption isotherm at low protein concentration has been previously interpreted in terms of the association of β-lact A protomer (A) in solution to form a stronger adsorbing oligomer (B) with a stoichiometry of two [6]:

$$2A \overset{K_e}{\rightleftharpoons} B \qquad [B] = K_e[A]^2 \tag{3}$$

$$A + mS \underset{k_{-a}}{\overset{k_a}{\rightleftharpoons}} AS_m \tag{4}$$

$$B + nS \underset{k_{-b}}{\overset{k_b}{\rightleftharpoons}} BS_n \tag{5}$$

where K_e is the apparent association equilibrium constant (l/mol) in solution from A to B, S is the available C_1-ether ligand concentration on the surface, k_a and k_{-a} are adsorption and desorption rate constants for the protomer A, respectively, k_b and k_{-b} are adsorption and desorption rate constants for the oligomer B, respectively, and m and n are the number of interaction sites between the surface and the protomer and oligomer, respectively.

Using low-angle laser light scattering (LALLS) [17], we found that under the same buffer conditions as in the isotherm measurement, at pH 4.5 and 5°C, a low concentration (< 1.0 mg/ml) of β-lact A appeared as the dimeric form (experimental MW $\approx$33 000). In the concentration range 1.0–10.0 mg/ml, the scattering function [17] could not be extrapolated to give an exact molecular weight because of changes in the relative amounts of two species in the association equilibrium with protein concentration. As the association was well characterized by a stoichiometry of two [6], it is reasonable to assume that an equilibrium between dimer and tetramer exists in this protein concentration range. Hence the above-discussed protomer represents the dimer (MW 36 800) and the oligomer represents the tetramer (MW 73 600).

According to the rate law, the adsorption rate of the dimer and tetramer can be expressed as

$$dq_A/dt = k_a C_A[S]^m - k_{-a}q_A \tag{6}$$

$$dq_B/dt = k_b C_B[S]^n - k_{-b}q_B \tag{7}$$

where q_A and q_B are the adsorbed concentrations of dimer [AS_m] and tetramer [BS_n] in mg/ml, respectively, and C_A and C_B are the solution concentrations of the dimer A and tetramer B, respectively. At steady state, $dq_A/dt = dq_B/dt = 0$, and eqns. 6 and 7 can be rearranged to

$$q_A = [S]^m(k_a/k_{-a})C_A \tag{8}$$

$$q_B = [S]^n(k_b/k_{-b})C_B \tag{9}$$

Assuming a constant surface availability ([S] = [S_0] = constant) during adsorption in the low concentration region, as applied by Lapidus and Amundson [18] and Golshan-Shirazi and Guiochon [19], we can obtain

$$Q = q_A + q_B = [S]^m(k_a/k_{-a})C_A + [S]^n(k_b/k_{-b})C_B \tag{10}$$

$$Q = K_A C_A + K_B C_B \tag{11}$$

where

$$K_A = [S_0]^m(k_a/k_{-a}) \tag{12}$$

$$K_B = [S_0]^n(k_b/k_{-b}) \tag{13}$$

and K_A and K_B are the apparent adsorption coefficients of dimer A and tetramer B, respectively. From the expression of the solution association constant and total concentration, C, C_A and C_B can be derived as follows:

$$C_B = K_e^* C_A^2 \tag{14}$$

$$C = C_A + C_B \tag{15}$$

where K_e^* is the apparent association constant (ml/mg) in solution from dimer to tetramer when C_A and C_B are in the units of mg/ml. From the model of the stoichiometry of dimer to tetramer, we can derive that

$$C_A = [(1 + 4K_e^*C)^{1/2} - 1]/2K_e^* \tag{16}$$

$$C_B = C - [(1 + 4K_e^*C)^{1/2} - 1]/2K_e^* \tag{17}$$

By substituting eqns. 16 and 17 into eqn. 11, we can obtain an explicit expression for the adsorption isotherm of this aggregating system:

$$Q = K_BC - (K_B - K_A)[(1 + 4K_e^*C)^{1/2} - 1]/2K_e^* \tag{18}$$

This is the same expression as that rearranged from eqn. 17 in ref. 6, except that a factor of 2 has been included in K_e^*. Fitting the experimental data to the isotherm equation and corresponding Scatchard plots, values of $1.8 \cdot 10^4$ ml/mg, 0.34 and 1.2 were obtained for K_e^*, K_A and K_B, respectively.

The desorption rate in an elution process of dimer and tetramer can be expressed as

$$-dq_A/dt = k_{-a}q_A - k_aC_A[S_0]^m(1 - Q/Q_{max}) \tag{19}$$

$$-dq_B/dt = k_{-b}q_B - k_bC_B[S_0]^n(1 - Q/Q_{max}) \tag{20}$$

assuming a saturation capacity Q_{max} for each of the desorption isotherm, Q/Q_{max} is the fractional surface coverage and $(1 - Q/Q_{max})$ represents the availability of the ligand for readsorption. At steady state, $-dq_A/dt = -dq_B/dt = 0$, and substituting eqns. 12 and 13 into eqns. 19 and 20, we obtain

$$q_A = K_AC_A(1 - Q/Q_{max}) \tag{21}$$

$$q_B = K_BC_B(1 - Q/Q_{max}) \tag{22}$$

and

$$Q = \frac{K_A C_A + K_B C_B}{1 + (K_A C_A + K_B C_B)/Q_{max}} \tag{23}$$

By substituting eqns. 16 and 17 into eqn. 23, the desorption isotherm can be expressed as

$$Q = \frac{K_B C - (K_B - K_A)[(1 + 4K_e^* C)^{1/2} - 1]/2K_e^*}{1 + (1/Q_{max})\{K_B C - (K_B - K_A)[(1 + 4K_e^* C)^{1/2} - 1]/2K_e^*\}} \tag{24}$$

Fitting the experimental data in Fig. 6 for the desorption isotherm at pH 4.5 according to the above equation and assuming the value of $1.8 \cdot 10^4$ ml/mg for K_e^*, the apparent adsorption coefficients K_A and K_B for the dimer and tetramer, respectively, during the elution branch of the hysteresis loop can be obtained. The results are given in Table I.

Interestingly, from the adsorption branch to the desorption side of the isotherm a 1.5-fold increase in the adsorption coefficient for the tetramer (K_B) was observed, while the binding constant for the dimer (K_A) remained constant. In addition, K_B for the desorption branches was found to be the same, within experimental error, independent of the adsorption–desorption loop. This result suggests that the increase in K_B from the adsorption branch to the desorption branch is characteristic of the system, as fundamentally an infinite number of loops can be obtained over the whole concentration range. It can thus be seen that the existence of hysteresis is accompanied by the formation of adsorbing species with a significant increase in the apparent adsorption coefficient, as found by others [11].

The increase in the apparent adsorption coefficient for the tetramer may be a consequence of reorientation, *e.g.*, from head-on to side-on or from edge-on to face-on. Based on X-ray scattering results Timasheff and co-workers [20,21] proposed a tetramer sturcture for β-lact A in which the four subunits lie in a distorted plane to form a non-spherical, asymmetric structure. Thus, the accommodation of the adsorbed tetramer from an edge-on to a face-on state on the hydrophobic surface could

TABLE I

PARAMETERS DERIVED FROM ISOTHERM CURVE FITTING

pH	Isotherm branch	Adsorption coefficient	
		Dimer	Tetramer
4.5	Adsorption	0.34	1.2
	Desorption, $C = 15.0 \rightarrow 0$, $Q = 12.6 \rightarrow 0$	0.34	1.9
	Desorption, $C = 10.0 \rightarrow 0$, $Q = 8.85 \rightarrow 0$	0.34	1.8
6.0	Adsorption	0.76[a]	–
	Desorption	0.76[a]	–

[a] Langmuir constant *a*, *i.e*, binding constant for the single species at pH 6.0.

occur with a relatively stronger interaction with the surface after reorientation. It should also be noted that there is no evidence to rule out the possibility of a conformational change on the surface. However, the on-line UV spectra and second-derivative spectra collected during the adsorption and desorption (see earlier) indicate that a major conformational change on the surface is less likely. The constant adsorption coefficient for the dimer, K_A, from the adsorption and desorption branches also points to unlikely unfolding. The larger size and the asymmetric shape of the tetramer may result in different strength upon reorientation on the surface.

CONCLUSIONS

This study has demonstrated the role of protein association on the adsorption of β-lactoglobulin A on a weakly hydrophobic surface. The observed hysteresis in the adsorption and desorption cycles has been analyzed in terms of an increase in the binding of the tetramer while in contact with the surface. Although a conformational change of the tetramer on the surface cannot be ruled out, the asymmetric shape and size of this species make it more likely that a surface reorientation has taken place. If this is so, the reorientation presumably leads to the stronger binding.

It is most interesting that a change in pH of the solution leads to a dramatic change in isotherm behavior. This result is a direct consequence of the significantly reduced tendency of β-lactoglobulin A to protein association at pH 6.0, relative to pH 4.5. A possible strategy for preparative-scale operation emerges from such behavior. Sample loading may take place at pH 4.5 where the anti-Langmuir isotherm leads to a relatively increased amount of adsorption with increased protein solution concentration. Desorption could then take place at pH 6.0 where the protein would presumably be dissociated and only a single species (dimer) would elute for a sharper band profile than if two species were present (*i.e.*, dimer and tetramer) (see Fig. 4). Clearly, full reversibility with change in pH is required for this strategy to be successful.

ACKNOWLEDGEMENTS

The authors gratefully acknowledge the support of this work by NIH under GM-15847 and by Merck, Sharp & Dohme Research Laboratories. They also thank R. Mhatre for assistance in the LALLS measurement of the molecular weight. This is contribution No. 461 from the Barnett Institute.

REFERENCES

1 J. D. Andrade, in J. D. Andrade (Editor), *Surface and Interfacial Aspects of Biomedical Polymers*, Vol. 2, Plenum Press, New York, 1985, p. 1.
2 T. A. Horbett and J. L. Brash, in J. L. Brash and T. A. Horbett (Editors), *Proteins at Interfaces: Physicochemical Aspects and Biomedical Studies*, American Chemical Society, Washington, DC, 1987, p. 1.
3 J. M. Jacobson, J. H. Frenz and Cs. Horváth, *Ind. Eng. Chem. Res.*, 26 (1987) 43.
4 G. Guiochon and A. Katti, *Chromatographia*, 24 (1987) 165.
5 N. Grinberg, R. Blanco, D. M. Yarmush and B. L. Karger, *Anal. Chem.*, 61 (1989) 514.
6 R. Blanco, A. Arai, N. Grinberg, D. M. Yarmush and B. L. Karger, *J. Chromatogr.*, 482 (1989) 1.
7 H. A. McKenzie, in H. A. McKenzie (Editor), *Milk Proteins: Chemistry and Molecular Biology*, Vol. II, Academic Press, New York, 1970, p. 304.

8 T. F. Kumosinski and S. N. Timasheff, *J. Am. Chem. Soc.*, 88 (1966) 5635.
9 H. P. Jennissen, in J. L. Brash and T. A. Horbett (Editor), *Proteins at Interfaces: Physicochemical Aspects and Biomedical Studies*, American Chemical Society, Washington, DC, 1987, p. 295.
10 H. P. Jennissen, in I. M. Chaiken, M. Wilchek and I. Parikh (Editors), *Affinity Chromatography and Biological Recognition*, Academic Press, New York, 1983, p. 281.
11 H. P. Jennissen and G. Botzet, *Int. J. Biol. Macromol.*, 1 (1979) 171.
12 J.-X. Huang, J. Schudel and G. Guiochon, *J. Chromatogr.*, 504 (1990) 335.
13 S.-L. Wu, K. Benedek and B. L. Karger, *J. Chromatogr.*, 359 (1986) 3.
14 N. T. Miller, B. Feibush and B. L. Karger, *J. Chromatogr.*, 316 (1984) 519.
15 F. Riedo and E. Kováts, *J. Chromatogr.*, 239 (1982) 1.
16 J. Jacobson, J. Frenz and Cs. Horváth, *J. Chromatogr.*, 316 (1984) 53.
17 R. Mhate, I. S. Krull and H. H. Stuting, *J. Chromatogr.*, 502 (1990) 21.
18 L. Lapidus and A. R. Amundson, *J. Phys. Chem.*, 56 (1952) 984.
19 S. Golshan-Shirazi and G. Guiochon, *J. Chromatogr.*, 506 (1990) 495.
20 T. T. Herskovits, R. Townend and S. N. Timasheff, *J. Am. Chem. Soc.*, 86 (1964) 4445.
21 S. N. Timasheff and R. Townend, *Nature (London)*, 203 (1964) 517.

Journal of Chromatography, 557 (1991) 383–389
Elsevier Science Publishers B.V., Amsterdam

CHROM. 23 290

High-performance liquid chromatography–atmospheric pressure ionization mass spectrometry of gymnemic acids

TOSHIAKI IMOTO*
Department of Physiology, Faculty of Medicine, Tottori University, Yonago 683 (Japan)
FUMIKO M. YAMAMOTO
Instrumental Analysis Research Center, Faculty of Science Kyoto University, Kyoto 606 (Japan)
AKIKO MIYASAKA
Department of Physiology, Faculty of Medicine, Tottori University, Yonago 683 (Japan)
and
HIROYUKI HATANO
Department of Chemistry, Kanagawa Dental College, Yokosuka 238 and International Institute of Technological Analysis, Health Research Foundation, Kyoto 606 (Japan)

ABSTRACT

Gymnemic acids (GAs), extracted from the leaves of *Gymnema sylvestre*, are a mixture of triterpene glucuronides possessing various physiological activities. The molecular masses of GA homologues were determined with high-performance liquid chromatography combined with atmospheric pressure ionization mass spectrometry.

A mixture of GAs was chromatographed on an octadecyl silica column eluted with an aqueous methanol solution containing ammonium acetate, and directly introduced into an atmospheric pressure ionization mass spectrometer. Quasimolecular ions of GAs were detected as ammonium adduct ions and/or proton adduct ions. Molecular masses of thirteen different GAs and five compounds not containing glucuronic acid in their molecules were evaluated. Three pairs of geometrical isomers of GAs were found.

INTRODUCTION

Gymnemic acids (GAs) are chemical compounds found in the leaves of the Indian plant *Gymnema sylvestre R. Br. (Asclepiadaceae)*. GAs have been found to inhibit various physiological functions, they affect in particular sweet taste sensing in humans as well as in some other species [1–3]. Furthermore, recent studies have revealed the inhibitory action of GAs against glucose uptake in the small intestine of the rat [4], and glucan synthesis by glucosyltransferase (GTase) from *Streptococcus mutans* [5]. These findings suggest that GAs interact with proteins that take part in sugar recognition.

Gymnemic acids are known to be a mixture of glucuronides of hexahydroxy-olean-12-en(triterpene) and some hydroxyl groups of the structural frame are acylated as shown in Fig. 1. The R groups (R_1–R_5) represent hydrogens (H) or acyl residues

0021-9673/91/$03.50

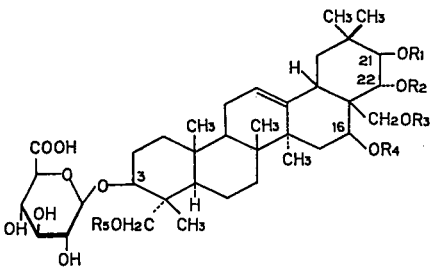

Fig. 1. Presumed molecular structure of gymnemic acid. R_1–R_5 are hydrogen atoms or acyl residues forming ester linkage with triterpene frame.

forming ester linkage with the triterpene framework. Recently, some GA homologues have been isolated, and acetyl, tigloyl and 2-methylbutanoyl residues have been identified as the constituents of R groups by nuclear magnetic resonance (NMR) and mass spectrometric (MS) techniques [6–8]. However, there are the least a few tens of homologues in the leaves, with structures as yet unknown.

In the present study, the GAs were divided into their homologues by molecular mass on an octadecyl silica (ODS) column. The molecular mass and the chemical structure of each GA homologue were investigated by using a combined system of high-performance liquid chromatography (HPLC) and MS.

EXPERIMENTAL

Dried leaves of *Gymnema sylvestre* imported from India were used in this work. Mixtures of GA homologues were extracted according to the method described by Kurihara [2].

The molecular masses of GAs were determined with a Hitachi 655A high-performance liquid chromatograph connected to a Hitachi M-80 mass spectrometer by an interface consisting of a nebulizer and a vaporizer through a PTFE tube (Hitachi, Tokyo, Japan). The vaporized sample and solvent molecules at 300°C were introduced into the ion source of the atmospheric pressure ionization (API) MS system. The drift voltage of spectrometer was set at 160 V.

Chromatography was done on a conventional ODS column (YMC-A312, 150 × 6 mm I.D.; Yamamura, Kyoto, Japan). Mobile phases were prepared as follows: mobile phase A, 0.1 *M* ammonium acetate–methanol (35:65, v/v); mobile phase B, 0.1 *M* ammonium acetate–methanol (10:90, v/v). Isocratic elution was used for 30 min after sample injection, followed by gradient elution from A to B in 10 min. The GA solution (10 mg/ml in the initial mobile phase) was injected via valve equipped with a 10-μl loop, and was eluted at a flow-rate of 1.0 ml/min at room temperature.

All chemicals were purchased from Wako (Tokyo, Japan) and Nacalai Tesque (Kyoto, Japan).

RESULTS AND DISCUSSION

Two HPLC chromatograms of GA mixtures on an ODS column are shown in Fig. 2. Chromatogram a was obtained by using acidic (pH 3.2) mobile phase (metha-

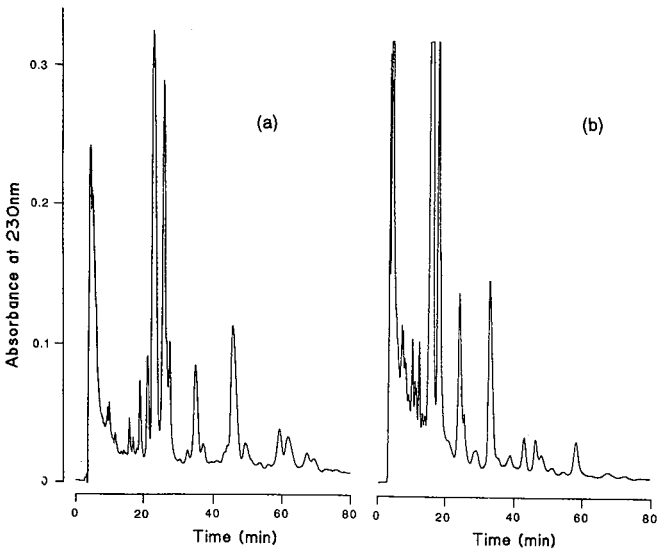

Fig. 2. Chromatograms of a mixture of GAs obtained with (a) the acidic mobile phase (methanol–water–acetic acid; 64:36:0.5 v/v/v, pH 3.2) and (b) the neutral mobile phase (methanol–0.02 *M* phosphate buffer; 60:40 v/v, pH 8.5) In each case, 1 mg of the sample was loaded on an ODS column (YMC A-312, 150 × 6 mm I.D. Temperature, 25°C; detection, UV at 230 nm.

nol–water–acetic acid, 64:36:0.5 v/v/v) and chromatogram b using a neutral (pH 8.5) mobile phase (methanol–0.02 *M* phosphate buffer, 60:40 v/v). In both chromatograms many peaks were observed. As the dissociation of the carboxyl group of glucuronic acid in the GA molecules progressed, the GA molecules became less hydrophobic in the neutral mobile phase than in the acidic mobile phase. In other words, the neutral mobile phase was a rather stronger eluent for GAs than the acidic mobile phase. We also examined the effect of the methanol concentration in the eluent on the retention of GAs. The retention volume of GAs depended on the methanol concentration in the eluent rather than the eluent pH. Therefore, we used a gradient for the methanol concentration in the eluent, as described under Experimental. Some components were much more hydrophobic and eluted with 90% (v/v) methanol, as shown in Fig. 3.

Components in Fig. 2 with retention times less than *ca.* 10 min were considered to be impurities. These were removed by semi-preparative ODS column chromatography before the experiment was performed in order to minimize contamination of the interface from extraneous materials.

Fig. 3 shows a total ion current (TIC) profile over the range *m/z* 400–1000 for the sample solution thus prepared and directly introduced from the column into the APIMS system. As shown, the concentration of methanol in the eluent was increased gradually from 65% to 90% in 10 min after 30 min from the start in order to shorten the analysis time. The addition of ammonium acetate to the eluent was useful to enhance the ionization efficiency of the sample molecule. Under the experimental conditions, quasimolecular ions were observed as ammonium adduct ions $[M + NH_4]^+$ and/or as proton adduct ions $[M + H]^+$.

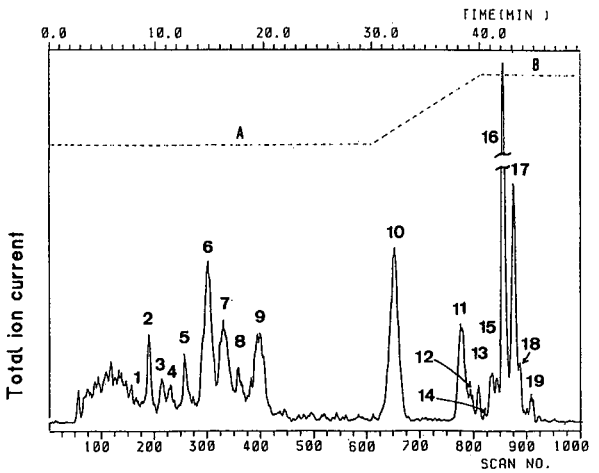

Fig. 3. Total ion current profile of LC–API-MS of GA mixture Total mass range, *m/z* 400–1000; column, ODS (YMC A-312, 150 × 6 mm I.D.); eluents: A = 0.1 *M* ammonium acetate–methanol (35:65, v/v), B = 0.1 *M* ammonium acetate–methanol (10:90 v/v). Gradient elution was begun after 30 min, from 100% A to 100% B in 10 min. Flow-rate, 1.0 ml/min.

The peaks numbered from 1 to 19 in Fig. 3 were selected for the analyses of their mass spectra. Some of these spectra are shown in Fig. 4. Ammonium adduct ions were observed at *m/z* 782 for component 3 and at *m/z* 784 for components 2 and 4: their molecular masses were determined to be 764, 766 and 766, respectively. As the calculated molecular mass of GAs with no acyl residues (R_1–R_5 = H) is 682, the molecular masses of 764 and 766 are consistent with molecular masses of GA homologues containing tigloyl (Tig, *m/z* 82) and 2-methylbutanoyl (MB, *m/z* 84) residues, respectively. The fragment ion at *m/z* 608 in the mass spectrum of component 2 differs from the quasimolecular ion at *m/z* 784 by 176 mass units. So this ion could be attributed to the ammonium adduct ion of the aglycone formed by loss of a glucuronic acid (glcUA) from the ammonium adduct molecular ion at *m/z* 784, which was represented as $[M + NH_4 - glcUA]^+$. The proton adduct ion of the aglycone was also observed at *m/z* 591 in the spectrum of component 2. Furthermore, the peak at *m/z* 471 of component 2 is 120 mass units lower than the fragment ion at *m/z* 591. This ion may be attributed to the fragment ion formed by successive loss of two molecules of water (*m/z* 36) and a 2-methylbutanoyl residue (*m/z* 84) from the proton adduct ion *m/z* 591, $[M + H - glcUA - MB - 2H_2O]^+$.

Similar fragment ions were observed for component 3 at *m/z* 589 and 471. The mass difference of 118 between these two fragment ions, which was two mass units lower than that in the case of component 2, was again consistent with the proposal that the component 3 contained a tigloyl residue. The fragment ions at *m/z* 589 and 471 were thus attributed to $[M + H - glcUA]^+$ and $[M + H - glcUA - tigloyl - 2H_2O]^+$, respectively. For component 4, which is a geometrical isomer of component 2, however, a fragment ion due to the loss of the acyl group was not found, although the fragment ion due to glycoside bond cleavage was clearly apparent at *m/z* 591.

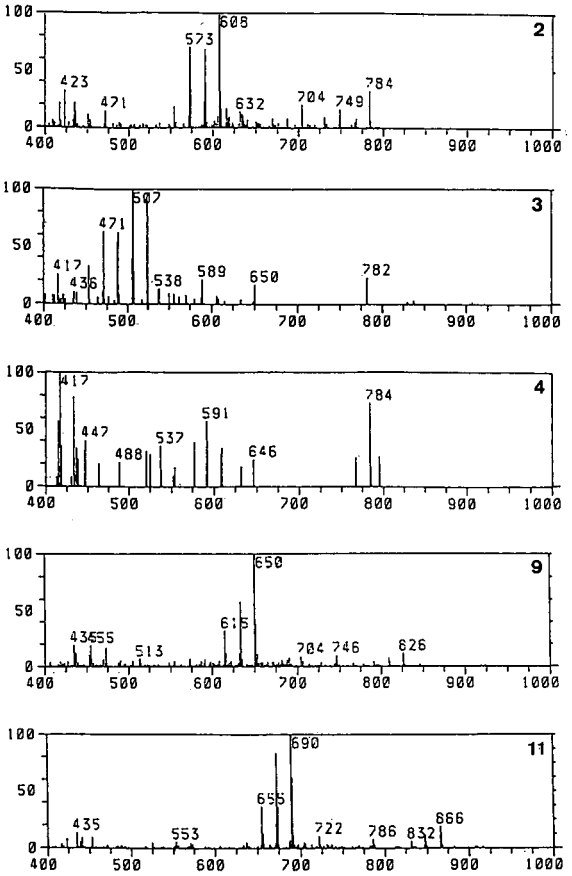

Fig. 4. Typical mass spectra obtained by LC–API-MS. Numbers in the upper right-hand corner of each spectrum correspond to the peak numbers in the total ion current profile in Fig. 3. In each spectrum, the percentage intensity of the ionic current compared with the maximum current in the mass range (m/z) from 400 to 1000 is shown as the ordinate.

Comparing the spectrum of component 9 with that of component 2, both the quasimolecular ion at m/z 826 and the fragment ions at 650, 615, and 513 differ by 42 mass units from those ions of component 2 at m/z 784, 608, 573, and 471, respectively. Therefore, component 9 was consistent with the compound containing an additional acetyl residue to component 2.

The peaks at m/z 866, 690 and 553 in the spectrum of component 11 correspond to those at m/z 784, 608 and 471, respectively, for component 2, increased by 82 mass units. This strongly suggests that component 11 is the homologue formed by further acylation of component 2 with the tigloyl residue. Similar analyses were done for the other fourteen components selected from Fig. 3.

Table I lists the quasimolecular ions, the presumed molecular masses, the fragment ions due to glycosidic bond cleavage and the presumed acyl residues for seventeen components. The data for components 7 and 8 are not listed because their mass spectra showed very complex patterns, indicating that these components were mix-

TABLE I

SUMMARY OF ANALYSIS OF MASS SPECTRA OBTAINED BY LC–API-MS

Component	Quasimolecular ion		Molecular mass	Fragment ion[a]		Presumed acyl residues[b]
	NH_4^+ adduct	H^+ adduct		NH_4^+ adduct	H^+ adduct	
1	782		764			Tig
2	784		766	608	591	MB
3	782		764		589	Tig
4	784		766		591	MB
5		791	790		615	
6[c]	826	(807)	808, (806)	648		MB, (Tig), Ac
9	826		808	650		MB, Ac
10	654		636			
11	866		848	690		MB, Tig
12	864		846		671	Tig, Tig
13	888		870	712		MB, Bz
14			766		573	
15		767	766	608		
16		591	590			
17	638		620			
18		591	590			
19		689	688			

[a] Formed by glycosidic bond cleavage.
[b] Abbreviations: Tig = tigloyl; MB = 2-methylbutanoyl; Ac = acetyl; Bz = benzoyl.
[c] Consist of two components.

tures of two or more compounds. Thirteen components in Table I were identified as GA homologues containing glcUA. Three pairs of isomers were found, whose molecular masses were 764, 766 and 808.

The molecular mass 870 of component 13 was the largest for GA homologues found in the present experiment. The mass difference between component 13 and components 2 and 4 was 104. NMR studies revealed some homologues that showed resonance lines attributable to the benzoyl residue (Bz, m/z 104). Therefore, component 13 was identified as the GA homologue derived by further acylation of component 2 or 4 with the benzoyl residue.

The presumed molecular masses of components 14 and 15 (both 766) are the same as those of components 2 and 4. However, these components could not simply be attributed to isomers of components 2 and 4. As shown in Fig. 3, components 14 and 15 were eluted by a higher methanol concentration in the eluent, suggesting that they passess a more hydrophobic structure than components 2 and 4. Therefore, the genins of components 14 and 15 may differ from gymnemagenin. For example, gymnestrogenin, which was proposed by Sinsheimer and Rao [9], is more hydrophobic than gymnemagenin, because gymnestrogenin lacks a hydroxyl group at C-22 of gymnemagenin (Fig. 1).

The molecular masses of components 16 to 19 were smaller than those of the compounds eluted before component 16. Furthermore, the fragment ions due to glycosidic cleavage were not observed in their spectra. It was suggested from these results that they corresponded to aglycones without a sugar moiety in the molecules.

In fact, the proton adduct molecular ion at *m/z* 591 of component 16 or 18 was the same as that of the fragment ion identified for component 2 or 4.

Present work showed that using LC–MS was quite useful for analysis of such a complex mixture of homologues as gymnemic acids. One of the advantages of using the API interface is that any conventional column can be used without placing a restriction on the choice of flow-rate or mobile phase. In fact, no special design was necessary in carrying out HPLC, except for the addition of ammonium acetate to the mobile phase.

In this study, the molecular masses of thirteen GA homologues and related components were determined. In addition, the acyl residues such as acetyl, tigloyl, 2-methylbutanoyl and benzoyl in GA molecules were identified by analysis of the fragmentation patterns. The GA homologue containing a benzoyl residue was the first one that we identified in the GA mixture. Moreover, we were able to identify three pairs of geometrical isomers in GA mixture. On the basis of the information obtained from the results of LC–API-MS, we are now investigating the complete chemical structures of each GA homologue by in-beam MS and NMR.

ACKNOWLEDGEMENTS

The authors thank Professor Yasutake Hiji for his support in this investigation. They also thank Dr. Shigetake Ganno, Mr. Yoshiaki Kato, and Ms Youko Numajiri, Hitachi Ltd., for their technical assistance with the LC–API-MS measurements and for helpful discussions.

REFERENCES

1 D. Hooper, *Pharm. J. Trans.*, 17 (1887) 867.
2 Y. Kurihara, *Life Sci.*, 8 (1969) 537.
3 D. Glaser, G. Hellekant, J. N. Brouwer and H. van der Wel, *Chem. Senses*, 8 (1984) 367.
4 S. Yoshioka, *J. Yonago Med. Assoc.*, 37 (1986) 142.
5 M. Miyoshi, T. Imoto and T. Kasagi, *J. Yonago Med. Assoc.*, 38 (1987) 127.
6 M. Maeda, T. Iwashita and Y. Kurihara, *Tetrahedron Lett.*, 30 (1989) 1547.
7 K. Yoshikawa, K. Amimoto, S. Arihara and K. Matsuura, *Chem. Pharm. Bull.*, 37 (1989) 852.
8 K. Yoshikawa, K. Amimoto, S. Arihara and K. Matsuura, *Tetrahedron Lett.*, 30 (1989) 1103.
9 J. E. Sinsheimer and G. S. Rao, *J. Pharm. Sci.*, 59 (1970) 629.

Journal of Chromatography, 557 (1991) 391–398
Elsevier Science Publishers B.V., Amsterdam

CHROM. 23 287

Isolation and determination of flavonol glycosides from *Epilobium* species

I. SLACANIN, A. MARSTON and K. HOSTETTMANN*
Institut de Pharmacognosie et Phytochimie, Université de Lausanne, B.E.P., CH-1005 Lausanne-Dorigny (Switzerland)
and
N. DELABAYS and C. DARBELLAY
Médiplant, Centre des Fougères, CH-1964 Conthey (Switzerland)

ABSTRACT

Centrifugal partition chromatography has been applied to the separation of flavonol glycosides from *Epilobium parviflorum* (Onagraceae). Using these glycosides, a method is described for their determination in different species of *Epilobium* by high-performance liquid chromatography on an octadecylsilyl column.

INTRODUCTION

The genus *Epilobium* (family Onagraceae) consists of over 200 species, sixteen of which are found in Switzerland and the most common being *E. angustifolium*. The commercially available plant drug *Epilobii herba* contains the dried aerial parts of several species, most notably *E. parviflorum*, *E. montanum* and *E. roseum*. Various members of the genus *Epilobium*, in particular *E. parviflorum*, have been used in folk medicine for the treatment of adenoma and inflammation of the prostate [1,2]. The constituents of *Epilobium* are not well known, but the presence of sterols [3], triterpenes and flavonoids (flavonol aglycones and glycosides) [4] has been reported. The active principles have not yet, however, been identified and it has been necessary to select suitable constituents for standardisation purposes. As the flavonoid glycosides occur in relatively large amounts, they have been chosen as markers.

The first part of this investigation involved the isolation of the major flavonoid glycosides quercitrin (1), myricitrin (2) and isomyricitrin (3) from *E. parviflorum*, using centrifugal partition chromatography (CPC) as the central separation step. This is a recently developed liquid–liquid technique which allows rapid separations without the problems of irreversible adsorption and decomposition which frequently occur in chromatography on solid supports [5,6]. CPC has multiple applications, especially in the area of polar natural products [7].

The determination of quercitrin, myricitrin and isomyricitrin in several different species of *Epilobium* was then undertaken. Finally, the extracts were hydrolysed to determine the principal aglycones formed.

0021-9673/91/$03.50

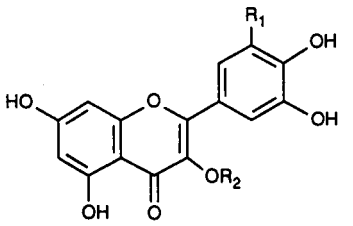

1	R_1 = H	R_2 = Rha	(quercitrin)
2	R_1 = OH	R_2 = Rha	(myricitrin)
3	R_1 = OH	R_2 = Glc	(isomyricitrin)
4	R_1 = H	R_2 = Glc	(isoquercitrin)
5	R_1 = H	R_2 = H	(quercetin)
6	R_1 = OH	R_2 = H	(myricetin)

EXPERIMENTAL

Apparatus

CPC was performed at *ca.* 20°C with an Ito multi-layer coil separator–extractor (P.C., Potomac, MD, USA), equipped with a 2.6 mm I.D. coil (volume 360 ml), sample loop and valve to allow switching of the solvent to the "head" or "tail" ends of the coil. Solvent delivery was by two Waters Assoc. 6000A high-performance liquid chromatography (HPLC) pumps [8]. The instrument was filled with 80% upper phase and 20% lower phase, and connected to a Büchi 683 detector (254 nm) (Büchi, Flawil, Switzerland), a Model 600 chart recorder (W + W Scientific, Basle, Switzerland) and an Ultrorac II fraction collector (Pharmacia, Bromma, Sweden).

HPLC–UV analyses were carried out on a system consisting of a Spectra-Physics 8700 pump (San Jose, CA, USA), a Rheodyne injector, a Hewlett-Packard (HP) 1040A photodiode array detector (Palo Alto, CA, USA), an HP-85 computer and an HP 7470A plotter. Quantitative analyses were performed with a Spectra-Physics 8800 pump connected to a Pharmacia 2151 variable-wavelength monitor and a Pharmacia 2221 integrator.

The chromatographic separations were run on Waters 4 μm NovaPak C_{18} (15 cm × 3.9 mm I.D.) and 10 μm μBondapak C_{18} (30 cm × 3.9 mm I.D.) columns and the samples were filtered over HV 0.45 μm units (Millipore, Bedford, MA, USA).

Plant material

Rosebay willowherb (*E. angustifolium*) was purchased from Siegfried (Zofingen, Switzerland), while the other species of *Epilobium* were collected at the Domaine expérimental de Bruson (Station fédérale de recherche agronomique, CH-1934 Bruson, Valais, Switzerland) in July 1989.

Isolation of flavonoid glycosides

The aerial parts (200 g) of *E. parviflorum* were extracted first with dichloromethane (3 × 2000 ml) and then with methanol (3 × 2000 ml). A part (2 × 2 g) of the

methanol extract (16.3 g) was chromatographed by CPC, using the solvent system chloroform–methanol–water (7:13:8, v/v), with the lower phase as the mobile phase. Four major fractions (I–IV) were obtained. Gel permeation chromatography (GPC) of fraction I on Sephadex LH-20 (methanol) yielded quercitrin (1) (25 mg), whereas GPC of fraction II under the same conditions gave myricitrin (2) (35 mg), isomyricitrin (3) (18 mg) and gallic acid (26 mg). The structures of 1–3 were confirmed by UV, mass spectrometry, ^{1}H and ^{13}C nuclear magnetic resonance spectroscopy, acidic hydrolysis and comparison with authentic samples.

Chromatographic conditions

The separations of glycosides were performed on a NovaPak column with a linear gradient of acetonitrile in water (10:90 to 25:75), each containing 2% orthophosphoric acid, over 30 min. The flow-rate was 1 ml/min and detection was at 350 nm. For the aglycones, a μBondapak column and a linear gradient of acetonitrile–water (20:80 to 60:40) over 20 min were used.

Quantitative analyses

The aerial parts (2.0 g) of each *Epilobium* species were extracted with 25% aqueous ethanol (200 ml) at room temperature for 24 h. After filtration, the solvent was removed by evaporation under reduced pressure and lyophilisation. A portion of the residue (10 mg) was taken up in methanol (1 ml).

Quantitative determinations were carried out with the flavonol aglycone myricetin as an internal standard. A 1 ml volume of a 1 mg/ml solution in methanol was added to 2 ml of a 10 mg/ml solution of *Epilobium* extract and 10 μl of the resulting solution was injected onto the HPLC column. A solution containing 0.25 mg/ml of the standard and each of the three flavonol glycosides 1–3 was used to calculate the correction factors. To obtain the standard correction factor (SCF) for the three glycosides, different volumes of the mixture were each injected three times and the SCF was calculated as follows:

$$\mathrm{SCF} = \frac{A(\mathrm{L})\ W(\mathrm{St})}{A(\mathrm{St})\ W(\mathrm{L})}$$

where $A(\mathrm{L})$ = peak area of flavonol glycoside, $A(\mathrm{St})$ = peak area of myricetin standard, $W(\mathrm{L})$ = weight of flavonol glycoside and $W(\mathrm{St})$ = weight of myricetin standard. The correction factors calculated were: quercitrin = 1.74, myricitrin = 1.67 and isomyricitrin = 1.73.

The linearity of the relationship between peak area and amount injected (over the range used for the determination) was checked by constructing calibration graphs for each of the flavonol glycosides.

The flavonol glycosides 1–3 in *Epilobium* extracts were determined by injecting samples with myricetin (prepared as described above) and calculating their content from the standard correction factors. HPLC runs were performed in triplicate to obtain the average results.

Hydrolyses

A portion (20 mg) of the 25% ethanolic plant extract was treated with 2 *M*

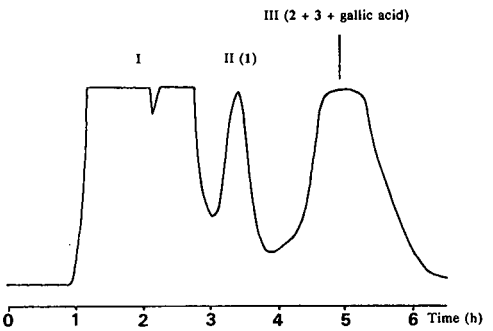

Fig. 1. CPC of a methanol extract of *E. parviflorum* (Onagraceae) aerial parts on a multi-layer coil separator–extractor. Solvent, chloroform–methanol–water (7:13:8) (mobile phase = lower phase; 80% stationary phase in coil); flow-rate, 3.5 ml/min; 700 rpm; detection, 254 nm; sample, 2 g.

hydrochloric acid (50 ml) at 70°C for 1 h. After cooling, the acidic solution was extracted with ethyl acetate (3 × 50 ml) and the organic layer was washed with water (2 × 50 ml). After evaporation, the residue was dissolved in methanol (1 ml) and 10 μl of this solution was injected for HPLC analysis.

RESULTS AND DISCUSSION

The initial isolation step for obtaining flavonol glycosides from the aerial parts of *E. parviflorum* was liquid–liquid partition chromatography on the Ito multi-layer coil separator–extractor. Using a chloroform–methanol–water solvent system, charges of 2 g could be loaded onto the instrument (Fig. 1). As the lower phase was used as the mobile phase, lipophilic compounds eluted at the beginning of the separation (band I). Of the glycosides, the first to elute was quercitrin (1), contained in band II (60 mg). This only needed a subsequent GPC step for final purification. Three substances eluted together under peak III (130 mg). This mixture of myricitrin (2), isomyricitrin (3) and gallic acid was separated by Sephadex LH-20 GPC. The three glycosides obtained in this way were used as reference compounds. The remainder of the extract injected into the chromatograph was eluted by running the upper phase of the two-phase system as the mobile phase and changing the direction of flow.

Quantitative analyses of the flavonol glycosides were performed with myricetin (6) (the aglycone of 2 and 3) as internal standard, as this compound elutes just after the glycosides and does not interfere with the peaks important for the determinations. A chromatogram of the 25% ethanolic extract of the aerial parts of *E. parviflorum* is shown in Fig. 2, with detèction at 350 nm. Myricitrin (2) is the major constituent, while quercitrin (1) and isomyricitrin (3) occur in smaller amounts. Trace amounts of other polyphenolic glycosides are present and chlorogenic acid elutes at 3.8 min (identified by co-elution and comparison of the UV spectra with an authentic sample). The UV spectra of the flavonol glycosides were obtained by the use of a diode-array detector.

A similar chromatogram for the ethanolic extract of the aerial parts of *E. roseum* is shown in Fig. 3. Again, myricitrin (2) is the major component. Chlorogenic acid (retention time 3.9 min) is present in higher concentrations than for *E. parviflorum*. The

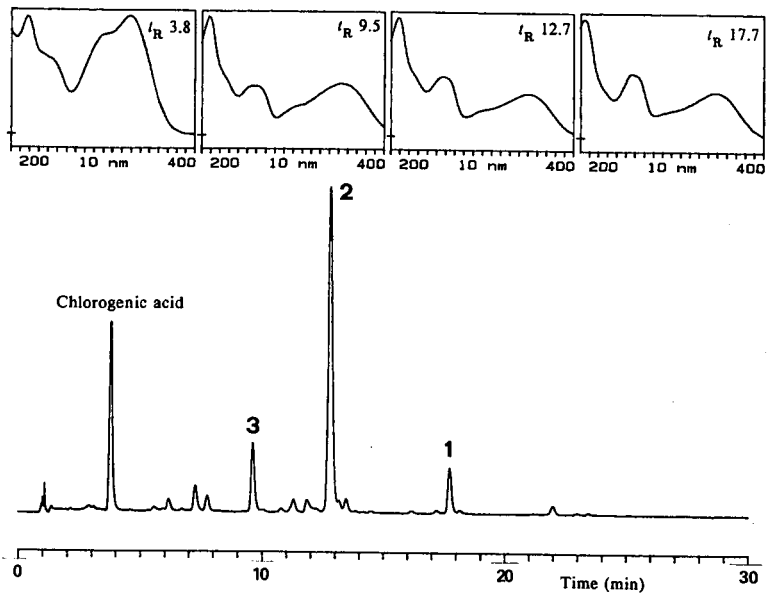

Fig. 2. HPLC separation of a 25% ethanol extract of the aerial parts of *E. parviflorum*. (1) Quercitrin, (2) myricitrin, (3) isomyricitrin. Column, NovaPak C_{18} (15 cm × 3.9 mm I.D.); eluent, 10% acetonitrile (containing 2% orthophosphoric acid) increasing to 25% acetonitrile over 30 min; flow-rate, 1 ml/min; detection, 350 nm.

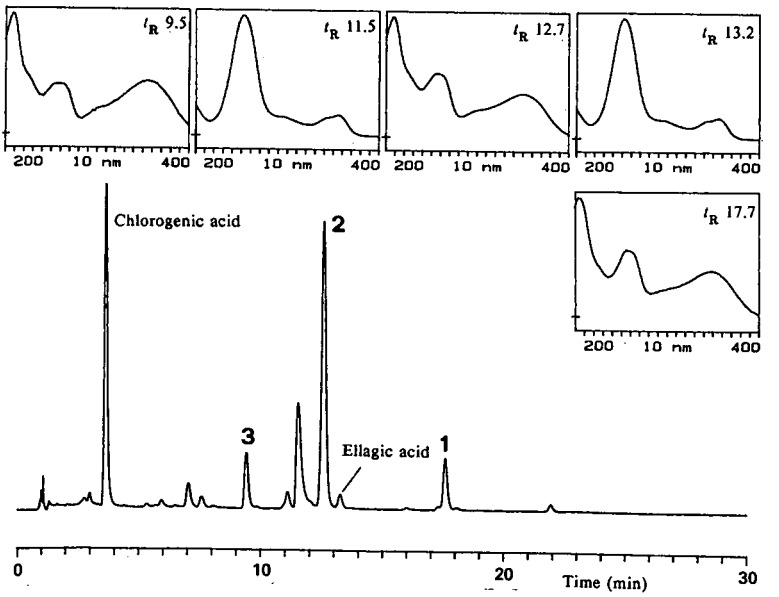

Fig. 3. HPLC separation of a 25% ethanol extract of the aerial parts of *E. roseum*. Conditions and peaks as in Fig. 2.

TABLE I

QUANTITATIVE DETERMINATION OF FLAVONOL GLYCOSIDES IN 25% ETHANOLIC EXTRACTS OF AERIAL PARTS OF EUROPEAN *EPILOBIUM* SPECIES

Species	Glycosides (%)		
	Quercitrin (1)	Myricitrin (2)	Isomyricitrin (3)
Epilobium parviflorum B1	0.24	2.13	1.31
Epilobium roseum C2	0.23	2.26	0.23
Epilobium montanum B1	0.23	2.08	1.23
Epilobium hirsutum B1	0.22	1.50	0.55
Epilobium hybridum B1	0.23	1.94	1.00
Epilobium dodonaei C1	0.22	1.49	0.92
Epilobium tetragonum B1	0.23	1.36	1.37
Epilobium alpinum C1	0.26	4.48	0.55

peak at 13.2 min was identified as ellagic acid by comparison with an authentic sample, whereas the peak eluting at 11.5 min has a UV spectrum very similar to that of ellagic acid and is not of a flavonoid nature.

The amounts of the three marker flavonol glycosides 1–3 in the aerial parts (ethanol extract) of eight different species of *Epilobium* collected in Valais, Switzerland, are shown in Table I. All contain differing amounts of the three glycosides. Except for *E. tetragonum*, myricitrin is always present in the largest amount. The highest percentage of myricitrin is found in *E. alpinum*. Myricitrin and isomyricitrin occur in equal amounts in *E. tetragonum* but, as in all the other species, the amount of quercitrin is the smallest of the three glycosides.

Analysis of the commonly found *E. angustifolium* gives a completely different flavonoid pattern from the other species. Instead of having myricitrin as the main

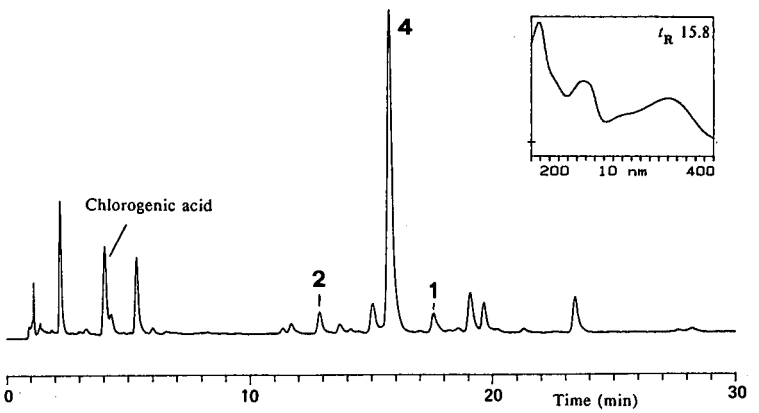

Fig. 4. HPLC separation of a 25% ethanol extract of the aerial parts of *E. angustifolium*. (4) Isoquercitrin. Conditions as in Fig. 2.

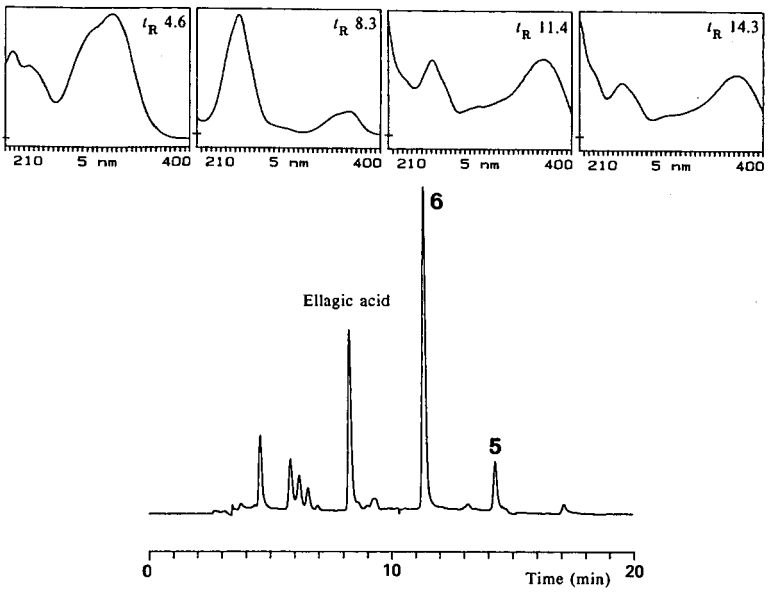

Fig. 5. Analytical HPLC of the acid hydrolysate from a 25% ethanolic extract of *E. parviflorum* aerial parts. 5 = Quercetin; 6 = myricetin. Column, μBondapak C_{18} (30 cm × 3.9 mm I.D.); eluent, 20% acetonitrile (containing 2% orthophosphoric acid) increasing to 60% acetonitrile over 20 min; flow-rate, 1 ml/min; detection, 350 nm.

constituent, isoquercitrin (4) (retention time 15.8 min) was identified as the most important flavonoid in the ethanolic extract (Fig. 4). A small amount of chlorogenic acid was also present (retention time, t_R 3.9 min). The analytical HPLC method described here thus provides a useful means of distinguishing the large-flowered *E. angustifolium* from the smaller-flowered species shown in Table I.

Acidic hydrolysis of the *Epilobium* extracts gave the corresponding aglycones, quercetin (5) and myricetin (6), of the glycosides 1–3. This can be seen in the HPLC chromatogram of the *E. parviflorum* hydrolysate (Fig. 5). Myricetin (6) is the predominant aglycone, with smaller amounts of quercetin (5). A trace of kaempferol elutes with a retention time of 17.2 min. The peak at t_R 4.6 min has a UV spectrum (diode-array detector) very similar to that of chlorogenic acid, while the slower-running peak (t_R 8.3 min) has a UV spectrum characteristic of phenolic acids; this was confirmed as ellagic acid by comparison with an authentic sample.

CONCLUSIONS

CPC is a very rapid and efficient technique for the fractionation of crude extracts. In the application illustrated here, the initial purification of a relatively large (2 g) amount of polar phenolic glycosides was possible, without encountering the problems of irreversible adsorption frequently encountered when using chromatography with solid supports. For the final purification of the glycosides, a single GPC step was necessary.

The three flavonol glycosides isolated are useful markers for the standardisation

of different batches of *Epilobium* plant material as they are present in all the small-flowered species analysed. Their determination is straightforward and involves a simple extraction step with ethanol. In all the samples investigated, no interference from other compounds was experienced. Thus, although the active principles in *Epilobium* are not yet known, a reliable method for the quality control of the crude plant drug now exists. This should be of considerable use when comparing different batches of *Epilobium* species from large-scale cultivation.

ACKNOWLEDGEMENT

Financial support has been kindly provided by the Swiss National Science Foundation.

REFERENCES

1 A. Hiermann, H. Juan and W. Sametz, *J. Ethnopharmacol.*, 17 (1986) 161.
2 K. Hostettmann and M. Hamburger, *Rev. Hort. Suisse*, 63 (1990) 8.
3 A. Hiermann and K. Mayr, *Sci. Pharm.*, 53 (1985) 39.
4 A. Hiermann, *Sci. Pharm.*, 51 (1983) 158.
5 Y. Ito, *Crit. Rev. Anal. Chem.*, 17 (1986) 65.
6 Y. Ito, *J. Biochem. Biophys. Methods*, 5 (1981) 105.
7 A. Marston, I. Slacanin and K. Hostettmann, *Phytochem. Anal.*, 1 (1990) 3.
8 I. Slacanin, A. Marston and K. Hostettmann, *J. Chromatogr.*, 482 (1989) 234.

Journal of Chromatography, 557 (1991) 399–411
Elsevier Science Publishers B.V., Amsterdam

CHROM. 23 252

Influence of mobile phase composition on evaluation of lipophilicity by partition chromatography

M. KUCHAŘ*, E. KRAUS and M. JELÍNKOVÁ
Research Institute for Pharmacy and Biochemistry, 130 60 Prague (Czechoslovakia)

ABSTRACT

The problems of the concentration dependence of retention indices and the applicability of extrapolated values in the evaluation of lipophilicity were studied. The reversed-phase high-performance liquid chromatography of arylalkanoic acids were carried out with experimental data for substituted estra-1,3,5 (10)-trienes, benzodiazepines, dermorphine derivatives and dansylamides selected from the literature for this purpose. Fair linear relationships between slopes of concentration dependences and extrapolated and non-extrapolated values of R_M and log k' were found. Equivalence of these indices in the evaluation of lipophilicity can be inferred. Statistically significant dependences of log P ($\Sigma\pi$) values on concentration slopes make it possible to use them as new parameters of lipophilicity. The goodness of fit of these relationships increases when the values of $E_T(30)$, as a measure of the solvatochromic solvent polarity of mobile phases, are used instead of the change in modifier concentration.

INTRODUCTION

Lipophilicity is one of the inherent properties of chemical compounds, affecting their biological activity. It plays a determinant role in the transport of compounds through a biological system and it may also influence the formation of a complex between a compound and a receptor or a biomacromolecule at the site of action. Partition chromatography is widely used in the evaluation of lipophilicity [1–4]. Application of partition chromatography for such a purpose follows from the relationship between suitable retention indices and partition coefficient, P_s, determined in the chromatographic system. A suitable index in thin-layer chromatography (TLC) is R_M, which is related to the experimental R_F value and depends linearly on log P_s [5]. The logarithm of the capacity factor, log k' [6,7], is equivalent to R_M in high-performance liquid chromatography (HPLC). R_M or log k' values can be used directly as lipophilicity parameters. Another possibility is the application of linear relationships between retention indices and log P, determined in the reference system octanol–water, for the calculation of log P from experimental values of R_M or log k'. In such a case, it is necessary that Collander's linear relationship [8] holds for the chromatographic and the reference system octanol–water:

$$\log P = a \log P_s + b \quad (1)$$

0021-9673/91/$03.50

It follows that

$$\log P = a R_M (\log k') + b \tag{2}$$

The statistical significance of these relationships depend on the type of chromatographic system and a suitable choice of the series of compounds tested.

The use of retention indices extrapolated to pure water as a mobile phase is a commonly discussed problem accompanying the utilization of chromatographic parameters for the evaluation of lipophilicity. Methanol, acetone or acetonitrile is usually used as a modifier and their concentration has a significant effect on the mobility of separated compounds. Soczewinski and Wachtmeister [9] found that R_M values are frequently linearly dependent on the composition of the mobile phase. For a binary mixture, this function can be expressed as

$$R_M = \varphi_1 R_M(1) + \varphi_2 R_M(2) \tag{3}$$

where φ_1 and φ_2 are the volume functions of the two components in the binary mobile phase and $R_M(1)$ and $R_M(2)$ are the R_M values in pure components of the mobile phase. It follows from eqn. 3 that

$$R_M = R_M^0 - a \varphi \tag{4a}$$

where φ is the fraction of the modifier and R_M^0 is the value of R_M when $\varphi = 0$. For reversed-phase HPLC, Schoenmakers *et al.* [10] suggested that the relationship between solute retention ($\log k'$) and the concentration φ of the modifier can be expressed by the equation

$$\log k' = \log k'_0 + A \varphi^2 - B\varphi \tag{4b}$$

where A and B are constants. Snyder *et al.* [11] showed that a linear relationship expressed by the equation

$$\log k' = \log k'_0 - a \varphi \tag{4c}$$

is valid over a limited range of concentration φ of the modifier.

Such expressions can be used for calculation of theoretical values of retention indices, R_M^0 and $\log k'_0$, extrapolated to pure water. A number of workers [12–15] consider that these values are more suitable as lipophilicity parameters than experimental values determined at a particular concentration of the modifier in the mobile phase. There are two reasons for this consideration: (a) R_M or $\log k'$ scales are extended, which allows better resolution in the characterization of lipophilicity; (b) lipophilicity is better expressed by R_M^0 or $\log k'_0$ calculated in the extrapolated system, as such a system is closer to the reference system octanol–water. Whereas the first reason is clear-cut, the second is less so. Chromatographic indices determined at different φ were often found to be equivalent for the evaluation of lipophilicity.

Some years ago, we compared [16] retention indices R_M and $\log k'$ obtained from TLC and HPLC, respectively, using mobile phase with a modifier or extrapolated to pure water. Eqns. 5 and 7 were obtained for non-extrapolated retention indices, and eqns. 6 and 8 for indices extrapolated to pure water. An increase in selectivity of the evaluation of lipophilicity is indicated by a decrease in the slopes in eqns. 6 and 8. At the same time, however, the statistical significance of both equations is slightly diminished.

	n^a	r^a	s^a	F^a	
$\log P = 1.990\ R_M^{50} + 2.399$	11	0.998	0.048	2048.8	(5)
$\log P = 0.797\ R_M^0 + 1.763$	11	0.991	0.097	494.7	(6)
$\log P = 1.790 \log k'_{60} - 1.971$	12	0.999	0.024	8353.2	(7)
$\log P = 1.103 \log k'_0 - 0.926$	12	0.991	0.097	527.0	(8)

This paper considers more deeply the problem of concentration dependences of retention indices in the evaluation of lipophilicity.

EXPERIMENTAL

TLC of compounds I–III

To prepare the stationary phase, silanized Kieselgel 60 F_{254} (E. Merck, Darmstadt, Germany) was impregnated by washing glass plates (20 × 10 cm) with a 5%

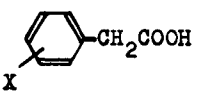

I

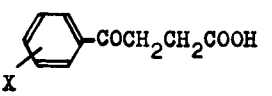

II

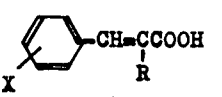

III

ethereal solution of silicone oil (Lukoil 100; VCHZ, Kolin, Czechoslovakia); the volatile components were evaporated within 16 h at 20°C. A citrate buffer (pH 3.4) containing various percentages of acetone was used as the mobile phase. Solutions (1%) of acids **I–III** in methanol were prepared and 5-μl samples were applied to the plates 3 cm from the lower edge. After evaporating off methanol at 20°C, ascending one-dimensional TLC was carried out. A chromatographic chamber was equilibrated with the mobile phase for 16 h at 20°C. After migration for 15 cm, the plates were removed and, after the remaining mobile phase had been evaporated off, the acids were detected under UV light (254 nm). Each chromatogram contained six compounds, two acids serving as reference samples. In the individual chromatogram, the R_F values of standards did not differ by more than 0.02.

TLC of compounds IV–VI

Experimental data were taken from the literature [17–20]. TLC of 16α-substituted estra-1,3,5(10)-trienes (**IV**) was performed [17] on silanized silica gel (PF_{254}) and the R_F values of androstane-type steroids were measured [18] on a silica gel G layer impregnated with silicone oil (DC 200). Acetone–water mixtures were used as the mobile phase in both instances. The R_M values of benzodiazepine derivatives **V** were obtained [19] on Silcoplat F_{254} impregnated with paraffin oil with acetonitrile–0.06 *M* KH_2PO_4 (pH 4.6) mixtures as mobile phases. The chromatography of dermorphine-related derivatives **VI** was performed [20] on silica gel G impregnated with silicone oil (DC 200) with methanol–aqueous buffer (pH 7.0) as mobile phase.

---

[a] The symbols *r*, *s* and *F* are explained under Experimental; *n* is the number of compounds.

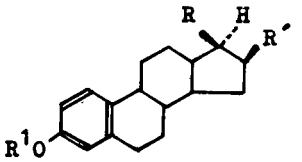

IV

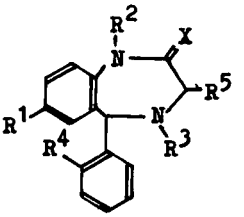

V

L-Tyr-D-Ala-L-Phe-NH-R^1-CONHR^2

VI

HPLC

Determination of acids **I** was carried out using a liquid chromatograph assembled from a Model 6000 A pump, U6K injector, a Model 440 fixed-wavelength detector and an N730 data module (Waters Assoc., Milford, MA, USA). A μBondapak C_{18} column (30 cm × 3.9 mm I.D.) (Waters Assoc.) and a custom-made column (25 cm × 3.9 mm I.D.), slurry-packed with 5-μm Spherisorb ODS (Phase Separations, Hauppage, NY, USA) were used as stationary phases. A phosphate buffer (pH 3.0) containing various percentages of methanol was used as the mobile phase. The eluent flow-rate was 1 ml/min. UV detection at 280 μm was used, range 0–0.01 a.u. The retention time of sodium nitrite (0.2% solution) was taken as t_o and the capacity factor, k', was evaluated from the retention time, t_r, of the solute, using the relationship $k' = (t_r - t_o)/t_o$.

HPLC of dansylamides **VII** was performed [21] on Spherisorb S5 ODS-2 with methanol–water as mobile phase.

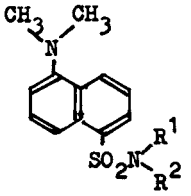

VII

Determination of partition coefficients

Experimental partition coefficients of acids **I–III** were determined by the shake-flask method [22] in octanol–acetate buffer (pH 3.4) at 20°C, with each phase being presaturated with the other. The concentration of acids in both phases was determined spectrophotometrically and the partition coefficients P were calculated as the ratio of concentrations in octanol and aqueous phases ($P = C_o/C_w$).

Determination of eluent polarity

The elution properties of the mobile phase were characterized by the change in its polarity. The values of $E_T(30)$, taken from paper of Johnson *et al.* [23], were used for this purpose. These values are based on the charge-transfer absorption (E_T-30) of 2,6-diphenyl-4-(2,4,6-triphenyl-N-pyridinio) phenolate (Reichardt's dye). This compound exhibits a very large solvatochromic effect on going from a very polar solvent (water, 453 nm) to a non-polar solvent (diphenyl ether, 810 nm). The values of $E_T(30)$ were calculated from corresponding wavelength of maximum absorption. The slopes $a(E_T)$ of the dependences $\log k' = a(E_T)E_T(30) + b$ were taken from ref. 23.

Sample preparation

Synthesis of arylacetic (**I**) [24,25], aryloxoalkanoic (**II**) (26) and cinnamic acids (**III**)[27] are described elsewhere. The origins of the compounds **IV–VII** are described in refs. 17–20.

Calculations

Log P values of the remaining acids **I**, **II** and **III** were calculated using parameters π according to the relationship $\log P = \log P_H + \Sigma\pi$, where P and P_H are the partition coefficients of a substituted and unsubstituted acid, respectively, and π is the substituent parameter of lipophilicity. Parameters π derived [28] for arylacetic acids were used for acids **I** whereas parameters π derived [28] for substituted benzoic acids were used for acids **II** and **III**. The sums of parameters π for 3-chloro-4-alkoxy derivatives were reduced by 0.23, in accordance with the results [16] of partition chromatography of these derivatives.

The coefficients in regression equations were calculated from the experimental results by multiple regression analysis. The statistical significance of the regression equations was tested by the standard deviation s, the coefficient of multiple correlation r and the Fischer–Snedecor criterion F.

RESULTS AND DISCUSSION

Eqns. 5–8 derived from chromatographic indices of arylacetic acids **I** [16] show statistical equivalence of both extrapolated and non-extrapolated values used as parameters of lipophilicity. Similar results were obtained also when using μBondapak as the stationary phase, as is evident from eqns. 9 and 10; the corresponding chromatographic indices are summarized in Table I.

	n	r	s	F	
$\log P = 1.548 \log k'_{50} + 1.562$	11	0.995	0.086	808.5	(9)
$\log P = 0.800 \log k'_0 + 0.326$	11	0.996	0.077	1014.8	(10)

The evaluation of the concentration dependences of R_M values (Table II) led to eqns. 11 and 12 for arylacetic (**I**), eqns. 13 and 14 for aryloxobutanoic (**II**) and eqns. 15 and 16 for cinnamic acids (**III**), respectively. The similarity of extrapolated and non-extrapolated R_M values as lipophilicity parameters is obvious.

	n	r	s	F	
$\log P = 1.362\ R_M^{40} + 2.004$	6	0.992	0.108	233.1	(11)
$\log P = 0.599\ R_M^{0} + 1.630$	6	0.995	0.081	415.6	(12)
$\log P = 1.940\ R_M^{45} + 1.931$	5	0.987	0.137	109.8	(13)
$\log P = 0.696\ R_M^{0} + 1.386$	5	0.968	0.211	44.9	(14)
$\log P = 1.792\ R_M^{45} + 2.306$	5	0.993	0.122	224.8	(15)
$\log P = 0.713\ R_M^{0} + 1.737$	5	0.989	0.157	134.6	(16)

Very different values of the slopes of the concentration dependences (cf. Table I) conflict with Snyder *et al.*'s [11] suggestion that the slopes depend only on the solvent strength of the organic modifier. Apparently, these slopes depend on the nature of the solutes. A decisive property is probably their lipophilicity, because the slopes correlate significantly with log P according to eqns. 17–19. Eqn. 17 was derived for the slopes of the concentration dependences of R_M values, eqn. 18 for log k' (Spherisorb) and eqn. 19 for log k' (μBondapak) in the series of acids **I** (values of slopes a are summarized in Table I).

	n	r	s	F	
$\log P = 0.557\ a + 1.431$	11	0.984	0.131	267.9	(17)
$\log P = 1.659\ a + 5.424$	12	0.929	0.261	63.4	(18)
$\log P = 0.908\ a - 1.420$	11	0.971	0.195	149.0	(19)

TABLE I

LIPOPHILICITY AND CHROMATOGRAPHIC BEHAVIOUR OF ACIDS I

Compound	X	Log P	a^a	a^b	μBondapak				
					Log k'_{60}[c]	Log k'_{50}	Log k'_{40}	Log k'_0	a
Ia	H	1.45	–	–	−0.293	−0.008	0.135	1.417	3.65
Ib	4-Cl	2.15	1.12	4.66	−0.008	0.245	0.570	2.110	3.73
Ic	4-C_2H_5	2.43	1.71	4.50	0.170	0.566	0.782	2.546	3.96
Id	3-Cl-4-*i*-C_3H_7O	2.71	2.16	4.86	0.269	0.717	0.954	2.957	4.48
Ie	4-*i*-C_3H_7	2.85	2.17	4.79	0.334	0.825	1.064	3.130	4.61
If	4-*t*-C_4H_9	3.13	2.73	5.08	0.536	1.024	1.276	3.464	4.88
Ig	4-*n*-$C_5H_{11}O$	3.46	3.56	5.01	–	–	–	–	–
Ih	3-Cl-4-CH_3O	1.91	1.12	4.66	−0.093	0.281	0.468	2.151	3.74
Ii	4-*i*-C_3H_7O	2.26	1.72	4.58	0.070	0.472	0.675	2.482	4.02
Ik	3-Cl-4-CH_2=$CHCH_2O$	2.61	2.11	4.89	0.222	0.675	0.900	2.940	4.53
Il	4-*i*-C_4H_9	3.35	–	5.08	–	–	–	–	–
Im	4-*c*-$C_6H_{11}O$	3.91	4.57	5.61	0.912	1.502	1.795	4.452	5.90
In	4-*n*-$C_6H_{13}O$	3.96	4.74	5.55	0.972	1.575	1.872	4.590	6.03

[a] Slopes of concentration dependences: $R_M = R_M^0 - a\varphi$; R_M values were measured [16] on silanized silica gel impregnated by silicone oil.

[b] Slopes of dependences: $\log k' = \log k'_0 - a\varphi$; log k' values were obtained [16] on Spherisorb ODS.

[c] Subscripts denote the concentration of modifier in mobile phase (in %, v/v).

Highly significant linear relationships between log P and slopes a (summarized in Table II) were also obtained from TLC data in the series of acids **I** (eqn. 20), **II** (eqn. 21) and **III** (eqn. 22):

	n	r	s	F	
$\log P = 0.425\,a + 1.314$	6	0.996	0.076	472.7	(20)
$\log P = 0.485\,a + 1.102$	5	0.951	0.259	28.6	(21)
$\log P = 0.530\,a + 1.358$	5	0.983	0.196	85.7	(22)

If the linear relationships of slopes a and parameters of lipophilicity, log P, are valid, it can be inferred that similar linear relationships exist also between the slopes and the respective chromatographic values. These dependences have been mentioned [29–31], especially for the extrapolated retention indices measured in methanol–water. The relationships expressed by eqns. 23–28 were calculated from the chromatographic indices of acids **I** (Table I). Letters A and B in parentheses denote Spherisorb ODS and μBondapak respectively, as stationary phases.

	n	r	s	F	
$R_M^0 = 0.770\,a - 0.474$	11	0.999	0.058	4310.2	(23)
$R_M^{50} = 0.281\,a - 0.489$	11	0.990	0.059	455.1	(24)
$\log k'_0$ (A) $= 1.584\,a - 4.333$	12	0.970	0.154	160.7	(25)
$\log k'_{60}$ (A) $= 0.944\,a - 4.129$	12	0.930	0.146	63.6	(26)
$\log k'_0$ (B) $= 1.139\,a - 2.197$	11	0.978	0.211	199.7	(27)
$\log k'_{60}$ (B) $= 0.589\,a - 1.937$	11	0.980	0.103	223.7	(28)

TABLE II

R_M VALUES OF ACIDS **I**, **II** AND **III** (R = H, CH_3) AT VARIOUS CONCENTRATIONS OF ACETONE IN MOBILE PHASE[a]

Compound	X (R[b])	Log P	R_M^{60}	R_M^{55}	R_M^{50}	R_M^{45}	R_M^{40}	R_M^0	a[c]
Ia	H	1.45[d]	–	−0.48	–	−0.44	−0.43	−0.297	0.33
Ie	4-*i*-C_3H_7	2.85	−0.05	−0.03	0.13	0.33	0.64	1.944	3.48
Io	4-$C_6H_5CH_2O$	2.85[d]	−0.03	0.04	0.345	0.48	0.76	2.299	3.98
If	4-*t*-C_4H_9	3.13	0.02	0.12	0.25	0.56	0.84	2.438	4.16
Ip	3-Cl-4-$C_6H_5CH_2O$	3.43[d]	0.02	0.21	0.45	0.77	0.95	2.900	4.84
Ig	4-*n*-$C_5H_{11}O$	3.46	0.05	0.25	0.50	0.85	1.04	3.118	5.16
IIa	H	1.30[d]	−0.38	–	−0.35	−0.315	−0.27	−0.068	0.53
IIb	4-*i*-C_3H_7O	2.18	0.31	−0.09	0.01	0.18	0.31	1.404	2.74
IIc	4-*i*-C_3H_7	2.70	−0.05	0.02	0.18	0.29	0.45	1.448	2.54
IId	3-Cl-4-*i*-C_3H_7O	2.78	0	0.14	0.35	0.46	0.72	2.094	3.52
IIe	4-*i*-C_4H_9	3.20	0.02	0.23	0.45	0.675	0.89	2.638	4.37
IIIa	H (H)	2.13[d]	−0.32	−0.30	−0.26	−0.16	−0.09	0.374	1.20
IIIb	4-*i*-C_3H_7 (H)	3.53	0.05	0.21	0.41	0.73	0.91	2.702	4.48
IIIc	4-*i*-C_4H_9 (H)	4.03	0.155	0.33	0.74	0.93	1.07	3.075	4.86
IIId	H (CH_3)	2.58[d]	−0.15	−0.04	0.075	0.23	0.37	1.407	2.62
IIIe	4-*t*-C_4H_9 (CH_3)	4.26	0.315	0.58	0.84	1.06	1.38	3.445	5.22

[a] Superscripts on R_M denote the concentration of acetone in mobile phase (in vol. %).
[b] R belongs to acids **III**.
[c] Slopes of concentration dependences $R_M = R_M^0 - a\varphi$.
[d] Experimental values.

A similar result was obtained in the TLC of acids **I–III** (Table II). The linear relationships between slopes and chromatographic values are highly significant, as is evident from eqns. 29 and 30 derived for acids **I**, 31 and 32 for acids **II** and 33 and 34 for acids **III**.

		n	r	s	F	
R_M^0	$= 0.710\ a - 0.525$	6	1.000	0.019	$>10^4$	(29)
R_M^{40}	$= 0.309\ a - 0.496$	6	0.995	0.061	385.3	(30)
R_M^0	$= 0.707\ a - 0.438$	5	0.998	0.080	638.9	(31)
R_M^{45}	$= 0.256\ a - 0.445$	5	0.988	0.066	123.2	(32)
R_M^0	$= 0.707\ a - 0.544$	5	0.999	0.078	1040.5	(33)
R_M^{45}	$= 0.298\ a - 0.537$	5	0.997	0.049	427.9	(34)

These relationships are of great importance for solving the question related to the equivalence of extrapolated and non-extrapolated retention indices, used as criteria of lipophilicity. If the linear relationship given by eqn. 4a holds and if, at the same time, the slope a is a linear function of extrapolated index according to eqn. 35:

$$a = m R_M^0 + n \tag{35}$$

then:

$$R_M = \varphi (mR_M^0 + n) + R_M^0 \tag{36}$$

$$R_M = (\varphi m + 1) R_M^0 + \varphi n \tag{37}$$

This result shows that there is a linear relationship between both indices:

$$R_M = a' R_M^0 + b' \tag{38}$$

Both parameters can be mutually substituted as criteria of lipophilicity in given range of concentrations of the modifier.

We have found that the validity of these relationships can be extended to other series of compounds, the retention characteristics of which were taken from the literature. Thirty structurally related 16α-substituted estra-1,3,5(10)-trienes (**IV**) [17] were used to derive eqns. 39 and 40. These equations characterize linear relationships between extrapolated and non-extrapolated R_M values and the slopes of the concentration dependences. Another series of compounds were selected from the paper by Biagi *et al.* [18]. Eqns. 41 and 42 were derived for androstane-type steriods (compounds **57–96** in Table I in ref. 18), whose R_M^{45} values were obtained experimentally and not by extrapolation. Also in this instance, a linear relationship exists between R_M and the slopes a of the concentration dependences.

		n	r	s	F	
R_M^0	$= 0.866\ a - 0.545$	30	0.988	0.124	1124.7	(39)
R_M^{45}	$= 0.415\ a - 0.540$	30	0.950	0.124	261.8	(40)
R_M^0	$= 0.801\ a - 2.099$	36	0.995	0.151	3182.3	(41)
R_M^{45}	$= 0.364\ a - 2.083$	36	0.971	0.155	566.7	(42)

Another example was taken from the series of benzodiazepine derivatives **V**. From the experimental results (Table III in ref. 19), the relationship between extrapolated R_M^0 values and slopes a of the concentration dependences is expressed by the equation

TABLE III

CHROMATOGRAPHIC INDICES OF DANSYLAMIDES VII[a]

Compound	R^1	R^2	a^b	Log k'_0	Log k'_{60}
VIIa	CH_3	H	3.64	2.78	0.535
VIIb	C_2H_5	H	3.78	3.02	0.70
VIIc	C_3H_7	H	4.03	3.34	0.905
VIId	C_4H_9	H	4.24	3.66	1.13
VIIe	C_5H_{11}	H	4.53	4.01	1.38
VIIf	C_6H_{13}	H	4.85	4.43	1.60
VIIg		$(CH_2)_4$	3.83	3.36	1.04
VIIh		$(CH_2)_5$	4.05	3.71	1.32
VIIi		$CH_2CH_2OCH_2CH_2$	3.63	3.06	0.82
VIIk	CH_3	CH_3	3.70	3.11	0.875
VIIl	C_2H_5	C_2H_5	3.99	3.55	1.18
VIIm	CH_3	t-C_4H_9	4.12	3.74	1.32
VIIn	CH_3	C_4H_9	4.33	3.98	1.46
VIIo	C_2H_5	i-C_3H_7	4.13	3.75	1.34
VIIp	C_3H_7	C_3H_7	4.54	4.23	1.62
VIIr	C_4H_9	C_4H_9	5.15	4.96	2.08
VIIs	CH_3	$C_6H_5CH_2$	4.47	4.12	1.54

[a] Experimental data were taken from ref. 21.

[b] Slopes of concentration dependences $\log k' = \log k'_0 - a\varphi$.

	n	r	s	F	
$R_M^0 = 0.524\,a - 1.040$	18	0.951	0.248	150.1	(43)

The statistical significance of the relationships between log P ($\Sigma\pi$) and lipophilic retention quantities generally increases with increasing structural similarity of the compounds studied. The same observation holds for the relationships between the slopes of concentrations dependences and corresponding retention indices. These concentration slopes of log k' values measured for dansylamides **VII** (Table III) [21] were correlated with extrapolated log k'_0 values. Eqn. 44 was derived for the whole series of amides[a], eqn. 45 for N-alkylamides and eqn. 46 for N,N-dialkylamides.

	n	r	s	F	
$\log k'_0 = 1.282\,a - 1.662$	17	0.975	0.131	283.6	(44)
$\log k'_0 = 1.350\,a - 2.101$	6	0.999	0.028	2488.1	(45)
$\log k'_0 = 1.246\,a - 1.424$	11	0.997	0.046	1413.2	(46)

The increase in statistical significance with increasing structural similarity in eqns. 45 and 46 is obvious. Even more significant results were obtained with eqns. 47–49 derived for retention indices evaluated in 60% methanol as mobile phase.

	n	r	s	F	
$\log k'_{60} = 0.839\,a - 2.280$	17	0.925	0.153	88.9	(47)
$\log k'_{60} = 0.884\,a - 2.653$	6	0.997	0.033	765.9	(48)
$\log k'_{60} = 0.816\,a - 2.079$	11	0.991	0.051	479.1	(49)

[a] Bis-2-hydroxyethylamide (compound **12** in ref. 21) was omitted as an outlier, probably owing to the presence of a hydroxy group in the alkylamide moiety.

Similar results were obtained from the chromatography of dermorphine related derivatives **VI** measured by Barbaro *et al.* [20]. The relationships were studied in structurally closed series of monoalkyl amides (Table IV). The dependences of $\Sigma\pi$ values on extrapolated and non-extrapolated R_M values are expressed by eqns. 50 and 51. The relationships between the slopes a of the concentration dependences and R_M values are also valid, as shown by eqns. 52 and 53. The corresponding relationship between slopes a and lipophilic parameters $\Sigma\pi$ is given by eqn. 54.

	n	r	s	F	
$\Sigma\pi = 0.976\ R_M^0 - 1.465$	12	0.980	0.207	247.8	(50)
$\Sigma\pi = 2.216\ R_M^{45} + 0.820$	12	0.970	0.256	158.2	(51)
$R_M^0 = 0.732\ a - 1.357$	12	0.987	0.168	384.7	(52)
$R_M^{45} = 0.298\ a - 1.493$	12	0.921	0.179	56.2	(53)
$\Sigma\pi = 0.705\ a - 2.739$	12	0.955	0.311	104.3	(54)

An interesting result was obtained when slopes a taken from different concentration ranges (for compounds **VIa, f** and **g**) were used. In this instance, eqn. 55 with lower significance was obtained:

	n	r	s	F	
$\Sigma\pi = 0.768\ a - 3.235$	12	0.866	0.527	29.9	(55)

The relationships between log P ($\Sigma\pi$) and the concentration slopes show the ability of this quantity to characterize the lipophilicity of the solutes evaluated. The fit of these relationships increases if the elution properties of the mobile phase are characterized by the change in polarity instead of the change in modifier concentration. Johnson *et al.* [23] used the values of $E_T(30)$ as a solvatochromic solvent polarity scale

TABLE IV

LIPOPHILICITY AND CHROMATOGRAPHIC INDICES OF DERMORPHINE-RELATED DERIVATIVES **VI**[a]

Compound	R^1	R^2	a[b]	R_M^0	R_M^{45}	$\Sigma\pi$
VIa	CH_2	C_2H_5	3.6 (3.9[c])	1.382	−0.28	0.08
VIb	CH_2	$C_6H_5CH_2$	4.8	2.241	0.02	0.78
VIc	CH_2	$C_6H_5CH_2CH_2$	6.3	3.087	0.17	1.34
VId	CH_2	$C_6H_5CH(CH_3)$	6.4	3.070	0.15	1.34
VIe	CH_2	*c*-C_5H_9	5.0	2.304	0.02	0.91
VIf	CH_2	$HOCH_2CH_2$	3.7 (5.2[d])	1.305	−0.42	−0.59
VIg	CH_2	$CH_3OCH_2CH_2$	3.8 (4.4[c])	1.518	−0.30	0.06
VIh	CH_2	4-HO-$C_6H_4CH_2$	4.7	1.931	−0.29	0.67
VIi	CH_2	1-Adamantyl	6.7	3.732	0.68	2.14
VIk	CH_2	1-Adamantyl-CH_2	7.0	4.017	0.86	2.70
VIl	CH_2CH_2	$C_6H_5CH(CH_3)$	6.4	3.145	0.26	1.62
VIm	CH_2CH_2	1-Adamantyl	7.3	4.065	0.77	2.42

[a] Experimental data and $\Sigma\pi$ values for chosen compounds were taken from ref. 20.

[b] Slopes of concentration dependences $R_M = R_M^0 - a\varphi$ from a wide concentration range (20–70%) of methanol.

[c] From concentration range 10–20% of methanol.

[d] From concentration range 0–20% of methanol.

TABLE V

LOG *P* VALUES AND SLOPES OF DEPENDENCES BETWEEN LOG *k'* AND $E_T(30)$ POLARITY SCALE[a]

Compound	$a(E_T)$	Log P^b	Compound	$a(E_T)$	Log P^b
Phenols			*Anilines*		
2-OH	0.159	0.88	H	0.195	0.90
3-OH	0.140	0.80	N-C_2H_5	0.330	2.16
4-OH	0.101	0.59	N,N-$(CH_3)_2$	0.384	2.31
4-CH_3	0.271	1.95	N,N-$(C_2H_5)_2$	0.541	3.31
4-NO_2	0.269	1.91	N-C_4H_9	0.529	3.58
H	0.209	1.48	2-CH_3	0.245	1.32
2,5-$(NO_2)_2$	0.318	2.00	3-CH_3	0.253	1.40
2,6-$(NO_2)_2$	0.294	1.55	4-CH_3	0.254	1.39
2-Br	0.311	2.35	2,4-$(CH_3)_2$	0.314	2.31
2-Cl	0.293	2.17	4-OCH_3	0.213	0.95
2-C_2H_5	0.342	2.47	3-Cl	0.321	1.90
2-CH_3	0.277	1.95	3,4-Cl_2	0.430	2.69
2-NO_2	0.292	1.79	4-Br	0.335	2.05
3,4-$(CH_3)_2$	0.322	2.23	3-NO_2	0.262	1.37
3,5-$(CH_3)_2$	0.332	2.35	1-Naphthylamine	0.361	2.22
3-Br	0.342	2.63	2-Naphthylamine	0.371	2.28
3-Cl	0.324	2.50	*Heterocyclics*		
3-C_2H_5	0.339	2.40	Pyridine	0.170	0.64
3-CH_3	0.273	1.95	2-NH_2-pyridine	0.125	0.20
3-NO_2	0.277	2.00	3-NH_2-pyridine	0.156	0.49
4-Br	0.340	2.60	4-CH_3-pyridine	0.236	1.22
4-Cl	0.320	2.35	4-C_2H_5-pyridine	0.282	1.69[c]
4-C_2H_5	0.341	2.58	Pyrazine	0.102	−0.22
1-Naphthol	0.383	2.98	2-CH_3-Pyrazine	0.142	0.23
2,4,5-Cl_3	0.448	3.72	2,5-$(CH_3)_2$-pyrazine	0.182	0.63
2,4,6-Cl_3	0.430	3.69	Quinoline	0.298	2.03
4-Cl-3-CH_3	0.370	3.10	2-CH_3-Quinoline	0.336	2.59
2,3,5,6-Cl_4	0.496	4.10	8-CH_3-Quinoline	0.347	2.60
4-*t*-C_4H_9	0.416	3.31			
2,4-Br_2	0.432	3.43			
2,3-$(CH_3)_2$	0.338	2.33			
2,6-$(CH_3)_2$	0.335	2.36			

[a] The slopes $a(E_T)$ were taken from ref. 23. HPLC measurements were performed on Unisil Q C_{18} as stationary phase; acetonitrile–water mixtures were used as mobile phase.
[b] Log *P* values were taken from ref. 32.
[c] Log *P* for 2-ethylpyridine.

for characterization of the mobile phase composition (see Experimental). The relationships of log *k'* *vs.* $E_T(30)$ gave statistically more significant linear equations than the corresponding concentration dependences. We have used these slopes, $a(E_T)$, to correlate them with corresponding values of log P^a in the series of phenols (eqn. 56), anilines (eqn. 57) and heterocyclics (eqn. 58). The corresponding data are summarized in Table V. For the common group of the mentioned compounds, the less significant

[a] The log *P* values were taken from ref. 32; only compounds with experimental log *P* were used in regression analysis.

eqn. (59) was derived. Taking into account that log P values were taken from the literature [32], and not measured in one laboratory, the correlations are very good.

	n	r	s	F	
$\log P = 9.330\ a(E_T) - 0.627$	32	0.975	0.184	572.4	(56)
$\log P = 7.350\ a(E_T) - 0.448$	16	0.981	0.157	351.0	(57)
$\log P = 11.262\ a(E_T) - 1.333$	11	0.996	0.099	995.2	(58)
$\log P = 9.088\ a(E_T) - 0.738$	59	0.951	0.295	534.4	(59)

The quantity $a(E_T)$ is the slope of the log k' *vs.* $E_T(30)$ relationships.

The experimental values of slopes $a(E_T)$ for the series of aromatic compounds measured on various types of stationary phase (Table VI) were taken from the same source [23]. Eqn. 60 for Sepralyte C_2, eqn. 61 for Sepralyte C_4 and eqn. 62 for Sepralyte C_8 were derived. The greatest deviation was observed for nitrobenzene; it decreases with the length of the silanizing group.

	n	r	s	F	
$\log P = 6.636\ a(E_T) - 0.049$	16	0.974	0.172	254.6	(60)
$\log P = 6.012\ a(E_T) - 0.219$	16	0.959	0.213	160.8	(61)
$\log P = 6.534\ a(E_T) - 0.991$	14	0.988	0.126	478.1	(62)

TABLE VI

LOG P VALUES AND SLOPES OF DEPENDENCES BETWEEN LOG k' AND $E_T(30)$ POLARITY SCALE[a]

Compound	$a(E_T)$[b]	$a(E_T)$[c]	$a(E_T)$[d]	Log P[e]
1,3,4-Trimethylbenzene	0.533	0.606	0.690	3.42
Anthracene	0.707	0.753	0.824	4.45
Benzene	0.331	0.395	0.472	2.13
Biphenyl	0.616	0.687	0.765	4.05
Ethylbenzene	0.461	0.548	0.670	3.15
Bromobenzene	0.451	0.510	0.591	2.99
Chlorobenzene	0.422	0.489	0.571	2.84
Iodobenzene	0.483	0.550	0.625	3.25
Naphthalene	0.519	0.547	0.644	3.37
Nitrobenzene	0.362	0.418	0.472	1.85
Toluene	0.392	0.467	–	2.73
Butylbenzene	0.651	0.778	0.826	4.26
Propylbenzene	0.546	0.684	0.733	3.68
p-Xylene	0.470	0.542	0.628	3.15
o-Xylene	0.454	0.612	–	3.12
Fluorobenzene	0.361	0.430	0.508	2.27

[a] The slopes $a(E_T)$ were taken from ref. 23. HPLC was performed on Sepralyte as stationary phase with methanol–water as mobile phase.
[b] Sepralyte C_2 was used.
[c] Sepralyte C_4 was used.
[d] Sepralyte C_8 was used.
[e] Log P values were taken from ref. 32.

CONCLUSIONS

It can be inferred from the fair linear regression relationships between the slopes of concentration dependences and extrapolated or non-extrapolated values of retention indices that there is an equivalence of these indices in the evaluation of lipophilicity. The statistically significant dependences of log P ($\Sigma\pi$) values on concentration slopes make it possible to use them as new parameters of lipophilicity. The goodness of fit of these relationships increased when a suitable measure of the polarity of mobile phases was used instead of the change in modifier concentration.

REFERENCES

1 E. Tomlinson, *J. Chromatogr.*, 111 (1975) 1.
2 M. Kuchař and V. Rejholec, *Česk. Farm.*, 28 (1979) 212.
3 C. F. Carney, *J. Liq. Chromatogr.*, 8 (1985) 2781.
4 R. Kaliszan, *Quantitative Structure–Chromatographic Retention Relationships*, Wiley, New York, 1987.
5 E. C. Bate-Smith and R. G. Westall, *Biochim. Biophys. Acta*, 4 (1950) 427.
6 J. M. McCall, *J. Med. Chem.*, 18 (1975) 549.
7 H. H. W. Thijssen, *Eur. J. Med. Chem.*, 16 (1981) 449.
8 R. Collander, *Acta Chem. Scand.*, 5 (1951) 774.
9 B. Soczewinski and C. A. Wachtmeister, *J. Chromatogr.*, 7 (1962) 311.
10 P. J. Schoenmakers, H. A. H. Billet, R. Tijssen and L. Galan, *J. Chromatogr.*, 149 (1978) 519.
11 L. R. Snyder, J. W. Dolan and J. R. Gant, *J. Chromatogr.*, 165 (1979) 3.
12 C. Altomare, A. Caretti, S. Cellamare and M. Ferappi, *Int. J. Pharm.*, 56 (1989) 273.
13 G. L. Biagi, A. M. Barbaro, M. C. Guerra, P. A. Borea and M. Recanatini, *J. Chromatogr.*, 504 (1990) 163.
14 T. Braumann, *J. Chromatogr.*, 373 (1986) 191.
15 H. Terada, *Quant. Structure–Activity Relat.*, 5 (1986) 81.
16 M. Kuchař, V. Rejholec, E. Kraus, V. Miller and V. Rábek, *J. Chromatogr.*, 280 (1983) 279.
17 J. Draffehn, B. Schoenecker and K. Ponsold, *J. Chromatogr.*, 205 (1981) 113.
18 G. L. Biagi, A. M. Barbaro, O. Gandolfi, M. C. Guerra and G. Cantelli-Forti, *J. Med. Chem.*, 18 (1975) 873.
19 K. Valko, S. Olajos and T. Cserhati, *J. Chromatogr.*, 499 (1990) 361.
20 A. M. Barbaro, M. C. Pietrogrande, M. C. Guerra, G. Cantelli-Forti, P. A. Borea and G. L. Biagi, *J. Chromatogr.*, 287 (1984) 259.
21 P. Lahtonen, *J. Chromatogr.*, 314 (1984) 141.
22 A. Leo, C. Hansch and D. Elkins, *Chem. Rev.*, 71 (1971) 525.
23 B. P. Johnson, M. G. Khaledi and J. G. Dorsey, *Anal. Chem.*, 58 (1986) 2354.
24 M. Kuchař, B. Brunová, J. Grimová, V. Rejholec, V. Čepelák and O. Němeček, *Česk. Farm.*, 29 (1980) 276.
25 M. Kuchař, B. Brunová, J. Grimová, J. Schlanger and O. Němeček, *Collect. Czech. Chem. Commun.*, 45 (1980) 1401.
26 M. Kuchař, B. Brunová, J. Grimová, V. Rejholec and V. Čepelák, *Collect. Czech. Chem. Commun.*, 51 (1986) 2617.
27 M. Kuchař, B. Brunová, V. Rejholec, Z. Roubal, J. Grimová and O. Němeček, *Collect. Czech. Chem. Commun.*, 40 (1975) 3545.
28 T. Fujita, J. Iwasa and C. Hansch, *J. Am. Chem. Soc.*, 86 (1964) 5175.
29 D. Reymond, G. N. Chung, J. M. Meyer and B. Testa, *J. Chromatogr.*, 391 (1987) 97.
30 T. L. Hafkenscheid and E. Tomlinson, *J. Chromatogr.*, 264 (1983) 64.
31 T. Braumann, G. Weber and L. H. Grimme, *J. Chromatogr.*, 261 (1983) 329.
32 C. Hansch and A. Leo, *Substituent Constants for Correlation Analysis in Chemistry and Biology*, Wiley, New York, 1979.

Journal of Chromatography, 557 (1991) 413–427
Elsevier Science Publishers B.V., Amsterdam

CHROM. 23 201

Characterization and determination of organic compounds in the mutagenic XAD-2 extracts of drinking water

SUKEO ONODERA

Faculty of Pharmaceutical Sciences, Tokyo University of Science, 12 Ichigaya-funagawara, Shinjuku-ku, Tokyo 162 (Japan)

ABSTRACT

Amberlite XAD-2 extracts, which exhibit mutagenicity in the Ames assays, of drinking water sampled each month during the period from April 1988 to March 1989 were studied in order to characterize and determine the organic pollutants. The major organic pollutants were phthalate ester plasticizers such as dibutyl and di(2-ethylhexyl) phthalate. Several polynuclear aromatic hydrocarbons (PAHs) and the organochlorine pesticide oxadiazon were also identified to be present at low concentrations. The XAD-extractable and chromatographable organic pollutants were found to be composed of PAHs with a mean concentration of 0.136 μg/l (*ca.* 10% of the total amount of organic compounds detected), phthalates with a mean value of 0.405 μg/l (*ca.* 30%) and other compounds with a mean value of 0.845 μg/l (*ca.* 60%). The concentrations and compositions of these organic pollutants were correlated with the effective rainfall content of the river and with the water temperature.

INTRODUCTION

Mutagenic and carcinogenic organic compounds found in source water [1] and drinking water [2] have recently caused concern as to their potential effects on human health. Mutagenicity in source water has generally been attributed to contamination by industrial waste or agricultural run-off, and to a lesser extent to naturally occurring substances. In comparison studies of raw water *vs.* finished water, Glatz *et al.* [3] and Maruoka and Yamanaka [4] suggested that chlorination may play a major role in the production of organic mutagens in potable water. Subsequent laboratory studies by Cheh *et al.* [5], in which a drinking water treatment process was simulated, clearly demonstrated that non-volatile mutagens were produced by chlorine disinfection. Several volatile compounds such as chloroacetones and 2-chloropropenal, and chlorinated hydroxyfuranone (MX), exhibiting mutagenicity have been identified to be present in chlorinated water [6–12], but many of the non-volatile mutagenic substances have not been fully characterized.

The potential health effects of organic contaminants in drinking water can be studied only after they have been isolated from the water and identified. However, because most of these compounds are present at micrograms per litre (ppb) levels or less in drinking water, a concentration step is necessary prior to the analytical identifi-

0021-9673/91/$03.50

cation of individual contaminants. Conventional techniques used for isolating organic compounds from the water for analytical purposes include liquid–liquid extraction [13–17], carbon adsorption [18–22] and resin adsorption [23–28]. These methods, like other concentration procedures, failed to provide a totally representative concentrate as one or more groups of organic components are not recovered effectively. Consequently, determining the variation in the types and amounts of organic substances present in drinking water is important in developing on effective concentration procedure.

This work was designed to characterize and determine the organic substances present in the mutagenic XAD-2 extract of drinking water collected each month during a 1-year period. These findings would provide background information that will be useful in assessing the health implications and trends of organic contaminant behaviour in water treatment process and drinking water distribution systems.

EXPERIMENTAL

Chemicals

Organic solvents (acetone, *n*-hexane, and methanol) were of analytical-reagent grade for pesticide residue analysis (Wako, Osaka, Japan). They were checked for purity by evaporating 100 ml to 100 μl and gas chromatographic (GC) analysis. The acetonitrile used for high-performance liquid chromatography (HPLC) was a Cica–Merck HPLC-grade solvent (Kantoh Chemicals, Tokyo, Japan). Water for HPLC was obtained from Nacalai Tesque (Kyoto,Japan). *n*-Alkane, phthalate ester plasticizer and polynuclear aromatic hydrocarbon (PAH) standards were commercially available. Standard solutions of these compounds both alone and as mixtures were prepared by dissolving the compounds in methanol or *n*-hexane, with subsequent serial dilutions.

Collection and preparation of XAD-2 resin extract

A 200-ml volume of Amberlite XAD-2 resin (Rohm and Hass, Philadelphia, PA, USA) was cleaned in a Soxhlet extractor with acetone–*n*-hexane (50:50, v/v) for 24 h, in order to remove interferences from the resin. During the cleaning, a portion of the solvent was evaporated and checked for interferences by GC. If necessary, the solvent washing in the Soxhlet extractor was repeated. When the blank chromatogram showed no interferences, the resin was removed from the extractor. The solvent remaining on the adsorbent was then evaporated completely in a vacuum desiccator for 24 h. The cleaned XAD-2 resin was placed in a glass column (16 cm × 4 cm I.D.) and washed with 10 l of purified water (distilled and filtered through a 0.45-μm membrane filter) before sample collection.

Drinking water was introduced bottom-to-top into the XAD-2 resin column, which was connected directly to the water tap in the laboratory. Water samples were continuously passed through the resin column at room temperature, at a flow-rate of 400 ml/min, during each sampling period (Table I) in order to collect XAD-2-extractable organic substances. The column was then washed with 2 l of distilled water and residual water was blown from the column with dry nitrogen.

The XAD-2 resin adsorbent was removed from the column and the organic substances on the resin were then extracted by sonication with 200 ml of acetone–*n*-

hexane (50:50, v/v). The sonication extractions were repeated twice more with a fresh 200-ml volume of the mixed solvent. These extracts were dried over anhydrous sodium sulphate and evaporated to dryness by means of a rotary evaporator at 40°C.The dry concentrate was dissolved, as rapidly as possible, in 5 ml of diethyl ether or methanol, producing a concentration factor of 10^6, and stored in a refrigerator at 4°C until the subsequent chromatographic analyses were performed.

The XAD-2 resin extracts of drinking water were fractionated into several fractions by thin-layer chromatography (TLC) on Polyamid 11 F_{254} (20 × 20 cm, thickness 0.15 mm) precoated TLC plates (Merck, Darmstadt, Germany) using chloroform as developing solvent [29]. The detection of the spots on the plates was performed by UV irradiation. The separated zones were scraped off by using special recovery tubes (Wako) and the adsorbed substances were then eluted with diethyl ether. The percentage recovery of individual fractions was determined by using GC and Ames assays [29].

Analysis of XAD-2-extractable organic pollutants

The XAD-2 resin extracts were analysed using a Shimadzu GC-6A gas chromatograph with flame ionization detection (FID). A glass column (2 m × 0.3 cm I.D.) packed with 2% silicone OV-1 on Uniport HP (60–80 mesh) was employed. The temperature of the column oven was increased from 80 to 260°C at 5°C/min. The injector and detector temperatures were 260°C. The carrier gas (nitrogen) flow-rate was 50 ml/min. A Shimadzu Model Chromatopac 1A data system was used to determine the retention times and the peak areas on the chromatograms. *n*-Alkanes, phthalate esters and PAHs were identified by comparison of their retention times with those of authentic standards injected under the same GC conditions (Table II).

PAHs in the XAD-2 resin extracts were analysed using a Shimadzu LC-9A liquid chromatograph with UV detection (Senshu Scientific, Tokyo Japan). The column (150 cm × 4.6 mm I.D.) packed with LiChrosorb RP-18 (Gasukuro Kogyo, Tokyo, Japan), grain size 5 μm. The following conditions were employed: column temperature, ambient; mobile phase, acetonitrile–water (60:40, v/v); flow-rate, 0.8 ml/min. A Shimadzu Chromatopac C-R6A data system was used to determine the retention times and the peak areas on the chromatograms. Individual PAHs were identified by comparison of their retention times with those of authentic samples (Table II).

A Hitachi M-80 combined gas chromatograph–mass spectrometer equipped with a Hitachi M-003 data-processing system was used for characterization of samples with the ion source operated at 250°C at a trap current of 70 μA and an electron energy of 70 eV. A Hewlett-Packard fused-silica capillary column (25 m × 0.25 mm I.D.) coated with OV-1 was used for the GC separations of the XAD-2-extractable organic compounds from drinking water. The oven temperature of the gas chromatograph was increased from 120 to 250°C at 5°C/min. Compounds were identified by comparison of their retention times and mass spectra with those of authentic standards.

Recovery tests were performed by spiking water with phthalate esters and PAHs at the 0.1 μg/l level and carrying out the entire procedure, in order to evaluate the total analytical precision for individual hydrocarbons. A small-scale column (20 cm × 2 cm I.D.) packed with clean XAD-2 resin (50 ml) was used for the recovery

tests. After processing with 100 l of the above spiking water at a flow-rate of 100 ml/min, the residual water was blown from the column with dry nitrogen. The hydrocarbons adsorbed on the XAD-2 resin were then extracted by sonication with acetone–*n*-hexane (50:50, v/v) (3 × 50 ml). The resulting extracts were concentrated to 100 μl using a Kuderuna–Danish concentrator for GC and HPLC analyses. Although drastic precautions were taken during the evaporation steps, loss of the more volatile compounds such as naphthalenes and biphenyl occurred (Table II).

The corresponding detection limits were 1 ng/l for phthalate esters by GC and 1 ng/l for PAHs by HPLC.

RESULTS AND DISCUSSION

Chemical characteristics of organic contaminants

The XAD-2 resin extracts were prepared from the laboratory tap water each month during spring (April, May and June 1988), summer (July, August and September), fall (October, November and December) and winter (January, February and March 1989). The drinking water in this area is distributed from Asaka water treatment plants (Saitama prefecture), which draw their water from midstream region of the Tone River. The flow-rate is generally low in the winter and high in the summer. There were heavy rainfalls in September and October 1988 in this river basin, before collecting samples. Data on mutagenicity, biochemical oxygen demand (BOD) and water temperature levels in the Tone River as source water are summarized in Table I.

The XAD-2 resin extracts of drinking water showed mutagenic levels ranging from 43 to 385 induced TA100 revertants per litre equivalent of the water, with a

TABLE I

DATA ON MUTAGENICITY, BIOCHEMICAL OXYGEN DEMAND (BOD) AND WATER TEMPERATURE LEVELS

Water sample	Sampling period	Volume of sample (l)	Mutagenicity[a] (revertants/l)	Water temperature (°C)	BOD (mg/l)
Spring					
a	16–20/04/88	4000	93	17.0	2.8
b	16–21/05/88	5000	53	15.0	2.5
c	20 and 25/06/88	3600	134	22.6	2.5
Summer					
a	12–18/07/88	4000	385	20.3	1.2
b	22–29/08/88	5000	97	23.0	1.3
c	17–24/09/88	4500	43	20.6	1.1
Fall					
a	15–21/10/88	5000	178	15.8	2.4
b	18–24/11/88	4500	233	13.8	3.7
c	13–19/12/88	4100	154	7.5	4.0
Winter					
a	17–23/01/89	5300	152	8.3	4.9
b	15–22/02/89	3600	177	9.9	4.0
c	10–16/03/89	4800	71	11.8	3.5

[a] Mutagenicity assays for each drinking water concentrate (XAD-2 extract) were conducted using Salmonella typhimurium TA100 strain in the absence of rat liver homogenate (S9).

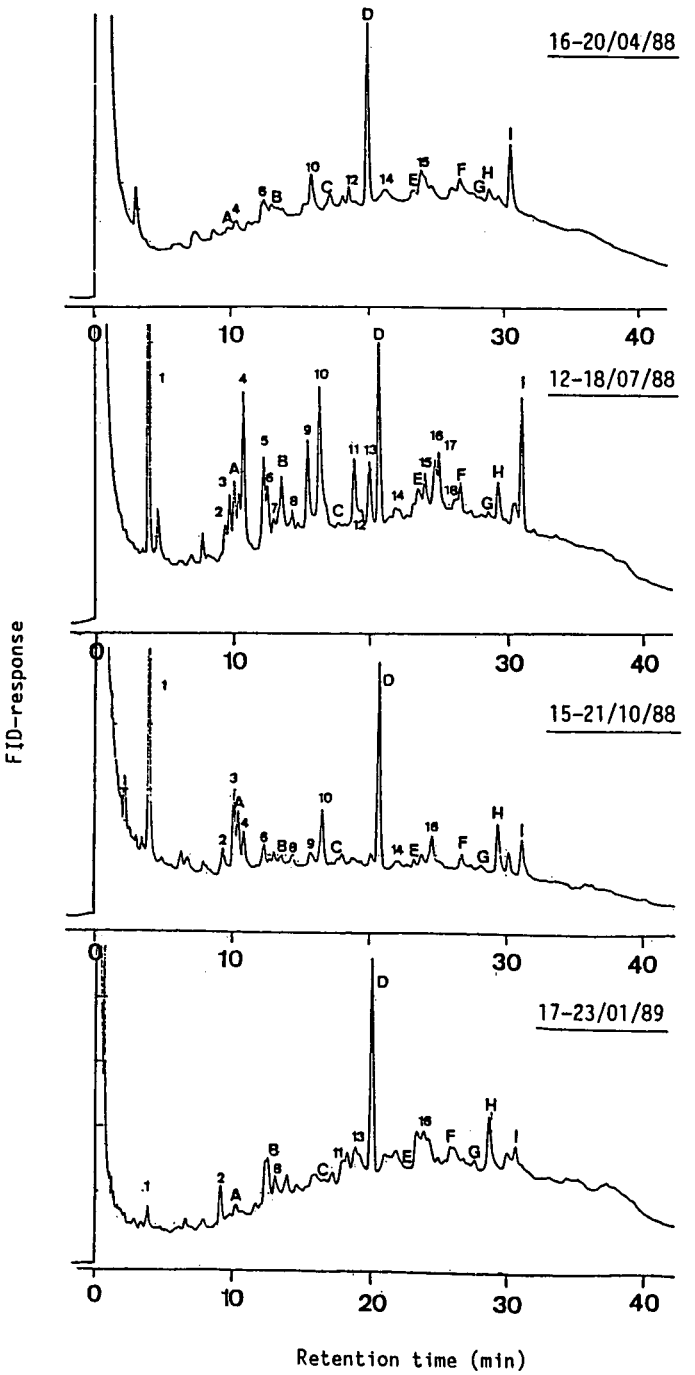

Fig. 1. Typical gas chromatograms (with FID) of XAD-2 extract of drinking water collected during spring, summer, fall and winter. The temperature of GC column (packed with 2% OV-1–Uniport HP) was raised from 80 to 260°C at 5°C/min. A 5-μl volume of the extract, equivalent to 5 l of drinking water, was injected into the column. Peaks: A = DMP; B = DEP; C = DDP; D = DBP; E = DAP; F = BBP; G = DHP; H = DCHP; I = DEHP. The numbered peaks were used for evaluation of seasonal variations in the concentrations of organic pollutants in water.

mean value of 134.8 revertants/l. Although the mutagenic levels in the extracts showed some seasonal scatter, it seems that the high levels were detected in the summer a and fall (a and b) water and low levels were observed in the spring (a and b), summer (b and c), and winter c samples. In general, it is assumed that an increase in water temperature during the warmer season would increase the formation of mutagenic substances on chlorination in water treatment processes. However, the reasons for the low levels of mutagenic activity in the summer (b and c) samples are still not clear.

Preliminary characterization of the mutagenic XAD-2 extracts of drinking water was performed by GC using a packed column and FID. Fig. 1 shows the gas

TABLE II

CHROMATOGRAPHIC BEHAVIOUR AND RECOVERY DATA FOR HYDROCARBONS WHICH MAY BE FOUND IN DRINKING WATER

Compound tested	Retention time (min)				Recovery (%)[b]
	GC[a]			HPLC[a]: 5 ng[c]	
	5 μg[c]	0.5 μg[c]	0.05 μg[c]		
PAHs					
Naphthalene	4.41	4.56	4.88	9.61	52
2-Methylnaphthalene	7.28	7.35	7.70	13.96	63
Biphenyl	8.80	8.94	9.20	13.00	65
2,3-Dimethylnaphthalene	10.42	10.67	10.89	17.05	74
Dibenzofuran	12.20	12.50	12.82	13.76	80
Fluorene	13.15	13.55	13.81	15.56	83
Benzophenone	14.70	15.13	15.50	7.55	82
9-Fluorenone	17.01	17.68	17.81	8.31	81
Anthracene	18.00	18.67	18.95	20.88	83
Phenanthrene	18.10	18.39	18.89	18.59	98
Carbazole	20.40	20.67	20.95	8.05	88
9,10-Anthraquinone	22.20	22.48	22.83	9.05	79
Fluoranthene	23.23	23.60	23.94	26.58	97
Pyrene	24.23	24.55	24.93	30.62	77
Chrysene	30.46	30.80	31.20	38.47	90
9,10-Phenanthraquinone	35.00	36.00	36.78	5.16	78
Phthalates					
Dimethyl phthalate (DMP)	10.63	11.00	11.29	–[d]	69
Diethyl phthalate (DEP)	13.80	14.20	14.53	–	78
Di-*n*-propyl phthalate (DPP)	17.95	18.20	18.42	–	83
Di-*n*-butyl phthalate (DBP)	20.95	21.40	21.63	–	88
Di-*n*-amyl phthalate (DAP)	25.23	25.41	25.95	–	90
Benzyl butyl phthalate (BBP)	28.36	28.56	28.77	–	88
Di-*n*-heptyl phthalate (DHP)	30.46	30.80	31.20	–	91
Dicyclohexyl phthalate (DCHP)	30.90	31.06	31.63	–	90
Di(2-ethylhexyl) phthalate (DEHP)	31.60	32.12	32.48	–	98

[a] For GC and HPLC operating conditions, see Experimental.
[b] Average of three recovery tests.
[c] Amount of compound chromatographed.
[d] Not determined.

chromatograms of the extracts, each of which is representative of four seasons. Over 50 compounds that respond to FID were detected in one extract collected during summer (summer a sample), whereas smaller numbers of compounds were found in the summer b and c samples. Some of the large peaks on the chromatograms could be identified tentatively as phthalate ester plastizers by comparison of their retention times with those of authentic compounds. However, the nature of the small peaks could not be determined because the GC retention times vary with the amounts of compounds injected under the given GC conditions (Table II).

Because of the complexity and the very low concentrations of individual compounds, the XAD-2 extracts of drinking water were further separated into several fractions on Polyamid 11 F_{254} precoated TLC plates, using chloroform as the developing solvent. Fig. 2 shows the typical thin-layer chromatograms of the extracts and several standard compounds of interest; the results of GC determinations and mutation tests for each separated component are summarized in Table III. The recovery of compounds in the fractions was *ca.* 80% (from comparison of GC peak areas) of the amount of sample applied, while the mutagenicity recovered of the amount of sample applied, while the mutagenicity recovered from the plates was about 80% of the overall acitivity applied.

As Table III shows, over 90% of compounds in the fractions recovered from the TLC plates were non-polar (R_F = 0.6–1.0), although compounds with a wide range of polarities can be seen on the chromatograms (Fig. 2). The mutagenicity detected in the original extracts was concentrated into the non-polar fractions, with a few exceptions (Table III). These results indicate that XAD-2 resin extracts of drinking water may be composed of mainly phthalate ester plasticizers and PAHs. Semipolar (R_F = 0.3–0.6) and polar fractions (R_F = 0.0–0.3), which may also include chlorophenols or chlorinated organic acids, exhibited no or weak mutagenicity.

Fig. 3 shows the reconstructed ion chromatogram of the non-polar fraction

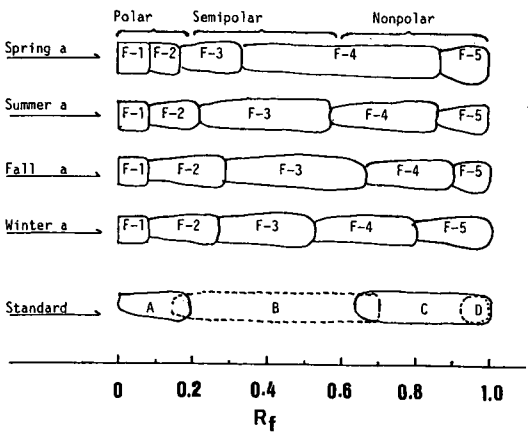

Fig. 2. Typical thin-layer chromatograms of XAD-2 extracts of drinking water and a mixture of chlorinated organic compounds of interest on a Polyamid TLC plate with chloroform as the developing solvent. A = Chlorinated organic acids; B = chlorophenols; C = phthalate ester plasticizers and PAHs; D = organochlorine pesticides and PCBs. For GC determinations and mutation tests for each fraction, see Table III.

TABLE III

DISTRIBUTION OF XAD-2-EXTRACTABLE ORGANIC CONTAMINANTS AND MUTAGENICITY OF DRINKING WATER ON POLYAMID 11 F_{254} TLC PLATE WITH CHLOROFORM

Water Sample	Distribution (%)									
	Organic contaminants[a]					Mutagenicity[b]				
	F-1[c]	F-2	F-3	F-4	F-5	F-1	F-2	F-3	F-4	F-5
Spring										
a	2.63	2.77	0.37	43.65	50.58	13.92	12.58	18.88	37.06	17.50
b	2.30	1.05	2.72	28.57	65.36	3.92	15.81	19.26	38.76	22.22
c	1.10	0.70	0.60	71.10	26.53	0	0	0	86.26	13.74
Summer										
a	14.50	0.91	0.92	61.74	21.84	0	0	1.85	94.46	3.69
b	0.86	2.48	1.18	56.74	38.74	4.10	5.45	5.53	77.35	7.57
c	1.52	7.08	3.87	70.59	16.93	7.50	7.92	9.68	65.20	9.70
Fall										
a	6.83	2.32	2.19	74.23	14.43	3.53	2.80	11.65	76.28	5.73
b	0.88	0.80	1.32	45.60	51.40	4.82	7.49	5.52	57.58	24.59
c	0.97	0.95	0.93	47.92	49.23	1.62	0	5.52	52.60	40.26
Winter										
a	2.10	1.05	0.99	47.56	48.30	3.21	13.20	7.50	47.50	28.53
b	2.50	1.88	1.53	43.21	52.88	5.00	6.93	13.25	45.31	29.51
c	3.83	2.14	0.68	39.36	55.00	3.83	12.20	11.50	37.00	35.47

[a] Amount of organic contaminants derived from the GC peak areas for each fraction, relative to the total peak areas for these fractionated components.

[b] Mutagenicity derived from the initial and linear portion of the dose–response curve for each fraction, relative to the total mutagenicity for these fractionated component.

[c] See Fig. 2.

obtained by the Polyamid TLC fractionations of the XAD-2 extract (summer a) and Table IV lists the compounds identified.

Phthalate ester plasticizers such as dibutyl and di(2-ethylhexyl) phthalate were the main organic contaminants detected by GC–FID of the extracts. As these phthalate esters are frequently encountered in the laboratory as artifacts, it should be pointed out that they were not found in the procedural blank; these widely used plasticizers do seem to be present in the water samples. Several PAH compounds such as naphthalenes, dibenzofuran, fluorene, anthracene, phenanthrene and fluoranthene and their oxygenated derivatives such as fluorenone, anthraquinone, chloromethylanthraquinone and phenanthraquinone (see Fig. 4) were also detected as minor components present in the extract. These compounds are generally introduced into the aquatic environment by petroleum activity and combustion processes [30,31]. Furthermore, several fatty acid esters such as palmitate and stearate, its chlorohydroxylated derivative and the organochlorine pesticide oxadiazon were found. These compounds may originate from domestic wastewater treatment plants and agricultural run-offs. A number of organic compounds, similar to those reported here, have been identified previously in drinking water [16,24,25,32,33].

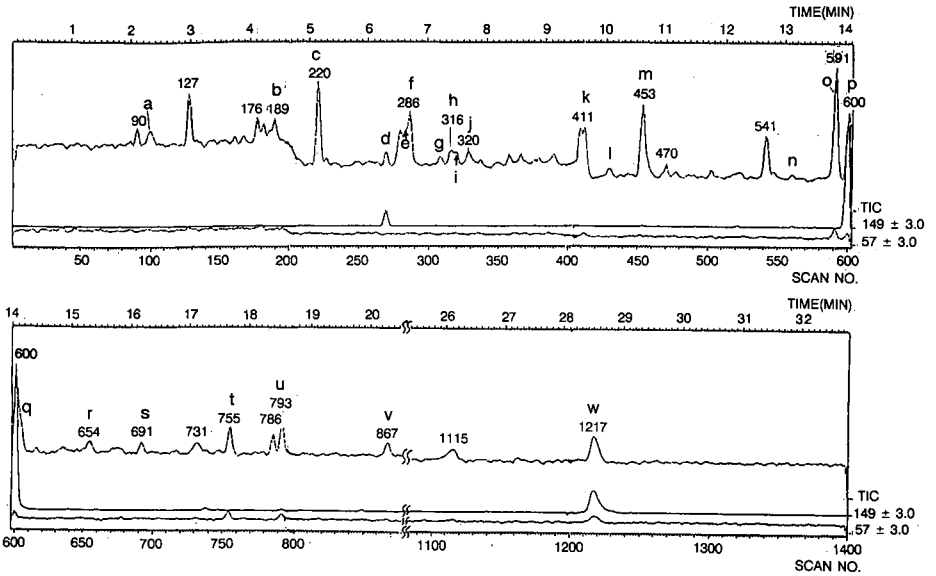

Fig. 3. Reconstructed ion chromatogram of the TLC-fractionated component (non-polar fraction in Fig. 2) of XAD-2 extracted collected during summer (summer a sample; 12–18 July 1988). The temperature of the GC column (fused-silica capillary coated with OV-1) was raised from 120 tot 240°C at 5°C/min. The letters above the peaks correspond to those in Table IV.

TABLE IV

COMPOUNDS INDENTIFIED IN THE XAD-2 EXTRACTS OF DRINKING WATER

Peak	Scan no.	M^+	Name	Formula	Identification[a]
a	100	154	Biphenyl	$C_{12}H_{10}$	a
b	189	168	Methylbiphenyl	$C_{13}H_{13}$	b
c	220	168	Dibenzofuran	$C_{12}H_8O$	a
d	269	220	Diethyl phthalate	$C_{12}H_{14}O_4$	a
e	280	166	Fluorene	$C_{13}H_{10}$	a
f	286	150	Methyl 3-methylbenzoate	$C_9H_{10}O_2$	b
g	308	182	Benzophenone	$C_{13}H_{10}O$	a
h	316	182	Methyldibenzofuran	$C_{13}H_9O$	b
i	320	156	Dimethylnaphthalene	$C_{12}H_{12}$	a
j	328	182	Methyldibenzofuran isomer	$C_{13}H_9O$	b
k	409	180	Fluorenone	$C_{13}H_8O$	a
l	430	170	Diphenyl ether	$C_{12}H_{10}O$	a
m	453	178	Anthracene/phenanthrene	$C_{14}H_{12}$	a
n	560	192	Methylanthracene	$C_{15}H_{14}$	a
o	591	270	Methyl palmitate	$C_{17}H_{34}O_2$	b
p	600	278	di-*n*-Butyl phthalate	$C_{16}H_{22}O_4$	a
q	605	208	Anthraquinone	$C_{14}H_{10}O_2$	a
r	654	256	Chloromethylanthraquinone	$C_{15}H_{11}ClO$	b
s	691	202	Fluoranthene	$C_{16}H_{10}$	a
t	755	298	Methyl stearate	$C_{19}H_{38}O_2$	a
u	792	344	Oxadiazon	$C_{15}H_{17}N_2Cl_2O$	a
v	867	348	Chlorohydroxymethyl stearate	$C_{19}H_{37}ClO_3$	b
w	1217	390	di(2-Ethylhexyl) phthalate	$C_{24}H_{34}O_2$	a

[a] Identification: a = comparison with authentic standard; b = tentative, based on interpretation of mass spectrum.

Organic pollutant levels in drinking water

On the basis of the qualitative information given above (Figs. 1–4 and Table IV), quantitative analyses of the XAD-2 extracts and their TLC-fractionated components of drinking water were performed by means of GC–FID and HPLC with UV

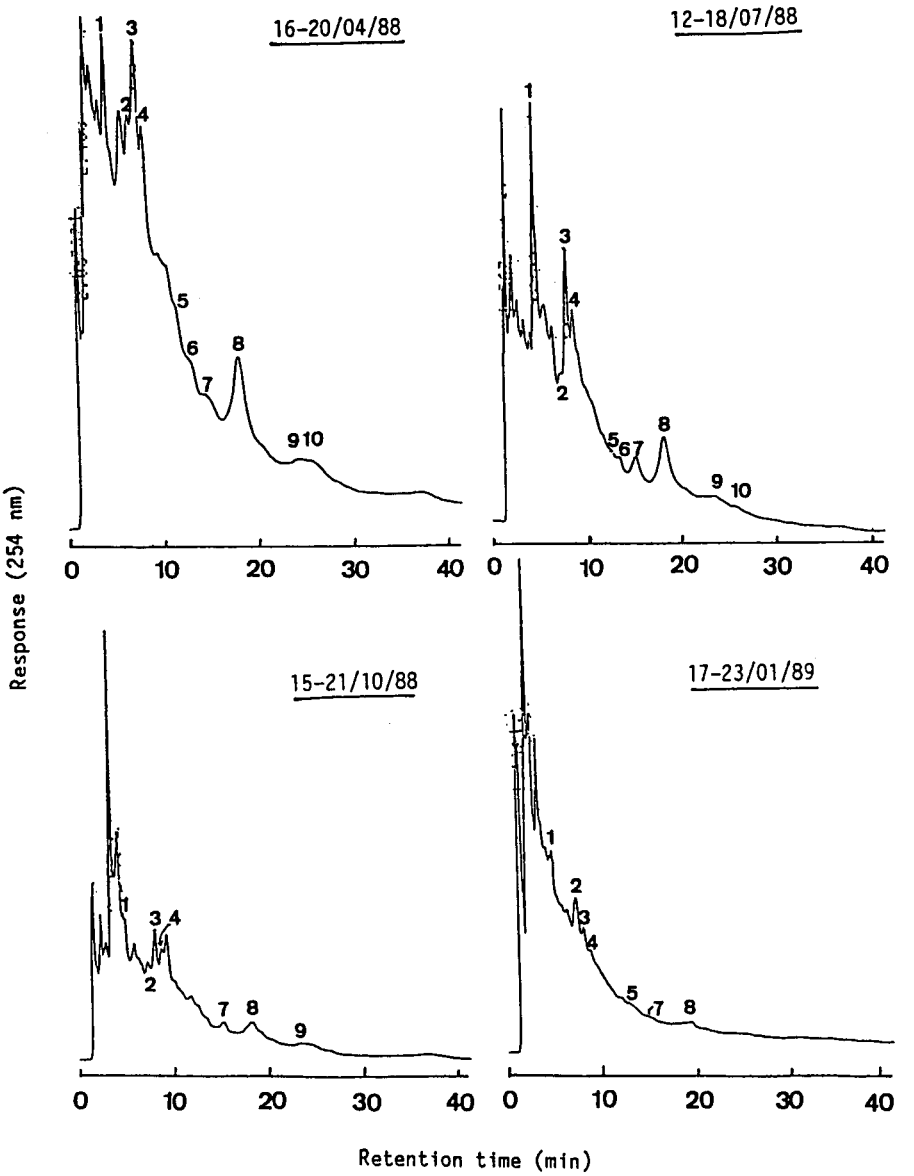

Fig. 4. Typical high-performance liquid chromatograms of the TLC-fractionated components (non-polar fractions in Fig. 2) of XAD-2 extracts. 1 = 9,10-Phenanthraquinone; 2 = benzophenone; 3 = fluorenone; 4 = anthraquinone; 5 = biphenyl; 6 = dibenzofuran; 7 = fluorene; 8 = phenanthrene; 9 = anthracene; 10 = fluoranthene.

detection. The results for these samples are listed in Table V as the concentrations of phthalate ester plasticizers, PAHs and other components. The concentrations of phthalate esters and other unknown components in drinking water were directly evaluated on the basis of the GC analyses of the XAD-2 extracts (Fig. 1), whereas the PAH levels were determined by HPLC analyses of their TLC-fractionated components (Fig. 4). Seasonal variations in the concentrations of these hydrocarbons in drinking water are also presented graphically in Figs. 5 and 6.

The range of total XAD-2-extractable organic pollutants in drinking water susceptible to chromatographic analysis was from 0.624 to 2.642 μg/l with a mean concentration of 1.389 μg/l, depending on the sampling periods (Table V and Fig. 5). As a general trend, high concentrations of these compounds were detected in the waters collected in summer and fall, whereas low values were observed for winter and spring samples, with the exception of three samples (summer c, fall and winter b). As already mentioned, there were heavy rainfalls in September and October 1988 in the Tone River basin, before sample collection [34]. Therefore, the low levels of these organic pollutants in the water samples collected in September and October can be explained by the heavy rains during the sampling periods.

Water samples taken from the laboratory tap showed phthalate ester levels ranging from 0.132 to 0.952 μg/l with a mean concentration of 0.409 μg/l, depending on the sampling period (Table IV and Fig. 5). High concentrations of these compounds were detected in the summer and fall samples, whereas low values were observed for the spring and late winter samples, with a few exceptions. The seasonal

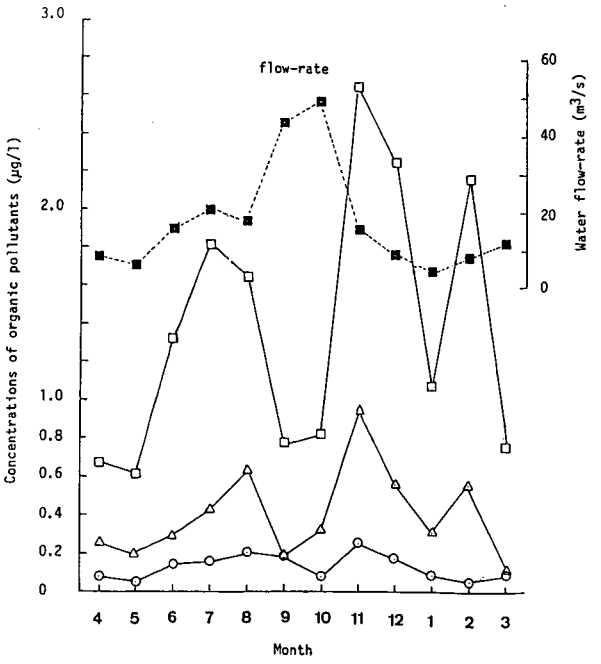

Fig. 5. Seasonal variations in the concentrations of ○ = PAHs, △ = phthalates and □ = total organic contaminants in drinking water, and ■ water flow-rate in the Tone River as source water.

TABLE V

CHROMATOGRAPHIC DETERMINATIONS OF PAHs, PHTHALATES AND OTHER COMPOUNDS IN THE XAD-2 RESIN EXTRACTS OF DRINKING WATER COLLECTED DURING APRIL 1988 to MARCH 1989

Compounds tested	Concentration (μg/l)												
	April	May	June	July	Aug.	Sept.	Oct.	Nov.	Dec.	Jan.	Feb.	March	Average
PAHs													
Naphthalene	0.012	0.022	0.020	0.051	0.013	0.060	0.003	0.002	0.003	0.002	0.001	0.002	0.016
2-Methylnaphthalene	0.004	0.004	0.008	0.018	0.024	0.026	0.024	0.070	0.044	0.025	0.001	0.006	0.021
Biphenyl	0.005	0.004	0.004	0.005	0.008	0.005	0.009	0.017	0.014	0.005	0.002	0.004	0.007
Benzophenone	0.011	0.010	0.005	0.006	0.023	0.005	0.008	0.081	0.058	0.032	0.027	0.015	0.023
Dibenzofuran	0.004	0.003	0.018	0.018	0.039	0.020	0.013	0.019	0.008	0.005	0.003	0.004	0.013
Fluorene	0.006	0.004	0.002	0.001	0.001	0.001	0.001	0.004	0.002	0.005	N.D.[a]	0.010	0.004
9-Fluorenone	0.005	0.003	0.011	0.011	0.024	0.021	0.008	0.023	0.014	0.008	0.005	0.010	0.012
Anthracene	0.001	N.D.	0.001	0.001	0.001	0.004	0.001	0.001	0.001	N.D.	N.D.	0.001	0.001
Anthraquinone	0.019	0.007	0.030	0.002	0.027	0.025	0.012	0.021	0.039	0.026	0.012	0.024	0.020
Phenanthrene	0.004	N.D.	0.018	0.019	0.024	0.014	0.006	0.019	0.010	0.001	0.002	0.007	0.010
9,10-Phenanthraquinone	0.005	N.D.	0.022	0.020	0.020	0.015	0.001	0.001	0.001	0.001	0.002	0.003	0.007
Fluoranthene	0.001	N.D.	N.D.	0.001	0.001	N.D.	N.D.	0.004	0.001	N.D.	N.D.	0.001	0.001
Subtotal	0.077	0.057	0.139	0.153	0.205	0.196	0.086	0.262	0.195	0.110	0.055	0.087	0.135
Phthalates													
Dimethyl phthalate	0.020	0.005	0.014	0.046	0.031	0.074	0.043	0.092	0.054	0.008	0.028	0.010	0.035
Diethyl phthalate	0.009	0.032	0.072	0.072	0.017	N.D.	0.007	0.037	0.060	0.034	0.048	0.016	0.034
Di-*n*-propyl phthalate	0.001	N.D.	N.D.	0.001	0.008	N.D.	0.010	0.018	0.020	0.011	0.036	0.004	0.010
D-*n*-butyl phthalate	0.140	0.046	0.110	0.134	0.197	0.073	0.147	0.279	0.180	0.159	0.403	0.008	0.156
Di-*n*-amyl phthalate	0.008	0.005	0.028	0.051	0.024	0.001	0.037	0.001	0.001	0.001	0.022	0.005	0.015
Benzyl butyl phthalate	0.001	0.074	N.D.	0.006	0.006	N.D.	0.001	0.031	0.016	0.007	0.037	0.031	0.017
Di-*n*-heptyl phthalate	0.013	N.D.	N.D.	0.001	0.019	0.014	0.001	N.D.	N.D.	0.001	N.D.	0.023	0.006
Dicyclohexyl phthalate	0.008	0.006	0.020	0.012	0.023	N.D.	0.016	0.032	0.006	0.027	N.D.	0.008	0.013
Di(2-ethylhexyl) phthalate	0.062	0.039	0.049	0.097	0.307	0.031	0.042	0.462	0.230	0.048	0.075	0.027	0.122
Subtotal	0.262	0.227	0.253	0.420	0.632	0.193	0.304	0.952	0.567	0.296	0.649	0.132	0.409
Unknown compounds[b]	0.331	0.360	0.906	1.244	0.811	0.401	0.446	1.428	1.494	0.679	1.462	0.573	0.845
Total	0.670	0.624	1.338	1.817	1.648	0.790	0.836	2.642	2.256	1.085	2.166	0.792	1.389

[a] Not detected.

[b] Amounts of these compounds were derived from GC–FID peak areas, relative to the area of di-*n*-butyl phthalate.

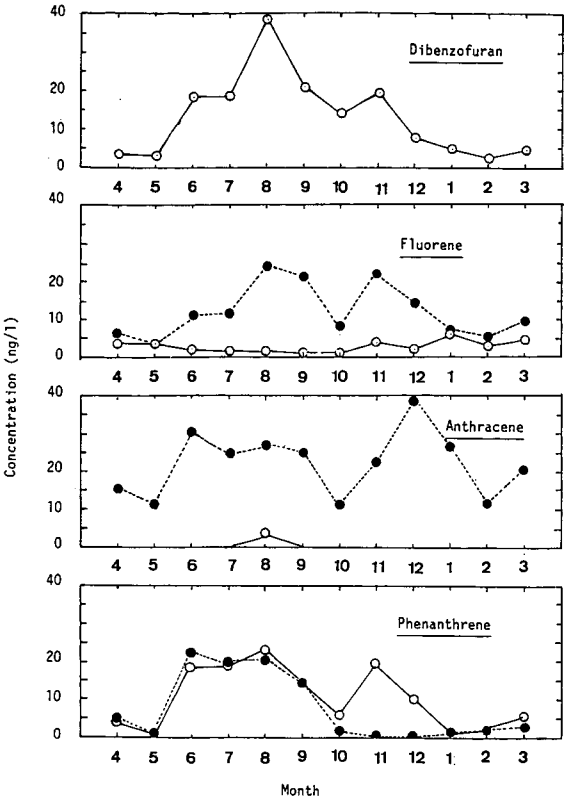

Fig. 6. Seasonal variations in the concentrations of PAHs in drinking water. Open circles represent the parent compounds and closed circles their oxygenated derivatives.

variations in the concentrations of total phthalate esters in drinking water were similar to those of total XAD-2-extractable and chromatographable compounds. The source of the phthalate esters is not yet known. Their concentrations are variable and seem to be correlated with the effective run-off. Locating their sources is of particular interest because their unusual ubiquity, their possible teratogenicity [35,36] and their mutagenicity [37].

The range of total PAH levels in water samples was from 0.055 to 0.262 μg/l with a mean concentration of 0.135 μg/l, depending on the sampling periods (Table V and Fig. 5). High concentrations of total PAHs were detected in the waters during the warmer months whereas low values were observed in those collected during the cooler months. This can be explained by an increase in water temperature (Table I), which may cause the leaching of PAHs from the coal tar coating inside pipes and water storage tanks [38,39] during warmer seasons. In addition, higher concentrations of fluorenone, anthraquinone and phenanthraquinone were detected in drinking water samples, as compared with the parent PAHs (Fig. 6). In general, reaction of chlorine with model PAHs produces oxygenated and chlorinated derivatives [40–43].

Fluorenone, anthraquinone and phenanthraquinone were reported as oxidation products of fluorene, anthracene and phenanthrene, respectively. PAHs have

also been suggested as the precursors of at least a portion of the mutagens produced in some chlorination processes [44].

CONCLUSION

Amberlite XAD-2 resin was used for the extraction of organic compounds from drinking water, in order to characterize and determine the organic pollutants. The XAD-2 extracts were further separated into several fractions on Polyamid TLC plates with chloroform as the developing solvent for GC–MS and HPLC analyses. The major organic pollutants were phthalate ester plasticizers such as dibutyl and di(2-ethylhexyl) phthalate. Several PAHs such as naphthalenes, biphenyl, benzophenone, dibenzofuran, fluorene, anthracene, phenanthrene and fluoranthene and their oxygenated compounds such as fluorenone, anthraquinone, phenanthraquione and chloromethylanthraquinone were also detected in drinking water samples. In addition, fatty acid methyl esters (palmitate, stearate and chlorohydroxystearate) were identified at low concentrations. The mean concentration of PAHs was 0.136 μg/l (*ca.* 10% of the total amount of organic compounds detected), phthalates comprised 0.405 μg/l on average (*ca.* 30%) and other components 0.845 μg/l on average (*ca.* 60%). The concentrations and compositions of organic pollutants were correlated with the effective rainfall content of the river and with the water temperature.

REFERENCES

1 W. Pelon, B. F. Whitman and T. W. Beasly, *Environ. Sci. Technol.*, 11 (1977) 619.
2 J. C. Loper, *Mutat. Res.*, 76 (1980) 241.
3 B. A. Glatz, C. D. Criswell, N. D. Arguello, H. T. Svec, J. S. Fritz, S. M. Grimm and M. A. Thomson, *J. Am. Water Works Assoc.*, 70 (1978) 465.
4 S. Maruoka and S. Yamanaka, *Mutat. Res.*, 79 (1980) 381.
5 A. M. Cheh, J. Skochpole, P. Koski and L. Cole, *Science (Washington, DC)*, 207 (1980) 381.
6 K. P. Kringstad, P. O. Ljungquist, F. de Sousa and L. M. Stronbeng, *Environ. Sci. Technol.*, 15 (1981) 562.
7 A. B. Mckagua, E. G.-H. Lee and G. R. Douglas, *Mutat. Res.*, 91 (1981) 301.
8 B. R. Holmbom, R. H. Voss, R. D. Mortimer and A. Wong, *Tappi*, 64 (1981) 172.
9 B. R. Holmbom, R. H. Voss, R. D. Mortimer and A. Wong, *Environ. Sci. Technol.*, 18 (1984) 333.
10 J. Hemming, B. Holmbom, M. Reunanen and L. Kronberg, *Chemosphere*, 15 (1986) 549.
11 J. R. Meier, R. B. Knohl, W. E. Coleman, H. P. Ringhand, J. M. Munch, W. H. Kaylor, R. P. Streicher and F. C. Kopfler, *Mutat. Res.*, 189 (1987) 363.
12 L. Kronberg and T. Vartiainen, *Mutat. Res.*, 206 (1988) 177.
13 M. Ahnoff and B. Josefsson, *Anal. Chem.* 46 (1974) 658.
14 M. Ahnoff and B. Josefsson, *Anal. Chem.*, 48 (1976) 1268.
15 B. Stachel, K. Baetjer, M. Cetinkaya, J. Duesein, U. Lahl, K. Lierse, W. Thiemann, B. Gabel, R. Kozicki and A. Podbielski, *Anal. Chem.*, 53 (1981) 1469.
16 H. Siraishi, N. H. Pilkington, A. Otsuki and K. Fuwa, *Environ. Sci. Technol.*, 19 (1985) 585.
17 B. G. Oliver and K. D. Nicol, *Int. J. Environ. Anal. Chem.*, 25 (1986) 275.
18 P. Van Rossum and R. G. Webb, *J. Chromatogr.*, 150 (1978) 381.
19 A. Tateda and J. S. Fritz, *J. Chromatogr.*, 152 (1978) 329.
20 C. Borra, A. D. Corcia, M. Marchetti and R. Samperi, *Anal. Chem.*, 58 (1986) 2048.
21 S. Onodera, K. Yoshimatsu, S. Nakano, H. Saitoh and S. Suzuki, *Eisei Kagaku (Jpn. J. Toxicol. Environ. Health)*, 34 (1988) 389.
22 S. Onodera, K. Yoshimatsu, H. Saitoh and S. Suzuki, *Eisei Kagaku (Jpn. J. Toxicol. Environ. Health)*, 35 (1989) 1.
23 G. A. Junk, J. J. Richard, M. D. Grieser, D. Witiak, J. L. Witiak, M. D. Arguello, R. Vick, H. J. Svec, J. S. Fritz and G. V. Calder, *J. Chromatogr.*, 99 (1974) 745.

24 R. Shinohara, A. Kido, S. Eto, T. Hori, M. Koga and T. Akiyama, *Water Res.*, 15 (1981) 535.
25 D. T. Williams, E. R. Nestmann, G. L. LeBel, F. M. Benoit and R. Otson, *Chemosphere*, 11 (1982) 263.
26 R. A. Moore and F. W. Karasek, *Int. J. Environ. Anal. Chem.*, 17 (1984) 187.
27 S. Maruoka, S. Yamanaka and Y. Yamamoto, *Water Res.*, 19 (1985) 249.
28 M. W. Tabor and J. C. Loper, *Int. J. Environ. Anal. Chem.*, 19 (1985) 281.
29 S. Onodera, M. Yamashita, S. Ishikura and S. Suzuki, *J. Chromatogr.*, 360 (1986) 137.
30 R. A. Hites, R. E. Laflamme and J. W. Farrinton, *Science (Washington, D.C.)*, 198 (1977) 829.
31 J. C. Marty, M. J. Tissier and A. Saliot, *Atmos. Environ.*, 18 (1984) 2183.
32 W. E. Coleman, R. G. Melton, F. C. Kopfler, K. A. Barone, R. A. Aurand and M. F. Jellison, *Environ. Sci. Technol.*, 14 (1980) 576.
33 K. Kveseth, B. Sortland and T. Boken, *Chemosphere*, 11 (1982) 623.
34 *Annual Report on Water Quality Survey of Natural Water and Drinking Water 1989*, Office of Environmental Preservation, Tokyo Metropolis, Tokyo, 1989.
35 R. K. Bower, S. Haberman and P. D. Minton, *J. Pharmacol. Exp. Ther.*, 171 (1970) 314.
36 A. R. Singh, W. H. Lawrence and J. Autian, *J. Pharm. Sci.*, 61 (1972) 51.
37 D. K. Agarwall, W. H. Lawrence, L. J. Nunes and J. Autian, *J. Toxicol. Environ. Health*, 16 (1985) 61, and references cited therein.
38 K. Alben, *Environ. Sci. Technol.*, 14 (1980) 468.
39 K. Alben, *Anal. Chem.*, 52 (1980) 1825.
40 A. R. Oyler, D. L. Bodenner, K. J. Weich, R. J. Liukkonen, R. M. Carlson, H. L. Kopperman and R. Caple, *Anal.Chem.*, 50 (1978) 837.
41 A. R. Oyler, R. J. Liukkonen, M A. Lukasewycz, D. A. Cox, D. A. Peake and R. M. Carlson, *Environ. Health Perspect.*, 46 (1982) 73.
42 S. Onodera, T. Muratani, N. Kobatake and S. Suzuki, *J. Chromatogr.*, 370 (1986) 259.
43 S. Onodera, K. Igarashi, A. Fukuda, J. Ouchi and S. Sizuki, *J. Chromatogr.*, 466 (1989) 233.
44 D. J. Schwartz, J. Saxena and F. C. Kopfler, *Environ. Sci. Technol.*, 13 (1979) 1138.

Journal of Chromatography, 557 (1991) 429–439
Elsevier Science Publishers B.V., Amsterdam

CHROM. 23 100

Analysis of industrial solvent mixtures in water using a miniature purge-and-trap device with thermal desorption and capillary gas chromatography–mass spectrometry

ALEXANDER P. BIANCHI*
Exxon Chemical Co., Department of Environmental Affairs, Fawley, Southampton (UK)
MARK S. VARNEY
Department of Oceanography, University of Southampton, Southampton (UK)
and
JOHN PHILLIPS
Department of Earth Sciences, The Open University, Walton Hall, Milton Keynes (UK)

ABSTRACT

A dynamic headspace stripping method for the determination of low levels of industrial hydrocarbon solvents in water is reported. Samples taken from industrial aqueous effluents and estuarine waters were sparged at 30 ml min^{-1} for 30 min at ambient temperature using a miniature all-glass stripping vessel. Solvent vapours were then sorbed on a Tenax-TA trap and subsequently analysed by thermal desorption and gas chromatography–mass spectrometry. Recoveries of five types of common industrial hydrocarbon solvent mixtures at 10, 100, 1000 and 5000 $\mu g\ l^{-1}$ in water were evaluated. Gasoline was included as a solvent as it is frequently used as an industrial cleaning and degreasing medium. The recoveries varied from 83.8 to 103.2% for gasoline and from 87.9 to 99.8% for hydrocarbon solvents such as kerosene and white spirit. Relative standard deviations between 2.8 and 9.6% were obtained for gasoline and between 2.2 and 8.9% for the remaining mixtures. The method has been used to detect traces of solvent mixtures as pollutants in industrial effluent streams and estuarine water, and more recently for investigating solvent contamination of potable water supplies.

INTRODUCTION

Many of the hydrocarbons discharged into effluent waters by chemical, manufacturing and allied industries are present as complex mixtures of compounds, rather than single compounds. Their measurement in water is typically conducted either by performing a crude quantification of total hydrocarbon content as oil-in-water, or by selective analysis of target compounds, based on legislative requirements and/or their relative mutagenicity or toxicity to river or estuarine ecosystems.

However, in some instances it is considerably more useful for the analytical environmental chemist to distinguish the nature and source of low levels of dissolved hydrocarbon mixtures in effluent waters. Strategies based on identification of individual compounds within mixtures may provide less useful information when there are

0021-9673/91/$03.50

several sources of contaminated effluents containing identical compounds. Indeed, for pollution control purposes, the chemist is often required to "fingerprint" the identity of the entire hydrocarbon mixture before determining the degree of contamination. Solvent mixtures are widely used in a variety of industries as diluents, fuels, reagents ans cleaning agents. Their flexibility of use is a major reason why they represent such a common source of hydrocarbon pollution in effluent waters. Typically, these may vary from kerosenes and fuel oils to aromatized solvents and, in some instances gasolines.

Dynamic "purge-and-trap" headspace analysis represents an expanding methodology available for the analysis of volatile hydrocarbon mixtures in water [1]. However, many analysts are reluctant to use these techniques, believing them to be relatively expensive, complex and time consuming [2]. Many applications of purge-and-trap methods, including those developed by the US Environmental Protection Agency laboratories, are centred on the determination of volatile organohalogens, volatile aromatics or volatile organosulphide compounds with low water solubilities and boiling points generally below 150°C [3]. There are comparatively few applications of purge-and-trap methods for stripping mixtures of organic substances with boiling point ranges extending above 200°C. One notable exception was demonstrated by Belkin and Esposito [4], who developed an elevated temperature purge-and-trap method for stripping Fuel Oil No. 2 and kerosene from water over three concentration ranges spanning from 10 to 1000 ppb.

In the laboratory, a simple miniature stripping device has been used at ambient temperatures to recover a variety of solvent mixtures from effluent water at low concentrations. The stripped compounds are trapped on Tenax-TA sorbent traps for subsequent analysis by thermal desorption and capillary column gas chromatography (GC) with flame-ionization detection (FID). The resulting chromatograms are then used to identify the nature and identity of the solvent(s) using a combination of "fingerprinting" techniques, comparison with reference mixture chromatograms and mass spectrometry (MS). Used in conjunction with standard infrared methods [5] for determining hydrocarbon oils in water, this technique provides a fast and sensitive means by which to assist in the identification of industrial solvent mixture in water.

EXPERIMENTAL

Standards

Standards were prepared by using commercial-grade solvent mixtures supplied by Esso Petroleum (Esso Research Centre, Abingdon, Oxford, UK) and Shell Oil (Thornton, Cheshire, UK) research laboratories. The usefulness of the method was assessed using five important industrial solvents *viz.*, (i) kerosene, (ii) white spirit, (iii) regular leaded gasoline and (iv) solvent 100 and (v) solvent 150, the last two being common aromatic solvent mixtures. Some common properties of these materials are summarized in Table I.

Industrial fresh water supplied by Southern Water Authority (SWA, Otterbourne, Winchester, UK) was purged under purified nitrogen overnight at 100 ml min^{-1}. Water blanks were analysed to ensure that interfering compounds had been removed. The solvent reference mixtures were gravimetrically added to 1-l volumes of stripped industrial fresh water. Serial dilutions were made in order to obtain standards at various concentration ranges.

TABLE I

COMMON PROPERTIES OF TYPICAL INDUSTRIAL HYDROCARBON SOLVENT MIXTURES

Solvent	Density ($g\ cm^{-3}$)	Molecular weight (mean)	Boiling range (°C)
Kerosene	0.75	200	150–325
White spirit	0.78	141	165–210
Gasoline	0.70	114	−0.5–216
Solvent 100	0.87	120	165–179
Solvent 150	0.89	138	190–210

Standard mixtures containing reference components present in the solvent mixtures were prepared according to certified ConCAWE methods [6], added to stripped water and used to assess recoverability and method response. These standard mixes were used as a secondary calibration check.

Adsorbents

Tenax-TA (60–80 mesh) (400 ± 10 mg) (Phase Separations, Clwyd, UK) was packed into 0.25-in. O.D. precleaned stainless-steel (ATD-50) thermal desorption tubes (Perkin-Elmer, Beaconsfield, Bucks, UK). These were conditioned by heating at 30°C for 10 min in a stream of oxygen-free prefiltered nitrogen at 15 ml min^{-1}. The temperature was then raised at 5°C min^{-1} to 350°C, held there for 1 h and allowed to cool. These tubes were analysed by thermal desorption and capillary GC in order to ensure the absence of background signals from contaminant peaks.

Sampling apparatus

The purge-and-trap device is shown in Fig. 1. The device, a miniature sparger, was developed from an original Bellar and Lichtenberg design intended for the determination of volatile priority pollutants in water [7]. The modified variant was developed and tested in the environmental laboratory [8] as a component part of a research programme investigating the occurrence and behaviour of volatile organic compounds in estuarine water [9].

Sample water was injected into the device using a 10-ml glass syringe (SGE, Milton Keynes, UK) with a Luer-Lok fitting according to Environmental Protection Agency recommended procedures. After removal of the all-glass stopper, the syringe needle and hub was inserted in the ground-glass neck of the vessel and located in place. The Luer-Lok was then opened and 7 ml of sample gently introduced to minimize the formation of pressure bubbles. The needle was then removed and the stopper replaced. The stopper was secured using two springs, as shown in Fig. 1, to ensure a leak-tight connection once stripping gas was introduced.

Ultrapure helium, used as the stripping gas, was metered via a metal–glass joint into the inlet arm of the stripping device. The gas passed through a 15-μm frit to produce a finely divided stream of gas bubbles. The effluent gas then passed through a bubble trap at the uppermost section of the device before flowing into the exit arm. A ground-glass insert connected the exit arm to a 0.125–0.25-in. Drallim reducing union. The stainless-steel tube containing the Tenax-TA sorbent was connected in turn to the 0.25-in. Drallim union. The design is leak-tight and permits a smooth

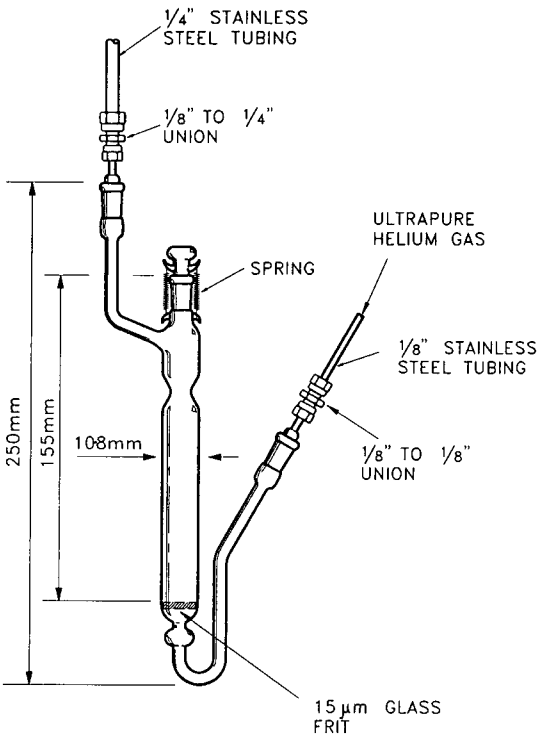

Fig. 1. Schematic diagram of the Bianchi miniature stripping vessel.

laminar flow of gas through the device. The flow-rate through the device can also be measured and adjusted by connecting a bubble flow-meter to the end of the Tenax-TA sorbent tube and altering the inlet flow accordingly. At the end of the stripping cycle, the gas is switched off and the Tenax-TA tube disconnected for thermal desorption–GC analysis.

Instrumentation and capillary column

An ATD-50 automated thermal desorber was connected to a Model 8700 gas chromatograph (Perkin-Elmer) via a 1-m length of fused-silica transfer line. This device was used for all thermal desorption analysis. A brief discussion of the principle of operation of the thermal desorber has been given in a previous paper [9].

The gas chromatograph was fitted with a cradle-mounted, 50 m × 0.22 mm I.D. OV-1701 wall-coated open-tubular fused-silica capillary column, 0.5-μm film thickness (SGE). The column effluent was connected to a twin-hole ferrule, allowing 50% of the column eluent to be routed to a flame-ionization detector. The remaining 50% was routed to an ion-trap detector–mass spectrometer (Finnigan MAT, Beaconsfield, UK).

Analytical operating parameters. The GC system conditions were as follows: carrier gas, ultrapure helium, 5.5 grade (Air Products, Basingstoke, UK); ATD-50, cold-trap packing, 20 mg of Tenax-TA; cold-trap low temperature, −30°C; cold-trap

high temperature, 280°C; splitting ratio, 300:1; desorption box temperature, 150°C; desorption oven temperature, 250°C; desorption time, 10 min; carrier gas pressure, 25 p.s.i.

Gas chromatograph. The detector temperature was 300°C, carrier gas flow-rate 1 ml min^{-1}, oven temperature isothermal at 50°C for 7 min then increased at 15°C min^{-1} to 250°C, final hold time 1 min.

Ion-trap detector. The ionization voltage was 70 eV, scan rate 0.5 s per scan, mass range 25–250 μ, transfer temperature 250°C, ion-source temperature 250°C, multiplier delay 200 s, mass defect 100 mu per 100 u and acquire time 30 min.

Chromatograms obtained by GC–FID and GC–MS were compared directly with a reference library of industrial solvent standards. The ion trap detector was used to identify and confirm major peaks in the chromatographic profiles and the presence of additional substances of environmental concern co-eluting with the solvent mixtures, *e.g.*, organohalogen compounds.

Analytical procedure

Wastewater samples were taken in precleaned 1-l amber-glass bottles capped with aluminium foil-lined inserts. A 10-ml glass syringe fitted with a removable plunger and Luer-Lok was used to transfer sub-samples to the stripping device. The syringe plunger was removed and the barrel filled with the water sample. The plunger was replaced and the sample flushed through the syringe needle to waste. The syringe barrel and needle were then flushed with ultrapure helium to remove any remaining sample. The Luer-Lok was closed and the filling procedure repeated. A 7-ml volume of water sample was then injected into the device as described previously. Water samples were stripped at flow-rates between 10 and 100 ml min^{-1} at 10 ml min^{-1} intervals. To complement these experiments, blank laboratory water was spiked with an ethoxyethanol solution (BDH, Poole, UK) of all five mixtures at concentration levels equivalent to 10, 100, 1000 and 5000 $\mu g\, l^{-1}$. Five replicates of each sample were purged and analysed to determine the accuracy and precision of the method. Quantification of recoveries was accomplished by summing the areas under all the integrated chromatographic peaks desorbed from the adsorbent tubes. The total peak area was then compared with the mass of solvent mixture added to the water standard. As no single component in the solvent mixtures can be considered as truly representative of the concentrations of the other solvent components in wastewater, summing the total peak area provides a more reliable measure of total solvent concentration.

Flow-rates were measured at the exit point of the Tenax-TA sorbent tube. All samples were stripped at room temperature. A second Tenax-TA sorbent tube was connected in series in order to investigate whether breakthrough of solvent mixture components occurred during the stripping step. On completion of stripping, the purge gas was gently closed off and the sorbent tube disconnected for immediate thermal desorption and GC-MS analysis.

RESULTS AND DISCUSSION

The results of the basic experiments show that the purge rate reaches an optimum value at 30 ml min^{-1} (see Table II). At flow-rates above 40 ml min^{-1} it was observed that the formation of the finely dispersed gas bubbles, which effect the

TABLE II

EFFECT OF STRIPPING FLOW-RATE ON RECOVERY USING THE MINIATURE STRIPPING VESSEL

Conditions: ultrapure helium gas; standard concentration, 10 $\mu g\ l^{-1}$; stripping time, 30 min.

Solvent	Purge flow-rate (ml min^{-1})	Recovery (%)	Breakthrough onto back-up trap (%)
Kerosene	10	80.1	0
	20	85.5	0
	30	95.7	0
	40	95.6	0
	50	95.5	0
	60	95.6	0
White spirit	10	82.4	0
	20	88.7	0
	30	96.5	0
	40	96.7	0
	50	96.2	0
	60	96.5	0
Gasoline	10	90.1	0
	20	93.5	6.1
	30	96.3	6.9
	40	96.1	7.1
	50	95.7	7.5
	60	95.5	7.7
Solvent 100	10	83.3	0
	20	89.5	0
	30	99.7	0
	40	99.4	0
	50	99.6	0
	60	99.3	0
Solvent 150	10	79.3	0
	20	85.8	0
	30	99.8	0
	40	99.3	0
	50	99.4	0
	60	99.4	0

TABLE III

VOLATILE COMPONENTS IDENTIFIED ON THE TENAX BACK-UP TUBE FOLLOWING GASOLINE PURGING ANALYSIS

n-Butane	2,3-Dimethylbutane
trans- + *cis*-2-Butene	2-Methylpentane
Isopentane	3-Methylpentane
n-Pentane	Cyclopentane
trans-2-Pentene	*n*-Hexane
2-Methyl-2-butene	Methylcyclopentane
2,2-Dimethylbutane	

stripping action, was disturbed by the formation of turbulence inside the vessel chamber. At flow-rates higher than this, channelling of the stripping gas was noted, leading to a single flow path of large gas bubbles. These are less effective at stripping than a stream of slower moving, evenly dispersed bubbles.

Except for gasoline, no breakthrough of any component from the solvent mixtures was found on the back-up adsorbent tube during these experiments. With gasoline, the amount of breakthrough is related directly to the purge rate. However, once the maximum recovery had been attained, further stripping did not yield higher overall recoveries. Only the most volatile components of gasoline broke through onto the back-up Tenax-TA adsorbent tube. These components, which were identified by retention time and ion-trap detection, are listed in Table III. Tenax has a low retention volume for very volatile compounds [10]. Accordingly, the loss of volatiles from Tenax adsorbents is theoretically predictable, based on several comprehensive and detailed studies of the retention volume characteristics of Tenax [11–14].

In general, recoveries increased with decreasing standard concentrations (see Table IV). Prolonged stripping for 60 and 90 min (*i.e.*, in excess of 30 min) afforded no improvements in recovery at any of the standard concentration levels. Recoveries for all five solvent mixtures varied from 83.8 to 103.2%. Gasoline exhibited the widest variation in recovery, *i.e.*, from 83.8 to 103.2%. This is due to the broad range of volatile components which constitute gasolines.

The experimental data on the accuracy and repeatability of the method are

TABLE IV

RECOVERY DATA FOR FIVE HYDROCARBON SOLVENT MIXTURES IN WATER AT DIFFERENT CONCENTRATION LEVELS

Mixture	Concentration level[a] ($\mu g\ l^{-1}$)	Recovery (%)
Kerosene	5000	89.7
	1000	91.9
	100	93.5
	10	95.7
White spirit	5000	90.8
	1000	94.8
	100	87.9
	10	96.5
Gasoline	5000	83.8
	1000	89.4
	100	97.8
	10	103.2
Solvent 100	5000	96.8
	1000	97.9
	100	98.3
	10	99.7
Solvent 150	5000	95.2
	1000	97.4
	100	99.2
	10	99.8

[a] Five samples at each concentration level.

TABLE V

ACCURACY AND REPEATABILITY DATA FOR THE STRIPPING METHOD FOR EACH SOLVENT MIXTURE OVER FOUR CONCENTRATION LEVELS

Mixture	Reference concentration[a] ($\mu g\ l^{-1}$)	Sample mean ($\mu g\ l^{-1}$)	Bias ($\mu g\ l^{-1}$)	Relative standard deviation (%)
Kerosene	4485	4499	14	8.9
	919	915	−4	5.8
	94	87	−7	5.1
	10	10	0	4.9
White spirit	4540	4558	18	6.3
	948	943	−5	8.3
	88	91	3	5.9
	10	9	−1	3.9
Gasoline	4190	4168	−22	9.6
	894	901	7	6.2
	98	100	2	7.0
	10	10	0	2.8
Solvent 100	4840	4851	11	4.9
	979	983	4	4.8
	98	96	−2	3.1
	10	10	0	2.8
Solvent 150	4760	4751	−9	7.2
	974	953	−21	6.4
	99	105	6	3.2
	10	10	0	2.2

[a] Five samples at each concentration level.

listed in Table V. Again, these data were based on the total summed peak area rather than on individual components. Accuracy and repeatability are expressed over four concentration ranges for each solvent mixture. Accuracy has been expressed as bias (bias = average value − reference value) for five replicates. Bias is a directional value which shows how much the sample results deviate from the known "true" value. The repeatability is expressed as the relative standard deviation (R.S.D., %).

Inspection of Table V shows that gasoline exhibits the greatest bias ($-22\ \mu g\ l^{-1}$). However, the bias values for all solvent mixtures at four concentration levels fall within 1% of the sample mean. All R.S.D.s were below 10%, with the lowest concentration standards yielding the smallest values.

Most of the individual compounds which constitute common solvent mixtures are non-polar and hydrophobic. Hence, despite the relatively high boiling point ranges of the mixtures, they can be purged from water at ambient temperature. Using this technique, it was possible to recover all five mixtures within the concentration range 10–5000 $\mu g\ l^{-1}$. Specimen gas chromatograms obtained with FID for kerosene and solvent 100 are shown in Fig. 2. Each of the chromatograms was obtained by stripping 10 $\mu g\ l^{-1}$ concentrations of each of the mixtures in water. A list of the principal components of these solvent mixtures is provided with each chromatogram.

CONCLUSIONS

The method described represents a novel application for an existing analytical protocol. Hydrocarbon solvent mixtures were recovered from both industrial effluent and estuarine water at trace concentrations by purging at ambient temperature. The method is also comparatively rapid, with each purging cycle taking only 30 min to complete. Small sample sizes (7 ml) are used, although the sample size can be readily increased. In some instances it would be acceptable to scale up the sparger in order to accommodate larger sample volumes. No solvents are required in the protocol, which eliminates the cost and laboratory effort required to use them for trace organic analy-

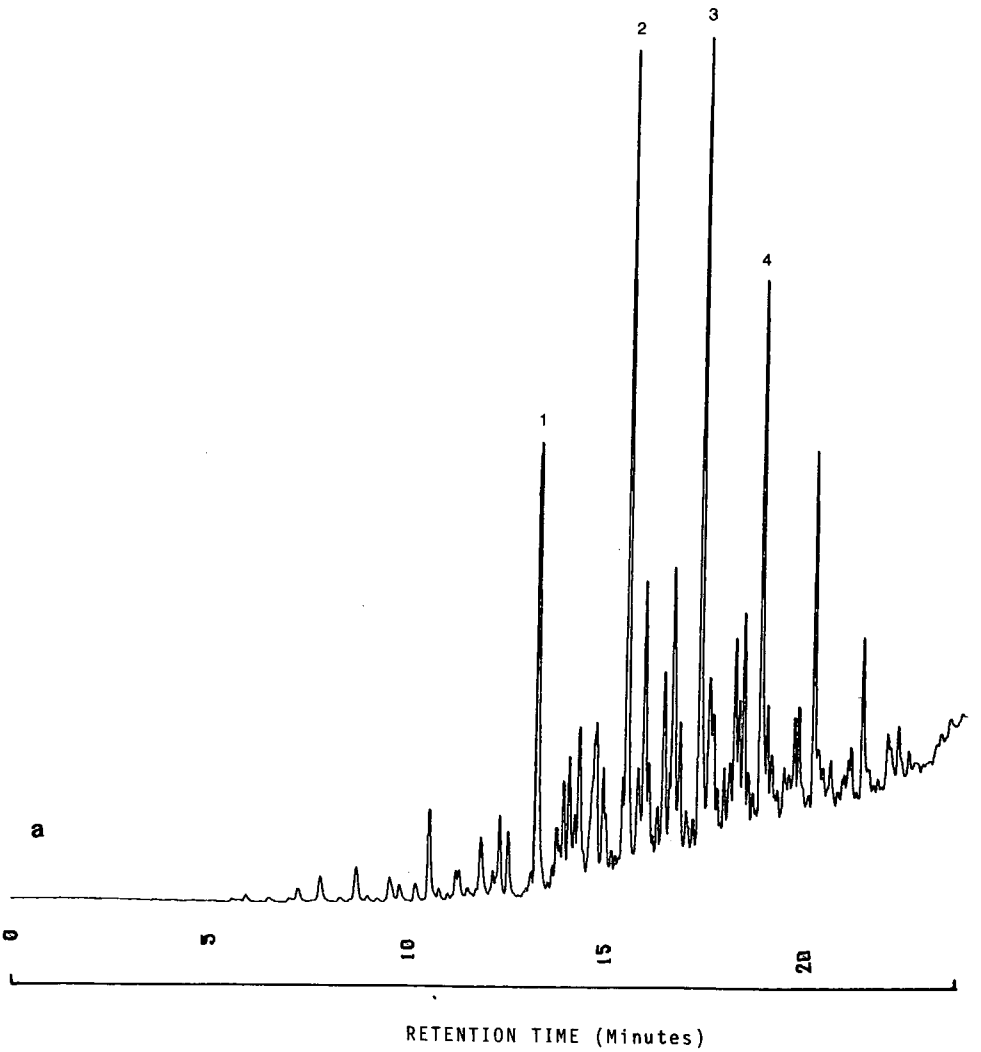

Fig. 2.

(*Continued on p. 438*)

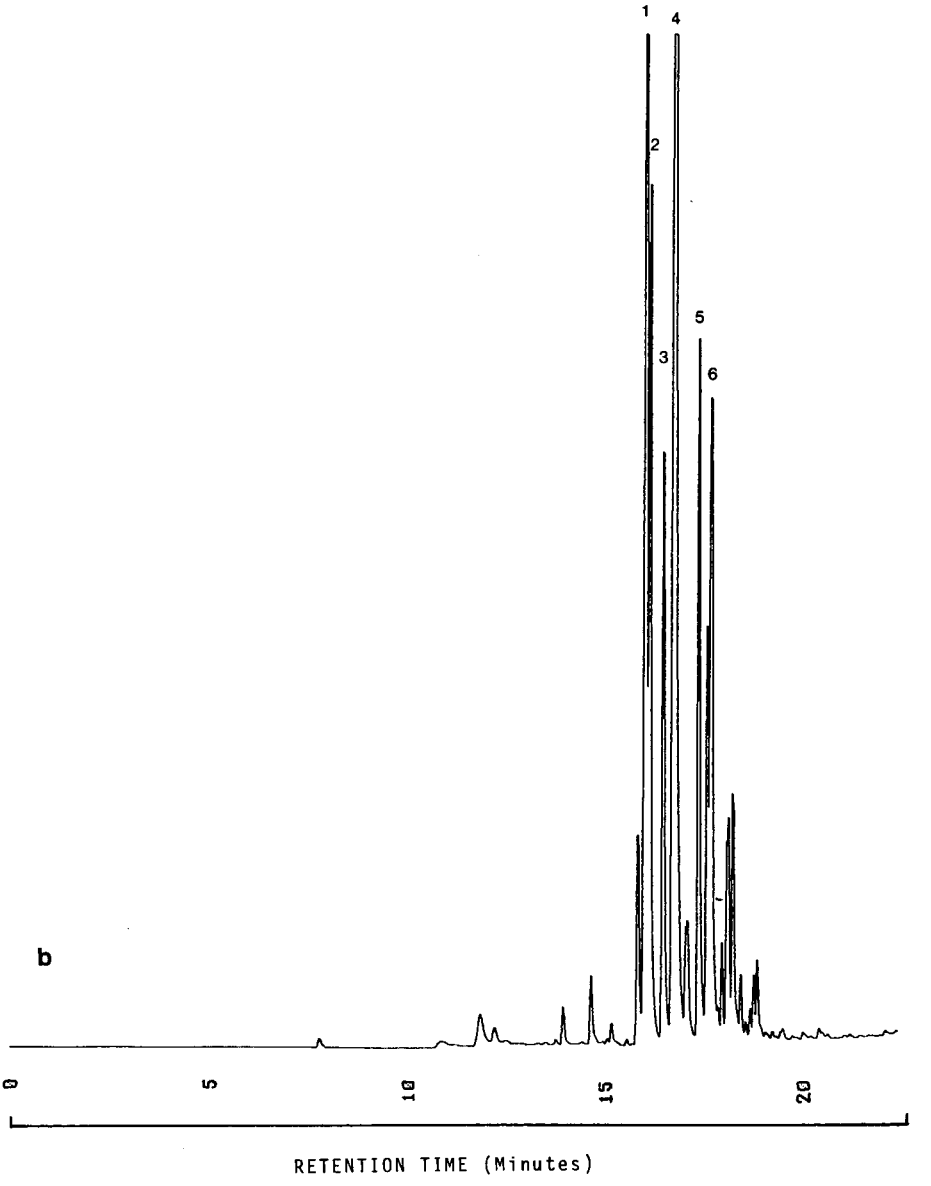

Fig. 2. Specimen purge chromatograms of each of the five standard hydrocarbon solvent mixtures in water (10 $\mu g\ l^{-1}$ of each). (a) Kerosene: 1 = *n*-nonane; 2 = *n*-decane; 3 = *n*-undecane; 4 = *n*-dodecane. (b) Solvent 100: 1 = 1-methyl-3-ethylbenzene; 2 = 1-methyl-4-ethylbenzene; 3 = 1,3,5-trimethylbenzene; 4 = 1,2,4-trimethylbenzene; 5 = 1,2,3-trimethylbenzene; 6 = 1-methyl-3-*n*-propylbenzene + 1-methyl-4-*n*-propylbenzene.

sis. The flexibility of the technique means that it can also be used to analyse for trace solvent mixture contamination in potable and fresh water supplies. The low cost and flexibility of the technique may also be useful for developing environmental lab-

oratories operating within Eastern Bloc countries, where rapid, reliable and cost-effective techniques are required to assist in pollution assessment and control measures within the aquatic environment.

REFERENCES

1 A. J. Núñez, L. F. González and J. Janak, *J. Chromatogr.*, 300 (1984) 127.
2 R. Pizzie, *Ph. D. Thesis*, University of Southampton, 1984.
3 R. L. Grob and M. A. Kaiser, *Environmental Problem Solving Using Gas and Liquid Chromatography*, (Journal of Chromatograhy Library, Vol. 21), Elsevier, Amsterdam, 1982, Ch. 4.
4 F. Belkin and G. E. Esposito, *J. Chromatogr. Sci.*, 24 (1986) 216.
5 *Methods for the Determination of Hydrocarbon Oils in Water*, H.M. Stationery Office, London, 1984.
6 Oil Companies International Study Group for the Conservation of Clean Air and Water (ConCAWE), *Report No. 8/86*, ConCawe, The Hague, 1986.
7 T. A. Bellar and J. J. Lichtenberg, *J. Am. Water Works Assoc.*, 66 (1974) 739.
8 A. P. Bianchi and M. S. Varney, *Int. Environ. Safety*, 6, No. 4 (1989) 12.
9 A. P. Bianchi, M. S. Varney and J. Phillips, *J. Chromatogr.*, 467 (1989) 111.
10 W. Bertsch, E. Anderson and G. Holzer, *J. Chromatogr.*, 112 (1975) 701.
11 J. F. Pankow, *Anal. Chem.*, 60 (1988) 950.
12 R. H. Brown and C. J. Parnell, *J. Chromatogr.*, 178 (1979) 79.
13 I. Maier and M. Fieber, *J. High Resolut. Chromatogr. Chromatogr. Commun.*, 11 (1988) 566.
14 A. Zlatkis, H. A. Lichtenstein and A. Tishbee, *Chromatographia*, 6 (1973) 67.

Journal of Chromatography, 557 (1991) 441–449
Elsevier Science Publishers B.V., Amsterdam

CHROM. 23 155

Analysis of nucleotides by high-performance liquid chromatography with phosphorus-selective detection

WENZHI HU and HIROKI HARAGUCHI
Department of Applied Chemistry, School of Engineering, Nagoya University, Chikusa-ku, Nagoya 464 (Japan)
and
TOYOHIDE TAKEUCHI*
Research Center for Resource and Energy Conservation, Nagoya University, Chikusa-ku, Nagoya 464 (Japan)

ABSTRACT

Phosphorus-selective detection based on the post-column molybdenum blue method was developed for the analysis of nucleotides in high-performance liquid chromatography. Orthophosphate generated from nucleotides reacted with molybdate to form a complex, which was detected by a visible absorption detector at 880 nm. Nucleotides were separated in the reversed-phase ion-pair mode, and operating conditions which influence the signal intensity were examined. Detection limits of 0.2–0.4 nmol per 12 μl were obtained for the examined nucleotides. The system was applied to the analysis of nucleotides in fish tissues.

INTRODUCTION

Nucleotides are often analyzed by high-performance liquid chromatography (HPLC) with UV detection. Ion-exchange [1], reversed-phase[2–8] and reversed-phase ion-pair chromatography [9,10] are the most commonly used methods. Nucleotides contain a mono-, di- or triphosphate group in the molecule, and there exist many species resulting from combination with different nucleosides and the position of the attached phosphate group. In addition, interferences from matrices make the analysis more complicated. One of the strategies for solving this problem is to develop a selective detection method for the nucleotides.

Complexation between orthophosphate (PO_4^{3-}) and molybdate, *i.e.*, the molybdenum blue method, has been utilized for the selective determination of phosphorus in various samples by means of an off-line method[11], flow-injection analysis [12–14] and continuous-flow analysis [15]. In these methods absorbance of the complex at a visible wavelength is measured to determine total phosphorus. Because it is orthophosphate that forms a complex with molybdate in the molybdenum blue method, condensed phosphoric acid and organophosphorus compounds should be decomposed to generate orthophosphate before the complexation. If the molybdenum blue

0021-9673/91/$03.50

colorimetry can be combined with a separation method, phosphorus compounds can be specified.

In this paper molybdenum blue colorimetry was combined with HPLC for the selective detection of nucleotides. The assembled system was applied to the analysis of nucleotides in fish tissues.

EXPERIMENTAL

Apparatus

A block diagram of the assembled system is shown in Fig. 1. An LC-6AD HPLC pump (No. 2) (Shimadzu, Kyoto, Japan) and a Minipuls 2 peristaltic pump (No. 16) (Gilson, Villiers-le-Bel, France) were used to deliver the mobile phase and the reagents, respectively. The line filter (No. 3) was composed of a 10 mm × 4.6 mm I.D. column packed with 30-μm porous silica (Develosil; Nomura Chemical, Seto, Japan). The loop injector (No. 4) was assembled by using a Model 7000 switching valve (Rheodyne, Cotati, CA, U.S.A.) in the laboratory, and the loop volume was 12 μl. Develosil ODS-5 (5 μm particle diameter, 250 mm × 4.6 mm I.D.; Noruma Chemical) was employed as the separation column (No. 5). The effluent from the separation column was monitored by a Uvidec-100 V UV spectrophotometer (No. 6) (Jasco, Tokyo, Japan) at 250 nm, followed by post-column reaction for the phosphorus-selective detection.

The eluent was first mixed with 4% (w/v) potassium peroxodisulfate aqueous solution (No. 14) and passed through the 8 m × 0.5 mm I.D. PTFE reaction coil (No. 10) heated in an EMG-1 aluminium block bath (No. 9) (Eyela, Tokyo, Japan), in order for the samples to undergo oxidative decomposition, in which orthophosphate was formed from nucleotides. The orthophosphate formed was then converted to the phosphorus–molybdenum complex by reaction with 2.5% (w/v) ammonium molybdate acidic solution (color-forming reagent; No. 15) in the 5 m × 0.5 mm I.D. PTFE reaction coil (No. 11) at room temperature. The color-forming reagent contained 0.36% (w/v) L-ascorbic acid and 1.5 *M* sulfuric acid. The molybdenum blue complex was monitored by a Uvidec-100 IV spectrophotometer (No. 12) (Jasco) at 880 nm. The flow cell of the latter detector as well as the hydraulic line for the post-column detection were metal-free because the reagents were strongly acidic.

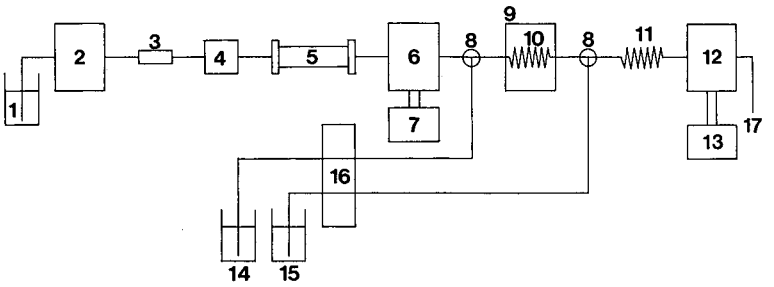

Fig. 1. Block diagram of the apparatus. 1 = Mobile phase; 2 = HPLC pump; 3 = line filter; 4 = loop injector; 5 = separation column; 6 = UV detector; 7 = chart recorder; 8 = T-joint; 9 = aluminum block bath; 10 = reaction coil (8 m × 0.5 mm I.D.); 11 = reaction coil (5 m × 0.5 mm I.D.); 12 = visible absorption detector; 13 = integrator; 14 = oxidative reagent; 15 = color-forming reagent; 16 = peristaltic pump; 17 = waste.

Reagents

All the reagents were of reagent grade and obtained from Wako (Osaka, Japan) or Tokyo Chemical Industry (Tokyo, Japan), unless otherwise stated. Purified water was prepared by using a Milli-Q reagent water system (Japan Millipore, Tokyo, Japan). The following nucleotides were obtained from Wako: adenosine 5′-monophosphate (AMP), adenosine 5′-diphosphate (ADP), adenosine 5′-triphosphate (ATP), cytidine 5′-monophosphate (CMP), guanosine 5′-monophosphate (GMP), inosine 5′-monophosphate (IMP), thymidine 5′-monophosphate (TMP) and uridine 5′-monophosphate (UMP).

Fish samples were prepared as follows: approximately 8 g of fish tissues were homogenized by adding 25 ml of 1 *M* perchloric acid, followed by centrifugation at 1600 *g* for 5 min. A 5-ml volume of the supernatant was taken, and its pH was adjusted to 6.5 with 1-*M* potassium bicarbonate. A portion of the supernatant was finally injected into the HPLC system.

The HPLC mobile phase was a mixture of a buffer and acetonitrile. The buffer contained tetrabutylammonium chloride, 20 m*M* boric acid, 10 m*M* sodium borate and 5 m*M* citric acid. The pH of the buffer was finally adjusted to 5.4 with sulfuric acid.

RESULTS AND DISCUSSION

Organophosphorus compounds must be decomposed to generate orthophosphate before complexation in molybdenum blue colorimetry, and thus several parameters could affect the signal intensity, for example mobile phase components, flow-rates of the mobile phase and the reagents, reaction conditions, etc. The effects of these parameters on the signal intensity were examined without the separation column. In reversed-phase ion-pair chromatography, the mobile phase is commonly composed of ion-pair reagent, buffer solution and organic solvent. In this work tetra-

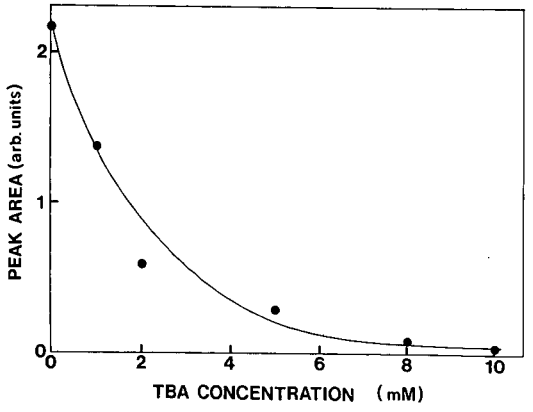

Fig. 2. Effect of the concentration of the ion-pair reagent in the eluent on the signal intensity. Eluent: borate buffer (pH 5.4) containing tetrabutylammonium chloride (TBA) and 5 m*M* citric acid–acetonitrile (98:2). Flow–rate of the eluent: 0.7 ml/min. Flow-rate of the oxidative reagent and color-forming reagent: 0.1 ml/min. Temperature of the aluminum block bath: 128°C. Solute: ATP. Wavelength of detection: 880 nm.

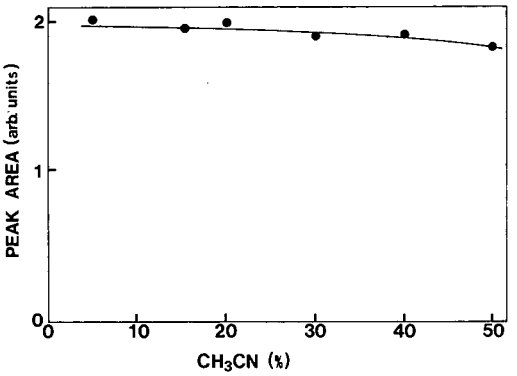

Fig. 3. Effect of acetonitrile concentration in the eluent on the signal intensity. Operating conditions as in Fig. 2 except the eluent composition (mixture of acetonitrile and borate buffer at pH 5.4 containing 1 m*M* TBA and 5 m*M* citric acid). Solute: ATP.

butylammonium chloride was used as the ion-pair reagent, and borate and acetonitrile were used as the buffer and the organic solvent, respectively.

Fig. 2 demonstrates the effect of the concentration of the ion-pair reagent in the eluent on the signal intensity. The peak heights observed without the separation column are plotted in the figure. The smaller is the concentration of the ion-pair reagent, the higher the signal intensity observed. In the reversed-phase ion-pair mode, the retention time of analytes decreases with decreasing ion-pair reagent concentration, which can be compensated for by decreasing acetonitrile concentration in the mobile phase. In the following experiments, the concentration of tetrabutylammonium chloride was kept constant at 1 m*M*.

Fig. 3 illustrates the effect of acetonitrile concentration in the eluent on the signal intensity. The results indicate that the effect of the acetonitrille concentration is not very significant up to 50% (v/v). Isocratic elution was carried out for the sep-

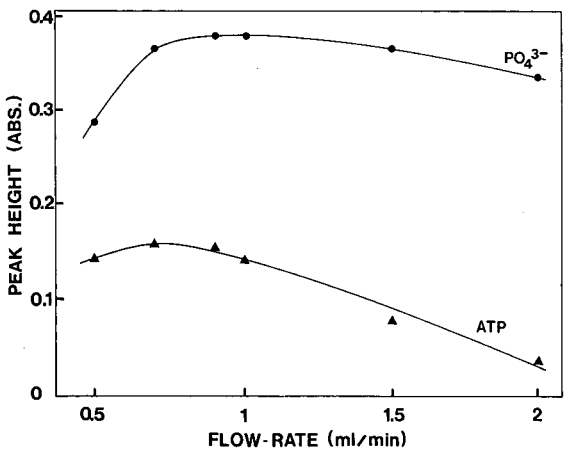

Fig. 4. Effect of the flow-rate of the mobile phase on the signal intensity. Operating conditions as in Fig. 2 except the solutes. (orthophosphate and ATP).

aration of nucleotides, and the mobile phase containing 1 m*M* tetrabutylammonium chloride and 2% (v/v) acetonitrile was mostly employed. The ionic strength of the mobile phase was adjusted with borate and citric acid as described in the Experimental section, and the pH of the mobile phase was adjusted to 5.4 with sulfuric acid.

The effect of the flow-rate of the mobile phase on the signal intensity is shown in Fig. 4. The flow-rates of both oxidative and color-forming reagents were kept constant at 0.1 ml/min. A flow-rate of approximately 0.7 ml/min was optimum for ATP, while around 1 ml/min was optimum for orthophosphate. The peak height decreases with increasing flow-rate, which is because the dispersion of the analyte in the hydraulic line becomes more significant and the concentration of the ion-pair reagent in the mixed solution increases.

The oxidative decomposition temperature remarkably influenced the signal intensity, especially for organophosphorus compounds. Fig. 5 shows the dependence of the signal intensity on the oxidative decomposition temperature. Potassium peroxodisulfate was employed as the oxidative reagent. The signal intensity increased with increasing decomposition temperature for ATP, while the signal was nearly constant for orthophosphate. The present system allowed heating to temperatures up to 135°C. At higher temperatures, the air bubble formed interfered with detection. The bubble formation could be eliminated by applying pressure from the downstream side of the flow cell of the detector, but the peristaltic pump employed in turn did not work well at several atmospheric pressures. Therefore, the oxidative decomposition was carried out at approximately 130°C. In addition, even without oxidation by potassium peroxodisulfate, the monophosphate-type nucleotides examined in this work (AMP, CMP, GMP, IMP, TMP and UMP) could be detected to some extent, *e.g.*, 40–50% of the signals observed using the oxidative decomposition process could be detected. However, diphosphate-type and triphosphate-type nucleotides could not be detected without the oxidative reaction process.

The effect of the flow-rate of the color-forming reagent on the signal intensity was examined. The flow-rate of the mobile phase was kept constant at 0.7 ml/min. The reagent employed was 1.5 *M* sulfuric acid solution containing 2.5% ammonium

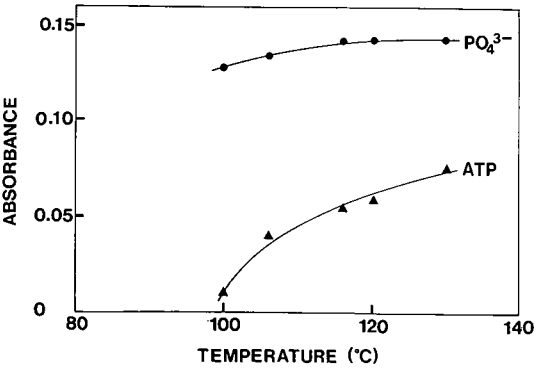

Fig. 5. Dependence of the signal intensity on the oxidative decomposition temperature. Operating conditions as in Fig. 2 except the solutes. (orthophosphate and ATP).

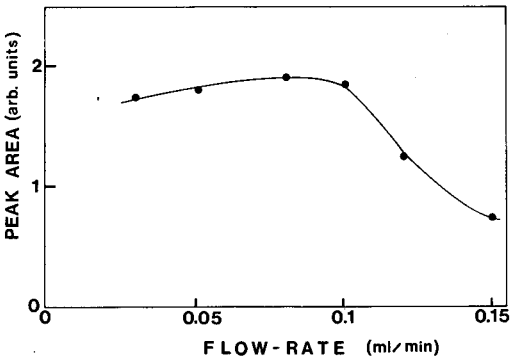

Fig. 6. Effect of the color-forming reagent on the signal intensity. Operating conditions as in Fig. 2 except the flow-rate of the color-forming reagent.

molybdate and 0.36% L-ascorbic acid. A flow-rate of approximately 0.08–0.1 ml/min gave a higher signal intensity, as shown in Fig. 6.

Using the compromise operating conditions determined by the above experiments, an artificial mixture of eight nucleotides was separated in the reversed-phase ion-pair mode, as shown in Fig. 7. The operating conditions are described in the figure legend. The wavelength of detection was 880 nm, and 0.7–12 nmol of the components were injected using a 12-μl loop injector. The detection limits for the examined nucleotides were 0.2–0.4 nmol under the operating conditions shown in Fig. 7.

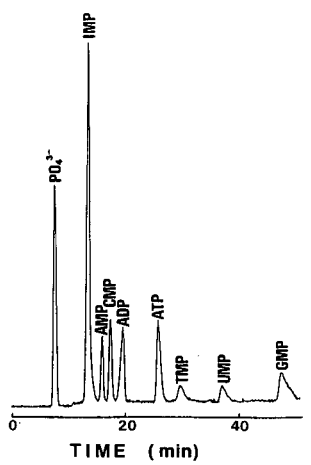

Fig. 7. Separation of an artificial mixture of nucleotides. Separation column: Develosil ODS-5, 250 mm × 4.6 mm I.D. Mobile phase: borate buffer (pH 5.4) containing 1 m*M* tetrabutylammonium chloride and 5 m*M* citric acid–acetonitrile (98:2). Flow-rate of the mobile phase: 0.7 ml/min. Flow-rates of the oxidative reagent and the color-forming reagent: 0.1 ml/min. Temperature of the aluminium bath: 128 °C. Wavelength of detection: 880 nm. Solutes: 12.2 nmol IMP; 4.9 nmol AMP; 4.9 nmol CMP; 4.7 nmol ADP; 4.4 nmol ATP; 0.7 nmol TMP; 0.7 nmol UMP; and 1.5 nmol GMP.

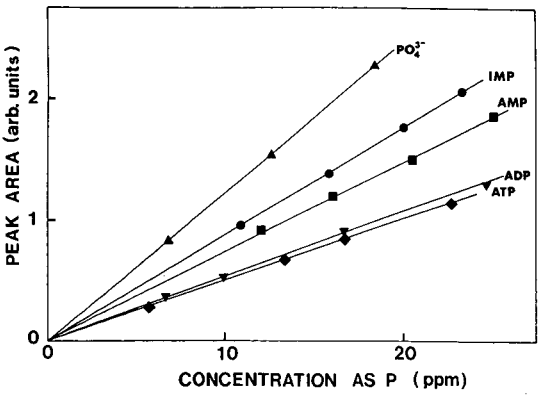

Fig. 8. Calibration graphs for nucleotides. Operating conditions as in Fig. 7.

Fig. 8 shows calibration graphs for orthophosphate, IMP, AMP, ADP and ATP. The peak areas are plotted *versus* the concentration of phosphorus in ppm. The results show that the conversion of the phosphate group of the nucleotides to orthophosphate is not perfect, *e.g.* 72% for IMP, 61% for AMP, 45% for ADP and 43% for ATP. A single calibration graph should be applicable to all the nucleotides if the conversion of all the phosphorus forms to orthophosphate is complete. The detection limits achieved by the molybdenum blue method were higher than those obtained by detection of inherent UV absorption. This is because the noise level of the phos-

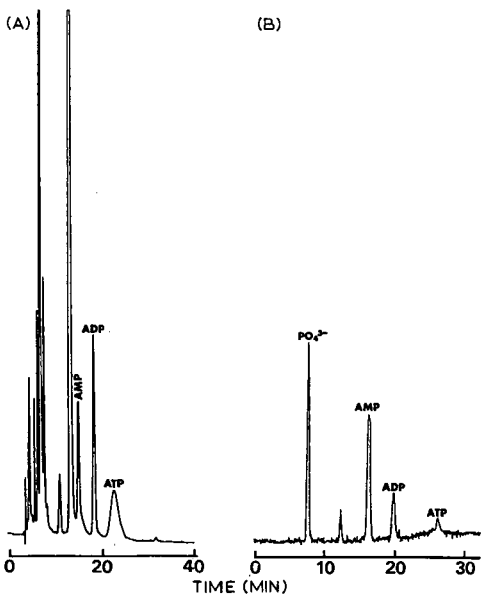

Fig. 9. (A) UV and (B) phosphorus-selective detection of components contained in fish tissues. Operating conditions as in Fig. 7 except the sample (tuna) and detection wavelengths. (A 250 nm; B, 880 nm).

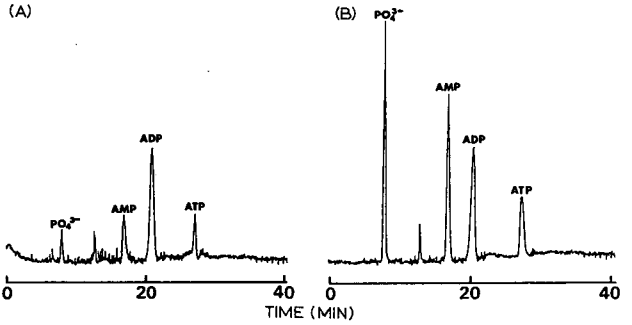

Fig. 10. Phosphorus-selective detection of components in fish tissues. Operating conditions as in Fig. 7 except the samples: (A) porgy; (B) yellowtail.

phorus-selective detection was much higher than that of UV detection owing to the pulsation in the post-column mixing. Howevere, UV detection is not selective, and thus matrices make the analysis of real samples more difficult.

The present system was applied to the analysis of nucleotides contained in raw fish tissues. Fig. 9 demonstrates UV (Fig. 9A) and phosphorus-selective detection (Fig. 9B) of components contained in tuna. The UV detection shows many peaks other than nucleotides, while the phosphorus detection shows a simple chromatogram. The latter detection method allows determination of the nucleotides without problems caused by the interferences from matrices. Orthophosphate, AMP, ADP and ATP could be identified from the retention times of the standard solutes, while the second peak could not be identified. By using the calibration graphs shown in Fig. 8, AMP, ADP and ATP concentrations were determined to be 5.4, 1.7 and 0.6 nmol respectively. The relative standard deviations of the peak area for five measurements of the reference analytes were 0.41 to 1.8%.

Applications to other fish samples, porgy and yellowtail, are shown in Fig. 10. The same components as in Fig. 9 are identified. For the porgy sample, amounts of 2.0 nmol AMP, 4.7 nmol ADP and 1.6 nmol ATP were observed, while 4.9 nmol AMP, 4.0 nmol ADP and 1.9 nmol ATP were observed for the yellowtail sample. The results are listed in Table I. The concentrations of the observed nucleotides were 0.3–3 μmol/g for the the examined raw fish tissues.

TABLE I

NUCLEOTIDES CONTAINED IN RAW FISH TISSUES

Fish	Concentration[a] (μmol/g)		
	AMP	ADP	ATP
Tuna	2.2	0.71	0.26
Porgy	1.0	2.4	0.81
Yellowtail	2.6	2.1	0.98

[a] Based on fresh weight of sample.

CONCLUSION

Phosphorus-selective detection based on the molybdenum blue method could be effectively applied to the analysis of nucleotides, but its detection limits were higher than the detection of inherent UV absorption of the analytes. This is because the former detection method has a higher noise level resulting from post-column mixing. If the pulsation could be eliminated, the sensitivity of the phosphorus-selective detection system would be improved. The present system will be applicable to the selective detection of other phosphorus compounds.

REFERENCES

1 M. McKeag and P. R. Brown, *J. Chromatogr.*, 152 (1978) 253.
2 F. S. Anderson and R. C. Murphy, *J. Chromatogr.*, 121 (1976) 251.
3 C. G. Horvath, W. Melander and I. Malnar, *Anal. Chem.*, 49 (1977) 142.
4 P. D. Schweinsberg and T. L. Loo, *J. Chromatogr.*, 181 (1980) 103.
5 M. W. Taylor, H. V. Hershey, R. A. Levine, K. Coy and S. Olivelle, *J. Chromatogr.*, 219 (1981) 133.
6 M. Zakaria, P. R. Brown and E. Grushka, *Anal. Chem.*, 55 (1983) 457.
7 D. L. Ramos and A. M. Schoffstall, *J. Chromatogr.*, 261 (1983) 83.
8 S. P. Assenza, P. R. Brown and A. P. Goldberg, *J. Chromatogr.*, 272 (1983) 373.
9 Z. El Rassi and C. G. Horvath, *Chromatographia*, 15 (1982) 75.
10 P. A. Perrone and P. R. Brown, *J. Chromatogr.*, 317 (1984) 301.
11 Japanese Industrial Standards Committee, *Testing Methods for Industrial Water JIS K 0102-1986*, Japanese Standards Committee Association, Tokyo, 1986, p. 158.
12 S. Motomizu and M. Oshima, *Analyst (London)*, 112 (1987) 295.
13 P. J. Worsfold, J. R. Clinch and H. Casey, *Anal. Chim. Acta*, 197 (1987) 43.
14 G. Shulze and A. Thiele, *Fresenius' Z. Anal. Chem.*, 329 (1988) 711.
15 M. Goto, W. Hu and D. Ishii, *Environ. Sci.*, 2 (1989) 41.

Journal of Chromatography, 557 (1991) 451–458
Elsevier Science Publishers B.V., Amsterdam

CHROM. 23 156

Structure determination of sesquiterpenes in Chinese vetiver oil by gas chromatography–tandem mass spectrometry

N. SELLIER* and A. CAZAUSSUS
Laboratoire de Spectrométrie de Masse, ENSCP–CNRS, 11 Rue Pierre et Marie Curie, 75231 Paris Cédex 05 (France)
H. BUDZINSKI
UA 348 CNRS, Université de Bordeaux I, 33405 Talence Cédex (France)
and
M. LEBON
Laboratoire de Spectrométrie de Masse, ENSCP–CNRS, 11 Rue Pierre et Marie Curie, 75231 Paris Cédex 05 (France)

ABSTRACT

In Chinese vetiver oil, 118 compounds were characterized according to their chromatographic (GC) and mass spectral (MS) data. Twenty of these compounds were completely identified (name, structure). The GC–MS technique applied involved the use of efficient capillary columns and the acquisition of mass spectra in three different ionization modes (electron impact and positive- and negative-ion chemical ionization). The specificity and sensitivity of the method were greatly enhanced by developing GC–MS–MS experiments under collisionally activated dissociation conditions, the results of which permitted the confirmation of the presence of minor constituents and the determination of the structures of previously undescribed compounds.

INTRODUCTION

The analysis of complex mixtures such as essential oils requires high-resolution chromatographic separation. However, even the use of very efficient columns cannot prevent the overlapping of some peaks. In order to overcome this difficulty, we used a relatively new technique that is particularly well suited to the analysis of complex mixtures, namely tandem mass spectrometry [1] coupled with capillary gas chromatography (GC–MS–MS).

Correct identification of sesquiterpenes is important as a means of checking the authenticity of essential oils, as the profile of sesquiterpenes provides a "fingerprint" for each oil and its particular origin.

In previous work we studied the alcoholic fraction of Bourbon vetiver oil from Reunion [2] and the acetylated fraction of the oil from Java [3]. The aim of this work was to identify the constituents of Chinese vetiver oil by using GC–MS with three different ionization methods: electron impact (EI), positive-ion chemical ionization

0021-9673/91/$03.50

(PCI) and negative-ion chemical ionization (NCI). However, in such complex mixtures as vetiver oil, a single chromatographic peak may contain several compounds, therefore making the recorded spectrum difficult to interpret. Tandem mass spectrometry (MS–MS) coupled with GC enables us to analyse each component of such peaks separately. Using GC–MS–MS we have confirmed the presence of minor compounds such as α-cedrene, acoradiene and khusimene and determined two new esters of molecular weights (MW) 324 and 436, which had not been described previously.

EXPERIMENTAL

Chinese vetiver oil was obtained from Sanofi (Grasse, France) and from L'Oréal (Chevilly-Larue, France) and reference compounds α-cedrene from Fluka (Buchs, Switzerland) and cadinenes from A. Michet of Clermont-Ferrand II University (Clermont-Ferrand, France).

Preliminary GC studies with flame ionization detection (FID) were performed on a Varian (Les Ulis, France) Model 3400 gas chromatograph.

GC–MS experiments were performed on a Nermag R10-10C combined gas chromatograph–mass spectrometer controlled by a Digital PDP11-23 Plus system (Delsi-Nermag, Agenteuil, France). Two fused-silica capillary columns were used, one (50 m × 0.23 mm I.D.) coated with SE-54 liquid phase (0.2 μm) (Chrompack-France, Les Ulis, France) and the other (60 m × 0.247 mm I.D.) coated with DB-WAX (0.15 μm) (J&W Scientific, Folson, CA, USA). The oven temperature was programmed from 100 to 160°C at 2°C/min, and then to 290°C at 5°C/min for the first column and to 250°C at 5°C/min for the second.

GC–MS analysis of the oxygenated fraction of Chinese vetiver oil was also carried out. This oil was retained on a column filled with silica (40 cm × 2.5 cm I.D.) with diethyl ether as eluent [4].

Different ionization methods were employed: EI, PCI using NH_3 [5] and N^2H_3 [6] (Air Liquide, Le Plessis-Robinson, France) as reagent gas at a pressure of 0.1 Torr (1 Torr = 133.3 Pa) in the ion source and NCI with OH^- as reagent from a nitrous oxide–methane (1:4) mixture (Air Liquide) [7,8].

Subsequent MS–MS studies were carried out using a Finnigan MAT (Hemel Hempstead, UK) TSQ70 triple quadrupole mass spectrometer under collisionally activated dissociation (CAD) conditions. Argon was used as collision gas at a pressure of $1.2 \cdot 10^{-3}$ Torr and the collision energy was 10 eV. Three different scan modes were used: daughter scan, parent scan and neutral loss scan.

The peak matching technique [9] was used to establish the exact mass of the esters and was carried out on a VG70E double-focusing mass spectrometer (VG Instruments, Le Chesnay, France) possessing electric and magnetic sectors.

RESULTS AND DISCUSSION

Gas chromatographic separation

The gas chromatogram of Chinese vetiver oil (Fig. 1) exhibits about 150 peaks, and 118 compounds were detected from these peaks and characterized according to their retention times and mass spectra obtained in the EI, PCI and NCI ionization modes. We identified specifically twenty of these compounds (name and structure)

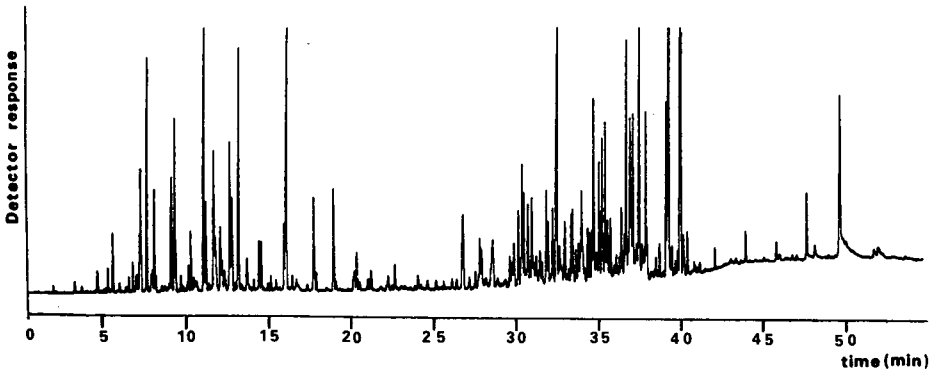

Fig. 1. GC–FID of Chinese vetiver oil. Column, DBWAX (60 m × 0.247 mm I.D.); pressure, 2.2 atm.

(Fig. 2) either with literature data [2,3,10–13] or with reference compounds when available [14].

Although we used a high-resolution capillary column, some peaks unfortunately overlapped (Fig. 3), making mass spectrum interpretation more difficult. GC–EI-MS–MS enabled us to analyse each component of such peaks separately [1].

Tandem mass spectrometry

Chinese vetiver oil does not have exactly the same composition as Bourbon vetiver oil. It was therefore necessary to confirm the presence of α-cedrene, acoradiene and khusimene, which are minor and isomeric compounds; their EI mass spectra are mixed together in the GC–MS analysis and consequently correct identification by comparison with EI spectra of the standards cannot be ensure.

α-Cedrene GC–EI-MS–MS. The EI mass spectrum of α-cedrene standard (Fig. 4a) does not fit the EI mass spectrum of α-cedrene in the mixture (Fig. 4b), which shows extra peaks.

To confirm the presence of this compound in the vetiver oil, GC–EI-MS–MS experiments were carried out. The CAD mass spectra daughter ions of *m/z* 204 and neutral loss of 28 u for standard α-cedrene (Fig. 4b and c) are very close to the CAD spectra obtained at the relevant point of α-cedrene in the mixture (Fig. 4e and f) and confirm that this compound is undoubtedly α-cedrene.

Acoradiene and khusimene GC–EI-MS–MS. The EI mass spectra of acoradiene (Fig. 5a) and khusimene (Fig. 5b) show base peaks at *m/z* 136 and 134, respectively, produced by a retro-Diels–Alder reaction. Consequently, the GC–EI-MS–MS experiments concerned the neutral loss of 68 u (Fig. 5c) and the parent ions of *m/z* 136 (Fig. 5e) for acoradiene and the neutral loss of 70 u (Fig. 5d) and the parent ions of *m/z* 134 (Fig. 5f) for khusimene. These results enabled us to assign the structures of acoradiene and khusimene for these two compounds.

GC–EI-MS–MS of two new products. The GC–EI-MS of Chinese vetiver oil (Fig. 6) shows the presence of unknown compounds of molecular weights 324 and 436, just at the end of the chromatogram. Two groups of peaks are observed in the chromatogram; we only analysed peaks A and B (Fig. 6) as the others are isomers of these compounds. Using GC–MS and GC–MS–MS we tried to establish the structure of these new, natural products observed in Chinese vetiver oil.

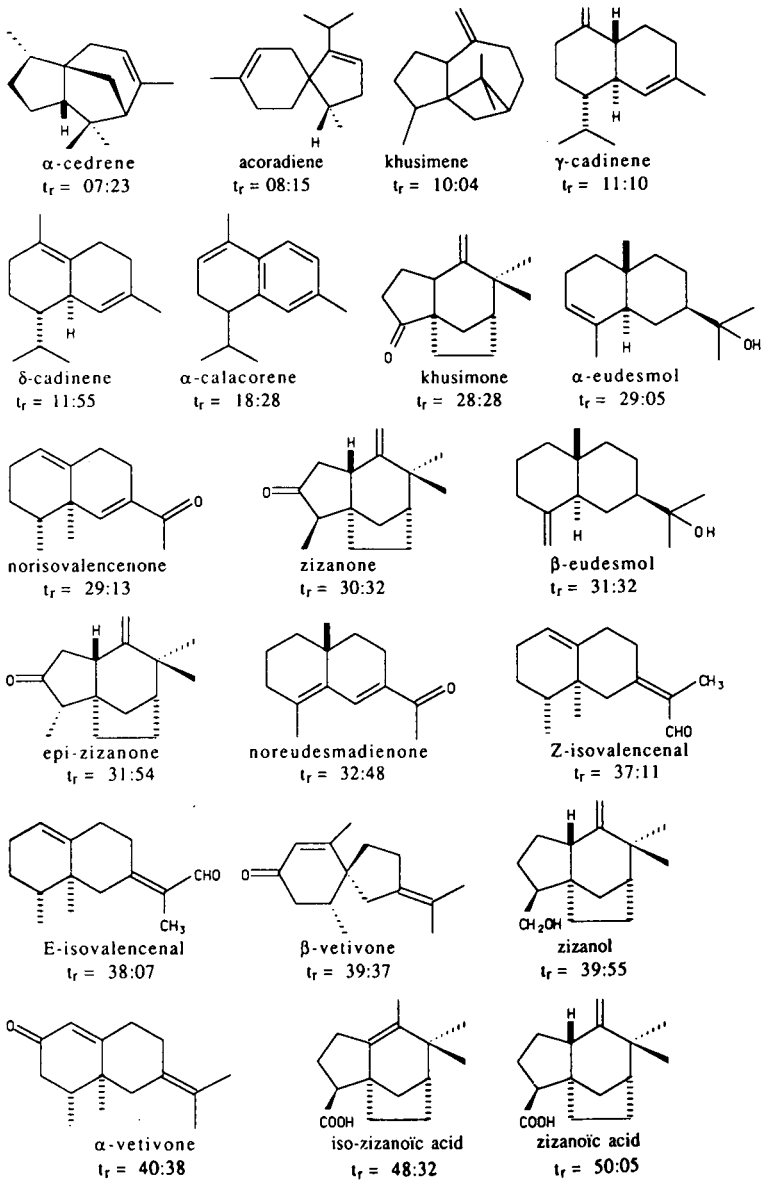

Fig. 2. Twenty sesquiterpenes identified in Chinese vetiver oil with names, formulae and retention times (min:s).

Figs. 7a and b show the EI mass spectra at 70 eV of the unknown compounds of molecular weights 324 (A) and 436 (B). We observed for A and B characteristic ions of sesquiterpenes such as at m/z = 131, 133, 145, 159, 173 and 187. For compound A, the base peak is m/z = 91 and an important fragment ion is observed at m/z = 233. For compound B, the base peak is m/z 202.

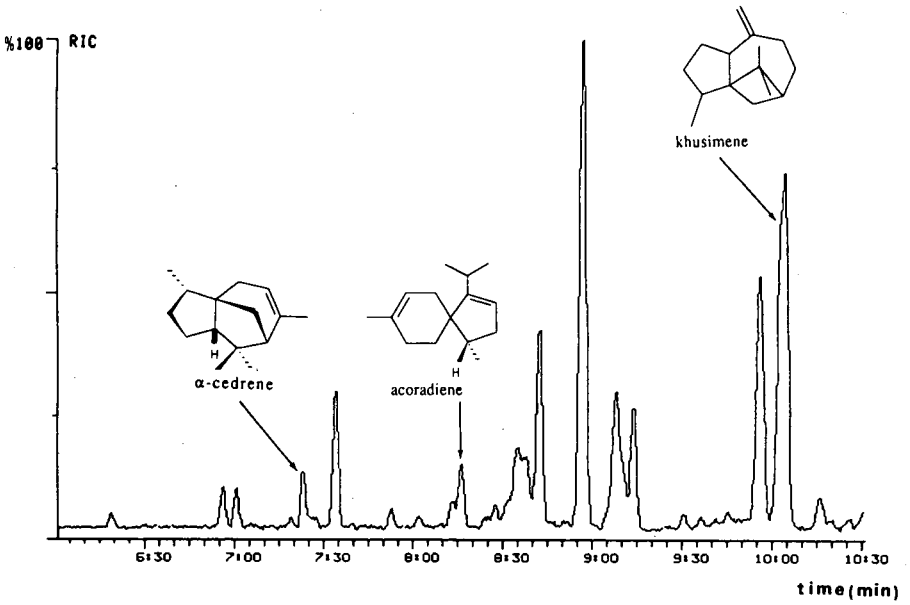

Fig. 3. GC–EI-MS expanded chromatogram of the region concerning α-cedrene, acoradiene and khusimene in Chinese vetiver oil.

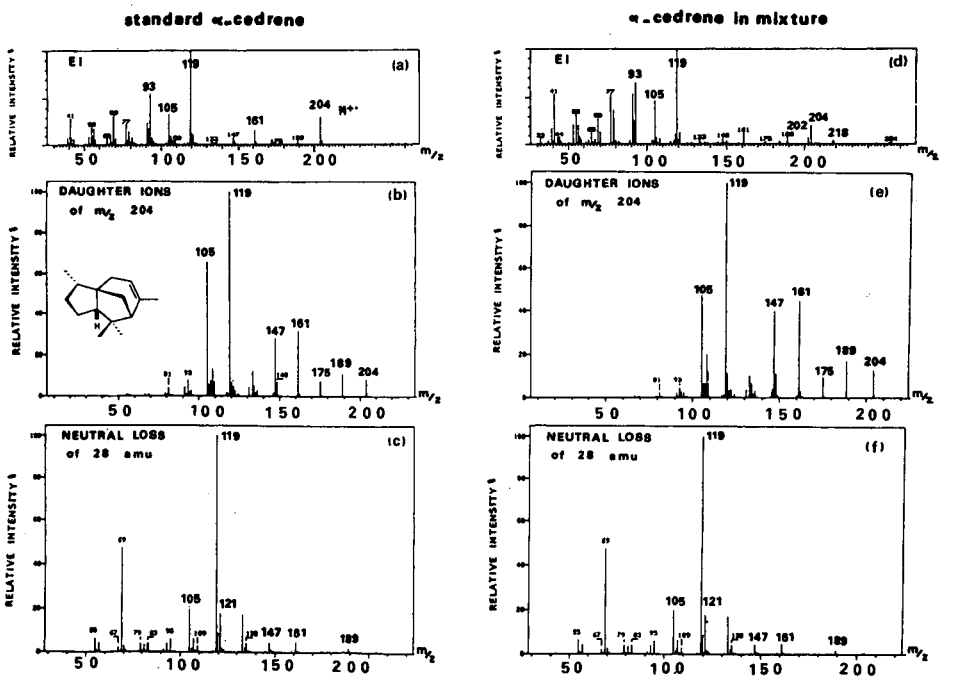

Fig. 4. (a) EI mass spectrum of standard α-cedrene at 70 eV; (b), (c) CAD mass spectra of standard α-cedrene at 10-eV collision energy; (d) EI mass spectrum of α-cedrene in the mixture at 70 eV; (e) (f) CAD mass spectra of α-cedrene in the mixture at 10-eV collision energy.

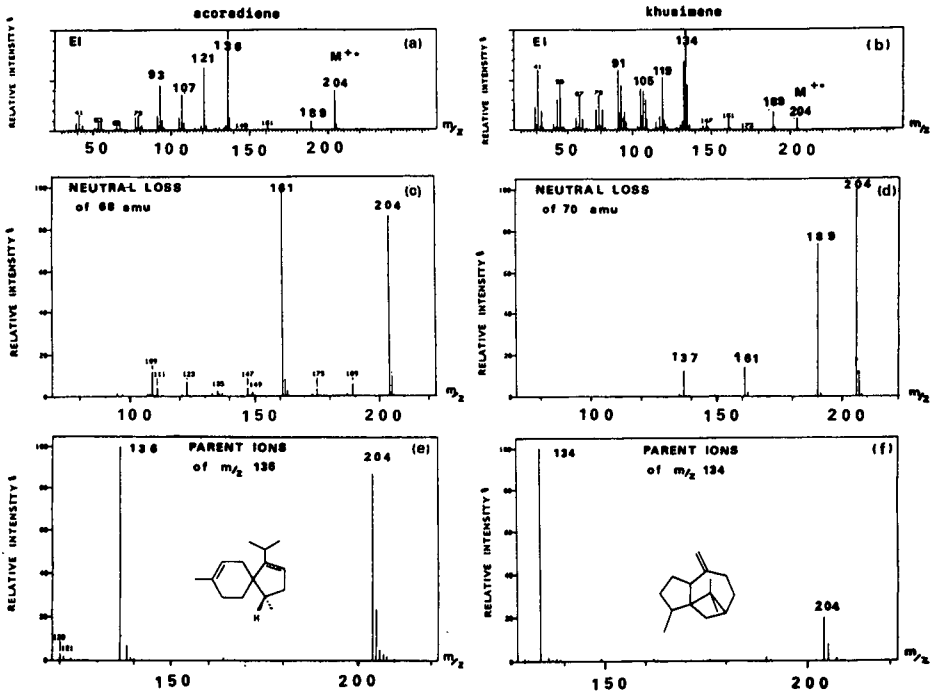

Fig. 5. (a) EI mass spectrum of acoradiene at 70 eV; (b) EI mass spectrum of khusimene at 70 eV; (c), (e) CAD mass spectra for acoradiene at 10-eV collision energy; (d), (f) CAD mass spectra for khusimene at 10-eV collision energy.

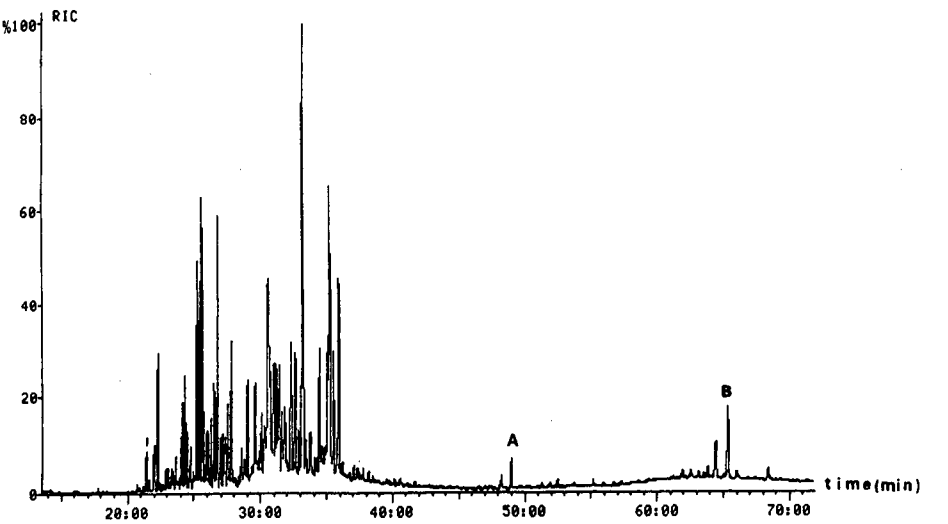

Fig. 6. GC–EI-MS chromatogram of Chinese vetiver oil. Column, SE-54 (50 m × 0.23 mm I.D.); pressure, 1.8 atm.

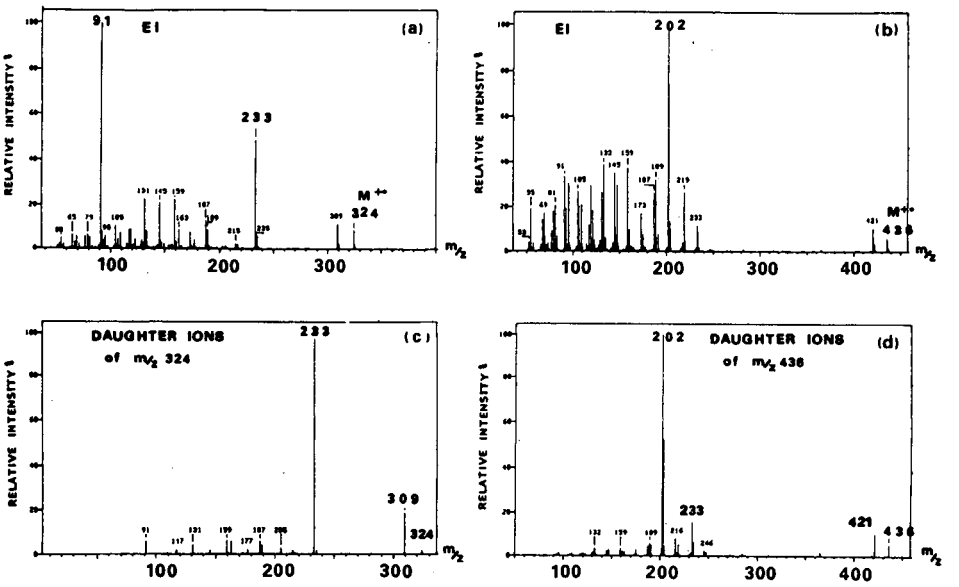

Fig. 7. (a) EI mass spectrum of compound A at 70 eV; (b) EI mass spectrum of compound B at 70 eV: (c) CAD mass spectrum daughter ions of m/z 324 for compound A at 10-eV collision energy; (d) CAD mass spectrum daughter ions of m/z 436 for compound B at 10-eV collision energy.

The spectra of compounds A and B were also obtained by GC–PCI ($N^2H_4^+$)-MS and this technique confirmed that no labile hydrogen exists in these two molecules.

To complete these investigations we used CAD experiments with a collision energy of 10 eV to examine the daughter ions of m/z 324 (Fig. 7c), the parent ions of m/z 233 and 91 and the neutral loss of 15 u from compound A. We also determined the daughter ions of m/z 436 (Fig. 7d) and the parents of m/z = 202 and 233 for compound B. In conclusion, the ions at m/z 233 from A and m/z 202 from B are only generated by the molecular ions of m/z 324 and 436, respectively.

Exact masses and formulae were obtained for compounds A and B by the peak matching technique. The results are given in Table I.

All the MS and MS–MS experiments confirmed the presence of esters of formula $C_{22}H_{28}O_2$ (MW = 324) and $C_{30}H_{44}O_2$ (MW = 436).

Two possible suggestions for compound A are $RCOOC_6H_4CH_3$-*p* or $RCOOCH_2C_6H_5$. If RCOOH is an acid of Chinese vetiver oil, it could be isozizanoic acid (Fig. 2), whose fragmentation under EI ionization is the same as that observed in the spectrum of compound A (Fig. 7a). The benzyl ester formula is the more likely of the two with regard to the base peak at m/z 91 observed in the EI mass spectrum (Fig. 7a).

For the ester B we propose the formula RCOOR′, in which RCOOH is an acid (MW = 234) and R′OH is an alcohol (MW = 218) both of which are present in vetiver oil.

It is difficult to determine the structures of the esters precisely because they are present in very small proportions in Chinese vetiver oil (0.27% of the total). There-

TABLE I

EXACT MASSES AND FORMULAE OF COMPOUNDS A AND B

Data were obtained on a VG70E double-focusing mass spectrometer.

Compound	Nominal mass	Exact mass	Formula
A	324	324.2087	$C_{22}H_{28}O_2$
	309	309.1853	$C_{21}H_{25}O_2$
	233	233.1540	$C_{15}H_{21}O_2$
B	436	436.3340	$C_{30}H_{44}O_2$
	421	421.3104	$C_{29}H_{41}O_2$
	203	203.1799	$C_{15}H_{23}$
	202	202.1720	$C_{15}H_{22}$

fore, GC–infrared measurements are not possible. Other vetiver oils from Bourbon Reunion, Java and Haiti were also analysed with the same techniques but the esters A and B were found only in Chinese vetiver oil.

In conclusion, although GC–MS is a very useful tool for the analysis of complex mixtures such as essential oils, a more sophisticated technique such as GC–MS–MS is required to confirm the presence and to determine the structures of minor compounds found in such oils. This paper has illustrated the successful application of tandem mass spectrometry and confirmed the specificity, sensitivity and speed of this technique.

ACKNOWLEDGEMENTS

The authors thank Henri Virelizier (CEA, Saclay, France) for his scientific support in peak matching analysis and Phil East and John Wellby of Finnigan MAT (Hemel Hempstead, UK) for their technical support in MS–MS analysis. They also thank A. Michet of Clermont-Ferrand II University (Clermont-Ferrand, France) for providing reference compounds of cadinenes and Jeannine Mauroy for her help and participation in this work. They express their gratitude to the CNRS for financial support.

REFERENCES

1 F. W. McLafferty, *Tandem Mass Spectrometry*, Wiley-Interscience, New York, 1983.
2 A. Cazaussus, R. Pes, N. Sellier and J. C. Tabet, *Chromatographia*, 25 (1988) 865.
3 A. Cazaussus, P. Y. Rozé and N. Sellier, *Chromatographia*, 28 (1989) 579.
4 S. Smadja, E. M. Gaydou, G. Lamaty and J. Y. Conan, *Parfums Cosmét. Arômes*, 86 (1988) 61.
5 J. B. Westmore and M. M. Alauddin, *Mass Spectrom. Rev.*, 5 (1986) 381.
6 D. F. Hunt and S. K. Sethi, *J. Am. Chem. Soc.*, 102 (1980) 6953.
7 D. F. Hunt and F. W. Crow, *Anal. Chem.*, 50 (1978) 1781.
8 G. George, *Parfums Cosmét. Arômes*, 43 (1982) 37.
9 K. S. Quisenberry, T. T. Scolman and A. O. Nier, *Phys. Rev.*, 102 (1956) 1071.
10 K. A. Plavcan, *Thesis*, Cornell University, 1985.
11 J. Smadja, *Thesis*, Université des Sciences et Techniques du Languedoc, 1987.
12 T. A. Van Beek, R. Kleiss, M. A. Posthumus and A. Van Veldhuizen, *Phytochemistry*, 28 (1989) 1909.
13 R. P. Adams, *Identification of Essential Oils by Ion Trap Mass Spectroscopy*, Academic Press, New York, 1989.
14 J. Biougne, J. C. Chalchat, R. Ph. Garry and A. Michet, *Parfums Cosmét. Arômes*, 73 (1987) 59.

Journal of Chromatography, 557 (1991) 459–468
Elsevier Science Publishers B.V., Amsterdam

CHROM. 23 097

Retention behaviour of polycyclic aromatic hydrocarbons on a liquid-crystal bonded phase in reversed-phase liquid chromatography

KIYOKATSU JINNO*, YOSHIHIRO SAITO and RENU MALHAN née CHOPRA
School of Materials Science, Toyohashi University of Technology, Toyohashi 441 (Japan)
JOSEPH J. PESEK
Department of Chemistry, San Jose State University, San Jose, CA 95192-0101 (USA)
and
JOHN C. FETZER and WILT B. BIGGS
Chevron Research and Technology Company, Richmond CA 94802 (USA)

ABSTRACT

The liquid chromatographic characteristics of polycyclic aromatic hydrocarbons on a recently reported liquid-crystal bonded phase were evaluated. The results clearly indicated that the material has a strong molecular planarity recognition capability because of its ordered bonded-phase structure. The recognition capability was dependent on mobile phase composition and column temperature. The behaviour can be explained by a so-called 'slot-like' structure used to describe retention of polycyclic aromatic hydrocarbons on polymeric octadecylsilica phases.

INTRODUCTION

It is necessary to have good separation and analytical methods for the recognition of molecular planarity and shape of polycyclic aromatic hydrocarbons (PAHs), because their physicochemical properties and biological activities are closely related to their molecular structures [1–3].

The most common method of PAH separation is reversed-phase liquid chromatography (RPLC) with chemically bonded octadecylsilica (ODS) phases as the universal choice of stationary phase. Commercially available ODS phases can be basically divided into two types, depending on the bonding chemistry: one is polymeric, synthesized from polyfunctional silanes, and the other is monomeric, based on monofunctional silanes as the starting material. The retention behaviour of PAHs has been reported to depend on the type of ODS stationary phases [4–10], and the conclusion is that polymeric phases are better able to recognize molecular planarity in PAHs. Planar molecules are retained longer than non-planar molecules with polymeric phases because of the "slot-like" structure on the surface, as described by Sander and Wise

0021-9673/91/$03.50

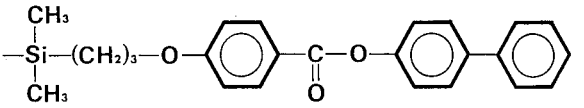

Fig. 1. Chemical structure of the liquid-crystal bonded phase.

[4–7]. Solid-state cross-polarization magic angle spinning nuclear magnetic resonance spectroscopy (CP-MAS-NMR) clearly reveals that the reduced molecular freedom of alkyl chains on the polymeric phase increases molecular planarity recognition [11]. It can be concluded that very ordered phases should have stronger molecular planarity recognition capability.

Extending the investigations of several previous publications [8–14], we evaluated a liquid-crystal bonded phase the structure of which is shown in Fig. 1 [15,16]. The phase has a very ordered structure in the normal temperature range and one can expect it to have strong molecular planarity recognition power. In this paper, we will describe the retention behaviours of PAHs with the liquid-crystal stationary phase in RPLC.

EXPERIMENTAL

Synthesis of (4-(allyloxy)benzoyl)biphenyl [17]

To a two-neck 250-ml round-bottom flask equipped with a 50-cm reflux condenser, a PTFE septum with a nitrogen line, a magnetic stirring bar and an oil bath were added, under nitrogen, 4.93 g of 4-phenylphenol dissolved in 50 ml of dry pyridine. Next, 6.13 g of 4-(allyloxy)benzoyl chloride was added with stirring. The mixture was stirred for 3 h at 25°C and then heated to 60°C for an additional 2 h. After the reaction mixture had cooled to 25°C, 200 ml of acidic (20% HCl) deionized water was added. The resulting precipitate was collected by vacuum filtration and washed with 200 ml of cold deionized water. The crude product was recrystallized from an acetone–ethanol (1:1) mixture yielding 8.45 g (88%, m.p. 138–140°C).

Synthesis of silane reagent and silica bonding [15,16]

The (4-(allyloxy)benzoyl)biphenyl (11.8 mmol) dissolved in 20 ml of dry toluene was added to a two-neck 100 ml round-bottom flask equipped with a 50-cm reflux condenser, a PTFE septum with a nitrogen line, a magnetic stirrer and an oil bath. Next, 11.8 mmol of dimethylchlorosilane were added to the reaction flask while stirring and purging with nitrogen. After 5 min, 8 mg of hexachloroplatinic acid were added. The reaction mixture was heated to 65°C and stirred for ten days under nitrogen. Then 20 ml of freshly distilled toluene were added followed by 6.5 g of silica (Nucleosil 300-10) and 0.5 ml of dry pyridine. The reaction mixture was stirred for ten days at 40°C under nitrogen. The solid was then collected and washed with 60 ml of toluene followed by 60 ml of ethanol. The wash procedure was repeated six times.

RPLC measurements

The synthesized liquid-crystal phase was packed into a fused-silica capillary of 200 mm × 0.52 mm I.D. by a slurry technique. For comparison two commercially

available stationary phases, TSK ODS-120T (Tosoh, Tokyo, Japan), representative of polymeric ODS, and Capcell ODS 120SG (Shiseido, Yokohama, Japan), representative of monomeric ODS, were also packed into the same size of capillaries.

The microcolumn LC system consisted of a microfeeder MF-2 pump (Azuma Electric, Tokyo, Japan), a Rheodyne 7513 injector (Cotati, CA, USA) and a Jasco Uvidec 100-III UV detector set at 254 nm. Mobile phases were pure methanol and mixtures of methanol and water, and the typical flow-rate was 2 μl/min. The column temperature was controlled by a home-made oven. The chromatographic measurements were performed at least in triplicate. The retention data used for the evaluation were mean values of these experimental data. The peak of dichloromethane, which was the sample solvent, was used to measure the column dead volume.

PAHs used for the evaluation were commercially available (Tokyo Kasei, Tokyo, Japan) except tetrabenzonaphthalene (TBN) and phenanthro[3,4-*c*]phenanthrene (PhPh), which were synthesized in the laboratory of Chevron Research and Technology Company (Richmond, CA, USA).

RESULTS AND DISCUSSION

To understand the basic chromatographic characteristics of the synthesized liquid-crystal bonded phase the separation of various PAHs was performed. The data obtained are summarized in Table I, in which the retention data with ODS-120T and Capcell ODS are also tabulated for comparison. The data for the liquid-crystal phase are shown in Fig. 2, in which log k' (capacity factor) values are plotted as a function of F number using 100% methanol as the mobile phase. A high linear correlation between log k' and F number was found [12] for the retention behaviour of PAHs with monomeric ODS phases in aqueous RPLC. The F number is defined by Schabron *et al.* [18] as follows: F = (number of double bonds) + (number of primary and secondary carbons) − 0.5 (for a non-aromatic ring). Fig. 2 clearly shows that planar PAHs are on the line, but the retention of non-planar PAHs such as *o*-terphenyl, PhPh and TBN shows a negative deviation from the line. This means that the phase

TABLE I

RETENTION DATA OF PAHs WITH THREE DIFFERENT BONDED PHASES

Mobile phase: methanol.

Solute	Capacity factor (k') on stationary phase		
	Liquid crystal	ODS-120T	Capcell ODS
Benzene	0.02	0.06	0.12
Naphthalene	0.09	0.16	0.21
Anthracene	0.47	0.38	0.41
Pyrene	0.53	0.66	0.59
o-Terphenyl	0.15	0.25	0.36
Triphenylene	0.72	0.75	0.61
BaP	2.48	1.81	0.80
TBN	2.12	1.94	1.86
PhPh	0.79	0.88	1.17

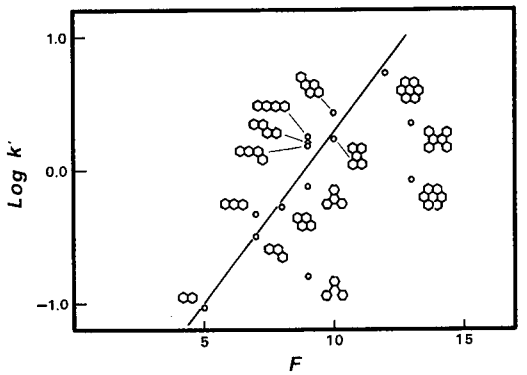

Fig. 2. Relationship between log k' and F number with the liquid-crystal stationary phase. Mobile phase, methanol, flow-rate, 2 μl/min.

has a strong planarity recognition capability. Planar solutes are retained longer, while non-planar solutes are eluted faster. Another interesting trend is the positive deviation from this line for the retention of rod-like PAHs. Although more detailed investigation will be required, it can be said that the liquid-crystal phase used in this study also has a shape selectivity for PAHs, as found by Chang *et al.* [19] in capillary supercritical fluid chromatography with a liquid-crystal stationary phase.

In order to examine in more detail the planarity recognition capability of the liquid-crystal phase, the separation factor of *o*-terphenyl and triphenylene was evaluated with the three phases shown in Table I, and the values are summarized in Table II. This factor has been confirmed by Tanaka and co-workers [20,21] and Jinno *et al.* [14] as a good indicator of the planarity recognition capability of the stationary phases in RPLC. Generally, polymeric ODS phases give a value of about 2–3, and monomeric phases a value of about 1–2 in aqueous mobile phase environments, although it has been observed that these values are larger when pure methanol is used as the mobile phase. The values reported in Table II are, therefore, in agreement with previous results. The value of the liquid-crystal phase is 4.8, and it suggests that this phase has very strong planarity recognition capability.

Mobile phase composition is one of major factors influencing the planarity recognition capability of the stationary phases in RPLC. The data summarized in

TABLE II

SEPARATION FACTORS BETWEEN *o*-TERPHENYL AND TRIPHENYLENE, AND BETWEEN TBN AND BaP

Stationary phase	Separation factors	
	Triphenylene/*o*-terphenyl	TBN/BaP
Liquid crystal	4.80	0.85
ODS-120T	3.00	1.07
Capcell ODS	1.69	2.33

TABLE III

RETENTION DATA OF *o*-TERPHENYL AND TRIPHENYLENE WITH DIFFERENT MOBILE PHASE COMPOSITIONS

Temperature: room temperature.

Mobile phase composition (methanol–water)	Capacity factor (k')		Separation factor
	o-Terphenyl	Triphenylene	
100:0	0.15	0.72	4.80
95:5	0.24	1.12	4.67
90:10	0.38	1.72	4.53
85:15	0.64	2.74	4.28
80:20	1.01	4.21	4.17

Table III indicate the effect of the water content in the mobile phase on the separation factor of *o*-terphenyl and triphenylene. For clarification the separation factors are plotted as a function of the water content in Fig. 3. It appears that increasing the water content in the mobile phase results in a decrease in the separation factor. The results can be explained as follows: In an aqueous environment, *o*-terphenyl will be more solvated by methanol. This makes the solute bulkier, so that the planarity difference between triphenylene and *o*-terphenyl will be smaller with increasing water content in the mobile phase.

Another measure of stationary phase planarity recognition in RPLC which has been proposed by Sander and Wise [6,7] is the retention ratios of benzo[*a*]pyrene (BaP), TBN and PhPh. These values are also calculated from the data in Table I and shown in Table II. These data also indicate strongly that the liquid-crystal phase has a greater capacity to recognize PAH molecular planarity.

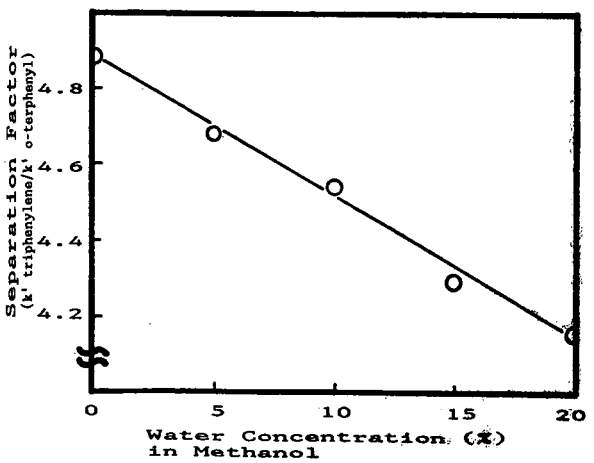

Fig. 3. Separation factor of *o*-terphenyl and triphenylene *versus* mobile phase compositions. Column temperature, room temperature.

TABLE IV

RETENTION DATA OF BaP, TBN AND PhPh WITH DIFFERENT MOBILE PHASE COMPOSITIONS

Temperature: room temperature.

Mobile phase composition (methanol–water)	Capacity factor (k')			Separation factor TBN/BaP
	BaP	TBN	PhPh	
100:0	2.48	2.12	0.79	0.85
95:5	4.18	3.83	1.32	0.92
90:10	6.99	7.11	2.21	1.02
85:15	12.00	12.90	3.71	1.08
80:20	19.80	23.37	6.21	1.18

Sander and Wise proposed [6,7,22] column selectivity based on the separation factor between BaP and TBN (k'_{TBN}/k'_{BaP}). They reported that monomeric ODS phases give values about 1.5–2, and polymeric ODS phases give a value less than 1 in aqueous mobile phase. As shown in Table II, the liquid-crystal phase gives a value of 0.85 in 100% methanol as the mobile phase. Therefore, the phase is quite similar to the typical polymeric ODS phases and has a strong planarity recognition capability.

For the separation factors between BaP and TBN the effect of the mobile phase

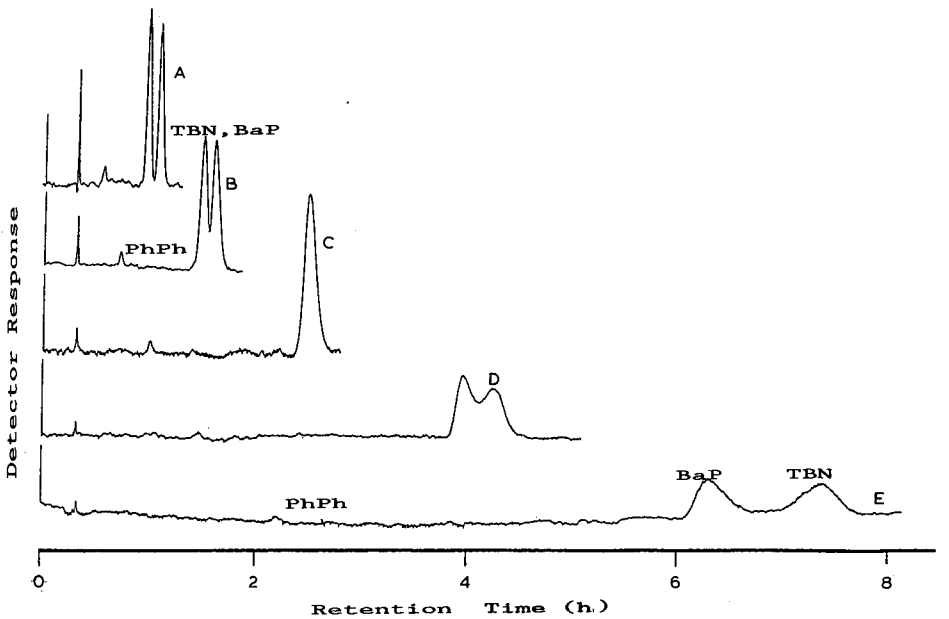

Fig. 4. Chromatograms for the separation of BaP, TBN and PhPh with different mobile phase (methanol–water) compositions. (A) 100:0;, (B) 95:5; (C) 90:10; (D) 85:15; (E) 80:20. Column temperature, room temperature; flow-rate, 2 μl/min; detection, UV at 254 nm.

TABLE V

SEPARATION FACTORS BETWEEN *o*-TERPHENYL AND TRIPHENYLENE WITH DIFFERENT COLUMN TEMPERATURES

Mobile phase: methanol–water (80:20).

Column temperature (°C)	Capacity factor (k')		Separation factor
	o-Terphenyl	Triphenylene	
0	1.94	8.82	4.55
27	1.03	4.44	4.31
40	0.74	3.04	4.11
50	0.66	2.56	3.88
60	0.59	2.21	3.75
70	0.56	2.01	3.59

composition was also evaluated. The results are summarized in Table IV. Increasing the water content in the mobile phase increases the separation factor. This means that the phase is changing to a monomer-like from a polymer-like structure, and this fact is in good agreement with that discussed above for the separation factors between *o*-terphenyl and triphenylene. In Fig. 4, the chromatograms clearly indicate the effect of the mobile phase composition on the elution order of BaP and TBN with the liquid-crystal stationary phase.

Temperature is also one of the major factors influencing the molecular recog-

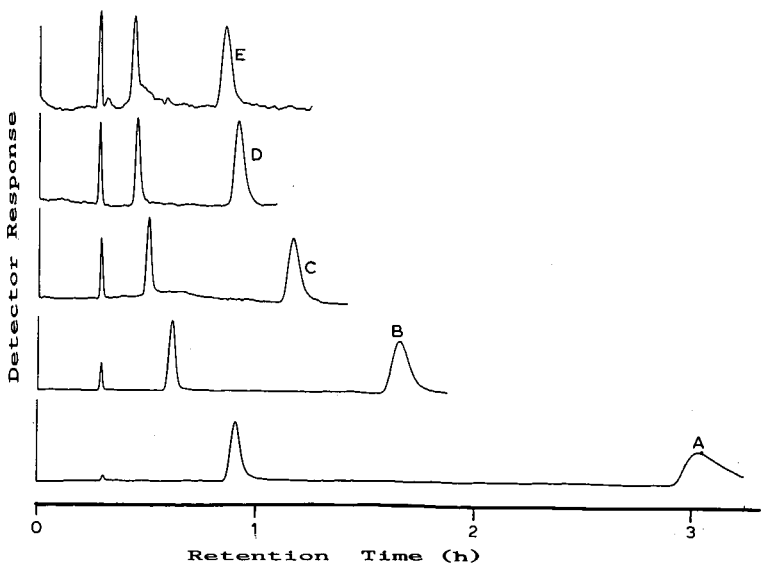

Fig. 5. Chromatograms for the separation of *o*-terphenyl and triphenylene with different column temperatures. (A) 0°C; (B) 27°C; (C) 40°C; (D) 60°C; (E) 70°C. Mobile phase, methanol–water (80:20); flow-rate, 2 μl/min; detection, UV at 254 nm.

nition capability of the stationary phase. In our previous work [8] and the work of Sander and Wise [6,22], increasing the temperature caused a decrease in the planarity recognition capability of polymeric ODS phases. Solid-state CP-MAS-NMR studies explained this fact by revealing that an increase in temperature caused the polymeric ODS phase to change from a solid-like to liquid-like structure [8]. This kind of behaviour would also be expected of the liquid crystal phase because it also undergoes a thermal phase change. Therefore, the separation factors between *o*-therphenyl and triphenylene were measured at various column temperatures. The results are tabulated in Table V. The corresponding chromatograms are illustrated in Fig. 5. An increase of the column temperature not only reduces the retention time but also causes a decrease in the separation factor between *o*-terphenyl and triphenylene. Fig. 6, in which the separation factors are plotted as a function of temperature, shows these effects clearly. A decrease of temperature increases the planarity recognition capability of the liquid-crystal phase in the same manner as polymeric ODS phases. It is possible to explain this fact by the same theoretical interpretation of the stationary phase structure change with the temperature. The orderlines of the bonded phase increases with the decrease of the temperature, and this orderliness or rigidity of the bonded phase offers higher planarity recognition capability. Although we did not measure the solid-state NMR spectra of the liquid-crystal phase at different temperatures, a situation similar to that which has been found in the polymeric ODS phase [8] may be present in this phase structure.

It was indicated in the above discussions that there are some similarities between polymeric ODS phases and the liquid-crystal phase in their planarity recognition capability. The similarity is better seen in the correlation matrix shown in Table VI, in which cross-correlations among the retention data sets obtained for the three different phases in Table I are summarized. The similarity between ODS-120T and the liquid-crystal phase is much higher than other correlations, and there is also a low correlation between Capcell and the liquid crystal phase. It is clear that the

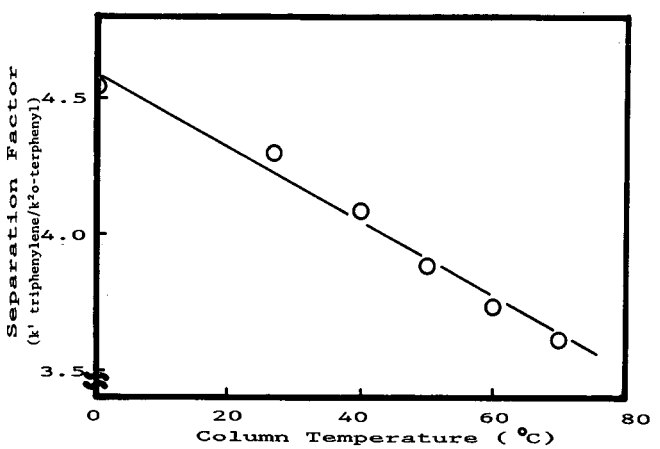

Fig. 6. Temperature dependency of the separation factors between *o*-terphenyl and triphenylene. Mobile phase, methanol–water (80:20); flow-rate, 2 μl/min.

TABLE VI

CORRELATION MATRIX OF THE RETENTION DATA WITH THREE DIFFERENT STATIONARY PHASES IN TABLE I

Mobile phase: methanol.

Stationary phase	Liquid crystal	ODS-120T	Capcell ODS
Liquid crystal	–		
ODS-120T	0.982	–	
Capcell ODS	0.740	0.844	–

liquid-crystal phase is very similar to the polymeric ODS phases and dissimilar to monomeric phases. This similarity is mainly due to the orderliness of the bonded-phase structures. This explains that the strong planarity recognition capability of the liquid-crystal phase is due to its ordered structure.

In conclusion, the liquid-crystal phase, like typical polymeric ODS phases, possesses a strong planarity recognition power, but its ability to recognize PAHs is much higher than that of polymeric ODS phases because its orderliness can be assumed to be tighter and more rigid than that of polymeric ODS phases, although more details should be known by structure studies of the liquid-crystal phase with spectroscopic measurements. This is currently being investigated in our laboratory.

ACKNOWLEDGEMENTS

Partial support for this work (J. J. P.) was provided by the National Science Foundation (Grant No. CHE-8814849). K. J. also thanks the Ministry of Education, Science and Culture of Japan (Grant No. 63550564) for its support.

REFERENCES

1 R. G. Harvey (Editor), *Polycyclic Hydrocarbons and Carcinogenesis (ACS Symposium Series*, No. 283), American Chemical Society, Washington, DC, 1986.
2 I. A. Smith, G. D. Berger, P. G. Seybold and M. P. Serve, *Cancer Res.*, 38 (1978) 2968.
3 G. H. Loew, J. Phillips, J. Wong, L. Hieldmeland and G. Pack, *Cancer Biochem. Biophys.*, 2 (1978) 113.
4 L. C. Sander and S. A. Wise, *Anal. Chem.*, 56 (1984) 504.
5 L. C. Sander and S. A. Wise, *J. Chromatogr.*, 316 (1984) 163.
6 L. C. Sander and S. A. Wise, *Anal. Chem.*, 59 (1987) 2309.
7 L. C. Sander and S. A. Wise, *LC·GC*, 8 (1990) 378.
8 K. Jinno, T. Ibuki, N. Tanaka, M. Okamoto, J. C. Fetzer, W. R. Biggs, P. R. Griffiths and J. M. Olinger, *J. Chromatogr.*, 461 (1989) 209.
9 K. Jinno, T. Nagoshi, N. Tanaka, M. Okamoto, J. C. Fetzer and W. R. Biggs, *J. Chromatogr.*, 392 (1987) 75.
10 K. Jinno, S. Shimura, N. Tanaka, K. Kimata, J. C. Fetzer and W. R. Biggs, *Chromatographia*, 27 (1989) 285.
11 K. Jinno, *J. Chromatogr. Sci.*, 27 (1989) 729.
12 K. Jinno, S. Shimura, J. C. Fetzer and W. R. Biggs, *J. High Resolut. Chromatogr. Chromatogr. Commun.*, 11 (1988) 673.
13 K. Jinno, S. Shimura, J. C. Fetzer and W. R. Biggs, *Poly. Arom. Comp.*, 1 (1990) 151.
14 K. Jinno, K. Yamamoto, H. Nagashima, T. Ueda and K. Itoh, *J. Chromatogr.*, 517 (1990) 193.

15 J. Pesek and T. Cash, *Chromatographia*, 27 (1989) 559.
16 J. Kohler, *Chromatographia*, 21 (1986) 573.
17 M. A. Apfel, H. Finkelmann, G. M. Janini, R. J. Laub, B. H. Luhman, A. Price, W. L. Roberts, T. H. Shaw and C. A. Smith, *Anal. Chem.*, 57 (1985) 651.
18 J. F. Schabron, R. J. Hurtubise and H. F. Silver, *Anal. Chem.*, 49 (1977) 2253.
19 H. C. K. Chang, K. E. Markides, J. S. Bradshaw and M. L. Lee, *J. Chromatogr. Sci.*, 26 (1988) 280.
20 K. Kimata, I. Iwaguchi, S. Onishi, K. Jinno, R. Eksteen, K. Hosoya, M. Araki and N. Tanaka, *J. Chromatogr. Sci.*, 27 (1989) 721.
21 N. Tanaka, K. Sakagami and M. Araki, *J. Chromatogr.*, 199 (1980) 327.
22 L. C. Sander and S. A. Wise, *Anal. Chem.*, 61 (1989) 1749.

Journal of Chromatography, 557 (1991) 469–479
Elsevier Science Publishers B.V., Amsterdam

CHROM. 23 098

Theoretical analysis for measurement of building pollution parameters by gas chromatography

N. A. KATSANOS* and Ch. VASSILAKOS
Physical Chemistry Laboratory, University of Patras, 26110 Patras (Greece)

ABSTRACT

The important parameters in gas–solid reactions can be determined simultaneously, under non-steady-state conditions using reversed-flow gas chromatography. A very simple experimental arrangement is required, with a slightly modified gas chromatograph. The distorted diffusion band obtained experimentally can be analysed mathematically giving, for the gas reactant, the values of adsorption, reaction and desorption rate constants, the overall mass transfer coefficients in the gas and in the solid and the adsorption equilibrium constant. All these parameters were determined at various temperatures for the reaction of sulphur dioxide with pieces of marble of two sizes, using two different air flow-rates.

INTRODUCTION

The main effects of air pollution on historic buildings and monuments are due to gas–solid reactions, and the important parameters in such reactions include the following:

(1) The rate constant for adsorption of the gas reactant on the external surface of the solid reactant, k_1.

(2) The overall mass transfer coefficient of the gas to the solid surface, K_G, related to k_1 by the equation

$$K_G = k_1 V'_G / A_s \tag{1}$$

where V'_G is the gaseous volume of void space in the solid bed and A_s is the total surface area of the solid.

(3) The rate constant for desorption of the gas reactant from the solid surface, k_{-1}.

(4) The overall mass transfer coefficient of the adsorbed gas in the solid, K_s, related to k_{-1} by

$$K_s = k_{-1} V_s / A_s \tag{2}$$

where V_s is the volume of the solid.

0021-9673/91/$03.50

(5) The adsorption equilibrium constant of the gas reactant between the solid and the gaseous phase:

$$K = K_G/K_s \tag{3}$$

(6) The first-order rate constant for the possible reaction of the adsorbed gas with the solid material, k_2.

If all above parameters can be measured simultaneously in the same experiment, under non-steady-state conditions, this will offer valuable information on the detailed mechanism of the action of air pollutants on historic buildings and monuments, thus providing a scientific basis for their conservation. This object can be achieved by employing reversed-flow gas chromatography (RF-GC), and it is the purpose of this paper to provide the necessary theoretical analysis so that the RF-GC technique be applied to the determination of the six parameters mentioned above.

The RF-GC method has been reviewed several times [1–4] and some more recent papers have been cited [5]. A preliminary synopsis of this paper has also been published [6].

THEORY

To help one follow the theoretical analysis, a brief description of the experimental outline is required, and is given in Fig. 1. Following the injection of a gaseous reactant, a diffusion current of it and of the possible gaseous products is set up inside column L_1, creating finite gas concentrations at the junction $x = l'$. On reversing the direction of the carrier gas flow at known times t_o, by means of the four-port valve, extra chromatographic peaks (sample peaks) appear superimposed on the continuous elution curve, thus forming a repeated sampling at $x = l'$ of

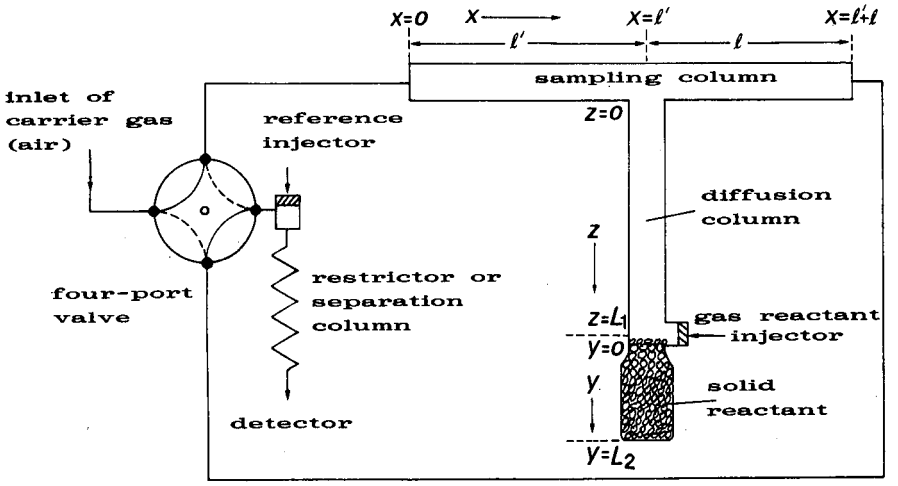

Fig. 1. Schematic representation of the columns and gas connections for studying gas–solid reactions by RF-GC under non-steady-state conditions.

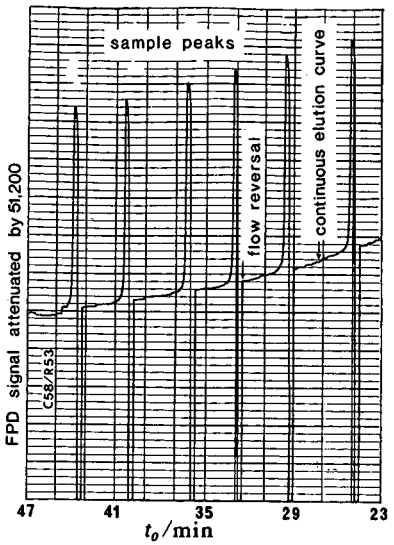

Fig. 2. Sample peaks due to simple flow reversals during the reaction of SO_2 with pieces of marble of 100–120 mesh at 323.2 K.

concentration $c(l', t_o)$ of the various substances present at this point at t_o. An example is given in Fig. 2.

The height h of the sample peaks, measured from the zero signal line, when plotted as $(1/m)\ln h$ *vs.* time t_o, where m is the response factor of the detector, gives a diffusion band, such as that shown in Fig. 3.

In the absence of any solid in vessel L_2 (*cf.*, Fig. 1), the diffusion band is determined by the geometric characteristics of the cell comprising sections l, l', L_1 and L_2, and the diffusion coefficient of the gas reactant into the carrier gas. When a solid

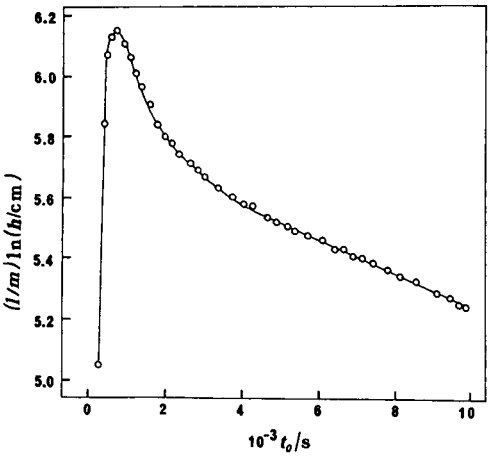

Fig. 3. A diffusion band for the reactant SO_2, obtained in the presence of pieces of marble (100–120 mesh) in vessel L_2 at 353.2 K.

reactant is present, the diffusion band is distorted in shape and/or in slope. It is this distortion which permits the calculation of the various kinetic and equilibrium parameters listed in the Introduction. The method is as follows.

The magnitude of $c(l', t_o)$ in each sampling act is related to the height h of the respective sample peak, measured from the baseline, by [4]

$$h = [2c(l', t_o)]^m \tag{4}$$

where m is the response factor of the detector. If $c(l', t_o)$ is found as an analytical function of the time, the mathematical equation describing the diffusion bands (previously mentioned) will be known. Under the slopes and the intercepts of these experimental bands are hidden all the physico-chemical parameters listed in the Introduction.

The function $c = c(l', t_o)$ has been derived in the past for many special cases pertaining to various physico-chemical parameters [4,5,7–11]. One particular publication [12] should be mentioned, as it deals with the same problem as that faced here, but under different experimental conditions and with different approximations. These led to the determination only of the adsorption rate constant k_1.

Now, one can combine, improve, modify and extend all the above derivations to serve the purposes of the present problem, adding the necessary new details to help readers follow the theoretical development.

The main idea of the technique, as outlined in Fig. 1, is to confine conventional chromatography used for separation purposes to the separation column, and reverse the direction of flow for sampling purposes only in the empty column $l' + l$. The effects of the gas–solid interaction in vessel y are not initially superimposed on the chromatographic stream running through the sampling and the separation column, but "sit" on the diffusion current of the reactant and the gaseous products into the carrier gas setting up inside the diffusion column z. The mathematical equation sought will be derived with the help of the coordinates in Fig. 1, by solving the diffusion equation first in the region z, then in the region y, and finally linking the two solutions by using appropriate boundary conditions at $z = L_1$ and $y = 0$.

Region z

The diffusion equation in this region is

$$\partial c_z/\partial t_o = D\partial^2 c_z/\partial z^2 \tag{5}$$

where $c_z = c_z(z, t_o)$ and D is the diffusion coefficient of the reactant into the carrier gas. If an amount m of the gas reactant is injected as an instantaneous pulse at $z = L_1$, the intial condition is

$$c_z(z, 0) = \frac{m}{a_G}\delta(z - L_1) \tag{6}$$

where a_G is the cross-sectional area in the columns z and $l' + l$ and δ is the Dirac delta function. The boundary conditions at $z = 0$ are

$$c_z(0, t_o) = c(l', t_o) \quad \text{and} \quad D(\partial c_z/\partial z)_{z=0} = vc(l', t_o) \tag{7}$$

where v is the linear velocity of the carrier gas in the sampling column. The solution of eqn. 5, with the initial condition 6 and subject to the boundary conditions 7, in the form of a Laplace transform with respect to time (parameter p_o), is

$$C_z = C(l', p_o)\cosh q_1 z + (v/Dq_1)C(l', p_o)\sinh q_1 z - (m/a_G Dq_1)\sinh q_1(z - L_1)\,u(z - L_1) \quad (8)$$

where

$$q_1^2 = p_o^0/D \quad (9)$$

and $u(z - L_1)$ is the unit step function. C_z and C denote the t_o Laplace-transformed functions of c_z and c, respectively.

For details of the derivation, see ref. 7.

Region y

The diffusion equation in this region is

$$\frac{\partial c_y}{\partial t_o} = D \cdot \frac{\partial^2 c_y}{\partial y^2} - \frac{K_s A_s}{V_G'}(c_s^* - c_s) \quad (10)$$

where c_y = concentration of the gaseous reactant in the gas phase of region y, c_s = concentration of the gaseous reactant adsorbed on the solid reactant, expressed in mol m^{-3}, c_s^* = concentration of the adsorbed reactant in equilibrium with that in the gas phase and D = diffusion coefficient of the gaseous reactant in the region y, assumed to be approximately equal to that in region z; for K_s, A_s and V_G' see Introduction.

The rate of change of c_s is given by

$$\frac{\partial c_s}{\partial t_o} = \frac{K_s A_s}{V_s}(c_s^* - c_s) - k_2 c_s \quad (11)$$

for V_s and k_2 see Introduction.

The system of eqns. 10 and 11, by applying Laplace transformation with respect to t_o, under the initial conditions $c_y(y, 0) = c_s(y, 0) = 0$, and then eliminating C_s between the transformed equations gives

$$d^2 C_y/dy^2 - q_2^2 C_y = 0 \quad (12)$$

where C_y is the transformed function c_y with respect to t_o, and q_2 is given by

$$q_2^2 = \frac{1}{D}\left(p_o + \frac{k_1 p_o + k_1 k_2}{p_o + k_{-1} + k_2}\right) \quad (13)$$

In proceeding from eqns. 10 and 11 to eqn. 12, eqns. 1, 2 and 3 were used, and also the definition $K = c_s^*/c_y$.

Eqn. 12 has been derived before [5,8], but not with the same content as here.

However, its solution is the same, *viz.*,

$$C_y'(0) = -C_y(0)q_2 \tanh q_2 L_2 \tag{14}$$

where $C_y(0)$ is the value of C_y at $y = 0$ and $C_y'(0) = (\mathrm{d}C_y/\mathrm{d}y)_{y=0}$.

Linking the solutions in regions z and y

Eqn. 8, valid in region z, is now linked with eqn. 14, holding in region y, by means of the boundary conditions at $z = L_1$ and $y = 0$, *viz.*, $C_z(L_1) = C_y(0)$ and $a_G(\partial C_z/\partial z)_{z=L_1} = a_G'(\partial C_y/\partial y)_{y=0}$, where a_G' is the cross-sectional area of the void fraction in region y. Using these two boundary conditions in eqn. 14, one obtains

$$(\partial C_z/\partial z)_{z=L_1} = -C_z(L_1)(a_G'/a_G)q_2 \tanh q_2 L_2$$

and calculating C_z and its z derivative at $z = L_1$ from eqn. 8, the result is

$$C(l', p_o) = \frac{m}{a_G D q_1}\left[\sinh q_1 L_1 + \frac{v}{Dq_1}\cdot\cosh q_1 L_1 + \frac{a_G'}{a_G}\cdot\frac{q_2}{q_1}\cdot\tanh q_2 L_2 \cdot \left(\cosh q_1 L_1 + \frac{v}{Dq_1}\cdot\sinh q_1 L_1\right)\right]^{-1} \tag{15}$$

This equation has exactly the same form as eqn. 21 in ref. 8, but the scientific content differs in that it now contains a gas–solid chemical reaction with rate constant k_2.

Approximations

In order that $c(l', t_o)$, and therefore h in eqn. 4, are found from eqn. 15, it is necessary to take the inverse Laplace transform of it. This can only be done, however, after introducing certain approximations in eqn. 15, most of which were used for an analogous equation recently [5], as follows:

(1) Omission of $\sinh q_1 L_1$ compared with $(v/Dq_1)\cosh q_1 L_1$, and also omission of $\cosh q_1 L_1$ compared with $(v/Dq_1)\sinh q_1 L_1$. Then eqn. 15 becomes

$$C(l', p_o) = \frac{m}{\dot{V}}\left[Dq_1 \sinh q_1 L_1\left(\frac{\coth q_1 L_1}{Dq_1} + \frac{a_G' q_2}{a_G D q_1^2}\cdot\tanh q_2 L_2\right)\right]^{-1} \tag{16}$$

where $\dot{V} = va_G$ is the volumetric flow-rate of the carrier gas.

(2) $Dq_1 \sinh q_1 L_1 \approx Dq_1 q_1 L_1 = L_1 p_o$

(3) $$\frac{\coth q_1 L_1}{Dq_1} \approx \frac{1}{L_1}\left(\frac{1}{p_o} + \frac{\pi^2}{3\beta}\right)$$

where

$$\beta = \pi^2 D/L_1^2 \tag{17}$$

(4) $\tanh q_2 L_2 \approx q_2 L_2$

Introducing approximations 2–4 into eqn. 16, it becomes, after rearrangement,

$$C(l', p_o) = \frac{m(\lambda + k'_{-1} + k'_2)}{\dot{V}\pi^2(^1/_3 + R)} \{\lambda^2 + [\pi^{-2}(^1/_3 + R)^{-1} + R(^1/_3 + R)^{-1}k'_1 + k'_{-1} + k'_2]\lambda + \pi^{-2}(^1/_3 + R)^{-1}(k'_{-1} + k'_2) + R(^1/_3 + R)^{-1}k'_1k'_2\}^{-1} \quad (18)$$

where

$$\lambda = p_o/\beta, \quad k'_1 = k_1/\beta, \quad k'_{-1} = k_{-1}/\beta, \quad k'_2 = k_2/\beta \quad (19)$$

β being the diffusion parameter, defined by eqn. 17, and

$$R = V'_G/V_G \quad (20)$$

i.e., the ratio of the gaseous volumes in vessel y (V'_G) and column z (V_G).

It should be noted that the time variable λ and the rate parameters k'_1, k'_{-1} and k'_2 are all dimensionless. The inverse transformation of eqn. 18 to find the analytical form of the function $c(l', t_o)$ depends on the relative values of the above four parameters. If the coefficient of λ in the denominator of eqn. 18 is set equal to

$$X = \pi^{-2}(^1/_3 + R)^{-1} + R(^1/_3 + R)^{-1}k'_1 + k'_{-1} + k'_2 \quad (21)$$

and the constant terms in the denominator are denoted by

$$(X^2 - Y^2)/4 = \pi^{-2}(^1/_3 + R)^{-1}(k'_{-1} + k'_2) + R(^1/_3 + R)^{-1}k'_1k'_2 \quad (22)$$

the two roots of the denominator are $-(X + Y)/2$ and $-(X - Y)/2$, and thus the inverse Laplace transformation of eqn. 18 gives the desired function of time as

$$c(l', t_o) = \frac{N_2}{2}\left[\left(1 + \frac{Z}{Y}\right)\exp\left(-\frac{X + Y}{2}\beta t_o\right) + \left(1 - \frac{Z}{Y}\right)\exp\left(-\frac{X - Y}{2}\beta t_o\right)\right] \quad (23)$$

where

$$N_2 = \frac{m\beta}{\dot{V}\pi^2(^1/_3 + R)} \quad (24)$$

and

$$Z = X - 2(k'_{-1} + k'_2) \quad (25)$$

This master equation, which has been derived in the same form for various other phenomena [3,5,7–10], the physical meaning of N_2, X, Y and Z being different each time, combines easily with eqn. 4 to give the mathematical description of distorted diffusion bands after the maximum, *i.e.*, only their descending branch (*cf.*, Experimental and Fig. 3).

Calculation of k_1, k_{-1}, k_2, K_G, K_s and K from the experimental data

The following steps are suggested for the calculation of these physico-chemical parameters, the meaning of which is explained in the Introduction.

(1) The value of the gaseous diffusion parameter β (eqn. 17) for each experimental arrangement and at each temperature is determined, by conducting an experiment without any solid in region y of the sampling cell (*cf.*, Fig. 1). The relevant diffusion band is constructed by plotting $(1/m)\ln h$ *vs.* t_o (*cf.*, Fig. 3), and the slope B_o of the last linear part after the maximum is computed. From this slope, β is found after division by r_2, $\beta = B_o/r_2$, where r_2 is the absolutely smaller root of the equation [9,10]

$$(1.29 + \pi^2 R)\lambda^2 + (4.29 + \pi^2 R)\lambda + 1 = 0 \tag{26}$$

and R is given by eqn. 20. Alternatively,

$$B_o = -\beta/\pi^2(^1/_3 + R) \tag{27}$$

as can be seen from eqn. 18 by setting $k'_1 = k'_{-1} = k'_2 = 0$ and taking the inverse transformation with respect to p_0. The result is

$$c(l', t_o) = N_2 \exp\left[-\frac{\beta}{\pi^2(^1/_3 + R)} t_o\right] \tag{28}$$

This coincides with eqn. 30 in ref. 5.

(2) An experiment is now conducted, under the same conditions as before, the only difference being that vessel y is filled with the solid reactant, as shown in Fig. 1.

The diffusion band is now distorted as compared with that of step 1, and is described (after the maximum) by eqn. 23. From the experimental band the two exponential coefficients $(X + Y)\beta/2$ and $(X - Y)\beta/2$, together with the two respective pre-exponential factors $N_2(1 + Z/Y)/2$ and $N_2(1 - Z/Y)/2$ are computed. This is done as described previously [5,7], *viz.*, by using a non-linear regression analysis computer program or, if the last part after the maximum is linear, by finding first the slope $-(X - Y)\beta/2$ and the intercept $\ln[N_2(1 - Z/Y)]$ of the last linear part of $(1/m)\ln h$ *vs.* t_o plot and then replotting the initial data of the non-linear part after the maximum as $(1/m)\ln\{h - N_2(1 - Z/Y)\exp[-(X - Y)\beta t_o/2]\}$ *vs.* t_o. Form the slope of the new straight line thus obtained, one finds $-(X + Y)\beta/2$ and from its intercept $\ln[N_2(1 + Z/Y)]$.

Dividing now the two slopes above by β, determined in step 1, one finds

$$B_1 = (X + Y)/2 \quad \text{and} \quad B_2 = (X - Y)/2 \tag{29}$$

By addition of these we find X and by subtraction we obtain Y:

$$B_1 + B_2 = X \quad \text{and} \quad B_1 - B_2 = Y \tag{30}$$

From the ratio ρ of the two pre-exponential factors, one finds

$$\rho = (1 - Z/Y)/(1 + Z/Y)$$

and from this

$$Z = \frac{1-\rho}{1+\rho} \cdot Y \tag{31}$$

The units used for the sample peak height, h, and any unknown proportionality factors do not influence the value of Z, as the latter is calculated from the ratio ρ of two intercepts pertaining to the same diffusion band.

(3) The values of X, Y and Z are now used in conjunction with eqns. 21, 22 and 25 to calculate the dimensionless rate constants k'_1, k'_2 and k'_{-1} with the help of the relationships

$$k'_1 = \frac{(X+Z)(^1/_3 + R) - 2\pi^{-2}}{2R} \tag{32}$$

$$k'_2 = \frac{(X^2 - Y^2)(^1/_3 + R) - 2(X-Z)\pi^{-2}}{2(X+Z)(^1/_3 + R) - 4\pi^{-2}} \tag{33}$$

$$k'_{-1} = X - \pi^{-2}(^1/_3 + R)^{-1} - R(^1/_3 + R)^{-1} k'_1 - k'_2 \tag{34}$$

The value of R used here is V'_G (packed)/V_G, in contrast to R in eqns. 26 and 27, which is V'_G (empty)/V_G.

The values of k_1, k_2 and k_{-1} are then found multiplying k'_1, k'_2 and k'_{-1} by β, respectively, according to the definitions 19.

(4) Finally, K_G, K_s and K are calculated from k_1 and k_{-1} by means of eqns. 1, 2 and 3, respectively.

EXPERIMENTAL

Materials and instruments

Sulphur dioxide and synthetic air, obtained form Linde Hellas (Athens, Greece), were of analytical-reagent grade. Marble was a sample from Penteli (Athens, Greece), approved as a reference material by the Commission of the European Communities.

A Pye Unicam (Cambridge, UK) PU 4500 gas chromatograph was used, equipped with a flame photometric detector. The sampling cell, consisting of the sampling column $l' + l$ (55 + 55 cm × 3.90 mm I.D.), the diffusion column L_1 (34.6 cm × 3.90 mm I.D.) and the vessel L_2 (5.1 cm × 18 mm I.D.), was accommodated inside the oven of the chromatograph. The carrier gas was dried with molecular sieve 12X.

Procedure

Before kinetic experiments, each marble sample was conditioned *in situ* by heating it at 200°C for 48 h, under a continuous carrier gas flow at a flow-rate of 0.283 or 0.583 cm^3 s^{-1}. Subsequently, the oven was adjusted to the working temperature and kept there overnight. Column L_1 was then filled with a uniform sulphur dioxide concentration by injecting into it 20 cm^3 of pure sulphur dioxide at atmospheric pressure. This was left for 1–2 days, until the signal at the detector decayed to a negligible height. Finally, 1 cm^3 of a gas mixture consisting of sulphur dioxide and

carrier gas (24%, v/v) was introduced through the injector, under a carrier gas flow, and the kinetic experiment was conducted by repeatedly reversing the flow direction at known times from the moment of injection.

The detector temperature was always 175°C and the pressure inside the cell was 1.04–1.05 atm (0.1054–0.1064 MPa).

RESULTS AND DISCUSSION

The methodology and equations given under Theory were applied to the action of sulphur dioxide at low concentrations in the carrier gas (synthetic air) on particles of Greek marble.

An example of the diffusion band for this particular case has already been given in Fig. 3. The response factor of sulphur dioxide for the flame photometric detector used had been determined previously [12], and its mean value was 1.92.

The values of the six physico-chemical parameters, calculated as described under Theory, are listed in Tables I and II for two sizes of marble particles, two flow-rates of the carrier gas, and four or five temperatures. It can be seen that there is a tendency for k_1 to decrease at the same temperature with increasing flow-rate of the air carrier gas, and this decrease is greater with marble particles of size 100–120 mesh, which have a larger specific surface area. Also, most of the other parameters for this size of particles decrease with increase in flow-rate, particularly at low temperatures. The changes observed when particles of size 22–30 mesh are used are less pronounced.

The negative values for k_2 observed with the smaller particles and a high flow-rate could mean that a chemical process leading to the release of sulphur dioxide from the marble is taking place, like the reverse of a chemisorption step.

In order that definite conclusions can be drawn about the mechanism of this particular gas–solid reaction, more experiments are required with other particle sizes

TABLE I

RATE CONSTANTS FOR ADSORPTION (k_1), DESORPTION (k_{-1}) AND CHEMICAL REACTION (k_2), MASS TRANSFER COEFFICIENTS IN THE GAS (K_G) AND IN THE SOLID (K_s), AND ADSORPTION EQUILIBRIUM CONSTANT (K) FOR THE GAS–SOLID REACTION OF SO_2 WITH MARBLE PARTICLES OF 22–30 MESH

T(K)	$10^5 k_1$ (s^{-1})	$10^5 k_{-1}$ (s^{-1})	$10^5 k_2$ (s^{-1})	$10^{10} K_G$ ($m\,s^{-1}$)	$10^{10} K_s$ ($m\,s^{-1}$)	K
Dry air as carrier gas with $V = 0.283$ $cm^3\ s^{-1}$						
323.2	11.2	5.70	7.32	2.99	1.82	1.65
353.2	13.2	8.52	6.00	3.51	2.72	1.29
373.2	14.2	5.93	7.39	3.77	1.89	1.99
393.2	13.2	7.52	7.36	3.51	2.40	1.46
423.2	17.1	8.46	10.46	4.55	2.70	1.69
Dry air as carrier gas with $V = 0.583$ $cm^3\ s^{-1}$						
323.2	9.77	4.88	7.75	2.59	1.55	1.66
353.2	10.56	7.05	5.43	2.81	2.24	1.25
373.2	8.33	6.58	3.65	2.21	1.16	1.90
393.2	12.92	8.77	6.09	3.43	2.79	1.23
423.2	16.30	7.94	10.46	4.33	2.53	1.71

TABLE II

RATE CONSTANTS FOR ADSORPTION (k_1), DESORPTION (k_{-1}) AND CHEMICAL REACTION (k_2), MASS TRANSFER COEFFICIENTS IN THE GAS (K_G) AND IN THE SOLID (K_s), AND ADSORPTION EQUILIBRIUM CONSTANT (K) FOR THE GAS–SOLID REACTION OF SO_2 WITH MARBLE PARTICLES OF 100–120 MESH

T(K)	$10^5 k_1$ (s^{-1})	$10^5 k_{-1}$ (s^{-1})	$10^5 k_2$ (s^{-1})	$10^{10} K_G$ ($m\,s^{-1}$)	$10^{10} K_s$ ($m\,s^{-1}$)	K
Dry air as carrier gas with $\dot{V} = 0.283$ $cm^3\ s^{-1}$						
323.2	10.5	8.00	3.09	1.94	1.78	1.10
353.2	17.8	8.89	5.23	3.30	1.97	1.67
373.2	19.1	8.32	6.80	3.54	1.85	1.92
393.2	19.9	9.31	8.20	3.68	2.07	1.79
423.2	21.0	10.98	8.41	3.89	2.44	1.60
Dry air as carrier gas with $\dot{V} = 0.583$ $cm^3\ s^{-1}$						
323.2	7.26	2.44	9.48	1.34	0.54	2.48
353.2	5.14	9.79	−1.04	0.95	2.17	0.43
393.2	7.58	12.82	−2.19	1.40	2.84	0.49
423.2	5.90	13.99	−2.23	1.09	3.10	0.35

or with single pieces of marble having particular shape, such as a sphere, cube, cone, cylinder or prism. Also, experiments with carrier gases loaded with water vapour should be conducted. Such work is in progress to elucidate the mechanism of the action of sulphur dioxide on marble.

ACKNOWLEDGEMENTS

This work was supported by a contract (No. EV 4V-0049 GR) of Environment and Waste Recycling of the Directorate-General for Science, Research and Development of the Commission of the European Communities, for which the authors express their gratitude. They also acknowledge the assistance provided by Mrs. M. Barkoula.

REFERENCES

1 N. A. Katsanos and G. Karaiskakis, *Adv. Chromatogr.*, 24 (1984) 125.
2 N. A. Katsanos and G. Karaiskakis, *Analyst (London)*, 112 (1987) 809.
3 N. A. Katsanos, *J. Chromatogr.*, 446 (1988) 39.
4 N. A. Katsanos, *Flow Perturbation Gas Chromatography*, Marcel Dekker, New York, Basle, 1988.
5 N. A. Katsanos and J. Kapolos, *Anal. Chem.*, 61 (1989) 2231.
6 N. A. Katsanos, G. Karaiskakis and Ch. Vassilakos, *Pure Appl. Chem.*, 61 (1989) 2057.
7 N. A. Katsanos and E. Dallas, *J. Phys. Chem.*, 91 (1987) 3103.
8 N. A. Katsanos, P. Agathonos and A. Niotis, *J. Phys. Chem.*, 92 (1988) 1645.
9 J. Kapolos, N. A. Katsanos and A. Niotis, *Chromatographia*, 27 (1989) 333.
10 N. A. Katsanos and J. Kapolos, in M. L. Occelli and R. G. Anthony (Editors), *Hydrotreating Catalysts*, Elsevier, Amsterdam, 1989, p. 211.
11 N. A. Katsanos and Ch. Vassilakos, *J. Chromatogr.*, 471 (1989) 123.
12 N. A. Katsanos and G. Karaiskakis, *J. Chromatogr.*, 395 (1987) 423.

Journal of Chromatography, 557 (1991) 481–487
Elsevier Science Publishers B.V., Amsterdam

CHROM. 22 966

Optimization of the gas chromatographic analysis of a standard mixture of polychlorodibenzo-*p*-dioxins and polychlorodibenzofurans

J. TABERA*
Instituto de Fermentaciones Industriales del CSIC, Calle Juan de la Cierva 3, 28006 Madrid (Spain)
and
B. JIMÉNEZ, L. M. HERNÁNDEZ and M. J. GONZÁLEZ
Instituto de Química Orgánica General del CSIC, Calle Juan de la Cierva 3, 28006 Madrid (Spain)

ABSTRACT

The separation of fifteen standard isomers of polychlorodibenzofurans (PCDFs) and polychlorodibenzo-*p*-dioxins (PCDDs) with a 2,3,7,8-substitution pattern by high-performance gas chromatography using capillary columns with bonded phases was studied in order to obtain better resolutions than those usually reported. The modified simplex method was used to improve the overall separation achievable with the analytical procedure by optimizing the experimental conditions that affect chromatographic resolution.

INTRODUCTION

Polychlorinated dibenzofurans (PCDFs) and dibenzo-*p*-dioxins (PCDDs) are two series of tricyclic, planar, aromatic compounds. Each series consists of a number of chloro homologues (mono- to octachlorinated) with a variable number of isomers for each group (135 PCDFs and 75 PCDDs) [1].

Because of the biological activity associated with small amounts of these compounds, specially the 2,3,7,8-substituted isomers, acceptable analytical methods have to be capable of providing qualitative identification and accurate quantification at low parts per 10^{12} (pg/g) levels in different matrices [2–4].

High-performance gas chromatography with capillary columns provides effective separations of many PCDF and PCDD isomers and a number of stationary phases have been used [5]. Optimization of the chromatographic separations requires great experimental effort as the number of variables involved increases. In such situations, it is essential to apply an optimization method for the simultaneous handling of several experimental variables in order to resolve as much as possible the chloro homologues and the isomers of PCDDs and PCDFs. The sequential simplex method [6] begins with a patterned set of experiments involving all the variables of interest. The pattern is an equilateral triangle in two variables, a regular tetrahedron in three variables or

0021-9673/91/$03.50

a simplex (*i.e.*, a regular multi-dimensional figure) in four or more variables. The effects on the performance of the process of changes in operating variables are measured according to a previously defined criterion or response function; from the results, the directions in which further changes should be made to obtain an improvement in process performance are inferred. The resulting new values of the variables are then tested and the procedure is repeated until no further improvement can be achieved. The sequential simplex method has been broadly recognized as a very efficient empirical optimization method [7,8] which can attain an optimum in a minimum number of experimental runs.

The objective of this work was the development of a GC method for analysing different complex matrices (biological materials, fly ash, etc.), resolving as much as possible the isomers of PCDDs and PCDFs. As a first step we used a mixture of 2,3,7,8-substituted isomers of PCDDs and PCDFs (tetra- to octadioxins and -furans). The optimization of the experimental conditions affecting the GC separation was performed by means of the modified simplex method.

EXPERIMENTAL

All measurements were carried out on a Perkin-Elmer Model 8310B gas chromatograph equipped with a ^{63}Ni electron-capture detector. A bonded-phase BP-5 fused-silica column (50 m × 0.22 mm I.D.) with a 0.25-μm film thickness (SGE, Victoria, Australia) was used. The BP-5 stationary phase is polyphenylsiloxane–polymethylsiloxane (5:95). The oven temperature programming was the object of optimization and Table I shows the variables included in the study. The detector temperature was 300°C and the injector temperature (splitless mode) was 280°C.

The PCDDs and PCDFs standards used were all purchased from Cambridge Isotope Labs. (Woburn, MA, U.S.A.) and Wellington Labs. (Ontario, Canada). Table II shows the mixture of 2,3,7,8-substituted isomers of PCDDs and PCDFs (tetra- to octachlorinated) used at a 1 ng/μl concentration of each in benzene.

Response function

The effect of modifying the experimental conditions on the overall performance of the method was evaluated in terms of the differences between the retention times of each chromatographic peak achievable in each analytical run. We are mainly interested in separations between chloro homologue groups, and therefore the

TABLE I

VARIABLES INCLUDED IN THE OPTIMIZATION STUDY, EXPERIMENTAL RANGES AND STARTING VALUES (BASE LEVEL)

Variable	Min.	Max.	Base
First oven temperature, T1 (°C)	90	150	100
First temperature gradient, G1 (°C/min)	15	30	20
Second oven temperature, T2 (°C)	160	200	180
Second temperature gradient, G2 (°C/min)	1	3	2
Third oven temperature, T3 (°C)	240	260	45

TABLE II

PCDD AND PCDF ISOMERS IN THE MIXTURE USED FOR OPTIMIZATION

Tetra-	Penta- (Pe)	Hexa- (Hx)	Hepta- (Hp)	Octa- (O)
2,3,7,8-TCDF	1,2,3,7,8-PeCDF	1,2,3,4,7,8-HxCDF	1,2,3,4,6,7,8-HpCDD	OCDD
2,3,7,8-TCDD	2,3,4,7,8-PeCDF	1,2,3,6,7,8-HxCDF		OCDF
	1,2,3,7,8-PeCDD	1,2,3,7,8,9-HxCDF		
		1,2,3,4,7,8-HxCDD		
		1,2,3,6,7,8-HxCDD		
		1,2,3,7,8,9-HxCDD		
		2,3,4,6,7,8-HxCDF		

differences in retention times between the first peak of a group and the last peak of the preceding group were weighted with a factor of 2 for the hepta–hexa and octa–hepta pairs and with a factor of 3 for the penta–tetra and hexa–penta pairs. Hence the response function can be expressed as

$$Y = \sum f(t_{Ri+1} - t_{Ri}) \tag{1}$$

where t_{Ri} is the retention time of the ith chromatographic peak and f is the weighting factor, equal to 1 for the peaks in the same group and to 2 or 3 for the extreme peaks in the above-mentioned groups. As is obvious, the objective was to maximize the value of the response function.

Optimization method

The variables subjected to the optimization procedure, their experimental ranges and starting values are shown in Table I.

The initial experimental design was established according to Spendley *et al.* [9]. Physical values of factors were calculated from their mathematical coordinates by applying

$$x_{\text{phys}} = x_0 + x_{\text{math}} \cdot \frac{x_2 - x_1}{s} \tag{2}$$

where x_{phys} is the physical value of the variable x, x_{math} is the corresponding mathematical coordinate, x_0 is its base level (starting physical value), x_1 and x_2 are the lower and upper limits of the range studied, respectively, and s is the number of mathematical units in which the range has been divided.

The initial simplex was moved in the directions given by the rules of movement of the modified simplex method [10] and the response function was subsequently evaluated. In this way, different sets of variables were tested until no further improvement was achievable. In all instances, two replicates of each analysis were carried out. The coordinates of a new vertex were calculated according to the expression

$$V_i^* = C + \alpha (C - V_i) \tag{3}$$

where V_i^* is the new vertex, C the centroid of the retained vertices in the movement, V_i the rejected vertex and α a factor with different values depending on whether a reflection ($\alpha = 1$), an expansion ($\alpha > 1$) or a contraction ($\alpha < 1$) was performed.

It should be pointed out that the self-directing nature of the optimization method makes possible a boundary violation (*i.e.*, a movement outside the experimental range initially established). In such a case, the corresponding vertex must be rejected before experimentation and the simplex forced to move back inside the boundaries by applying a factor $\alpha = -0.5$ [11].

RESULTS AND DISCUSSION

Table III summarizes the sets of values tested for optimizing the peak resolution in the chromatogram. The base level of each variable (*i.e.*, the starting point of the optimization study) is also included (vertex No. 1). The s value was set at 3. The values attained for the response function (eqn. 1) in each chromatogram are included in the response column in Table III.

The optimization study was initiated by performing at random the first seven

TABLE III

EXPERIMENTAL RUNS AND RESULTS FOR THE SIMPLEX OPTIMIZATION OF THE GC ANALYSIS OF A MIXTURE OF PCDDs AND PCDFs

Vertex No.	Simplex No.	Retained vertices	Experimental variable levels						Response, Y (min)
			T1 (°C)	G1 (°C/min)	T2 (°C)	G2 (°C/min)	T3 (°C)	IST1 (min)	
1	1		100	20.0	180	2.0	250	45.0	117.98
2	1		118	21.0	183	2.1	251	47.0	116.56
3	1		104	24.5	183	2.1	251	47.0	116.50
4	1		104	21.0	192	2.1	251	47.0	116.42
5	1		104	21.0	183	2.6	251	47.0	113.79
6	1		104	21.0	183	2.1	256	47.0	108.84
7	1		104	21.0	183	2.1	251	54.0	120.94
8	2	1, 2, 3, 4, 5, 7	107	21.8	185	2.2	246	48.6	157.93
9	2	1, 2, 3, 4, 5, 7	109	22.2	186	2.3	241	49.5	165.45
10	3	1, 2, 3, 4, 7, 9	109	22.2	186	1.7	247	49.5	162.22
11	4	1, 2, 3, 7, 9, 10	111	22.7	175	2.0	247	50.4	162.37
12	5	1, 2, 7, 9. 10, 11	113	18.5	181	1.9	244	51.5	167.06
13	5	1, 2, 7, 9. 10, 11	118	15.5	181	1.8	241	53.8	174.91
14	6	1, 7, 9, 10, 11, 13	99	20.3	181	1.8	241	53.8	174.67
15	7	7, 9, 10, 11, 13, 14	116	21.3	183	1.9	239	58.6	182.39
16	7	7, 9, 10, 11, 13, 14	124	22.0	185	1.9	240	65.5	198.69
17	8	9, 10, 11, 13, 14, 16	119	20.1	182	1.7	232	53.5	–
18	9	9, 10, 11, 13, 14, 16	108	20.9	182	2.0	247	53.9	164.53
19	10	9, 11, 13, 14, 16, 18	114	20.9	182	2.0	246	53.8	–
20	11	9, 11, 13, 14, 16, 18	110	21.4	184	1.8	245	52.0	166.42
21	12	9, 13, 14, 16, 18, 20	112	18.1	192	1.9	237	59.1	–
22	13	9, 13, 14, 16, 18, 20	111	21.5	179	2.0	244	52.5	167.11
23	14	9, 13, 14, 16, 20, 22	116	20.1	182	1.8	235	55.1	–
24	15	9, 13, 14, 16, 20, 22	110	20.7	182	2.0	244	54.2	169.20

experiments defined in Table III, which constitute the initial simplex. The assessment of the values obtained for the response function in each analysis allows the worst vertex to be rejected (No. 6). A new simplex was then formed with the retained vertices and a new one resulting from the mirror image of the rejected vertex ($\alpha = 1$). The procedure must be repeated to move from one simplex into another by rejecting the worst observation and by utilizing an adequate α value.

It should be noted that vertices Nos. 9, 13 and 16 were obtained from eqn. 3 with $\alpha = 2$ because their preceding $\alpha = 1$ vertices (Nos. 8, 12 and 15, respectively) were the best in their simplexes and then an expansion is indicated. Vertices Nos. 9, 13 and 16 achieve higher response values than the $\alpha = 1$ vertices, and therefore were maintained, rather than vertices Nos. 8, 12 and 15, to form the next simplex. In vertices Nos. 17, 19, 21 and 23 boundary violations in variable T3 occur, and therefore they were rejected without previous experimentation and a contraction was performed in the subsequent

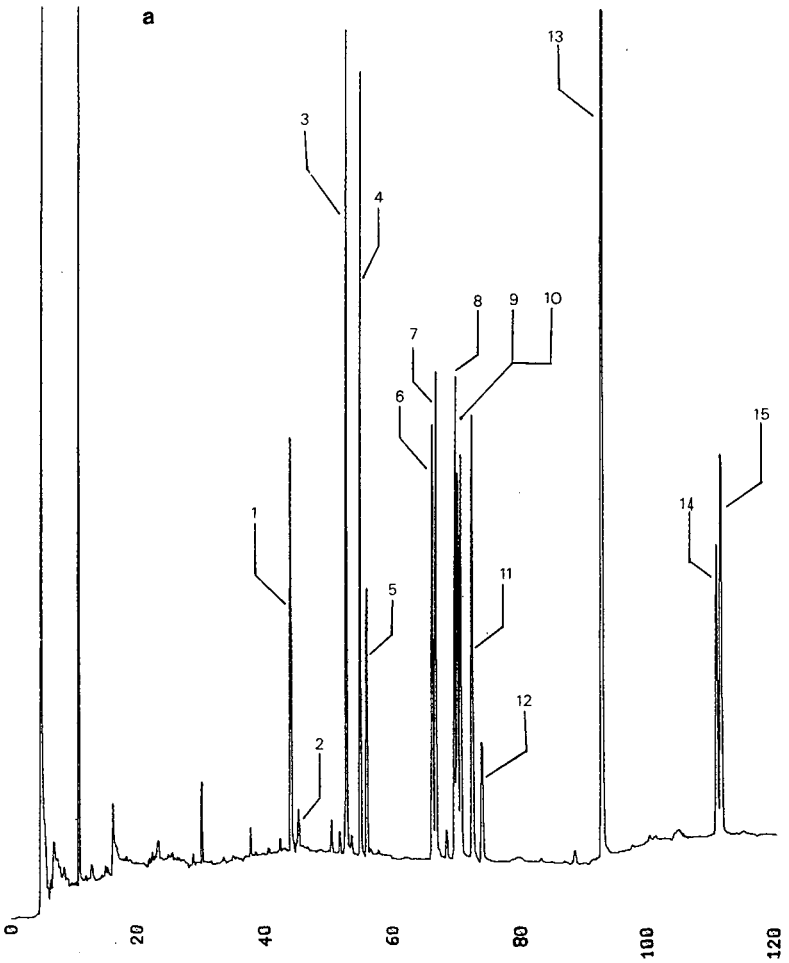

Fig. 1.

(Continued on p. 486)

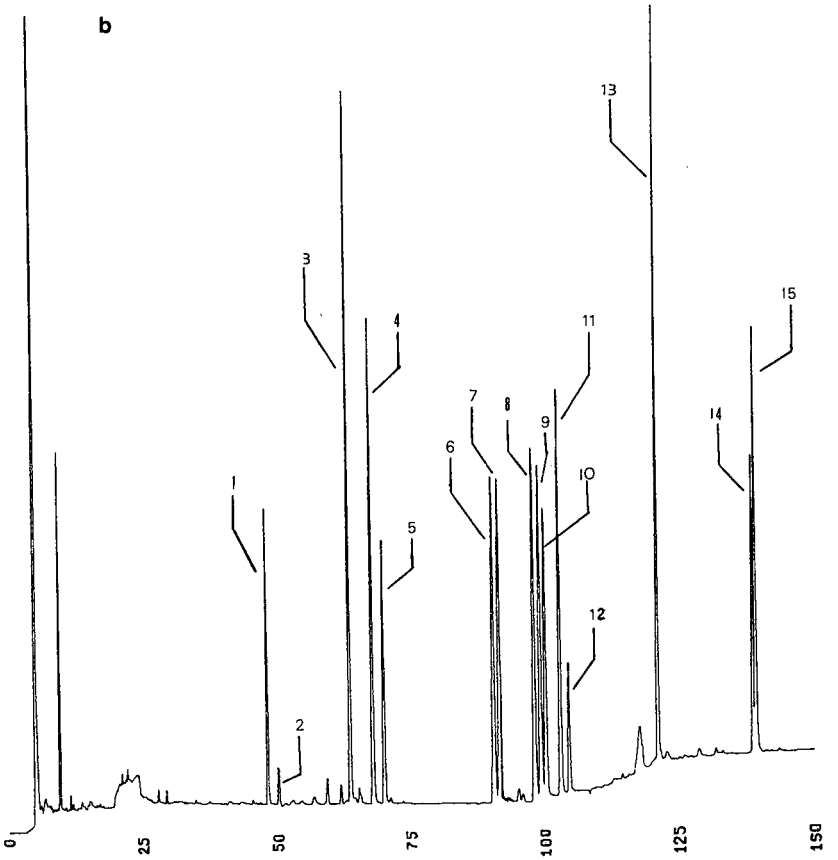

Fig. 1. High-performance GC separation of a mixture of standards PCDDs and PCDFs. (a) Initial conditions, (b) after simplex optimization. Peaks: 1 = 2,3,7,8-TCDF; 2 = 2,3,7,8-TCDD; 3 = PeCDF; 4 = PeCDF; 5 = PeCDD; 6 = HxCDF; 7 = HxCDF; 8 = HxCDF; 9 = HxCDD; 10 = HxCDD; 11 = HxCDD; 12 = HxCDF; 13 = 1,2,3,4,6,7,8-HpCDD; 14 = OCDD; 15 = OCDF. Time scale in min.

simplexes by applying eqn. 3 with $\alpha = -0.5$ as mentioned before. A re-incidence of boundary violations in addition to no significant improvements in response registered in the last vertices led us to end the search and to establish that the experimental conditions of vertex No. 16 were the optimum for our objective.

Fig. 1 shows the initial and final chromatograms resulting from optimizing the GC conditions. It is evident that the optimization process allows a significant increase in the overall peak separations, mainly between penta–tetra and hexa–penta groups, as was desired. It must be emphasized that in only 20 experimental runs (24 vertices generated minus 4 rejected without experimentation) an optimum zone was achieved with six variables involved in the optimization study.

CONCLUSIONS

The application of the modified simplex method to the variables involved in the

oven temperature programming results in an improvement of the overall peak separation of PCDF and PCDD isomers. As a direct consequence, a better differentiation from interferences generally due to some much more abundant compounds (*e.g.*, polychlorobiphenyls) of similar structural characteristics, present in natural samples, would be obtained.

REFERENCES

1 H. R. Buser, *Environ. Health Perspect.*, 60 (1985) 259–268.
2 R. W. Baughman and M. Meselson, *Environ. Health Perspect., Exptl. Issue*, 5 (1973) 27–35.
3 A. Poland, E. Glover and A. S. Kende, *J. Biol. Chem.*, 251 (1976) 4936–4946.
4 A. Poland and J. C. Knutson, *Annu. Rev. Pharmacol. Toxicol.*, 22 (1982) 517–554.
5 C. Rappe, *Environ. Sci. Technol.*, 18, No. 3 (1984) 78A–95A.
6 C. Hendrix, *ChemTech.*, (1980) 488–497.
7 J. C. Berridge, *Anal. Chim. Acta*, 191 (1986) 243–259.
8 R. J. Fisher, *Food Technol.*, 43, No. 3 (1989) 90–94.
9 W. Spendley, G. R. Hext and F. R. Himsworth, *Technometrics*, 4 (1962) 441–461.
10 J. A. Nelder and R. Mead, *Comput. J.*, 7 (1965) 308–313.
11 S. L. Morgan and S. N. Deming, *Anal. Chem.*, 46 (1974) 1170–1181.

Journal of Chromatography, 557 (1991) 489–494
Elsevier Science Publishers B.V., Amsterdam

CHROM. 23 377

Short Communication

Confirmation of the structure of by-products in the synthesis of Modafinil by liquid chromatography–mass spectrometry

Th. BECUE
S.A.M.M. Centre d'Études Pharmaceutiques, 5 Rue J. B. Clément, 92296 Chatenay, Malabry (France)
and
M. BROQUAIRE*
Centre de Recherches du Laboratoire Lafon, 19 Avenue du Professeur Cadiot, BP 22, 94701 Maisons-Alfort Cedex (France)

ABSTRACT

By-products formed during the synthesis of Modafinil, a new awakening drug, were analysed by liquid chromatography–mass spectrometry with thermospray interface; the working conditions were optimized, in particular the value of the tension of repeller. The obtained mass spectra, giving in three cases out of four not only molecular adducts but lower ones, furnished structural information concerning these by-products. Through comparison of spectra with standards, confirmation of their structure was achieved.

INTRODUCTION

Modafinil, (diphenylmethyl)sulphinyl-2 acetamide, a new awakening drug [1], is thermally unstable and cannot be analysed by gas chromatography (GC). So its purity was studied by high-performance liquid chromatography (HPLC) and three by-products were detected: their structures were deduced from the synthetic pathway of Modafinil. These supposed impurities were synthesized: their retention times were equal to those of Modafinil by-products, but no further proof of their structure could be given.

The present study involving thermospray HPLC–mass spectrometry (MS) was developed to confirm the structure of these impurities. After having optimized the equipment and the chromatographic separation, the tension of repeller was optimized to obtain not only molecular adducts, but lower ones, able to give structural information.

0021-9673/91/$03.50

EXPERIMENTAL

Solvents

HPLC-grade acetonitrile and analytical-grade ammonium acetate used for the mobile phase were purchased from Prolabo (Paris, France).

Standards

Modafinil and impurities, the structures of which are given in Fig. 1, were synthesized in the laboratories of Laboratoire L. Lafon (Maisons-Alfort, France). These impurities are (1) (diphenylmethyl)sulphonyl-2 acetamide (sulphone), (2) (diphenylmethyl)sulphinyl-2 acetic acid (acid) and (3) methyl(diphenylmethyl)sulphinyl-2 acetate (ester).

Equipment

Analyses were carried out on a HPLC–MS system consisting of a Waters Model 600 MS solvent delivery system, a Waters Model U6K injector (Waters, Division of Millipore, Trappes, France) equipped with a 50-μl loop, a Vestec thermospray interface (Vestec, Houston, TX, USA) and a Nermag R 10-10 L quadrupolar mass spectrometer (Delsi-Nermag, Argenteuil, France).

A six-port Rheodyne valve, used as injector shunt, allowed the chromatographic column to be bypassed in order to calibrate the mass spectrometer and to optimize the working conditions of the thermospray interface. The second solvent delivery system, originally used after the chromatographic column to introduce the ionization reagent ammonium acetate, was removed in order to maintain the efficiency of the chromatographic separation, to avoid dilution of the analyte, and to increase the sensitivity. Ammonium acetate was put directly into the chromatographic mobile phase.

Chromatographic analysis and mass spectrometry

The mobile phase [acetonitrile–0.1 *M* ammonium acetate (4:6, v/v)], degassed prior to use and kept under a stream of helium, was adjusted to a flow-rate of 1.00 ± 0.01 ml/min through a stainless-steel column (15 cm × 4.6 mm I.D.) packed with

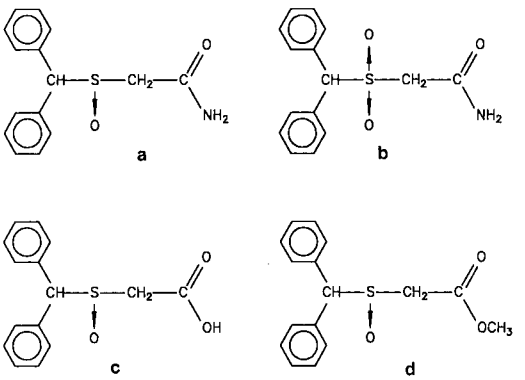

Fig. 1. Chemical formulae of Modafinil and its supposed impurities. (a) Modafinil (molecular mass 273); (b) sulphone (289); (c) acid (274); (d) ester (288).

Ultrabase C_8, 5 μm (S.F.C.C., Neuilly-Plaisance, France), maintained at a temperature of 40°C. Ammonium acetate was only used as ionization reagent for the thermospray interface and did not affect chromatographic separation.

The conditions of use for the thermospray interface, optimized from a direct injection of Modafinil (30 μl of a 5 mg/ml solution of Modafinil in the mobile phase) through the injector shunt, were as follows: control temperature: 128°C; vaporizer tip temperature: 250°C; tension of repeller: + 130 V and source temperature: 170°C. Mass spectra were scanned from m/z = 150 a.m.u. to m/z = 350 a.m.u.

RESULTS AND DISCUSSION

The mass spectrum of Modafinil (Fig. 2), obtained as described above, was characterized by an $[M+H]^+$ at m/z 274 (44%) and an $[M+NH_4]^+$ adduct at m/z 291 (100%). Note the presence of an ion at m/z 332 (5.5%) corresponding to M + 59. It is an $[M+(CH_3CN)NH_4]^+$ adduct resulting from reaction with a primary $(CH_3CN)NH_4^+$. The intensity of such an $[M+(CH_3CN)NH_4]^+$ depended on repeller voltage and source temperature [2].

Three fragments with lower m/z values gave structural information. The ion at m/z 167 (70%) was the result of cleavage from the SO group in the α position: it corresponded to the fragment $(C_6H_5)_2CH^+$. The ion at m/z 184 (6.1%) was the result of migration of the $(C_6H_5)_2CH$ group on the oxygen atom, followed by a cleavage at the S–O bound to give a secondary alcohol, $(C_6H_5)_2$ $CH–OH^+$ [3]. The fragment at m/z 225 (9.4%) resulted in a loss of SO [3]. The occurrence and the relative intensity of fragments 167–184 and 225 were closely bound to the value of the tension of repeller. The relative intensity of such fragments *versus* tension of repeller was a complex function depending on the fragment itself and on the analysed compound [4]. The importance of such optimization in thermospray LC–MS has already been pointed out [5].

The chromatographic conditions, described above, were directly derived from those previously optimized to analyse the purity of Modafinil in the Centre de Recherches du Laboratoire Lafon; only the mobile phase was different: acetonitrile–water (50:50, v/v). The addition of ammonium acetate as ionization reagent directly into the mobile phase did not modify the chromatographic separation, but the k' (capacity factor) value of impurity acid decreased to zero. To avoid this, the amount of acetonitrile in the mobile phase was reduced as described above.

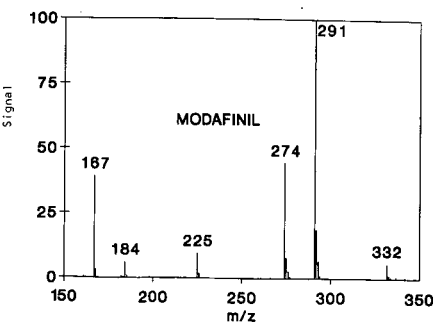

Fig. 2. Mass spectrum of Modafinil.

The total ionic current, obtained after injection into the chromatographic column of 30 μl of a Modafinil solution (8 mg/ml in mobile phase) (Fig. 3a), showed three peaks of impurity at retention time 1 min 36 s (impurity 1), 5 min 36 s (impurity 2) and 9 min (impurity 3). The peak close to 3 min was an artefact due to perturba-

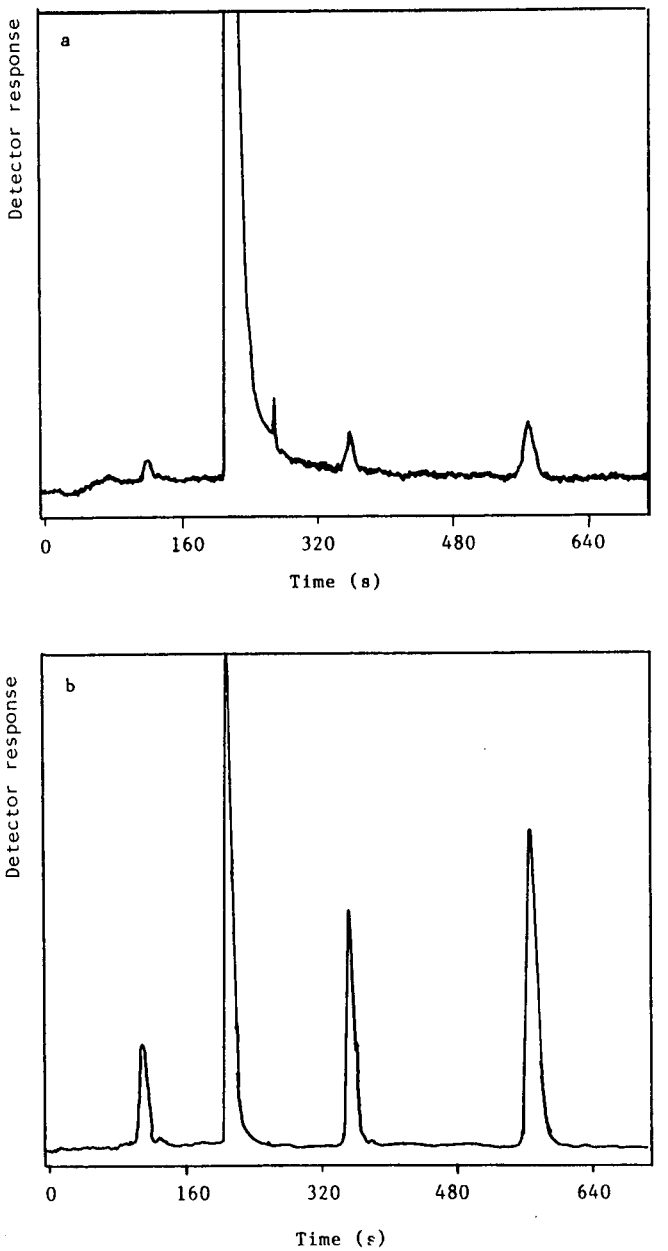

Fig. 3. Reconstructed chromatogram of Modafinil. Conditions: see text. (a) Modafinil solutions (240 μg injected). (b) Modafinil spiked with impurities.

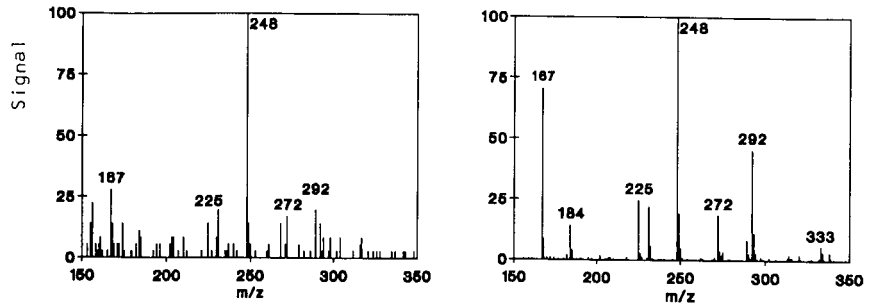

Fig. 4. Mass spectra of impurity 1 (left) and acid (right).

tions created in thermospray regulation by the large amount of Modafinil to be vaporized. Its mass spectrum was exactly the same as that of Modafinil. Fig. 3b shows the total ionic current obtained after an injection of Modafinil (12.5 μg) spiked with acid (12.5 μg), sulphone (4 μg) and ester (7.5 μg). Retention times were, respectively, 1 min 48 s, 3 min 23 s and 5 min 39 s for acid, sulphone and ester. These values are quite similar to those of, respectively impurity 1, impurity 2 and impurity 3.

On the mass spectra of impurity 1 and acid (Fig. 4), the ions at *m/z* 167, 184 and 225, already described for Modafinil, appeared together with ions at *m/z* 231, 248 (100% on both spectra), 272 and 292. Despite the fact that the impurity 1 spectrum was largely noisy (because of the very small amount of this impurity), the two spectra were rather similar: the ion at *m/z* 292 corresponded to the $[M+NH_4]^+$ adduct. The ion $[M+H]^+$ at *m/z* 275, present in the acid spectrum (3.36%), was masked by the noise in the impurity 1 spectrum. In the same way, the $[M+(CH_3CN)NH_4]^+$ adduct appeared at *m/z* 333 only on the acid spectrum. Fragments at *m/z* 231 and 248 (100% in both cases) were due to decarboxylation of $[M+H]^+$ and the $[M+NH_4]^+$ adduct.

The mass spectra of impurity 2 and sulphone (Fig. 5) were identical. They were characterized by an $[M+NH_4]^+$ adduct at *m/z* 307 (100% in both cases) and an $[M+(CH_3CN)NH_4]^+$ adduct at *m/z* 348. The two spectra did not exhibit any important fragmentation at lower values: on the sulphone spectrum, the fragment at *m/z* 167 had relative abundance of only 0.34%. Whatever the working conditions of thermospray, no additional fragment occurred.

The mass spectra of impurity 3 and ester (Fig. 6) were quite similar. They gave the same kind of information as the Modafinil spectrum: three fragments at *m/z* 167,

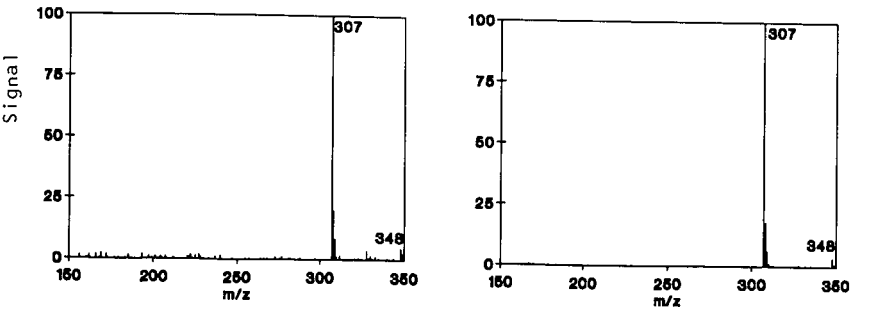

Fig. 5. Mass spectra of impurity 2 (left) and sulphone (right).

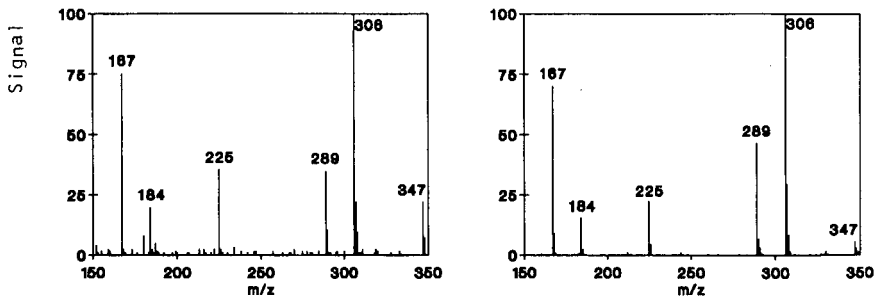

Fig. 6. Mass spectra of impurity 3 (left) and ester (right).

184 and 225, an $[M+H]^+$ at *m/z* 289, an $[M+NH_4]^+$ adduct at *m/z* 347; their relative intensities exhibited the same kind of dependency on repeller voltage.

The results described above show the importance of identification of adducts for determining molecular mass. But, for a given set of thermospray working conditions, the presence of these adducts seemed to be bounded to molecular structure: all four studied compounds gave $[M+18]$ and $[M+59]$ adducts but sulphone did not exhibit an $[M+1]$ ion.

The most important result was to demonstrate the ability of thermospray HPLC–MS to obtain fragments lower than the molecular adduct and giving structural information. On first approximation, their relative intensity, related to the tension of the repeller, increased when the relative intensity of molecular and bigger adducts decreased [4].

On the other hand, under the conditions described above for the thermospray interface regulation, the mass spectra were rigorously reproducible from day to day. But any minor change in these conditions could drastically modify the profiles of spectra [4], some of the fragments or of the adducts being able to disappear from the spectra.

CONCLUSIONS

The results described above show the total similarity between impurity 1 and acid, impurity 2 and sulphone and impurity 3 and ester and confirm the structure of the impurities occurring in the synthesis of Modafinil. But the most important result of this work is probably the demonstration that the technique of LC–MS with thermospray interface is able to provide not only molecular mass information but also structural information if optimization of thermospray parameters can be achieved.

REFERENCES

1 J. Duteil, F. A. Rambert, J. Pessonnier, J. F. Hermant, R. Gombert and E. Assous, *Eur. J. Pharmacol.*, 180 (1990) 49–58.
2 M. Lesieur, *Thesis*, Conservatoire National des Arts et Métiers, Paris, 1987.
3 H. Budzikiewicz, C. Djerassi and D. H. Williams, *Mass Spectrometry of Organic Compounds*, Holden-Day, London, 1967, p. 552.
4 Th. Becue and M. Broquaire, in preparation.
5 C. E. M. Heeremans, R. A. M. van der Hoeven, W. M. A. Niessen, U. R. Tjaden and J. van der Greef, *J. Chromatogr.*, 474 (1989) 149–162.

Journal of Chromatography, 557 (1991) 495–499
Elsevier Science Publishers B.V., Amsterdam

CHROM. 23 375

Short Communication

Study of salt hydrates by gas–solid chromatography

T. A. MILLS and C. S. G. PHILLIPS*
Inorganic Chemistry Laboratory, Oxford University, South Parks Road, Oxford OX1 3QR (UK)

ABSTRACT

Gas–solid chromatographic experiments were conducted with salt hydrate systems [particularly those of copper(II) sulphate] in order to study the chromatographic consequences of phase transition in the solid. The results reflect the equilibrium phase diagrams of the hydrates involved, but can be strongly affected by non-attainment of equilibrium under the chromatographic conditions. It is suggested that chromatographic methods could be of value in the determination of phase diagrams, and as an alternative to thermogravimetric analysis.

INTRODUCTION

Hitherto, experiments in gas–solid chromatography have been virtually limited to systems in which no phase change occurs in the solid: indeed, for the most part such studies have been concerned only with adsorption at solid surfaces. However, it is possible to pack a chromatographic column with a solid which undergoes a complete compositional and thus a phase change throughout its bulk. If equilibrium is then achieved within the chromatographic time scale, two kinds of useful and informative experiments may be performed. In the first, which provides an alternative to thermogravimetric analysis (TGA), the temperature of the column is raised continuously and the evolved gases are monitored by a chromatographic detector: we shall call this method thermal evolved-gas analysis (TEGA). Similar experiments with copper(II) sulphate hydrates were mentioned by Wendlandt [1], although he seems to have made no attempt to measure the exact amounts of water vapour evolved and to have assumed that the dehydration took place simply from 5 to 3 to 1 to 0 H_2O. In the second, carried out isothermally, it should be possible (again under equilibrium conditions) for the chromatogram simply to reflect and thus determine the phase diagram. Each step height would then give an equilibrium pressure and the dehydration step areas would measure the compositional changes. In order to investigate these techniques, we have made a particular study of hydrated copper(II) sulphate. Fig. 1 shows the isothermal chromatogram expected, and its relation to the phase diagram.

0021-9673/91/$03.50

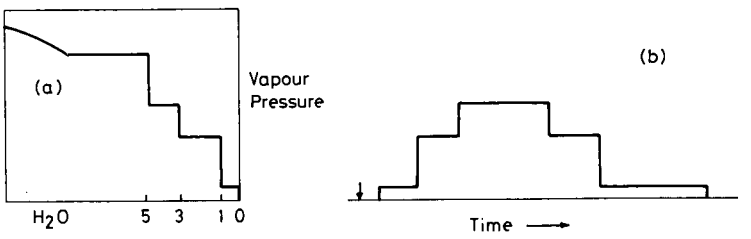

Fig. 1. (a) Phase diagram and (b) the chromatogram expected following an injection of the appropriate amount of water on to a column of anhydrous $CuSO_4$ with dry carrier gas under conditions which are both isothermal and at equilibrium. In the chromatogram, the water vapour pressure rises to the 0:1 phase diagram value after the dead time of the column. Any water vapour pressure larger than this value will be reduced in order to produce hydrated $CuSO_4$. The second chromatographic step starts when all the anhydrous $CuSO_4$ has disappeared, and corresponds to the 1:3 phase diagram value; it continues until all the $CuSO_4 \cdot H_2O$ has disappeared. The highest chromatographic step in (b) corresponds to the 3:5 equilibrium value. Thereafter the column dehydrates under continued flow of dry carrier gas.

In practice, the results obtained show up the effects of non-attainment of equilibria under the conditions of the chromatographic experiments.

EXPERIMENTAL

The chromatographic work was carried out with a Pye Model 104 gas chromatograph (Pye Unicam, Cambridge, UK), but using a thermal conductivity detector (Gow-Mac, Madison, NJ, USA) with matched tungsten filaments to measure the water released. It was necessary to calibrate this detector carefully with known water vapour concentrations, and to house it separately from the column. Oxygen-free nitrogen was used as the carrier gas. The temperature measurements refer generally to those of the oven rather than the sample in the chromatographic column. There is, of course, some lag in the temperature of the sample behind that of the oven. To determine this a second thermocouple was placed inside the column and compared with the thermocouple in the oven. The differences in temperature are illustrated in Fig. 2,

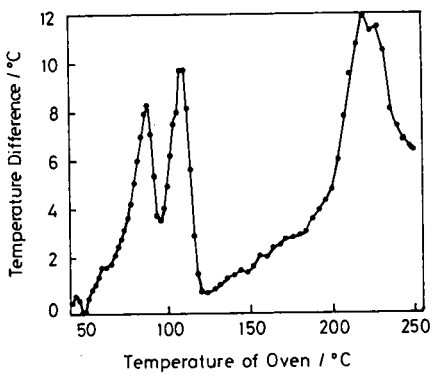

Fig. 2. Differences in temperature between column and oven during the temperature-programmed dehydration of $CuSO_4 \cdot 5H_2O$.

which thus corresponds to a differential thermal analysis (DTA), the three peaks arising from the three dehydration steps. Normal TGA and DTA experiments were made with a Stanton Redcroft (London, UK) simultaneous thermal analyser.

Salts of AnalaR grade were obtained from BDH (Poole, UK).

RESULTS AND DISCUSSION

In the TEGA studies, the chromatographic column was packed with, *e.g.*, 0.0299 g of $CuSO_4 \cdot 5H_2O$ (AnalaR grade). This was held in place by two plugs of silanized glass-wool. The oven was heated at 1°C/min from 30 to 105°C and then at 5°C/min to 270°C. A typical result is shown in Fig. 3. If the heating rate is increased to 2°C/min the first two peaks for $CuSO_4$ are incompletely resolved. Fig. 4 gives the related TGA and DTA curves.

In the TGA experiments, the weight losses were found to be in the ratios 2.02:1.97:1.01, corresponding closely to the 5 to 3, 3 to 1 and 1 to 0 dehydration steps expected. However, in the TEGA experiments, the water vapour released in the three stages corresponded to ratios of 2.27:1.68:1.06, as is shown in Table I. It is of interest that ratios of 2.5:1.5:1.0 and 2.12:1.84:1.00 have been reported by Mu and Perlmutter [2] and by Reisman and Karlak [3], respectively, for analyses conducted in connection with DTA studies.

We believe that the TEGA results are caused by a first-stage dehydration (under the dry carrier gas), which goes beyond the $CuSO_4 \cdot 3H_2O$ expected, to give a "trihydrate" phase in which some of the $CuSO_4$ has been dehydrated to the monohydrate, and on the surface to the anhydrous material which then blocks any further dehydration until a higher temperature is reached. The particular slowness of the trihydrate decompostion has been commented upon by Langfelderova *et al.* [4] in kinetic studies of the dehydration process. The difference between the TEGA and the TGA results can be explained by the rapid removal of water vapour in the former instance. It was found that proper equilibrium could be established in the chromatography system in one of two ways. In the first, the gas flow is stopped for a period of time. In the second, the temperature is first raised and then lowered back to the original temperature.

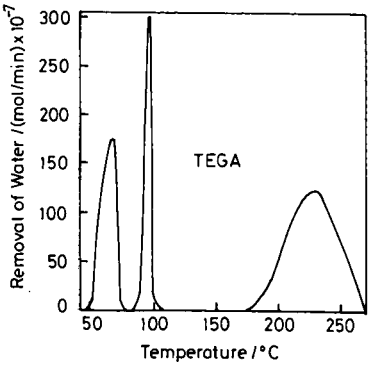

Fig. 3. TEGA study of the dehydration of $CuSO_4 \cdot 5H_2O$.

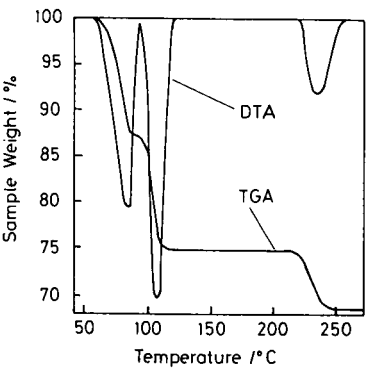

Fig. 4. TGA and DTA curves for the dehydration of $CuSO_4 \cdot 5H_2O$.

TABLE I

WATER LOSS IN SUCCESSIVE STEPS IN TEGA OF $CuSO_4 \cdot 5H_2O$

	Dehydration step		
	1	2	3
Ratio of areas	2.26	1.63	1.11
	2.25	1.72	1.03
	2.27	1.72	1.04
	2.28	1.66	1.07
Average ratio	2.27	1.68	1.06

For $BeSO_4 \cdot 4H_2O$, three dehydration steps were found in TEGA, corresponding to weight ratios of water of 2.0:0.9:1.1. TGA indicates that 2 mol of water are removed at 100°C and a further 2 mol between 150 and 300°C. Some evidence for the latter involving two separate losses of 1 mol of water is provided by DTA. All three techniques give one peak for $LiSO_4 \cdot H_2O$ and $MgSO_4 \cdot 7H_2O$. A double-humped trace for $CaSO_4 \cdot 2H_2O$ is more clearly shown by DTA than by TEGA.

Fig. 5 is an example of the behaviour found when dry nitrogen is passed isothermally (60°C) through a column of $CuSO_4 \cdot 5H_2O$ (in this instance 3.939 g). The regions of pentahydrate, "trihydrate", monohydrate and anhydrous $CuSO_4$ can be clearly distinguished by their colours, namely dark blue, pale blue, very pale blue and white. These changes are also shown in Fig. 5. After *ca.* 14 h, dehydration to the "trihydrate" appears to be complete, but instead of dropping to a value corresponding to the 3:1 equilibrium pressure, the water vapour pressure now leaving the column falls to zero. This is in agreement with our earlier postulate of surface blocking by dehydration to some anhydrous $CuSO_4$. In the particular experiment illustrated in Fig. 5, nucleation of the 3 to 1 dehydration then started accidentally at about a quarter of

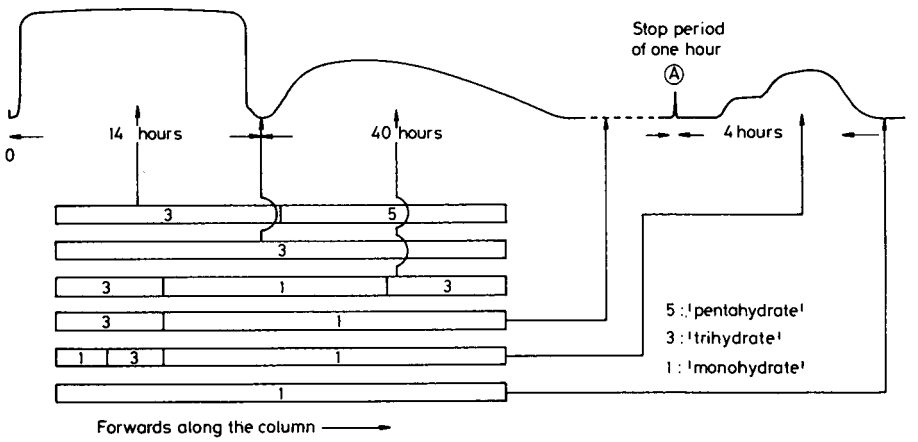

Fig. 5. "Isothermal" chromatographic dehydration of $CuSO_4 \cdot 5H_2O$. For details, see text.

the way along the column, and further water then left the column over a period of *ca.* 40 h, corresponding to the dehydration of the last three quarters of the column to "monohydrate" (*i.e.*, presumably also blocked with a surface layer of anhydrous material). At the point marked A in Fig. 5 the gas flow was stopped for a period of 1 h, so enabling equilibrium to be re-established. After this the remaining water could be removed as shown, the first step corresponding to the 1 to 0 dehydration vapour pressure at the column outlet. It was also found that the dehydration of the "trihydrate" could be restarted by using moist carrier gas with a water vapour content lower than the 3 to 1 dehydration equilibrium pressure.

CONCLUSIONS

We believe that the methods developed in this work have much wider application. Dehydration was chosen as the behaviour of salt hydrates is already well known, but from a chromatographic point of view water is particularly difficult because of the detector problems which it causes. As our experience with $CuSO_4$ shows, care must always be taken to allow for the possibility of non-equilibrium processes occurring in the special circumstances of the chromatographic experiment.

REFERENCES

1 W. W. Wendlandt, *Anal. Chim. Acta*, 27 (1962) 309.
2 J. Mu and D. D. Perlmutter, *Ind. Eng. Chem., Process Des. Dev.*, 20 (1981) 640.
3 A. Reisman and J. J. Karlak, *J. Am. Chem. Soc.*, 80 (1958) 6500.
4 H. Langfelderova, M. Linkesova and E. Jona, *J. Thermal. Anal.*, 19 (1980) 117.

Journal of Chromatography, 557 (1991) 501–505
Elsevier Science Publishers B.V., Amsterdam

CHROM. 23 300

Short Communication

Analyse par chromatographie en phase gazeuse de la réaction de macrolactonisation de Mukaiyama

K. HALVORSEN, J. C. ADER, I. RICO* et A. LATTES
Université Paul Sabatier, Lab. IMRCP, URA CNRS No. 470, 118 Route de Narbonne, 31062 Toulouse Cedex (France)

ABSTRACT

GAS CHROMATOGRAPHIC ANALYSIS OF THE MACROLACTONISATION REACTION OF MUKAIYAMA

Macrocyclic chemistry has been studied for many years. For example, Mukaiyama optimised the synthesis of macrolides by using high dilution and special activation to promote lactonisation of ω-hydroxycarboxylic acids relative to polymerisation. In order to suppress high dilution in this reaction, we conducted the first kinetic study of Mukaiyama's reaction by gas phase chromatography.

INTRODUCTION

La chimie des macrocycles connait depuis plusieurs années un grand intérêt comme en témoigne le prix Nobel qui a été attribué sur ce thème en 1987, conjointement à C.J. Pedersen, D. J. Cram et J. M. Lehn. Le principe bien connu selon lequel la technique de la "haute dilution" favorise la cyclisation intramoléculaire aux dépens de la polymérisation intermoléculaire a guidé toutes les démarches synthétiques dans ce domaine [1–3].

Corey et Nicolaou [4] et Mukaiyama *et al.* [5,6] ont, pour leur part, optimisé la

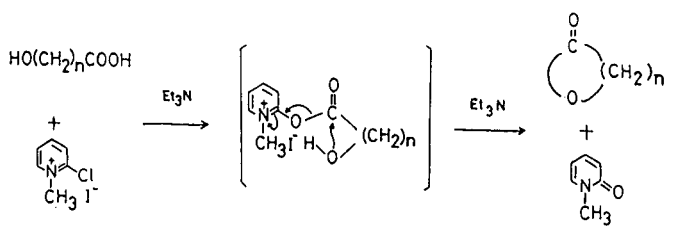

Fig. 1. Formation de macrolactones selon la réaction de Mukaiyama. Et = C_2H_5.

synthèse de macrolactones par cyclisation d'hydroxyacides à longue chaîne en couplant la technique de haute dilution et la "double activation" du substrat (Fig. 1).

Une série de macrolactones de différentes tailles a été ainsi obtenue avec de bons rendements [5].

Dans le cadre d'une étude de la réaction de Mukaiyama visant à supprimer la haute dilution, nous avons mis au point pour la première fois une méthode d'analyse directe de la cinétique de la réaction par chromatographie en phase gazeuse (CPG).

PARTIE EXPÉRIMENTALE

L'iodure de chloro-2 méthyl-1 pyridinium 97%, l'acide hydroxy-16 hexadecanoïque 98%, la triéthylamine > 99% (Aldrich, Strasbourg, France) et l'hexadécanolide 97% (Lancaster Synthesis, Mundolsheim, France) ont été utilisés sans purification complémentaire. L'acétonitrile > 99,5% (Prolabo, Subra, Toulouse, France) a été distillé sur CaH_2, puis conservé sur tamis 4 Å.

Expérience 1

A une solution de 510 mg (2 mmol) d'iodure de chloro-2 méthyl-1-pyridinium dans 50 ml d'acétonitrile anhydre est additionnée une solution de 136 mg (0,5 mmol) d'acide hydroxy-16 hexadecanoïque et 404 mg (4 mmol) de triéthylamine dans 40 ml d'acétonitrile sur une période de 6 min.

Expérience 2

A une solution de 510 mg (2 mmol) d'iodure de chloro-2 méthyl-1 pyridinium dans 10 ml d'acétonitrile anhydre est additionnée une solution de 136 mg (0,5 mmol) d'acide hydroxy-16 hexadecanoïque et 404 mg (4 mmol) de triéthylamine dans 8 ml d'acétonitrile sur une période de 6 min. (Les réactifs sont donc en concentration cinq fois plus grande que dans l'expérience 1.)

Etude cinétique

L'apparition de l'hexadecanolide est suivie au cours du temps par prélèvements d'échantillons du milieu réactionnel qui sont analysés par chromatographie en phase gazeuse. Une courbe d'étalonnage a été établie au préalable avec une gamme de concentrations en hexadecanolide allant de 0,005 à 0,03 *M*.

L'appareil de CPG est un Di 200 (Delsi-Nermag, Argenteuil, France) couplé à un intégrateur Shimadzu C-R4A (Touzart-Matignon, Vitry-sur-Seine, France). Les analyses ont été réalisées à l'aide d'une colonne SE 30 à 10% de silicone sur chromosorb PAW 80/100 mesh (2 m de longueur). Les conditions d'analyse sont: T_{four} = 220°C; $T_{\text{injecteur}}$ = 280°C; $T_{\text{détecteur}}$ (ionisation de flamme) = 290°C. Dans ces conditions le temps de rétention de l'hexadecanolide formé est de 10,3 min (Fig. 2).

RÉSULTATS ET DISCUSSION

La cinétique de la réaction de formation de l'hexadecanolide à partir de l'acide hydroxy-16 hexadecanoïque (n = 15 dans la Fig. 1) a été suivie par CPG. Deux expériences ont été ainsi analysées:

(i) Les conditions opératoires retenues pour l'expérience 1 sont analogues à

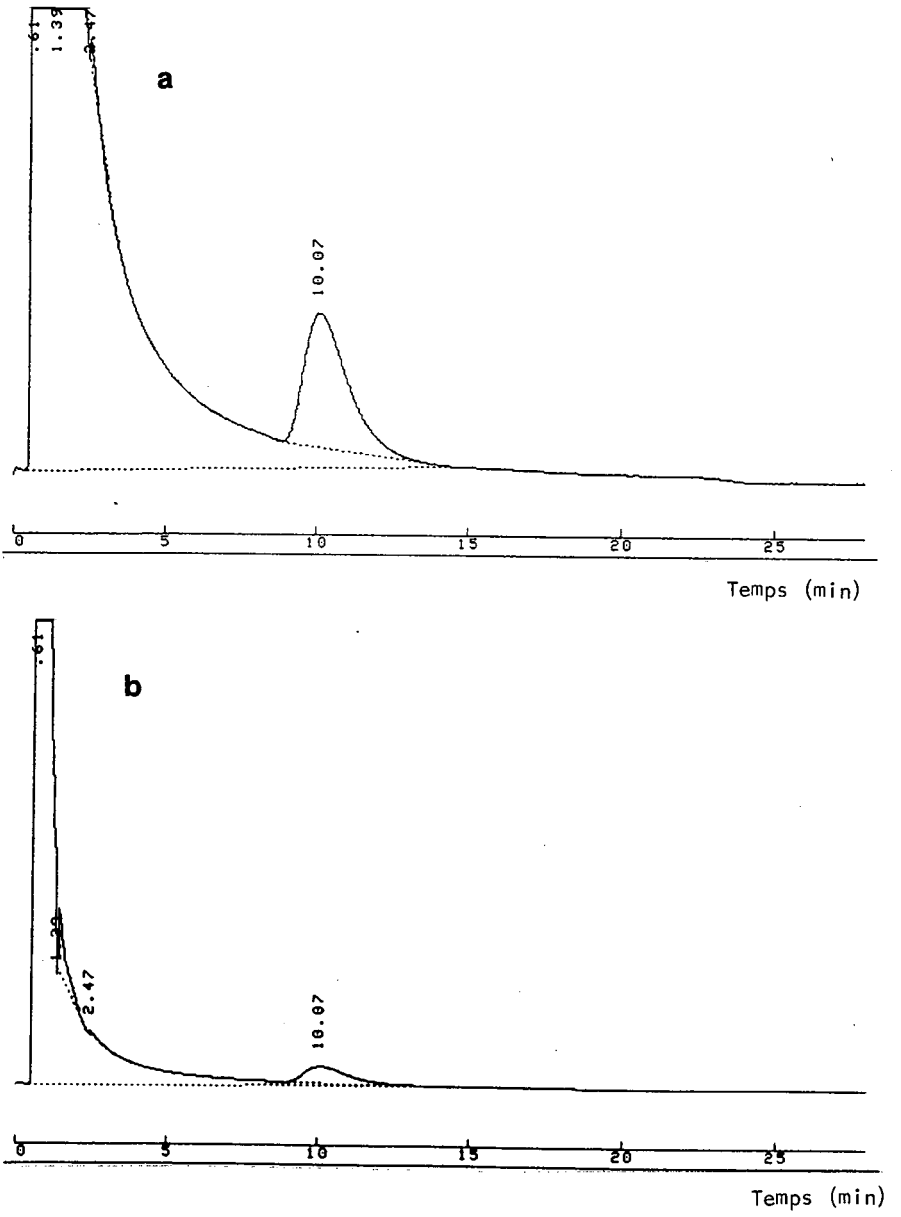

Fig. 2. Chromatogramme du milieu réactionnel. Le temps de rétention de l'hexadécanolide formé est de 10,07 min dans l'exemple choisi. (a) Attenuation 3; (b) attenuation 5.

celles décrites par Mukaiyama *et al.* [5]. Dans le but de supprimer la haute dilution, nous avons cependant remplacé l'addition lente de l'hydroxyacide et de la triéthylamine (8 h selon Mukaiyama) par une addition rapide (6 min).

(ii) Pour l'expérience 2, nous avons augmenté les concentrations en réactifs d'un facteur cinq par rapport à celles de l'expérience 2, tout étant équivalent par ailleurs.

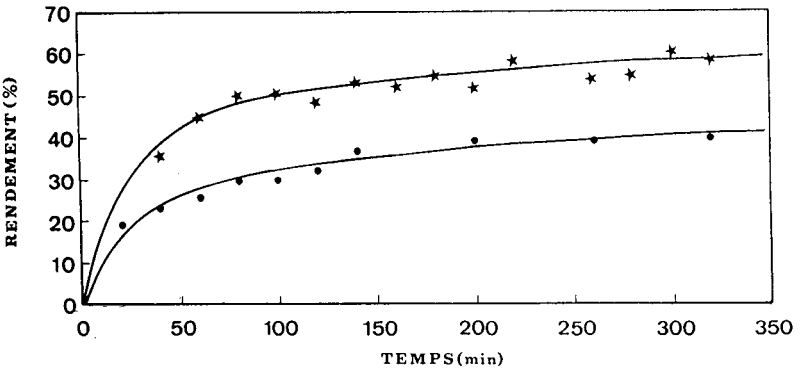

Fig. 3. Rendement en hexadecanolide en fonction du temps pour l'expérience 1 (★) et l'expérience 2 (●) (N.B.: $t = 0$) correspond à la fin de l'addition de l'hydroxyacide; *cf.* Partie expérimentale.

Les cinétiques de la réaction ont été suivies par CPG. Les courbes obtenues (rendement en lactone en fonction du temps) pour les deux expériences sont rassemblées dans la Fig. 3.

L'examen de la Fig. 3 conduit aux conclusions suivantes:

(i) Quelles que soient les conditions (expériences 1 ou 2) la réaction est rapide; elle est pratiquement terminée au bout de 3 h.

(ii) La cinétique de la réaction apparait d'un ordre complexe comme le laissait prévoir le mécanisme de la réaction [5].

(iii) Au terme de la réaction, le rendement (Rdt.) en lactone diminue selon la séquence suivante: conditions de Mukaiyama (Rdt. 80%); expérience 1 (Rdt. 60%); expérience 2 (Rdt. 40%).

L'étude de la réaction de Mukaiyama, réalisée ici, met donc en évidence les limites de ce procédé: l'addition lente de l'hydroxyacide ainsi que des concentrations faibles en réactifs sont nécessaires pour obtenir les macrolactones avec de bons rendements.

CONCLUSIONS

Nous avons mis au point dans ce travail une technique d'analyse directe par CPG de la réaction de macrolactonisation de Mukaiyama.

Cette étude met clairement en évidence l'importance de la haute dilution dans le déroulement de cette réaction. Notre but étant de nous affranchir de cet impératif couteux et malaisé à mettre en oeuvre, nous nous proposons dans un deuxième temps de modifier le milieu réactionnel en particulier par l'utilisation de systèmes organisés tels que les microémulsions [7,8].

RÉSUMÉ

La chimie des macrocycles connait depuis plusieurs années un grand interêt. Mukaiyama a ainsi optimisé la synthèse de macrolactones par cyclisation d'hydroxyacides à longue chaîne en couplant la technique de haute dilution et la double

activation du substrat. Dans le cadre d'une étude de la réaction de Mukaiyama visant à supprimer la haute dilution, nous avons mis au point pour la première fois une méthode d'analyse directe de la cinétique de la réaction par chromatographie en phase gazeuse.

BIBLIOGRAPHIE

1 G. Ercolani, L. Mandolini et P. Mencarelli, *Gazz. Chim. Ital.*, 119 (1989) 209.
2 C. J. Pedersen, *Science (Washington, D.C.)*, 241 (1988) 536.
3 C. Galli et L. Mandolini, *J. Chem. Soc. Chem. Commun.*, (1982) 251; et références citées dans cet article.
4 E. J. Corey et K. C. Nicolaou, *J. Am. Chem. Soc.*, 96 (1974) 5614.
5 T. Mukaiyama, M. Usui et K. Saigo, *Chem. Lett.*, (1976) 49.
6 T. Mukaiyama, *Angew. Chem. Int. Ed. Engl.*, 18 (1979) 707; et références citées dans cet article.
7 A. Lattes, *J. Chim. Phys. Phys Chim. Biol.*, 84 (1987) 1061.
8 A. Lattes et I. Rico, *Colloids Surf.*, 35 (1989) 221.

Journal of Chromatography, 557 (1991) 507–513
Elsevier Science Publishers B.V., Amsterdam

CHROM. 23 234

Short Communication

Cyclooxygenase and lipoxygenase arachidonic acid metabolism by monocytes from human immune deficiency virus-infected drug users

ISABEL RAMIS, JOAN ROSELLÓ-CATAFAU and GLORIA GÓMEZ
Department of Neurochemistry, Eicosanoid Branch, Centro de Investigación y Desarrollo, CID, CSIC, Jordi Girona 18-26, 08034 Barcelona (Spain)
JOSÉ MARÍA ZABAY and EDUARDO FERNÁNDEZ CRUZ
Immunology Department, Hospital General Gregorio Marañon, Madrid (Spain)
and
EMILIO GELPÍ*
Department of Neurochemistry, Eicosanoid Branch, Centro de Investigación y Desarrollo, CID, CSIC, Jordi Girona 18-26, 08034 Barcelona (Spain)

ABSTRACT

Prostaglandin E_2, thromboxane B_2 and leukotriene B_4 monocyte production have been determined in human immune deficiency virus (HIV)-infected drug users ($n = 36$) and healthy subjects ($n = 29$). Eicosanoids were extracted from the incubates using C_{18} solid-phase cartridges and determined by radioimmunoassay. An enhanced production of prostaglandin E_2 and thromboxane B_2 was detected in monocytes from HIV-positive drug users whether or not they had been previously stimulated with zymosan. Concomitant leukotriene B_4 increases were not observed. The results reported in this paper indicate that altered cyclooxygenase arachidonic acid metabolism in monocytes from HIV-infected drug users is associated with the severe cellular immunodysfunction characteristic of AIDS. In contrast, leukotriene B_4 does not seem to play a role in AIDS-associated immunosuppression.

INTRODUCTION

Prostaglandins of the E series are important arachidonic acid (AA) metabolites involved in the immune response [1]. Recent studies have demonstrated their immunosuppressor role in immunological functions. Furthermore, it is known that prostaglandin E_2 (PGE_2) and thromboxane B_2 (TXB_2) are the major cyclooxygenase metabolites of AA produced by human monocytes [2] and that these mononuclear cells can be infected by the human immunodeficiency virus (HIV) [3]. In line with previously reported work on increased PGE_2 and TXB_2 production by unstimulated

0021-9673/91/$03.50

monocytes from eight AIDS patients [4], that study has now been extended to a much larger population of HIV-infected drug users ($n = 36$, including the eight earlier reported cases). The *in vitro* effects of zymosan and indomethacin (a stimulant and inhibitor of AA metabolism, respectively) on monocyte PGE_2 and TXB_2 production from seven HIV infected drug users has also been evaluated.

As no data are available on leukotriene B_4 (LTB_4) production by monocytes from HIV-infected drug users, this lipoxygenase metabolite of AA was also included in this study. It is known that LTB_4 induces the T-lymphocyte suppressor cell population [5]. More recently it has been reported that LTB_4 induces lymphokine and monokine production by various T-cell types [6], although its effect on T-cell activation remains unclear [7].

Briefly, the aim of this further study was to validate the results obtained with eight patients and to expand the scope of the first study [4] to an additional number of new HIV-positive (HIV+) cases to strengthen the implications of altered arachidonic acid metabolism in patients suffering from AIDS.

EXPERIMENTAL

Chemicals

Tritiated PGE_2 (186 Ci/mmol), TXB_2 (210 Ci/mmol) and LTB_4 (150 Ci/mmol) were purchased from Amersham International (Amersham, UK). Methanol, acetonitrile and light petroleum (b.p. 40–60°C) were from Merck (Darmstadt, Germany). Methyl formate was from Fluka (Buchs, Switzerland). The C_{18} cartridges were obtained from Waters Assoc. (Milford, MA, USA).

Subjects

Arachidonic acid metabolism by monocytes was studied in a group of 36 HIV-infected drug users with or without AIDS, selected according to the Criteria of the Center for Disease Control Classification. In all cases HIV antibodies were assessed by two different enzyme-linked immunosorbent assays (Abbot-Elisa and Elavia-Institute Pasteur Tests) and confirmed by Western blotting. The absolute numbers of CD4+, the blastogenic response to mitogens *in vitro* and the response to antigens in delayed type hypersensitivity skin testing were evaluated in all patients. A group of 29 healthy volunteers (HIV−), both male and female, were studied as controls.

Monocyte incubations

Monocyte preparations from 36 HIV-infected drug users and 29 healthy controls were carried out as described elsewhere [8]. More than 95% of the adherent cells thus obtained were shown to be monocytes by May–Grünwald–Giemsa staining and positive reaction for esterase. The monocyte preparations were incubated for 24 h in RPMI-1540 medium supplemented with 1% fetal calf serum. Incubate supernantants were analysed for PGE_2, TXB_2 and LTB_4 as described in the following sections. Moreover, in monocyte preparations from seven of these HIV-infected drug users and healthy subjects, four monocyte cell preparation aliquots were incubated under the following conditions: basal, indomethacin (1 μg/ml), zymosan (160 μg/ml) and zymosan (160 μ/ml) + indomethacin (1 μg/ml); zymosan and indomethacin were added to study the synthesis and release of PGE_2 and TXB_2 in stimulated and non-stimulated cells, respectively.

Extraction of arachidonic acid metabolites

Tritiated standards (52 pg of PGE_2, 46 pg of TXB_2 and 58 pg of LTB_4) were added to the monocyte cell culture supernatants. The samples were acidified to pH 3 and directly processed through Sep-Pak C_{18} cartridges. After washing with 10 ml of water (pH 3.15) and 20 ml of light petroleum, the arachidonic acid metabolites were finally eluted with 8 ml of methyl formate. The residues, obtained after the evaporation of organic eluates to dryness, were resuspended in chromatographic or radioimmunoassay (RIA) buffer and subjected to high-performance liquid chromatography (HPLC) and/or RIA [7]. The recoveries were determined by scintillation counting.

HPLC purification

HPLC separation of the cyclooxygenase arachidonic acid metabolites PGE_2 and TXB_2 was carried out under isocratic conditions using 40 m*M* formic acid, pH 3.15, with triethylamine–acetonitrile (67:33, v/v) as the mobile phase at a flow-rate of 1.5 ml/min. A Spherisorb ODS-2, 10 μm, 25 × 0.46 cm I.D. column (Phase Separations, Deesire, UK) was used.

The biological samples were injected into a Kontron liquid chromatograph (Kontron Analytical, Zurich, Switzerland) and the appropriate fractions were collected at the elution time of the tritiated standards, established by a radioactivity detector (Ramona, Issomess, Straubenhardt, Germany) directly coupled to the HPLC system. After collection of the appropriate eluates, these 60-s fractions containing PGE_2 and TXB_2 were lyophilized and resuspended in RIA buffer.

RIA determinations

Resuspended extracts, either directly obtained from the Sep-Pak cartridges or previously purified by HPLC, were subjected to RIA quantification. TXB_2, PGE_2 and LTB_4 were determined in duplicate using specific antisera. The PGE_2 and TXB_2 antisera showed a cross-reactivity for TXB_2 and PGE_2 of less than 0.01 and 0.1%, respectively.

RESULTS

The C_{18} solid-phase extraction, HPLC and overall recoveries for PGE_2, TXB_2 and LTB_4 are given in Table I.

The immunoreactive peaks detected in the HPLC eluate fractions from the monocyte supernatants correspond to those eluates collected at the elution times of tritiated authentic standards of PGE_2 and TXB_2 (Fig. 1). No significant difference in the results was observed when the HPLC purification step was omitted. Linear correlations (r = 0.9899 and 0.97623, respectively) were observed for the RIA values of TXB_2 and PGE_2 obtained with and without prior HPLC purification.

Fig. 2 shows the TXB_2 and PGE_2 levels determined in monocyte preparations obtained from HIV infected drugs users (n = 7) and healthy volunteers (n = 7), in both instances incubated individually with indomethacin or zymosan as well as with a mixture of these two compounds. TXB_2 is the major cyclooxygenase AA metabolite synthesized by human monocytes under these conditions. A significant inhibitory effect on TXB_2 and PGE_2 production was observed in the presence of indomethacin

TABLE I

TXB_2, PGE_2 AND LTB_4 RECOVERIES (%) FROM MONOCYTE SUPERNATANTS EXTRACTED AND PURIFIED BY HPLC

Values are expressed as mean ± S.D. $n = 5$.

Metabolite	Recovery (%)		
	Extraction	HPLC	Extraction + HPLC
TXB_2	92.7 ± 3.8	64.6 ± 2.1	59.7 ± 1.7
PGE_2	93.7 ± 3.8	78.8 ± 4.7	72.4 ± 4.7
LTB_4	90.3 ± 2.3	80.6 ± 5.5	72.7 ± 6.1

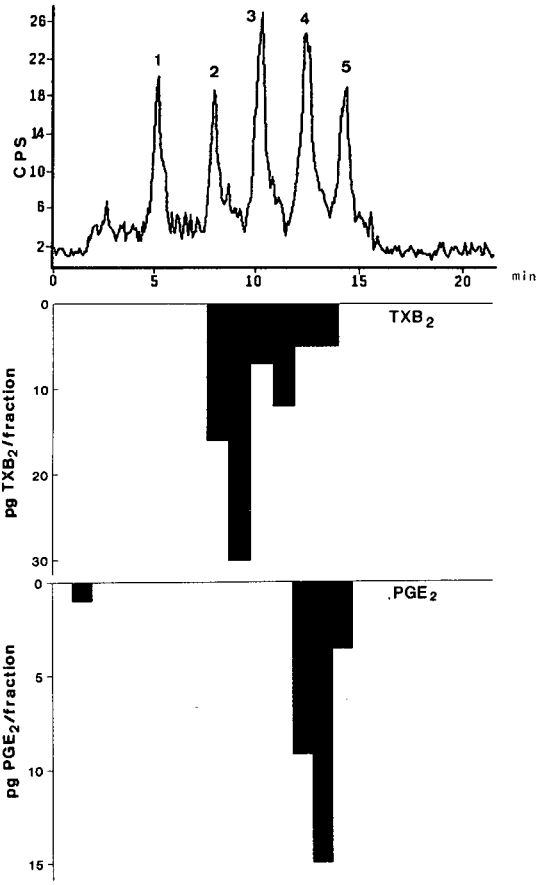

Fig. 1. On-line radiochromatogram of five prostanoids (top panel) and reconstructed immunochromatographic profiles of TXB_2 and PGE_2 (centre and lower panels) obtained by RIA of collected 60-s HPLC eluates of monocyte incubate supernatants. Mobile phase: 40 m*M* formic acid, pH 3.15, with triethylamine–acetonitrile (67:33, v/v), at a flow-rate of 1.5 ml/min. Peaks: 1 = 6-Keto-$PGF_{1\alpha}$; 2 = TXB_2; 3 = $PGF_{2\alpha}$; 4 = PGE_2; 5 = PGD_2.

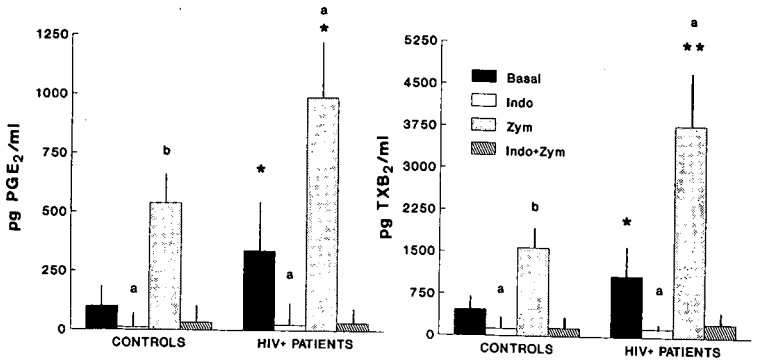

Fig. 2. PGE_2 (left) and TXB_2 (right) synthesized by monocytes from HIV-infected drug users ($n = 7$) and controls ($n = 7$), incubated under basal conditions and with the addition of indomethacin, zymosan or a mixture of both. ★: $p<0.1$; ★★: $p<0.05$ *versus* controls (Student's *t*-test); a: $p<0.05$; b: $p<0.005$ *versus* basal (*t*-paired test).

in both groups of subject ($p< 0.05$ *versus* basal). Also, a significant increase in TXB_2 and PGE_2 production was observed in the presence of zymosan ($p< 0.005$ in the control group and $p< 0.05$ in the HIV+ groups *versus* basal). In all instances prostanoid production in monocytes from HIV-infected drug users was higher than in the controls ($p< 0.1$, *versus* control), including monocytes incubated with zymosan ($p< 0.1$ for PGE_2 and $p< 0.05$ for TXB_2 *versus* controls).

Fig. 3 shows the basal production of PGE_2, TXB_2 and LTB_4 corresponding to HIV+ drug users ($n = 36$) and controls ($n = 29$). In agreement with earlier work [4], monocytes from these HIV-infected drug users also show an altered production of PGE_2 and TXB_2 ($p< 0.05$),but there were no variations in LTB_4, the major lipoxygenase AA metabolite synthesized by human monocytes.

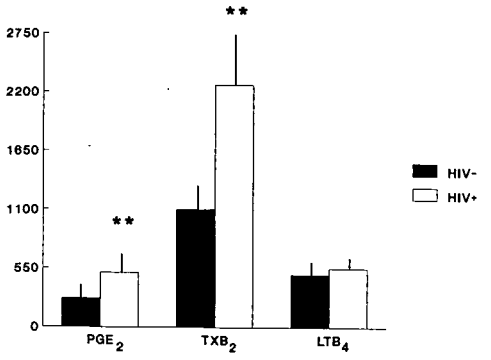

Fig. 3. Eicosanoid biosynthesis by monocytes from HIV+ drug users ($n = 36$) and healthy subjects ($n = 29$) with values including the seven cases described in Fig. 2. ★★: $p<0.005$ *versus* monocytes from HIV+ drug users (Student's *t*-test).

DISCUSSION

The immunochromatograms shown in Fig. 1 and the linear correlation between TXB_2 and PGE_2 values obtained pre- and post-HPLC, suggest that, contrary to recommended procedures [9], the HPLC purification of samples before RIA could be omitted in this instance, thus simplifying the experimental procedure. The direct RIA of biological extracts is often made difficult by lack of absolute specificity of the antibodies. This leads to well known instances of erroneous values as a result of cross-reactivity between structurally related compounds present in the samples [9]. However, in instances where the sample matrix is both relatively simple in its composition and free of analyte interferences, direct RIA could become a valid alternative. Nevertheless, for analytical reliability, the results of direct RIA should always be validated against the corresponding values from HPLC-purified fractions. These data, obtained as shown in Fig. 1 from a single pool of monocyte incubates, confirm that cyclooxygenase immunoreactivity is higher for TXB_2 than for PGE_2 and that the RIA quantitation is not affected by mutual interferences because of the extremely low cross-reactivity of the respective antibodies. This has been verified although TXB_2 shows considerable tailing, as shown by the corresponding immunochromatogram in Fig. 1 and the lower HPLC recovery values (Table I). This tailing effect, as previously discussed, is very difficult to counteract due to the dynamic equilibrium established between the open and closed forms of the oxane ring in TXB_2 [10,11]. However, the contribution of the approximately 5 pg TXB_2 present in each of the two 60-s fractions (collected between 12 and 14 min in Fig. 1) does not add more than 0.05 pg per fraction to the RIA values of PGE_2.

The pattern of prostanoid synthesis in human monocytes depends on the *in vitro* culture conditions. From this point of view, these results (see Fig. 2) agree with data reported previously [8,12]. The results in Fig. 2. show that monocytes from HIV-infected drug users (in basal or stimulated conditions) show a significant cyclooxygenase activation which is reflected in a concomitantly increased production of PGE_2 and TXB_2, the latter being the major cyclooxygenase AA metabolite. Although this tendency observed in a groups of seven patients is significant at $p = 0.1$, when the study was extended to a group of 36 patients and 29 controls (see Fig. 3), the observed differences were conclusive, showing a clear overproduction of prostanoids by monocytes from HIV-infected drug users with a higher statistical significance ($p < 0.05$).

PGE_2 has been accepted as an immunosupressing factor in cellular immunity [13]. However, the role of TXB_2 in immune regulation is unknown. TXB_2 seems to be involved in severe immunological responses such as organ rejection [14] and septicaemia [15]. With respect to the latter, it is known that the suppressed immune response of the patients with sepsis is also associated with enhanced TXB_2 plasma levels when compared to healthy subjects [15]. It is not known whether TXB_2 plays an immunosuppressive role in HIV-infected drug users. Further studies are necessary to elucidate whether this elevated TXB_2 production could contribute to increased immune deficiency in AIDS patients.

One interesting result of this study is that the LTB_4 production by monocytes is unaltered in the presence of HIV infection. These data seem to indicate a higher specific cyclooxygenase activity in monocytes from HIV-infected drug users, in con-

trast to the non-specific activation of human monocytes by several stimuli such as calcium ionophore or zymosan, which indistinctively potentiate both the cyclo and the lipoxygenase pathways. Thus, these results suggest that LTB_4 is not directly involved in the immunosuppressive mechanisms of AIDS, although it has been reported that, in addition to being a potent pro-inflammatory agent, LTB_4 can affect immunorregulatory functions [6].

In conclusion, an enhanced prostanoid production by monocytes from HIV-infected drug users has been confirmed. Moreover, these results also confirm that PGE_2 and TXB_2 are associated with HIV infection and suggest that altered cyclooxygenase AA metabolism may be one of the factors involved in the progressive and severe immunosuppression associated with AIDS.

ACKNOWLEDGEMENTS

This work was supported by the Fondo de Investigacion Sanitaria de la Seguridad Social, grant no. 89/0386.

REFERENCES

1 J. S. Goodwin and D. R. Weeb, *J. Clin. Immunol. Immunopathol.*, 15 (1980) 106.
2 J. I. Kurland and R. Buckman, *J. Exp. Med.*, 147 (1987) 952.
3 S. Gartner, D. M. Markovitz, M. H. Kaplan, R. C. Gallo and M. Popovic, *Science*, 233 (1986) 215.
4 E. Fernandez-Cruz, E. Gelpí, N. Longo, B. Gonzalez, M. T. de la Morena, M. Garcia Montes, J. Roselló, I. Ramis, A. Suarez, A. Fernandez and J. M. Zabay, *AIDS*, 3 (1989) 91.
5 M. Rola-Pleszczynski, P. Borgeat and P. Sirois, *Biochem. Biophys. Res. Commun.*, 113 (1982) 531.
6 M. Rola-Pleszczynski, L. Gagnon and P. A. Chavaillez, *Ann. NY Acad. Sci.*, 524 (1988) 218.
7 J. S. Goodwin, *Immunol. Res.*, 5 (1986) 233.
8 N. A. Pawlowski, G. Kaplan, A. L. Hamill, Z. A. Cohn and W. A. Scott, *J. Exp. Med.*, 158 (1983) 393.
9 E. Gelpí, I. Ramis, G. Hotter, G. Bioque, O. Bulbena and J. Roselló, *J. Chromatogr.*, 492 (1989) 223.
10 R. Freixa, J. Casas, J. Roselló and E. Gelpí, *J. High Resolut. Chromatogr. Chromatogr. Commun.*, 7 (1984) 156.
11 J. Abian and E. Gelpí, *J. Chromatogr.*, 562 (1991) 153.
12 M. S. Kennedy, J. D. Stobo and M. E. Goldyne, *Prostaglandins*, 20 (1980) 135.
13 S. Chouaib, L. Chatenoud, D. Klatzmann and D. Fradelizi, *J. Immunol.*, 132 (1984) 1851.
14 H. B. Steinhauer, H. Wilms, M. Rüther and P. Schollmeyer, *Transplant. Proc.*, 18 (suppl 4) (1986) 98.
15 H. A. Ball, J. A. Cook, W. C. Wise and P. V. Halushka, *Intens. Care Med.*, 12 (1986) 116.

Journal of Chromatography, 557 (1991) 515–522
Elsevier Science Publishers B.V., Amsterdam

CHROM. 23 102

Short Communication

Structural investigation of oligomeric *n*-octylsilyl reversed phases

S. O. AKAPO*,[a] and C. F. SIMPSON

Analytical Science Group, Chemistry Department, Birkbeck College, University of London, 20 Gordon Street, London WC1H 0AJ (UK)

ABSTRACT

The structural characteristics of a series of oligomeric bonded phases prepared by the fluidised bed technique have been determined using ^{29}Si and ^{13}C CP-MAS-NMR spectroscopy. The porous properties of these materials were also investigated using GPC and it was shown that the size separation characteristics of the various oligomers were substantially the same irrespective of the carbon load.

INTRODUCTION

Surface modification of silica gels with organochlorosilanes has become popular in reversed-phase high-performance liquid chromatography (RP-HPLC). Depending on the functionality (chlorine atoms) of the silane reagent and the reaction conditions, the surface of the derivatized silica gel may vary from a bonded monolayer to polymerized layers with a cross-linked structure of the silanizing agent on the silica surface [1,2].

The percentage carbon load of the modified silica gel is obtained by elemental analysis, and other parameters such as specific surface area, pore volume, particle size and size distribution are determined by BET nitrogen adsorption measurement, Coulter counter and other techniques [3,4]. However, none of these techniques provides useful information about the surface structure of the bonded phases.

Solid-state ^{29}Si and ^{13}C cross-polarization and magic angle spinning nuclear magnetic resonance ($^{29}Si/^{13}C$ CP-MAS-NMR) spectrometry has proved to be a useful technique for a quantitative and qualitative description of the surface structure of chemically modified silica gels [2,5–12]. Such studies exploit the short relaxation time

[a] Present address: Chemical Sciences Department, Ogun State University, P.M.B. 2002, Ago-Iwoye, Nigeria.

0021-9673/91/$03.50

of ^{13}C and the ability of ^{29}Si–H cross-polarization to restrict detection to surface nuclei that are nearer the available protons of the hydroxyl groups. Hence the method is capable of differentiating the various binding sites on the silica surface.

As an extension of our previous work [13,14], this paper reports an investigation of the surface structure of oligometric *n*-octylsilyl reversed phase using ^{29}Si and ^{13}C CP-MAS-NMR spectrometry. In addition, the porous properties of the bonded phases were further examined by gel permeation chromatography (GPC).

EXPERIMENTAL

The bonded phases were prepared by the fluidized bed technique [15] and details of the original synthesis, physical characterization and column packing can be found in a previous paper [13]. The characteristics of the bonded phases are given in Table I.

Solid-state ^{29}Si and ^{13}C CP-MAS-NMR spectra of the unmodified and selected modified silica gels were obtained on a Bruker MSL-300 Fourier transform spectrometer. The $^{29}Si/^{13}C$ spectra were obtained at 59.60 and 75.47 MHz, respectively, using a zirconia rotor (7 mm I.D.) containing 100–200 mg of sample. To overcome excessive NMR line widths and overlapping lines, magic angle spinning was performed at 4 kHz. A cross-polarization contact time of 10 ms and a recycling time of 5 s were used. Chemical shifts were referenced to liquid tetramethylsilane.

Gel permeation chromatographic studies were performed on a chromatograph consisting of a Shimadzu LC-5A pump and SPD 2AM variable-wavelength UV detector (Shimadzu, Kyoto, Japan) operated at 254 nm. The columns were evaluated at ambient temperature using tetrahydrofuran (THF) (Fisons, Dorset, UK) as the mobile phase. Benzene (Fluka, Buchs, Switzerland) and polystyrenes (Waters Assoc. USA, and Polymer Labs., UK) of narrow molecular-mass distribution served as the standard test solutes. The solutes were made up singly in the mobile phase (*ca.* 1 mg/ml in THF) and injected into the column via a Rheodyne (Berkeley, CA, USA)

TABLE I

CHARACTERISTICS OF THE BONDED PHASES [13]

Column No.	C (%, w/w)	Surface area, S_{BET} ($m^2\ g^{-1}$)	Pore volume	
			$V_{P(N_2)}$ ($cm^3\ g^{-1}$)	$V_{P(GPC)}$ cm^3
Silica	–	250.00	1.00	0.87
1	7.58	153.04	0.82	0.76
2	9.69	144.99	0.71	0.65
3	11.14	132.69	0.60	0.58
4	12.18	126.59	0.63	0.56
5	12.69	118.64	0.59	0.54
6	14.43	115.97	0.59	0.53
7	14.90	107.11	0.54	0.49
8	15.80	106.50	0.49	0.47
9	16.79	105.21	0.48	0.46
10	17.45	105.14	0.45	0.45

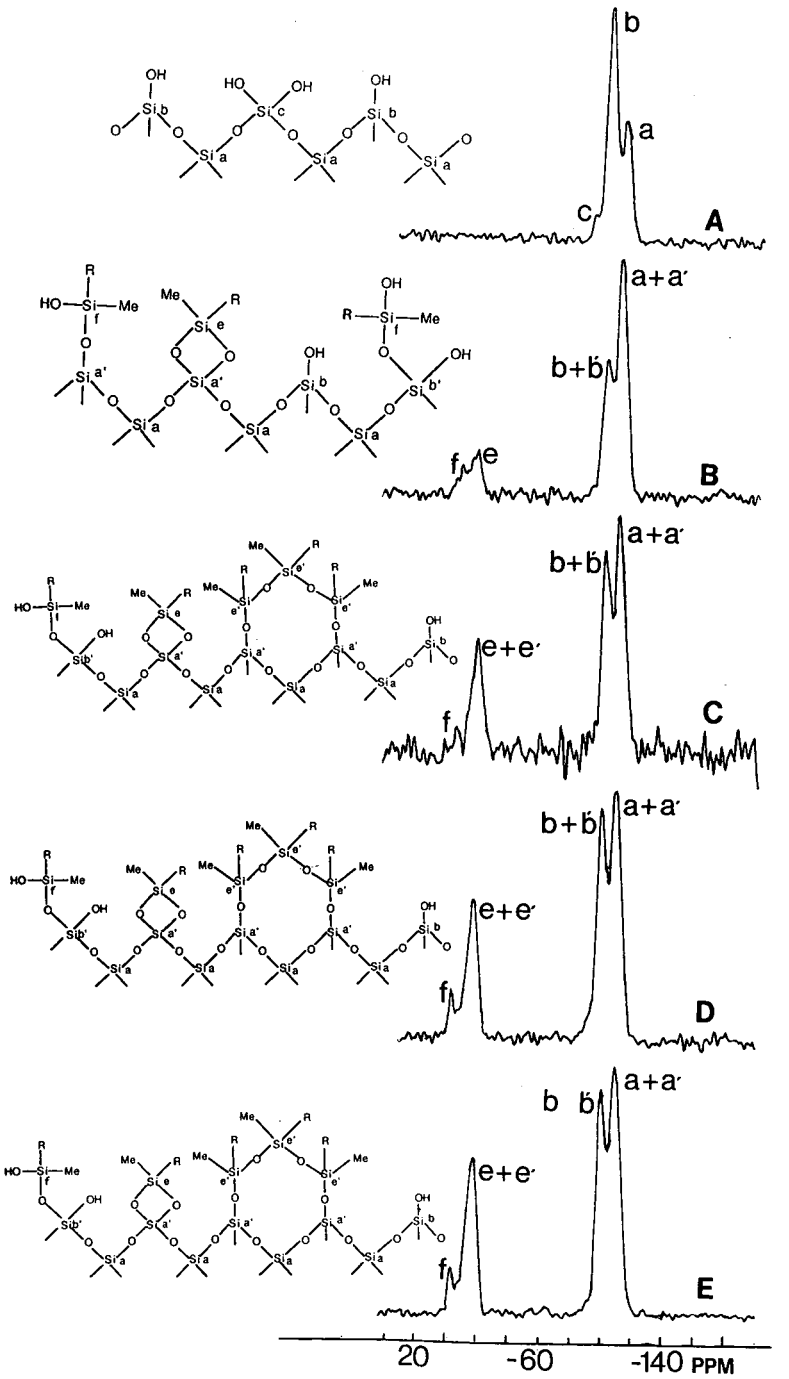

Fig. 1. ^{29}Si CP-MAS-NMR spectra of (A) silica after hydrothermal treatment at 200°C and of the bonded phases; (B) column 1; (C) column 3; (D) column 5; (E) column 10. Me = Methyl.

7125 valve fitted with a 20-μl loop. Benzene and polystyrene standard (molecular mass $1.2 \cdot 10^6$) were used to determine the void or mobile phase volume V_o and the exclusion volume V_{ex}, respectively. The relative retention R and the solute probe diameter $\varnothing$ were calculated by [16]

$$R = [(V_e - V_{ex})/(V_o - V_{ex})]100$$
$$\text{and } \varnothing = 0.62\ (\text{MW})^{0.59}$$

where V_e is the retention volume of the test solute.

RESULTS AND DISCUSSION

Fig. 1 shows the ^{29}Si CP-MAS-NMR spectra of the unmodified and modified silica gels. The NMR data were obtained by on-line computer acquisition and processing. The chemical shifts (labelled a–f) were assigned according to the literature [6,7,10]. The proposed surface structure of the bonded phases are given beside each figure. The chemical shifts and the structural environment of the silicon atom of interest (Si*) are given in Table II.

As shown in Fig. 1A, the ^{29}Si spectra showed the dominant silica resonances at -110 (peak a = a'), -100 (peak b = b') and -90 (peak c) ppm, and these has been assigned to the surface silicon, $(\equiv SiO)_4Si^*$, single hydroxyl sites, $(\equiv SiO)_3Si^*OH$, and geminal hydroxyl sites, $(\equiv SiO)_2Si^*(OH)_2$, respectively. The weak absorbance at -90 ppm indicates that the silica contains a relatively small amount of geminal silanols.

The ^{29}Si spectra of the representative packings (columns 1,3,5 and 10) are shown in Fig. 1B–E. The absence of peak c in these spectra suggests that the geminal hydroxyls are more reactive, although present in smaller proportion. In general, there is a rapid transfer of intensity between adjacent peaks with increase in carbon load due to an increase in the formation of secondary siloxane bonds, *i.e.*, bonds labelled a', b' and e'. The resonance at -19 ppm (peak e) in Fig. 1B is assigned to silane molecules characterized by two siloxane bonds formed via a 1:2 reaction with the silanols. The presence of peak f, assigned to a silicon atom bonded to siloxane bond and a hydroxyl group, indicates that the silane reagent also undergoes a 1:1 reaction with the silanols and the hydroxyl groups arises from the hydrolysis of the unreacted chlorine atom of the reagent. Consequently, it can be concluded that the silane reagent undergoes mixed reactions with the silica surface, *i.e.*, 1:1 and 1:2 stoichiometry.

TABLE II

STRUCTURAL ENVIRONMENT OF Si* ATOM

Chemical shift (ppm)	Peaks	Species
-110	a(a')	$Si^*(OSi\equiv)_4$
-101	b(b')	$HOSi^*(OSi\equiv)_3$
-91	c	$(OH)_2Si^*(OSi\equiv)_2$
-19	e(e')	$-O-Si^*(CH_3)(R)-O-$
-8 to -4	f	$HO\ Si^*(CH_3)(R)-O-$

As can be seen from Fig. 1B–E, the intensity of peak e increased with increasing carbon load whereas that of peak f remained relatively unchanged between Fig. 1A and B and Fig. 1C and D, respectively. As it becomes more difficult for the silane molecules to react with the surface silanols owing to steric hindrance on increasing the reaction step, therefore, the above phenomena indicate that further silanization occurred on the newly formed silanols. Consequently, the increase in siloxane peak intensity (peak e) suggests a possible 1:2 reaction mechanism between the silane molecules and the hydroxyl groups of two adjacent siloxane bonds (labelled e'), that is, the

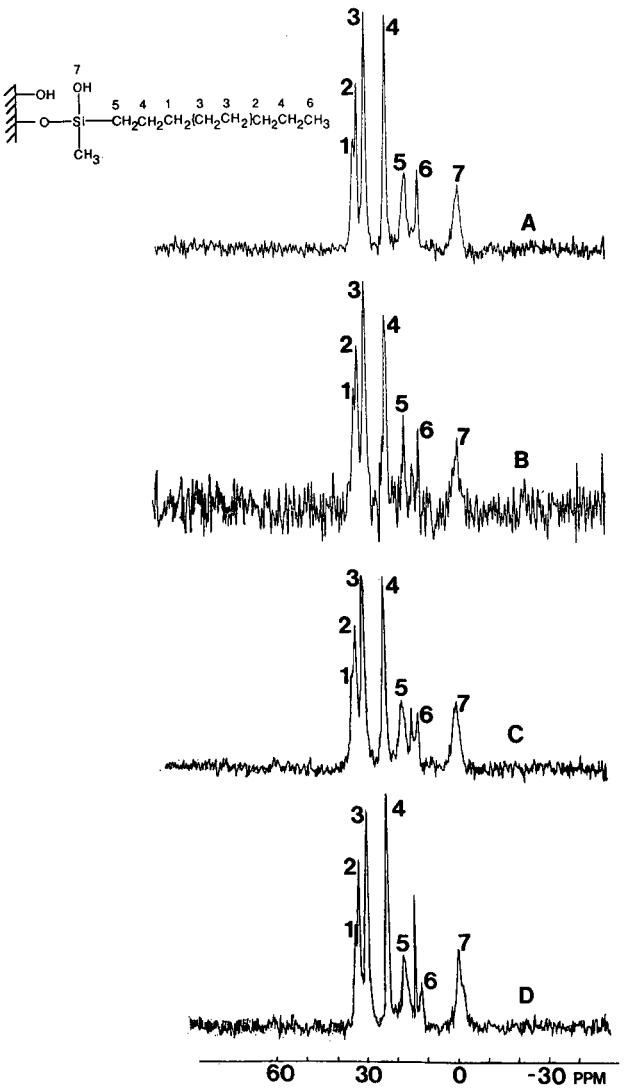

Fig. 2. ^{13}C CP-MAS-NMR spectra of the bonded phases: (A) column 1; (B) column 3; (C) column 5; (D) column 10.

newly formed silanols. This is further confirmed by the absence of the silicon peak at −47 ppm associated with one ≡Si–O–group, two hydroxyl groups and an alkyl group [2].

Fig. 2 shows the ^{13}C CP-MAS-NMR spectra of the representative packings and the chemical shifts (labelled 1–7) were assigned according to the literature [7,11,17]. The resonances at 34 and 32 ppm are assigned to methylene carbons 1 and 2, respectively, owing to their slower cross-polarization rate than methylene carbon 3 in the same chemical environment [10].

The dominant peaks at 22 and 29 ppm can be identified with the methylene groups adjacent to the terminal methyl C (peak 4) and internal methylene carbon atom (peak 3) of the hydrocarbon chain, respectively. The absorption at 17, 12 and −0.56 to −1.04 ppm are assigned to the methylene carbon atom attached to Si atom (peak 5), terminal methyl C (peak 6) and the methyl carbon attached to Si atom (peak 7), respectively.

In general, the chemical shifts of the carbon atoms were affected by their chemical environments and not the carbon load, except the carbon atoms near the silica surface (peak 7), which cross-polarize faster with increasing carbon load. The lower field shift in carbon 7 resonances with increasing carbon load further substantiate the polymeric nature of the bonded phases and consequent increase in steric interaction between the methyl groups possibly with the silica surface and/or the other attached silane moieties. The gradual decrease in the intensities of peaks 5 and 6 may be attributed to the short relaxation time of carbon atoms near the silica surface.

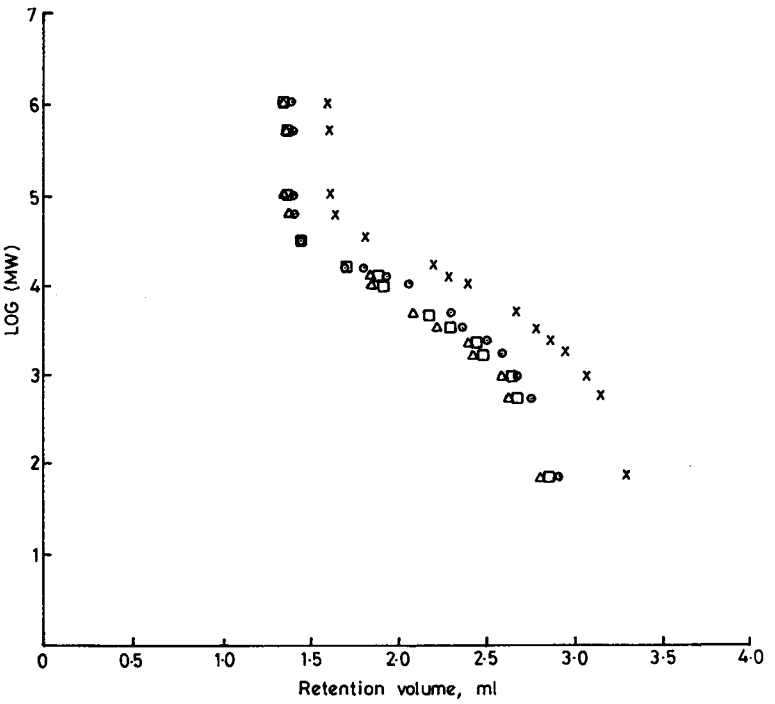

Fig. 3. Polystyrene calibration graphs for (×) silica gels, (○) column 1, (□) column 3 and (△) column 5 by GPC.

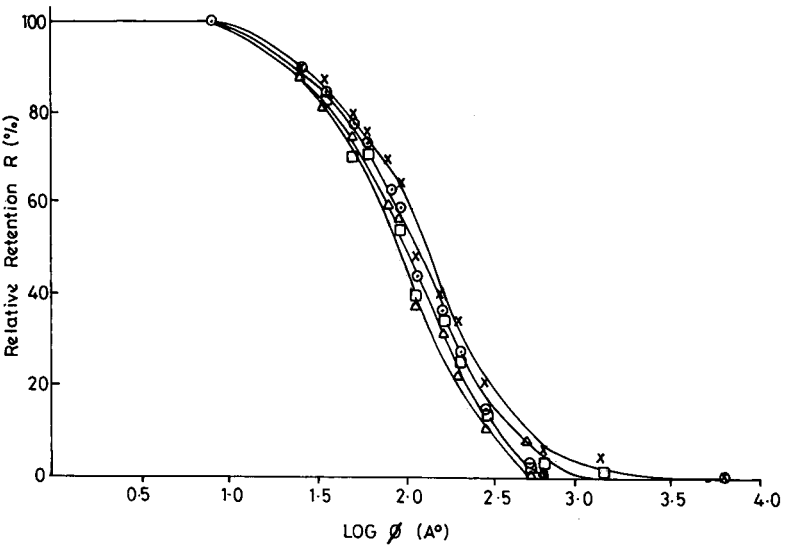

Fig. 4. Pore-size distribution by GPC. Symbols as in Fig. 3.

Considering the resonance pattern in Fig. 1 and 2, it is proposed that the bonded phases consists essentially of cyclic structures of the type $(–Si–O–Si(CH_3)(R)–O–)_n$ and $[(–Si–O–Si(CH_3)(R)–O–)_2Si(CH_3)(R)]_n$, where n is the number of siloxane units and R is the alkyl chain length (C_8).

The molecular mass calibration graphs of the packings, as illustrated in Fig. 3, are substantially the same except that of the unmodified silica gels. This further confirms the retention properties of the phases in the reversed-phase mode as reported in an earlier paper [13]. The shift in the calibration graphs reflects the effect of surface modification on the size-exclusion properties of silica gels and possible operation of a mixed retention mechanism [18]. Irrespective of the carbon load and the shift in the calibration graphs, the bonded phases have the same molecular mass separation range (molecular mass 580–68 000) and similar pore-size distribution as illustrated in Fig. 4.

Whilst the effect of surface modification on surface area and pore volume [$V_{p(N_2)}$] has been explained earlier [13], it is further observed that the GPC experiments produced lower pore volumes than the BET nitrogen adsorption isotherm as shown in Table I. The differences in the pore volumes measured by the two methods may be ascribed to possible alteration of the pore structure by the mobile phase (THF) or the penetration of the micropores by nitrogen [18].

ACKNOWLEDGEMENTS

The authors are grateful to Dr. C. Groombridge and Mr. D. B. Butler of the Royal Holloway and Bedford New College, ULIRS, Egham, UK, for their assistance with the NMR measurements and to Mr. E. B. Orgunseye of the Earth Sciences Department, Ogun State University, Ago-Iwoye, for drawing some of the figures.

REFERENCES

1 J. Nawrocki and B. Buszewski, *J. Chromatogr.*, 449 (1988) 1.
2 S. O. Akapo and C. F. Simpson, *J. Chromatogr.*, 28 (1990) 186.
3 K. K. Unger, *Porous Silica*, Elsevier, Amsterdam, 1979.
4 R. K. Iler, *The Chemistry of Silica*, Wiley-Interscience, New York, 1979.
5 G. E. Marciel and D. W. Sindorf, *J. Am. Chem. Soc.*, 102 (1980) 7606.
6 D. W. Sindorf and G. E. Marciel, *J. Am. Chem. Soc.*, 103 (1981) 4263.
7 G. E. Marciel, D. W. Sindorf and V. J. Bartuska, *J. Chromatogr.*, 205 (1981) 438.
8 D. W. Sindorf and G. E. Marciel, *J. Phys. Chem.*, 86 (1982) 5208.
9 D. W. Sindorf and G. E. Marciel, *J. Am. Chem. Soc.*, 105 (1983) 3767.
10 D. W. Sindorf and G. E. Marciel, *J. Am. Chem. Soc.*, 105 (1983) 1848.
11 E. Bayer, K. Albert, J. Reiners, M. Nieder and D. Muller, *J. Chromatogr.*, 264 (1983) 197.
12 A. A. Claessens, J. W. de Haan, L. J. M. van de Ven, P. C. de Bruyn and C. A. Cramers, *J. Chromatogr.*, 436 (1988) 345.
13 S. O. Akapo, A. Furst, T. M. Khong and C. F. Simpson, *J. Chromatogr.*, 471 (1989) 283.
14 S. O. Akapo and C. F. Simpson, *Anal. Proc.*, 26 (1989) 394.
15 T. M. Khong and C. F. Simpson, *Chromatographia*, 24 (1987) 385.
16 I. Halasz and K. Martin, *Angew. Chem. Int. Ed. Engl.*, 17 (1978) 901.
17 M. E. McNally and L. B. Rogers, *J. Chromatogr.*, 331 (1985) 23.
18 J. V. Dawkins and M. Hemming, *Makromol. Chem.*, 176 (1975) 1795.

Journal of Chromatography, 557 (1991) 523–530
Elsevier Science Publishers B.V., Amsterdam

CHROM. 23 233

Short Communication

Chromatographic trace analysis of some organic compounds in the environment using derivatization–sorption concentration techniques

I. Gas chromatographic analysis of acrylates in air

J. CHURÁČEK*, H. PECHOVÁ, A. HORNA, R. KOTRLA and K. VENTURA
University of Chemical Technology, CS-53210 Pardubice (Czechoslovakia)
(First received , 1990; revised manuscript received , 1991)

ABSTRACT

Derivatization–sorption concentration techniques for the gas chromatographic analysis of acrylates are described. Acrylates are accumulated and derivatized in the trapping absorber. The sorption and derivatization yield of thioethers is 71 ± 2.6%.

Two different procedures are recommended: (1) direct selective derivatization–sorption, and (2) universal sorption of all organic compounds in the first step, followed by a thermal desorption and selective derivatization in the second step.

INTRODUCTION

Methods for thin-layer chromatography (TLC) and gas chromatography (GC) separation of alkyl esters of acrylic and methacrylic acids [1–3] and for preparation and separation of their derivatives with diazomethane [4–6] *n*-butylmercaptan [7–9] and hydrogen chloride [10] have been published previously.

Perfect separation and identification of acrylate can be achieved by gas chromatography–mass spectrometry on an OV-101 glas capillary column [11] in less than 20 min provided, of course, a 2–10% solution of the esters is available. These conditions are impossible to meet under practical application of trace analysis. The compounds are contained in the atmosphere in concentrations of after ppm or less. In this case their direct analysis is not feasible and, consequently, it is necessary to treat the sample in order to concentrate it.

Two different procedures and their combination for identification and deter-

0021-9673/91/$03.50

mination of trace amounts of acrylates in the environment have been tested in this paper.

It was demonstrated that the "trapping" procedure offers the best results if the chemical reaction and formation of derivatives are used. Universal sorption of all organic compounds on solid state sorbent (Tenax, Porapak, Separon) can help to improve the procedure further.

EXPERIMENTAL

A number of sorbents of different origin were used as specified: Tenax GC 60–80 mesh (200–250 μm) was obtained from Serva (Heidelberg, Germany) Porapak S 80–100 mesh and Porapak R 80–100 mesh were purchased from Milipore Waters Chromatography Division (Milford, MA, U.S.A.), Chromosorb 102 100–120 mesh and Chromosorb 105 80–100 mesh was from Serva and Separon CHN 200–300 μm, Separon SE 150 μm and Separon SDA 90–125 μm were purchased from Tessek, (Prague, Czechoslovakia). All anaytical-grade solvents and pure-grade butylmercaptane were obtained from Lachema (Brno, Czechoslovakia).

Apparatus

A Fractovap GW gas chromatograph (Carlo Erba, Milan, Italy) and Chrom 5 gas cromatograph–flame ionization detector (Laboratorní přístroje, Prague, Czechoslovakia) were used.

Enrichment procedure

Air sample collection

Procedure (a). A defined amount of air (1–40 l) was sucked through the trapping absorber filled with an alkaline solution of *n*-butylthiol in acetone (sodium hydroxide concentration 0.04 mol/l, *n*-butylthiol concentration 0.03 mol/l). On-line derivatization–sorption hardware (Fig. 1a) was home-made (diffuser bubbler trapping absorber 250 mm × 25 mm O.D.).

Procedure (b). Glass tubes (60 mm × 3.2 mm I.D.) containing 80–140 mg of solid sorbent were used. The air was sampled at a flow-rate of 100–400 ml/min. The flow-rate was calibrated with a soap bubbler flowmeter (Fig. 1b).

Procedure (c): This represents a combination of procedures (b) and (a): The entrapped organic compounds (by procedure b) were desorbed by thermal desorption and flushed with inert gas into a derivatization–sorption apparatus. Of the many organic compounds which were trapped on solid sorbent, only acrylates would react in the trapping absorber. Hydrocarbons and other organic compounds (not containing a double bond) did not react and were not retained.

Absorpton solution was concentrated, transferred quantitatively into 5-ml or 1-ml volumetric vessels; if the concentration of the contaminant was extremely small then it was necessary to use even smaller vials.

RESULTS AND DISCUSSION

The role of derivatization in modern chromatographic analysis is not only to increase the sensitivity of detection but also in possibly to concentrate the substances being followed in the course of sampling.

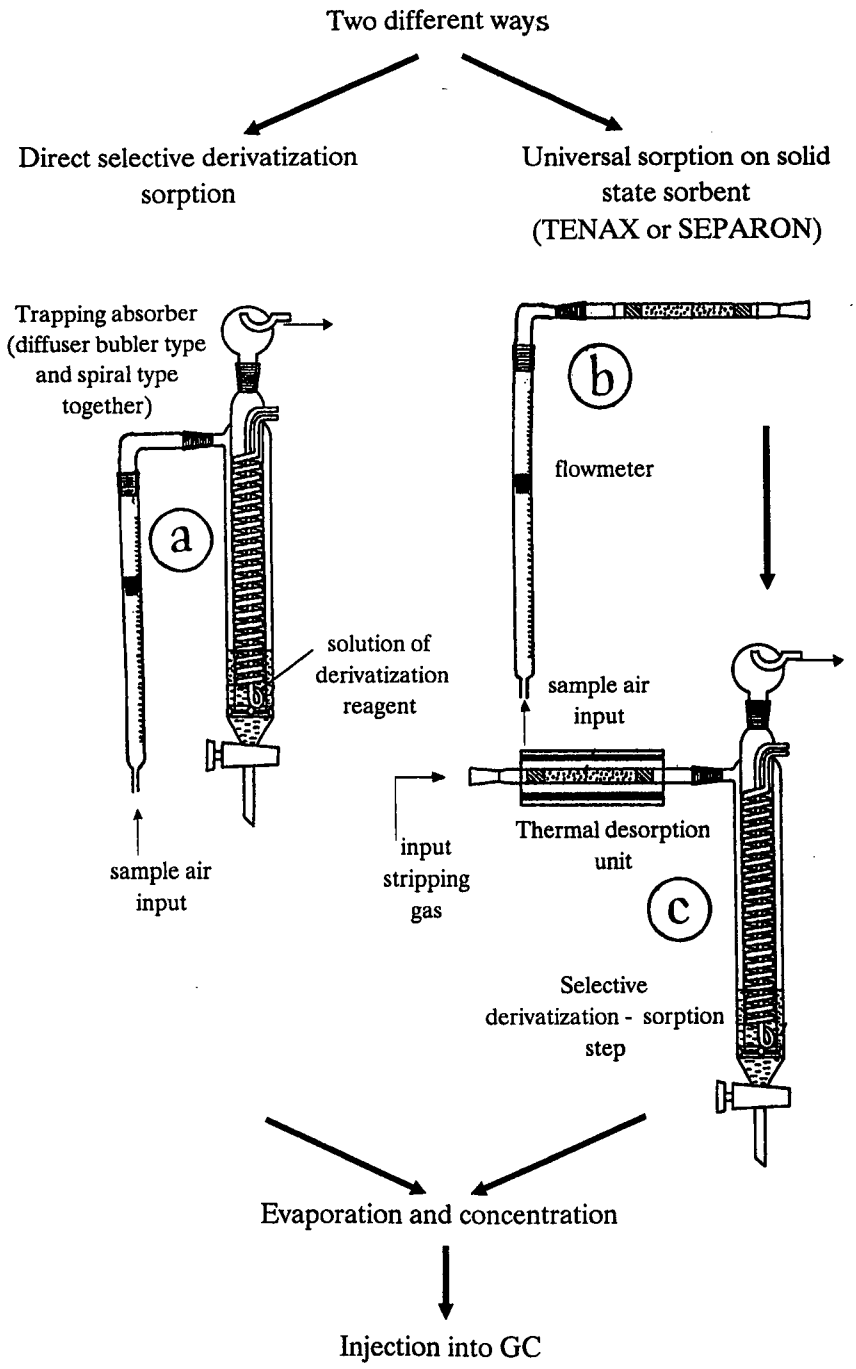

Fig. 1. A schematic representation of the sorption system assembly.

The principle of the derivatization–sorption procedure is obvious. A certain amount of air is sucked through the trapping absorber filled with the solution of the reagent (selective derivatization–sorption method) (Fig. 1a). The best are diffuser bubblers having an absorbent solution capacity of 10–100 ml working at a sampling rate from 100 ml to thousands of milliliters per minute. They are easy to use and have a good gas–liquid contact time, but are subject to plugging. One disadvantage of this method is considerable evaporation of the solvent from the absorption apparatus during suction of a larger amount of air.

This problem does not occur if the sorption tube (Fig. 1b) is used with a solid sorbent (Tenax, Porapak, Chromosorb or some new sorbent type like Separon) (Table I). In the first step, preliminary concentration is carried out. In the tube of the solid sorbent, all organic compounds contained in the air are entrapped. In the next step (Fig. 1c) the entrapped organic compounds are removed, *i.e.* desorbed, from the solid sorbent by thermal desorption and flushed with inert gas into a derivatization–sorption apparatus. Here only acrylates are selectively entrapped and concomitantly converted into corresponding derivatives. Other organic compounds pass through the reactor. The absorption solution is then concentrated, transferred quantitatively into a volumetric flask and, finally, the solution is injected into the gas chromatograph.

The main question is which reagents can be used for derivatization. In our case *n*-butylthiol and diazomethane appeared the to be the best, but we limited ourselves to *n*-butylthiol.

For optimization of the sorption–derivatization process, it was necessary to take into account the following facts:

(a) The flow-rate of the air sample through the absorption unit must be kept at its optimum. In our case the optimum flow rate of the gaseous sample was 210 ml/min.

(b) The absorption (reaction) temperature must be also optimized and should represent a compromise between the need to ensure sufficiently fast reaction and tolerable evaporation of the reaction solution. Though one would propose an operating temperature of 40°C, for practical reasons we have worked at 25–35°C.

TABLE I

EXTRAPOLATED RETENTION VOLUMES (V_g) AND SAFE SAMPLING VOLUMES (V_{max}) [12] OF *n*-BUTYLACRYLATE ON POROUS POLYMERS

Sorbent	V_g (l/g) at 293 K	V_{max} (l/g) at 293 K	Ref.
Tenax GC	1630	1540	This paper
	63	32	13[a]
	238	120	14[b]
Porapak S	2150	1980	This paper
Porapak R	6670	6350	This paper
Chromosorb 102	1190	1120	This paper
Chromosorb 105	1490	1890	This paper
Separon SE	1140	940	This paper
Separon SDA	560	520	9
Separon CHN	4830	4210	This paper

[a] For methyl- and ethylacrylate.

[b] For methylacrylate (7.96 ml of Tenax was used).

TABLE II

RELATIVE WEIGHT RESPONSE (RWR) AND RELATIVE STANDARD DEVIATION (R.S.D.) FOR ACRYLATE DERIVATES USING FLAME IONIZATON DETECTION (n = 6)

Butylthioether of acrylic acid ester C_1–C_8	RWR	R.S.D. (%)
1	1.20	2.05
2	1.16	2.31
3	1.08	2.89
4	1.00	–
5	1.20	2.67
6	1.12	2.65
7	1.15	2.40
8	1.10	2.55

TABLE III

REPRODUCIBILITY OF DERIVATIZATION TRAPPING PROCEDURE BY OPTIMAL CONDITIONS

Flow: 200 ml/min; sodium hydroxide concentration: 0.04 mol/l; n-butylthiol concentration: 0.03 mol/l; temperature: 35°C. SA4 = n-butylthioether of n-butylacrylate; ρSA4 = concentration (mass) of injected solution; c_{SA4} = concentration (volume) of injected solution; R.S.D. = relative standard deviation; i.u., integration unit.

SA4 sample no.	Area (A) (i.u.) A	ρSA4 (mg/ml^{-1})	$c_{SA4} \cdot 10^{-3}$ (mol l^{-1})	Yield (%)	Average yield (%)	R.S.D. (%)
1	185 307	1.628	7.457	66.07		
	185 748	1.632	7.475	66.23	66.15	0.171
2	191 863	1.686	7.721	68.41		
	190 884	1.677	7.681	68.06	68.24	0.363
3	196 424	1.726	7.904	70.04		
	195 009	1.696	7.707	68.82	69.43	1.243
4	184 572	1.622	7.427	65.81		
	189 214	1.663	7.614	67.46	66.64	1.751
5	211 200	1.856	8.499	75.30		
	218 586	1.921	8.796	77.94		
	207 178	1.820	8.337	73.87	75.70	2.727
6	215 378	1.892	8.667	76.79		
	223 153	1.961	8.980	79.57	78.18	2.514
7	190 576	1.674	7.669	67.95		
	196 650	1.728	7.913	70.12		
	201 910	1.774	8.125	71.99	70.02	2.888
8	193 489	1.700	7.786	69.00		
	197 138	1.732	7.933	70.29	69.65	1.310
9	219 130	1.925	8.818	78.13		
	194 317	1.707	7.819	69.28		
	209 066	1.837	9.413	74.54	73.98	6.016
10	211 219	1.856	8.499	75.31		
	208 470	1.832	8.389	74.33	74.82	0.926
11	199 692	1.755	8.036	71.20		
	203 366	1.767	8.183	72.51	71.86	1.289

Optimization of conditions should always be carried out for a given reagent and for each sorption apparatus. The sorption efficacy of the bubbler trapping absorber can be most simply evaluated by connecting a second absorber to the system.

Enrichment procedure

Acrylates present in an air sample were simultaneously accumulated and derivatized in the trapping absorber. A given amount of air (1–40 l) was sucked through the trapping absorber (reactor) filled with 25–50 ml of acetone solution containing 0.04 mol/l sodium hydroxide and 0.03 mol/l *n*-butylthiol. The sorption and derivatization yield was 71.3 ± 2.6% ($n=10$). The absorption solution was concentrated and transferred quantitatively into a 5-ml volumetric flask (it is also possible to use volumetric vessels of 1 ml or less if necessary).

Estimation of the determination limit and quatitative aspects

The limit of determination was established by using an absorption unit equipped with a stripping vessel into which 0.3–900 μg of acrylic acid butyl ester was gradually added. The minimum amount of corresponding thioether assayed was 1.5 μg. The relative weight response of the analysed derivatives is summarized in Table II. As indicated, the relative standard deviation for each derivative on the packed GC column

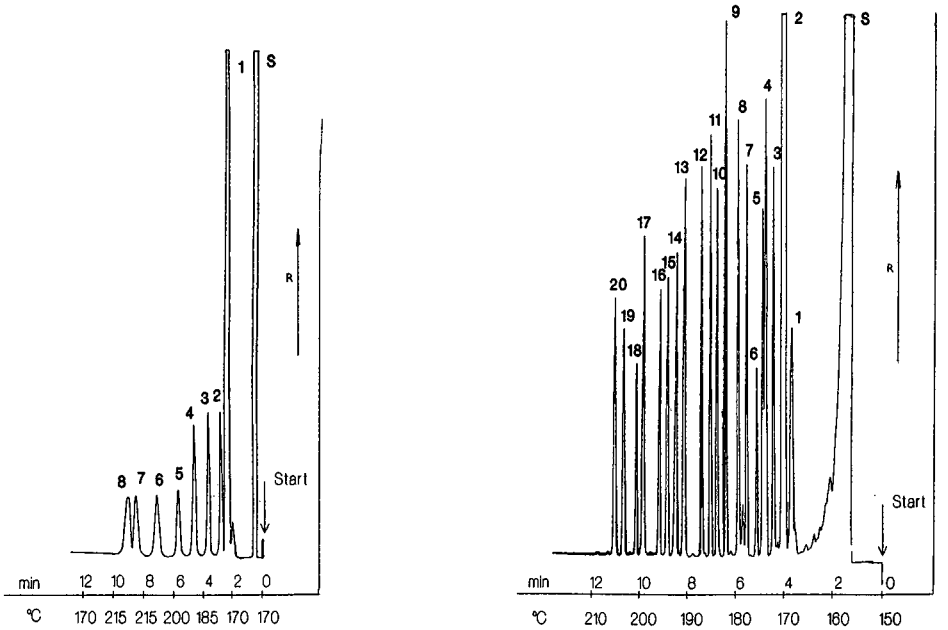

Fig. 2. GC gradient temperature separation of methyl- to octylacrylate butylthioethers (SA 1–8). Chrom 5–flame ionization detector: column 2.4 m × 3 mm I.D., Chromosorb W AW with 20% DC-200, nitrogen flow 48 ml/min, hydrogen flow 30 ml/min, air flow 500 ml/min. Temperature programme: 170°C at 2 min, 7.5°C min^{-1}, 210°C at 2 min. S = solvent; 1–8 = methyl- to octylacrylatethioethers. R = Response.

Fig. 3. Separation of C_1–C_6 *n*-alkyl and C_3–C_6 isoalkyl esters of acrylic and methacrylic acid on a fused-silica capillary column. For experimental conditions and peak identification, see Table IV.

TABLE IV

RETENTION TIME (t_R) AND RELATIVE RETENTION (RRT) OF *n*-BUTYLTHIOETHERS OF C_1–C_6 *n*-ALKYL AND C_3–C_6 ISOALKYL ESTERS OF ACRYLIC ACID AND METHACRYLIC ACID ON FUSED-SILICA CAPILLARY COLUMN, 32 m WITH OV-101

Temperature gradient 5°C min^{-1}, from 150 to 220°C. Bu_2S_2 = dibutyldisulphide; SA 1–6 = thioether from C_1–C_6 acrylates; SMA 1–6 = thioether from C_1–C_6 methacrylates; i = iso.

No of peak	Compound	t_R (s)	RRT
S	Solvent	(88.0)	(0.16)
1	SA 1	277.5	0.52
2	SMA1 + Bu_2S_2	298.2	0.55
3	SA2	336.2	0.63
4	SMA2	361.6	0.67
5	SAi3	363.7	0.68
6	SMAi3	392.4	0.73
7	SA3	430.0	0.80
8	SMA3	457.0	0.85
9	SAi4	493.3	0.92
10	SMAi4	519.3	0.96
11	SA4	538.3	1.00
12	SMA4	553.2	1.03
13	SAi5	612.6	1.14
14	SMAi5	633.4	1.18
15	SA5	657.0	1.22
16	SMA5	680.7	1.26
17	SAi6	729.8	1.36
18	SMAi6	749.6	1.39
19	SA6	782.6	1.45
20	SMA6	804.3	1.49

was less than 3%. The reproducibility of the derivatization–sorption trapping procedure is shown in Table III.

Gas chromatographic separation

For identification and quantitative trace analysis of acrylate and methacrylate derivatives (thioethers), an analytical column packed with Chromosorb W AW with 20% DC 200 (Fig. 2) or a capillary fused-silica column with OV-101 silicone phase (Fig. 3) appeared to be the best. Retention times and relative retention times (with respect to *n*-butylacrlate) of corresponding butylthioethers are presented in Table IV. Each derivative displayed a single sharp symmetrical chromatographic peak with no significant peak tailing and did not indicate any signs of decomposition on the column.

CONCLUSIONS

The application of universal sorption on Tenax or Separon only does not solve the problem of determining nanogram concentrations of acrylates in 1 litre of air. This is because a great number of a whole series of organic compounds, mostly hydrocarbons, which are sorbed on a solid sorbent may be present in the sampled

atmosphere. During the desorption step these are released and flushed into the chromatographic column, resulting in much overlapping of the tiny peaks of acrylates.

Not does the application of derivatization–sorption procedures for the analysis of trace amounts of acrylates in air solve this problem because a large volume of air (100–1000 l) must be sucked through the derivatization sorption apparatus, leading to sorption solution and time losses.

To follow trace amounts of acrylates in the atmosphere, of the order of ng/l, both universal concentration techniques (sorption on solid sorbent) and subsequent selection connected with chemical derivatization should be used in combination.

Two different procedures for identification and determination of acrylates in the environment are recommended (Fig. 1):

(1) Direct selective derivatization–sorption method (Fig. 1a).

(2) Universal sorption of all organic compounds on a solid sorbent in the first step (Fig. 1b) followed by a thermal desorption and selective derivatization sorption in the second step (Fig. 1c).

The main advantage of the second procedure is that, of the many organic compounds which are trapped on the solid sorbent, only acrylates will react with *n*-butylthiol.

The last step is common to both procedures: the sorption solution is partly evaporated, the entrapped solutes are concentrated and the resulting sample is subjected to GC analysis.

ACKNOWLEDGEMENTS

We thank the personnel of Chemical Works, Sokolov, Czechoslovakia, for assistance and fruitful discussion.

REFERENCES

1 A. Horna, H. Pechová, A. Tůmová and J. Churáček, *J. Chromatogr.*, 288 (1984) 230.
2 A. Horna, J. Táborský, O. Dufka, P. Matoušek and J. Churáček, *J. Chromatogr.*, 325 (1985) 367.
3 A. Horna, H. Pechová and J. Churáček, *J. Chromatogr.*, 330 (1985) 439.
4 D. S. Matteson, *J. Org. Chem.*, 27 (1962) 4293.
5 A. Ledwith and D. Parry, *J. Chem. Soc. C*, (1966) 1408.
6 A. Horna, H. Pechová, A. Pikulová, L. Hornová and J. Churáček, *J. Chromatogr.*, 367 (1986) 155.
7 F. D. Snell and C. L. Hilton, *Encyclopedia of Industrial Chemical Analysis*, Vol. 4, Wiley-Interscience, New York, 1966, p. 181.
8 D. Hurt and L. Gershbein, *J. Am. Chem. Soc.*, 69 (1947) 2328.
9 A. Horna, H. Pechová, O. Kašpar and J. Churáček, *Sb. Ved. Pr., Vys. Sk. Chemickotechnol.*, Pardubice, 1991, in press.
10 A. Horna, J. Táborský, J. Churáček and O. Dufka, *J. Chromatogr.*, 348 (1985) 141.
11 A. Horna, J. Táborský and J. Churáček, *J. Chromatogr.*, 360 (1986) 89 and references cited therein.
12 A. Raymond and G. Guiochon, *J. Chromatogr. Sci.*, 13 (1975) 173.
13 R. H. Brown and C. J. Purnell, *J. Chromatogr.*, 178 (1979) 79.
14 K. J. Krost, E. D. Pellizzari, S. G. Walburn and S. H. Hubbard, *Anal. Chem.*, 54 (1982) 810.

Author Index Vols. 556 and 557

PUBLICATION SCHEDULE FOR 1991

Journal of Chromatography and Journal of Chromatography, Biomedical Applications

MONTH	D 1990–M 1991	J	J	A	S	O	N	D
Journal of Chromatography	Vols. 535–545/1	545/2 546/1 + 2 547/1 + 2	548/1 + 2 549/1 + 2 550/1 + 2	552/1 + 2 553/1 + 2 554/1 + 2 555/1 + 2	556/1 + 2 557/1 + 2 558/1	558/2 559/1 + 2		
Cumulative Indexes, Vols. 501–550				551/1 + 2				
Bibliography Section	560/1	560/2			561/1			561/2
Biomedical Applications	Vols. 562–566	567/1	567/2 568/1	568/2	569/1 + 2 570/1	570/2	571/1 + 2	572/1 + 2

[1]The publication schedule for further issues will be published later

INFORMATION FOR AUTHORS

(Detailed *Instructions to Authors* were published in Vol. 522, pp. 351–354. A free reprint can be obtained by application to the publisher, Elsevier Science Publishers B.V., P.O. Box 330, 1000 AH Amsterdam, The Netherlands.)

Types of Contributions. The following types of papers are published in the *Journal of Chromatography* and the section on *Biomedical Applications:* Regular research papers (Full-length papers), Review articles and Short Communications. Short Communnications are usually descriptions of short investigations, or they can report minor technical improvements of previously published procedures; they reflect the same quality of research as Full-length papers, but should preferably not exceed six printed pages. For Review articles, see inside front cover under Submission of Papers.

Submission. Every paper must be accompanied by a letter from the senior author, stating that he/she is submitting the paper for publication in the *Journal of Chromatography*.

Manuscripts. Manuscripts should be typed in double spacing on consecutively numbered pages of uniform size. The manuscript should be preceded by a sheet of manuscript paper carrying the title of the paper and the name and full postal address of the person to whom the proofs are to be sent. As a rule, papers should be divided into sections, headed by a caption (*e.g.*, Abstract, Introduction, Experimental, Results, Discussion, etc.). All illustrations, photographs, tables, etc., should be on separate sheets.

Introduction. Every paper must have a concise introduction mentioning what has been done before on the topic described, and stating clearly what is new in the paper now submitted.

Abstract. All articles should have an abstract of 50–100 words which clearly and briefly indicates what is new, different and significant.

Illustrations. The figures should be submitted in a form suitable for reproduction, drawn in Indian ink on drawing or tracing paper. Each illustration should have a legend, all the *legends* being typed (with double spacing) together on a *separate sheet*. If structures are given in the text, the original drawings should be supplied. Coloured illustrations are reproduced at the author's expense, the cost being determined by the number of pages and by the number of colours needed. The written permission of the author and publisher must be obtained for the use of any figure already published. Its source must be indicated in the legend.

References. References should be numbered in the order in which they are cited in the text, and listed in numerical sequence on a separate sheet at the end of the article. Please check a recent issue for the layout of the reference list. Abbreviations for the titles of journals should follow the system used by *Chemical Abstracts*. Articles not yet published should be given as "in press" (journal should be specified), "submitted for publication" (journal should be specified), "in preparation" or "personal communication".

Dispatch. Before sending the manuscript to the Editor please check that the envelope contains four copies of the paper complete with references, legends and figures. One of the sets of figures must be the originals suitable for direct reproduction. Please also ensure that permission to publish has been obtained from your institute.

Proofs. One set of proofs will be sent to the author to be carefully checked for printer's errors. Corrections must be restricted to instances in which the proof is at variance with the manuscript. "Extra corrections" will be inserted at the author's expense.

Reprints. Fifty reprints of Full-length papers and Short Communications will be supplied free of charge. Additional reprints can be ordered by the authors. An order form containing price quotations will be sent to the authors together with the proofs of their article.

Advertisements. Advertisement rates are available from the publisher on request. The Editors of the journal accept no responsibility for the contents of the advertisements.

Eleventh International Symposium on HPLC of Proteins, Peptides and Polynucleotides

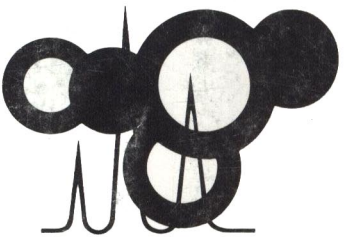

PRELIMINARY PROGRAM

October 20-23, 1991
Washington, DC USA

SUNDAY, OCTOBER 20, 1991

Registration and Welcome Reception

MONDAY, OCTOBER 21, 1991

Column Technology and Support Materials
Speakers: K.K. Unger, G.G. Wallace, B.E. Boyes, N.B. Afeyan, D.E. Williams
Protein Surfaces and Separation Processes
Speakers: K.D. Caldwell, A.W. Purcell, L. Haggerty, X. Geng
Poster Session
Discussion Session
Quality Control in Analytical Biotechnology
Guest Speaker: R.L. Garnick

TUESDAY, OCTOBER 22, 1991

Isolation and Purification Techniques I
Speakers: R.D. Sitrin, B. Sebille, S.M. Cramer, T.B. Tennikova
Isolation and Purification Techniques II
Speakers: G.B. Cox, G. Guiochon, E.P. Kroeff, M. Hessing, P. Karsnas
Poster Session
Discussion Session
Analytical Methodologies I
Speakers: F.E. Regnier, M. Trucksess, J.J. Dougherty, Jr.

WEDNESDAY, OCTOBER 23, 1991

Electroseparation Techniques
Speakers: B.L. Karger, S. Hjerten, H. Irth
Instrumental Methods
Speakers: R.D. Smith, I.S. Krull, C. Miller-Stein, R.A. Kornfeld
Poster Session
Discussion Session
Analytical Methodologies II
Speakers: R.R. Townsend, L. Otvos, K.-I. Kasai
Adjourn

SECRETARIAT, 11TH ISPPP:

Mrs. Janet Cunningham
Barr Enterprises
P.O. Box 279
Walkersville, Maryland 21793 USA
Phone: 301-898-3772
Fax: 301-898-5596